The Viscoelastic Behaviour Of Tendon

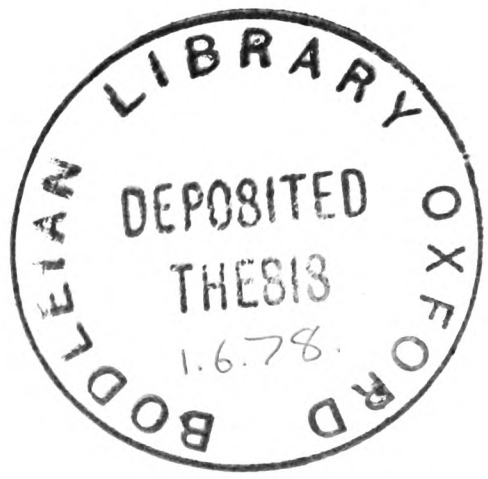
by

C.J. Hooley

Hertford College

1977

A thesis submitted for the degree of Doctor of Philosophy at the University of Oxford



The Viscoelastic Behaviour of Tendon

by C.J. Hooley, Hertford College. D.Phil. Thesis. Submitted Michaelmas 1977

Abstract

The viscoelastic deformation of tendon has been studied in the 'toe' and 'linear' regions of the stress-strain curve. The extent to which the behaviour of the material can be considered to be linear viscoelastic has been determined. It was found that the tendon exhibited non-linear viscoelastic behaviour in both the 'toe' and 'linear' regions and the observed non-linearity was in contrast to that found for synthetic polymeric solids.

The apparent activation energy, ΔH_a, of the viscoelastic deformation process of tendon was determined by the temperature change (or T-jump) technique. A gradual transition was observed from the value of ΔH_a = 12 kcal/mol in the 'toe' region to ΔH_a = 32 kcal/mol in the 'linear' region in creep, recovery and stress relaxation experiments for a variety of tendon specimens. These values indicated that the viscoelastic mechanism of tendon deformation was one of shear of the mucopolysaccharide gel in between the collagen ribbons in the 'toe' region followed by fibrillar extension in the 'linear' region.

A theoretical model based on this hypothesis and the assumptions of linear viscoelasticity was developed to explain the observed viscoelastic behaviour of tendon, using the normal viscoelastic parameters of the constituents of the tendon, the structural constants of the material and the appropriate form for the retardation spectrum. Excellent agreement between experiment and theory was found for a variety of experimental circumstances.

A critical examination of the T-jump experiment was made. Generalised non-isothermal linear viscoelastic equations in creep were developed and the validity of these equations for the case of a ramp temperature change was tested on a specimen of poly(methylmethacrylate). The predicted increase in the experimentally obtained value of ΔH_a was observed as the duration of the ramp temperature change increased. For the case of the instantaneous temperature change (T-jump) experiment, these equations were used, together with an appropriate form for the retardation spectrum, (either a box or a wedge distribution) to predict the creep rate dependence on time. Excellent fit of the creep rate data for tendon was obtained with these equations. Using a box distribution for the spectrum of retardation times in these equations, it was shown that the effect of b_T on the creep rate behaviour could be neglected under most experimental circumstances.

Abstract

The viscoelastic deformation of tendon has been studied in the 'toe' and 'linear' regions of the stress-strain curve. The extent to which the behaviour of the material can be considered to be linear viscoelastic has been determined in isothermal creep, recovery, 2-step loading and cycling experiments. It was found that tendon exhibited non-linear viscoelastic behaviour in both the 'toe' and 'linear' regions and the observed non-linearity was in contrast to that found for synthetic polymeric solids.

The apparent activation energy, ΔH_a, of the viscoelastic deformation process of tendon was determined by the temperature change (or T-jump) technique. A gradual transition was observed from the value of $\Delta H_a = 12 \pm 3$ kcal/mol in the 'toe' region to $\Delta H_a = 32 \pm 3$ kcal/mol in the 'linear' region in creep, recovery and stress relaxation experiments for a variety of specimens. The value of $\Delta H_a = 0$ found by Rigby et al[1] in the 'toe' region by the method of time-temperature superposition was thus rejected. The values which were found for ΔH_a indicated that the viscoelastic mechanism of tendon deformation was one of shear of the mucopolysaccharide gel in between the collagen ribbons in the 'toe' region followed by fibrillar extension in the 'linear' region.

A theoretical model based on this hypothesis and the assumptions of linear viscoelasticity was developed to explain the observed viscoelastic behaviour of tendon using the normal viscoelastic parameters of the constituents of the tendon, the structural constants of the material and the appropriate form for the retardation spectrum. It was found that the following parameters played an important part in the resulting viscoelastic process, namely; the initial crimp angle, θ_o, the measure of the width of the distribution of the crimp angles, Γ, and the magnitude of the compliance difference of the gel, ΔJ_G, and the fibres, ΔD_F. Excellent agreement between

experiment and theory was found for a variety of experimental circumstances, (creep, creep cycling and T-jump experiments) and the parameters θ_o, $\bar{\lambda}$, ΔJ_G and ΔD_F were determined for a number of specimens from fitting the theoretical equations to the experimental data. The theory illustrates the effects on the viscoelastic properties of changes in these parameters as a result of disease and age, for instance, and provides a challenge for the future in that an independent determination of the parameters, θ_o, $\bar{\lambda}$, ΔJ_G and ΔD_F will confirm the predictions of the theory.

A critical examination of the T-jump experiment was made; in particular, the effect of a non-instantaneous temperature change and the effect of b_T on the observed creep rates were determined. Generalised non-isothermal linear viscoelastic equations in creep were developed and the validity of these equations for the case of a ramp temperature change was tested on a specimen of poly(methylmethacrylate). The predicted increase in the experimentally obtained value of ΔH_a was observed as the duration of the ramp temperature change increased.

For the case of the instantaneous temperature change (or T-jump) experiment, these equations were used, together with an appropriate form for the retardation spectrum (either a box or wedge distribution) to predict the creep rate dependence on time. It was shown that a straight line is to be expected on a plot of log creep rate against log time before the time of the temperature change, t', and that in general, a curve will be seen after t', the exact form of which depends on the value of ΔH_a and the slope of the wedge distribution. Excellent fit of the creep rate data for tendon was obtained with these equations, the values of ΔH_a found from the theory agreeing well with those determined experimentally. Using a box distribution for the spectrum of retardation times, the effect of b_T on the creep rate behaviour was found not to be as great as had been previously thought and

could be neglected under most experimental circumstances. A method was suggested for overcoming the problem when the b_T effect was significant. The equations for the stress relaxation and the recovery T-jump were also presented.

References

1 Rigby B.J., Hirai N., Spikes J.D. and Eyring H., J.Gen.Physicl., 43,265,1959.

2 McCrum N.G. and Pearce D.L.,Nature, Physical Sci.,243,52,1973.

Acknowledgements

The work described in this thesis was carried out at the Department of Engineering Science, Oxford University, under the supervision of Dr. N.G. McCrum, between 1972 and 1975, and afterwards at the Department of Chemical Engineering, Massachusetts Institute of Technology. The work was supported by the Science Research Council, a Kennedy Memorial Trust Scholarship to M.I.T., and a grant from the National Science Foundation.

The thesis would not have been possible but for the assistance of a number of people. I am particularly grateful to Dr. N.G. McCrum, Professor R.E. Cohen, Professor J.M. Caruthers and Dr. C.P. Buckley for their help, advice and encouragement during the course of the thesis. I would also like to thank : Dr. A.H.T. Robb-Smith for providing the tendon specimens; Dr. B.B. Doyle, Dr. A. Miller and Mr. S. White for taking the X-ray measurements; Dr. M.F. Venn for performing the collagen and uronic acid analysis; Mr. T. Parry for his help in unravelling the mysteries of the computer; Mr. R.S. Stone for designing various parts of the apparatus and Mr. D. Saxton for making the apparatus glassware.

Finally, I would like to thank my wife for making the drawings for the thesis, and for her patience and understanding throughout the course of this work.

Contents

		Page
Abstract		i
Acknowledgements		iv
Contents		v
Chapter 1	The Structure and Properties of Tendon	
1.1	Introduction	1
1.2	The Structure of Tendon	2
1.2.1	The Constituents of Tendon	2
1.2.2	The Structure of Collagen	3
1.2.3	The Formation of Collagen	5
1.2.4	The Mucopolysaccharides (Glycosaminoglycans) of Tendon	6
1.2.5	The Elastic Tissue of Tendon	8
1.2.6	The Crimp in Tendon Collagen	8
1.3	The Mechanical Properties of Tendon	10
1.3.1	The Stress-Strain Curve	10
1.3.2	The 'Toe' Region	10
1.3.3	The 'Linear' and Yield Regions	12
1.4	Viscoelasticity of Polymers	12
1.4.1	Linear and Non-linear Viscoelasticity	12
1.4.2	Temperature Dependent Viscoelastic Behaviour of Polymers	16
1.4.3	The Viscoelastic Behaviour of Tendon	21
	References	23
	Tables	
	Figures	
Chapter 2	Materials and Methods	
2.1	Introduction	27
2.2	Specimens	27
2.3	Creep Experiments	28
2.3.1	Apparatus	28
2.3.2	Isothermal Experiments	31
2.3.3	T-jump Experiments	34
2.3.4	Analysis of the Data	36
2.3.5	Thermal Expansion Measurements	38
2.4	Recovery T-jump	39
2.5	Stress Relaxation	40
	References	44
	Tables	
	Figures	
Chapter 3	The Influence of Finite Rates of Temperature Change in the Creep T-jump Experiment	
3.1	Introduction	45
3.2	Theoretical	47
3.3	Experimental	52
3.4	Results	54
3.5	Discussion	56
3.6	Summary	57
	References	59
	Figures	

		Page
Chapter 4	The Instantaneous Temperature Change Experiment	
4.1	Introduction	60
4.2	The Creep T-jump	60
4.2.1	General Equations for the T-jump	60
4.2.2	Equations with a Box Distribution for the Spectrum of Retardation Times	62
4.2.3	The Log Rate-Log Time Curve	66
4.2.4	The Effect of A* on the Determination of ΔH_a	67
4.2.5	The Effect of A* on the Log Creep Rate-Log Time Curve	71
4.2.6	The Wedge Distribution for the Spectrum of Retardation Times	72
4.2.7	The Determination of ΔH_a when A* is Significant	75
4.3	Stress Relaxation T-jumps	76
4.4	Recovery T-jumps	79
4.5	Summary	82
	References	83
	Figures	
Chapter 5	Isothermal Creep Behaviour of Tendon	
5.1	Introduction	84
5.2	Results	85
5.3	Discussion	94
5.4	Summary	99
	References	101
	Figures	
Chapter 6	The Non-isothermal Viscoelastic Behaviour of Tendon in Creep	
6.1	Introduction	102
6.2	The Apparent Activation Energy, ΔH_a, for Tendon	103
6.2.1	ΔH_a in the 'Toe' Region	103
	(a) The T-jump Experiment	103
	(b) Time-Temperature Superposition	106
6.2.2	ΔH_a at High Loads by T-jump	110
6.2.3	ΔH_a of a Preloaded Tendon by T-jump	113
6.3	ΔH_a of Collagen Tape	114
6.4	ΔH_a of Gelatin	114
6.5	Discussion	115
	References	119
	Tables	
	Figures	
Chapter 7	Theoretical Model for the Creep Behaviour of Tendon	
7.1	Introduction	120
7.2	Creep Deformation with a Single Retardation Time	121
7.2.1	The 'Toe' Region	121
7.2.2	The 'Linear' Region	126
7.2.3	Distribution of Crimp Angles	128
7.3	Creep Behaviour with a Distribution of Retardation Times	130
7.3.1	Isothermal Behaviour	130
7.3.2	Temperature Dependent Behaviour	133
7.4	Discussion	137
	References	140
	Figures	

		Page
Chapter 8	Experimental Verification of the Predictions of the Theoretical Model for the Creep of Tendon	
8.1	Introduction	141
8.2	Application of the Theoretical Model to Experimental Data	142
	8.2.1 Determination of the Crimp Angle	142
	8.2.2 Determination of the Distribution of Crimp Angles and the Compliance Differences of the Fibres and Gel	142
	8.2.3 The Dependence on Strain of the Slope of the Log Creep Rate-Log Time Curve	146
	8.2.4 The Dependence of ΔH_a on Strain	147
	8.2.5 The Dependence of the Log Creep Rate on Log Time	147
	8.2.6 Cycling and Recovery Behaviour	151
8.3	Summary	153
	References	155
	Tables	
	Figures	
Chapter 9	The Stress Relaxation Behaviour of Tendon	
9.1	Introduction	156
9.2	Isothermal Behaviour	156
9.3	T-jumps in Stress Relaxation	157
9.4	Theoretical Model for Stress Relaxation	159
9.5	The Stress-Strain Curve of Tendon	162
9.6	Discussion	164
	References	166
	Tables	
	Figures	
Suggestion for Further Work on the Viscoelastic Behaviour of Tendon		167
Appendix:	Non-isothermal Viscoelastic Constitutive Equations	170

Chapter 1

The Structure and Properties of Tendon

1.1 Introduction

This thesis is a study of the viscoelastic behaviour of tendon and in particular

(i) the mechanisms of the deformation processes of tendon,

(ii) the extent to which the behaviour of tendon is linear viscoelastic,

(iii) the formulation of a theoretical model to explain the viscoelastic behaviour of tendon,

(iv) the development of the equations of non-isothermal viscoelasticity with particular reference to the temperature change(or T-jump) experiment used for evaluating the apparent activation energy, ΔH_a, of the viscoelastic deformation process.

The T-jump experiment lies at the heart of the thesis and is a most powerful tool for determining the apparent activation energy. The value of ΔH_a gives an indication of the type of viscoelastic deformation mechanism which is occurring in a material at a given level of stress. The T-jump method is particularly useful for determining whether different viscoelastic deformation processes are taking place in the 'toe' and 'linear' regions of the stress-strain curve of tendon. The method is applicable to both linear and non-linear viscoelastic materials and does not suffer from any of the disadvantages of time-temperature superposition, the latter method being totally unsuitable for use on tendon.

Our interest in tendon lies in its major protein constituent, collagen. Collagen is a fibrous protein and a major component of both vertebrates and invertebrates. It is found in a wide variety of tissues such as skin,cartilage, bone, cornea as well as tendon, i.e. in the mass of tissues called connective tissue which exist to contain,support and interconnect the body tissues. The role of these organs and collagen in particular is almost entirely mechanical and like any other polymer, whether biological or synthetic, collagen will display

viscoelastic behaviour.

Tendons attach muscle to bone and transmit the forces developed by muscular contractions to the skeleton. In this way, the muscle is able to be situated at a convenient distance from the joints over which it acts, and the forces, which are transmitted with little loss from the muscle to the joint, can act over a small region of the bone. The tendon also acts as a buffer to abrupt stresses, thus helping to prevent injury.

1.2 The Structure of Tendon

1.2.1 The Constituents of Tendon.

Fibroblasts are the most common cells in tendon and these cells are associated with the deposition and growth of collagen. The water content of tendon decreases with age from 80-85% in babies to between 55 and 75% in mature human tendon.[1] The extracellular components of tendon include the following:

1) collagen fibres, which are the main extracellular constituent, and are aligned in parallel in the tendon. The collagen content increases with age of the animal and varies between species. For tendon, it was found to be ~96% of the dry weight (see chapter 2).
2) elastic fibres, whose main protein constituent is elastin, which are located between the tendon bundles. These amount to only~2% of the dry weight of human tendons.
3) mucopolysaccharides (or glycosaminoglycans), mainly hyaluronic acid, chondroitin 4-sulphate and chondroitin 6-sulphate, which occur in tendon as a gel. The content in the tendon is ~1%.

The amounts and organisation of the above constituents in a tissue is related to its function.[2] The skin is required to contain all the other organs of the body and to have a certain degree of flexibility in all directions. The collagen fibres are thus arranged in a three dimensional mesh and contain more of the mucopolysaccharide and elastin than does tendon.

Bone is composed of collagen and calcium salts to give the structure both strength and rigidity, the collagen being arranged in concentric lamellae. For cartilage, a smooth lubricating, load-bearing surface is required and it is composed of mainly mucopolysaccharide gel (~80%) with the surface collagen fibres parallel to the surface. Arteries require perfect elastic recovery as well as possessing a certain rigidity. Hence the elastic content is large (~50%) and collagen content only ~30%.

1.2.2 The Structure of Collagen.

The structure of collagen is extremely complex, far more so than any synthetic polymer. Collagen is a highly ordered protein, exhibiting more than five levels of order, and exists in tissues as fine, translucent fibres.[3,4] The primary structure describes the sequence of amino acids in a single polypeptide chain of the protein and analyses of collagens from a large number of different animals show the composition to be remarkably constant.[5] The polypeptide chain contains 18 different amino acids, the total number of residues in the chain being over 1000. The amino acid glycine accounts for one third of these residues and there is an unusual amount of the imino acids proline and hydroxyproline (~20%). A typical sequence can thus be represented by[6]

GLY-X-Y-GLY-PRO-HYPRO-GLY-PRO-Y

where X and Y are any amino acid. The number of acidic, basic and hydroxylated residues is very large and accounts for the hydrophilic nature of collagen.[3]

The shape in space of the polypeptide chain is called the secondary structure. For collagen this is a left-handed helix designated an α-helix[7]. The abundance of proline and hydroxyproline, which because of their ring structure distort the CO-NH bond, distorts the regularity of the helix. The pitch of the helix is 9 Å as opposed to 5.4Å for the true α-helix

and there are ~3 residues per turn (the axial translation between residues is 2.86Å). Most collagens have two types of α-chain called α1 and α2 and are found in tendon in the ratio 2:1.[8] The amino acid sequence of the α2 chain is slightly different from the α1 chain. The molecular weight of collagen was found to be ~300000[9,10] and the molecular weight of an α1 chain to be 95000. The composition for tendon, skin and bone is $(\alpha 1)_2 \alpha 2$.[11] The complete amino acid sequence for the α1 chain has been collated.[4,5,12]

The arrangement of the α-chains into the collagen molecule is called the tertiary structure. The three chains, which are themselves coiled, wind around each other in a right-handed helix with ~30 residues per turn to form a coiled coil molecule termed 'tropocollagen'[13,14] (figure 1-1(a)). The molecule is stabilised by hydrogen bonds between the chains and by restricted rotation about the proline and hydroxyproline linked bonds. The length of the tropocollagen molecule is ~3000Å and has a diameter of ~15 Å.[9.10] The molecule contains short non-helical regions (telopeptides) at both ends of length 16 and 25 amino acid residues.[5] These non-helical regions are the sites for crosslinks between the tropocollagen molecules.[15,16,17]

The tropocollagen molecules aggregate into microfibrils to form the quaternary structure. The molecules are aligned in parallel in a quarter stagger and overlap manner[18] (figure 1-1(b)). This stagger (0.6D) combined with the overlap (0.4D) is thought to be responsible for the characteristic 65 nm (i.e. D) repeat observed in both electron microscopy[18,19] and low angle X-ray diffraction.[20] The length of the tropocollagen molecule is 4.4D. It is at present thought that there are five tropocollagen molecules per microfibril (figure 1-1(b)) and arranged in the five stranded rope like structure proposed by Smith.[21] Support for this has come from X-ray diffraction[20] which showed that the collagen molecules are packed laterally on a cylinder of diameter 38 Å. The five tropocollagen molecules are thought to intertwine by a slow helical twist.[22] The microfibrils are packed on a square lattice with a tetragonal cell (figure 1-1(c)) of side

38 Å [22,23] to form the collagen fibril, the diameter of which at maturity is of the order 100-500 nm (figure 1-1(d)). There is some evidence that there may be discrete subfibrils of diameters 30 nm [24] within these fibrils (figure 1-1(d)). The fibrils are surrounded by an extrafibrillar matrix [24,25] consisting largely of the mucopolysaccharides and glycoproteins. A mucopolysaccharide matrix within the fibrils has also been proposed. [26] The details of how these fibrils are packed together to form a tendon will be described later.

The amorphous form of collagen is called gelatin. [3] This has the levels of order up to the secondary structure and has the same amino acid content as collagen. It exists in space as a random coil [3,4] and exhibits rubberlike behaviour. On heating a collagen fibre to about 60°C, shrinkage occurs and the resulting fibre appears to be largely gelatin. On stretching, the tertiary structure is recovered but not the quaternary.

1.2.3 The Formation of Collagen

The three peptide chains of the collagen molecule are synthesised in the fibroblasts and associate to form a protocollagen molecule. This molecule contains additional non-helical amino acid residues in addition to those in the final molecule. Hydroxylation of some of the proline and lysine residues occurs as well as addition of carbohydrate groups to specific hydroxylysine residues. [15] This molecule (procollagen) is released from the fibroblast where the extra non-helical part of the molecule is removed by an enzyme, procollagen peptidase. Subsequent oxidation of the lysine residues and crosslink formation between the tropocollagen molecules occurs to give the mature fibre. The intermolecular crosslink sites are thought to occur in the N and C terminal non-helical regions. [15,16,17]

It can be seen that if this sequence is not followed, and the crosslinks not formed, then a fragile and disordered fibre will result.

The disorders produced by defective collagen have been recently reviewed.[27] An abscence of lysyl hydroxylase results in a hydroxylysine deficient collagen and medically observed tissue fragility (Ehlers Danlos Syndrome Type VI). A similar result is found for a deficiency in procollagen peptidase activity. Scurvy results from vitamin C deficiency which prevents hydroxylation. Copper is essential for the enzyme lysyl oxidase and its deficiency results in Menkes kinky hair and lathyrism in other mammals which disrupts and fragments the arteries. Other diseases which suggest defective crosslinking are certain types of Ehlers Danlos Syndrome in which the skin is hyperextensible, Marfans Syndrome in which the aorta ruptures and Osteogenesis Imperfecta in which the bones are brittle. Degradation of the normal fibre can also occur, a common disease resulting from this being arthritis. Rapid proliferation of the collagen results in diseases such as Osteoarthritis or Skin Scheleroderma.

1.2.4 The Mucopolysaccharides (Glycosaminoglycans) of Tendon.

The connective tissue polysaccharides[28] are linear chains built from disaccharide units. One of these is an hexosamine (usually glucosamine (GlcNac) or galactosamine (GalNac)) with the amino group usually acetylated, (Nac), and the other is usually an hexuronic acid (glucuronic acid (GlcUA) or iduronic acid (IdUA)). A list of the glycosaminoglycans is shown in Table 1-1 and the chemical composition of the disacchride units of the more common ones in tendon are shown in figure 1-2. All the polysaccharides except hyaluronic acid are sulphated.

Hyaluronic acid is the major polysaccharide in tendon along with small amounts of chondroitin 4- and 6-sulphates.[29] It has a molecular weight several orders of magnitude higher than the other polysaccharides and a simple structure given by the formula $(GlcUA\text{-}GlcNac)_n$ where $n \sim 40000$. The molecule is thought to occur as a kinked randomly coiled structure[30].

All of the other polysaccharides except hyaluronic acid are covalently linked to protein by a glycopeptide linkage usually of the form shown in figure 1-3. Little information is known about the protein moities to which these polysaccharides are linked but glycine, alanine and glutamic acid have been found close to the glycosidic linkage in chondroitin 4-sulphate for cartilage [31] (figure 1-3). The term proteoglycan has been coined for these substances where the polysaccharides are covalently linked to protein molecules. These proteoglycans are more compact than the linear hyaluronic acid but exist, like hyaluronic acid,as solvent imbibed coils[31]. Under physiological conditions the polysaccharide coils entangle and form a continuous network of chains. This entanglement helps to keep the molecule from being removed from the tissue. There is also evidence to suggest that the protcoglycans interact to form bands around the collagen fibre[32] and that there are various collagen-polysaccharide interactions, the nature of these being electrostatic binding between the collagen and certain glycosaminoglycans and by steric exclusion[33]. The glycosaminoglycan-proteoglycan gel matrix is often referred to as the ground substance.

The major role of the glycosaminoglycans is that of a lubricant for interacting surfaces, most notably in the synovial fluid of the joints. Hyaluronic acid can be stretched to several times its original length and still return to its original shape, the shear stress for such a deformation being small[34]. It was suggested that at low stresses it acts as the only viscoelastic element between the tendons and the tendon sheath[34]. The viscoelastic behaviour of hyaluronic acid was studied by Gibbs et al[35,36] at concentrations, pH and ionic strength similar to that of the body. In particular,they found that the activation energy for the relaxation process at 25 °C to be ~9 kcal/mol.

1.2.5 The Elastic Tissue of Tendon

The elastic tissue content of tendon is small and does not affect the viscoelastic properties of this material and so it will only be briefly described. It is important in the mechanical properties of arteries, skin and ligament. It is thought that the elastic properties of these tissues derive from two constituents; a microfibrillar component thought to be a glycoprotein* with a diameter of ~110 Å [37] [38,39] which serves as a framework on which the second amorphous component, elastin, is deposited. Elastin appears as an amorphous material [37] and the evidence at present is that it exists at a molecular level as a network structure [40] and that the behaviour is typical of rubberlike materials. A globular structure has also been proposed [41,42] and there is some debate as to which is correct. The microfibrils do not contribute significantly to the mechanical properties of adult elastic tissue. [37]

1.2.6 The Crimp in Tendon Collagen

There is one very important feature of the packing of the collagen fibrils into the macroscopic tendon which plays a major part in the explanation of the elastic mechanical behaviour at small stresses and strains. The tendon is composed of bundles of tendon fibres of diameter 100-500 μm, packed laterally to form the whole tendon. [25] It was observed by Rigby et al [43] that the tendon fibres in their unstretched length appeared to have a wavy pattern. Recently, Diamant et al [44] made a more detailed study of this wavy structure, or crimp, of the fibres. It was found that

---

* Glycoproteins are proteins which contain sugars covalently linked to certain amino acids. The carbohydrate side chains are usually oligosaccharides which contain more than one type of sugar.

by taking a rat-tail tendon fibre of diameter ~200 μm and viewing by polarised light microscopy, a planar waveform, resembling more a zig-zag than a sine wave could be seen along the length of the tendon fibre (figure 1-4(b)). The period of this zig-zag, or crimp, was ~200 μm and the crimp angle, θ_c, between the planar fibrils and the tendon axis was in the range 15-20° depending on the age of the specimen. On teasing the tendon fibre into units of smaller and smaller diameter, crimped subunits could be discerned down to the level of the optical microscope detection. The subunits, or ribbons (figure 1-4(b) and (c)) still displayed the 200 μm period and appear to have cross sectional dimensions of the range of a few microns to tens of microns.[45,46] It is thought that these ribbons all crimp in phase with their ribbon planes parallel throughout the tendon fibre,[46] although this is unlikely. The connection between the ribbons and the fibrils mentioned earlier has not been made but has been suggested[46] as shown in figure 1-4(c) where the fibrils are seen within the ribbon. Since the larger, wavy tendon fibre is composed of smaller and smaller crimped entities, there must ultimately be a crimped ribbon which is not subdivisible and this may be the fibril. It has been determined by Diamant et al[44] that the load bearing unit in the mechanical deformation is of the order of the size of the fibril.

The crimp is not confined to rat-tail tendon alone. Dale et al[47] showed that four types of tendon (rat-tail, kangaroo tail, human diaphragm and achilles tendon) all exhibited the same kind of crimped waveform. More recently, Gathercole and Keller[25] have studied a wide variety of collagenous tissue and it seems that the 'crimp' is present whenever the tissue is subjected to a tensile stress.

It should be remembered that the polysaccharides of the tendon are thought to be situated on the level between the fibrils and the ribbons and form the matrix in which the fibrils and ribbons are embedded.

Torp et al[24] showed that the matrix is a 10-30 nm belt around each fibril in rat-tail tendon. There is also some suggestion that there are other links between the fibrils.[24,25,48]

1.3 The Mechanical Properties of Tendon

1.3.1 The Stress-Strain Curve

The crimp structure is very important in explaining the elastic deformation of the tendon. A typical stress-strain curve for tendon is shown in figure 1-5 and has been described by various workers.[3,43,45,49,50] It is composed of three regions:

Region A. The material deforms easily under a small applied stress and becomes gradually stiffer as the stress (or strain) increases. This is the characteristic 'toe' region of the curve.

Region B. The 'toe' region is followed by a 'linear' region where the strain (or stress) response to an applied stress (or strain) is approximately linear.

Region C. At still higher stresses the fibres begin to yield and fracture as shown by the bending over of the stress-strain curve.

1.3.2 The 'Toe' Region

This has been the region of most of the research performed on tendon as it is thought to be the region of physiological behaviour since the strains in this region are recoverable.[51] It has been shown that the muscle in the hind leg of a rabbit transmits a maximum tension equal to $\frac{1}{4}$ of the tensile strength of the tendon.[52] Gathercole and Keller[25] using available data from muscle forces of frogs, found that in no case did the resulting strains exceed the 'toe' region. It is highly likely, however, that stresses will be exerted on the tendon of sufficient magnitude to

take it into the 'linear' region of the stress-strain curve, and, as will be seen in chapter 5, the tendon will recover from such deformation.

The straightening of the crimped fibres and ribbons seems to account for the 'toe' region of the stress-strain curve. Diamant et al[44] observed a direct correlation between the strain of a rat-tail tendon specimen and the crimp angle, (i.e. the angle which the planar ribbons make with the tendon axis).[49,50] Viidik points out that the 'toe' is actually longer than that observed in constant strain-rate experiments since he observed some fibres straightening before a load reading was registered and the transition from 'toe' to 'linear' region can only be seen as a gradual change since different tendon fibres straighten before others.

Diamant et al[44] proposed an elastica model to explain the elastic deformation in the 'toe' region. The planar zig-zag was considered rigid with inflexible hinges and the fibres deform as cantilevers. Experimental fit was found if they assumed a value of the load bearing unit in the range 100-500 nm, which ties in with the diameter of the fibril. More recently, Comninou and Yannas[53] have shown that the 'toe' behaviour will result from considering the crimp as a sinusoidal beam which bends under the applied stress. Although this has not been fitted to any experimental data it predicts a curve of the correct form and is a more physically realistic model.

The physical significance of the crimp would appear to provide the body with a mechanism to reduce injury from large, rapidly imposed forces, i.e. it acts as a shock absorber. The geometry produces an initially compliant region which will have a decelerating effect on the motion of the tendon resulting from a rapidly contracting muscle and will reduce the likelihood of permanent injury to the bone.

1.3.3 The 'Linear' and Yield Regions.

The 'linear' and yield regions of the stress-strain curve have been extensively studied by Baer and coworkers [24,54] in the respect that they looked at the effects of certain parameters, namely the age and strain cycling on the ultrastructure of the tendon. Rigby [55] and Abrahams [51] studied the effect of strain cycling in the 'linear' region. These workers suggest that the collagen fibres themselves are responsible for the deformation in these regions. Further evidence for this has been shown by X-ray diffraction by Cowen et al [56] who explained the changes in their wide and low angle diffraction patterns with increasing strain by the increased orientation of the fibrils and by extension of the triple helix itself. The modulus of the rat-tail tendon, obtained from the slope of the 'linear' region is $8 \pm 2 \times 10^8$ Pa when wet [4,43] and $\sim 10^{10}$ Pa when dehydrated. [45]

When the tendon is subjected to large mechanical deformation, Torp et al [24] observed that the primary mechanism of failure of the tendon was by dissociation of the fibrils into subfibrils of diameter 150 Å and sometimes further into the 38 Å microfibrils of Miller and Wray [20]. These subfibrils were also crimped with crimp length 100 μm. A secondary failure mechanism was reported. This was on the next higher level of organisation where fissures were observed to fragment the tendon structure. These fissures appear to initiate at the fibroblasts and propagate between the collagen fibrils. The dissociation of the fibrils is thought to result from a slippage between the longitudinal units within the fibril.

1.4 Viscoelasticity of Polymers

1.4.1 Linear and Non-linear Viscoelasticity

The stress-strain curve of tendon as determined from constant strain-rate experiments [3] is clearly non-linear in the 'toe' region and is followed by a region which may be linear. To determine whether the visco-

elastic response of the tendon is linear or not we must measure its response to certain loading patterns in creep (or stress relaxation) experiments at different levels of stress (or strain) and determine the extent to which the Boltzmann Superposition Principle is obeyed. These loading patterns are creep-recovery and 2-step proportional loading.

For a linear viscoelastic solid, the strain $\epsilon(t)$ at any time, t, is given by the Boltzmann integral[57,58]

$$\epsilon(t) = \int_{-\infty}^{t} D(t-u) \frac{d\,\sigma(u)}{du}\, du \qquad (1.1)$$

where D(t) is the tensile compliance, $\sigma(u)$ is the stress applied at time t=u. Two necessary and sufficient conditions must be satisfied before the Boltzmann Linear Superposition Principle can be said to apply to a material.[57,58] The first is that at any fixed time after the application of a stress, the strain should be directly proportional to the stress. The second is that the strain generated (or recovered from) a load currently applied (or removed) should be independent of any previous loading. Non-linear viscoelasticity is observed when one or both of these two conditions is not obeyed.

For a linear viscoelastic solid, the isochronal creep and recovery compliances and rates will be equal in the creep-recovery experiment and the creep and 'additional' compliances and rates will be equal in the proportional 2-step loading experiment.[58] Non-linear viscoelastic behaviour in synthetic polymers is characterised by the isochronal creep compliance increasing with stress and at times short compared with the loading time, the creep compliance is less than the recovery and 'additional' compliances.[59] Hence, by performing creep-recovery and 2-step proportional loading tests on tendon at various stresses, we can compare the results with those of synthetic polymers.

Numerous non-linear viscoelastic theories have been proposed

for solid polymers and reviews of these have recently appeared.[57,60,61] A widespread empirical approach to non-linearity is based on assuming that, in a creep test, the effect of stress and time can be separated and the creep data can be fitted by an expression of the form[57]

$$\epsilon(t) - \epsilon_o = A(\sigma)\, t^k \qquad (1.2)$$

where ϵ_o is the instantaneous strain and $A(\sigma)$ is a function of stress alone. Numerous forms for $A(\sigma)$ and k have been used.[62,63]

Another expression which separates the time and stress dependence of the viscoelastic behaviour was proposed by Tobolsky and Andrews.[64]

$$\sigma(t) = \frac{\epsilon}{f_1(\epsilon)} f(t) \qquad (1.3)$$

where the non-linearity is in the form of a non-linear strain function and a time function. Later, Smith showed that the large strain behaviour of elastomers could be represented by an expression of this form, and[65] Ferry has reviewed the use of this equation for stress relaxation data of rubbers.[66]

The above empirical equations are of limited value as they are specific for one loading pattern and give no physical insight into the nature of non-linearity. The theoretical representations of non-linear viscoelasticity have centred around modifications of the Boltzmann integral or a multiple integral approach. In order to explain the creep-recovery behaviour of certain textile fibres, Leaderman[67] proposed that the strain was of the form

$$\epsilon(t) = \sigma/E + \int_{-\infty}^{t} D(t-u) \frac{d}{du} f(\sigma(u))du \qquad (1.4)$$

where σ/E is the instantaneous deformation and the second term is a modified Boltzmann integral in which an unknown function of stress history now appears. This type of equation was proposed by Fung[68] for soft connective tissue , the equation being of the form (for constant strain-

rate tests)

$$\sigma(t) = \int_0^t G(t-u) \frac{d\sigma^e(\epsilon(u))}{d\epsilon(u)} \frac{d\epsilon(v)}{du} du \qquad (1.5)$$

By incorporating a relaxation function $G(t) = A'\ln t + B'$ and a non-linear time independent, elastic response $\sigma^e = c\epsilon^2$, Haut and Little[69] predicted the effect of strain rate and hysteresis on rat-tail tendon fibres.

Much attention has been paid in the past to the multiple integral representation of non-linear viscoelasticity as presented by Green and Rivlin[70]

$$\epsilon(t) = \int_{-\infty}^{t} D_1(t-u_1) \frac{d\sigma(u_1)}{du_1} du_1 + \int_{-\infty}^{t}\int_{-\infty}^{t} D_2(t-u_1, t-u_2) \frac{d\sigma(u_1)}{du_1} \frac{d\sigma(u_2)}{du_2} + \ldots. \qquad (1.6)$$

The application of this theory has been numerous, particularly by Ward and coworkers.[59,71,72] These theoretical methods also suffer from the lack of physical insight into the problem of non-linear viscoelasticity.

More recently, Buckley and coworkers[73,74,75] have shown that the non-linear viscoelastic behaviour of polypropylene in creep can be attributed to the shear creep compliance $J(t)$ being stress history sensitive and that $J(t)$ depends on both the deviatoric and hydrostatic components of stress. The shear compliance has been seen to jump to a new value following a step change in tensile stress and then decay.[75]

It is extremely difficult to apply any of these foregoing theories to tendon viscoelastic behaviour. The best we can do is to try and determine how the behaviour differs from that expected for synthetic polymers and try to explain this on our knowledge of linear and non-linear viscoelasticity and the structure of the material, the latter being expected to have a large effect. In the theory we present for the viscoelastic deformation of tendon (chapters 7 and 8) the structure will be seen to account for the observed non-linearity.

1.4.2 Temperature Dependent Viscoelastic Behaviour of Polymers

The thermorheological behaviour of polymeric materials is of widespread interest and much attention has been paid to this for synthetic polymers.[66] During the processing of many polymeric materials, the polymer is subjected to large changes in temperature. Control of these changes in temperature is important for the ultimate use of the polymer and an understanding of the mechanical deformations which occur as a result of the temperature fluctuations during the processing is of enormous value. The end product will in many cases be used in non-isothermal surroundings, e.g. in automobile engines, bodies and tyres and it is important that failure of the component will not occur under these temperature varying conditions.

The equations of non-isothermal viscoelasticity relate various measurable quantities to certain material parameters. The most important of the material parameters is the time-temperature shift factor a_T which relates the relaxation time at any temperature, T, to that at a reference temperature. Obtaining a value for a_T and determining its variation with temperature and time is the major goal of any experiment on non-isothermal rheology.

For a material which is thermorheologically simple, i.e. one for which temperature affects all the relaxation times equally (in other words, a_T is a function of temperature only and not of time), various means are available for determining a_T. The standard technique is the time-temperature superposition method.[66] By performing isothermal creep (or stress relaxation) experiments at various temperatures and shifting the resulting compliance-time (or modulus-time) curves along the time axis so that they all superpose, we can determine a_T from the amount of this shift on the time axis. This method suffers from a variety of shortcomings which will be described in more detail below. Another technique has recently been developed for obtaining the time-temperature shift factor a_T. This is the

temperature change, or T-jump experiment.[76,77] It will be seen that this experiment has enormous advantages over time-temperature superposition for determining a_T for biological polymers.

The dependence of a_T on temperature can be presented in two ways.

i) at temperatures in the region of the glass to rubber transition, it has been shown that, for various polymers, a_T obeys the empirical relation known as the WLF equation[66] given by

$$\log a_T = \frac{-C_1(T-T_o)}{C_2 + T-T_o} \qquad (1.7)$$

where T is the temperature of the data, T_o is a reference temperature, and C_1 and C_2 are empirical constants.

ii) for amorphous and semicrystalline polymers well below and well above the glass transition, the temperature dependence can be expressed in the form of an Arrhenius type equation of the form[66,78]

$$a_T = \exp \frac{\Delta H_a}{R}\left(\frac{1}{T} - \frac{1}{T_o}\right) \qquad (1.8)$$

where ΔH_a is the apparent activation energy of the deformation process. If the temperature intervals are small enough then this can also be used for the region around T_g.

The advantages of the use of an apparent activation energy to describe the temperature dependence of the material behaviour are as follows. In the glassy and rubbery regions, where large changes in configuration do not occur, the value of the apparent activation energy found from equation (1.8) is constant for a given deformation process and the value of ΔH_a found can be associated with a particular mechanism. It is thus much more convenient to refer to ΔH_a than to a_T since the value of a_T will vary with temperature in a manner described by equation (1.8), but as long as the deformation mechanism remains the same, the value of ΔH_a will remain constant. If the mechanism changes, then a change in ΔH_a may be observed, depending

on the value of ΔH_a for the new mechanism.

This concept of an apparent activation energy (ΔH_a) being associated with a given process is very useful for the study of the viscoelastic behaviour of tendon since it is thought that two different types of deformation behaviour will be occurring in the 'toe' and 'linear' regions and we would expect to observe two different values of ΔH_a in these regions.

We will now describe in more detail the T-jump technique and its advantages over time-temperature superposition in determining the apparent activation energy. In the T-jump experiment, a specimen is allowed to creep under a given load at temperature T_o. At a specified time, t', after the application of the load, the temperature is suddenly changed to temperature T. The ratio of the creep rate at t' at temperature T, $\dot{\epsilon}_T(t')$, to that at t' and temperature T_o, $\dot{\epsilon}_{T_o}(t')$, is related to the time-temperature shift factor by the McCrum and Morris equation

$$r \equiv \frac{\dot{\epsilon}_T(t')}{\dot{\epsilon}_{T_o}(t')} = \frac{1}{a_T}\left[1 + (b_T - 1)A\right] \qquad (1.9)$$

where

$$A = \int_{-\infty}^{\infty} \frac{L(\ln \tau)}{\tau} d\ln\tau \;\Big/ \int_{-\infty}^{\infty} \frac{L(\ln \tau)}{\tau} \exp(-t'/\tau)\, d\ln\tau \qquad (1.10)$$

and $L(\ln \tau)$ is the retardation spectrum at temperature T_o and b_T is the ratio of the compliance difference at temperature T and T_o, i.e.

$$b_T = \frac{\Delta D_T}{\Delta D_{T_o}} \qquad (1.11)$$

where $\Delta D = D_R - D_U$ and D_R and D_U are the relaxed and unrelaxed compliances respectively. Hence for the case where $(b_T - 1)A$ can be neglected in comparison to unity (this assumption will be discussed fully in chapter 4) we have that

$$r = \frac{1}{a_T} = \exp\ \Delta H_a \left(\frac{\Delta T}{RTT_o}\right) \qquad (1.12)$$

If we perform a series of T-jumps at various values of $\Delta T = T-T_o$, we will obtain various values of r and a plot of ln r against $\Delta T/RT_o$ will give a straight line of slope ΔH_a. The advantages of the T-jump over time-temperature superposition for tendon are as follows.

i) Time-temperature superposition requires the accurate determination of the compliance-time curves at two different temperatures in two different experiments and the shifting of one relative to the other. Hence extremely good reproducibility of the data from one experiment to another is necessary. For tendon, this is extremely difficult because of the nature of the crimp structure. Slight deviations in the zero load crimp position from one experiment to another at the same temperature and load will give different values of strain. This problem is well known for tendon.[43,50,51] Any technique which requires two separate experiments to determine a_T will be of no use for tendon.

ii) During the creep of tendon, structural changes are taking place in that the crimp is straightening out. Hence it is not clear whether superposition is valid, since we would be shifting data obtained at one structure to that obtained at another. In the T-jump technique, however, we determine the ratio of the rates at a specific time, t', and thus at a specific structure.

iii) In the abscence of any universally valid non-linear theory (see section 1.4.1)[60] the T-jump offers us a useful tool in the non-linear region because in this experiment we determine ΔH_a at one time and structure. For small enough displacements about that structure at t', the material will be linear viscoelastic[75] so that the equations for the T-jump will still apply. The validity of time-temperature superposition in the non-linear region is questionable although Morgan and Ward[72] successfully superposed non-linear data for oriented polypropylene monofilament, and found a value for ΔH_a which agrees with that found by T-jump.[81]

iv) Time-temperature superposition also suffers from the complication introduced by the temperature dependences of the relaxed and unrelaxed compliances D_R and D_U. The theoretical incorporation of the parameters b_T, c_T, and d_T into the time-temperature shift has been made to account for this.[78,82] These last two parameters are defined as

$$c_T = \frac{D_{U_T}}{D_{U_{T_o}}} \quad ; \qquad d_T = \frac{D_{R_T}}{D_{R_{T_o}}} \tag{1.13}$$

and introduce a vertical shift to the data in addition to the ordinary a_T horizontal shift and the rotation by b_T.

The T-jump equations have a problem with b_T as can be seen from equation (1.9).[83] The term A can be large and even if b_T is close to unity, the product $(b_T - 1)A$ may still be significant. This was seen by McCrum and Pearce[77] who found that an error of ~100% could be introduced by this term. This problem will be dealt with more thoroughly in chapter 4 where it will be seen that the b_T effect is negligible for most experimental circumstances.[79]

The McCrum and Morris equation and the T-jump technique has been restricted in its past use to synthetic polymers.[80,84,85] Hutchinson et al determined the apparent activation energy for polypropylene in torsional creep and recovery in the linear and non-linear regions. This work has recently been superceded[81] and a value of ΔH_a =34.5 kcal/mol found for polypropylene. Pearce[77,86] performed T-jump experiments in tensile creep and found that for both linear polyethylene and polypropylene, the value of ΔH_a decreased as the stress increased. For the former the decrease was from 30 to 20 kcal/mol, which indicates that there are different mechanisms for the high stress and low stress behaviour. The low stress mechanism was assigned to inter-lamellar shear and the high stress value to intermolecular shear. Caruthers and Cohen[87] found a value of ΔH_a=10 kcal/mol for lightly crosslinked cis 1-4 polybutadeine for all levels of stress used, a value they associated with entanglement coupling.

1.4.3 The Viscoelastic Behaviour of Tendon

Few people have looked at the viscoelastic deformation of tendon or tried to assign mechanisms to the deformation processes occurring in the 'toe' and 'linear' regions. This thesis is aimed at determining the viscoelastic behaviour in these two regions, in particular whether the viscoelastic mechanisms are the same in the two regions and whether linear viscoelasticity is exhibited at any stage.

Some previous studies will be mentioned in this respect. Laban[88] performed creep experiments on canine calcanian tendon and found that in the 'linear' region the strain which was recovered immediately after removal of the load was approximately 50% of the strain immediately before removal of the load. For increasing stress, this elastic recovery was proportional to the stress. Stromberg et al[89] found the amount of creep over 100s to be less than 0.1% of the initial elastic response. A linear relationship between the creep rate and stress was also found, the values for the creep rate varying between 1 and 4×10^{-5} s^{-1}. Rigby et al[43] performed time-temperature superposition on rat-tail tendon at temperatures from 0 to 45 °C and found that the relaxation behaviour did not change in the range 0 to 35 °C, (i.e. the apparent activation energy $\Delta H_a = 0$), but at 40 °C they found a marked increase in relaxation. They postulated a mechanism of entropic flow in the range up to 35 °C and suggested that the observed increase in relaxation at a temperature just above physiological could have serious effects if the body was subjected to a severe fever.

These observations by these three workers[88,89,43] will be examined more thoroughly with our own data. In particular, it will be seen that

(i) the method of time-temperature superposition cannot be used to provide an accurate determination of ΔH_a for tendon.

(ii) the value of ΔH_a for tendon found by the more accurate method of T-jump

is non-zero.

(iii) the isochronal recovery strain of the tendon is at all observable times not less than 95% of the isochronal creep strain and the isochronal recovery strain against load curve is of the same form as for creep.

(iv) the values for the isochronal creep rate are $\sim 10^{-5}$ s^{-1} and the creep rate dependence on load shows two distinct regions, namely a monotonically decreasing concave downward curve at strains in the 'toe' region followed by an approximately linear region.

Two other pieces of work are of interest in elucidating the role played by the various constituents of tendon in the mechanical properties. Minns et al[90] removed the ground substance from tendon by treatment with an α-amylase preparation or by a solution of E.D.T.A. in water. It was found that the tendon was easier to deform in the 'toe' region and the amount of relaxation was reduced. From this it was concluded that the ground substance contributes significantly to the mechanical behaviour of the tendon. Partington and Wood[91] used pure hyaluronidase to remove the hyaluronic acid and chondroitin 4- and 6-sulphates from rat-tail tendon. They found that this had no effect on the slope of the linear portion of the stress-strain curve.

It appears from these data that the mucopolysaccharides are important in the deformation process in the 'toe' region but not in the 'linear' region. It will be seen in chapter 6 that the values found for the activation energy in the 'toe' and 'linear' regions confirms this suggestion. More importantly, the values of ΔH_a indicate the type of deformation which is occurring in these two regions and a model can then be developed to explain the viscoelastic deformation of tendon.

References

1 Bailey A.J., In Comprehensive Biochemistry, (ed. M. Florkin), 26B,297,1968. Elsevier, Amsterdam.

2 Bailey A.J., In Colston Papers, 'The Structure of Fibrous Biopolymers', (ed. Atkins E.D.T. and Keller A.), 26,115,1975. Butterworths, London.

3 Yannas I.V., Collagen and Gelatin in the Solid State., J.Macromol.Sci.-Revs.Macromol.Chem., C7(1),49,1972.

4 Chien J.C.W., J.Macromol.Sci.-Revs.Macromol.Chem., C12.1,1975.

5 Piez K.A., In Biochemistry of Collagen. (ed. Ramachandran G. N. and Reddi A.H.) Plenum Press, New York,1976.

6 Piez K.A., Thule Int.Symp. on Aging of Connective and Skeletal Tissue, Nordiska,Bokhandelns,Forlag,Stockholm,1969.

7 Ramachandran G.N. and Ramakrishnan C., In Biochemistry of Collagen,(ed. Ramachandran G.N. and Reddi A.H.) Plenum Press, New York, 1976.

8 Piez K.A., Eigner E.A. and Lewis M.S., Biochemistry,2,58,1963.

9 Boedtker H. and Doty P., J.Amer.Chem.Soc.,78,4267,1956.

10 Rice R.V., Cassassa E.F., Kerwin R.E. and Maser M.D., Arch.Biochem.Biophys., 105,409,1964.

11 Traub W. and Piez K.A., 'The Chemistry and Structure of Collagen', Adv.Prot.Chem.,25,243,1971.

12 Hulmes D.J.S., Miller A., Parry D.A.D., Piez K.A., and Woodhead-Galloway J., J.Mol.Biol.,79,137,1973.

13 Ramachandran G.N. and Kartha G., Nature,176,593,1955.

14 Rich A. and Crick F.H.C., Nature,176,915,1955.

15 Bailey A.J., Robins S.P. and Balian G., Nature,251,105,1974.

16 Bailey A.J. and Robins S.P., Front.Matrix.Biol., (ed. Robert L.) 1,130,1973. Karger, Basle.

17 Tanzer M.L., Science,180,561,1973.

18 Hodge A.J. and Petruska J.A., In Aspects of Protein Structure, (ed. Ramachandran G.N.) Academic Press, New York, 1963.

19 Hodge A.J. and Schmitt F.O., Proc.Nat.Acad.Sci., U.S.,46,186,1960.

20 Miller A. and Wray J.S., Nature,230,437,1971.

21 Smith J.W., Nature,219,157,1968.

22 Miller A. and Parry D.A.D., J.Mol.Biol.,75,441,1973.

23 Fraser R.D.B., Miller A., and Parry D.A.D., J.Mol.Biol. 83,281,1974.

24 Torp S., Baer E. and Friedman B., In Colston Papers (ed.Atkins E.D.T. and Keller A) 26,223,1975. Butterworths, London.

25 Gathercole L.J. and Keller A., In Colston Papers (ed. Atkins E.D.T. and Keller A.) 26,153,1975. Butterworths, London.

26 Pease D.C. and Bouteille M., J.Ultrastructure Res.,35,314,1971.

27 Lapiere C.M. and Nusgens B., In Biochemistry of Collagen, (ed. Ramachandran G.N. and Reddi A.H.) Plenum Press, New York, 1976.

28 Balazs E.A.,ed., Chemistry and Molecular Biology of the Intercellular Matrix, Vol 2,1970. Academic Press, London.
Gardell S., Fransson L. and Heinegard D., Thule Int.Symp., 'Aging of Connective and Skeletal Tissue', Nordiska, Bokhandelns, Forlag, Stockholm. 1969.

29 Meyer K. and Rapport M.M., Science, 113,599,1951.

30 Laurent T.C., Wasteson A. and Obrink B., Thule Int.Symp., 'Aging of Connective and Skeletal Tissue', Nordiska, Bokhandelns, Forlag, Stockholm,1969.

31 Laurent T.C., In Colston Papers, 'The Structure of Fibrous Biopolymers', (ed. Atkins E.D.T. and Keller A.) 26,27,1975. Butterworths, London.

32 Serafim-Fracassini A., Wells P.J. and Smith J.W., In Chemistry and Molecular Biology of the Intercellular Matrix,(ed. Balazs E.A.) vol 2, 1970. Academic Press, London.

33 Obrink B., In Colston Papers, Structure of Fibrous Biopolymers', (ed. Atkins E.D.T. and Keller A.) 26,81.1975. Butterworths, London.

34 Balazs E.A., Thule Int.Symp., 'Aging of Connective and Skeletal Tissue', Nordiska, Bokhandelns, Forlag, Stockholm, 1969.

35 Gibbs D.A., Merrill E.W., Smith K.A. and Balazs E.A., Biopolymers, 6,777,1968.

36 Gibbs D.A., Sc.D. Thesis, M.I.T., 1966.

37 Gosline J.M., Int.Rev.Conn.Tiss.Res.,7,211,1976.

38 Ross R. and Bornstein P., Scient. Amer., 224,44,1971.

39 Ross R. and Bornstein P., In Chemistry and Molecular Biology of the Intercellular Matrix, (ed. Balazs E.A.) 1,641,1970.

40 Hoeve C.A.J. and Flory P., Biopolymers, 13,677,1974.

41 Partridge S.M., Scient. Amer., 224,13,1971.

42 Weiss-Fogg T. and Anderson S.O., Nature,227,718,1970.

43 Rigby B.J., Hirai N., Spikes J.D. and Eyring H., J.Gen.Physiol.,43,265,1959.

44 Diamant J., Keller A., Baer E., Litt M., and Arridge R.G.C., Proc.Roy. Soc., London, B180, 293, 1972.

45 Yannas I.V. and Huang C., J.Polymer Sci., Part A-2, 10, 577, 1972.

46 Baer E., Gathercole L.J. and Keller A., In Colston Papers, 'Structure of Fibrous Biopolymers', (ed. Atkins E.D.T. and Keller A.) 26, 189, 1975. Butterworths, London.

47 Dale W.C., Baer E., Keller A. and Kohn R.R., Experientia, 28, 1293, 1972.

48 Myers D.B., Highton T.C. and Rayns D.G., J.Ultrastructure Res., 42, 87, 1973.

49 Viidik A., Z.Anat.Entwicklungsgesch, 136, 204, 1972.

50 Viidik A., Int.Rev.Conn.Tiss.Res., 6, 127, 1973.

51 Abrahams M., Med.Biol.Eng., 5, 443, 1967.

52 Elliot D.H. and Crawford G.N.C., Proc.Roy.Soc., B162, 137, 1965.

53 Comninou M. and Yannas I.V., J.Biomech., 9, 427, 1976.

54 Torp S., Arridge R.G.C., Armeniades C.D. and Baer E., In Colston Papers, 'Structure of Fibrous Biopolymers', (ed Atkins E.D.T. and Keller A.), 26, 197, 1975. Butterworths, London.

55 Rigby B.J., Nature, 202, 1072, 1964.

56 Cowen D.M., North A.C.T. and Randall J.T., Symp.Soc.Exp.Biol., 9, 115, 1955.

57 Yannas I.V., J.Polymer Sci., Macromolecular Revs., 9, 163, 1974.

58 Ward I.M., Mechanical Properties of Solid Polymers, Wiley, London, 1971.

59 Ward I.M. and Onat E.T., J.Mech.Phys.Solids, 11, 217, 1963.

60 Hadley D.W. and Ward I.M., Rep.Prog.Phys., 38, 1143, 1975.

61 Lockett F.J., Proc.Symp.Mechanics of Viscoelastic Media and Bodies. Gothenburg.IUTAM. Berlin, Springer-Verlag.1974.

62 Findley W.N. and Khosla G.J., J.Appl.Phys., 26, 821, 1955.

63 Marin J., Pao Y.H. and Cuff G., Trans.ASME, 73, 705, 1951.

64 Tobolsky A.V. and Andrews R.D., J.Chem.Phys., 13, 3, 1945.

65 Smith T.L., Trans.Soc.Rheol., 6, 61, 1962.

66 Ferry J.D., Viscoelastic Properties of Polymers, Wiley, New York, 1970.

67 Leaderman H., Elastic and Creep Properties of Filamentous and Other High Polymers, The Textile Foundation, Washington, 1943.

68 Fung Y.B., Appl.Mech.Rev., 21, 1, 1968.

69 Haut R.C. and Little R.W., J.Biomech.,5,423,1972.

70 Green A.E. and Rivlin R.S., Arch.Ration.Mech.Anal.,1,1,1957.

71 Hadley D.W. and Ward I.M., J.Mech.Phys.Sol.,13,397,1965.

72 Morgan C.J. and Ward I.M., J.Mech.Phys.Sol.,19,165,1971.

73 Buckley C.P. and McCrum N.G., J.Mater.Sci.,9,2064,1974.

74 Buckley C.P. and Green A.E., Phil.Trans.Roy.Soc.,A281,543,1976.

75 Buckley C.P., To be published.

76 Hutchinson J.M. and McCrum N.G., Nature,Phys.Sci.,236,115,1972.

77 McCrum N.G. and Pearce D.L., Nature,Phys.Sci.,243,52,1973.

78 McCrum N.G., Read B.E., and Williams G., Anelastic and Dielectric Effects in Polymeric Solids, Wiley, London, 1967.

79 McCrum N.G. and Morris E.L., Phil.Mag.,7,2115,1962.

80 Hutchinson J.M., McCrum N.G., Pearce D.L. and Matthews J.F., Plastics and Polymers, Apr.1974,p76.

81 McCrum N.G. and coworkers. To be published.

82 McCrum N.G. and Morris E.L., Proc.Roy.Soc.,A281,258,1964.

83 Hooley C.J., Caruthers J.M. and Cohen R.E., Rheol.Acta,16,69,1977.

84 Hutchinson J.M., D.Phil.Thesis, Oxford University, 1974.

85 Hutchinson J.M., McCrum N.G. and Pearce D.L., J.Polymer Sci.,12,1255,1974.

86 Pearce D.L., D.Phil. Thesis, Oxford University, 1976.

87 Caruthers J.M. and Cohen R.E., J.Polymer Sci.,14,1891,1976.

88 Laban M.M., Arch.Phys.Med.Rehabil.,43,461,1962.

89 Stromberg D.D. and Weiderhielm C., J.Appl.Physiol.,26,857,1969.

90 Minns R.J., Soden P.D. and Jackson D.S., J.Biomech.,6,153,1973.

91 Partington F.R. and Wood G.C., Biochim.Biophys.Acta,69,485,1963.

Table 1-1

The Connective Tissue Polysaccharides.

Name	Sugars	Mol.Wt.
Hyaluronic Acid	GlcNac,GlcUA	10^6-10^7
Chondroitin 4-sulphate	GalNac,GlcUA	1-5x10^4
Chondroitin 6-sulphate	GalNac,GlcUA	1-5x10^4
Dermatan sulphate	GalNac,IdUA	1-5x10^4
Heparan sulphate	(GlcNac,$GlcNSO_4$),GlcUA	1-5x10^4
Keratan sulphate	GlcNac,Gal	5-20x10^3

Symbols:

GlcNac	N-acetyl glucosamine
GalNac	N-acetyl galactosamine
GlcUA	Glucuronic Acid
IdUA	Iduronic Acid
Gal	D-Galactose

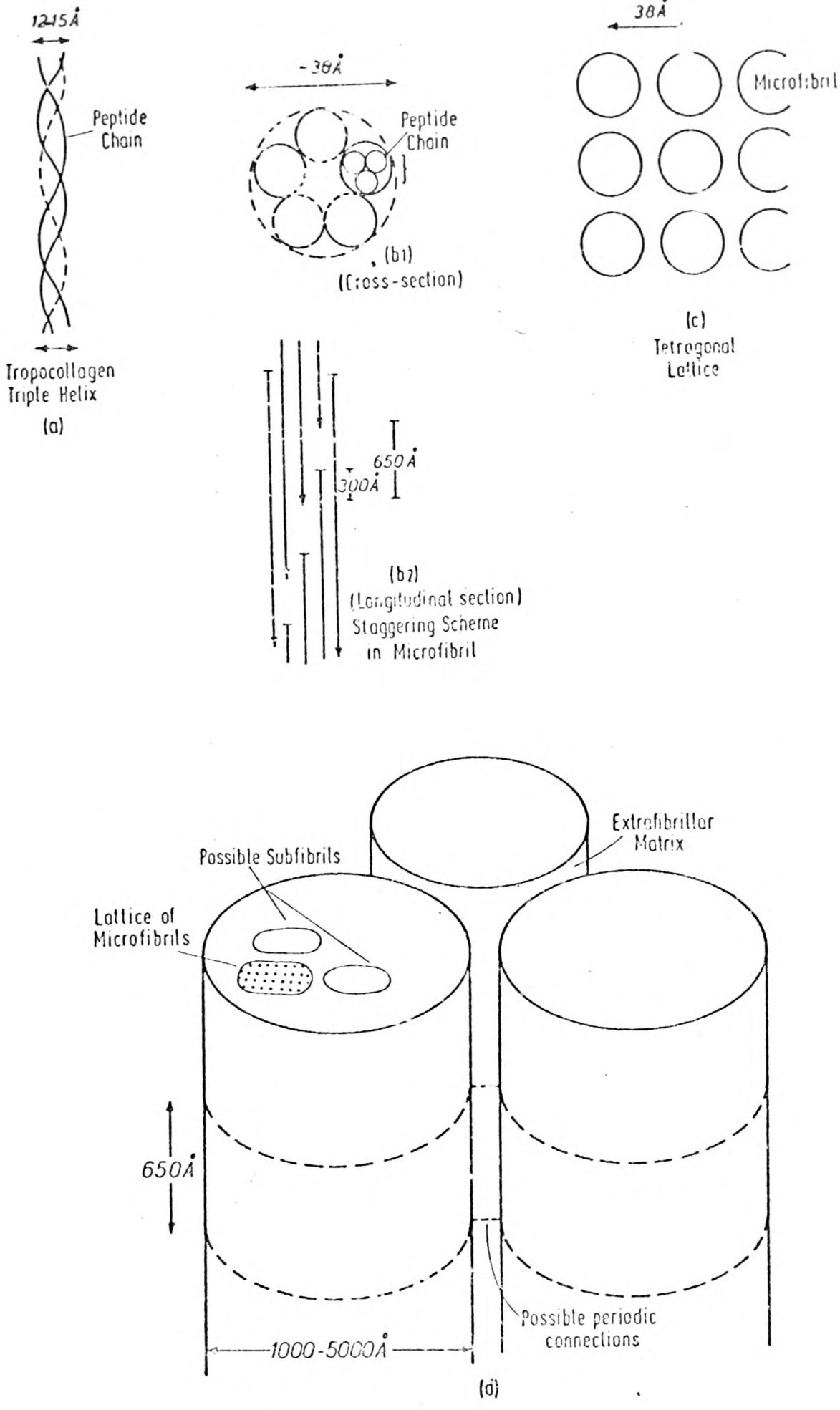
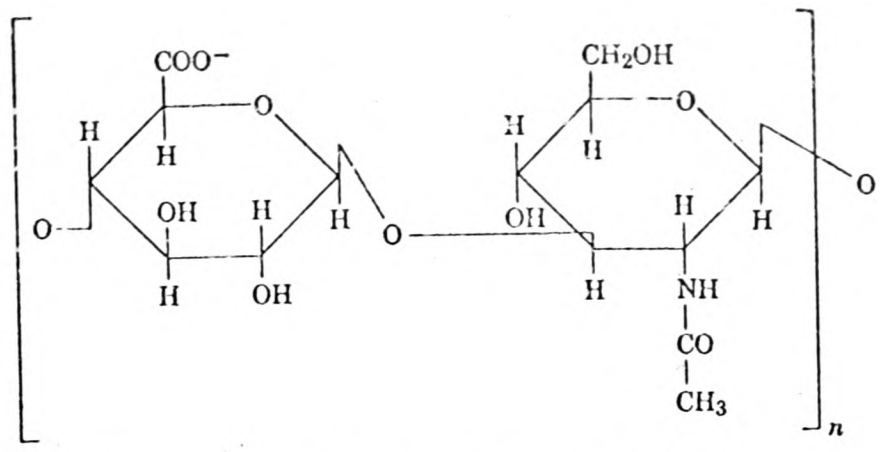
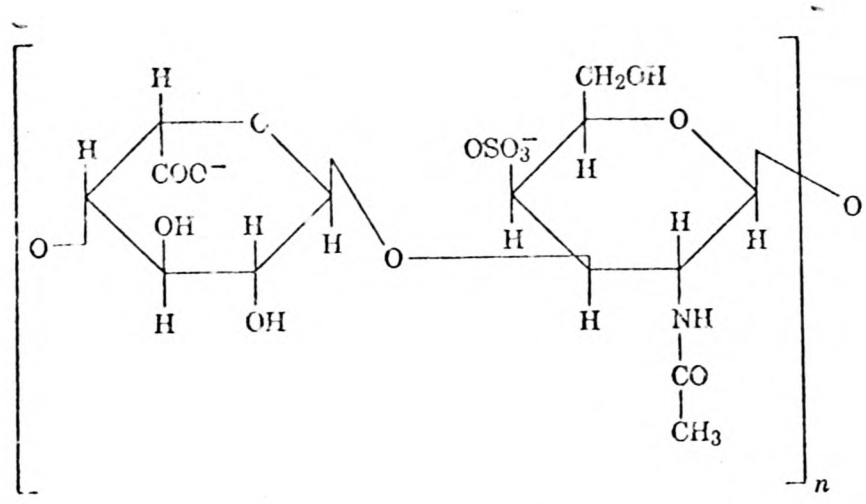


Figure 1-1

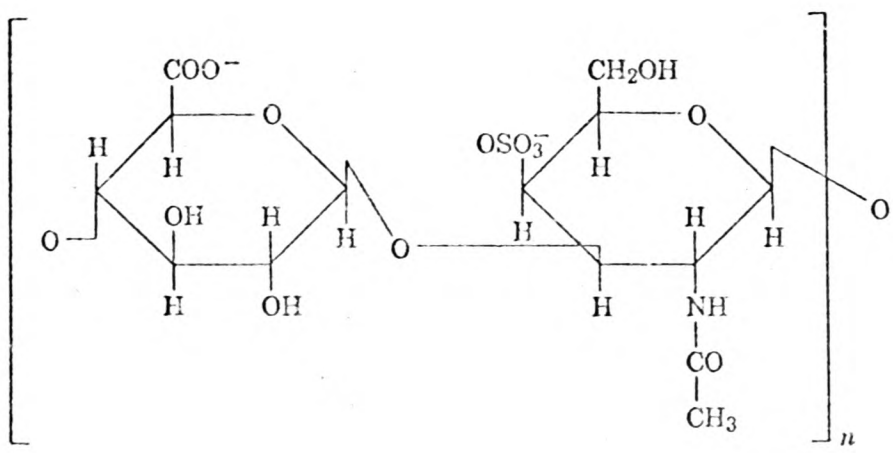
Schematic diagram of the levels of structure of collagen. (after ref. 46)
a) the tropocollagen molecule
b) the microfibril; (b_1) in cross section and (b_2) in longitudinal view, the arrow-headed lines corresponding to the tropocollagen molecule of a)
c) the packing of the microfibrils on a tetragonal lattice.
d) the collagen fibril formed by the microfibrils and possible subfibrils.



The structure of the repeating unit of the hyaluronic acid chain.



The structure of the repeating unit of the dermatan sulfate chain.



The structure of the repeating unit of the chondroitin-4-sulfate chain.

Figure 1-2

The chemical composition of the more common glycosaminoglycans of tendon.

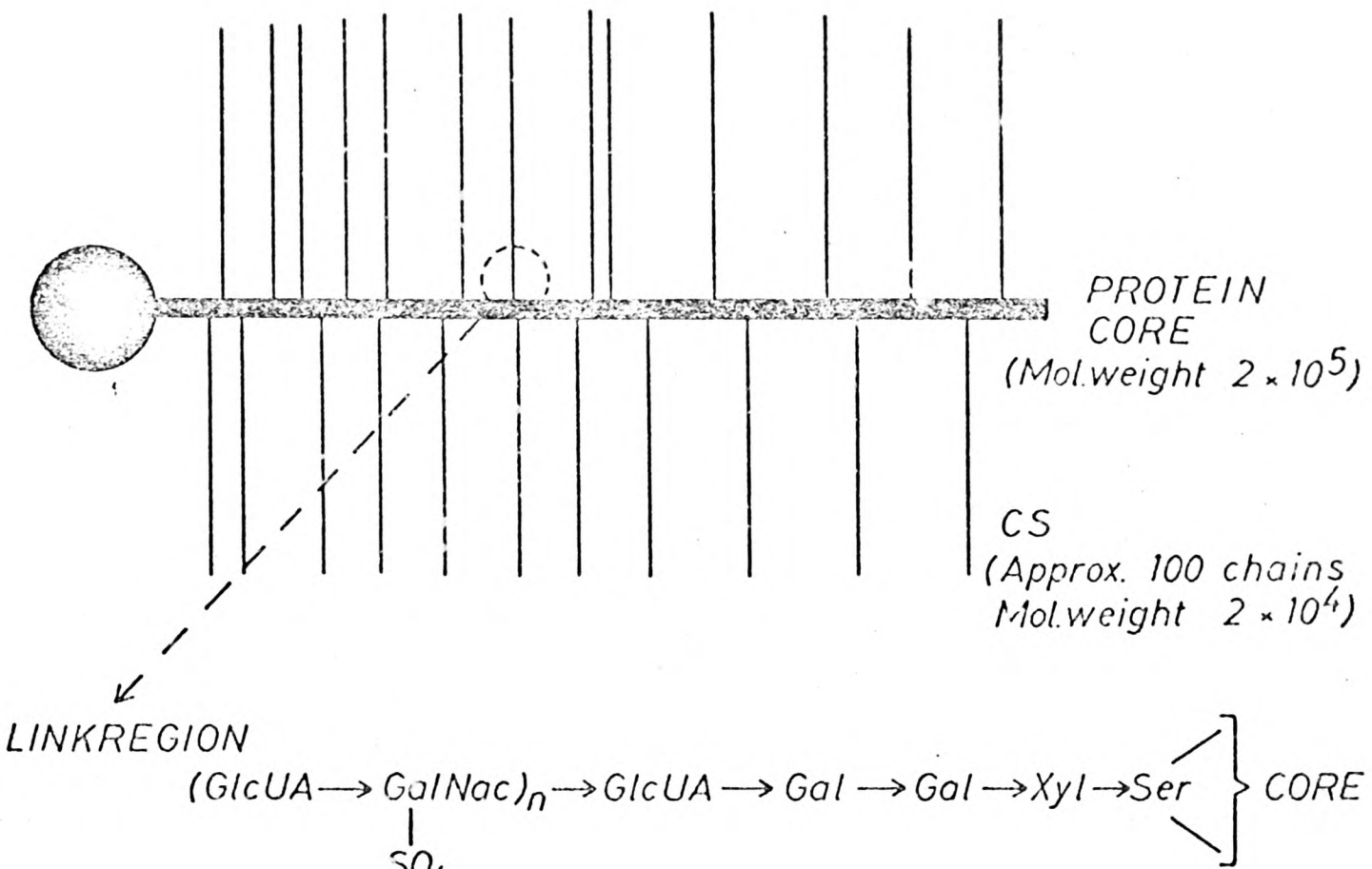


Figure 1-3

Schematic diagram of the structure of a cartilage proteoglycan, (after ref. 31). The chondroitin sulphate chains (CS) are attached to the linear portion of the protein core through the link region shown.

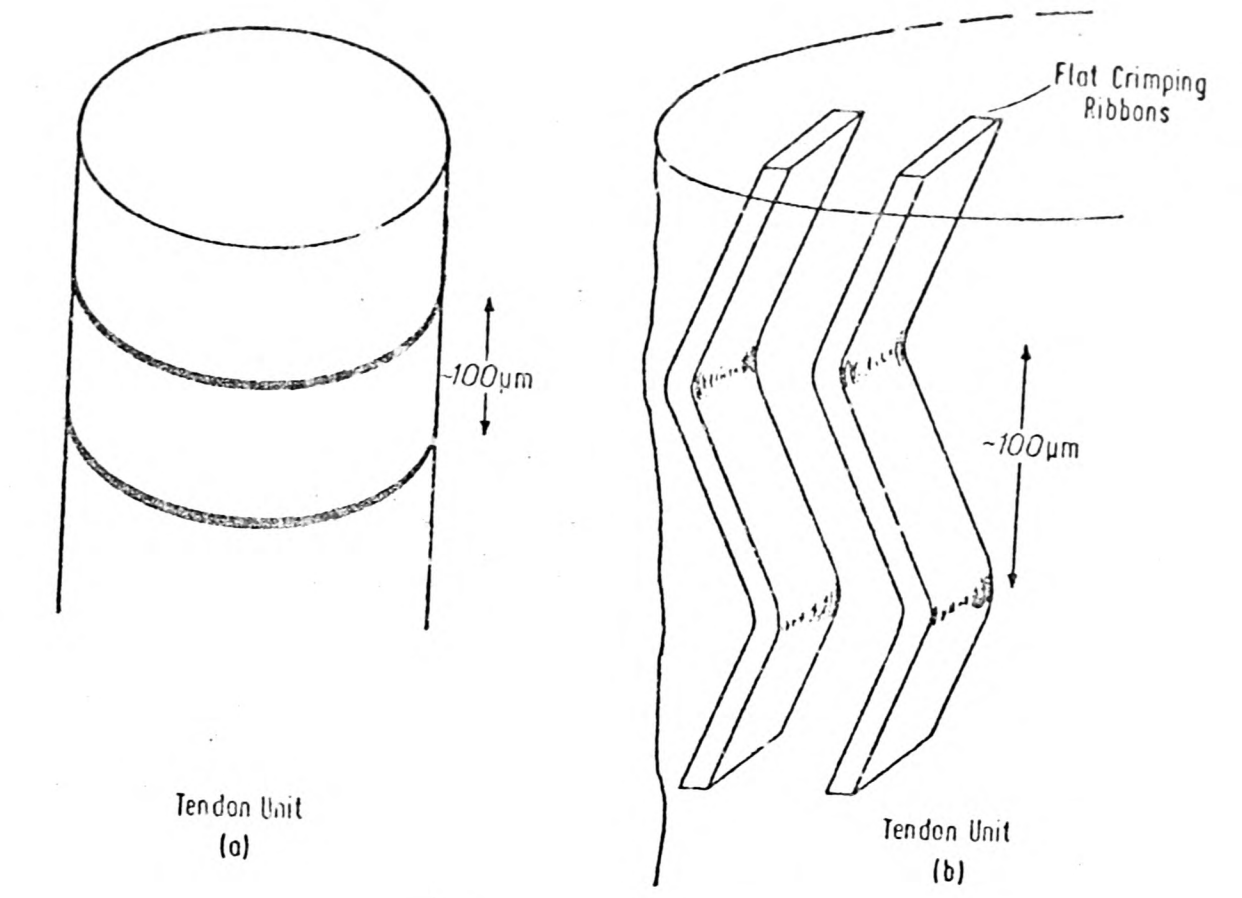


Figure 1-4

a) the tendon
b) flat crimped ribbons within the tendon unit
c) an individual ribbon showing the fibrils within.
(after ref 46)

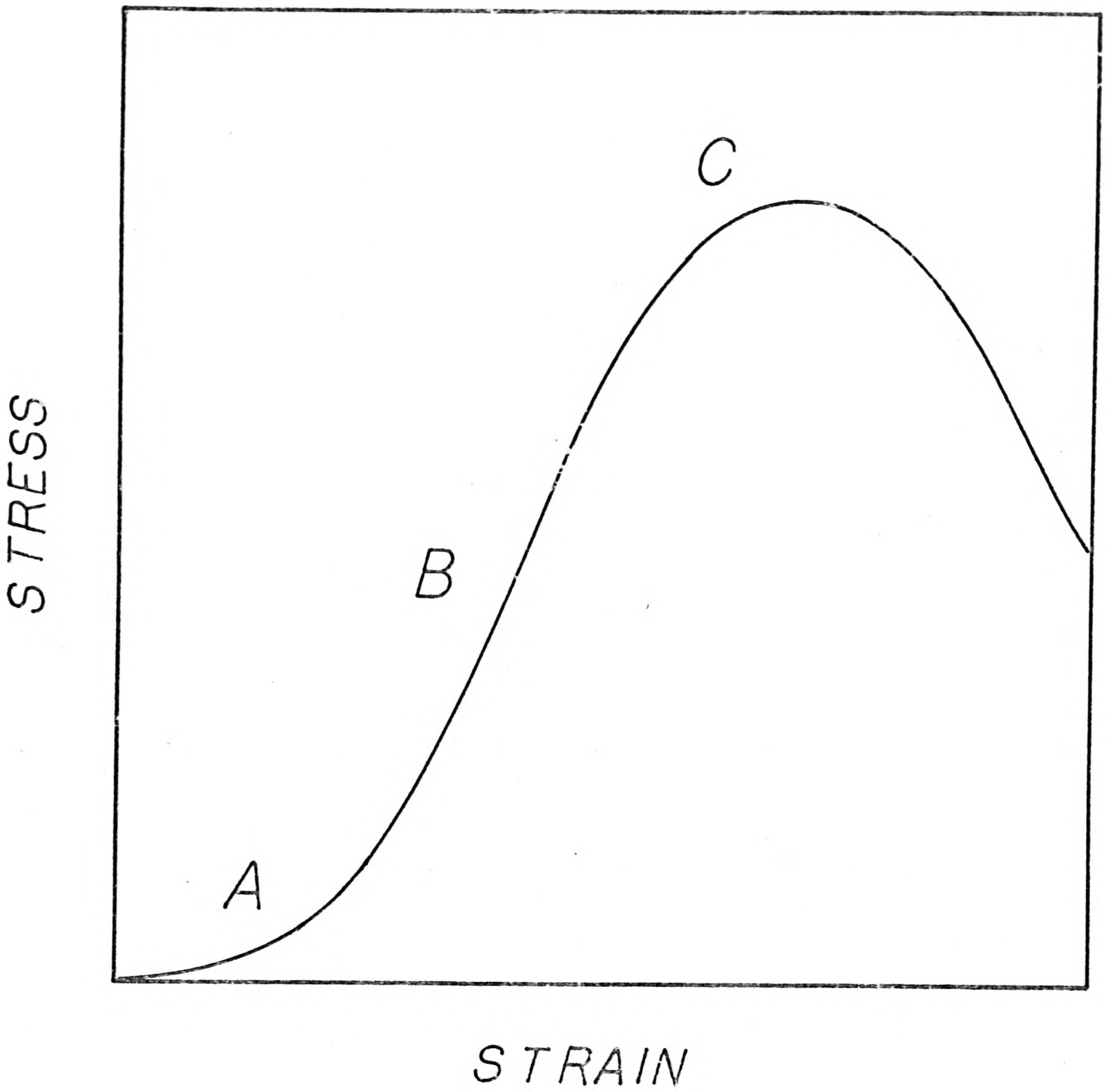


Figure 1-5

Schematic diagram of the stress-strain curve of tendon, showing
A the 'toe' region
B the 'linear' region
C the yield and failure regions.

Chapter 2

Methods and Materials

2.1 Introduction

The two experimental techniques used in this thesis were tensile creep and stress relaxation. The creep apparatus has been used in the past for a variety of measurements on synthetic polymers and its performance and accuracy have been evaluated earlier.[1] For the stress relaxation (or more correctly load relaxation) experiments, we used an Instron tensile tester. Various modifications of the basic equipment had to be made in order to perform tests on tendon, both for isothermal and T-jump experiments.

2.2 Specimens

Most of the experiments on tendon were performed on specimens of human digital extensor or flexor tendons. These were chosen mainly for their convenient size and they required loads to deform them, in the 'toe' and 'linear' regions, that were of the right order for our apparatus. Rat-tail tendons were used at first since most studies on tendons have used this source, but they broke at loads ~100 gm. The specimens used are listed in Table 2-1 with their type, origin, age and sex. We also performed tests on toe tendons from humans and bovine deep flexor tendons which are also described in Table 2-1. A specimen of collagen tape, 3500 denier, was also used. This was prepared by Ethicon Inc., Somerville, New Jersey, U.S.A. from purified steer tendon and was devoid of all mucopolysaccharides. As it was difficult to obtain an accurate measure of the cross-sectional area of the tendons, we instead measured the wet weight per unit length to obtain some comparison of sizes. These values are also shown in Table 2-1 along with the lengths of specimen used in the experiments.

A collagen and uronic acid analysis was performed on a human

digital tendon in the CH2-16-series. The results are shown in Table 2-2. The collagen content of the dry weight is thus ~96%. The elastin and mucopolysaccharide content can be seen to be low, ~3% for the former and ~1% for the latter.

An attempt was also made to determine whether the X-ray pattern for human digital tendon was similar to that for rat-tail tendon on which most of the X-ray work has been performed. The results showed that the major reflections for rat-tail tendon and human digital tendon coincide.[2]

2.3 Creep Experiments

2.3.1 Apparatus

A schematic diagram of the creep apparatus is shown in figure 2-1. The specimen was held between two clamps (A and M). The lower clamp, A, was attached rigidly to the apparatus support B through an invar tube C which was slotted at the bottom. Invar was used to minimise the thermal expansion of the apparatus in contact with the thermostating fluid. Heat losses through the tube to the main support were reduced by introducing a bakelite disk in between the two. The circular base of the lower clamp which had a pin to locate in the slot of the outer tube had four quadrants cut out of it and was held in place by a threaded locking nut in the shape of a ring. Both of these features allowed fluid flow through the base of the tube and past the specimen. The outer tube had vertical slots so that the thermostating fluid could flow past the specimen.

The upper clamp, M, was attached through a thin walled invar tube (0.4 m long) to a yoke into which was screwed the core of an Hewlett Packard linear voltage differential transducer, type 7DCDT-100. The transducer had a displacement-output voltage characteristic linear to 99.5%. The core passed centrally through the transducer coil D which was fixed to a bracket fitted with a micrometer barrel head used for calibrating

the LVDT and also to allow for simultaneous measurements of the creep strain and rate of the specimens. The transducer coils were supplied by a 6V DC voltage from a Farnell stabilised power supply, type L30A. The vertical displacement of the transducer core and thus of the specimen was converted to a DC millivolt output which was measured on a Graphispot pen recorder, the normal operating range for the recorder for the specimens being in the region 50 mV to 1 V. This allowed strains $\sim 10^{-5}$ to be measured.[3]

The micrometer read to 5 microns but there was some backlash on the barrel which moved the micrometer of up to 3 microns if the direction of rotation of the barrel was reversed. To overcome this error during calibration , the barrel was moved in one direction only to obtain the transducer displacement to output voltage characteristic. Care was taken not to reverse the direction of rotation during this calibration. The process was repeated with the barrel rotated in the opposite direction. The characteristics observed in this way were identical. The calibration was repeated before each new specimen was tested. Little variation around a value of 1.25 ± 0.01 volts/mm was found over the course of the experiments.

The loads were applied to the specimen by a motor with an eccentric cam device which lowered the weights at point E with minimal impact on to the lever H which was balanced on a knife edge F. The weight of the transducer yolk, invar pull rod and support on the left side of the fulcrum was balanced by weights at position G. The positions of G and E was such that the lever ratios were 1:1 and 2:1 respectively. The apparatus support B was arranged so that the outer tube C was in a vertical plane and the transducer and pull rod assembly was adjusted to be vertically above the centre of the bottom clamp. Care was also taken so as to avoid errors in the voltage output due to sticking.

The tendon specimens were immersed in physiological saline

solution (0.9 wt % NaCl) buffered with $NaHCO_3$ to pH7 ($\pm$ 0.2). This is the standard medium in which to test tendons[4] although little difference was found in tests using distilled water instead of saline, (see chapter 6). The saline solution was contained in a small glass cavity J (~7 cm long) with a double wall which acts as a thermal jacket. The temperature of the saline in the jacket was kept constant by pumping distilled water from a bath at temperature T_o through the double wall. The temperature for all isothermal experiments was controlled in this way.

In order to perform the creep temperature change (T-jump) experiments the thermal jacket was made with an entrance K through which saline from a second bath at temperature T could be pumped directly into the cavity containing the specimen. The cavity was always maintained full of saline and excess overflowed into the outer cylinder from which it flowed under gravity back into the saline reservoir at temperature T. The top clamps were streamlined so as to reduce the buoyancy effect from the fluid flow past them. The saline was pumped from the T-bath by submersible centrifugal pumps and the temperature was controlled by Gallenkamp thermostirrers to $\pm$ 0.1 °C. Both baths were supplied with adequate stirring to provide thorough mixing.

Bacterial degradation of the tendon was reduced by using in the saline solution an antibiotic recipe similar to that used for ordinary tissue culture, namely 100 units of penicillin and 100 units of streptomycin per ml of circulating fluid[5]. As a secondary precaution, the antibiotic-saline solution was changed every four days. No specimen was tested for more than three weeks.

Corrosion of the apparatus metal by the saline solution was reduced to a minimum by various means. All the metal parts were covered with a polyurethane coating. P.V.C. tubing was used to connect the pump in

the bath at temperature T to the glass cavity and to return the saline back to that reservoir. The lower clamp was constructed of high quality stainless steel. All pumps used for circulating the thermostating fluid were constructed of polypropylene except for several titanium screws which were wrapped with Teflon tape as were the screws in the lower and upper clamps. The saline in the bath at temperature T was not heated directly with the temperature controller but was contained in a larger bath of distilled water heated to the required temperature.

2.3.2 Isothermal Experiments

All isothermal experiments were conducted with the temperature controlled by the outer jacket with fluid from the bath at T_o which was normally at 28 °C. A small preload was normally applied to the specimen to remove any buckling caused by clamping. In order to obtain reproducible results and complete recovery of the specimen, a conditioning procedure, similar to that of Rigby et al[4] was necessary as follows:

the specimen was allowed to creep for 1000s at various loads up to the maximum load to be used in the experiments. The maximum load to be used was determined for each specimen by simultaneously plotting the isochronal load-strain curve from these creep experiments. In all cases it was no higher than what we estimated to be the linear region of the load-strain curve, i.e. no yielding was observed. After all experiments, whether it was the conditioning or the isothermal creep or the T-jump experiments, the specimen was annealed at 34 °C for at least 2 hours or sufficient time so that no further recovery of the specimen could be detected. For the early experiments we did not extend the specimens past the 'toe' region as this was thought to be the limit of recoverable behaviour[4,6-8]. This was found not to be so. For creep experiments performed in the 'toe' and 'linear' regions

of the tendon deformation after the conditioning, we could obtain recovery of the specimen to $<0.5\%$ of the specimen strain for all applied loads. It was found that unless the above conditioning was adhered to, the specimen did not recover back to its original length by as much as 5% of the 20s strain. This was unacceptable when trying to compare creep and recovery behaviour at different loads.

The values of the strains from one creep experiment to another at the same load were found to be reproducible to 2% and the rates to 4%. Much of this variation arises from the crimp nature of the tendon at zero stress. Any slight non-recovery of the specimen is magnified during the creep process in that the creep strain will be different from that found previously since the specimen is at a slightly different internal structure than before. This is one of the reasons why the T-jump experiment is so valuable for this type of material since the parameter ΔH_a can be obtained from a single experiment.

For the earlier experiments on the tendons at loads in the 'toe' region, a hook was used in place of the upper clamp so that the specimen formed an inverted 'U' and the two free ends were clamped in the bottom clamp with a spacer in between equal to the thickness of the hook. This was chosen as some previous workers had employed this geometry which is also used successfully for elastomers.[4,9] Once the conditioning experiments had been performed, we could obtain reproducibility of strain and rates of the order stated before, so it was thought that the errors introduced by the hook geometry were no greater than those from the two clamps. As we attempted to go to higher applied loads, which took the specimen into the 'linear' region, we found that the hook was not adequate for these high loads (usually those greater than 1.5 kg) since the tendon became squashed at the hook and this was contributing to the measured creep rate.

In preliminary work on tendon, we tried to determine whether there was any slippage from the grips. Bench marks (usually ink marks, sometimes epoxy marks) were placed on the specimen before mounting in the apparatus between the clamps. The values of strain at various loads as measured with a cathetometer and the LVDT were identical within the random experimental error (limited by the cathetometer readings), showing no slipping had occurred. Some slipping out of the grips was later observed at high loads, usually ~10 kg and this was immediately obvious as a sudden, slight non-recoverable jump in the transducer output. Once this was observed, no further experiments were performed on that sample.

The cross-sectional area of the tendon samples could not be measured accurately. The most reproducible measure that has been found is the dry weight per unit length of tendon [10] (which can be related through the density of the collagen and water content to the cross-sectional area of the specimen). This is not practical for our purposes since once the tendon has been dried, it is not clear whether irrecoverable damage has been done to the specimen. We did, however, make measurements of the wet weight per unit length [11] in order to make some sort of comparison from specimen to specimen. The values for the area calculated from (i) the specific weight of rat-tail tendon = 1.16 [12] and (ii) from the density of collagen = 1.33 [13] and water content of 75% are shown in Table 2-3 and are of the same order as that estimated from the dimensions of the specimen CH2-O-1. These values gave us some indication of the order of magnitude of loads required for looking at the 'toe' region or to take the specimen into the 'linear' region. We thus always worked in loads rather than stresses. Even if the stress was known, direct comparison of the stress-strain curves for various tendons is fruitless (except perhaps for the modulus in the 'linear' region but this measurement will suffer from non-uniformity of cross-sectional area), since so much depends on the initial crimp angle once the specimen

has been clamped, this being different for each specimen. On clamping, the tendons are unavoidably squashed at the clamps which unfortunately makes the area over the whole length of the specimen non-uniform.

2.3.3 T-jump Experiments.

The T-jump experiment requires that the temperature of a specimen creeping under a given load be rapidly changed from that temperature T_o to another temperature T. In order to do this, the following procedure was followed: at time t=0, a load was applied via the eccentric cam motor to the specimen which had been kept at temperature T_o by the fluid in the outer thermal jacket for at least one hour. The saline at temperature T was circulating on a bypass line. At time t' (or really t'-5s, since it took ~5s to open the valve fully and for the saline at temperature T to reach the specimen) after the application of the load, the valve K was opened and the saline at temperature T was pumped past the specimen at a velocity of ~10 cm s^{-1} so that the saline surrounding the specimen could be changed in a time of the order of 1s. The cavity design produced a pattern approaching plug flow[3,14], thus reducing the time to change the temperature. As soon as the fluid at temperature T was flowing through the cavity, the pump on the bath at temperature T_o was switched off. This precaution, along with the low conductivity of the glass wall of the cavity, meant that the presence of fluid in the thermal jacket disturbed the new constant temperature to a negligible degree. All temperatures were measured with a mercury in glass thermometer calibrated to 0.1 °C which was immersed in the cavity. The value of t' throughout these experiments was 60s. This was chosen so that the creep rates would be high enough both before and after the T-jump so that the rate could be determined accurately and so that the extrapolation to t' (as described later) was relatively short. The total loading time in the T-jump experiments was normally ~600s, (i.e. t'x10).

It has been estimated that the time to change the temperature of the fluid surrounding the specimen is ~1s. (The effect of having a non-instantaneous change in temperature will be dealt with more thoroughly in the next chapter). The specimen itself will not change temperature as rapidly. Hutchinson[3], by a torsional pendulum technique, found the time taken for a thin walled tube of thickness ~0.4 mm to reach the new temperature was less than 3s. Pearce[14] estimated that the time would be ~0.5s for a blade of linear polyethylene (c.s. area ~3mmx0.5mm). Caruthers and Cohen[15] calculated the upper limit for the time for heat penetration into specimens of cis 1-4 polybutadeine (c.s. area ~5mmx2mm) and found that in 15s the temperature of the centre line of the specimen differed from the surface temperature by less than 5%. The time scale for our sample would not be much different and so no experimental points were taken in the period less than 15s after the T-jump. The speed of the Graphispot response was another reason for not taking readings immediately after the change in temperature.

In order to obtain the creep rate with accuracy it was necessary to be able to work on a voltage scale sufficiently low so that the pen traversed the chart at least once during the creep process. This scale was normally 50-100 mV. This was achieved by either (i) appropriately setting the initial voltage at the desired point on the transducer characteristic and/or (ii) moving the micrometer barrel during an experiment by a determined amount. Care was always taken to move the barrel continuously in one direction as this was found to reduce the backlash errors mentioned earlier. The error due to this for a specimen of length 30 mm would be <0.01% strain. As most strains measured were greater than 1% this was a negligible error. The rates will not be affected by this.

2.3.4 Analysis of the Data

The creep strain values were obtained quite simply from the voltage change in the output of the transducer and converting this to a length change by the transducer calibration constant. Any movement of the micrometer was added onto this. The creep rates were less easily determined. The method adopted was similar to that used by Hutchinson[3] and by Pearce,[14] i.e. by numerical differentiation of the strain. The creep rate, $\dot{\epsilon}(t)$, at time t is approximated by the difference in the creep strain at $t+\frac{\Delta t}{2}$ and at $t-\frac{\Delta t}{2}$ divided by the time interval, Δt, and is given by

$$\dot{\epsilon}(t) = \left(\epsilon\left(t+\frac{\Delta t}{2}\right) - \epsilon\left(t-\frac{\Delta t}{2}\right)\right) / \Delta t \qquad (2.1)$$

where $\dot{\epsilon}$ is the creep rate and ϵ is the creep strain. The rates obtained from this formula were smoothed using the equation[16]

$$\dot{\epsilon}(t) = \tfrac{1}{4}\left(2\dot{\epsilon}(t) + \dot{\epsilon}(t+\Delta t) + \dot{\epsilon}(t-\Delta t)\right) \qquad (2.2)$$

where $\dot{\epsilon}(t)$ is now the smoothed value of the creep rate at time t. With this method, the first and last data points were lost but the smoothing made a reduction in the random scatter of the data points particularly at long times.

It was also found that by reading the values of strain from the Graphispot chart by means of a graduated eyepiece, with divisions of 0.1mm, the random errors in the creep rates calculated were significantly reduced. The time interval was normally chosen so that the difference between points on the chart on the voltage scale was greater than 1 mm. The creep rates so determined were plotted on a log (creep rate) against log (time) graph. For isothermal tests it was always found that a straight line resulted. The reason for this will be shown in chapter 4. This type of plot is very important and reference will frequently be made to the log rate-log time plots for various loads, temperatures and specimens.

For the T-jump experiment we need to know the ratio of the creep rate immediately after t' at temperature T, $\dot{\epsilon}_T(t')$, to the rate immediately before t' at temperature T_o, $\dot{\epsilon}_{T_o}(t')$. A typical T-jump experiment is shown in figure 2-2(a) where the strain, ϵ, is plotted against time. The temperature was changed abruptly at time t'=60s from $T_o=28^\circ C$ to $T=34.3^\circ C$. It will be seen that there is a change in slope of the strain-time curve at t'. There will thus be a discontinuity in the rates. In order to determine the rates at t', extrapolation of the data before and after t' to the value at t' is required since data points cannot be obtained in the immediate vicinity of t'. This is due to two factors, (i) before t', the smoothing technique cuts out the points closest to t' and (ii) after t', the thermal expansion of the specimen introduces a large sudden increase in the strain which the graphispot does not follow closely. The first data point taken was usually 15-20 s after the time of the T-jump. The first creep rate point is thus at 80-90 s. The problem of thermal expansion is not a simple one and this will be dealt with later.

A typical plot of log (creep rate) against log time is shown in figure 2-3 for tendon specimen CH2-8-2 at a load of 500 gm (i.e. in the 'toe' region) and $\Delta T=6.9^\circ C$. Here it will be seen that the data before t'=60 s is a straight line and so we can extrapolate this line to t' to obtain $\dot{\epsilon}_{T_o}(t')$. After t', the observed creep rates (circled points) are seen to lie on a curve concave upwards for time close to t' and then become a straight line. Once the rates due to thermal expansion of the specimen and apparatus have been subtracted from this, the squared points result and all the data is seen to lie on the same straight line. Extrapolation of the rate data after t' back to t' to obtain $\dot{\epsilon}_T(t')$ is now straightforward. This shape of curve after t' will be predicted in chapter 4 for a low value of ΔH_- (< 15 kcal/mol).

The log rate-log time curve for specimen CH2-8-2 at a load in the 'linear' region of the load-strain curve is shown in figure 2-4. Again, the straight line before t' is observed. After t', even when the thermal expansion is subtracted off, the rates no longer fall on a straight line. There is a gentle concave upwards curvature. This behaviour was observed for all the high load experiments and will again be predicted in chapter 4.

For each value of ΔT ($=T-T_o$) the values of the ratio of the rates $r= \dot{\epsilon}_T(t')/ \dot{\epsilon}_{T_o}(t')$ are plotted on what we call a ln r- ΔT plot. From equations(1.9) and (1.12) and the theory of the T-jump presented in chapters 3 and 4, it will be seen that if the effect of b_T is negligible, a straight line will result on this plot, the slope of which gives the apparent activation energy, ΔH_a. The values of ΔH_a for the tendon specimens were all obtained in this manner and comparisons made at various stages between these values and those obtained from fitting the log creep rate-log time curve with the viscoelastic equations (see chapters 4 and 8).

2.3.5 Thermal Expansion Measurements

In order to determine the thermal expansion in creep, the following experiments were performed on each specimen.[14] With the specimen under zero load* and fully recovered from any previous loading, a series of T-jumps were performed (ΔT +ve). The time dependence of the change in the sample length was monitored, usually on a Graphispot mV scale ten

---

* It should be noted that the observed thermal expansion of the tendon under zero load, i.e. when the collagen fibres are crimped, will be less than when the fibres are straight. The error in the thermal expansion measurements introduced by taking the zero load values will only be 4% for an initial crimp angle of 15° (i.e. a crimp angle of the order of that found by Diamant et al[17])

times lower than that normally used to monitor the creep rates. The results for one ΔT for the specimen CH2-0-1 are shown in figure 2-2(b). The value measured for the thermal expansion coefficient of the tendon was $\sim 0.4 \times 10^{-4} °C^{-1}$ The rate of thermal expansion was calculated from the length changes as a function of time after the temperature change for the various ΔT. For each value of time (usually 10s apart) the isochronal thermal expansion rate was plotted against the value of ΔT in a manner similar to Caruthers and Cohen[15]. An approximate straight line resulted and the slope of the line was obtained by a least squares fit to give the isochronal thermal expansion rate per °C temperature rise. This value is shown for specimen CH2-16-1 as a function of time in figure 2-5. It can be seen to decrease rapidly and is negligible compared with most of the creep rates after ~50s. The thermal expansion rates were subtracted from the observed creep rate after t' in a T-jump experiment to give the true creep rate of the specimen under the applied load at temperature T.

2.4 Recovery T-jump

The purpose of performing the recovery T-jump is to ascertain whether the effect of b_T is present in the creep T-jump experiment. The theory of the recovery T-jump has been developed by Hutchinson et al[18] and will be dealt with in chapter 4 along with the shape of the log rate-log time curves. Here, it will be sufficient to describe the experimental procedure. A load is applied to the specimen for a time, t_o, when it is removed. After a further period of time t', the temperature is jumped to T. The residual rates, $\dot{\epsilon}_r$[19], before and after the T-jump are found in a similar manner to creep. A typical log $(-\dot{\epsilon}_r)$ against log (time after removal of the load) curve is shown in figure 2-6 for specimen CH2-8-3, load 5 kg (in the 'linear' region), $\Delta T = 6.05$ °C. It will be seen here that the thermal expansion rates must be added to the observed rate to obtain the

true residual rate. The squared corrected points lie on a curve, concave upwards, as before for creep. The rates before t' lie on an approximate straight line. It was much harder to obtain good rate data from the recovery T-jumps. The buffeting of the upper clamp by the thermostating fluid when the specimen was unloaded produced scatter of the data, particularly for low applied loads where the rate was lower. It was rarely possible to obtain a value for $\dot{\epsilon}_{r_T}(t')$ for a -ve T-jump.

2.5 Stress Relaxation

An Instron tensile tester was used for studying the load relaxation behaviour of tendon. The Instron was supplied with a zero suppression control which moves the zero load position by a given amount depending on the value required by the experimenter. With this feature, it was possible to look at the observed relaxation rates on the smallest load scale and much better rate data was obtained. By always noting how much load was suppressed, it was possible to calculate both loads and load rates.

The Instron was modified to be able to perform isothermal and T-jump tests by attaching to the cross-head an apparatus essentially the same as the part below the transducer in the creep apparatus of figure 2-1, where B will now be the bottom of the crosshead. The pull rod went through the centre of the crosshead and attached to the load cell. The invar tube was replaced, because of availability, by three $\frac{1}{2}$ inch diameter, ~12" long invar rods which were securely bolted in recessed holes to a $\frac{1}{2}$" steel plate, which attached to the crosshead and to the base of the lower clamp, this now being a solid triangular piece of stainless steel, $\frac{1}{2}$"thick. The rods were located at the corners of the triangle. The temperature control was provided in the same manner as for creep except that the cavity had to be made wider and longer to accomodate the larger bottom clamp and its

movements when stretching the sample. Since the upper clamp did not move, the cavity was positioned so that the whole of the upper clamp was just immersed in fluid. The movement of the crosshead was measured by a dial guage reading to 0.01 mm.

The main experiments performed on the Instron were T-jumps. A typical one for specimen CH2-16-3 is shown in figure 2-7 where the load is plotted as a function of time after the specimen was strained to 4.96%. The temperature was changed at t'=60s from 28 °C to 30.05 °C. A change in slope at t' is observed and the load rates calculated from these values of load exhibit a discontinuity at t' as shown in figure 2-8 where the log(-load rate) is plotted against log(time). The rates before t' fall on a straight line. After t', when thermal expansion has been subtracted off, a curve concave upwards (squared points) is observed for times close to t' which becomes a straight line for longer times. These data will later be fitted with the linear viscoelastic theory (chapter 9). From the ratio of the load rates, r, immediately before and after the T-jump, a ln r- ΔT plot can be constructed as before for creep and the value of ΔH_a obtained from the slope.

Thermal expansion presents a more difficult problem in stress relaxation T-jumps than in creep. This arises from the length change accompanying the temperature change at t'. Although the actual specimen length does not change during the stress relaxation process, the temperature change effectively alters the length of the unstressed sample, l_o, at temperature T_o. For a +ve ΔT, this means that the strain in the sample changes by

$$\Delta\epsilon = \frac{l}{l_o + \Delta l} - \frac{l}{l_o} \qquad (2.3)$$

where l is the length of the sample at the time of the temperature change, Δl is the length change which would be introduced by the temperature change ΔT in a freely hanging specimen, i.e.

$$\frac{\Delta l}{l} \sim \frac{\Delta l}{l_o} = \alpha \Delta T \qquad (2.4)$$

where α is the linear coefficient of thermal expansion of the tendon. Hence

$$\Delta \epsilon \sim -\alpha \Delta T \qquad (2.5)$$

and the stress is decreased by

$$\Delta \sigma = E_{T_o}(t') \alpha \Delta T \qquad (2.6)$$

where $E_{T_o}(t')$ is the relaxation modulus at the strain and time of the temperature change at the temperature T_o.

An added complication is that for tendon, the modulus changes with stress up to the 'linear' region. Hence what is required is to determine the thermal expansion load rates for several ΔT's at each level of load at which the temperature is changed or to find the load rate at one level of load and strain and relate it to that which would be obtained at the other loads through the slope of the isochronal stress-strain curve, $(d\sigma/d\epsilon)_{t',T_o}$ as described below. To do the former for tendon would be totally impractical since by the time all the thermal expansion data had been obtained at the various load levels, the specimen would have been in the apparatus for probably 3 weeks or longer. What was done instead was the second method. A prestrain was applied of sufficient magnitude to take the specimen to the lower end of the 'linear' region. When the load had completely relaxed to its equilibrium level, temperature change experiments (with zero additional applied strain) were performed for various ΔT's and the change in the load monitored. The resulting isochronal load rate against ΔT plots were found to be straight lines as for creep and the least squares fit of the slope of the straight line for each time was found and shown in figure 2-9 for specimen CH2-16-3 for a prestrain of 4.96%. It is seen that after ~50s, the thermal expansion is negligible. The thermal expansion load rate, $\dot{F}_\epsilon(t)$, for another strain at a given time t is found from equation (2.6) to be

$$\dot{F}_{\epsilon_2}(t) = \dot{F}_{\epsilon_1}(t) \left[\left(\frac{dF}{d\epsilon} \right)_{\epsilon_2} / \left(\left(\frac{dF}{d\epsilon} \right)_{\epsilon_1} \right] \right. \qquad (2.7)$$

where F is the load, ϵ is the strain, subscript 1 refers to the data for the above prestrain and subscript 2 refers to any other strain and $(dF/ d\epsilon)_{\epsilon}$ is the slope of the load-strain curve at ϵ . The thermal expansion load rates for all the applied strains in the T-jumps were calculated in this way.

References

1 Duckley C.P., D.Phil. Thesis, Oxford University, 1971.

2 Doyle B.B., White S. and Miller A., Private Communication.

3 Hutchinson J.M., D.Phil. Thesis, Oxford University, 1974.

4 Rigby B.J., Hirai N., Spikes J.D. and Eyring H., J.Gen. Physiol., 43, 265, 1959.

5 Robb-Smith A.H.T., Private Communication.

6 Abrahams M., Med.Biol.Eng., 5, 443, 1967.

7 Viidik A., Int.Rev.Conn.Tiss.Res., 6, 127, 1973.

8 Partington F.R. and Wood G.C., Biochim.Biophys.Acta, 69, 485, 1963.

9 Sharda S.C., Ph.D. Thesis, Caltech, 1974.

10 Ellis D.G., J.Biomech., 2, 175, 1969.

11 Viidik A., Scand.J.Plast.Reconstruct.Surg., 1, 141, 1967.

12 Miller A. and Parry D.A.D., J.Mol.Biol., 75, 441, 1973.

13 Chien J.C.W., J.Macromol.Sci.-Revs.Macromol.Chem., C12(1), 1, 1975.

14 Pearce D.L., D.Phil. Thesis, Oxford University, 1976.

15 Caruthers J.M. and Cohen R.E., Poly.Eng.Sci., 16, 41, 1976.

16 Whittaker E.T. and Robinson G., The Calculus of Observations, Blackie, London, 1924.

17 Diamant J., Keller A., Baer E., Litt M. and Arridge R.G.C., Proc.Roy.Soc. London, B180, 293, 1972.

18 Hutchinson J.M., McCrum N.G. and Pearce D.L., J.Polymer Sci., Polym. Phys., 12, 1255, 1974.

19 Ward I.M., Mechanical Properties of Solid Polymers, Wiley, London, 1971.

Table 2-1 Specimens

Specimen No	Source	sex	age	type	l_o cm	w_o cm	t_o cm	w/l gm/cm
CH2-0-1	Human	m	21	flexor, hand	2.52	0.6	0.17	
CH2-1-1	"	m	55	extensor, hand	1.98			
CH2-2-1	"	f	89	extensor, hand	2.38			
CH2-2-2	"	"	"	extensor, toe	1.67			
CH2-8-2	"	m	23	extensor, hand	2.95			0.065
CH2-8-3	"	"	"	"	3.35			0.073
CH2-9-1	"	m	77	flexor, hand	3.31			0.124
CH2-10-1	"	m	44	extensor, hand	2.87			0.117
CH2-16-1	"	m	71	flexor, hand	3.00			0.122
CH2-16-4	"	"	"	"	3.15			0.197
BT2	Bovine			deep flexor, foot	2.20			
Collagen Tape	Steer				3.70	0.48	0.009	
Instron								
CH2-5-1	Human	m	54	extensor, hand	4.41			0.086
CH2-5-2	"	"	"	"	4.11			0.090
CH2-16-3	"	m	71	flexor, hand	3.22			0.172

Table 2-2 Collagen and Uronic Acid Analysis of Human Tendon(CH2-16-series)

Wet weight	= 582.1	mg
Dry weight	= 145.0	mg
Water content	= 75%	
Total hydroxyproline	= 18.35	mg
Total collagen (hpx7.46)	= 139.9	mg
Total uronic acid	= 0.276	mg

Table 2-3 Estimate of Cross-sectional Area

Specimen	Area Based on specific weight =1.16 (mm^2)	Area Based on collagen density = 1.33 gm/cc and water content = 75% (mm^2)
CH2-8-2	5.60	6.00
CH2-8-3	6.29	6.74
CH2-9-1	10.69	11.45
CH2-10-1	10.09	10.81
CH2-16-4	16.98	18.20
CH2-5-1	7.41	7.94
CH2-5-2	7.76	8.31
CH2-16-3	14.83	15.89

CH2-0-1 Area from width and thickness measurements is 10.20 mm^2

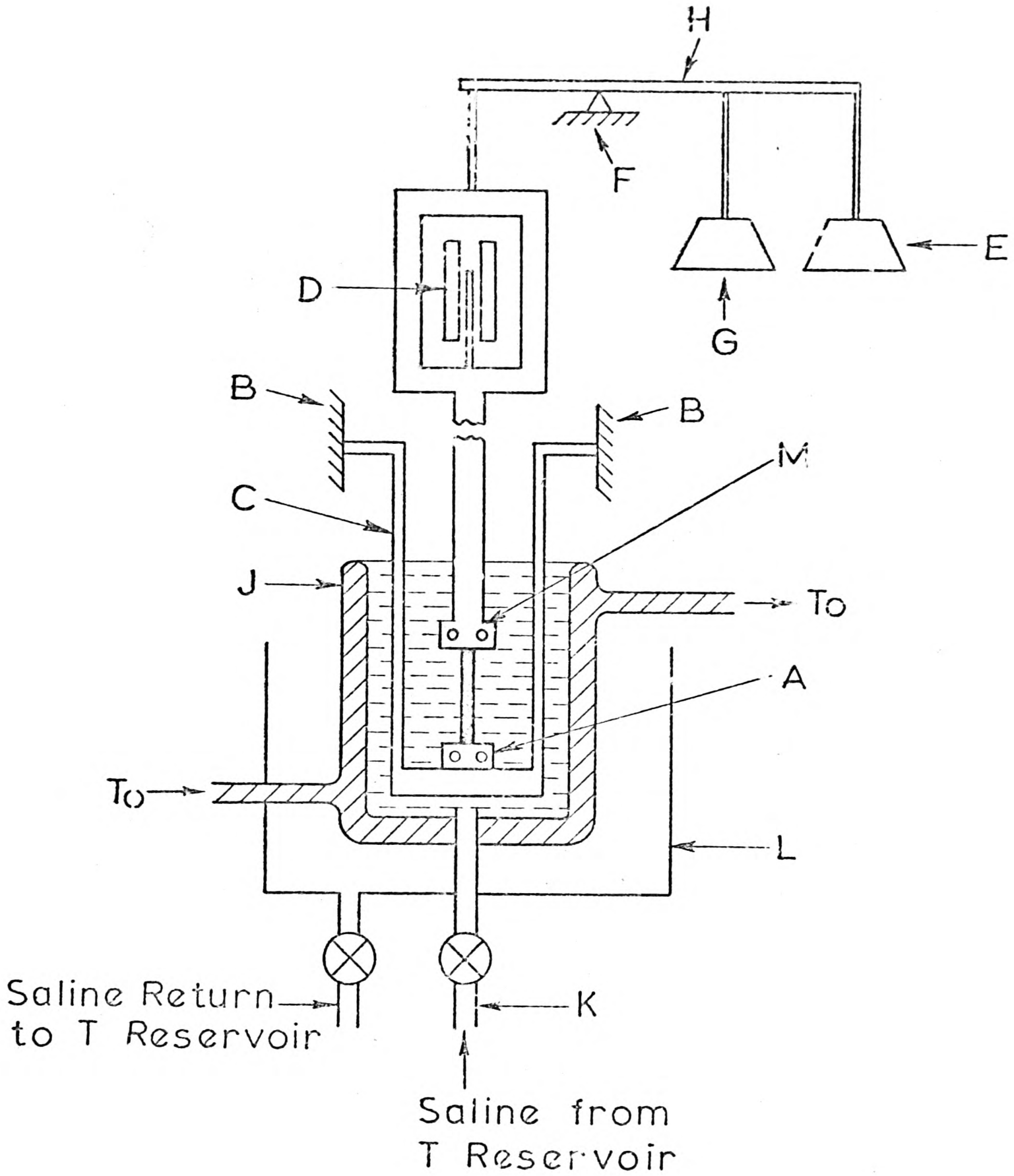


Figure 2-1

Schematic diagram of the tensile creep apparatus.

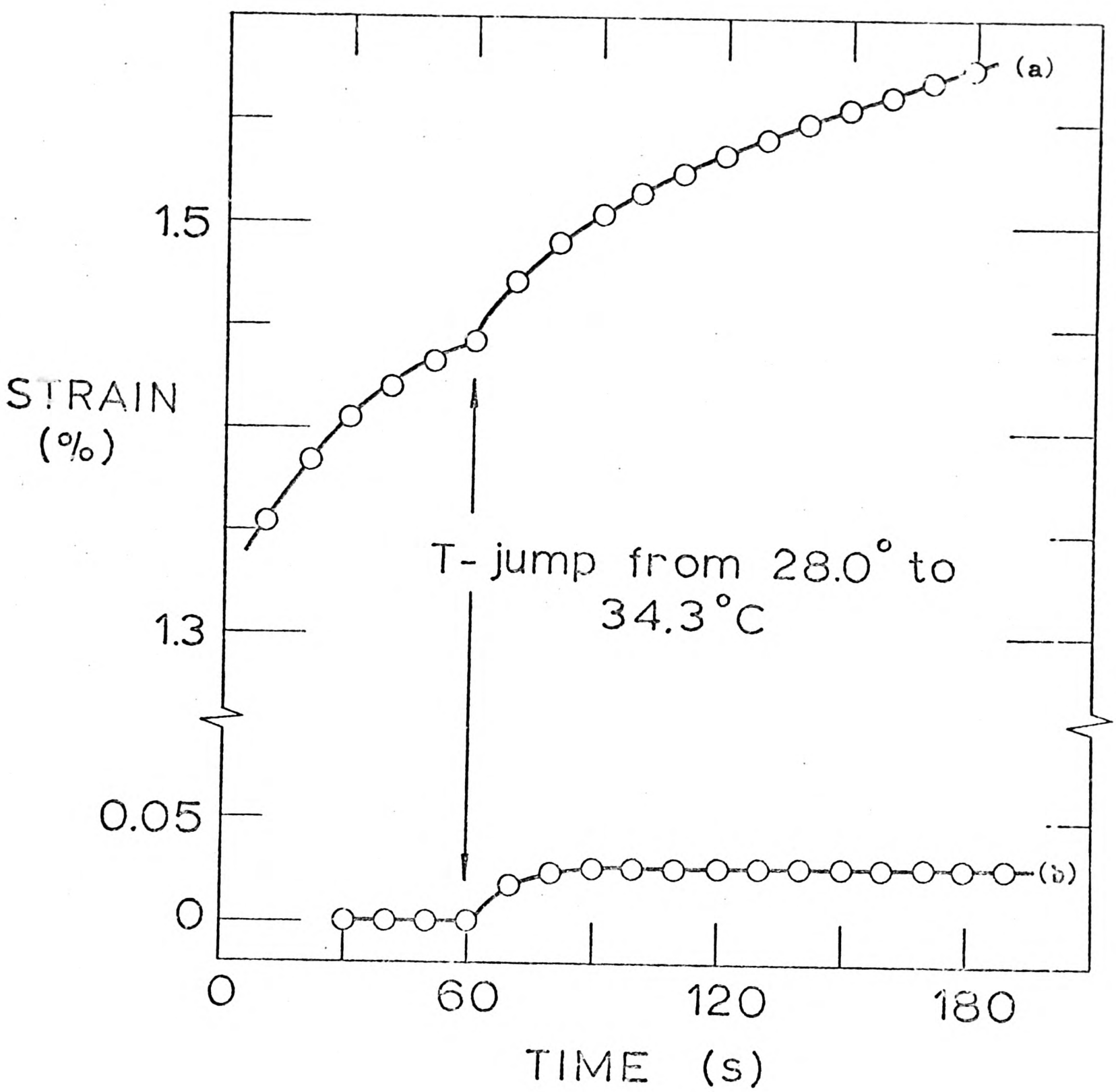


Figure 2-2

Dependence of strain on time during a creep experiment for specimen CH2-O-1, with a T-jump at t' = 60s.
a) under constant load of 0.76 kg.
b) under zero load showing the time dependence of the thermal expansion

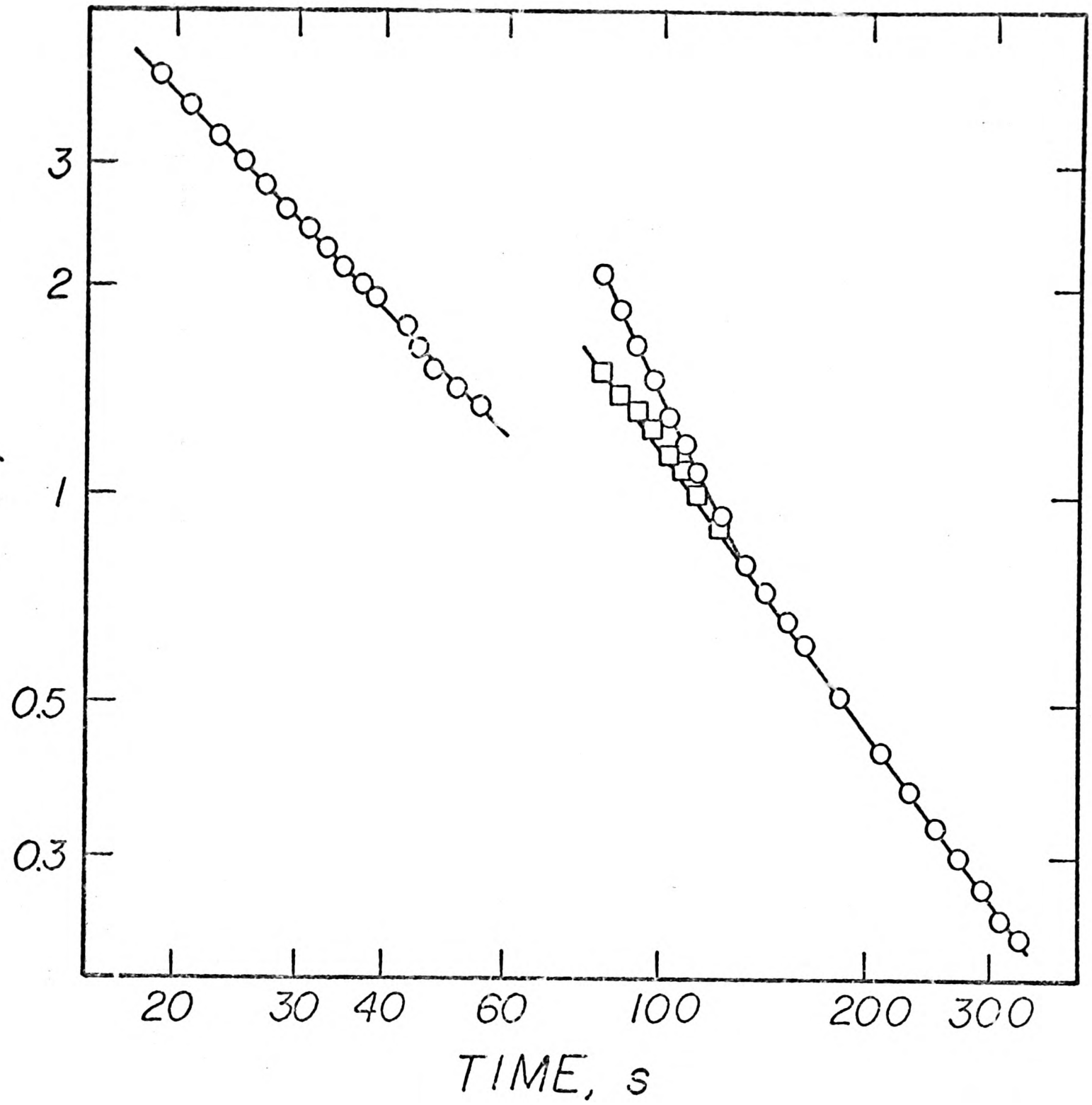


Figure 2-3

Plot of log (creep rate) against log time for specimen CH2-8-2 in creep T-jump, t'=60s, load= 0.5 kg, i.e. in the 'toe' region, $\Delta T=6.9^{\circ}C$.
Circled points: experimental data before thermal expansion correction
Squared points: experimental data after thermal expansion correction.

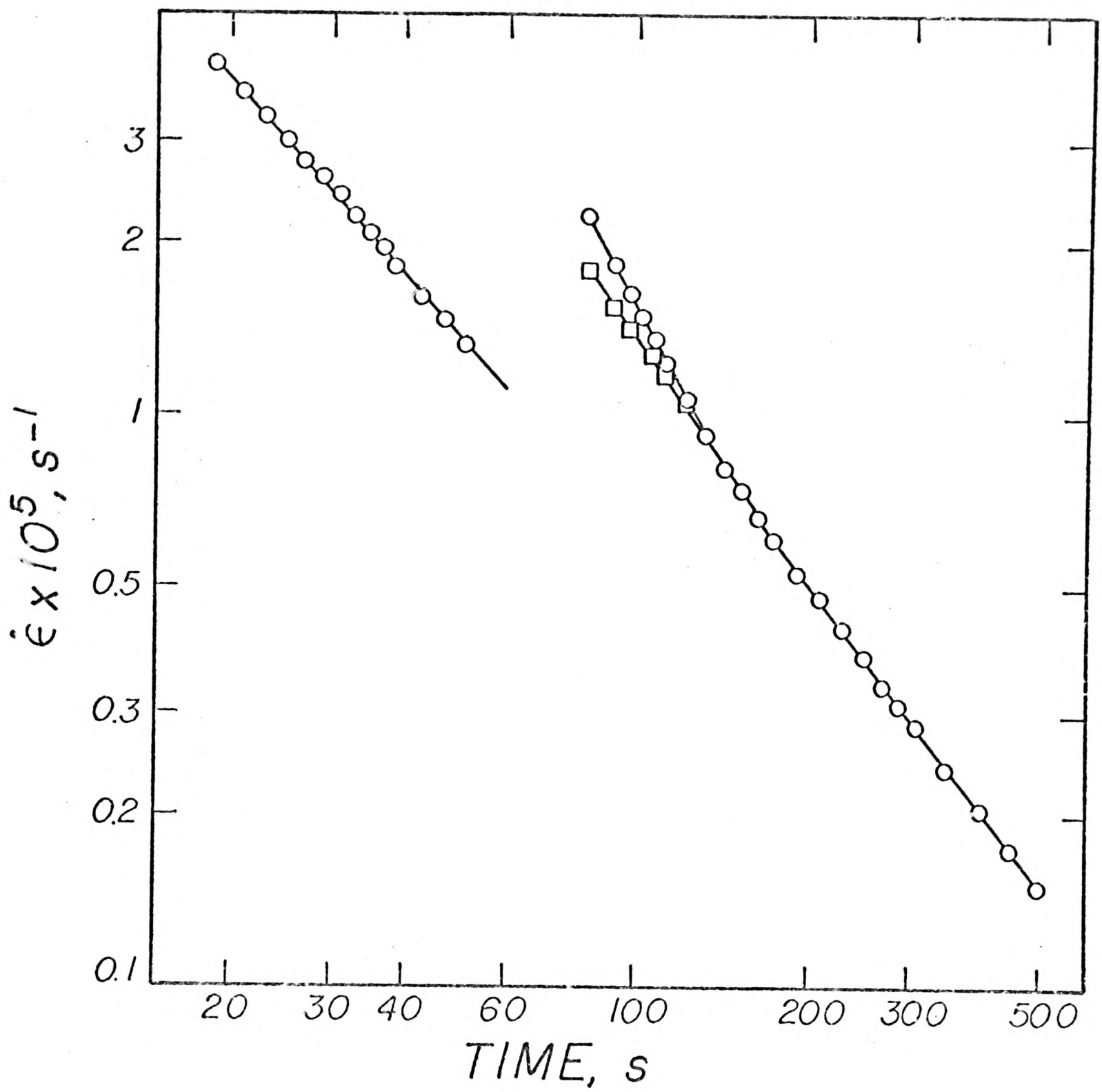


Figure 2-4

Plot of log (creep rate) against log time for specimen CH2-8-2 in creep T-jump, load = 3 kg, ('linear' region) $\Delta T = 5.7\,^{\circ}C$.
Circled points: experimental data before thermal expansion correction.
Squared points: experimental data after thermal expansion correction.

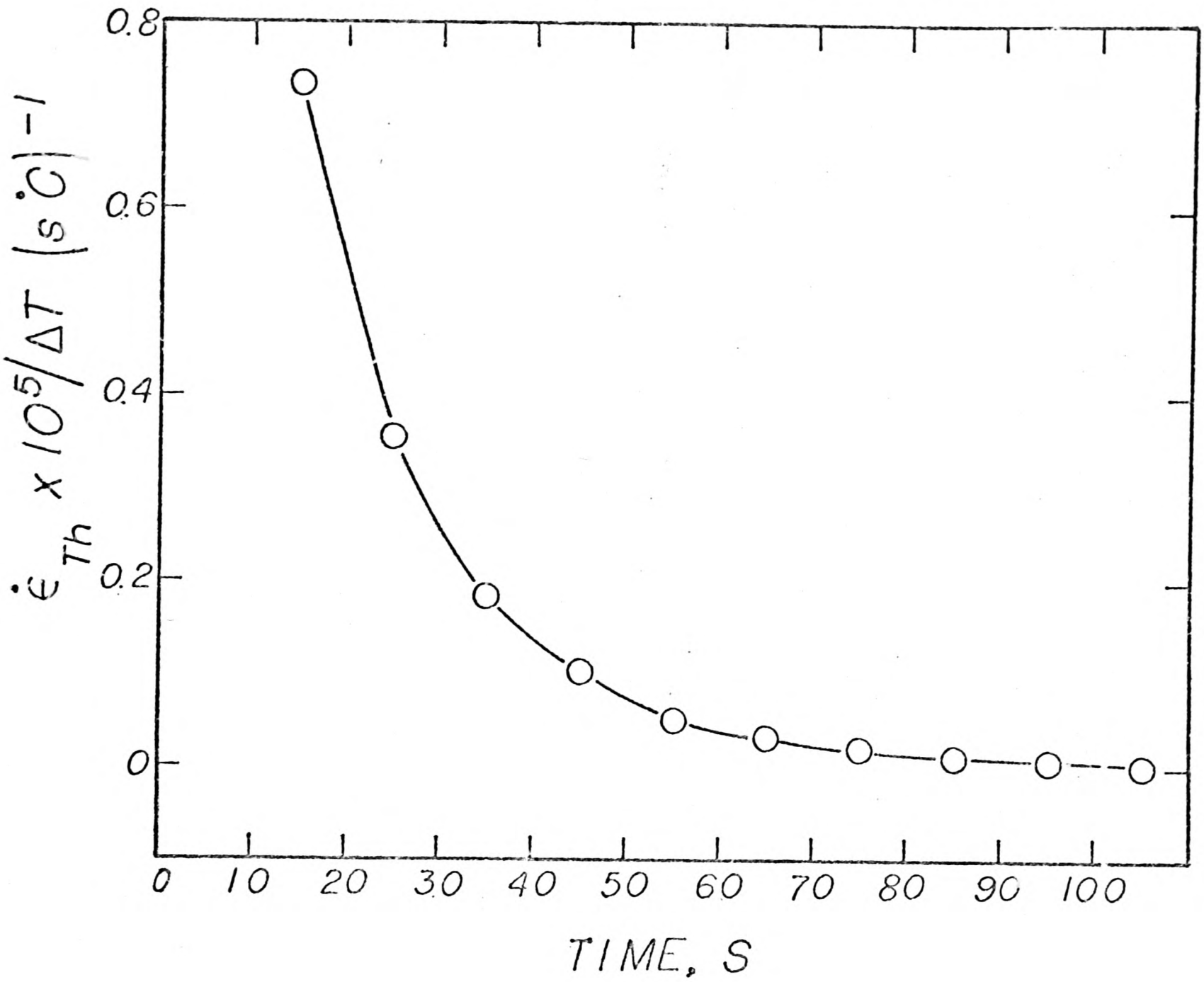


Figure 2-5

Thermal expansion rate per °C rise in temperature against time, specimen CH2-16-1, zero load.

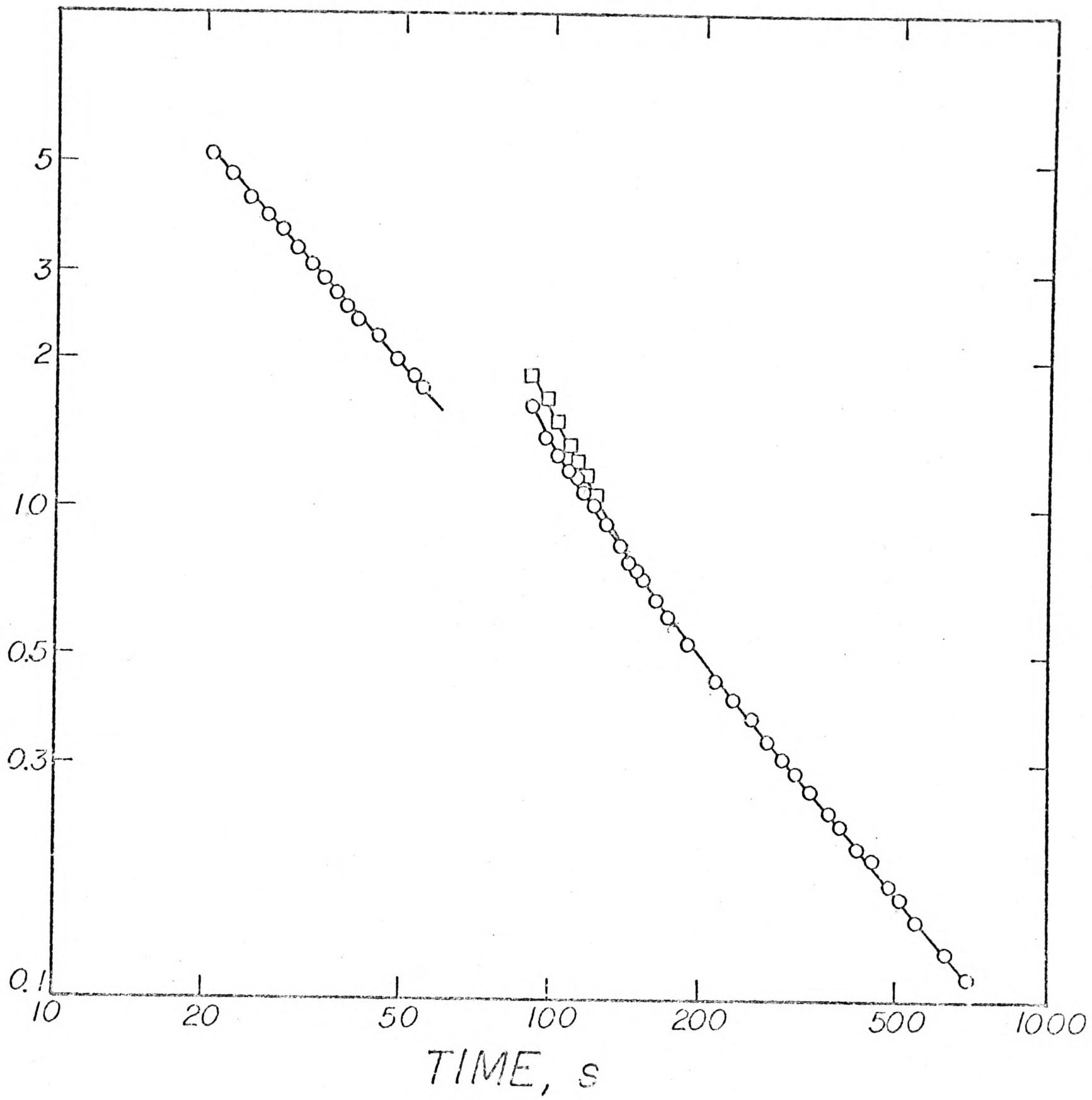


Figure 2-6

Dependence of log(residual rate ($-\dot{\epsilon}_r$)) against log (time after removal of the load) for a recovery T-jump, specimen (H2-8-3, load = 5 kg; ΔT= 6.05°C.
Circled points: data before thermal expansion correction.
Squared points: data after thermal expansion correction.

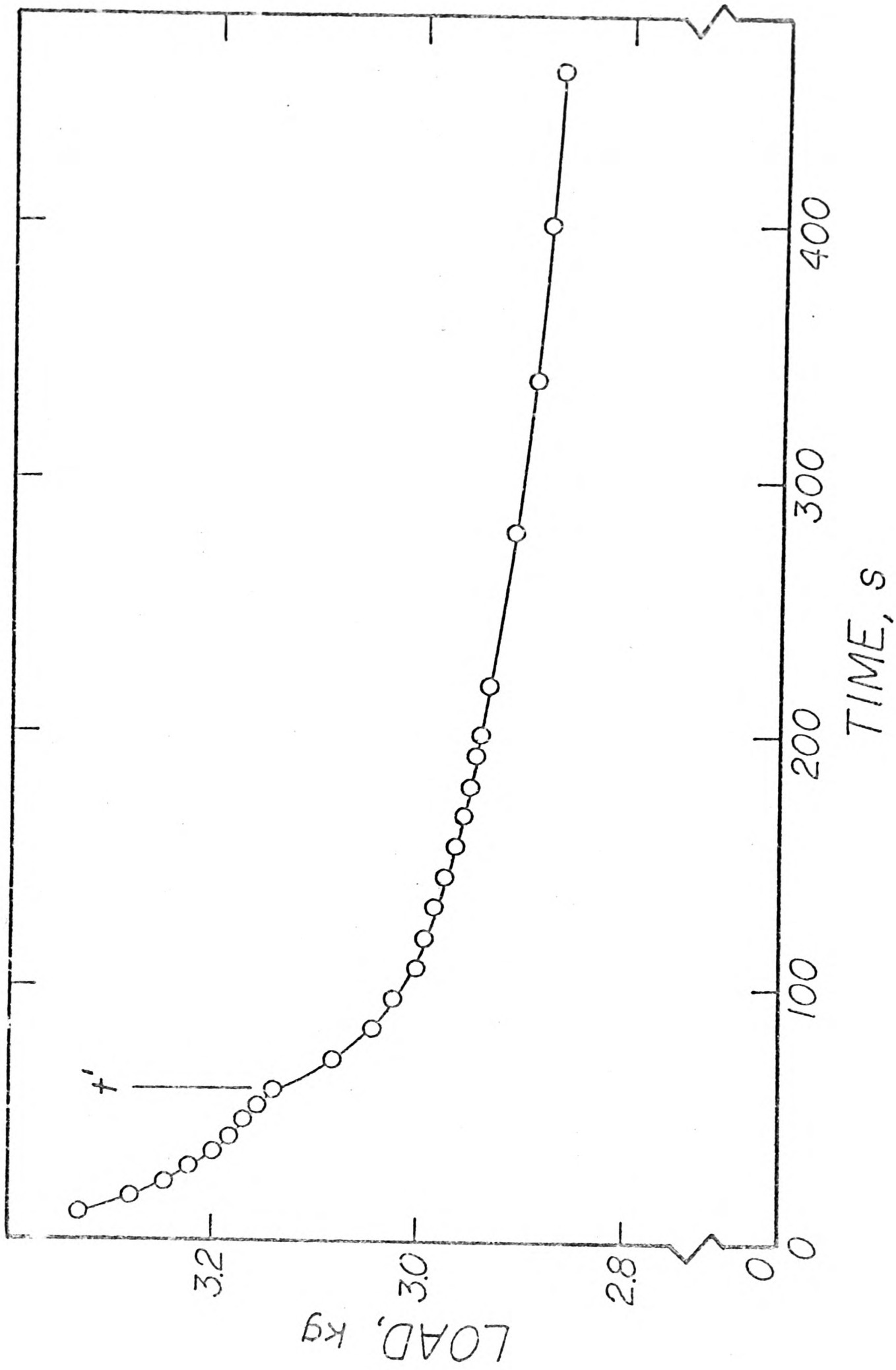


Figure 2-7

Dependence of load on time during a stress relaxation T-jump experiment, specimen CH2-16-3, t' = 60s, ΔT = 2.05 °C, strain = 4.96%.

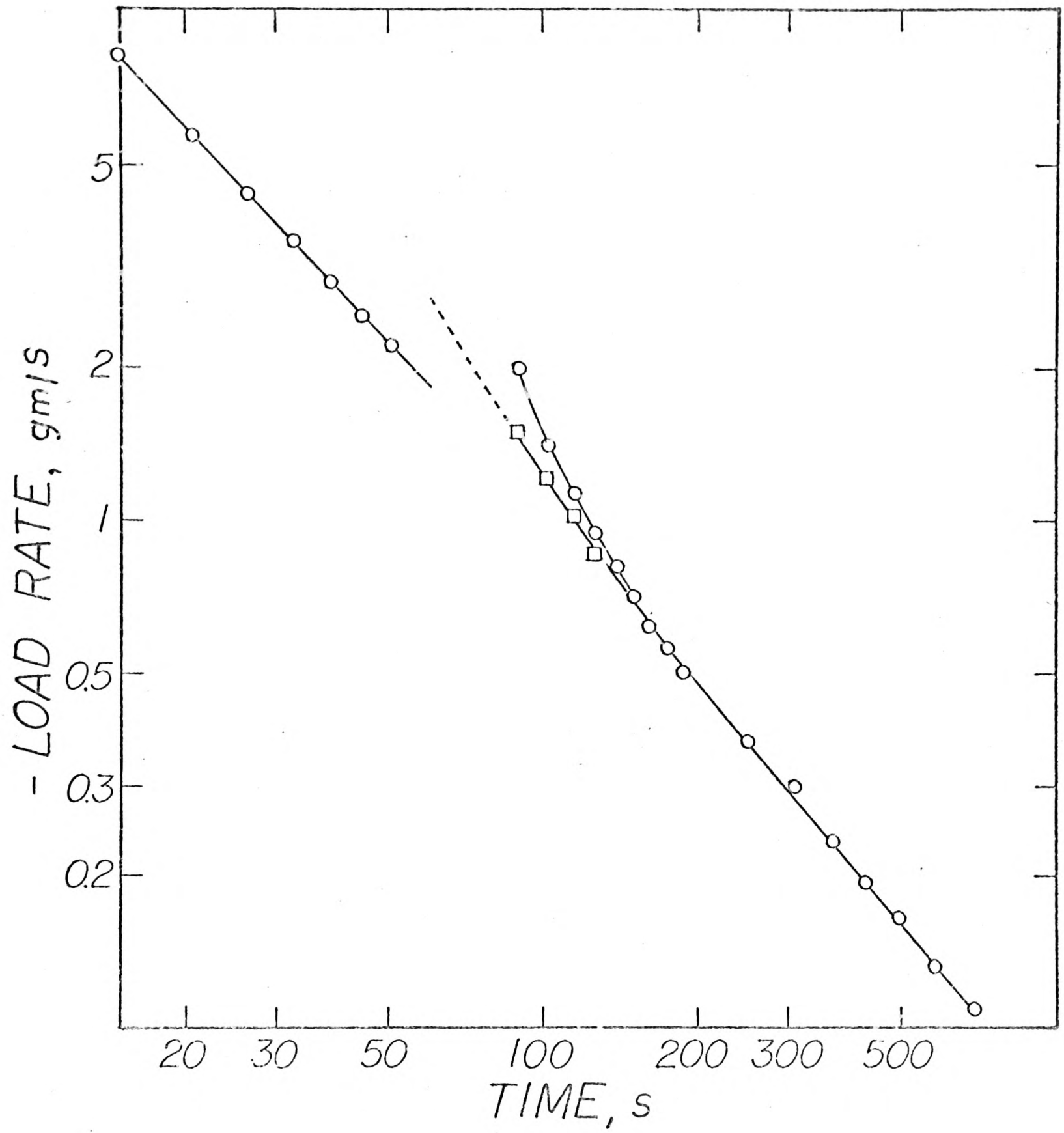


Figure 2-8

Dependence of log (load relaxation rate) on log time for specimen CH2-16-3 in stress relaxation T-jump, strain = 4.96%. ΔT= 2.05 °C.
Circled points: data before thermal expansion correction.
Squared points: data after thermal expansion correction.

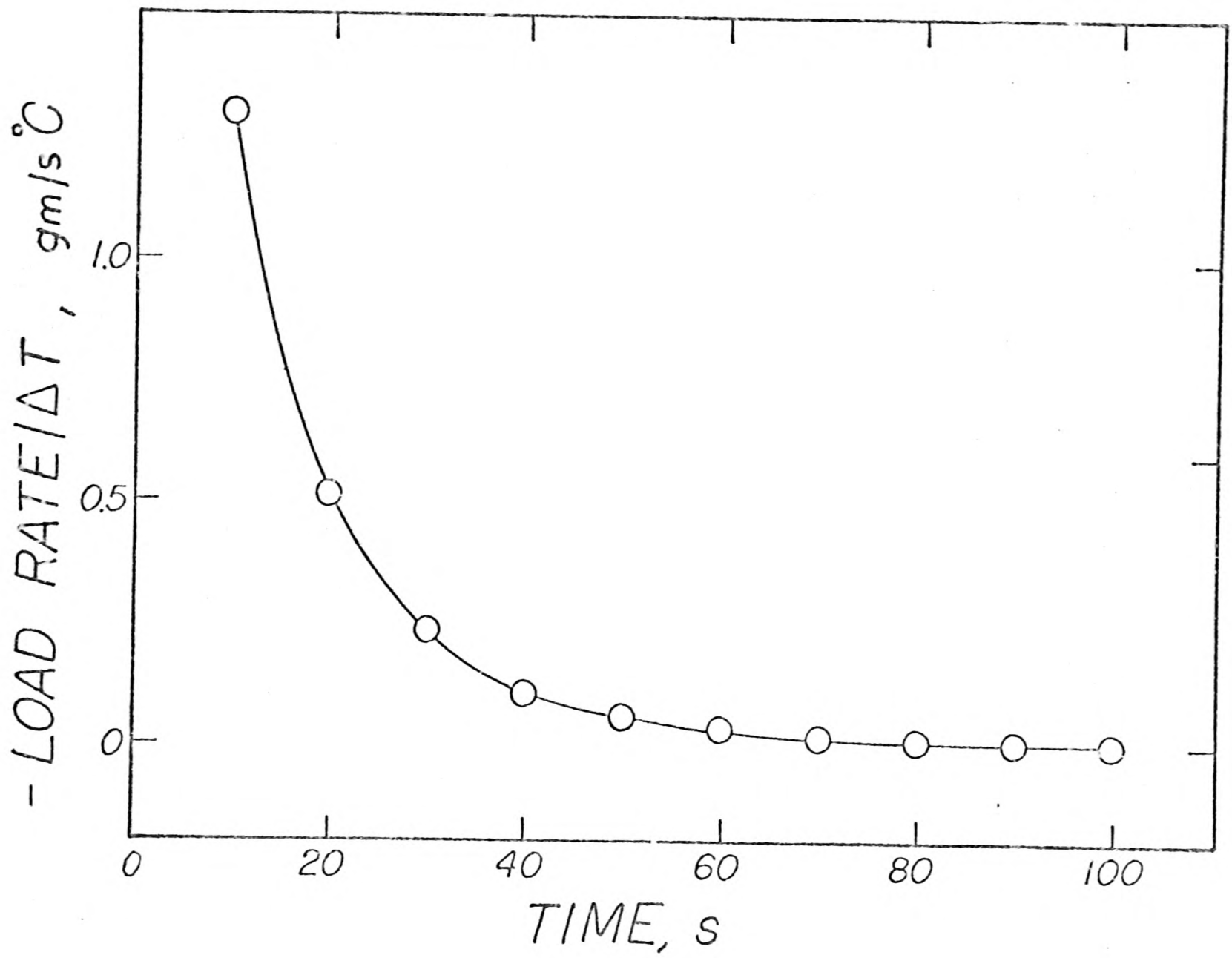


Figure 2-9

Dependence of(thermal expansion load rate per °C temperature rise for stress relaxation)on time, specimen CH2-16-3, prestrain = 4.96%.

Chapter 3

The Influence of Finite Rates of Temperature Change in the Creep T-jump Experiment.

3.1 Introduction

The creep T-jump technique[1] has been employed by various workers to determine the activation energy of viscoelastic deformation processes in synthetic polymers[2] with low activation energies (~10 kcal/mol) and in the investigation of the deformation mechanisms of amorphous and semi-crystalline thermoplastics[3,4,5] in which the activation energies are considerably larger (30-60 kcal/mol). The T-jump experiment requires that an abrupt temperature change be imposed on a specimen which is creeping isothermally at a reference temperature T_o. The creep rates at the final temperature T and at the original temperature, T_o, are determined as a function of time. The creep rates before and after the temperature change are extrapolated to the time of the temperature change, t', to obtain $\dot{\epsilon}_{T_o}(t')$ and $\dot{\epsilon}_T(t')$ respectively.

For the case of an instantaneous change in temperature at t', McCrum and Morris[1] have shown

$$r \equiv \frac{\dot{\epsilon}_T(t')}{\dot{\epsilon}_{T_o}(t')} = \frac{\beta}{a_T} \qquad (3.1)$$

where

$$\beta = 1 + (b_T - 1)A$$

and

$$A = -\frac{\int_{\infty}^{\infty} \frac{L(\ln \tau)\, d \ln \tau}{\tau}}{\int_{-\infty}^{\infty} \frac{L(\ln \tau)}{\tau} \exp(-\frac{t'}{\tau})\, d \ln \tau}$$

In the above equation $L(\ln \tau)$ represents the retardation spectrum at the reference temperature, T_o. The time-temperature shift factor, a_T is a

temperature dependent function defined by

$$\tau_T = a_T \tau \qquad (3.2)$$

where τ_T and τ are the retardation times at T and the reference temperature T_o respectively. The parameter b_T embodies the temperature dependence of the material compliances:

$$b_T = \frac{(D_R - D_U)_T}{(D_R - D_U)_{T_o}} = \frac{\Delta D_T}{\Delta D} \qquad (3.3)$$

D_R and D_U are the relaxed and unrelaxed compliances, respectively, which bound the viscoelastic transition under consideration.

The temperature dependence of the a_T shift factor may be expressed by an Arrhenius equation

$$a_T = \exp \frac{\Delta Ha}{R} \left(\frac{1}{T} - \frac{1}{T_o} \right) \qquad (3.4)$$

where ΔH_a is the apparent activation energy. In the glass to rubber transition it is necessary to allow for variation of ΔH_a with temperature. In this discussion, we assume that ΔH_a is not a function of temperature and combine equations(3.4) and (3.1) to obtain

$$\ln r = \ln \frac{\dot{\epsilon}_T(t')}{\dot{\epsilon}_{T_o}(t')} = \frac{\Delta H_a \Delta T}{RTT_o} + \ln \beta \qquad (3.5)$$

where $\Delta T = T - T_o$. From equation (3.5) it can be seen that if β is assumed to be unity, then a plot of ln r against $\frac{\Delta T}{RTT_o}$ results in a straight line of slope ΔH_a. The anticipated effect of a significant β term on the slope of the plot has been illustrated by McCrum and Pearce[5] and experimentally verified by T-jump experiments on linear polyethylene and will be dealt with in more detail in chapter 4.

This chapter is a critical examination of the experimental problems associated with imposing an abrupt temperature change in the creep T-jump experiment. In all previous investigations employing T-jump

experiments the results were analysed using equation (3.5) which assumes an instantaneous temperature change; however, the actual time of the temperature change was between 1 and 100 seconds.[4,6,7] Using linear viscoelastic theory, the effects of a noninstantaneous temperature change will be determined and experimental confirmation of these theoretical predictions will be obtained. It will be found that a non-instantaneous temperature change introduces a systematic error in the determination of ΔH_a from T-jump experiments, and that the error is most significant at high activation energies. A method is suggested by which this unavoidable experimental error may be accounted for in a quantitative manner.

3.2 Theoretical

The effect of an arbitrary temperature history on the creep behaviour of a linear viscoelastic solid has been derived. Two different models have been postulated to describe the viscoelastic behaviour of the material: Case 1 is a single retardation time model with a temperature dependent compliance difference ($b_T \neq 1$). Case 2 is similar to Case 1 but includes a distribution of retardation times. Normalised creep rates $\Upsilon(t)$ for these two cases are given in equations (3.6-1) and (3.6-2). The digit following the dash in the equation number refers to the two cases described above. The two possible forms of the normalised non-isothermal creep rate are

$$\Upsilon_1(t) = \frac{a_T(t=0)}{b_T(t=0)} \frac{1}{a_T(t)} \left[b_T(t) - \int_0^t \frac{b_T(\xi)}{a_T(\xi)\tau} \exp\left\{ -\int_\xi^t \frac{d\zeta}{a_T(\zeta)\tau} \right\} d\xi \right] \qquad (3.6\text{-}1)$$

$$\Upsilon_2(t) = \frac{a_T(t=0)}{b_T(t=0)} \frac{1}{a_T(t)} \frac{-\int_{-\infty}^{\infty} \frac{L(\ln \tau)}{\tau} \left[b_T(t) - \int_0^t \frac{b_T(\xi)}{a_T(\xi)\tau} \exp\left\{ -\int_\xi^t \frac{d\zeta}{a_T(\zeta)\tau} \right\} d\xi \right] d \ln \tau}{\int_{-\infty}^{\infty} \frac{L(\ln \tau)}{\tau} d \ln \tau} \qquad (3.6\text{-}2)$$

In the above equations, the temperature dependence of the retardation time and the limiting compliance difference are respectively a_T and b_T as defined in equations (3.2) and (3.3). A complete derivation of equation(3.6) may be found in the appendix. It should be noted that equation(3.6) involves no assumptions regarding the form of a_T or b_T or the form of the time varying temperature history. Also, we note that equation(3.1) carries the tacit assumption that the reference temperature, T_o, is also the temperature before t' in a T-jump experiment. Equation (3.6) has been derived to account for the more general case in which the initial temperature in a non-isothermal experiment is not identical with the arbitrarily selected reference temperature.

We now assume that the temperature dependence of a_T is given by the Arrhenius expression given in equation (3.4). The temperature dependence of b_T is assumed[5] to be of the form

$$b_T = 1 + \lambda\left[T(t) - T_o\right] \tag{3.7}$$

where λ is a constant with dimensions $(^{\circ}C)^{-1}$. For analysis of the creep T-jump experiment a piecewise continuous ramp function was chosen for the temperature change history, since this is a reasonable approximation to the non-instantaneous T-jump generated experimentally. Thus we have

$$\Delta T(t) \equiv T(t) - T_o = \begin{cases} 0 & t < t' \\ k(t - t') & t' < t < t'' \\ k(t'' - t') \equiv \Delta T & t > t'' \end{cases} \tag{3.8}$$

The rise time of the temperature ramp is given by t'' - t' with k being the appropriate slope needed to achieve the maximum temperature change, ΔT.

Using equations (3.4) and (3.8) the form of the time-temperature shift factor is

$$a_T(t) = \begin{cases} 1 & t < t' \\ \exp\ -\Delta H_a\, k(t-t')/RT_o^{\,2} & t' < t < t'' \\ \exp\ -\Delta H_a\, k(t''-t')/RT_o^{\,2} & t > t'' \end{cases} \qquad (3.9)$$

where the product TT_o is approximated by $T_o^{\,2}$. The form of b_T is given by equations (3.7) and (3.8).

$$b_T(t) = \begin{cases} 1 & t < t' \\ 1 + \lambda\, k(t-t') & t' < t < t'' \\ 1 + \lambda\, k(t''-t') & t > t'' \end{cases} \qquad (3.10)$$

Inserting equations (3.9) and (3.10) into equations (3.6-1) and (3.6-2) and integrating the resultant expressions either analytically or numerically, we obtain the time dependent creep rate of a viscoelastic material subjected to a piecewise continuous ramp function of temperature. For Case 1, this becomes the equations(A.12), (A.13) and (A.14) of the appendix. For an instantaneous temperature change (i.e. t'' = t') these properly reduce to the McCrum and Morris[1] expression shown in equation (3.5) and for Case 1 to that of Caruthers et al.[8]

First we shall consider Case 1, the single retardation time model but with temperature independent compliance difference (i.e. $b_T = 1$). Figure 3-1 shows the time dependence of the normalised creep rate, $\Upsilon_1(t) = \frac{\tau\,\dot{\epsilon}(t)}{\Delta D\,\sigma_o}$ (where σ_o is the applied stress, and τ the single retardation time). The creep rate is shown for $\Delta T = +4.0\,^{\circ}C$, t' =100s, ΔH_a=40 kcal/mol, τ =1000s and various rise times. As can be seen from figure 3-1 the plot of log $\Upsilon_1(t)$ versus t gives straight lines of differing slopes for values of t before t' and after t''. In the region between t' and t'' the lines are curved and omitted for clarity in figure 3-1. By extrapolating the line $\Upsilon_1(t)$ for times greater than t'' back to t', a value of $\dot{\epsilon}_T(t')$ is obtained.

As the temperature ramp rise time is increased, the extrapolated value of $\dot{\epsilon}_T(t')$ also increases and the activation energy calculated

from equation (3.5), denoted as ΔH_{calc}, deviates from the true value of ΔH_a. The magnitude of this difference can be seen in figure 3-2 where ΔH_{calc} is plotted against rise time for several values of ΔH_a. The difference between ΔH_{calc} and ΔH_a becomes more important as ΔH_a is increased. Thus, for a high activation energy material it is necessary to do a very rapid T-jump or do a series of experiments in which the rise time is varied at a constant ΔT and extrapolate a plot of the activation energy, determined by equation (3.5), versus rise time to zero rise time. The extrapolated value of the activation energy is ΔH_a.

The effect of a non-instantaneous temperature change will also manifest itself on a plot of ln r against $\Delta T/RTT_o$ where r is the ratio of creep rate at t' defined in equation (3.1). The non-instantaneous T-jump results in a curved plot as shown in figure 3-3. The extrapolated values of r have been computed for various values of ΔT at each rise time using values of b_T=1.0 and ΔH_a=40 kcal/mol. For rise times greater than zero, the curve bends away from the straight line of the instantaneous T-jump and this effect is most pronounced at large positive values of ΔT. For negative ΔT's the computed values of ln r are close to the value obtained for zero rise time; therefore, if experiments are performed at only one rise time, the down T-jumps should give closer approximation of ΔH_a.

Let us summarise the major results obtained so far. For a linear viscoelastic material described by a single retardation time model and with a limiting compliance difference independent of temperature, the activation energy calculated from a non-instantaneous creep T-jump experiment via equation (3.5) will be different from the true activation energy. This error in the calculated activation energy will be most significant for a material with a high activation energy, for large positive temperature changes, and for long rise times. However, by constructing a

plot of ΔH_{calc} versus rise time at a constant ΔT, one can in principle extrapolate to zero rise time and obtain the true activation energy.

The effect of β on the non-instantaneous creep T-jump experiment can be investigated using Case 1, with $b_T \neq 1$, i.e. a single retardation time model with a temperature dependent limiting compliance difference. In figure 3-4, a plot of ΔH_{calc} against rise time for various values of λ (see equation(3.7)) illustrates the combined effect of β and a non-instantaneous rise time. As λ is increased, the slope of ΔH_{calc} vs. rise time is imperceptibly increased while the intercept is increased significantly. The increase in the intercept is a manifestation of the β effect described by McCrum and Pearce[5]. The effect of rise time on the model in this case can be handled in a manner analogous to that presented earlier for Case 1 with $b_T = 1$.

A plot of ln r against $\Delta T/RTT_o$ is shown in figure 3-5 for $\lambda = 0.0168$ and in figure 3-6 for $\lambda = 0.084$. As can be seen from figure 3-5 the ln r vs. $\Delta T/RTT_o$ curves for various rise times are rotated counterclockwise from the positions shown earlier in figure 3-3 ($\lambda = 0$) and deviate more from the straight line of $\Delta H_a = 40$ kcal/mol. For still larger values of λ as shown in figure 3-6, the rotation of the curves becomes more pronounced and this is particularly clear for negative temperature changes. As expected, the curve calculated for an instantaneous T-jump with $\lambda = 0.084$ deviates significantly from the straight line for the instantaneous T-jump with $\lambda = 0$. The shape of this calculated curve is similar to that found experimentally by McCrum and Pearce[5].

The analysis has been extended to include a distribution of retardation times as described in Case 2 with $b_T = 1$. As a first approximation a box distribution was used. The creep rates obtained for this case were plotted on a log rate-log time graph for various rise times. The resulting

curves were found to be straight lines for t less than t' and approximately straight lines for t greater than t". The values of ΔH_{calc} obtained from extrapolation of these lines to t' showed a similar effect to that described for the single retardation time model, i.e. an increase in ΔH_{calc} as the rise time increased.

3.3 Experimental

In order to test the validity of the theoretical results presented above, experiments were performed on a thin strip of poly(methyl methacrylate), PMMA, of dimensions 15.85 cm x 0.222cm x 0.089cm. The same specimen of PMMA was employed throughout the experimental investigation. This material was chosen because the activation energy is known to be about 40 kcal/mol at 45°C,[9] a convenient operating temperature for our equipment. The tensile creep apparatus and silicone oil flow system have been described elsewhere.[10] Both silicone oil reservoirs were controlled to within 0.05°C by immersion heaters. One heater had a power control which allowed the amount of heat input to the bath to be varied. This feature enabled us to make controlled ramp changes in the bath temperature. In this way, the time to change the temperature from an initial temperature T_o to a final temperature T could be varied to give temperature ramp rise times between 15s and 500s.

The time required to complete the temperature change was monitored in two ways. (1) The temperature of the specimen environment was measured via thermocouple emf and (2) the thermal expansion of the unstressed specimen was monitored via the creep strain transducer output. For rise times greater than 20 s the thermal expansion output followed the thermocouple output identically. For times shorter than 20s a lag in the thermal expansion was observed. A typical thermal expansion trace and the

corresponding thermocouple output are shown in figure 3-7. The appropriate heater settings which would produce the required rise times were determined from experiments of this type on the unstressed sample.

In order to perform an experiment with a rise time greater than 20s with a negative temperature change, a cooling coil was placed in the silicone oil bath. Cooling water was passed through this coil and the flow rates required for the desired rise times were again determined from the experiments at zero load described above.

The fastest T-jumps were performed in approximately 15s by employing two baths, one at T_o and the other at T, and using techniques described in detail elsewhere.[10,11] Briefly, the experiment proceeds as follows: Before the time of the T-jump, oil from the bath at T_o is circulated past the specimen; at t=t', the fluid from the bath at T is pumped past the specimen by simultaneously opening and closing various solenoid valves. Appropriately designed recirculation lines ensure that fluid from the two baths does not mix and the temperature control is maintained throughout the experiment.

A value of $T_o = 45^{\circ}C$ was chosen as the initial temperature. At this temperature, the T-jump is conducted at the start of the α relaxation region for PMMA.[9] A lower value for T_o would shift the creep response into the β relaxation region, in which there is some controversy over the value of ΔH_a.[12] At higher temperatures, ($80^{\circ}C$ upwards), ΔH_a becomes a strong function of temperature which would introduce unwanted complications in the interpretation of the experiments.

The specimen was annealed at $55^{\circ}C$ for 3 hours (i.e. $5^{\circ}C$ above the maximum value used for T), after each T-jump to ensure complete recovery of the specimen. Subsequently the specimen was allowed to equilibrate at T_o for at least one hour before performing the next experiment.

3.4 Results

In the theoretical development of non-isothermal creep presented above is the implicit assumption of linear viscoelasticity. Thus, it was first necessary to determine the limits of the linear viscoelastic region for the PMMA specimen. An isochronal stress-strain curve was constructed and is shown in figure 3-8. As can be seen in figure 3-8, the PMMA specimen exhibits linear viscoelastic behaviour up to a stress of 15 MPa. We chose to operate at a stress of 13.5 MPa in all subsequent experiments. The stress is still in the linear viscoelastic region but large enough to give easily measured creep rates.

A more critical test of the applicability of linear viscoelasticity is the observance of the Boltzmann Superposition Principle when applied to isothermal creep and recovery data. Isothermal creep recovery behaviour of PMMA was monitored in order to test the validity of the Boltzmann Superposition Principle. The material was allowed to creep at 45°C for 200s. After removal of the load and sufficient annealing to allow for complete recovery of the specimen, the same load was applied for 100s. The load was then removed and the specimen was allowed to recover with both creep and recovery data being recorded. This creep and recovery data is presented in figure 3-9 for a stress of 13.5 MPa. The validity of Boltzmann Superposition is observed at this level of stress.

A series of rapid T-jumps, rise time = 15s, were performed on the PMMA specimen with T_o = 45 °C and t'=100s. Values of ln r were obtained for the rapid T-jumps for values of ΔT from +4 °C to -4 °C. As a first approximation, the data were analysed according to the instantaneous T-jump solution of equation (3.5) with $\beta = 1$. These results are plotted in figure3-10. A best fit straight line through the points gives a ΔH_{exp} = 43 $\pm$ 2 kcal/mol.

To determine if a significant β effect was present, creep recovery T-jumps were performed. Linear viscoelastic theory indicates that the β effect is nonexistent for recovery T-jump.[13] Therefore, if β is significant the recovery T-jumps should exhibit a lower value of ΔH_{exp} than that obtained from the creep T-jumps.[13] In the recovery T-jump experiment, the specimen was allowed to creep at T_o=45 °C for 500s, the load was removed and after another 100s the temperature was abruptly changed to T and the recovery behaviour was recorded. A plot of ln r against $\Delta T/RTT_o$, shown in figure 3-11 for the recovery data, indicates a $\Delta H_{exp} = 43 \pm 6$ kcal/mol. The increased scatter of the recovery data can be attributed to the low creep rates involved. For recovery T-jumps with negative ΔT's the recovery rates were too low for accurate extrapolation . Since, within experimental error, the value of ΔH_{exp} is the same for both creep and recovery T-jumps it is clear that β is not large. Although it is not conclusive that $\beta = 1$, its magnitude is sufficiently close to unity so as not to introduce a large error into the determination of ΔH_a by the T-jump technique for this PMMA sample.

Non-instantaneous T-jump experiments were performed using rise times of 20, 212, 364, and 510s with a constant ΔT = 3.6 °C. The logarithm of the observed rates are plotted against log t as shown in figure 3-12. The rate data at T_o are extrapolated forward to t' to give $\dot{\epsilon}_{T_o}(t')$ while the data after the temperature change are extrapolated back to t' to give $\dot{\epsilon}_T(t')$. The creep rate data during the ramp temperature change are ignored. Using the values of $\dot{\epsilon}_{T_o}(t')$ and $\dot{\epsilon}_T(t')$ with equation (3.5), ΔH_{exp} was calculated for each rise time. The values of ΔH_{exp} for the various rise times are shown in figure 3-13. As expected from the previous analysis, the longer the rise time the larger the value of ΔH_{exp}. The intercept of ΔH_{exp} versus rise time plot is 42 kcal/mol in good agreement with the rapid T-jump experiment presented in figure 3-10. The solid line

in figure 3-13 is calculated from a single retardation time model (Case 1) with ΔH_a = 42 kcal/mol, τ = 750s and b_T=1.

Additional experimental confirmation of the theoretical predictions for non-isothermal creep of a linear viscoelastic material is presented in figure 3-14. As theoretically predicted and shown in figure 3-3, when the duration of the temperature change is increased, curvature is introduced on a ln r versus $\Delta T/RTT_o$ plot. We have performed experiments at one rise time, 370s, and various values of ΔT. These data are presented in figure 3-14 and the expected curvature of a ln r versus $\Delta T/RTT_o$ plot is observed. The solid line in figure 3-14 is calculated using the Case 1 model with ΔH_a = 42 kcal/mol, τ =750s and b_T=1. It should be noted that these are the same constants used to fit the results shown in figure 3-13.

3.5 Discussion

We have determined the apparent activation energy for deformation of PMMA in the α relaxation region at 45 °C and a stress of 13.5 MPa to be 43 $\pm$ 2 kcal/mol. This activation energy was observed in rapid (nearly instantaneous) creep and recovery T-jumps. These values are in good agreement with those of Sherby and Dorn[14] and Bueche.[9]

However, the most important finding of the experiment is not the actual magnitude of ΔH_a for PMMA, but the effect of the temperature ramp rise times on the creep T-jump technique. If a non-instantaneous T-jump is performed, the value of the activation energy, ΔH_{exp}, obtained from extrapolation of the log rate-log time data is always greater than that for the instantaneous T-jump. This result has been predicted from considerations of the appropriate equations of non-isothermal linear viscoelasticity and has been clearly demonstrated in the data acquired for PMMA. We have seen excellent agreement between experimental results and

the theoretical prediction for two sets of data:

(1) values of ΔH_{exp} versus rise time at a constant ΔT and

(2) values of $\ln \dot{\epsilon}_T(t')/\dot{\epsilon}_{T_o}(t')$ versus $\Delta T/RTT_o$ at a constant rise time.

From the experimental results and the preceeding analysis, it is clear that for high activation energy processes, the T-jump experiment must be very rapid (almost instantaneous) or one must do T-jump experiments at different rise times and extrapolate the result to zero rise time.

As a further test of the theory, we obtained a fit of the experimental data by a single retardation time model with $b_T = 1$, (Case 1). It was found that the best fit straight line through the data corresponded to $\tau = 750s$ and $\Delta H_a = 42$ kcal/mol; this line is shown in figure 3-13. The same parameters were used in equation (3.6-1) to calculate the theoretical line shown in figure 3-14. Again, this line closely fits the experimental points.

3.6 Summary

General equations for nonisothermal creep of a linear viscoelastic solid have been presented. Both the time dependent strain and strain rate were predicted for an arbitrary temperature history. The creep T-jump experiment (imposition of a sudden temperature change on a creeping specimen) was analysed using these equations in order to understand the influence of non-instantaneous temperature changes on the experimental observations. It was shown that an increase in the time required to impose the temperature change caused an increase in the activation energy, ΔH_{exp}, determined via creep T-jump. This effect was most pronounced for materials with large activation energies. Appropriate extrapolation techniques can be used to obtain the result expected for an instantaneous temperature change. Verification of the theoretical prediction was obtained from isothermal and non-isothermal creep experiments

on poly(methyl methacrylate) in the linear viscoelastic region. The activation energy for a nearly instantaneous temperature change was 43 ± 2 kcal/mol. As the rise time of the temperature change was increased to 600s, ΔH_{exp} increased to 70 ± 2 kcal/mol. The effects of the rate of temperature change on other aspects of the creep T-jump experiment were also found to be in keeping with the predictions of the nonisothermal linear theory.

References

1 McCrum N.G. and Morris E.L., Phil.Mag.,7,2115,1962.

2 Caruthers J.M. and Cohen R.E., J.Polymer Sci.,14,1891,1976.

3 Tietz T.E. and Dorn J.E., Trans.Am.Inst.Min.Met.Eng.,206,156,1956.

4 Hutchinson J.M. and McCrum N.G., Nature, Physical Sci.,236,115,1972.

5 McCrum N.G. and Pearce D.L., Nature, Physical Sci.,243,52,1973.

6 Morris E.L., D.Phil. Thesis, Cambridge University, 1963.

7 Sherby O.D., Lytton J.L. and Dorn J.E., Acta.Met.,5,219,1957.

8 Caruthers J.M., Hooley C.J. and Cohen R.E., Proc. 7th Int.Cong. on Rheology, C.Klason and J. Kubat eds, Gothenburg, August 1976, page 389.

9 Bueche F., J.Appl.Phys.,26,738,1955.

10 Caruthers J.M. and Cohen R.E., Polymer Preprints, 16:1,746,1975.
" " Polymer Eng. Sci.,16,41,1976.

11 Matthews J.F. and McCrum N.G., J.Physics E: Sci.Instrum.,6,583,1973.

12 McCrum N.G. and Morris E.L., Proc.Roy.Soc.,A281,258,1964.

13 Hutchinson J.M., McCrum N.G. and Pearce D.L., J.Polymer Sci.,Polym.Phys., 12,1255,1974.

14 Sherby O.D. and Dorn J.E., J.Mech.Phys.Solids,6,145,1968.

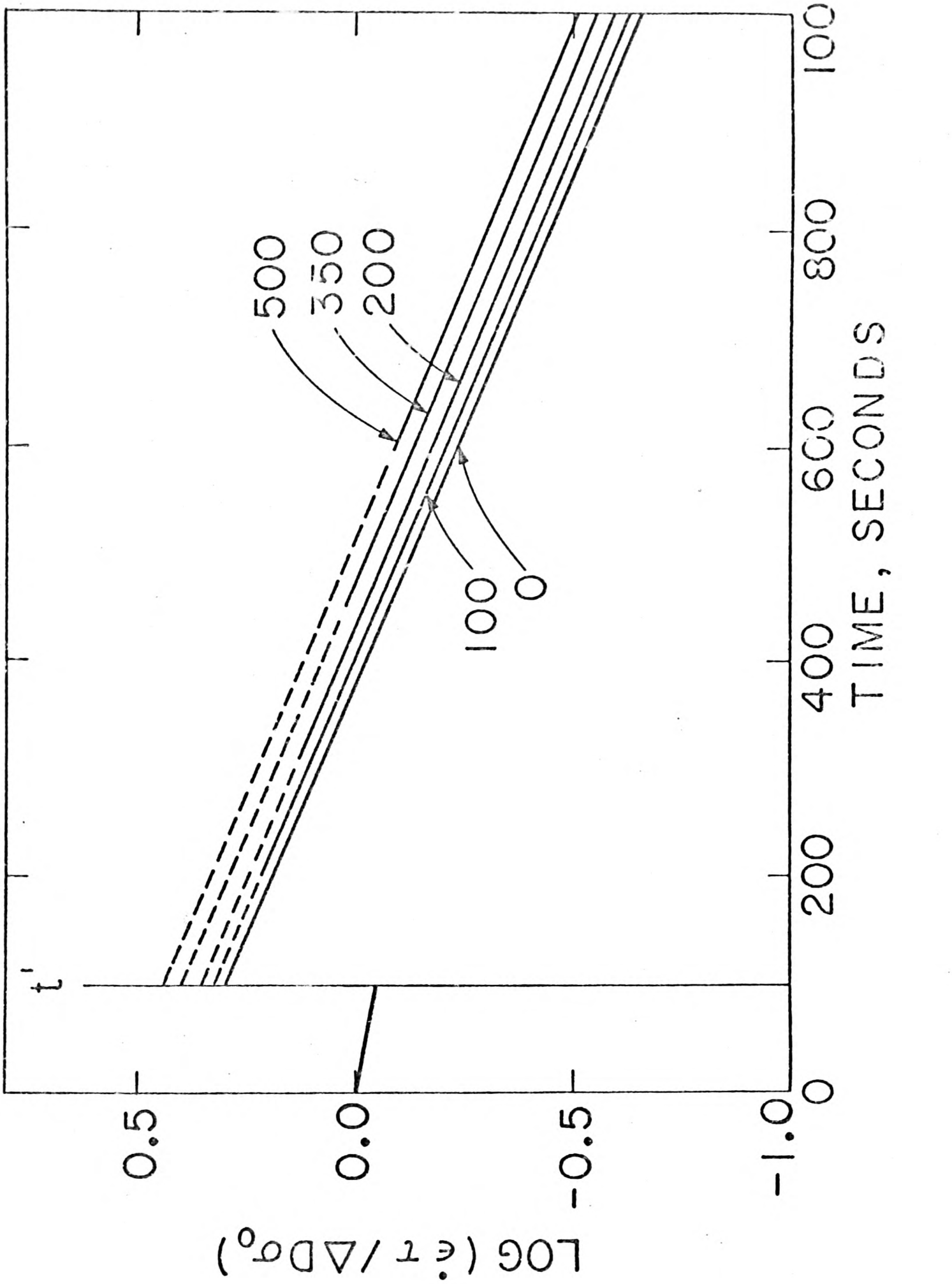


Figure 3-1

Plot of ln ($\dot{\epsilon}\tau$ / $\Delta D\sigma_o$) against t for the single retardation time model with ΔH_a = 40 kcal/mol, t'= 100s, τ=1000s, λ= 0, and for rise times (t'' - t') = 0, 100, 200, 350, 500s, with ΔT = 4 °C.

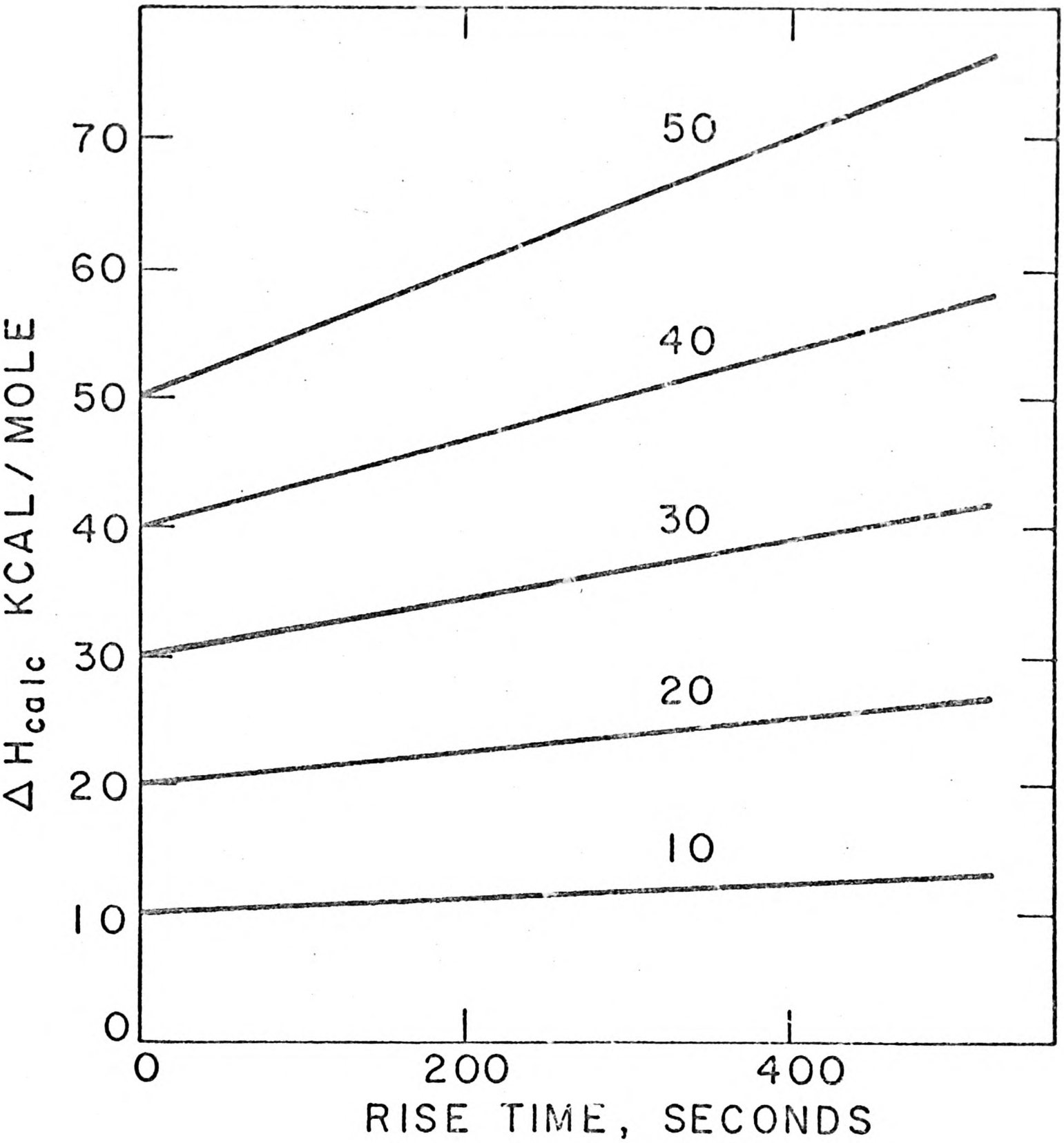


Figure 3-2

ΔH_{calc} against rise time for single retardation time model for several values of ΔH_a = 10, 20, 30, 40, 50 kcal/mol with t' = 100s, τ = 1000s, λ = 0 and $\Delta T = 4^{\circ}C$.

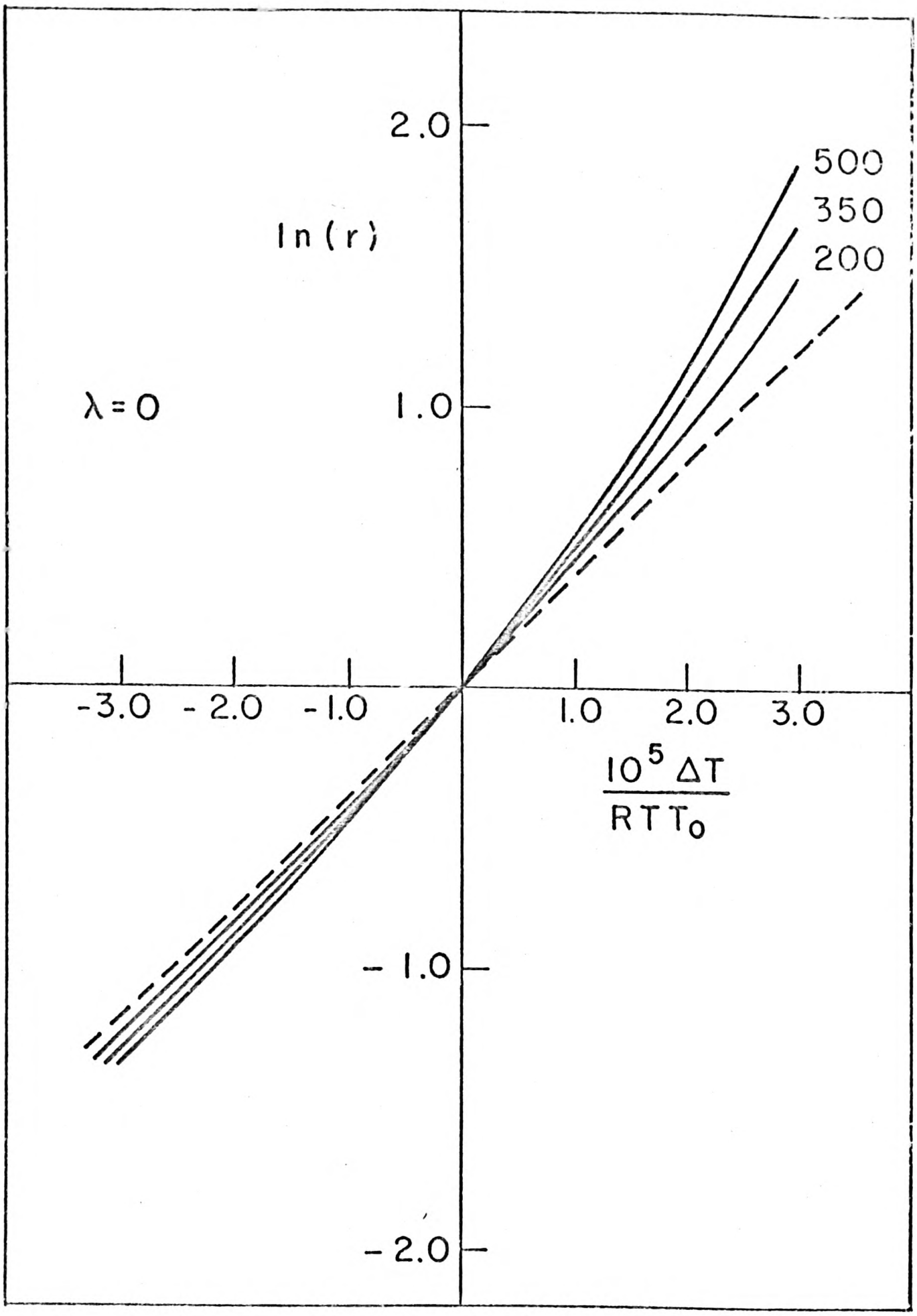


Figure 3-3

Plot of ln r against $\Delta T/RTT_0$ for single retardation time model for various rise times $(t'' - t') = 0$, 200, 350, 500s, with $t' = 100$s, $\tau = 1000$s, $\lambda = 0$, $\Delta H_a = 40$ kcal/mol.

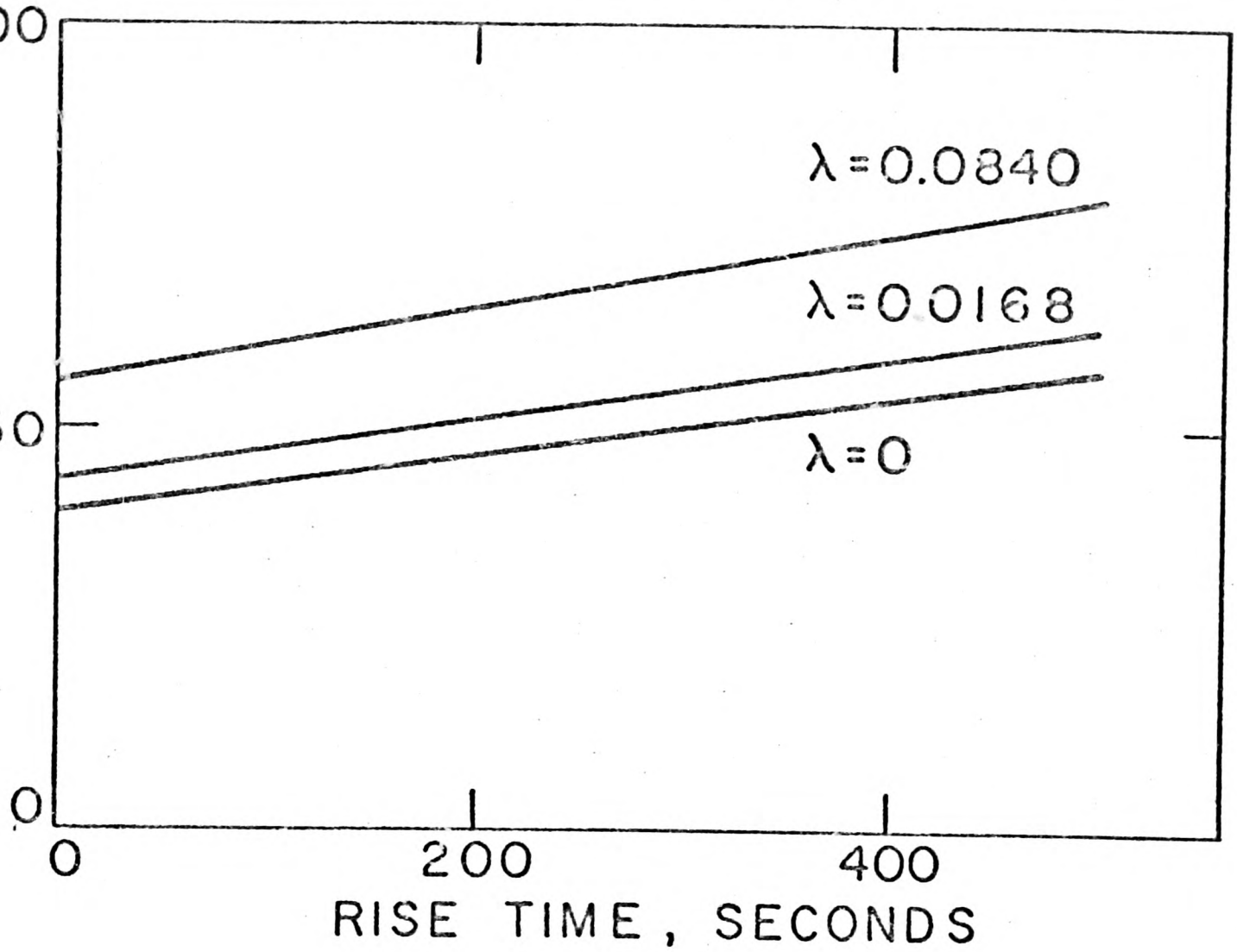


Figure 3-4

ΔH_{calc} against rise time for single retardation time model with ΔH_a = 40 kcal/mol, and various values of λ = 0.0, 0.0168, 0.0840. τ = 1000s, t' = 100s, and ΔT = +4 °C.

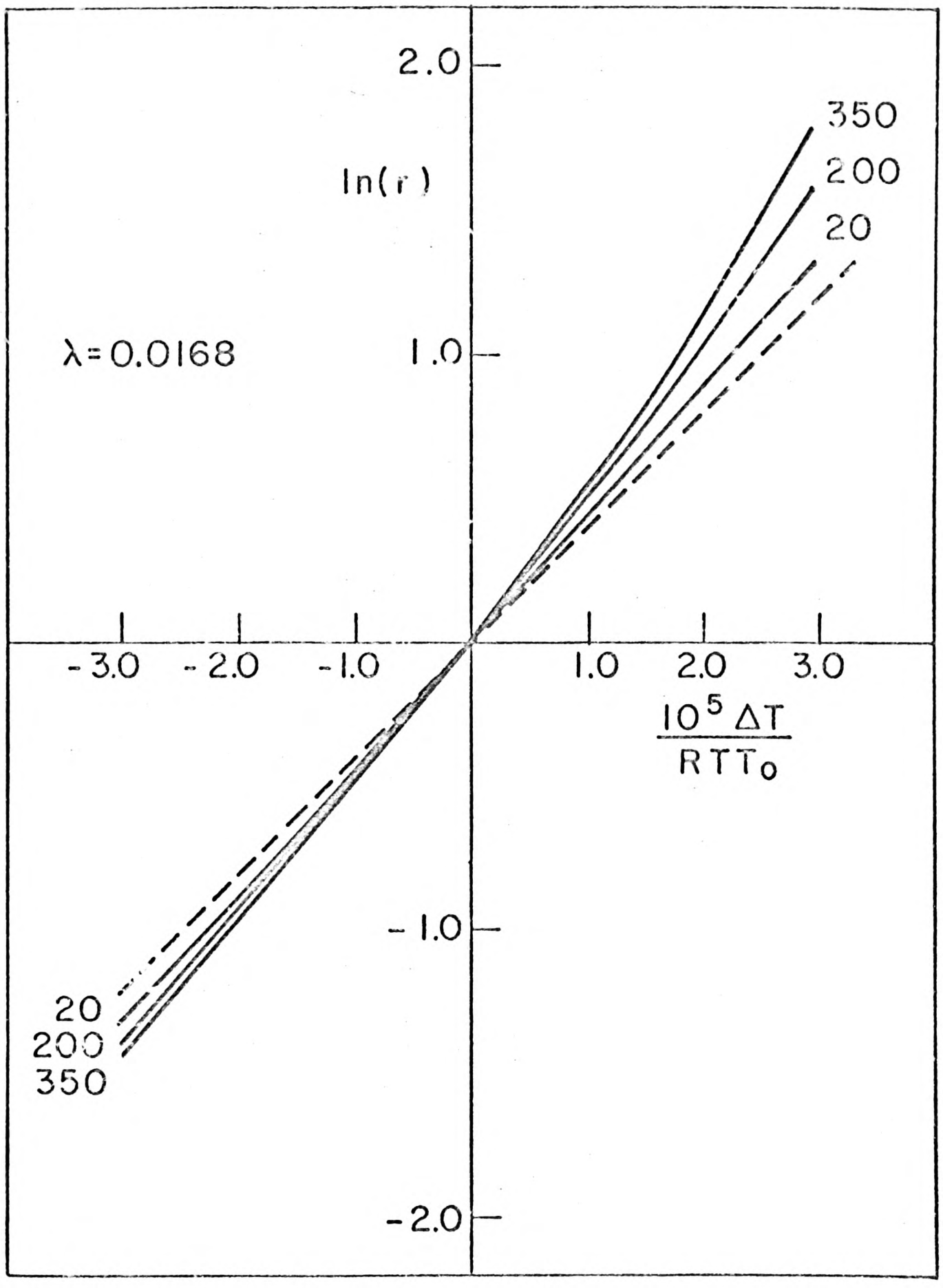


Figure 3-5

Plot of ln r against $\Delta T/RTT_o$ for single retardation time model for rise times $(t'' - t') = 0, 20, 200, 350s$, and $\lambda = 0.0168$, $t' = 100s$, $\tau = 1000s$.

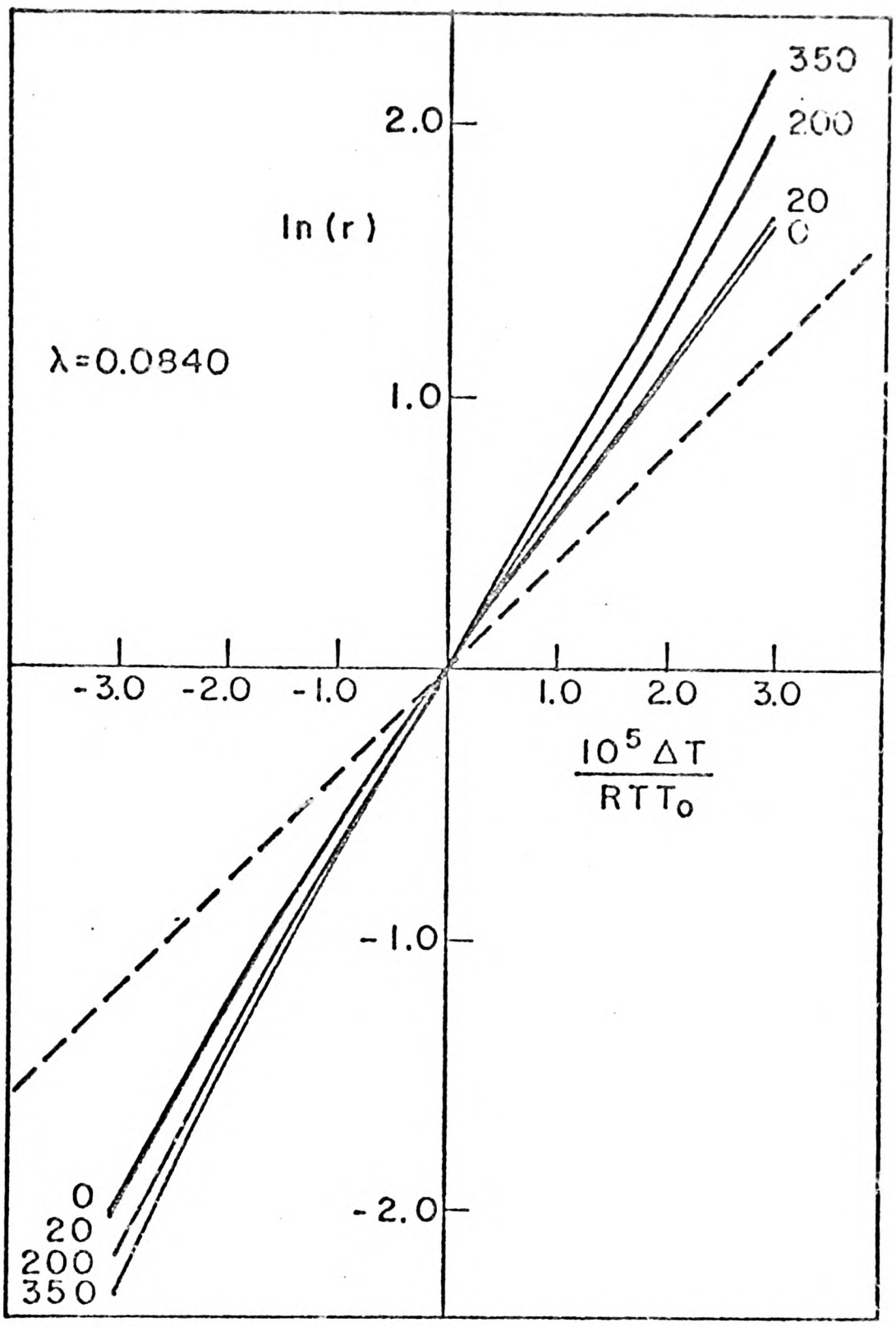


Figure 3-6

Plot of ln r against $\Delta T/RTT_o$ for single retardation time model for rise time $(t'' - t') = 0$, 20, 200, 350s, and $\lambda = 0.0840$, $t' = 100s$, $\tau = 1000s$.

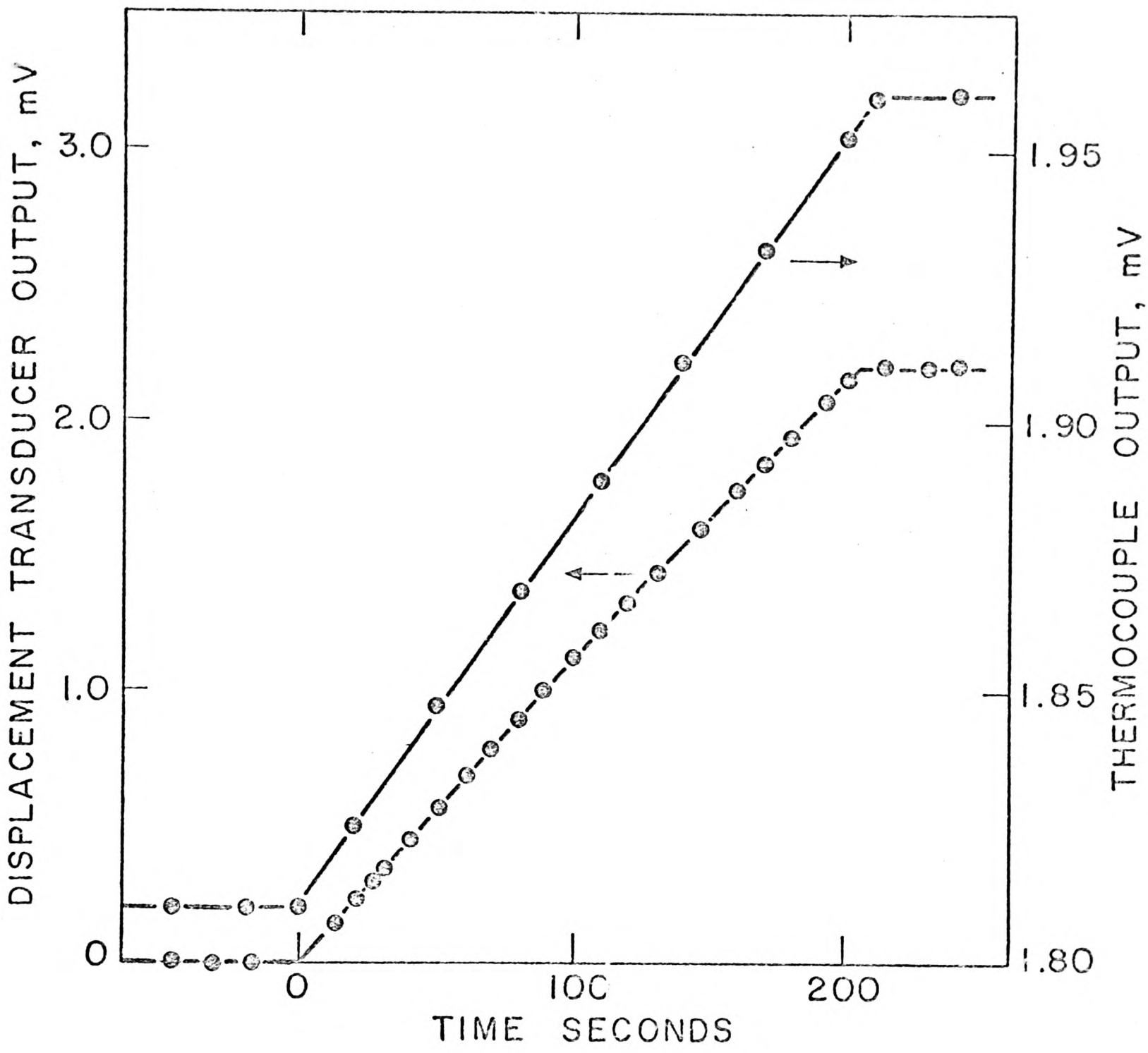


Figure 3-7

Thermal expansion output from LVDT plotted against time for PMMA showing a rise time of 206s for a ΔT of +3.6 °C; also shown is the corresponding thermocouple emf.

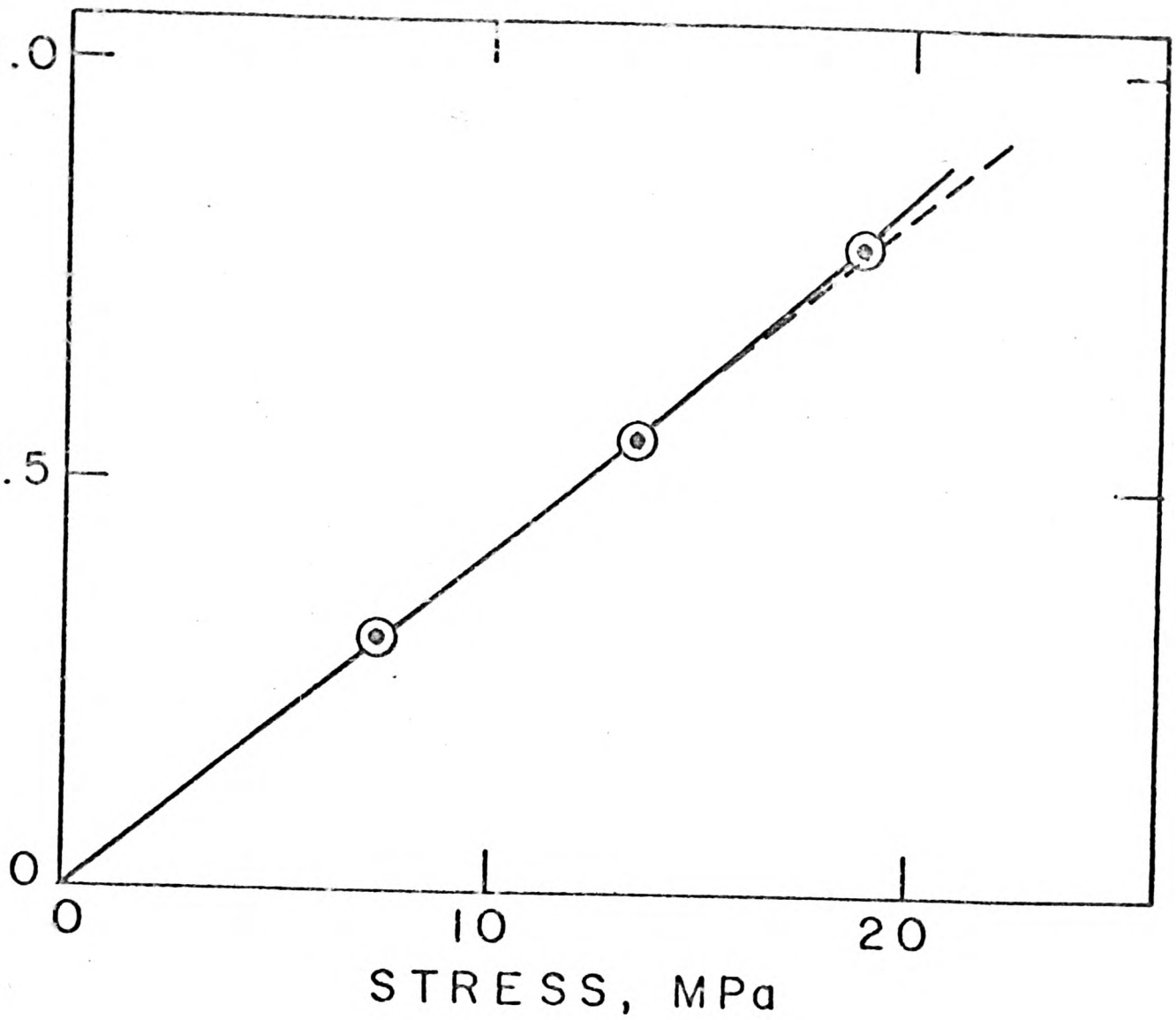


Figure 3-8

20s isochronal stress-strain curve for PMMA at 45 °C. Dotted line shows extension of linear region.

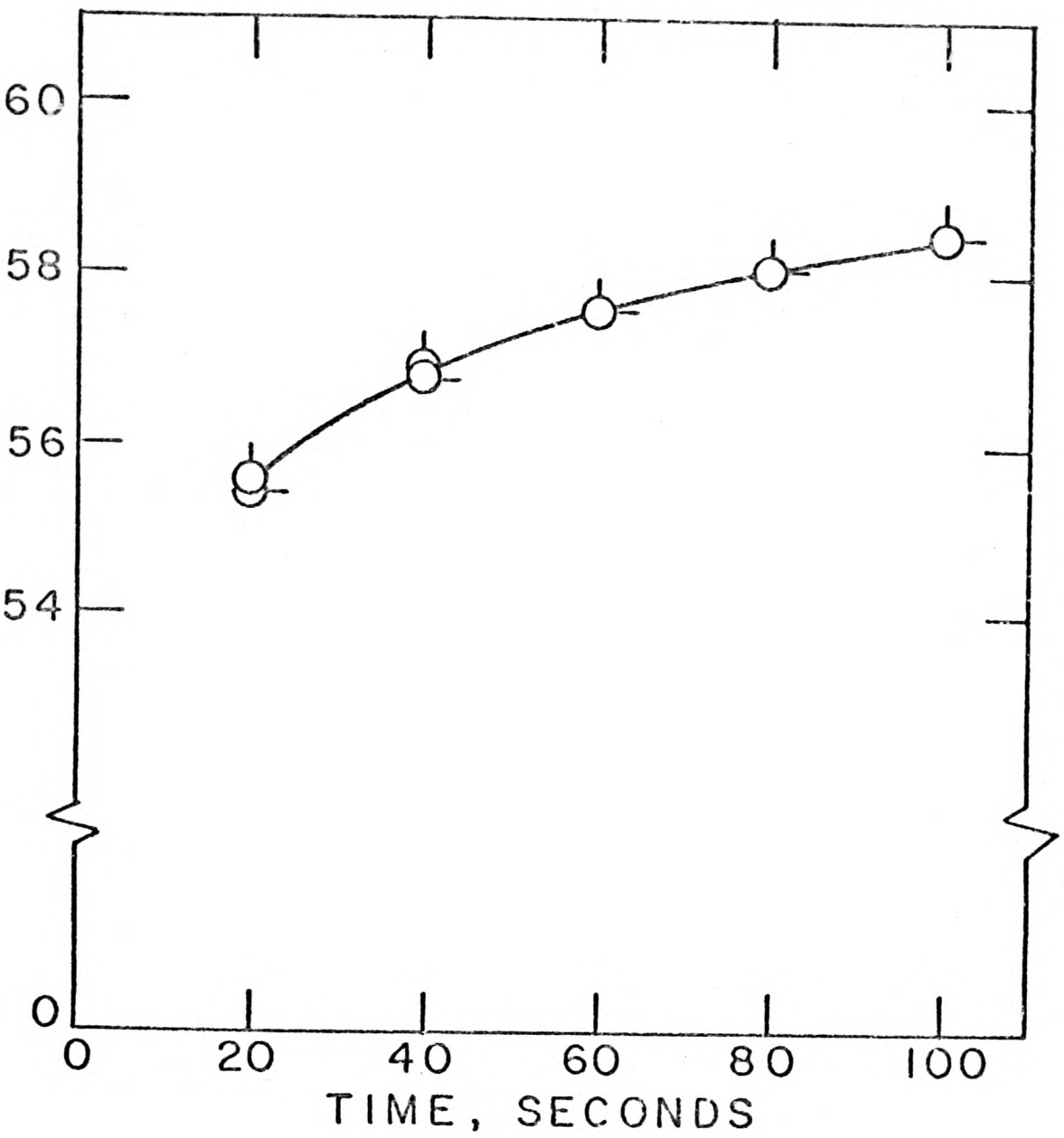


Figure 3-9

Plot of creep and recovery strain against time for PMMA at a stress of 13.5 MPa, at 45°C, ● creep strain; ○ recovery strain.

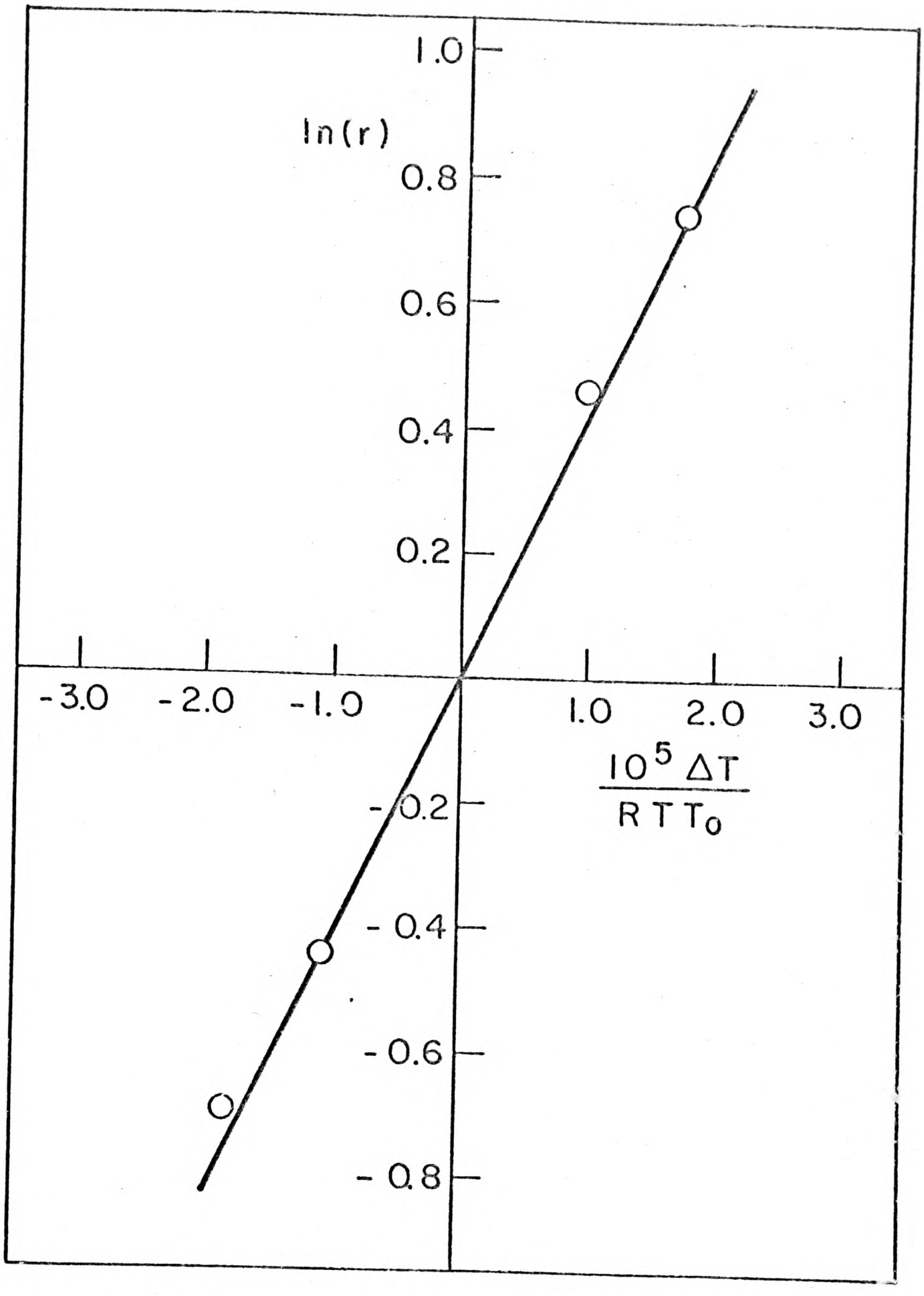


Figure 3-10

Experimental values of ln r against $\Delta T/RTT_o$ for PMMA. $T_o = 45^\circ C$, $\sigma_o = 13.5$ MPa, rise time < 15s, $t' = 100$s. Best fit line corresponds to $\Delta H_a = 43 \pm 2$ kcal/mol.

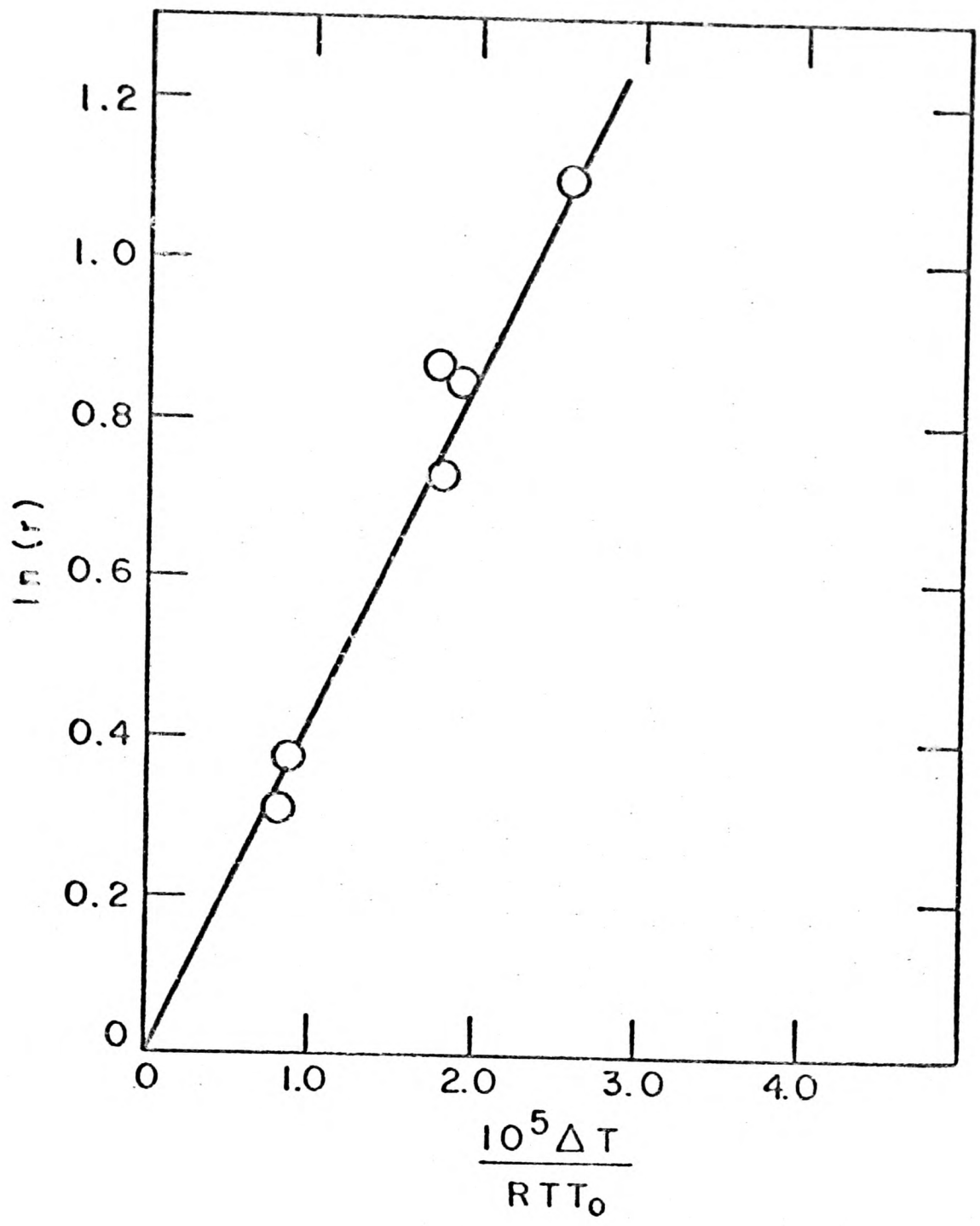


Figure 3-11

Experimental values of ln r against $\Delta T/RTT_o$ for recovery T-jumps on PMMA. T_o = 45°C, σ_o = 13.5 MPa, rise time <15s, loading time = 500s, t' = 100s after removal of the stress. ΔH_a = 43 ± 6 kcal/mol.

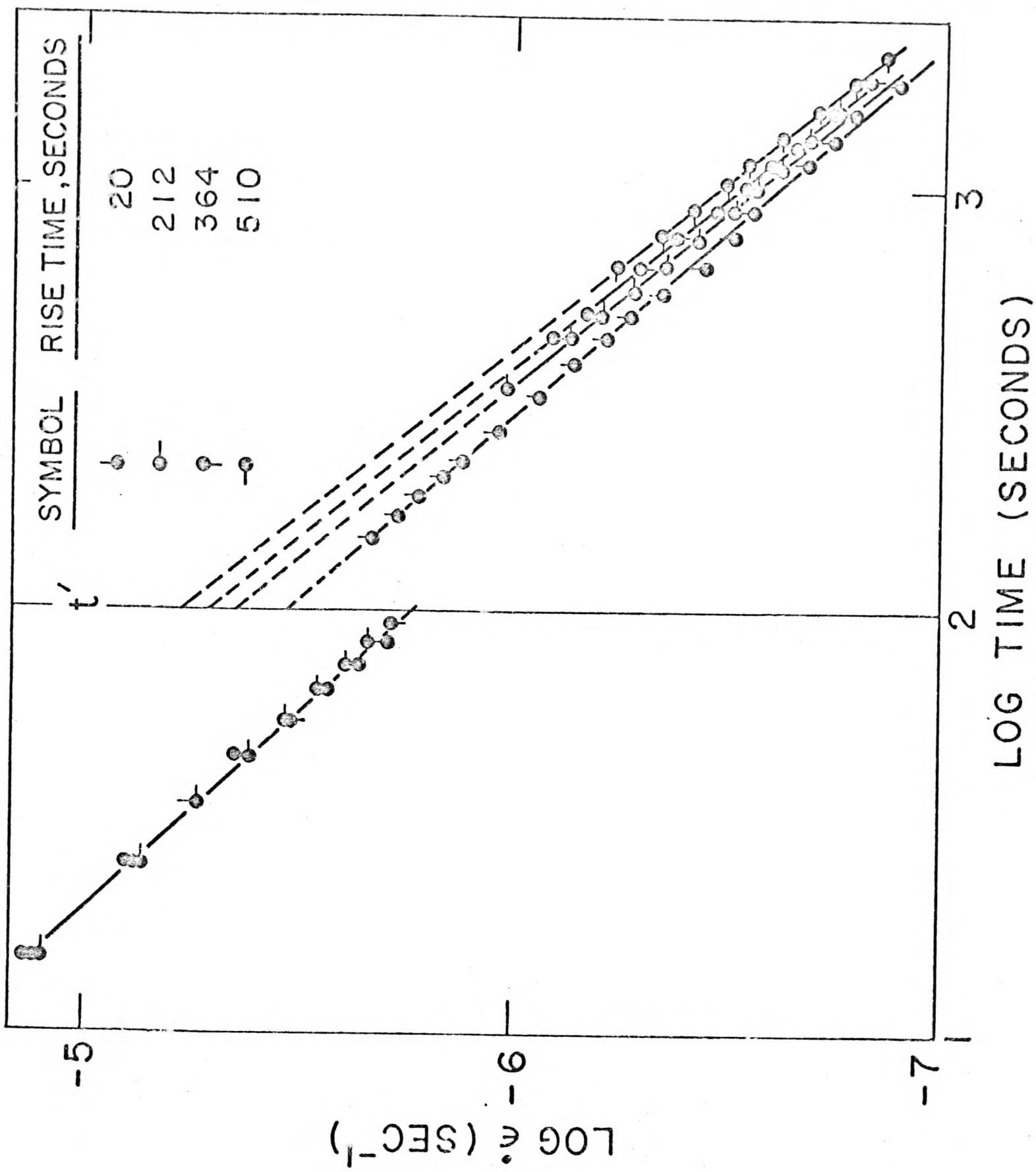


Figure 3-12

Log $\dot{\epsilon}$ against log t obtained from creep T-jumps on PMMA for various values of rise time; (t" - t') = 20, 212, 364, and 510s. ΔT = + 3.6 °C, t'= 100s, T_c = 45°C, σ_o = 13.5 MPa.

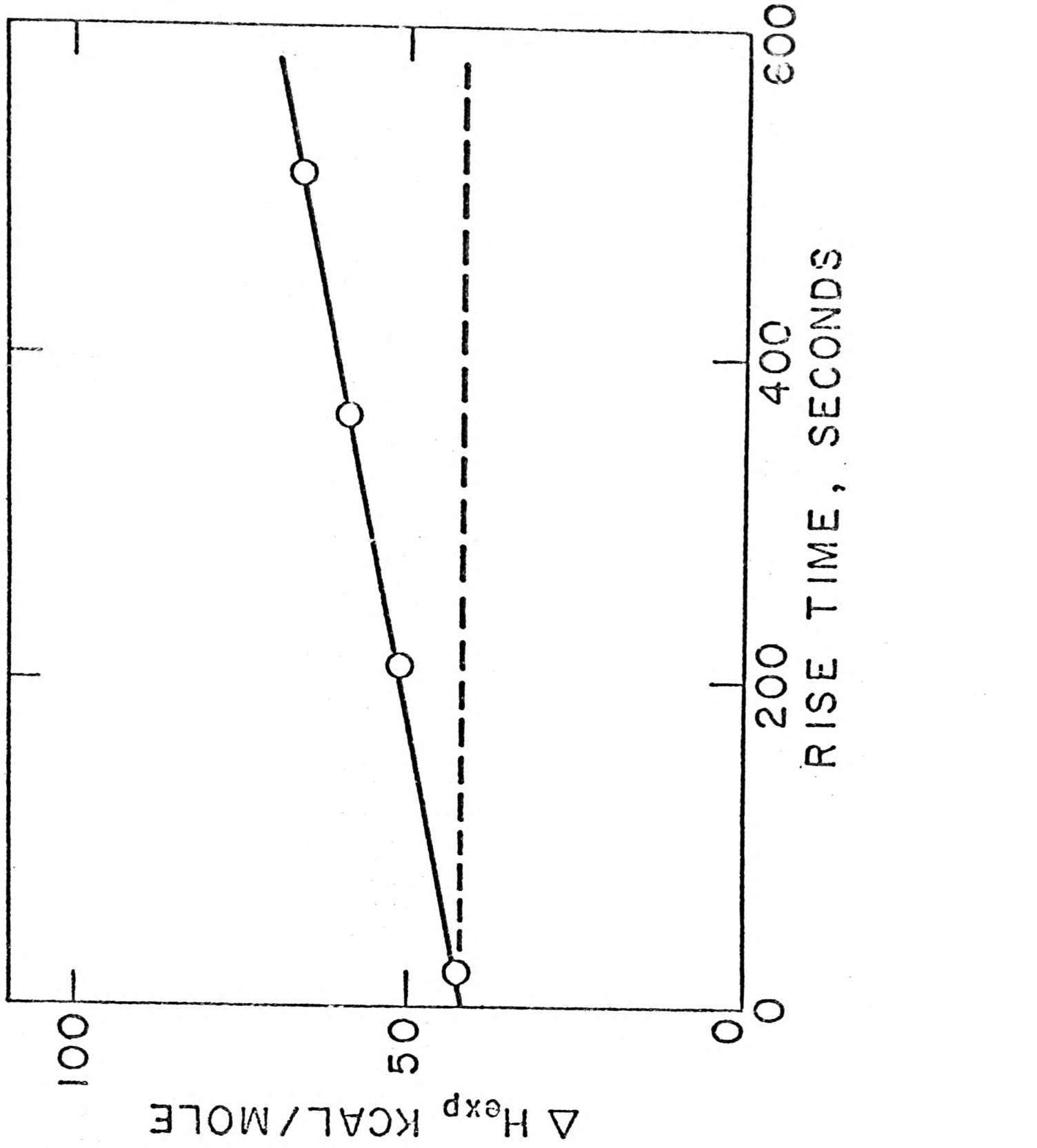


Figure 3-13

Plot of ΔH_{exp} against rise time of PMMA, using one value of $\Delta T = +3.6\ ^{\circ}C$, $T_o = 45\ ^{\circ}C$, $\sigma_o = 13.5$ MPa. Also shown through the points is the theoretical line for $\Delta H_a = 42$ kcal/mol, $\tau = 750$s.

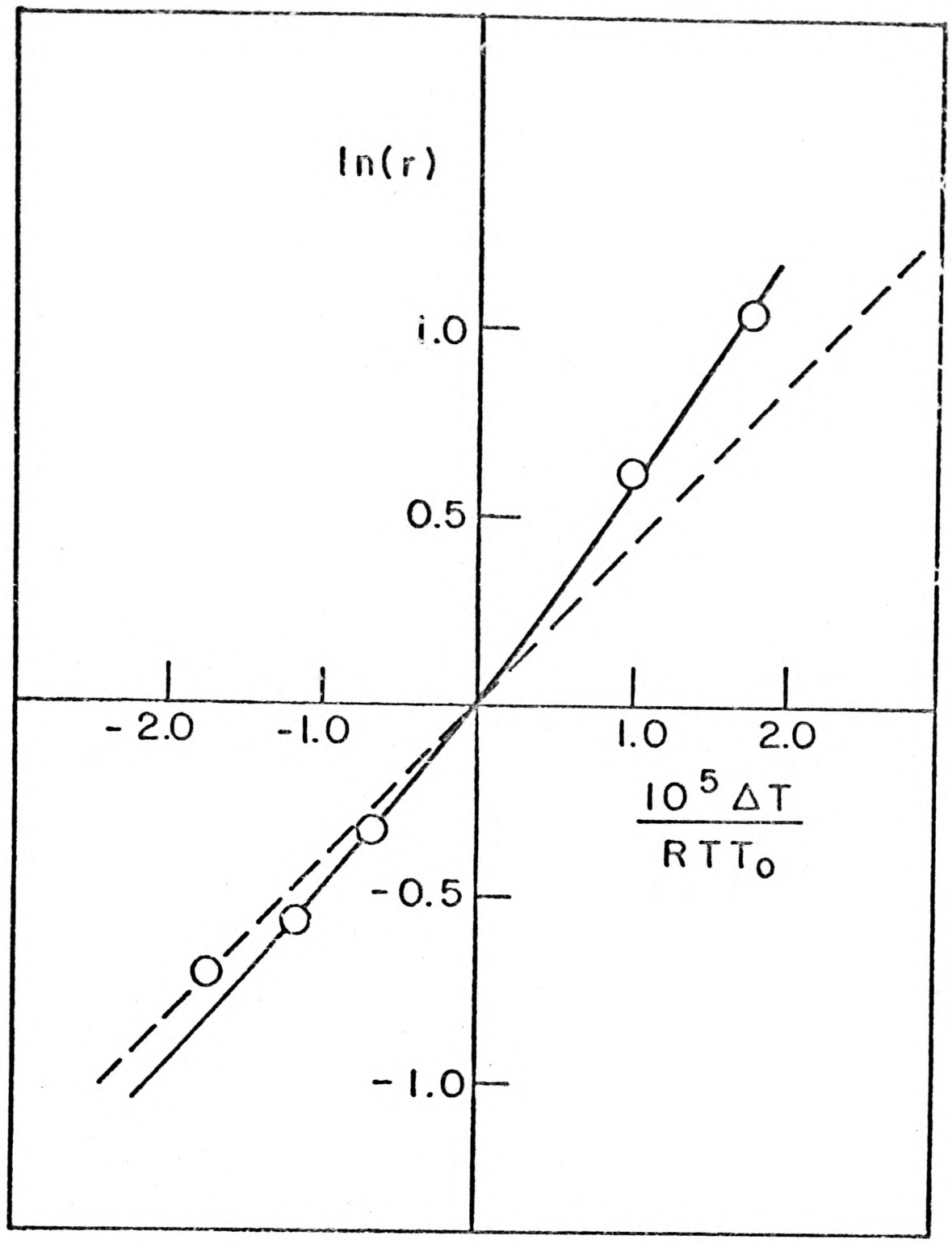


Figure 3-14

Plot of experimental values of ln r against $\Delta T/RTT_o$ for a rise time = 370s. Also shown is the theoretical line for ΔH_a = 42 kcal/mol, τ = 750s and the dashed line for an instantaneous T-jump with ΔH_a = 42 kcal/mol.

Chapter 4

The Instantaneous Temperature Change Experiment

4.1 Introduction

The linear viscoelastic equations for the creep T-jump, which were developed by McCrum and Morris[1] and used by various workers[2,3,4], describe the creep rates at the time of the T-jump. The equations for the creep rates at any time, t, before and after the T-jump can also be obtained. This chapter will develop the use of these equations for the creep rates to determine the shape of the theoretical creep rate against time curves. It will be seen that the best method of plotting the creep rate data is on a log rate-log time graph and the theoretical curves can be compared with those obtained experimentally. The discussion will be extended to the problem of the terms containing b_T and A[1,3] in the McCrum and Morris equation (3.1), and by considering the equations for the creep rate after the T-jump, a method is suggested by which this problem may be overcome. The equations for the rates in stress relaxation and recovery T-jump[5] are also presented.

The development of these equations is important since, for a linear viscoelastic solid, they can be used to fit the whole of the creep rate against time curve for the parameters a_T (or ΔH_a) and b_T instead of just using the two points at t=t' obtained from extrapolation of the data before and after t' to that time. It will be seen in chapters 8 and 9 that these equations can be used to fit the experimental data obtained from T-jumps on tendon.

4.2 The Creep T-jump

4.2.1 General Equations for the T-jump

For a linear viscoelastic material creeping under a constant stress, σ_o, at temperature T_o, the creep rate $\dot{\epsilon}_{T_o}(t)$ at any time, t, is given by

$$\frac{\dot{\epsilon}_{T_o}(t)}{\sigma_o} = \int_{-\infty}^{\infty} \frac{L(\ln \tau)}{\tau} \exp\left(-\frac{t}{\tau}\right) \quad d \ln \tau \tag{4.1}$$

where $L(\ln \tau)$ is the spectrum of retardation times τ. If the temperature is suddenly changed to T at time t', then the creep rate at any time t after t' will be

$$\frac{\dot{\epsilon}_T(t)}{\sigma_o} = \int_{-\infty}^{\infty} \frac{L(\ln \tau)}{a_T \tau} \left[\exp\left\{ -\frac{1}{\tau}\left(t' + \left(\frac{t-t'}{a_T}\right)\right)\right\} + (b_T - 1) \exp - \left(\frac{t-t'}{a_T \tau}\right)\right] d\ln \tau \tag{4.2}$$

A convenient method of looking at these rates will be to refer them all to the creep rate at t' at temperature T_o. Thus we have the ratio of the creep rate after t' at temperature T and time t, $\dot{\epsilon}_T(t)$ to the creep rate at t' before the T-jump at temperature T_o, $\dot{\epsilon}_{T_o}(t')$ as

$$\frac{\dot{\epsilon}_T(t)}{\dot{\epsilon}_{T_o}(t')} = \frac{1}{a_T}\left[\frac{\int_{-\infty}^{\infty} \frac{L(\ln \tau)}{\tau} \exp\left(-\frac{t^*}{\tau}\right) \, d \ln \tau}{\int_{-\infty}^{\infty} \frac{L(\ln \tau)}{\tau} \exp\left(-\frac{t'}{\tau}\right) \, d \ln \tau} + (b_T - 1) A^* \right] \tag{4.3}$$

where A^* is the factor which multiplies $(b_T - 1)$ and is

$$A^* = \int_{-\infty}^{\infty} \frac{L(\ln \tau)}{\tau} \exp -\left(\frac{t^* - t'}{\tau}\right) d \ln \tau \quad / \int_{-\infty}^{\infty} \frac{L(\ln \tau)}{\tau} \exp\left(-\frac{t'}{\tau}\right) d \ln \tau \tag{4.4}$$

and

$$t^* = t' + \left(\frac{t - t'}{a_T}\right) \tag{4.5}$$

At t=t', equation (4.3) becomes that of McCrum and Morris[1] giving the ratio of the rates as

$$r \equiv \frac{\dot{\epsilon}_T(t')}{\dot{\epsilon}_{T_o}(t')} = \frac{1}{a_T}\left[1 + (b_T - 1) A \right] \tag{4.6}$$

where A is the value of A^* at t=t' and is

$$A = \int_{-\infty}^{\infty} \frac{L(\ln \tau)}{\tau} \, d \ln \tau \quad / \quad \int_{-\infty}^{\infty} \frac{L(\ln \tau)}{\tau} \exp\left(-\frac{t'}{\tau}\right) d \ln \tau \qquad (4.7)$$

The problem in interpreting all previous T-jumps has been the question of the value of A and the magnitude of the product of (b_T-1) and A. For most cases the value of b_T has been assumed so close to unity that the product $(b_T - 1)$ A is close to zero. The value of A can be large depending on the position within the distribution of retardation times at which the T-jump is performed (see section 4.2.2) The following analysis will show how the difficulty may be overcome in experimental measurements of the creep rates. We will show that for all intents and purposes, the value of A to be used in equation (4.6) will be much less than the actual value of A given by equation (4.7). It is the value of A^* as $t \to t'$ which is important in the analysis. In almost all practical cases, the value of A^* is independent of the position of the time of the temperature change within the distribution. The exceptions will be pointed out. The analysis will also show the shape of curve to be expected on the log rate-log time plot in a T-jump experiment used to compute the ratio r. The function a_T is assumed to take an Arrhenius form, i.e.

$$a_T = \exp \frac{\Delta H_a}{R} \left(\frac{1}{T} - \frac{1}{T_o} \right) = \exp \left(- \frac{\Delta H_a \, \Delta T}{R T T_o} \right) \qquad (3.4)$$

where ΔH_a is the apparent activation energy of the deformation process and ΔT is the temperature change $T-T_o$. In future discussion, we will refer to both ΔH_a and a_T.

4.2.2 Equations with a Box Distribution for the Spectrum of Retardation Times.

For the simplest case for our modelling, we take a box distribution for the retardation spectrum i.e. $L(\ln \tau) = C$ = constant between the limits of the distribution $\ln \tau = \ln a$ and $\ln \tau = \ln b$.

Equation (4.1) then becomes

$$\frac{\dot{\epsilon}_{T_o}(t)}{\sigma_o} = \int_a^b \frac{C}{\tau^2} \exp\left(-\frac{t}{\tau}\right) d\tau \qquad (4.8)$$

$$= \frac{C}{t}\left\{\exp\left(-\frac{t}{b}\right) - \exp\left(-\frac{t}{a}\right)\right\} \qquad (4.9)$$

which at t' is

$$\frac{\dot{\epsilon}_{T_o}(t')}{\sigma_o} = \frac{C}{t'}\left\{\exp\left(-\frac{t'}{b}\right) - \exp\left(-\frac{t'}{a}\right)\right\} \qquad (4.10)$$

With the box distribution, equation (4.2) becomes

$$\frac{\dot{\epsilon}_T(t)}{\sigma_o} = \frac{C}{a_T}\frac{1}{t'}\left[\frac{\exp(-\frac{t^*}{b}) - \exp(-\frac{t^*}{a})}{t^*/t'} + (b_T-1)\frac{\exp-\left(\frac{t^*-t'}{b}\right) - \exp-\left(\frac{t^*-t'}{a}\right)}{\left(\frac{t^*}{t'}-1\right)}\right] \qquad (4.11)$$

Hence, using equations (4.10) and (4.11), equation(4.3) becomes

$$\frac{\dot{\epsilon}_T(t)}{\dot{\epsilon}_{T_o}(t')} = \frac{1}{a_T}\left[\frac{D_1}{(t^*/t')} + (b_T-1)\frac{D_2}{\left(\frac{t^*}{t'}-1\right)}\right] \qquad (4.12)$$

where

$$D_1 = \frac{\exp(-\frac{t^*}{b}) - \exp(-\frac{t^*}{a})}{\exp(-\frac{t'}{b}) - \exp(-\frac{t'}{a})} \qquad (4.13)$$

$$A^* = \frac{D_2}{\left(\frac{t^*}{t'}-1\right)} \qquad (4.14)$$

and

$$D_2 = \frac{\exp-(\frac{t^*-t'}{b}) - \exp-(\frac{t^*-t'}{a})}{\exp(-\frac{t'}{b}) - \exp(-\frac{t'}{a})} \qquad (4.15)$$

At t=t', D_1=1 and t^*=t', so on expanding the terms in $\exp-(\frac{t^*-t'}{b})$ and $\exp-(\frac{t^*-t'}{a})$, equation (4.12) becomes

$$\frac{\dot{\epsilon}_T(t')}{\dot{\epsilon}_{T_o}(t')} = \frac{1}{a_T}\left[1 + (b_T - 1)\frac{\left(\frac{t'}{a} - \frac{t'}{b}\right)}{\exp(-\frac{t'}{b}) - \exp(-\frac{t'}{a})}\right] \qquad (4.16)$$

From equations (4.6), (4.14) and (4.16), it can be seen that the value of A for the box distribution is given by

$$A = \left(\frac{t'}{a} - \frac{t'}{b}\right) \Big/ \left\{\exp(-\frac{t'}{b}) - \exp(-\frac{t'}{a})\right\} \qquad (4.17)$$

For times before t', from equation (4.9) we see that

$$\frac{\dot{\epsilon}_T(t)}{\dot{\epsilon}_{T_o}(t')} = D_3\left(\frac{t}{t'}\right)^{-1} \qquad (4.18)$$

where

$$D_3 = \frac{\exp(-\frac{t}{b}) - \exp(-\frac{t}{a})}{\exp(-\frac{t'}{b}) - \exp(-\frac{t'}{a})} \qquad (4.19)$$

Equations (4.12) to (4.19) will be used for much of the following modelling.

An important simplification can be made to the above equations by considering the form of the expressions for D_1, D_2 and D_3 and determining the effect on these parameters of the position within the distribution of the time of the temperature change. For the modelling which follows, we assumed the distribution to extend over 20 decades of τ . Thus for various values of t'/a, where ln τ = ln a is the beginning of the distribution, we computed values of D_1, D_2 and D_3 as shown in figures 4-1 and 4-2. Looking first at times after the T-jump we see from figure 4-1 that the two quantities D_1 (equation(4.13)) and D_2 (equation (4.15)) are equal to unity for the following conditions:

$$10^2 < \frac{t'}{a} < 10^{18} \qquad (4.20\text{-}1)$$

and

$$\frac{t}{t'} > 1.005 \qquad (4.20\text{-}2)$$

Before t' we see from figure 4-2 that the quantity D_3 of equation (4.19) is equal to unity for the condition (4.20-1) and values of

$$\frac{t}{t'} > 0.1 \qquad (4.20\text{-}3)$$

If equations (4.20) do hold for a given experiment, and this is likely for many cases, then equations (4.12) and (4.18) simplify to

$$\frac{\dot{\epsilon}_T(t)}{\dot{\epsilon}_{T_o}(t')} = \frac{1}{a_T}\left[\frac{1}{(t^*/t')} + (b_T - 1)\,A^*\right] \qquad (4.21)$$

where

$$A^* = \frac{1}{\left(\frac{t^*}{t'} - 1\right)}$$

and for times $t < t'$,

$$\frac{\dot{\epsilon}_{T_o}(t)}{\dot{\epsilon}_{T_o}(t')} = \frac{1}{(t/t')} \qquad (4.22)$$

Since most experiments on polymers will occur under the conditions outlined above, then equations (4.21) and (4.22) describe the creep rates before and after a T-jump and allow for a simple fitting of the experimental data for a_T and b_T. It is worth noting that the condition (4.20-2) means that for a T-jump occurring at t'=100s, then t must be greater than 100.5s before this condition holds. Since the first data points obtainable from the T-jump experiment are >10s after the temperature change (i.e. at t/t'> 1.1) then all experimental points will obey this criteria. For criteria (4.20-3)

to hold, then the first data point should be taken at a time $t > 10s$ after application of the load. This is always obeyed in our experiments.

The most important aspects of the equations (4.12) to (4.22) are

(i) we have an expression for the value of A^* for all times after the T-jump and not just at the time of the T-jump.

(ii) we have expressions for the creep rates before and after the time of the T-jump which can be used to fit experimental data. We can thus find the values of a_T and b_T from fitting the whole creep rate-time curve after t' and not merely rely on one specific point at t=t'.

(iii) equation (4.22) for the creep rate before t' is a straight line on a log (normalised rate, $(\dot{\epsilon}_{T_o}(t)/\dot{\epsilon}_{T_o}(t'))$) against log (normalised time, (t/t')) plot with a slope equal to -1.

(iv) for the case where the b_T terms of equation (4.21) are negligible, then the equation for the creep rate after t' (equation (4.21)) is identical to the equation for the rate before t' if we simply replace t by $a_T t^*$.

4.2.3 The log rate-log time curve

As a preliminary look at the equations (4.12), (4.18), (4.21) and (4.22) it will be interesting to see what shape of curve is predicted for the log creep rate-log time curve with b_T=unity. In figure 4-3, using equations (4.12) and (4.18) we see the change in shape of the log (normalised rate, $(\dot{\epsilon}(t)/\dot{\epsilon}_{T_o}(t'))$) against log (normalised time, (t/t'))★ curve both before and after t' as t' moves within the distribution (i.e. as t'/a increases) for a +ve T-jump with $\Delta T = 4\,^{\circ}C$. The important thing to note is that in the

---

★ It is convenient to use these normalised functions since both $(\dot{\epsilon}_{T_o}(t)/\dot{\epsilon}_{T_o}(t'))$ and t/t' are unity at t=t'. They will be used throughout the modelling.

range $10^2 < \frac{t'}{a} < 10^{18}$ the creep rate curve is independent of t'/a. This is a result of D_1 in equation (4.13) being unity in this range. It should also be noticed that for the same range of t'/a, the curve before t' is a straight line since D_3 in equation (4.19) is unity. A similar effect is seen for the -ve temperature jumps with $\Delta T = -4^{\circ}C$ in figure 4-4. As expected the creep rates from equations (4.21) and (4.22) coincide with those from equations (4.12) and (4.18) in the region where criteria (4.20) are obeyed in figures 4-3 and 4-4.

We can now use equations (4.21) and (4.22) to determine the change in the creep rate for various values of ΔT and ΔH_a, again with $b_T = 1$. Figure 4-5 shows the creep rate before and after a temperature change from these equations for several typical values of ΔT and with $\Delta H_a = 30$ kcal/mol. The rates before t' fall on a straight line of slope -1 and after t' approach the straight line that would have resulted if no temperature change had occurred. It can also be seen that slight curvature is introduced into the rate curve after t'. Figure 4-6 shows the theoretical curves of log creep rate against log time for one value of ΔT but different values for ΔH_a. The distinction between the curves for determining ΔH_a by extrapolation is clear for times $(t/t') < 5$, but the lines merge for longer times. Hence it is clear that for a good determination of the activation energy by the extrapolation technique, it is necessary to have good data in the time region for $t/t' < 5$. Reliance can not be placed on the long time data alone. It is important to note at this stage that the form of the creep rate against time curves of figures 4-5 and 4-6 is similar to that found experimentally in the T-jump experiments on tendon.

4.2.4 The Effect of A^* on the determination of ΔH_a

Let us now consider the terms A of equations (4.7) and (4.17)

and A^* of equations (4.14) and (4.21). If we again assume the distribution in τ ranges over 20 decades, we can plot the variation of A with the position of t' within the distribution from equation (4.17). This is shown in figure 4-7 where log A is plotted against log(t'/a) from which it can be seen that when log (t'/a) = 2, (i.e. t' is 2 decades into the distribution), then A has already reached the value of 100, a value which can have a significant effect on the value of r obtained from equation (4.6).

More insight into the problem can be gained if we look at A^* of equation (4.14) and how it varies with time after the T-jump. The values of A^* for various values of t'/a were computed at times after the T-jump, the result of which is shown in figure 4-8. Here log A^* is plotted against (t/t') for values of a_T=0.518 and 1.965. Using the Arrhenius equation (3.4), for the variation of a_T with temperature, this corresponds to an activation energy, ΔH_a, of 30 kcal/mol and a ΔT of $\pm$ 4 °C. Other combinations of ΔH_a and ΔT which give the same value of a_T will also show the same time dependence of A^* as that shown in figure 4-8. This figure illustrates that as t'/a becomes greater than 10^2 then the curve for A^* is independent of the value of (t'/a) except at times very close to t/t' = 1 (i.e. t/t' < 1.005) where a singularity occurs. It can also be seen from figure 4-8 that the massive increase in A^* as t/t' approaches unity will not be observed experimentally as was previously thought. We will actually observe what would be the extrapolation of the value of A^* from a value of t/t' > 1.0 back to t/t' = 1.0.

This can more easily be seen when we plot the values for A^* on a time scale more appropriate to the experimental time scale. For all the subsequent modelling, we will take criteria (4.20) to hold (i.e. t' is more than two decades into the distribution) and we can again use equations (4.21) and (4.22). Figure 4-9 shows the variation of A^* over one decade of values of t/t' after the temperature change for various values of a_T. (This would

correspond to a plot of log A^* against log time for a T-jump at t'=100s and the abscissa would range from t=100s to 1000s). It is clear from this curve that for a_T=1.25 (say) that, by extrapolating from a time t/t'=1.5 to t/t'=1, (dashed line), the value of A^* at t=t' will be of the order of 10 and not equal to A given by equation (4.7). Hence the value of A to be used in the T-jump equation as proposed by McCrum and Morris[1] (equation(4.6)) is for experimental purposes the value found from the extrapolation of the log A^* -log (t/t') curve back to t=t', and not that found from the evaluation of A from equation (4.7). Hence we replace A in equation (4.6) by the extrapolated value of A^* at t=t' denoted from now on by A'. From a plot of log A^* against log (t/t') for various values of a_T we can obtain the value of A' to be used in the McCrum and Morris equation (4.6) for any value of a_T.

The values of A' found from extrapolating the curves of figure 4-9 back to t=t' from t/t' =1.5 are plotted against a_T in figure 4-10 (line 3) and the resulting straight line shows that as a_T increases, so does A'. This means that any effect due to A' in equation (4.6) will be greater for -ve temperature changes (for a given ΔH_a) which will bring about curvature of the ln r - ΔT plot as described by McCrum and Pearce[3], but this curvature will arise from the temperature dependence of b_T and of A'. This curvature on the ln r- ΔT plot is shown in figure 4-11, (line 3) using values of A' found from line 3 of figure 4-10, with ΔH_a=30 kcal/mol and various ΔT, for values of b_T given by the equation[3]

$$b_T = 1.0 + \lambda \Delta T \qquad (4.23)$$

λ was taken to be 0.005. Also shown in figure 4-11 is the straight line for λ=0.0 and ΔH_a=30 kcal/mol. If a straight line was drawn through the points of line 3 for $\Delta T > 0$, this would give a value of ΔH_a ~2-3 kcal/mol greater than the true value of 30 kcal/mol. A larger error (~8 kcal/mol)

will be obtained for $\Delta T < 0$. The error decreases as λ decreases and if the first experimental creep rate point after the T-jump is taken at $\sim t/t' = 1.5$ and if λ is ~ 0.002 (which is the case for PMMA for example [6]) then the experimental value of ΔH_a will be quite close (< 2 kcal/mol) to the true value of ΔH_a for both +ve and -ve ΔT.

The effect of A is thus much less than was at first thought. However, if we extrapolate back to t' from data obtained in the region $t/t' < 1.5$, the errors increase. For example, if the first creep rate data point was at $t/t' = 1.25$, we would obtain line 2 in figure 4-10 which in turn gives line 2 of figure 4-11 (again with $\lambda = 0.005$). Similarly for extrapolation from $t/t' = 1.1$ we obtain line 1 of figures 4-10 and 4-11. With these last two lines (1 and 2) the error in ΔH_a obtained for +ve ΔT T-jumps is 10 and 20 kcal/mol respectively.

In summary, we have seen that the effect of A in the McCrum and Morris equation (4.6) can be small if

(i) the increase in b_T per °C (i.e. λ) is less than 0.005, and

(ii) the creep rate points in the region $t/t' < 1.5$ are ignored and extrapolation back to $t/t' = 1$ is obtained by using the points for $t/t' > 1.5$.

These criteria are often obeyed in many T-jump experiments. The above criteria arise because, for experimental purposes, we need to consider the value of A^* as $t \to t'$ (i.e. A') given by equation (4.21) rather than the value of A in equation (4.6). If the value of λ is much less than that given in criteria (i) above, then the creep rate data at times $t/t' < 1.5$ can be used and vice versa.

4.2.5 The Effect of A^* on the Log Creep Rate-Log Time Curve

It would appear from figure 4-9 that the effect of A^* on the observed creep rate dies out at sufficiently long times. But what is important to the creep rate is the magnitude of the product $\frac{1}{a_T}(b_T-1)A^*$ compared to the creep rate which would be observed if $b_T=1.0$. The creep rate after t' can be written in the form (using equations(4.23) and (4.21)).

$$\frac{\dot{\epsilon}_T(t)}{\dot{\epsilon}_{T_o}(t')} = \frac{1}{a_T}\left[\frac{1}{(t^*/t')} + \frac{\lambda\Delta T}{(\frac{t^*}{t'}-1)}\right] \qquad (4.24)$$

and so the addition to the creep rate due to b_T divided by the creep rate which would occur if $b_T=1$ is

$$\frac{\text{Addition to creep rate}}{\text{Creep rate}} = (b_T-1)A^*(\frac{t^*}{t'}) = \lambda\Delta T\,\frac{(t^*/t')}{(\frac{t^*}{t'}-1)} \qquad (4.25)$$

Hence the function $(\frac{t^*}{t'})/(\frac{t^*}{t'}-1)$ will give the fractional addition to the creep rate for unit $\lambda\Delta T$. From figure 4-12, where the function $(\frac{t^*}{t'})/(\frac{t^*}{t'}-1)$ is plotted against (t/t'), it is seen that this function approaches unity for times $t/t' > 10$. This means that the effect of a non-unity b_T is to provide a vertical shift of the creep rate on a log rate-log time plot, the shift decreasing to a constant value of magnitude $\lambda\Delta T$ for values of $t/t' > 10$.

This shift of the creep rate curves is shown in figure 4-13 using equations (4.22) and (4.24). In this figure the log of the normalised creep rate before and after t' is plotted against log(t/t') for a value of ΔH_a =30 kcal/mol (the same as in figures 4-3 to 4-6) for temperature changes of $\Delta T = \pm 4^\circ C$, and for values of b_T which could typically be found in polymeric materials. Note that b_T is obtained from equation (4.23) with ΔT a constant at either $+4^\circ C$ or $-4^\circ C$ and λ taking values of 0.005, 0.02 and 0.05. These values of λ could arise in different materials or from the same material when λ varies with T_o. Figure 4-13 illustrates the addition

to the creep rate due to the $(b_T-1)A^*$ term in equation (4.24) which adds more curvature at times close to $t/t'=1$. This is equivalent to the factor $(\frac{t}{t'}^*)/(\frac{t}{t'}^*-1)$ (see figure 4-12) being much greater than unity. For the +ve ΔT T-jumps, the curvature bends the curves upwards, this increasing as λ increases. For the -ve ΔT T-jumps, the curves are bent downwards. The curves of figure 4-13 become parallel for larger values of t/t' illustrating the constant vertical shift arising from b_T for these longer times.

4.2.6 The Wedge Distribution for the Spectrum of Retardation Times.

We can now introduce a more general form of the spectrum of retardation times. If we assume the distribution takes the form

$$\ln L(\ln \tau) = \ln C + m \ln \tau \qquad (4.26)$$

i.e a straight line on a $\ln L(\ln \tau)$ against $\ln \tau$ plot of slope m, between $\ln \tau = \ln a$ and $\ln b$, and zero elsewhere, we can obtain for the creep rate in equation (4.1)

$$\frac{\dot{\epsilon}_{T_o}(t)}{\sigma_o} = \int_a^b \frac{C \tau^m}{\tau^2} \exp\left(-\frac{t}{\tau}\right) d\tau \qquad (4.27)$$

This integral is unfortunately only solved by use of numerical analysis techniques. If, however, we assume the limits of the integration of τ to be from 0 to ∞, then we can solve the equation to give

$$\frac{\dot{\epsilon}_{T_o}(t)}{\sigma_o} = C\, t^{-n}\, \Gamma(n) \qquad (4.28)$$

where $n=1-m$ and Γ is the Gamma function. Hence

$$\frac{\dot{\epsilon}_{T_o}(t)}{\dot{\epsilon}_{T_o}(t')} = \left(\frac{t}{t'}\right)^{-n} \qquad (4.29)$$

This means that if we can assume that the time scale of the experiment is such that the material 'sees' the distribution as stretching from 0 to ∞ , then a straight line will result on the log rate-log time curve of slope -n. When is this a valid approximation? For the case of the box distribution it was seen that once the time of the experiment is 2 decades into the distribution, then the effect of the position in the distribution no longer affects the result. There is no reason to suppose that there will be any difference from that case to the present one. So if we assume that we are more than 2 decades into the distribution, then equations(4.28) and (4.29) will hold. Equation (4.29) reduces to equation (4.18) for the case n=1 and D_3=1.

We can perform a similar analysis for the time after the T-jump. In this case, substituting the form of the distribution of equation (4.26) into equation (4.2) gives

$$\frac{\dot{\epsilon}_T(t)}{\sigma_o} = \int_a^b \frac{C\tau^m}{a_T \tau^2} \exp(-\frac{t^*}{\tau})\, d\tau + \int_a^b \frac{C\tau^m}{a_T \tau^2} (b_T - 1) \exp -(\frac{t^* - t'}{\tau})\, d\tau \qquad (4.30)$$

To integrate this other than by numerical techniques we again have to assume the limits of the integration to run from 0 to ∞ and we obtain

$$\frac{\dot{\epsilon}_T(t)}{\dot{\epsilon}_{T_o}(t')} = \frac{1}{a_T}\left[\frac{1}{(t^*/t')^n} + \frac{(b_T - 1)}{(\frac{t^*}{t'} - 1)^n}\right] \qquad (4.31)$$

Equations (4.29) and (4.31) compare with equations (4.21) and (4.22) for the box distribution when n=1 and when criteria (4.20) hold. Thus equations (4.29) and (4.31) represent the solution to the creep rate dependence on time for a more realistic distribution of retardation times. In figure 4-14 we have plotted the log normalised creep rate (i.e log ($\dot{\epsilon}(t)/\dot{\epsilon}_{T_o}(t')$)) against log normalised time (i.e. log(t/t')) from equations (4.29) and (4.31) for various values of n with b_T =1, ΔH_a=30 kcal/mol and $\Delta T = \pm 4^{\circ}C$. The

following can be seen:

(i) For the rates before t', equation (4.29) gives straight lines of slope -n.

(ii) For the rates after t', we have three situations for each pair of curves of equal +ve and -ve ΔT at a given value of n.

(a) n=1; (full lines) the curves approach each other and a slope of -1.

(b) n<1; (long dashed lines) the curves approach a line of slope -n but do not merge.

(c) n>1; (short dashed lines) the lines cross over each other and at long times approach the slope -n.

The results also have more significance than might at first be apparent. It is important to realise that in most of the experiments performed so far by various workers employing the T-jump technique on a variety of polymers[4,7,8,9], it has been observed that the creep rate before t' obeys a relation of the form shown in equation (4.29), i.e. a straight line on a plot of log rate against log time. One such plot for tendon is shown over two decades of time in figure 4-15. Similar straight lines have been observed by Caruthers et al[4,9] for carbon black filled elastomers, by Hutchinson[7] for polypropylene and by Pearce[8] for linear polyethylene. It will be seen in chapter 8 (see figures 8-9 to 8-15) that the creep rates obtained from T-jumps on tendon can be fitted with equations (4.29) and (4.31) and show exactly the behaviour shown in figure 4-14. It is interesting to note from equation (4.31) that if log ($\dot{\epsilon}_T(t)/\dot{\epsilon}_{T_o}(t')$), (i.e. log normalised creep rate after t') is plotted against log (t^*/t') then a straight line will result of slope -n, which is equal to that before t', and differs from the line before t' only by a vertical shift of magnitude log a_T.

4.2.7 The Determination of ΔH_a when A^* is Significant

We found earlier that A^* does not assume such a large value as was previously thought. Under certain circumstances, however, it does have a significant effect and,in this case, two methods suggest themselves for solution of the problem. The first is on similar lines to that used by McCrum and Pearce[3] and is to extrapolate the experimental log rate-log time curves to obtain $\dot{\epsilon}_T(t')$ and $\dot{\epsilon}_{T_o}(t')$ and plot their ratio ln r (as defined before) against $\Delta T/RTT_o$ for a given stress level and fit the resulting curve for the parameters ΔH_a and λ . This now has to be done in the following manner since we have found that the value of A' depends on a_T (and thus on ΔH_a and ΔT) and the slope (-n) of the log rate-log time curve.

From the first determined experimental creep rate point which is available after t' on the log rate-log time curve, we can determine which line on figure 4-10 (or the equivalent one for $n \neq 1$) should be used to determine A' as a_T varies. Hence, for the first point on the ln r- ΔT curve, ($\ln r_1$, ΔT_1), say, and for a trial value of ΔH_a we can determine a_T from equation(3.4) and thus A' from figure 4-10. Along with a trial value of λ these values can be used in equation(4.6) (with A' replacing A) to give a value of ln r to compared with that found experimentally ($\ln r_1$). Similarly for all the other points on the ln r- ΔT plot and in this way, the best fit for ΔH_a and λ can be found. The major source of error from this method lies in the choosing of t/t' at which A' is determined. McCrum and Pearce[3] assumed that A' would be the same for all points on the ln r- ΔT curve and found values of ΔH_a = 30 kcal/mol and $\lambda A'$=0.168 on fitting their ln r- ΔT curve. For an average of A' =10 over the range involved, this would give λ=0.015, a figure quite within the range for polymeric materials.

The second method to obtain the activation energy (or a_T) and b_T from the experimental data is to fit each experimental log creep rate against log time curvefor these two parameters,at a given stress level, with equations (4.29) and (4.31). This will only be valid for a linear viscoelastic material and for the cases where the log creep rate-log time curve before t' is linear, which as stated before has been shown to be true for several polymeric materials. The values of a_T found from the best fit of each log rate-log time curve can be plotted against $\Delta T/RTT_o$, the slope of which will be ΔH_a. Similarly, by plotting the best fit values of b_T against ΔT will give λ . This will be the more preferable technique when the data allows, since we are not now relying on one extrapolated point at t=t', but on the data during the entire experiment.

4.3 Stress Relaxation T-jump

The equivalent expressions for an instantaneous temperature jump in stress relaxation are as follows. Before t', at temperature T_o, the stress relaxation rate, $\dot{\sigma}_{T_o}(t)$, is

$$\frac{\dot{\sigma}_{T_o}(t)}{\epsilon_o} = -\int_{-\infty}^{\infty} \frac{H(\ln \tau)}{\tau} \exp\left(-\frac{t}{\tau}\right) \, d \ln \tau \qquad (4.32)$$

where $H(\ln \tau)$ is the spectrum of relaxation times, and ϵ_o the strain. After the temperature jump at temperature T, the rate is

$$\frac{\dot{\sigma}_T(t)}{\epsilon_o} = -\int_{-\infty}^{\infty} \frac{H(\ln \tau)}{a_T \tau} \exp\left(-\frac{t^*}{\tau}\right) d \ln \tau \; - \int_{-\infty}^{\infty} \frac{H(\ln \tau)}{a_T \tau} (b_T^{SR} - 1) \exp-\left(\frac{t^* - t'}{\tau}\right) d \ln \tau \qquad (4.33)$$

where b_T^{SR} is defined as $\dfrac{\left(E_U - E_R\right)_T}{\left(E_U - E_R\right)_{T_o}}$. E_R and E_U are the relaxed and unrelaxed moduli. b_T^{SR} can be seen to be related to the parameters b_T, c_T

and d_T in creep by

$$b_T^{SR} = b_T / c_T\, d_T \tag{4.34}$$

where c_T and d_T are as defined in equation (1.13). These equations reduce at t=t' to

$$\frac{\dot{\sigma}_T(t')}{\dot{\sigma}_{T_o}(t')} = \frac{1}{a_T}\left[\, 1 + (b_T^{SR} - 1)\, A_{SR} \,\right] \tag{4.35}$$

where

$$A_{SR} = \int_{-\infty}^{\infty} \frac{H(\ln \tau)}{\tau}\, d \ln \tau \;\Big/ \int_{-\infty}^{\infty} \frac{H(\ln \tau)}{\tau} \exp\left(-\frac{t'}{\tau}\right) d \ln \tau \tag{4.36}$$

This is the same equation as for creep except $H(\ln \tau)$ replaces $L(\ln \tau)$ and b_T^{SR} replaces b_T in creep. Introducing a box distribution as in creep we obtain the analogous equations to equations (4.21) and (4.22) with σ replacing ϵ and b_T^{SR} replacing b_T. The major difference lies in the b_T term. For creep

$$b_T = 1 + \lambda \Delta T \tag{4.23}$$

and for stress relaxation

$$b_T^{SR} = 1 - \lambda^{SR} \Delta T \tag{4.37}$$

where λ^{SR} is a +ve quantity.

Hence for stress relaxation

$$\frac{\dot{\sigma}_T(t)}{\dot{\sigma}_{T_o}(t')} = \frac{1}{a_T}\left[\, \frac{1}{(t^*/t')} + (b_T^{SR} - 1)\, A^* \,\right] \tag{4.38}$$

where, as for creep

$$A^* = \frac{1}{\left(\frac{t^*}{t'} - 1\right)} \tag{4.21}$$

Using equation (4.37), equation (4.38) becomes

$$\frac{\dot{\sigma}_T(t)}{\dot{\sigma}_{T_o}(t')} = \frac{1}{a_T}\left[\frac{1}{(t^*/t')} - \frac{\lambda^{SR}\,\Delta T}{\left(\frac{t^*}{t'} - 1\right)}\right] \qquad (4.39)$$

When $\lambda^{SR}=0$, (or $b_T^{SR}=1.0$) the curves for stress relaxation and creep will be identical at any given ΔT and ΔH_a and the log relaxation rate-log time curves will be as in figures 4-5 and 4-6 (i.e. the same curves as for creep). When $b_T \neq 1$, however, the effect on the relaxation rate-time curve will be as shown in figure 4-16 where it can be seen that, for increasing λ, the -ve T-jump curves (figure 4-16(a)) are shifted vertically upwards whereas the +ve T-jump curves (figure 4-16(b)) are shifted downwards. As $t/t' \to 1$, the down jump curves (figure 4-16(a)) bend upwards for $\lambda > 0.005$, (in creep they bend downwards) and vice versa for the up jumps. It can be seen that a pair of curves for equal +ve and -ve ΔT will cross if there is a significant b_T term, something which did not happen in creep. Hence the stress relaxation experiment could show the presence of a non-unity b_T term better than creep.

For the case of the more general distribution of the form

$$\ln H(\ln \tau) = \ln C_{SR} + m_{SR} \ln \tau \qquad (4.40)$$

we obtain expressions for the stress relaxation rate similar to equations (4.29) and (4.31), namely

$$\frac{\dot{\sigma}_{T_o}(t)}{\dot{\sigma}_{T_o}(t')} = \left(\frac{t}{t'}\right)^{-n} \qquad (4.41)$$

and

$$\frac{\dot{\sigma}_T(t)}{\dot{\sigma}_{T_o}(t')} = \frac{1}{a_T}\left[\frac{1}{(t^*/t')^n} + \frac{(b_T^{SR} - 1)}{\left(\frac{t^*}{t'} - 1\right)^n}\right] \qquad (4.42)$$

where $n=(1-m_{SR})$

Equation (4.41) again shows a straight line on a log rate-log time plot before t' and equation (4.42) can be used to fit the experimental data after t'. Extrapolation of the data to t' can be done in the same way as for creep and the resulting values of $(\ln r)^{\star}$ and ΔT fitted for λ_{SR} and ΔH_a. The shape of the ln r- ΔT curve when A' is significant will be different from creep and of the form shown in figure 4-17. The solid lines show the curves which result from various values of λ and taking A' (again as defined for creep) as found from line 3 of figure 4-10 for each ΔT and with ΔH_a=30 kcal/mol. Thus A' is varying along the curve as ΔT varies. The dotted lines result from taking the same values for λ but keeping A' constant at a value of 10. There is thus a marked difference between the two cases. Hence stress relaxation tests could well indicate whether the procedure of introducing the variation of A' is the valid method to adopt.

4.4 Recovery T-jump

The equations for the recovery T-jump have been presented by Hutchinson et al[5] who calculated the ratio of the rates at the time of the T-jump. We will present the equations for the rate at any time before and after t' and determine the shape of the residual rate against time curve in a similar manner as for creep. We will use the notation of Hutchinson et al.[5]

In the recovery T-jump, the load is applied at temperature T_o

---

$\star$ The parameter r will be used to define the ratio of the rates at the time of the T-jump in all three types of T-jump experiment, namely creep, stress relaxation and recovery. It will always be clear to which experiment the parameter r applies.

for a time t_o and removed. After a further time, t', the temperature is suddenly changed to T. The linear viscoelastic equations developed assume that a positive stress, σ_o, applied at t=0 followed by an equal negative stress, $-\sigma_o$, applied at time $t=t_o$ will give the creep-recovery behaviour. In this way, the observed (residual) rate after the removal of the load will be, before t'

$$\frac{\dot{\epsilon}_{T_o}(t)}{\sigma_o} = \int_{-\infty}^{\infty} \frac{L(\ln \tau)}{\tau} \exp\left(-\frac{t}{\tau}\right)\left(1 - \exp\left(\frac{t_o}{\tau}\right)\right) \, d \ln \tau \qquad (4.43)$$

and after t'

$$\frac{\dot{\epsilon}_{T}(t)}{\sigma_o} = \int_{-\infty}^{\infty} \frac{L(\ln \tau)}{a_T \tau} \exp\left(-\frac{1}{\tau}\left(t' + \frac{(t-(t_o+t'))}{a_T}\right)\right)\left(1 - \exp\left(\frac{t_o}{\tau}\right)\right) d \ln \tau \qquad (4.44)$$

The terms containing b_T disappear for all time after the T-jump and not only at the time of the T-jump. From equations (4.43) and (4.44) and using a box distribution as before, we obtain the residual rates before and after the time of the temperature jump as

$$\frac{\dot{\epsilon}_{T_o}(t)}{\dot{\epsilon}_{T_o}(t_o+t')} = \frac{\left(\frac{t}{t'} - \frac{t_o}{t'}\right)^{-1} - \left(\frac{t}{t'}\right)^{-1}}{1 - \left(\frac{t_o}{t'} + 1\right)^{-1}} \qquad (4.45)$$

and

$$\frac{\dot{\epsilon}_{T}(t)}{\dot{\epsilon}_{T_o}(t_o+t')} = \frac{1}{a_T}\left(\frac{t_o}{t'}\right)^{-1}\left[\left\{\left(\frac{t_o}{t'} + 1\right)^{-1} + \left(\frac{\frac{t}{t'}\left(\frac{t_o}{t'} + 1\right)^{-1} - 1}{a_T}\right)\right\}^{-1} - \left\{1 + \left(\frac{\frac{t}{t'}\left(\frac{t_o}{t'} + 1\right)^{-1} - 1}{a_T}\right)\right\}^{-1}\right] \qquad (4.46)$$

Equations (4.45) and (4.46) are plotted against $(t-t_o)/t'$ (i.e. normalised time after removal of the load) in figure 4-18 for various values of t_o/t' and ΔH_a = 30 kcal/mol, $\Delta T = \pm 4^{\circ}C$. It can be seen that for $t_o/t' < 0.1$, there is little change in the rate curves. The rates after t' are curved as for the creep T-jumps.

When $t=t_o+t'$, i.e. at the time of the T-jump, and using the Arrhenius equation (3.4), equation (4.46) reduces to that of Hutchinson et al[5]

$$\frac{\dot{\epsilon}_T(t_o+t')}{\dot{\epsilon}_{T_o}(t_o+t')} = \frac{1}{a_T} = \exp \Delta H_a \left(\frac{\Delta T}{RTT_o} \right) \qquad (4.47)$$

The recovery T-jump can thus be used to determine the apparent activation energy ΔH_a from the rates at the time of the temperature jump without any effects from b_T. In this case, a plot of $\ln r = \ln(\dot{\epsilon}_T(t_o+t')/\dot{\epsilon}_{T_o}(t_o+t'))$ against $\Delta T/RTT_o$ will have the slope ΔH_a. The recovery T-jump is thus an important experiment for determining whether there is any effect of b_T on the creep T-jump data.

4.5 Summary

The T-jump equations for creep, stress relaxation and creep-recovery have been presented. The equations describe the rate at any time, t, before and after the time of the temperature change, and were solved using realistic forms for the retardation spectrum,(namely a box and wedge distribution). This enabled us to determine the form of the creep (or stress relaxation) rate dependence on time and showed that the best method to plot the data was on a log rate- log time graph. The theoretical equations for the rate dependence on time will be seen to fit the experimental data for tendon in chapters 8 and 9. The box distribution was used to find the effect of b_T on the creep rate at times after the T-jump and on the determination of ΔH_a in experimental circumstances. The effect was not as great as had been previously thought[3] and a method by which the problem could be overcome was suggested. The difference between the log rate-log time curves for creep and stress relaxation when the b_T terms in the T-jump equations were significant suggested a method for detecting the b_T effect. The recovery T-jump equations do not contain any b_T terms.

References

1 McCrum N.G. and Morris E.L., Phil.Mag.,7,2115,1962.

2 Hutchinson J.M. and McCrum N.G., Nature, Phys.Sci.,236,115,1972.

3 McCrum N.G. and Pearce D.L., Nature Phys.Sci.,243,52,1973.

4 Caruthers J.M. and Cohen R.E., J.Polymer Sci.,14,1891,1976.

5 Hutchinson J.M., McCrum N.G. and Pearce D.L., J.Polymer Sci.,Polymer Phys.,12,1255,1974.

6 McCrum N.G. and Morris E.L., Proc.Roy.Soc.,A281,258,1964.

7 Hutchinson J.M., D.Phil. Thesis, Oxford University, 1974.

8 Pearce D.L., D.Phil. Thesis, Oxford University, 1976.

9 Caruthers J.M., Ph. D. Thesis, M.I.T., 1977.

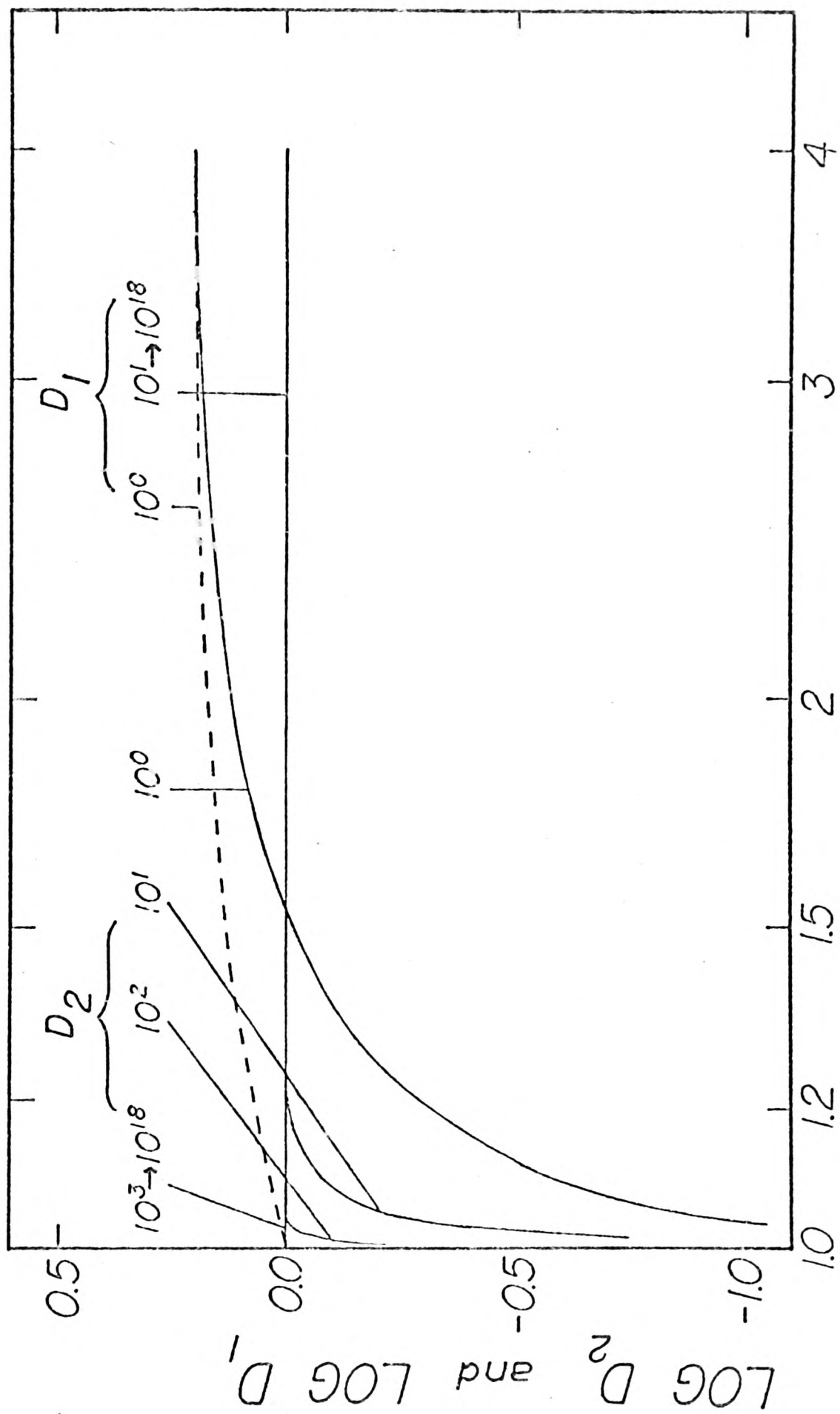


Figure 4-1

Plot of log D_1 and log D_2 against log (t/t') for various values of t'/a. (--- D_1 ; —— D_2)

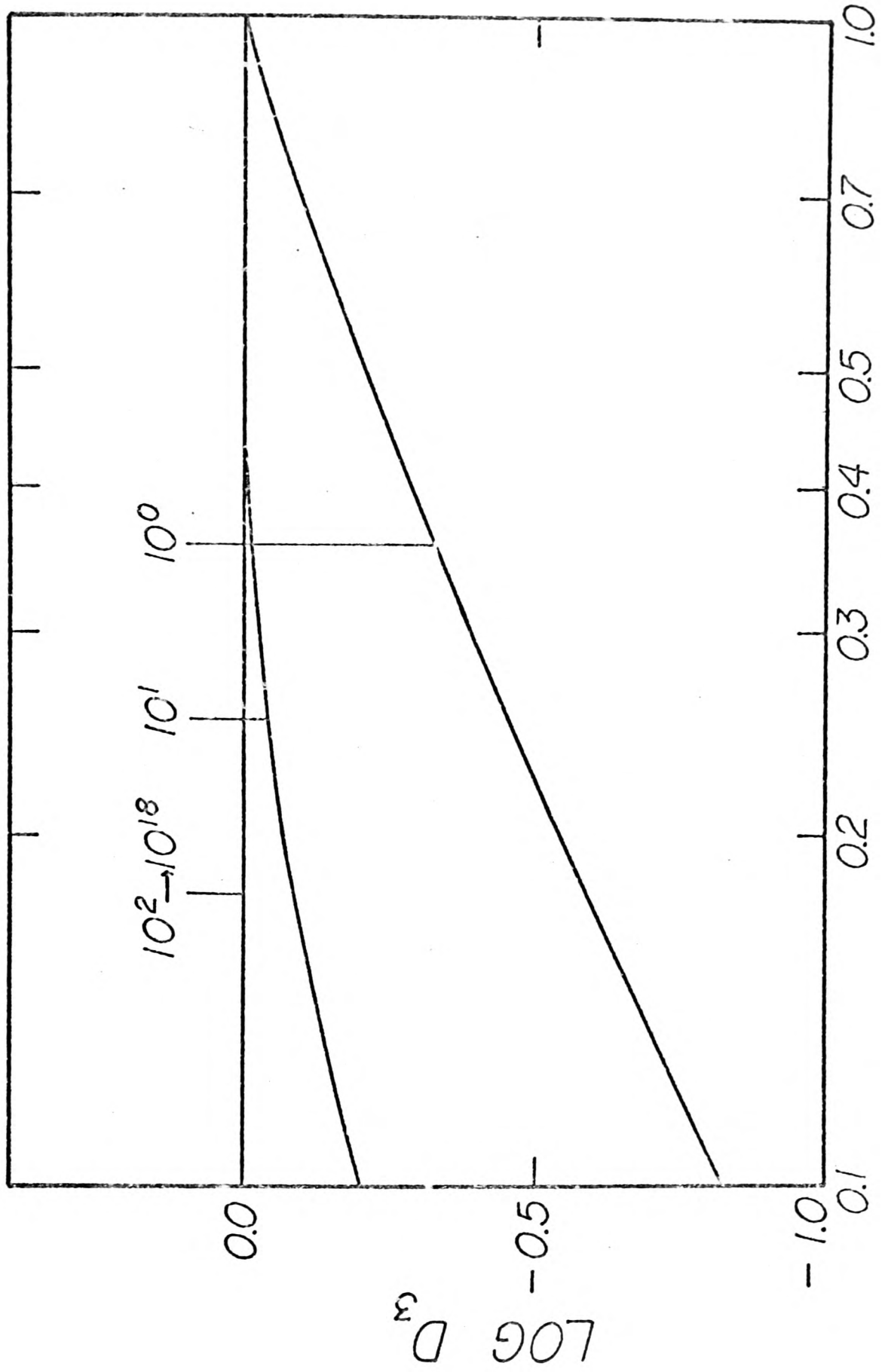


Figure 4-2

Plot of log D_3 against log (t/t') for various values of t'/a.

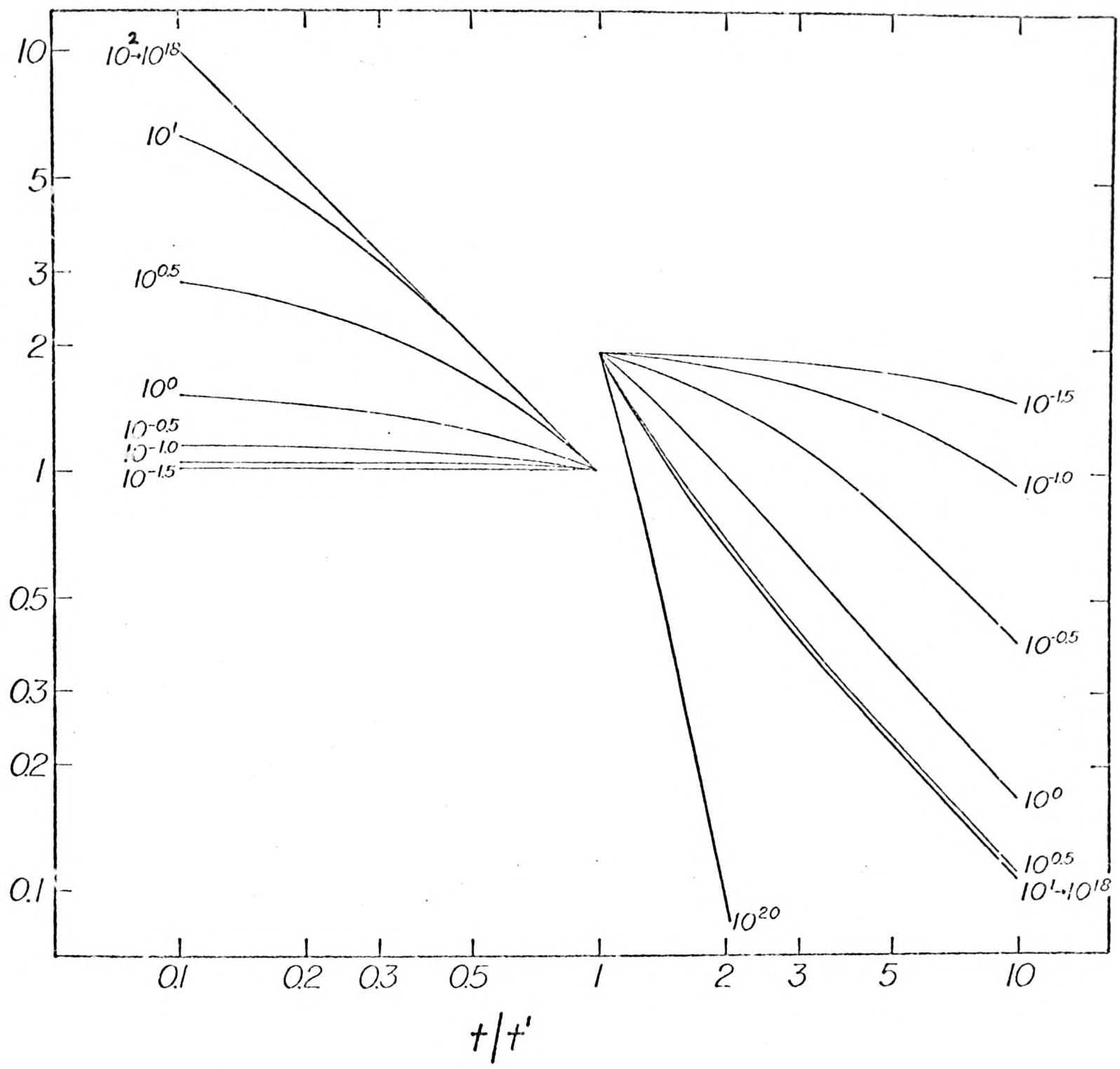


Figure 4-3

Plot of log (normalised creep rate, $\dot{\epsilon}(t)/\dot{\epsilon}_{T_o}(t')$) against log (normalised time, t/t') both before and after the T-jump for values of t'/a as shown. ΔH_a = 30 kcal/mol, ΔT = +4 °C, b_T = 1.0.

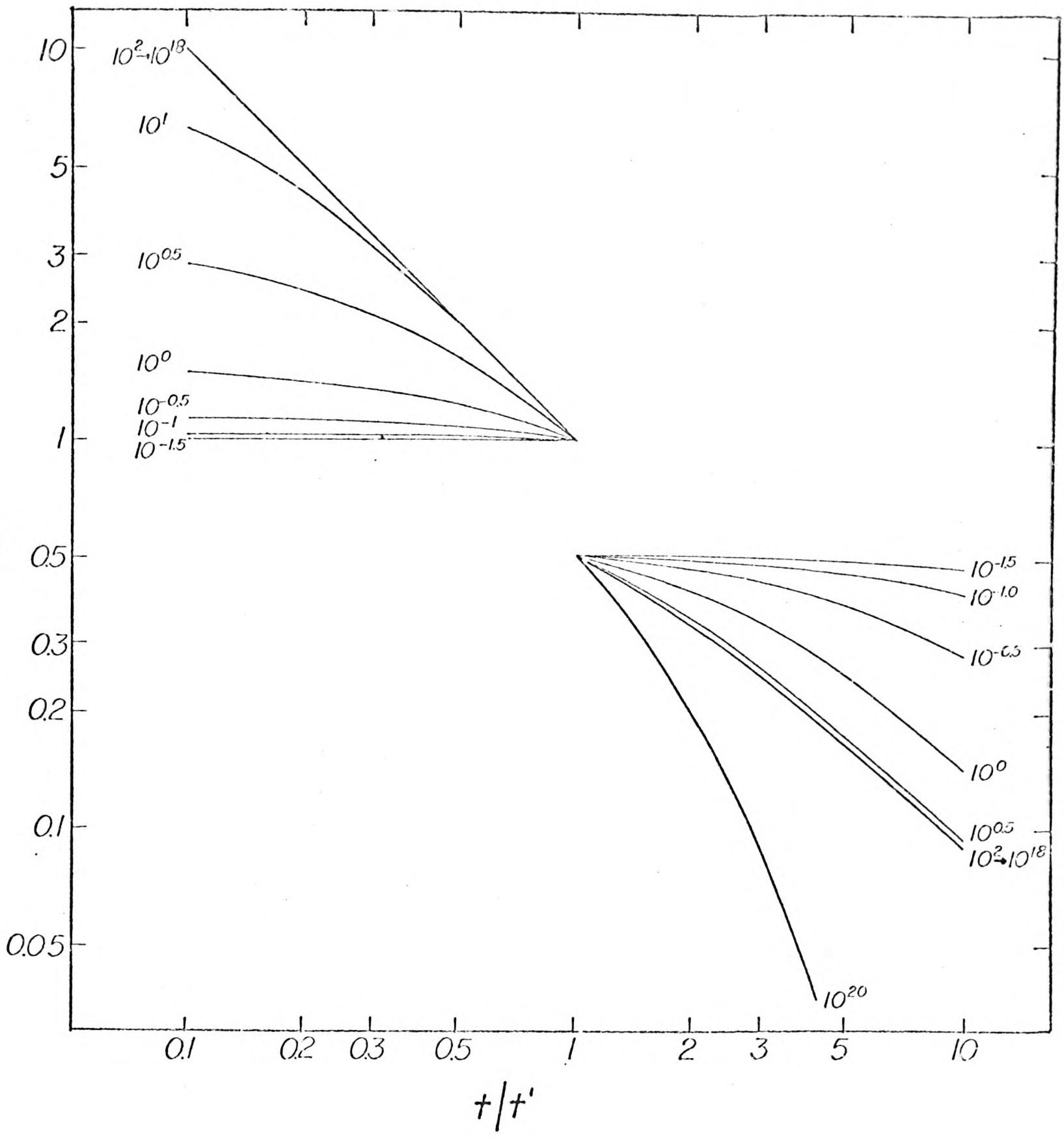


Figure 4-4

Plot of log (normalised rate, $\dot{\epsilon}(t)/\dot{\epsilon}_{T_o}(t')$) against log (normalised time, t/t') both before and after the T-jump for values of t'/a as shown. ΔH_a = 30 kcal/mol, ΔT = -4 °C, b_T = 1.0

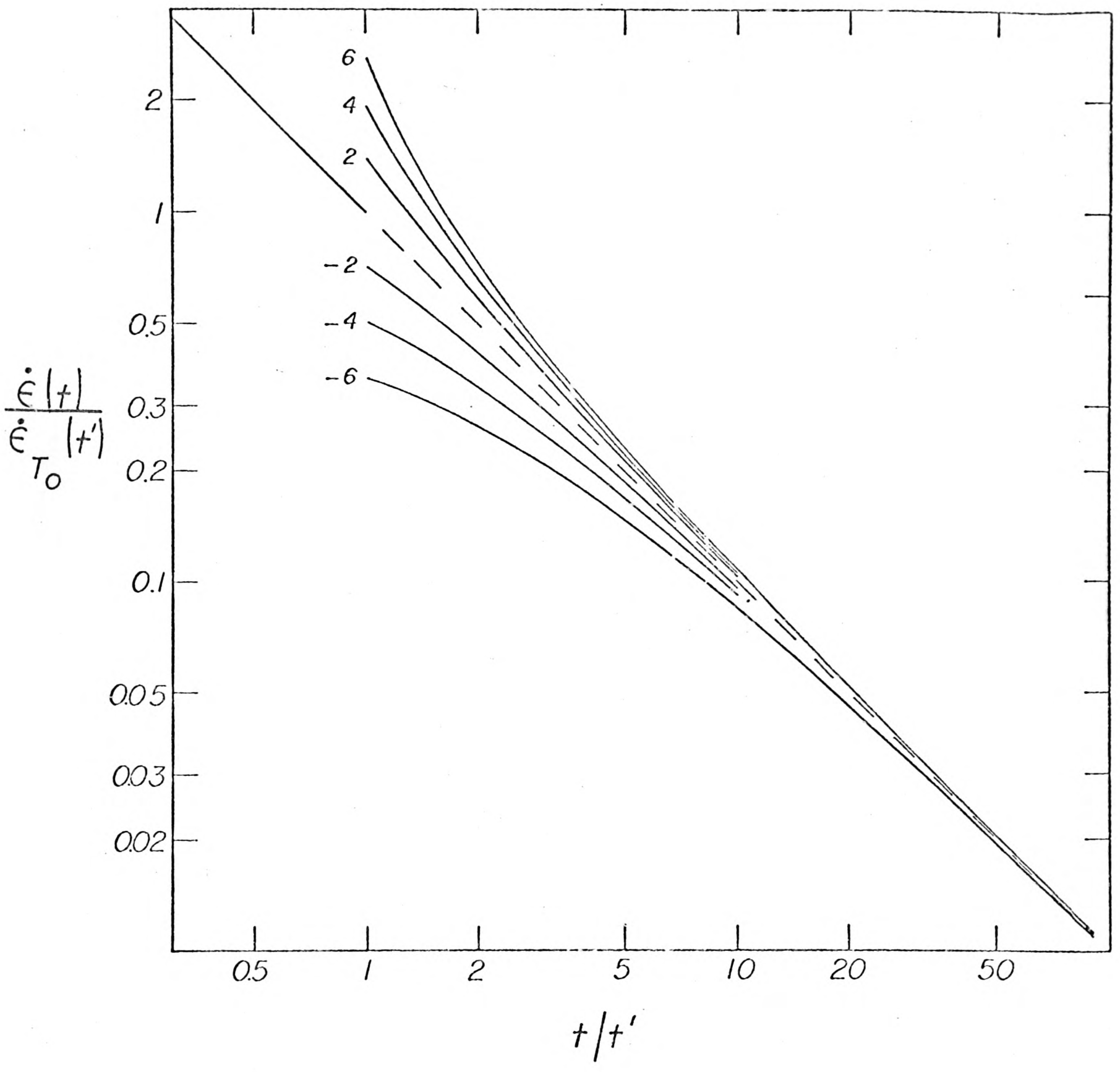


Figure 4-5

Plot of log(normalised rate, $\dot{\epsilon}(t)/\dot{\epsilon}_{T_o}(t')$,(or $\dot{\sigma}(t)/\dot{\sigma}_{T_o}(t')$))against log (normalised time, t/t'), for ΔH_a = 30 kcal/mol, and various values of ΔT (in °C) as shown. The curves correspond to values of a_T of 0.37, 0.52, 0.71, 1.405, 1.95, 2.72. b_T = 1.0.

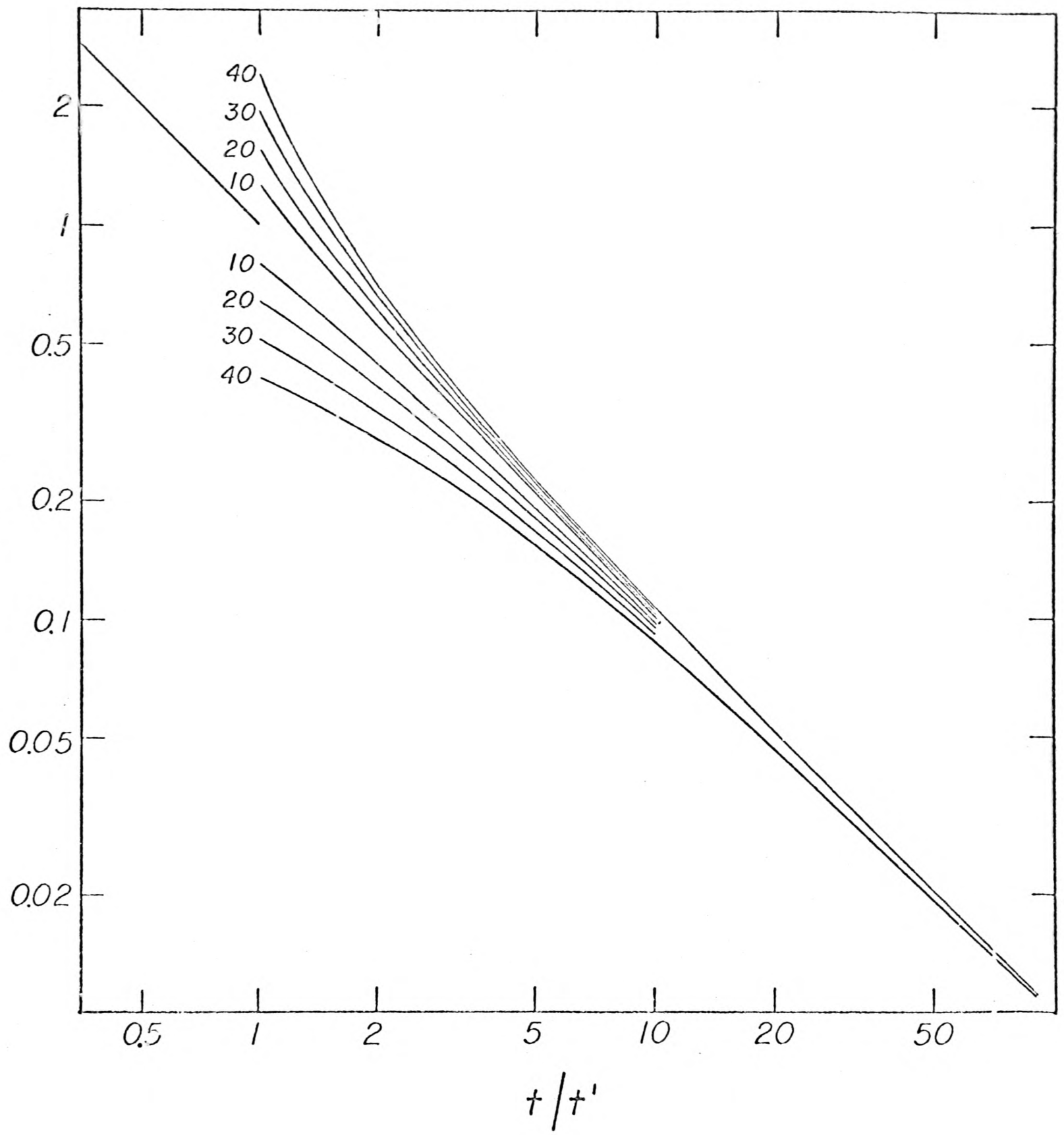


Figure 4-6

Plot of log (normalised rate, $\dot{\epsilon}(t)/\dot{\epsilon}_{T_o}(t')$, (or $\dot{\sigma}(t)/\dot{\sigma}_{T_o}(t')$)) against log (normalised time, t/t') for various values of ΔH_a and one $\Delta T = \pm 4\ ^\circ C$. The curves correspond to values of a_T = 0.41, 0.52, 0.64, 0.80, 1.25, 1.56, 1.95, 2.43. a_T = 1.0. ΔH_a= 40, 30, 20, 10 kcal/mol

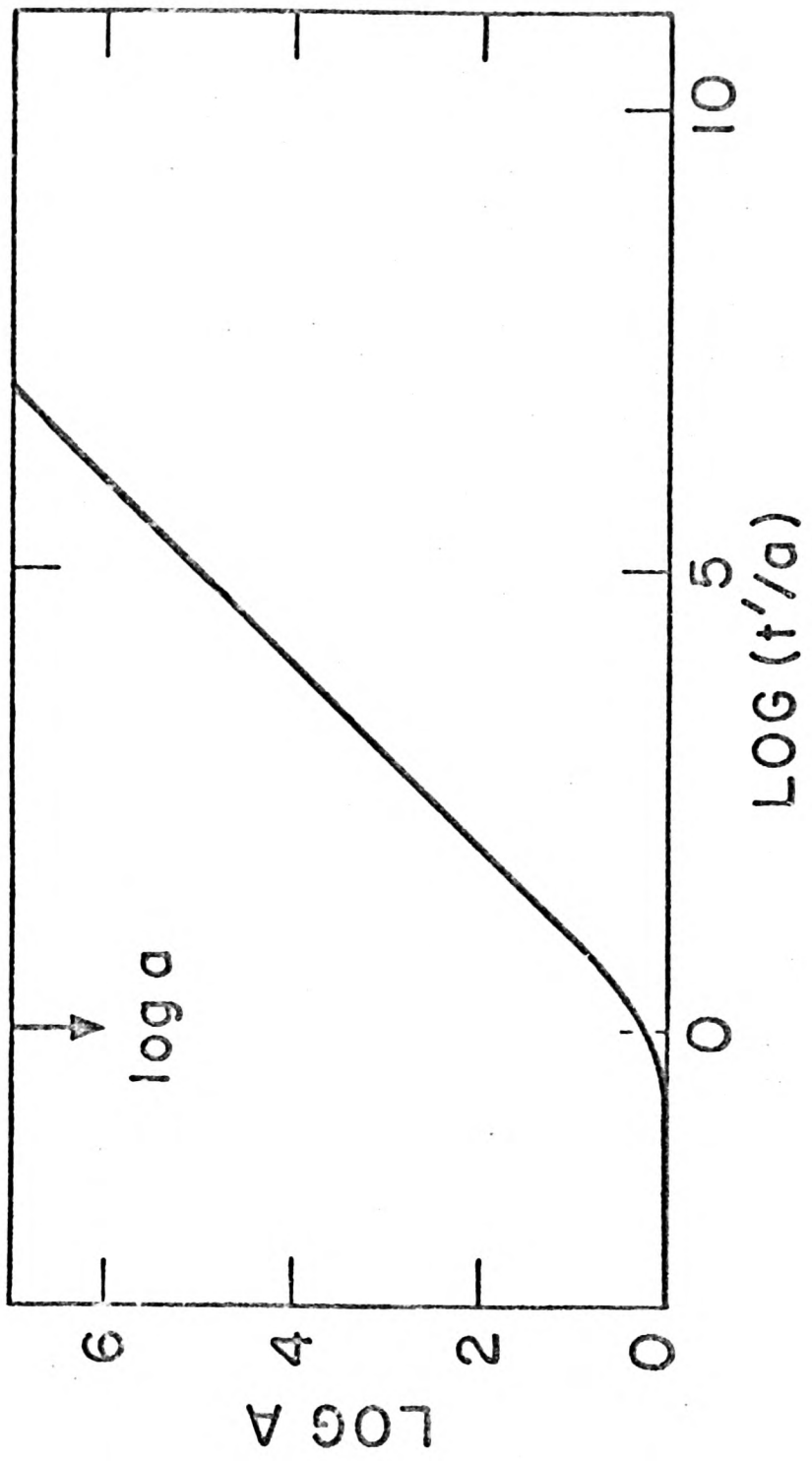


Figure 4-7

Plot of log A against log (t'/a) calculated from the box distribution of retardation times.

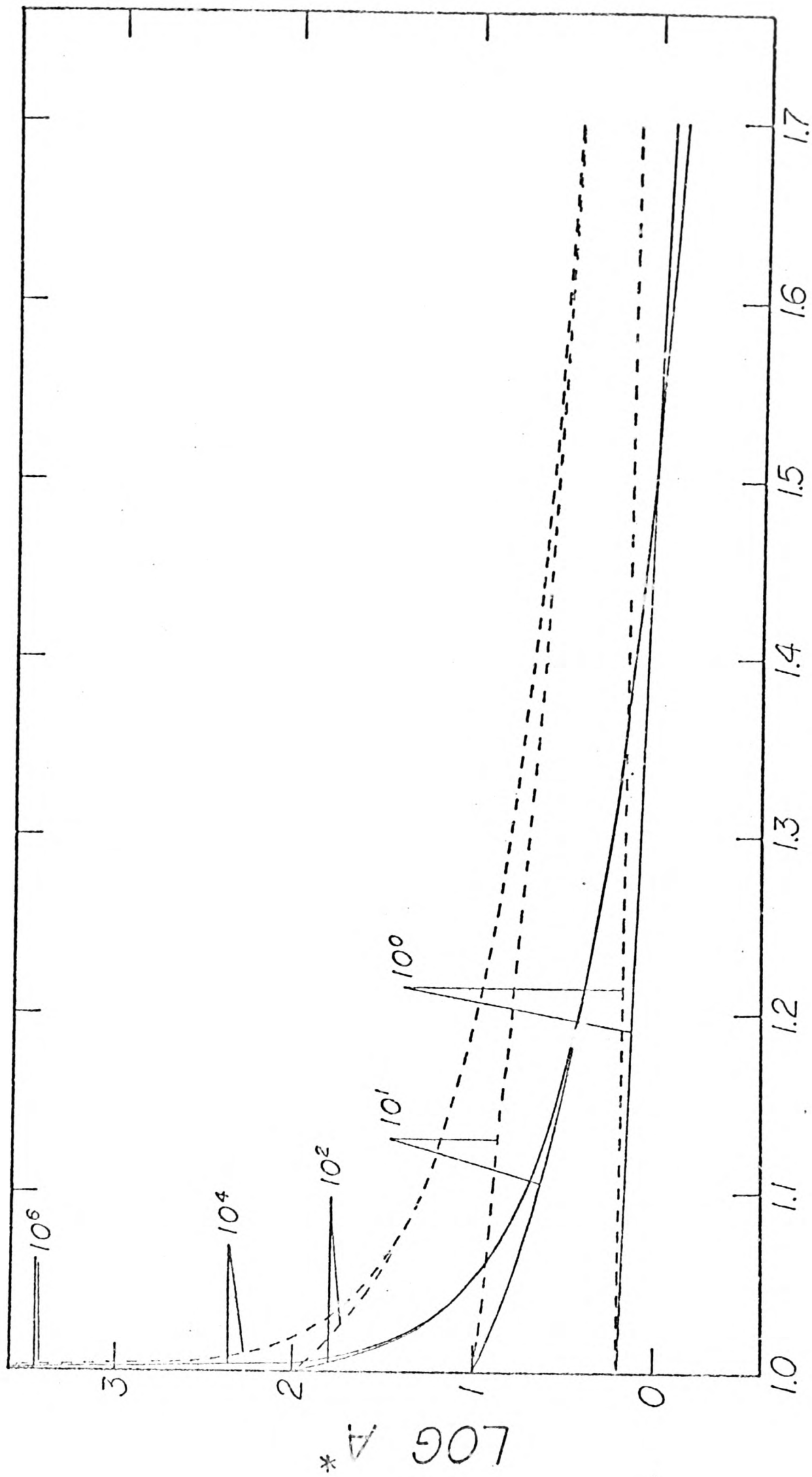


Figure 4-8

Plot of log A^* against (t/t') for different values of (t'/a) as shown.
——— ΔH_a = 30 kcal/mol and ΔT = +4 °C, (i.e. a_T = 0.52)
---- ΔH_a = 30 kcal/mol and ΔT = -4 °C, (i.e. a_T = 1.95)

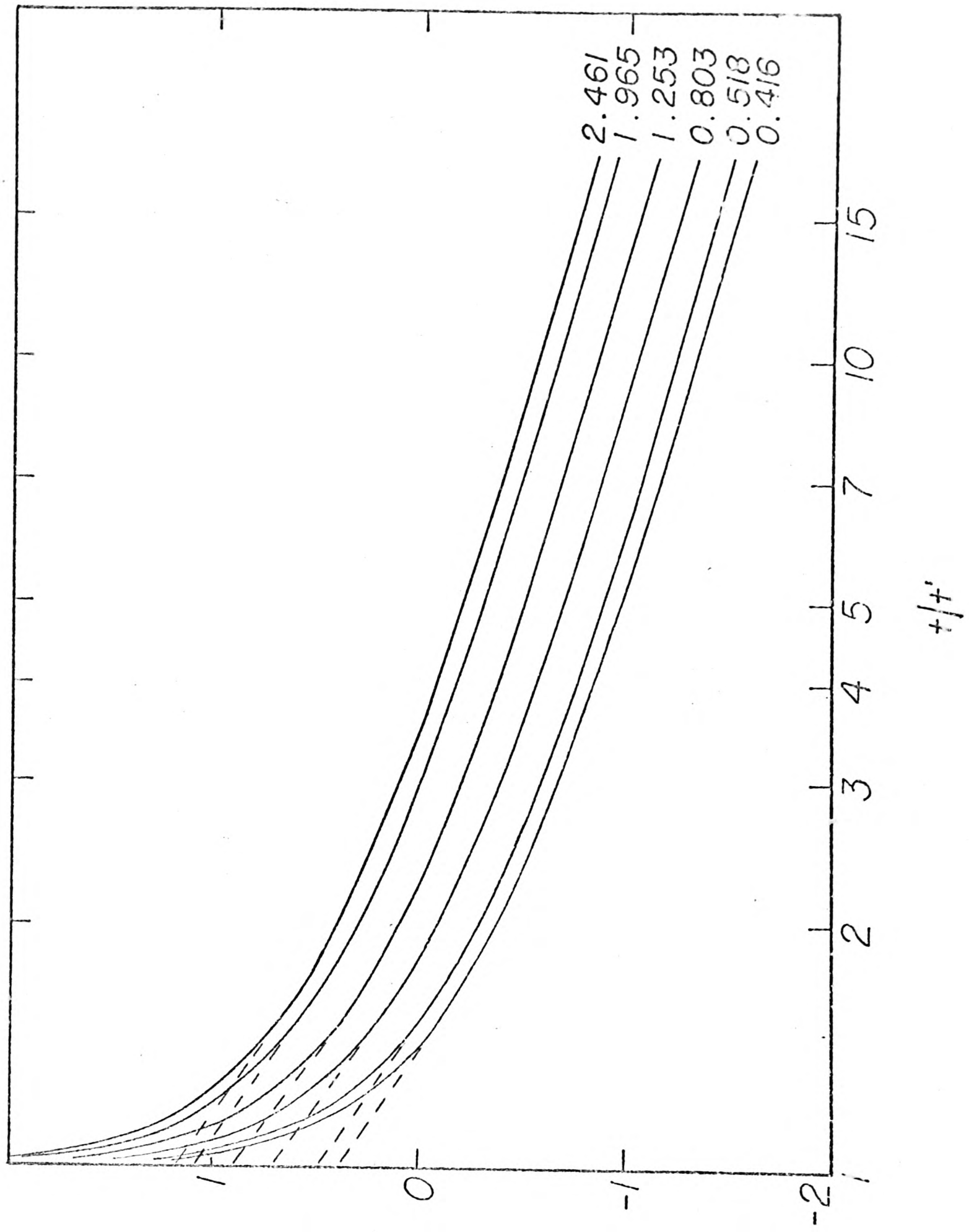


Figure 4-9

Plot of log A^* against log (t/t') for various values of a_T as shown. Dotted lines are the extrapolation of the curves from t/t' = 1.5 back to t/t' = 1.0. The values of a_T correspond to values of ΔH_a and ΔT below.

ΔH_a = 40 kcal/mol, ΔT = -4 °C, i.e. a_T = 2.461.
= 30 " , = -4 °C, = 1.965.
= 10 " , = -4 °C, = 1.253.
= 10 " , = +4 C, = 0.803.
= 30 " , = +4 C, = 0.518.
= 40 " , = +4 C, = 0.416.

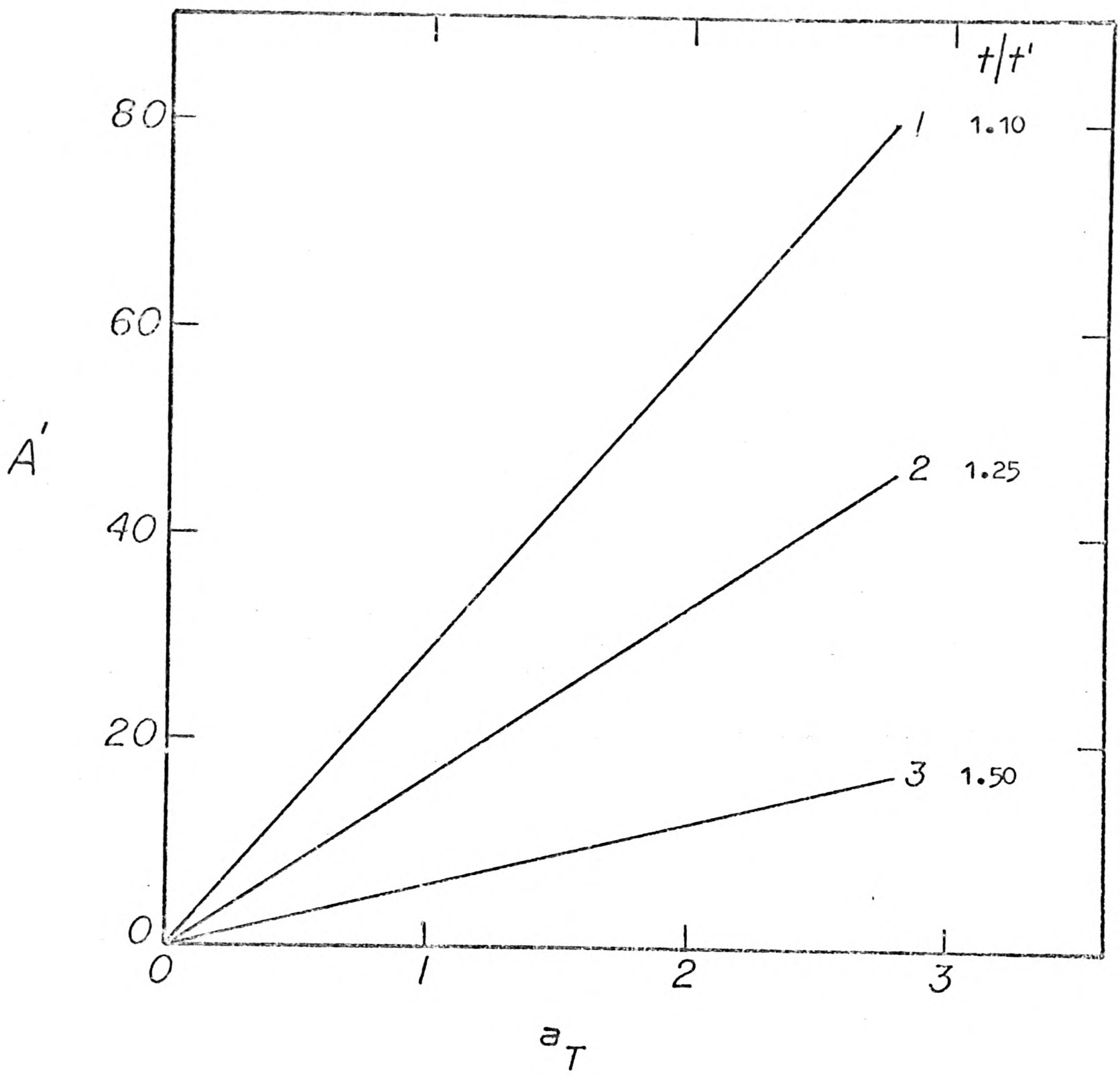


Figure 4-10

Plot of A' against a_T found from extrapolation of the curves of figure 4-9 to t/t' = 1.0, The three lines were obtained by extrapolating from (1) t/t' = 1.1; (2) t/t' = 1.25; (3) t/t' = 1.5.

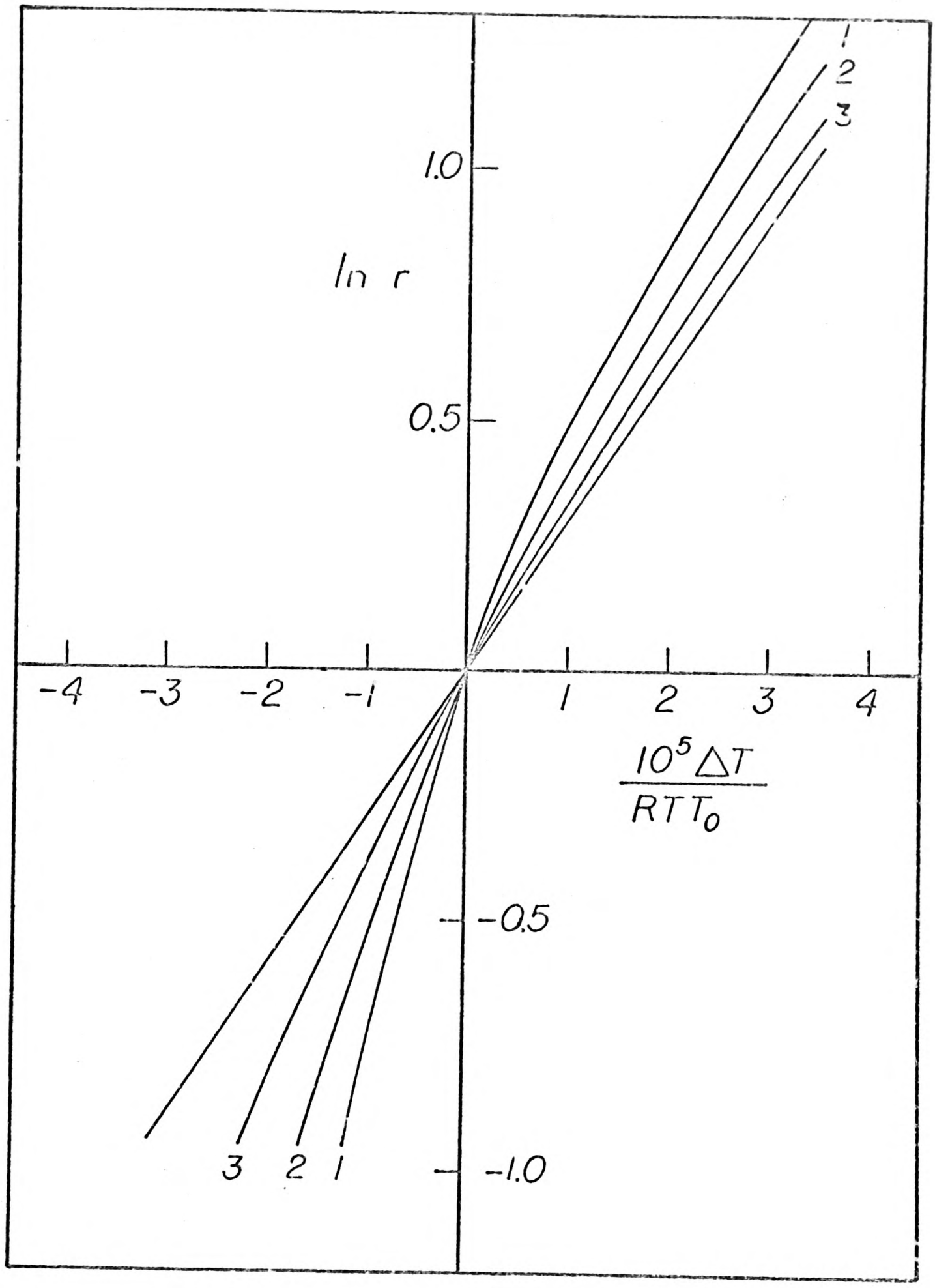


Figure 4-11

Plot of ln r against $\Delta T/RTT_o$ for the values of A' found from the three lines of figure 4-10, with ΔH_a = 30 kcal/mol and λ=0.005. Also shown is the straight line for b_T = 1.0

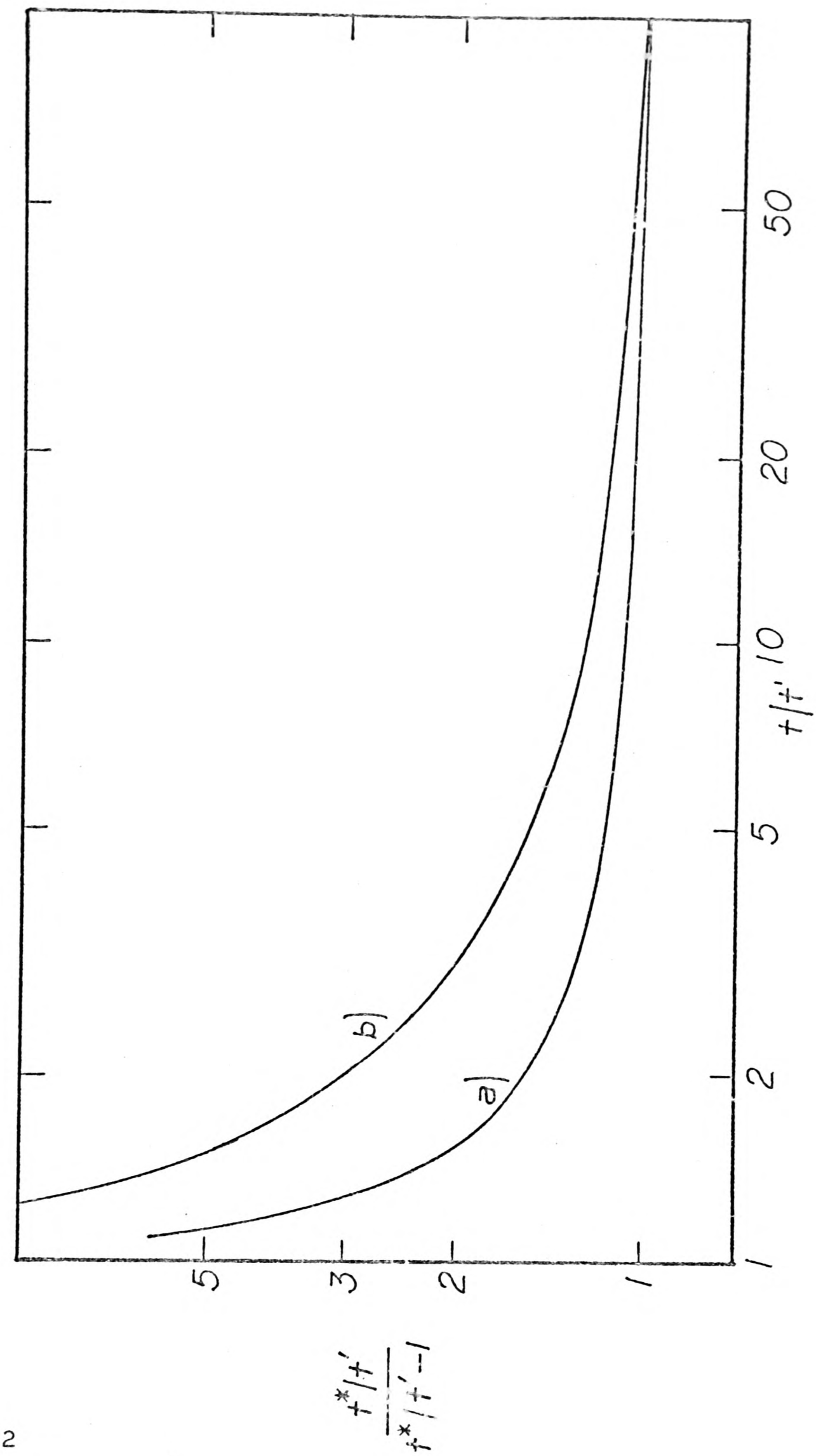


Figure 4-12

Plot of $\log((t^*/t')/(\frac{t^*}{t'} - 1))$ against log (t/t') for two values of a_T

a) $a_T = 0.518$, (i.e. $\Delta H_a = 30$ kcal/mol, and $\Delta T = +4\ ^\circ C$).
b) $a_T = 1.965$, (i.e. $\Delta H_a = 30$ kcal/mol, and $\Delta T = -4\ ^\circ C$).

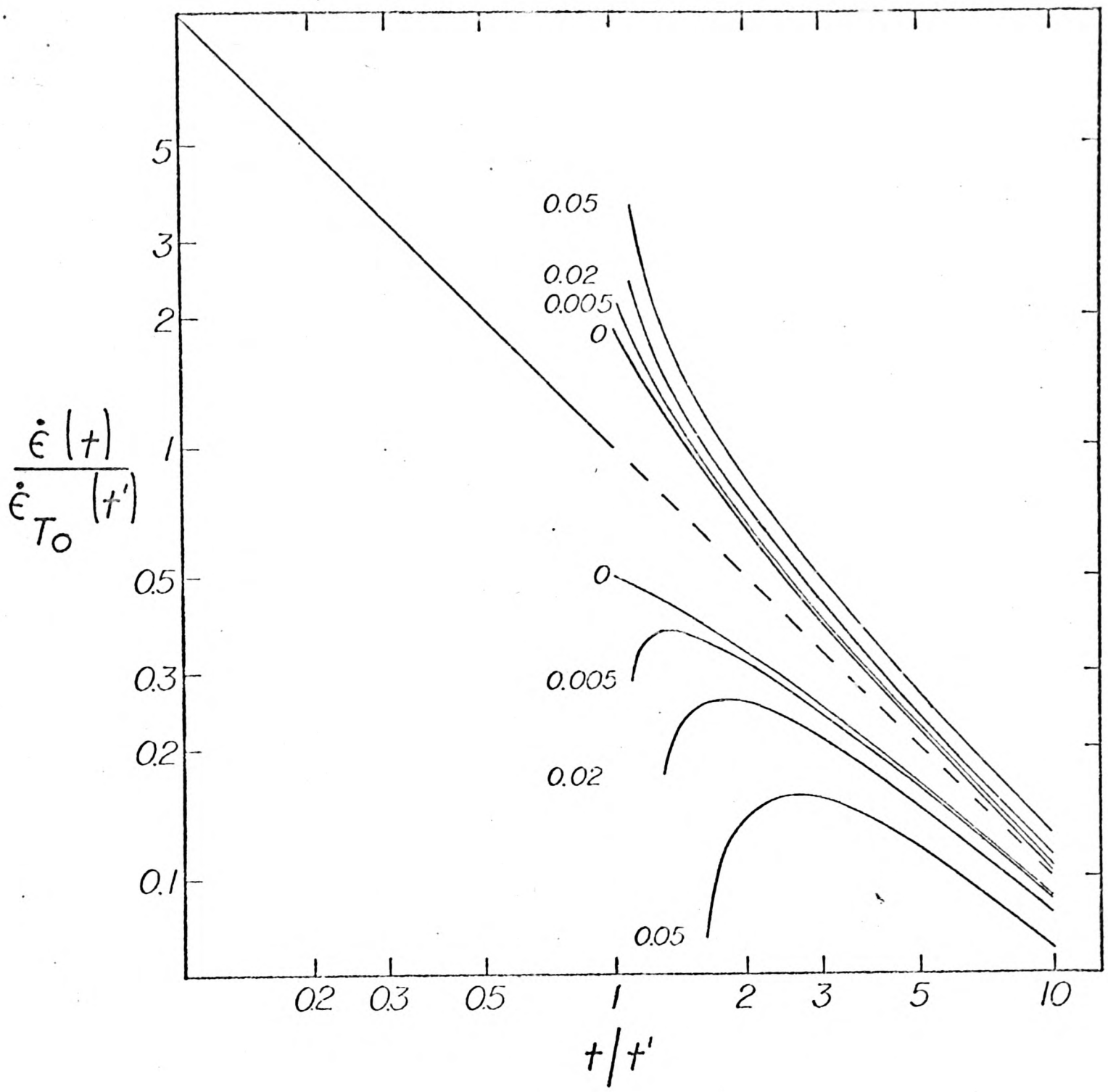


Figure 4-13

Plot of log (normalised rate, $\dot{\epsilon}(t)/\dot{\epsilon}_{T_0}(t')$) against log(t/t') before and after a T-jump for values of λ = 0.00, 0.005, 0.02, 0.05, for +ve (ΔT = +4 °C) and -ve (ΔT = -4 °C) T-jumps and ΔH_a = 30 kcal/mol.

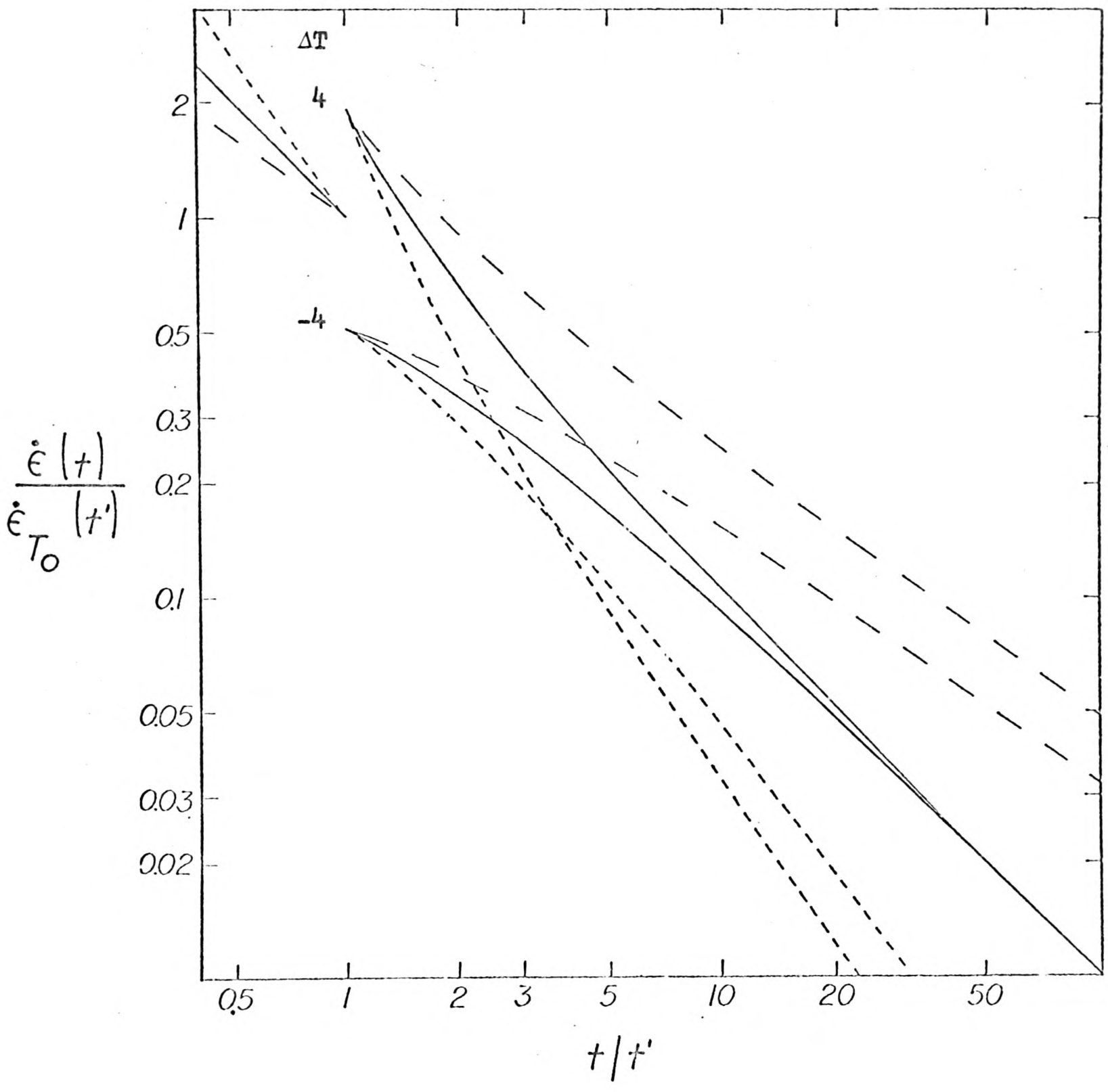


Figure 4-14

Plot of log(normalised creep rate, $\dot{\varepsilon}(t)/\dot{\varepsilon}_{T_o}(t')$) against log (t/t') before and after a T-jump from equations (4.29) and (4.31) with various values of n; — — — n = 0.7; ——— n = 1.0; ---- n = 1.4.
ΔH_a = 30 kcal/mol, $\Delta T = \pm 4\,^{\circ}C$.

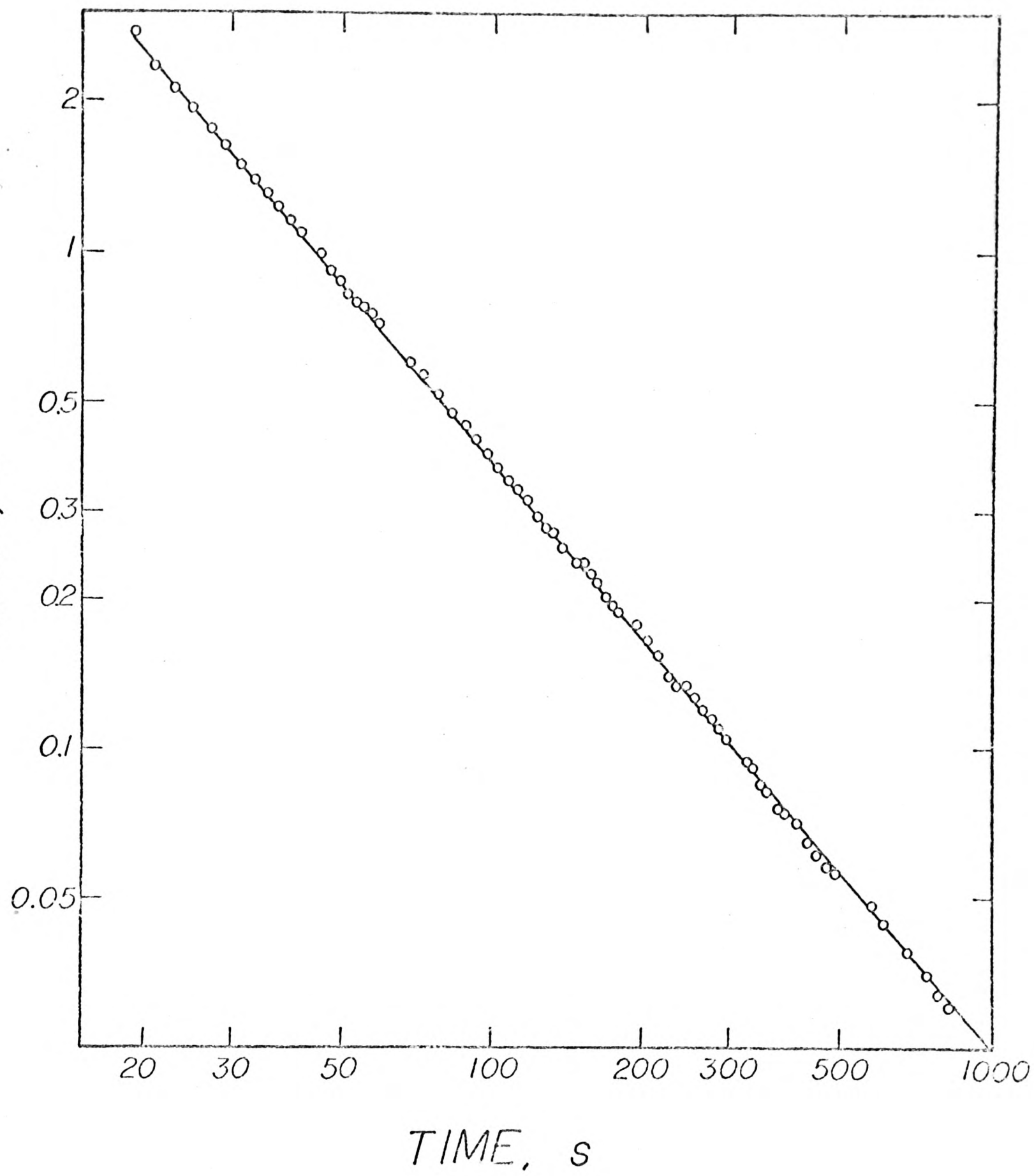


Figure 4-15

Experimental determination of log creep rate against log time for human tendon, specimen CH2-8-3, (male 23yrs, extensor, hand tendon). T_o = 28 °C and load = 2.1 kg. Straight line through the points has a slope of -1.17.

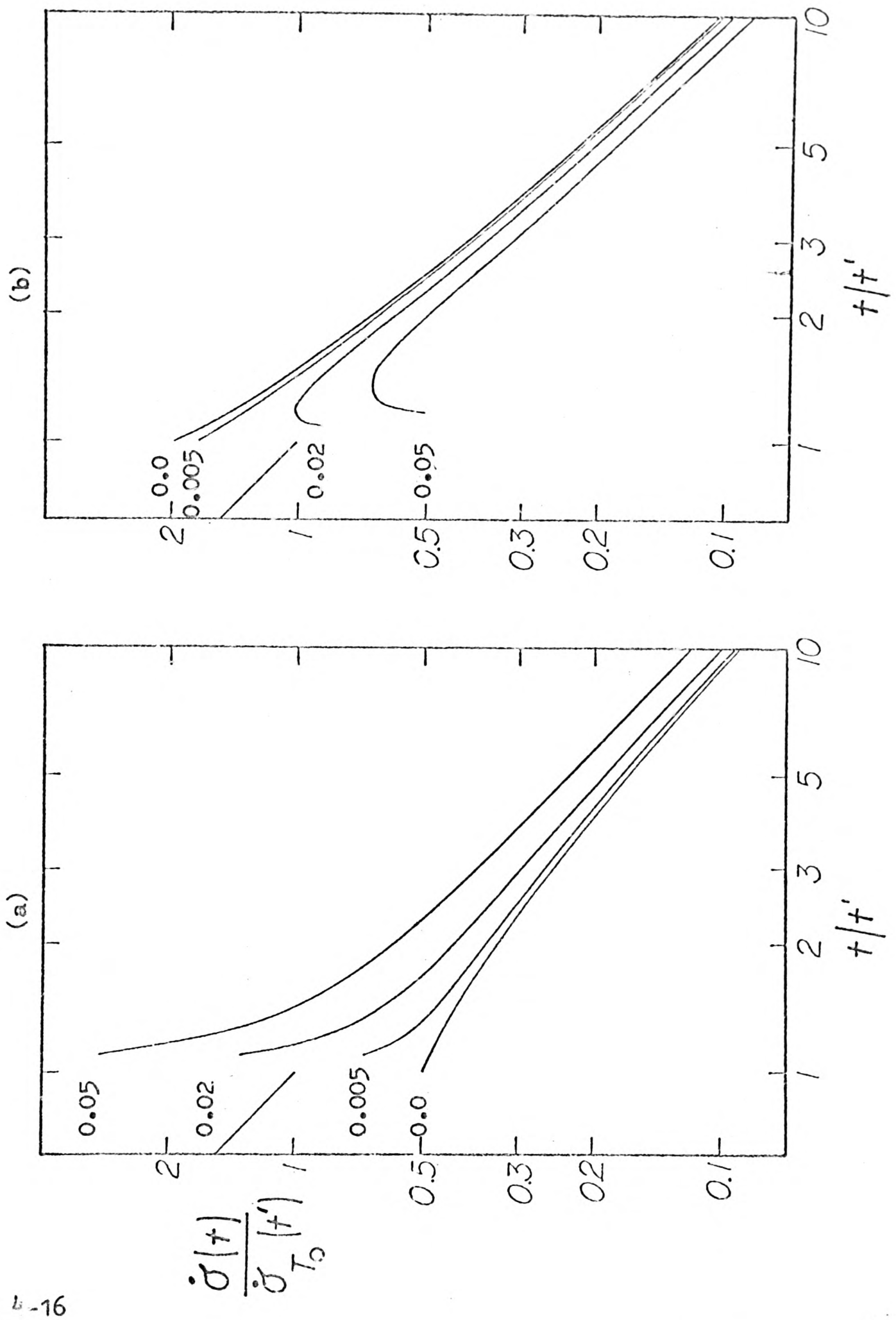


Figure 4-16

Plot of log ($\dot{\sigma}(t)/\dot{\sigma}_{T_o}(t')$) against log (t/t') for a stress relaxation T-jump before and after the T-jump for a) a down jump, ($\Delta T = -4\,^{\circ}C$) and b) an up jump ($\Delta T = +4\,^{\circ}C$), ΔH_a = 30 kcal/mol, and various values of λ^{SR} = 0.000, 0.005, 0.02, 0.05.

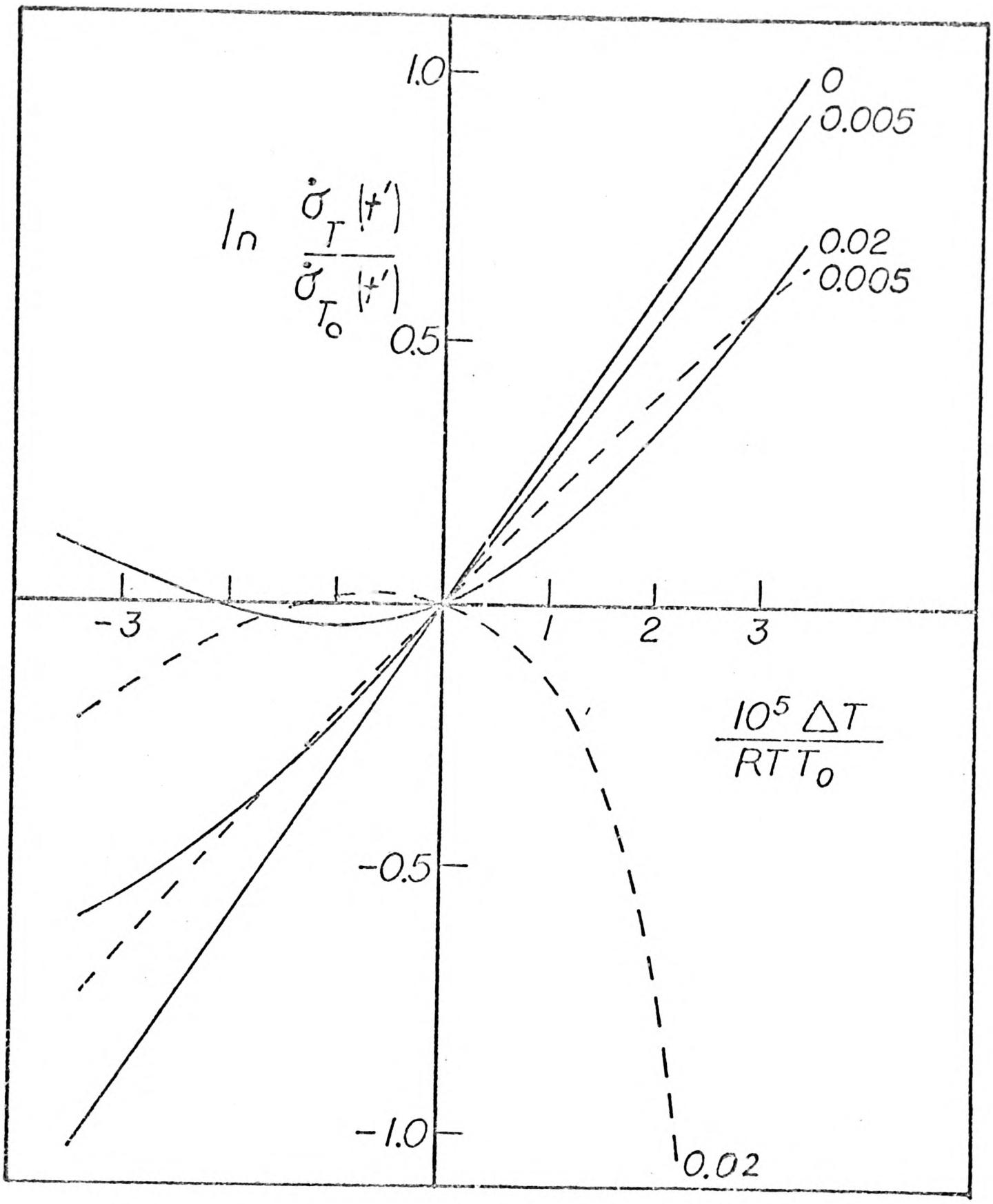


Figure 4-17

Plot of ln r against $\Delta T/RTT_0$ for stress relaxation T-jumps, for values of λ^{SR} = 0.005 and 0.02, with ΔH_a = 30 kcal/mol.

——— found from taking the values of A' from line (3) of figure 4-10

---- found from assuming A' is a constant = 10.

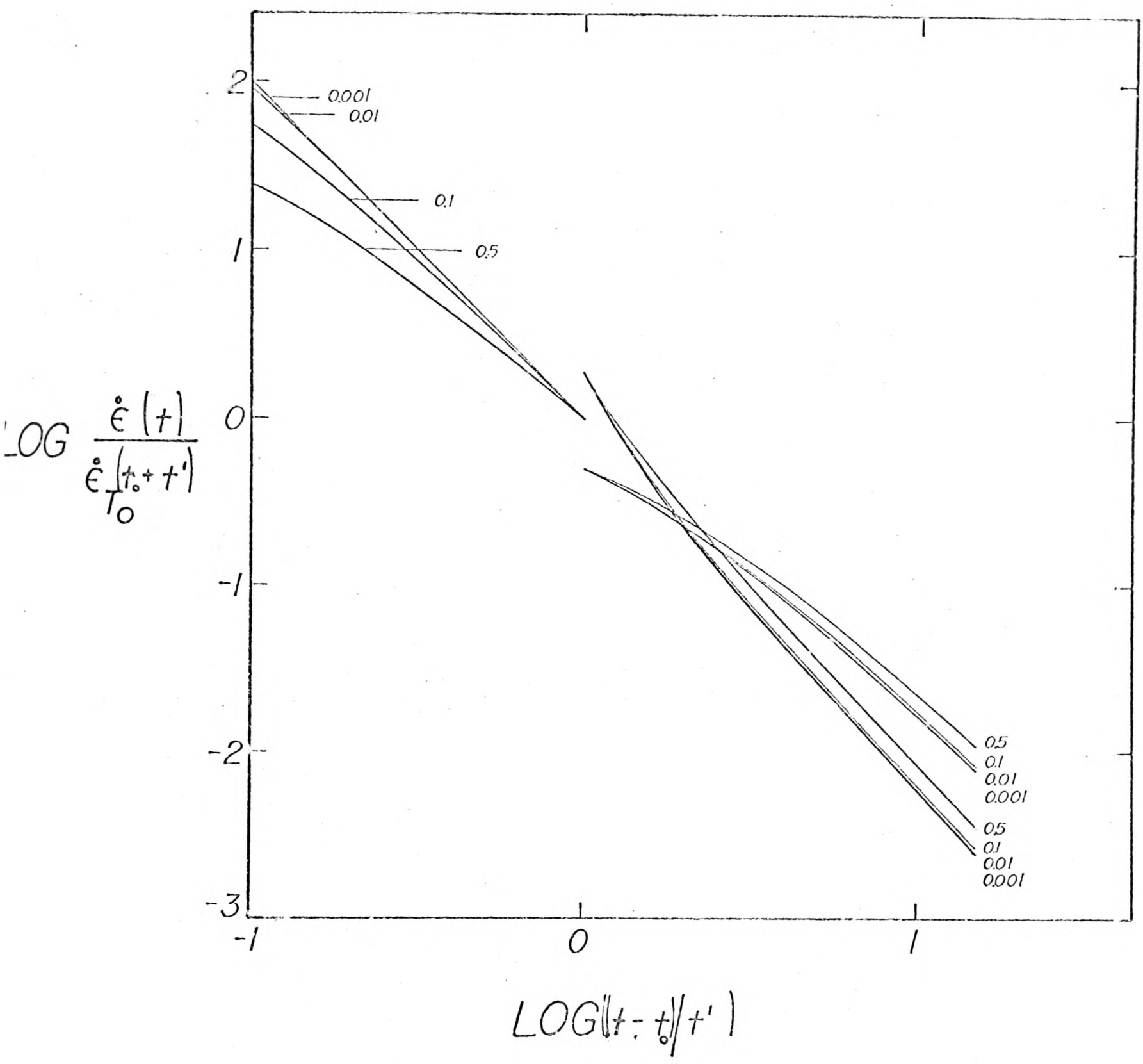


Figure 4-18

Plot of $\log(\dot{\epsilon}(t)/\dot{\epsilon}_{T_o}(t_o+t'))$ against $\log((t-t_o)/t')$ for various values of $t_o/t' = 0.5, 0.1, 0.01, 0.001$, for recovery T-jumps, from equations (4.45) and (4.46). $\Delta H_a = 30$ kcal/mol and $\Delta T = \pm 4\,^{\circ}C$.

Chapter 5

Isothermal Creep Behaviour of Tendon

5.1 Introduction

This chapter will describe the isothermal behaviour of tendon in tensile creep. It was necessary to conduct isothermal experiments to obtain

(i) the loads required to take the specimen into the 'toe' and 'linear' regions of the stress-strain curve.

(ii) the extent to which recovery of the specimen was taking place.

(iii) the magnitude of the creep and recovery rates at a given load, which must be sufficiently large to give good rate data in the T-jump experiment after a change in temperature.

In addition to this, it is necessary to determine whether the viscoelastic deformation of tendon is linear or non-linear. Any difference between the tendon behaviour and that of synthetic polymers will be important. The isothermal data plays an essential part in the verification of any theoretical model which may be developed to explain the viscoelastic behaviour of tendon.

As outlined in chapter 1, a material can be considered to be linear viscoelastic if it obeys the Boltzmann Superposition Principle. This can be tested by performing creep-recovery and 2-step loading experiments. The extent to which the properties of tendon deviate from linear viscoelastic behaviour was found by studying the creep and recovery behaviour of tendon under various loads from the 'toe' region into the 'linear' region of the stress-strain curve. Both strains and strain rates were obtained and deviations from the Boltzmann Superposition Principle and thus linear viscoelasticity were determined. The dependence of the strain rate on load will be seen to be composed of two regions which coincide with the 'toe' and 'linear' regions of the stress-strain curve. Two-step loading and

creep cycling experiments were performed and a comparison made with the normal behaviour of linear and non-linear viscoelastic solids. We also studied the creep behaviour in the 'linear' region by performing creep experiments on a prestressed tendon.

5.2 Results

The creep and recovery strain behaviour of tendon for various applied loads is shown in figure 5-1 for the specimen CH2-16-1(m71,Hfh)★ with a loading time t_o of 100s. The temperature for this and all subsequent isothermal experiments in this chapter was 28 °C. The creep part of this behaviour is shown in greater detail in figures 5-2 and 5-3. In figure 5-2 the creep strain is plotted against log time and the increase in strain over the period of the loading time is seen more clearly. Figure 5-3 shows the log creep rate against log time curve for these various loads. It can be seen that a straight line can be drawn through the points for each load as predicted by equation (4.29), the slope of which depends on the level of stress and is close to -1. The value of this slope is found by least squares and a typical variation with isochronal strain is shown in figure 5-4 for the specimen CH2-8-2(m23,Heh) where the slope at low loads is -0.95 ± 0.05 and begins to change at a strain level of $\sim 4\%$ until a slope of -1.17 ± 0.05 is reached.

The isochronal load-20s creep strain curve taken from the data of figure 5-2 for specimen CH2-16-1(m71,Hfh) is shown in figure 5-5(a),

---

★This notation will be used throughout the thesis. The specimen number (see chapter 2) is followed by its description in brackets, namely sex (male,m, or female,f), age (e.g. 71 years), source (Human H), type (flexor,f,or extensor,e), and location (hand,h,or toe,t) respectively.

circled points, and the characteristic 'toe' region of the tendon behaviour is seen for loads up to ~2 kg and 3% strain. In this region, a small increase in load produces a large increase in strain. An approximately 'linear' region is observed for loads greater than 2 kg and here the material is much stiffer and requires considerably more load than in the 'toe' region to produce a given increment of strain.

It is important to note that once the conditioning procedure, as outlined in chapter 2, was carried out, we obtained recovery of the specimen to less than 1% of the 20s creep strain observed for each load and this occurred for all load levels applied for this particular specimen including those strains well into the'linear' region. In fact slippage of the tendon from the grips occurred before we observed any non-recoverable behaviour. This is in conflict with data produced before where reproducibility and recovery was only observed in the 'toe' region.[1,2,3] It is to be expected that the strength of the collagen fibres is utilised 'in vivo' and although the normal flexing and stretching of the fingers exerts only a small load on the tendon, there are many occasions when people carry weights of 3 kg of more in their hands, e.g. a shopping bag with items including a 10 lb bag of potatoes. In this case, the tendon will be in the 'linear' region of the load-strain curve and the fibres are being stretched. The tendon will be able to recover from these loads as seen in figures 5-1 and 5-9.

The 20s isochronal creep rate of the specimen CH2-16-1(m71,Hfh) can be obtained as a function of load from figure 5-3 and plotted against the load as shown in figure 5-5(b), circled points. It will be seen that for loads up to ~2 kg and 3% strain a curved region is displayed followed by an approximately linear region. At all levels of load, the creep rate increases with load, but what is startling is the direction of the curvature

at loads up to 2 kg. The curvature is away from the tangent to the curve at the origin in a direction opposite to that normally seen for polymeric materials.[4,5]

In order to determine deviations of the behaviour of a polymeric material from the Boltzmann Linear Superposition Principle, it is usual to perform two experiments at each load.[5]

(i) a creep experiment of duration in time equal to $2t_o$ and

(ii) after the load has been removed and the specimen fully recovered, a creep experiment for time t_o (figure 5-6(a)) at which time the load is removed.

The recovery strain $\epsilon_R(t-t_o)$ can be determined from the difference between the creep strain $\epsilon_c(t)$ in experiment (i) and the residual strain[5] $\epsilon_r(t)$ in experiment (ii) after time t_o (figure 5-6(a)). The recovery rate $\dot{\epsilon}_R(t-t_o)$ can be similarly calculated from the rates $\dot{\epsilon}_c(t)$ and $\dot{\epsilon}_r(t)$.

For creep experiments on tendon it was found that the isochronal creep strain and creep rate from one experiment to another at the same load could differ by 2% and 4% respectively, even though the tendon recovered to less than 1% of the creep strain after each experiment. This will introduce errors in the determination of the recovery strains and rates from the above method of 2% and 4% respectively. In order to obtain the recovery strain $\epsilon_R(t-t_o)$ more accurately, the following procedure was adopted: a typical output of strain against log time for a creep experiment on specimen CH2-16-1(m71,Hfh) is shown in figure 5-7(a). It can be seen that the line is a gentle curve over a reasonable time scale. If this curve is extrapolated to the time at which we wish to calculate the recovery strain (e.g. at $t-t_o$=20s) we can obtain the creep strain $\epsilon_c(t)$ at the time t ($=t_o+20s$), which would have resulted if the load had been left on, with an error of less than 0.2%. The recovery strain can then be calculated from subtracting

this value from the residual strain $\epsilon_r(t)$ in figure 5-7(b) where the strain after the removal of the load is plotted against the time after removal of the load (i.e. $t-t_o$). We can thus calculate both the creep and recovery strains from one experiment and the accuracy of the recovery strain determination has been improved by a factor of ~ 10.

We also performed a similar extrapolation procedure for the rates. The rates obtained in the experiment of figure 5-7 are shown in figure 5-8 during creep (figure 5-8(a), circled points), and after the load was removed (figure 5-8(b)). By extrapolating the creep rates of figure 5-8(a) we obtained the value of the creep rate which would have resulted if the load had remained on the specimen after time t_o. The accuracy obtained for this value is $\sim 4\%$, the same as that found earlier from the two experiment method.

Although there is little to choose between the above methods in determining the recovery rate, the extrapolation technique provides a significant improvement in accuracy when calculating the recovery strain, and was thus used in all isothermal creep experiments to determine the recovery strains and rates. Another important advantage in the use of the extrapolation method for tendon is that only one experiment is required for determining creep recovery behaviour at a given load which reduces the amount of time required to keep the specimen in the apparatus.

The recovery strain and strain rates for the specimen CH2-16-1(m71,Hfh) at various times were found by the extrapolation method from data similar to those shown in figures 5-7 and 5-8 for various loads. In figure 5-9(a), the creep strain in a creep-recovery experiment is plotted against time for two loading times, 100s and 200s and for the load 2 kg (the same as in figures 5-7 and 5-8). The strain after removal of the load at t_o=100s is also shown and the recovery strain $\epsilon_R(t-t_o)$ was

obtained for times up to 200s and compared to the creep strain as shown in figure 5-9(b). It is clear that for all times up to 200s, the recovery strain is less than the creep strain. This difference is not due to the non-recovery of the sample, the amount of which is shown in figure 5-9(a). It is clearly due to the viscoelastic properties of the tendon. It can be seen from figure 5-9(b) that the isochronal creep and recovery strains merge as the time increases and will be equal for some time longer than we were able to observe.

The creep rate for the same experiment just outlined with loading time 100s and load 2 kg was shown in figure 5-8(a) (circled points) along with the residual strain rate $-\dot{\epsilon}_r(t)$ after the load was removed in figure 5-8(b). By the extrapolation technique, the recovery rate $\dot{\epsilon}_R(t-t_o)$ is found for times $t-t_o$ up to the loading time 100s and plotted on figure 5-8(a) , (squared points) where it can be seen that for all times shown the recovery rate is greater than the creep rate. It can also be seen that as the time increases, the recovery and creep rate curves diverge, indicating that at some time less than we are able to observe, the two rates could have been equal.

The 20s isochronal recovery strain and recovery rate taken from graphs such as figures 5-7, 5-8 and 5-9 are shown in figure 5-5 (squared points) for the various loads applied to the specimen CH2-16-1(m71,Hfh). When these are compared to the creep behaviour in the same figure it is clear that

(i) the recovery strain is less than the creep strain at all load levels and

(ii) the recovery rate is greater than the creep rate at all load levels.

This is observed for the times less than the loading times. If these data are plotted in the form as shown in figure 5-10, then two regions are apparent.

In figure 5-10(a), the ratio of isochronal $\epsilon_R(t-t_o)/\epsilon_C(t)$ is plotted against load for two times 20s and 90s. The values of $\epsilon_R(t-t_o)/\epsilon_C(t)$ range between 0.975 and 0.955 for t=20s (the linear viscoelastic value would be 1.0) and a minimum in the curve is seen at around 1 kg load. For the rates in figure 5-10(b) where the ratio $\dot{\epsilon}_R(t-t_o)/\dot{\epsilon}_C(t)$ is plotted against load for the same times, the maximum in the curve is found at around the same value of load, namely 1 kg, after which the ratio approaches the linear viscoelastic value of 1.0 as the load increases. The 90s strain ratio ϵ_R/ϵ_C is closer to unity than the 20s ratio and vice versa for the rates. (It should be noted that both ratios for strains and rates are well outside the errors of the experiment).

It is clear that the viscoelastic behaviour of the tendon in the 'toe' and 'linear' regions is non-linear viscoelastic. This has been observed in both the strains and the rates for specimen CH2-16-1. In 2-step loading experiments, shown schematically in figure 5-6(b), where a load, σ_o, is applied for time t_o, when another load is applied, this non-linear viscoelastic behaviour is also observed. Figure 5-11(a) shows the creep response to a step load of 1 kg (lower curve (i)) as a function of log time, followed by a step load of 1 kg applied at 100s (upper curve(ii)). For the upper curve, log $(t-t_o)$ is plotted on the abscissa, where t_o is the loading time, in this case 100s. The lines are approximately straight, thus allowing extrapolation to obtain the 'additional' creep strain ϵ'_C. The loading programme is shown in figure 5-11(b) with the creep response for this specimen, this time plotted against linear time. It is obvious that the increase in strain on imposition of the second load is far less than for the first step load of 1 kg and the magnitude of the 'additional' strain, $\epsilon'_C(t)$ is shown as the squared points. Different step loadings were applied to the specimen as follows: 0.1 kg + 0.1 kg ; 0.5 kg + 0.5 kg ; 4 kg + 2 kg.

[5]

In all cases, it was found that the 'additional' creep compliance was less than that expected from the linear viscoelastic case and corresponds to the fact that the slope of the isochronal strain-stress curve (or compliance) is decreasing as the level of stress increases.

The creep and recovery behaviour of another specimen CH2-16-4 (m71,Hfh), (i.e. from the same donor as CH2-16-1) is shown in figure 5-12. This was obtained from creep-recovery experiments with t_o=30s. The same sort of behaviour is observed as with CH2-16-1. Slight differences are however apparent. The 'toe' region is longer for specimen CH2-16-4, (figure 5-12(a), circled points). This illustrates the difficulty of obtaining the same starting point with regards to the initial crimp angle from specimen to specimen, and thus the need to determine for each specimen its load-strain characteristic and its creep rate-load behaviour. As well as the longer 'toe' region, the creep rate against load curve (figure 5-12(b), circled points), shows a distinctly flat region from a load of 2 to 3 kg. It was observed that for specimens for which the 'toe' region was even longer (as a result of a smaller preload applied to straighten the sample, or the preload for one sample straightening it more than the same preload for another sample, or simply from sample to sample variation of the crimp angle), this flat region turned into a distinct 'hump' shape on the creep rate against load curve at the low levels of strain corresponding to the 'toe' region. This can be seen in figure 5-13 for the specimen CH2-9-1(m77,Hfh) where the 'hump' is clearly visible. The load-strain curve for this specimen is shown in the inset and the longer 'toe' region can be seen. This 'hump' was also observed for specimens CH2-8-2(m23,Heh) and CH2-8-3(m23,Heh), (see figures 6-15 and 6-17). This is a very important feature of the tendon behaviour and it will be seen that the model developed to explain the creep behaviour of tendon in chapter 7 predicts exactly this behaviour.

In order to try and determine the viscoelastic properties of the fibres themselves, a preload was applied to specimen CH2-16-4(m71,Hfh) of sufficient magnitude to take the specimen into the 'linear' region of the load-strain curve. The load-strain behaviour of this material is shown in figure 5-12 from which we ascertained the correct preload to be applied. A preload of 3 kg was chosen, and once the specimen had achieved mechanical equilibrium at this load (i.e. when no further increase in strain could be observed over a period of 3 hours on the smallest scale of the chart recorder used for determining the rates), creep-recovery experiments were performed with loads of 2 kg and 3 kg as shown in figures 5-14. The 20s isochronal creep strain is plotted against load and shown in figure 5-15(a), solid line, where a straight line can be drawn through the points. The 20s creep rate against load curve (figure 5-15(b), solid line) is also a straight line as are the 30s and 60s lines. It would appear that the material might be linear viscoelastic. However, on determining the 20s recovery strain, a straight line was observed on a strain-load plot but the level of recovery strain was less than the creep strain at each level of load (figure 5-15(a), dashed line). The 20s and 30s recovery rates were less than the creep rates even though the lines were straight on the creep rate-load curve (figure 5-15(b), dashed lines). At 60s, the creep and recovery rates coincided, but the 60s creep and recovery strains were not equal. It is clear that the creep-recovery behaviour of the preloaded tendon does still not observe the Boltzmann Superposition Principle.

Creep cycling experiments were performed on specimen CH2-9-1 (m77,Hfh) which was subjected to 10 cycles of creep-recovery, each cycle 120s long and loading time t_o=60s. The values of the isochronal creep and recovery strains and rates at a given load were not equal, a result found before. The variation of the creep and recovery strains with cycling for

various loads are shown in figure 5-16. Both creep and recovery strains decrease with cycling. For the lower loads they settle down to a steady value after about 3 cycles, but for the higher loads, the decrease is still occurring after 10 cycles, but are levelling out. In all cases the creep strain is larger than the recovery strain. For the rates shown in figure 5-17, we see that they also decrease with cycling and are steady for the low loads after about 4 cycles and are still levelling out at 10 cycles at the high loads. This approach to a steady value agrees with other cycling data. Lockett and Turner[6] found that for polypropylene the creep and recovery strains increased with cycling and approached a steady value. Here we see the opposite behaviour, i.e. the isochronal strains and rates decrease with cycling.

This decrease in creep rate with cycling for other applied loads can be seen in figure 5-18 where the creep rate is plotted against load. The 'hump' in the curve is clear for the first few cycles, but seems to disappear after the fifth cycle. The variation with time of the observed rate in creep, $\dot{\epsilon}(t)$ and the residual rate $\dot{\epsilon}_r(t)$ after removal of the load is plotted in figure 5-19. The abscissa is log $t-t_{sw}$, where t_{sw} is the time at which the load is changed; for the case of creep it is the time at which the load is applied at the start of a given cycle, and for recovery it is the time at which the load is removed on that cycle. It will be seen in figure 5-19(a) for creep that the curves for the first two cycles are somewhat higher than subsequent cycles and that the curves are close together for further cycles. In figure 5-19(b), the residual rate, $-\dot{\epsilon}_r(t)$, after removal of the load is plotted against log $(t-t_{sw})$. The first cycle is lower than subsequent cycles which all fall close to one another. This behaviour was observed for all loads tested up to 5 kg.

5.3 Discussion

The non-linear viscoelastic behaviour of most polymeric materials exhibits the following general features.[5,6,7,8]

(i) the isochronal creep strain and creep rate against stress curves bend upwards with increasing stress.

(ii) the isochronal recovery strain (for times short compared with the loading time) is greater than the isochronal creep strain.

(iii) the isochronal recovery rate (for times short compared with the loading time) is less than the isochronal creep rate.

(iv) the isochronal 'additional' compliance in a 2-step loading programme is greater than the isochronal creep compliance.

(v) the isochronal creep and recovery strains increase with cycling to a steady value.

We have seen that the non-linear viscoelastic behaviour of tendon is, in all of these five cases, opposite to that found for normal polymeric materials. This leads us to believe that the non-linearity is merely the result of the structure of the tendon rather than anything extra-ordinary about the viscoelastic properties of either the collagen fibres or the mucopolysaccharides of the tendon.

If we consider the creep-recovery experiment, then for a material obeying the simple Boltzmann Linear Superposition Principle, the compliance D(t) at any stress level will be given by

$$D(t) = D_U + \int_0^\infty \Delta D \left(1 - \exp\left(-\frac{t}{\tau}\right)\right) d\tau \qquad (5.1)$$

in which D_U, ΔD and τ are not dependent on the level of stress and thus the compliance is not dependent on stress. Now, for the case of tendon, we have a curved isochronal stress-strain behaviour, i.e. the compliance D(t) is strongly stress dependent. This non-linearity can be introduced in 3 ways;

either D_U, ΔD or τ may be functions of stress. For most polymeric materials, the value of D_U is thought not to be stress dependent. For tendon, however, D_U is a function of stress as a result of the uncrimping of the collagen fibres. Yannas[9] has shown that, by considering the elastic bending of a sinusoidal beam, the stress-strain curve in the 'toe' region can be predicted, and that the elastic modulus increases as the strain increases, i.e. as the crimp angle decreases. Hence the modulus E_U is a function of strain and so will the compliance D_U.

In a creep-recovery experiment, the specimen will creep under the applied stress with a value D_U determined by the value of the crimp angle at time $t=0^+$. As the specimen is creeping, the angle of the fibres to the tensile axis, θ, will change and by the time the load is removed, the internal arrangement of the fibres is different from the time just after the load was applied; the crimp angle will be smaller. The compliance in any subsequent loading pattern will be lower than it was at the start of the experiment. Hence, if the load is removed, the material will recover, but the compliance D_U for the recovery will be less than that for the creep. Thus the initial recovery strain will be less than the initial creep strain, (figures 5-5(a), 5-9(b), 5-10(a), 5-12). Similarly for the step loading experiments, the strain after imposition of the second load will be less than that expected for the case when the compliance D_U does not change, (figure 5-11), and for the cycling experiments, the creep strain on the nth cycle will be less than that on the n-1 th cycle, (figure 5-16).

Even though a 'linear' region is seen on the stress-strain curve, the straightening of some of the crimps will still be occurring in this region, which will introduce non-linear viscoelastic effects on the recovery behaviour (figure 5-15) even though the fibres themselves may exhibit linear viscoelastic behaviour. It is seen that the behaviour approaches the linear

case for the higher loads (figure 5-10) which suggests that the non-linear crimp straightening process is now being dominated by the fibre stretching process.

In order to look at the rates, it is important to know the viscoelastic parameters which contribute to the creep. For a material with a single retardation time, τ , the creep rate is given by

$$\frac{\dot{\epsilon}(t)}{\sigma_o} = \frac{\Delta D}{\tau} \exp\left(-\frac{t}{\tau}\right) \qquad (5.2)$$

and we need to know what the ΔD's and τ's refer to. Can we associate them with the fibres or the gel? Do they change with stress or can they be assumed to be linear viscoelastic? In chapters 7 and 8 we will see that much of the creep rate data can be explained by assuming two processes to be occurring in the viscoelastic deformation:

(i) the interfibrillar shear of the mucopolysaccharide gel at low strains and stresses and

(ii) fibrillar extension at high stresses.

Qualitatively, we can see that if the low strain behaviour is governed by interfibrillar shear, then the creep rate will depend of the shear stress on the gel in between the collagen ribbons.[10] As the strain increases, and the crimp angle decreases, the shear stress on the gel decreases, and hence we obtain the concave downward curve for the creep rate against load behaviour, (figures 5-5(b), 5-12(b), 5-13).

The creep-recovery rate behaviour will also depend on the crimp angle. In recovery, the net stress on the material is zero, but the creep-recovery process may be envisaged as a combination of a +ve stress applied at time t=0 and an equal and opposite stress at time $t=t_o$. After the load is removed at time t_o, the crimp angle will be larger and hence

the shear stress on the gel will be greater than in creep. The contribution of the gel to the viscoelastic process will be greater in recovery than in creep, thus giving a larger recovery rate than creep rate,(figures 5-5(b), 5-8(a), 5-10(b), 5-12(b)). These ideas will be put on a more quantitative footing in chapters 7 and 8.

The behaviour of a linear viscoelastic material undergoing creep-recovery can be described as follows. We found in chapter 4 that the creep rate could be described by the equation

$$\frac{\dot{\epsilon}_{T_o}(t)}{\sigma_o} = C\, t^{-n}\, \Gamma(n) \qquad (4.28)$$

where the constants n and C are given by equation (4.26) which describes the form of the retardation spectrum, and Γ is the Gamma function. We have used this equation (4.28) to calculate the response to a cycling load as shown in figure 5-20 with $C = \sigma_o = n=1$. The length of each cycle is 120s with the loading time 60s. We have plotted the log rate against log $(t-t_{sw})$ curves, where t_{sw} is as defined before: figure 5-20(a) shows the observed rate in creep, $\dot{\epsilon}(t)$, and figure 5-20(b) shows the residual rate , $-\dot{\epsilon}_r(t)$. It can be seen that after the first cycle in both creep and recovery, the lines fall very much on top of each other and experimentally no difference would be detected. In creep, the first cycle is above and for recovery the first cycle is below subsequent cycles. The tenth cycle values of $\dot{\epsilon}(t)$ and $-\dot{\epsilon}_r(t)$ are hardly distinguishable from each other, with $-\dot{\epsilon}_r(t)$ being slightly less than $\dot{\epsilon}(t)$.

The experimental results for specimen CH2-9-1(m77,Hfh) agree qualitatively with this behaviour as was shown in figure 5-19 for a cycling load of 0.2 kg. It was seen that the level of the log rate-log time curves decreased with cycling for creep and increased with cycling

for data after the load was removed.

The creep rate behaviour in cycling experiments as shown in figure 5-18 can be qualitatively explained by the following; we earlier observed that specimens CH2-16-1(m71,Hfh) and CH2-16-4(m71,Hfh) displayed a smaller 'toe' region than specimen CH2-9-1(m77,Hfh). The initial crimp angle for specimen CH2-9-1 will thus be larger than that of the other two specimens. When it is cycled, it does not recover back to the initial crimp angle before the next cycle is imposed. Hence the situation can be reached on the 5th cycle, say, where the crimp angle is of the order of that for specimens CH2-16-1 and 4 (which showed no 'hump' in the creep rate against load curve) and hence the 'hump' will disappear, (figure 5-18). Since the material gets stiffer and the shear stress on the gel reduces as the crimp angle reduces, then there will be a reduction in both the isochronal creep strain (figure 5-16) and rate (figures 5-17 and 5-18) with cycling. This decrease in the rate with cycling will be shown thecretically in chapter 8.

5.4 Summary

It has been shown that the non-linear viscoelastic behaviour of tendon is contrary to that of normal synthetic polymers. In particular, we have observed the following creep behaviour for tendon at times short compared to the loading time:

(i) the isochronal load-20s strain curve showed the characteristic 'toe' and 'linear' regions.

(ii) the isochronal creep rate against stress curve showed a concave downwards curvature at loads corresponding to the 'toe' region, followed by an approximately linear region.

(iii) the isochronal creep strain is greater than the recovery strain.

(iv) the isochronal creep rate is less than the recovery rate.

(v) the isochronal creep compliance is greater than the 'additional' compliance.

(vi) the isochronal creep and recovery strains and rates decrease with cycling.

From these data it appears that different processes are contributing to the deformation of tendon in the 'toe' and 'linear' regions of the stress-strain curve. It is difficult to discern purely from the isothermal behaviour what the viscoelastic mechanisms might be. The indications are that the mucopolysaccharide gel plays a major role in the 'toe' region and that the collagen fibres themselves are being deformed in the 'linear' region.

In the next chapter, we will obtain the important parameter, the apparent activation energy, ΔH_a, of tendon by the T-jump technique. From the values of ΔH_a in the 'toe' and 'linear' regions of the stress-strain curve, we can provide stronger evidence to support the hypothesis for the deformation of tendon presented above, since each deformation process has

an associated value of ΔH_a. It will be seen in chapters 7 and 8 that the isochronal creep rate data presented in this chapter can be predicted by the theoretical model, based on the above hypothesis of tendon deformation, which was developed to explain the creep behaviour of tendon

References

1 Rigby B.J., Hirai N., Spikes J.D. and Eyring H., J.Gen.Physiol.,43,265,1959.

2 Abrahams M., Med.Biol.Eng.,5,443,1967.

3 Rigby B.J., Nature,202,1072,1964.

4 McCrum N.G., Read B.J. and Williams G., 'Anelastic and Dielectric Effects in Polymeric Solids', Wiley, London. 1967.

5 Ward I.M., Mechanical Properties of Solid Polymers, Wiley, London.1971.

6 Lockett F.J. and Turner S., J.Mech.Phys.Solids,19,201,1971.

7 Yannas I.V., J.Polymer Sci.-Macromol.Revs.,9,163,1974.

8 Ward I.M. and Onat E.T., J.Mech.Phys.Solids,11,217,1963.

9 Comninou M. and Yannas I.V., J. Biomech.,9,427,1976.

10 Baer E., Gathercole L.J. and Keller A., In Colston Papers, Structure of Fibrous Biopolymers (ed. Atkins E.D.T. and Keller A.) 26,189,1975. Butterworths, London.

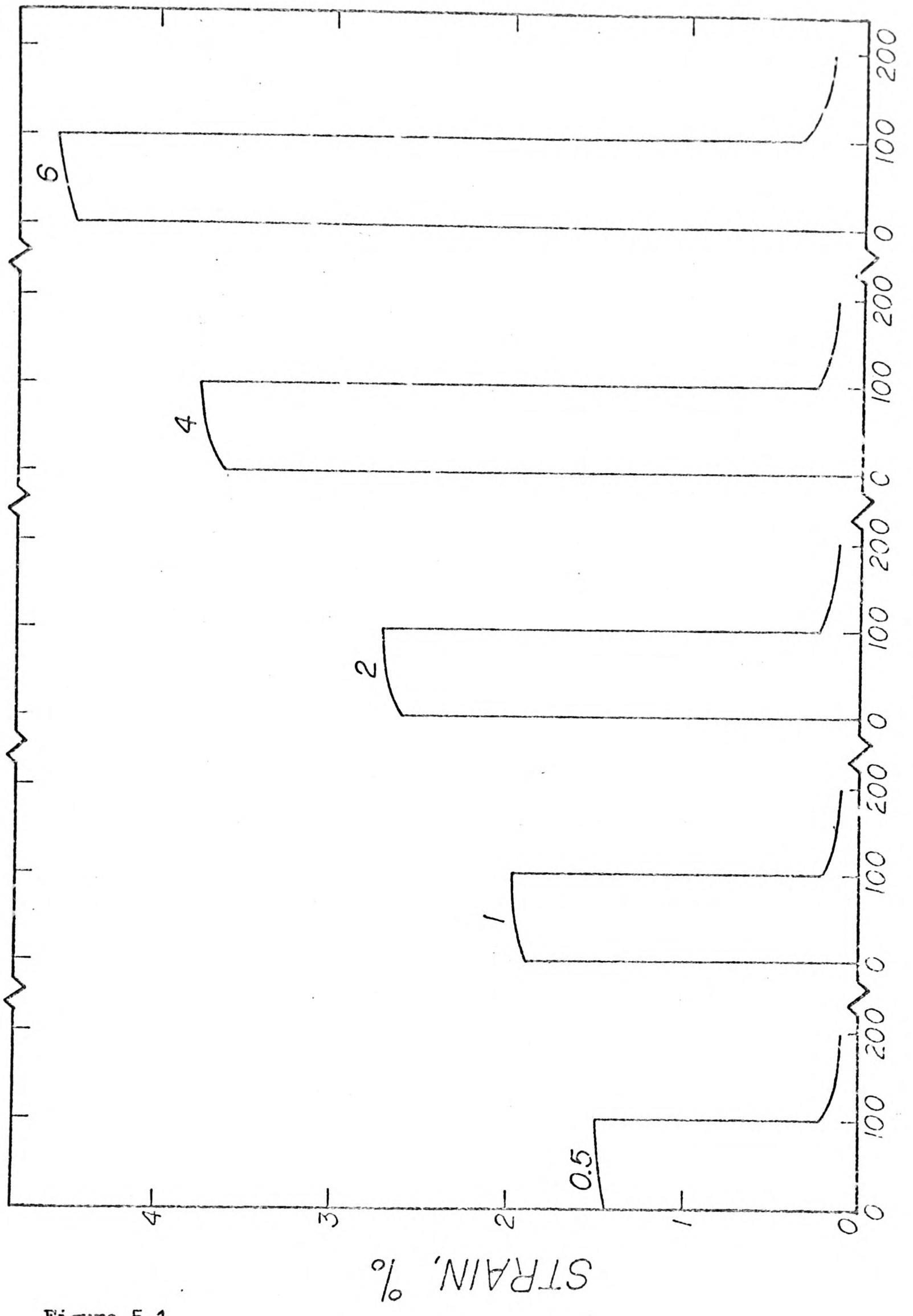


Figure 5-1

Dependence of strain on time in isothermal creep experiments for the various step loads as shown, specimen CH2-16-1(m71,Hfh), T_o = 28 °C, loads are in kg.

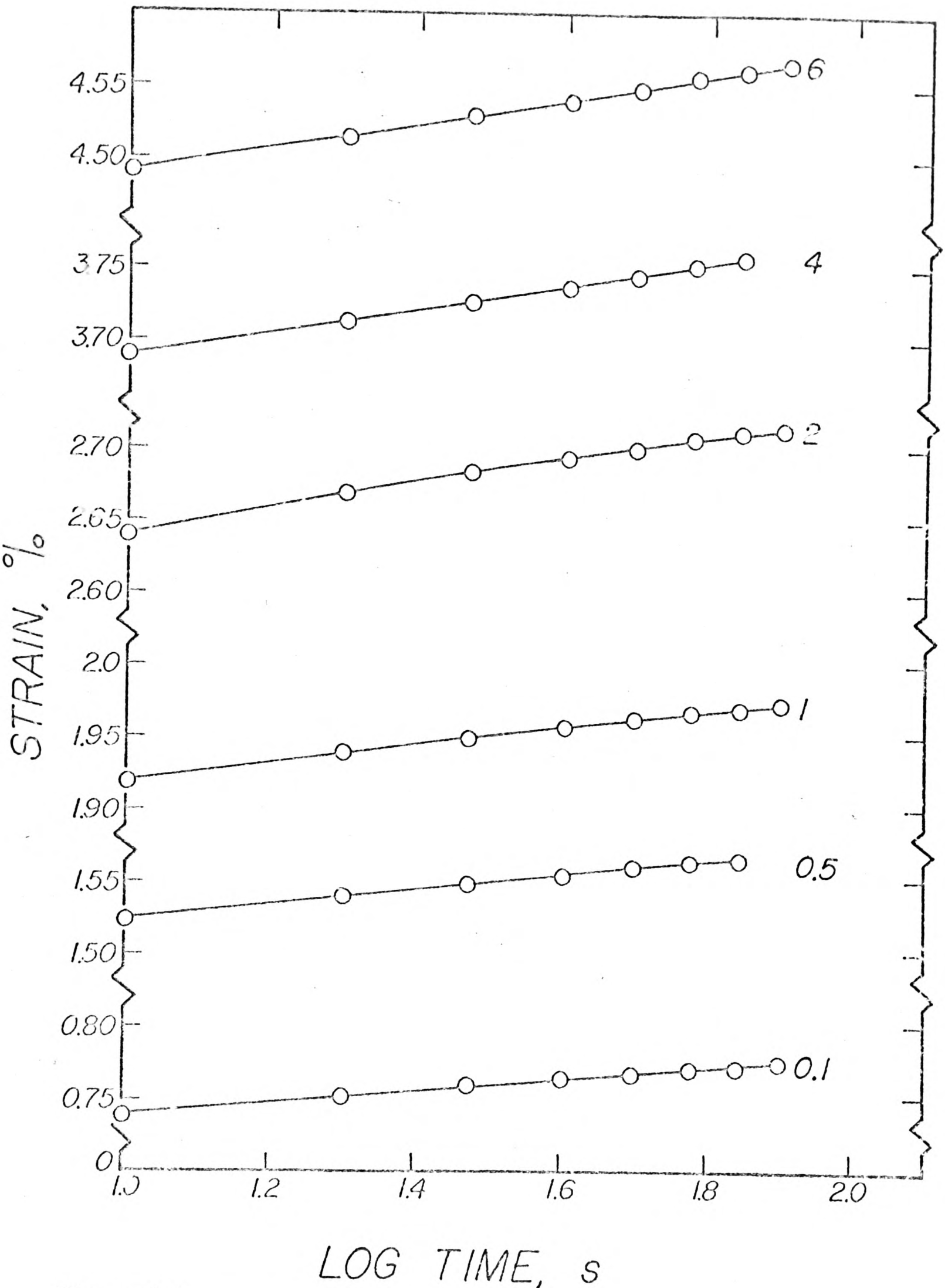


Figure 5-2

Dependence of strain on log time for the experiments shown in figure 5-1, specimen CH2-16-1(m71,Hfh), isothermal creep, loads (in kg) as shown.

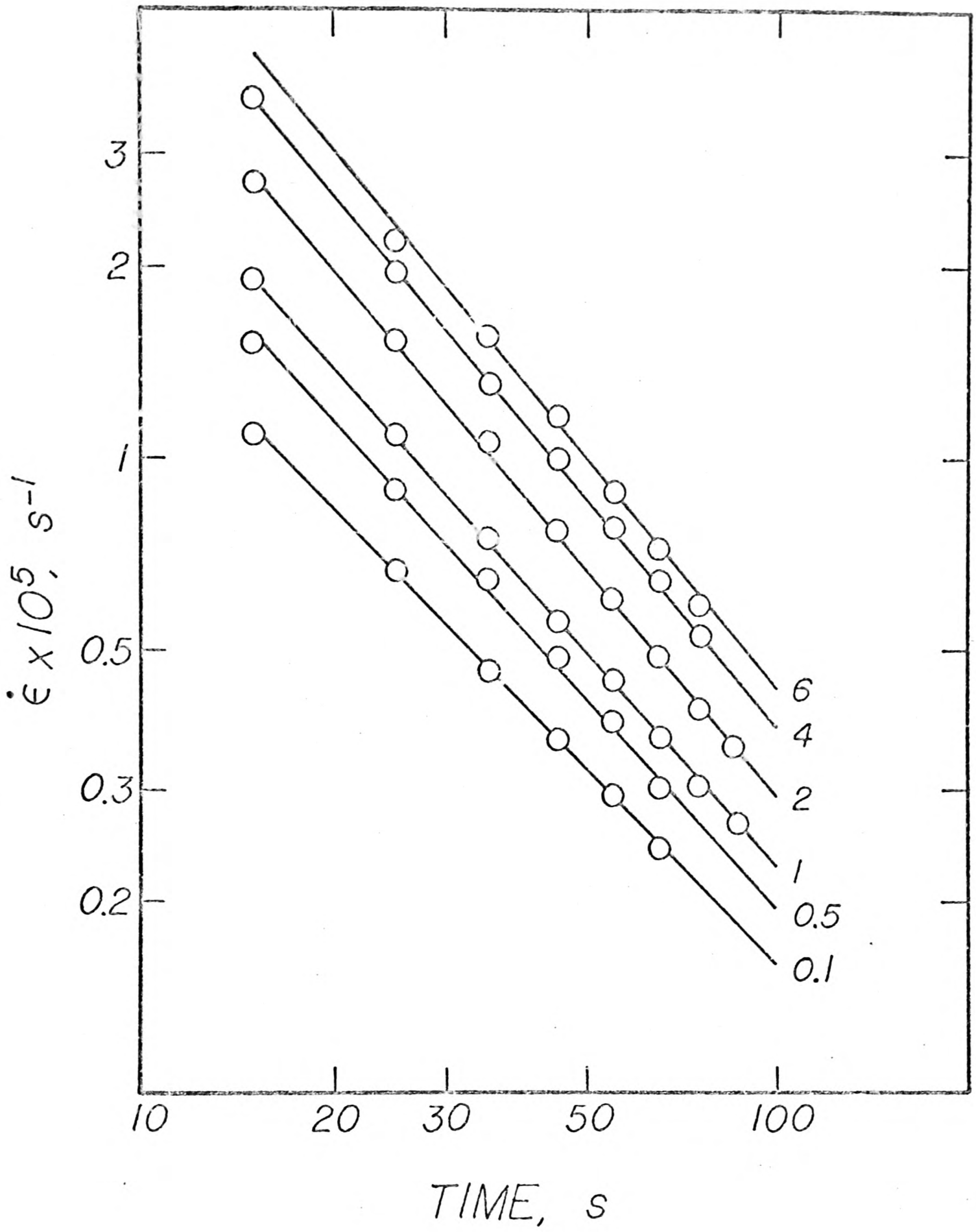


Figure 5-3

Dependence of log (creep rate) on log time for the isothermal creep experiments shown in figure 5-1, for the loads (in kg) as shown. Specimen CH2-16-1(m71.Hfh).

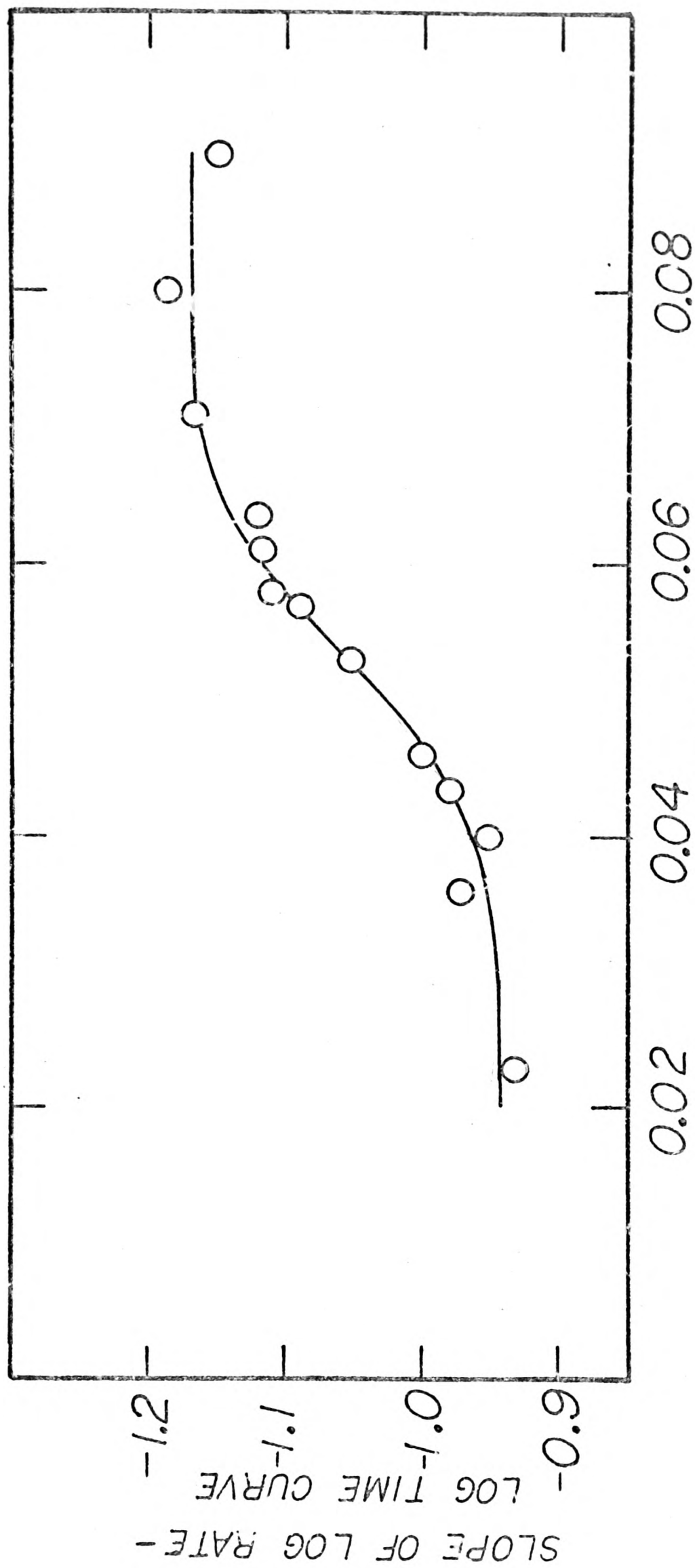


Figure 5-4

Dependence of(the slope of the log rate-log time curves) on 20s strain, specimen CH2-8-2(m23,Heb)

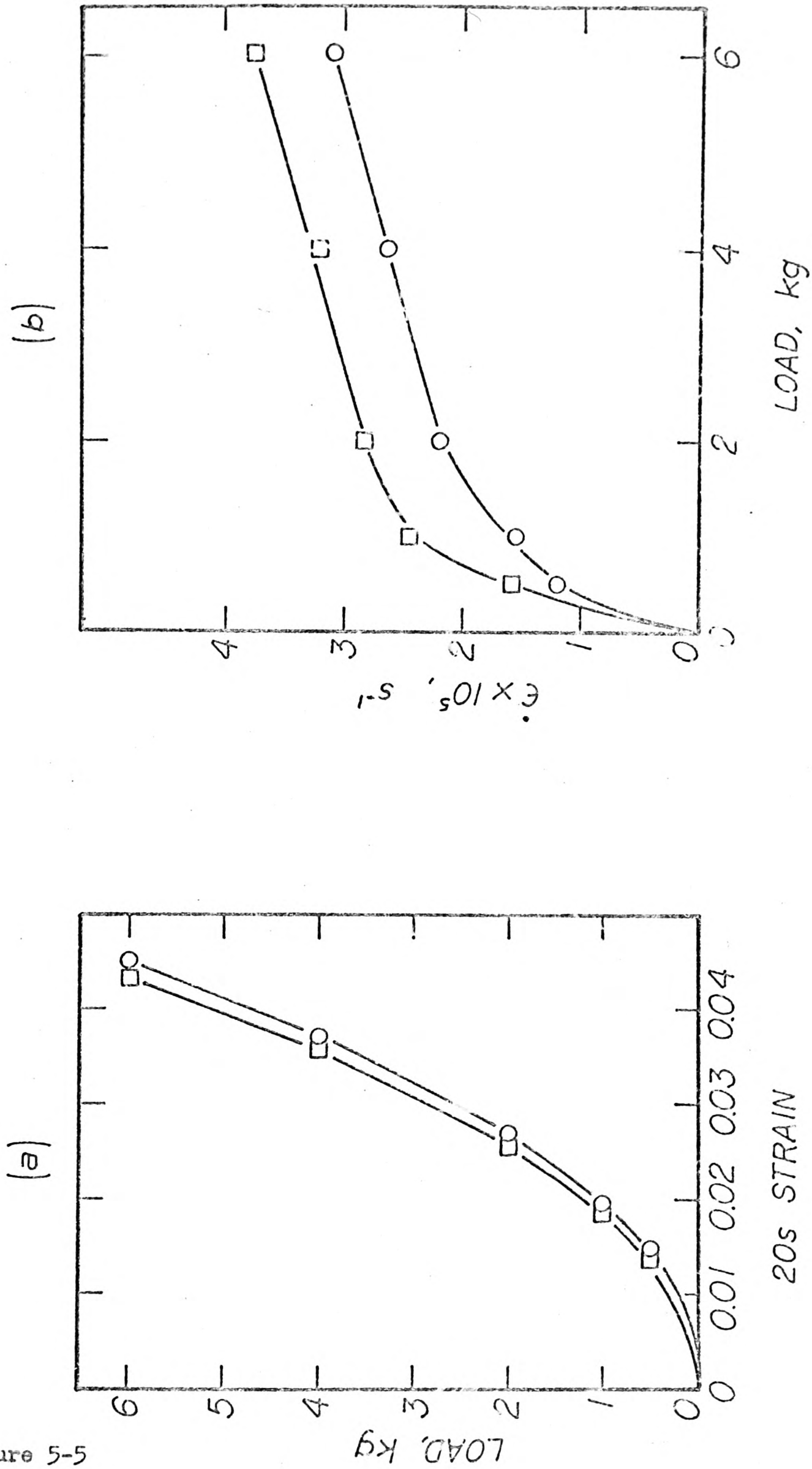


Figure 5-5

a) 20s isochronal load-strain curve
b) 20s isochronal rate-load curve
specimen CH2-16-1(m71,Hfh)
Circled points: creep strain, ϵ_C, and creep rate $\dot{\epsilon}_C$.
Squared points: recovery strain, ϵ_R, and recovery rate, $\dot{\epsilon}_R$.

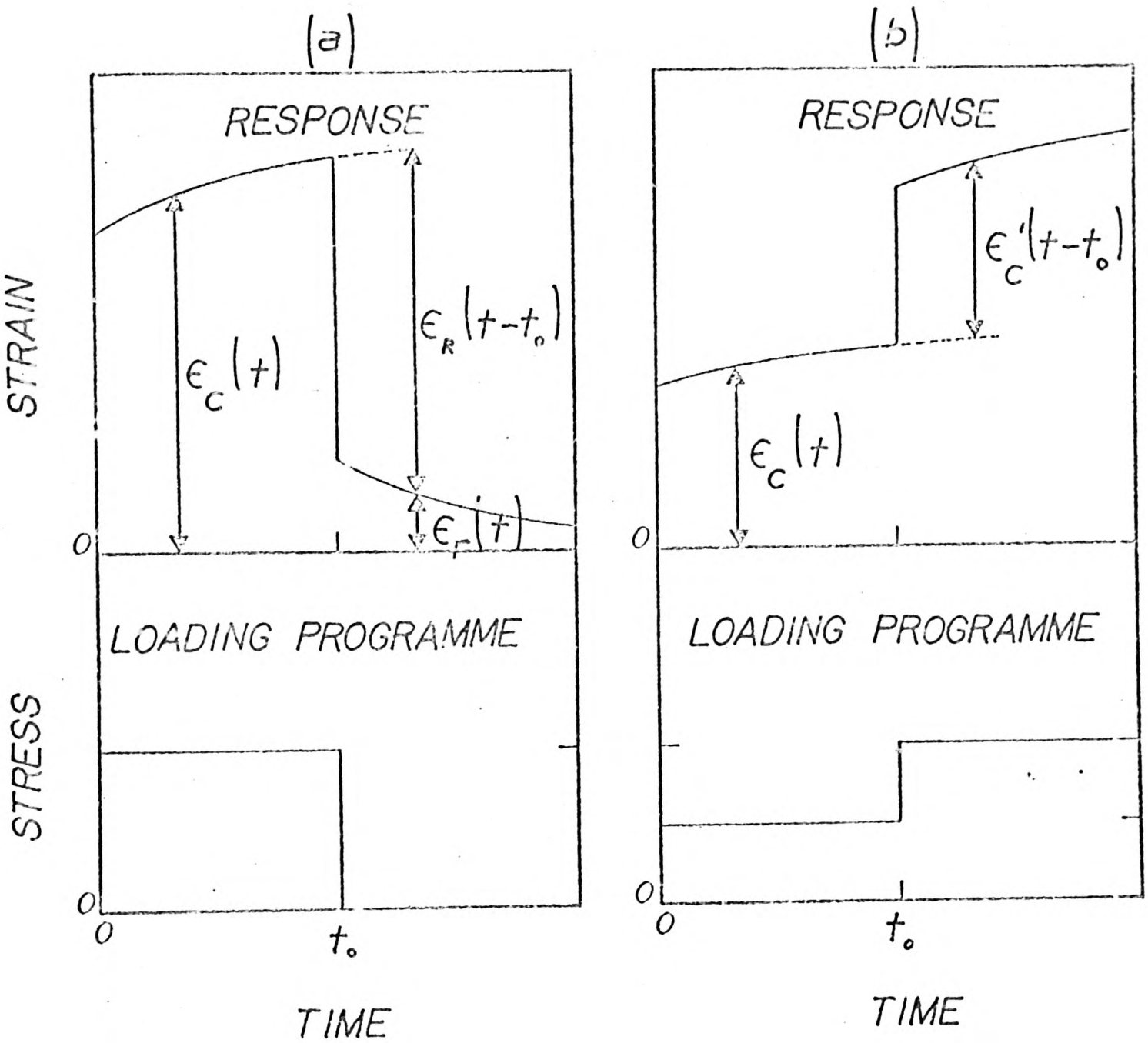


Figure 5-6

Schematic diagram to show the definitions of
a) creep (ϵ_C), residual (ϵ_r) and recovery (ϵ_R) strains for creep recovery experiment.
b) 'additional' strain, (ϵ_C') for the 2-step loading programme.

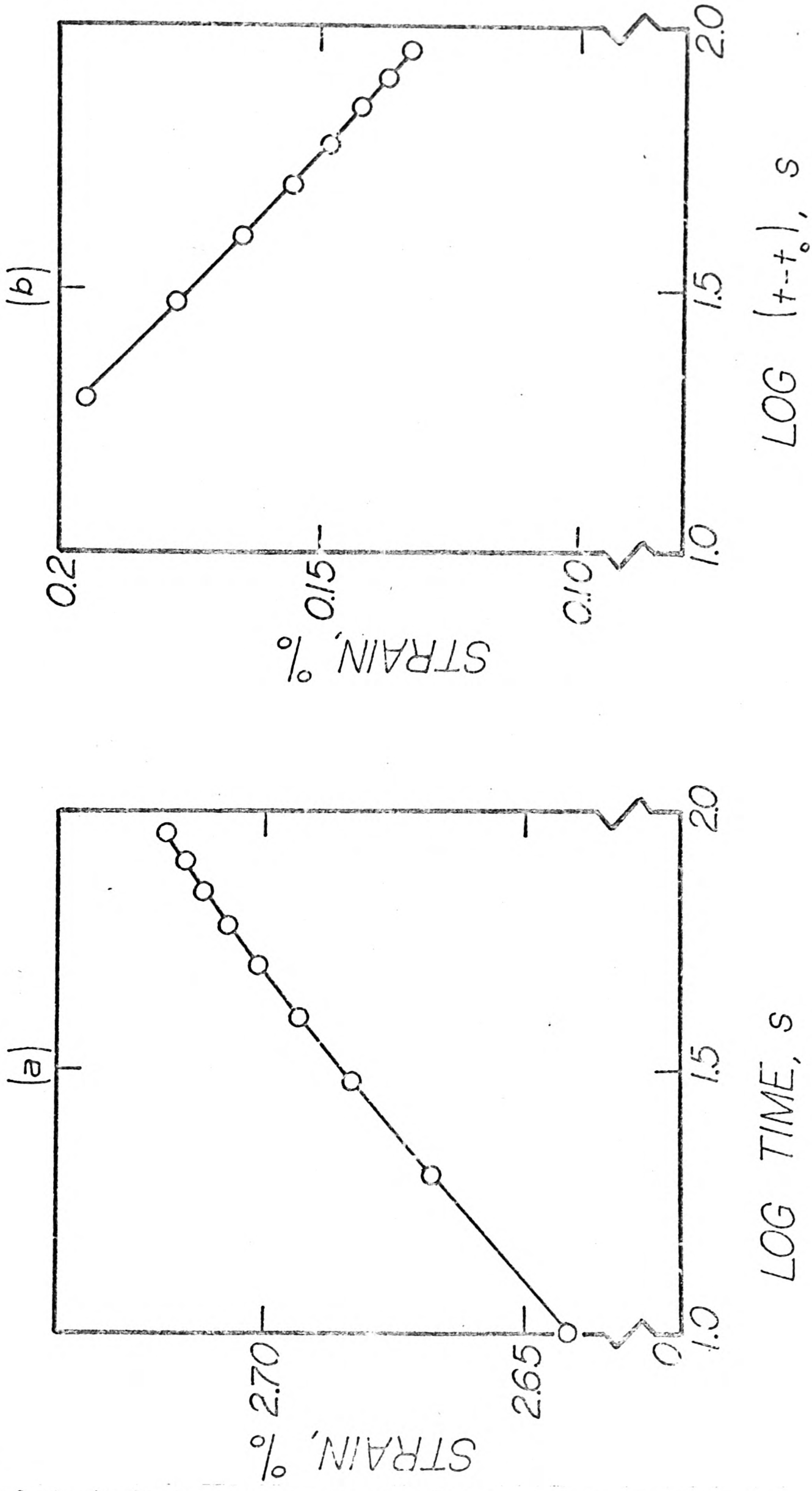


Figure 5-7
Dependence of strain in creep recovery experiment on a) log time during creep and b) log (time after removal of the load), specimen CH2-16-1 (m71,Hfh), load = 2 kg, T_o = 28 °C.

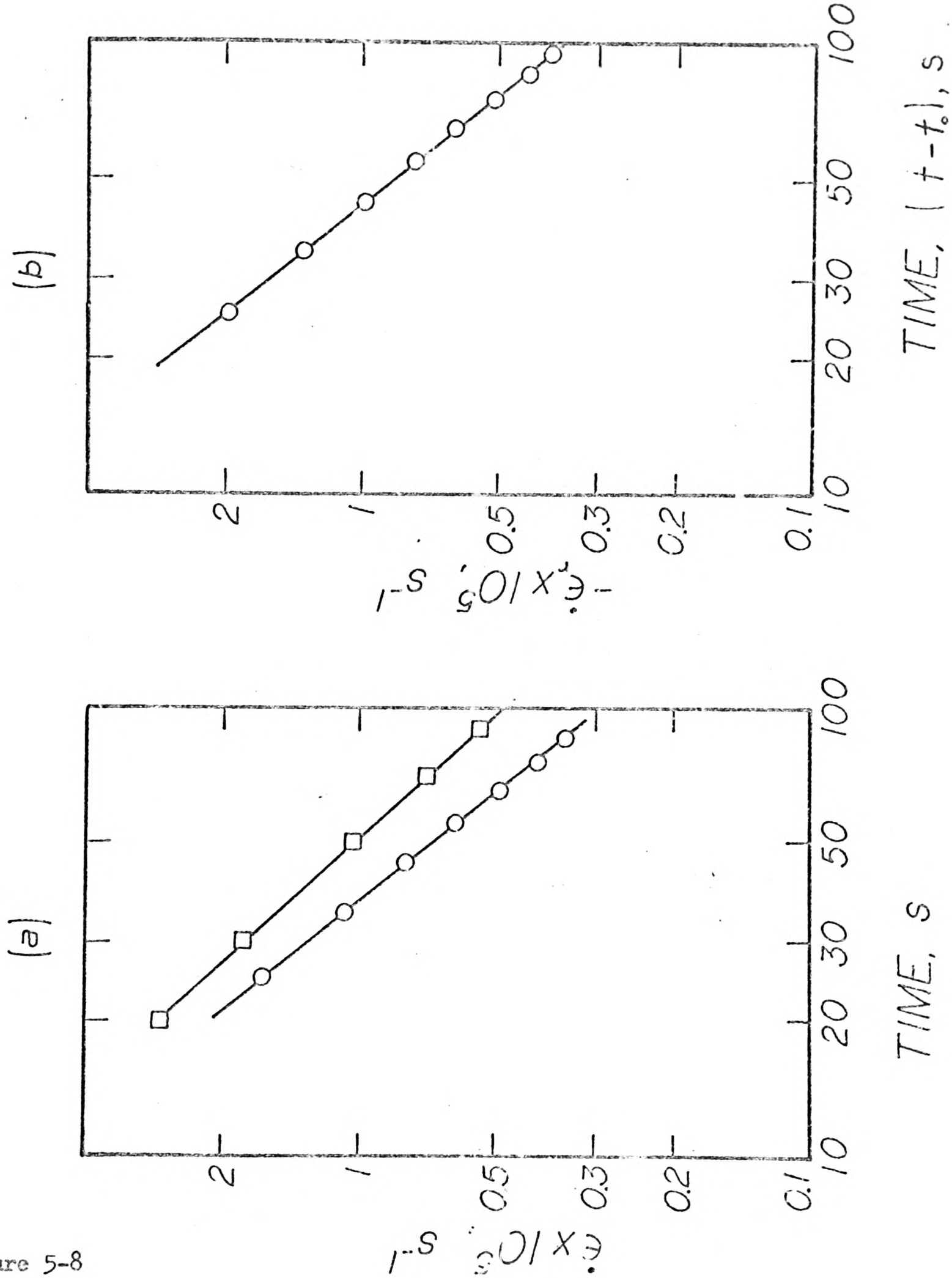


Figure 5-8

Dependence of
a) circled points; log creep rate on log time.
squared points; log (calculated recovery rate) on log time.
b) log (residual rate in recovery, $-\dot{\varepsilon}_r$), on log (time after removal of the load.)
in creep recovery experiment, specimen C52-16-1(m71,Hfb), load = 2 kg.
T_o = 28°C

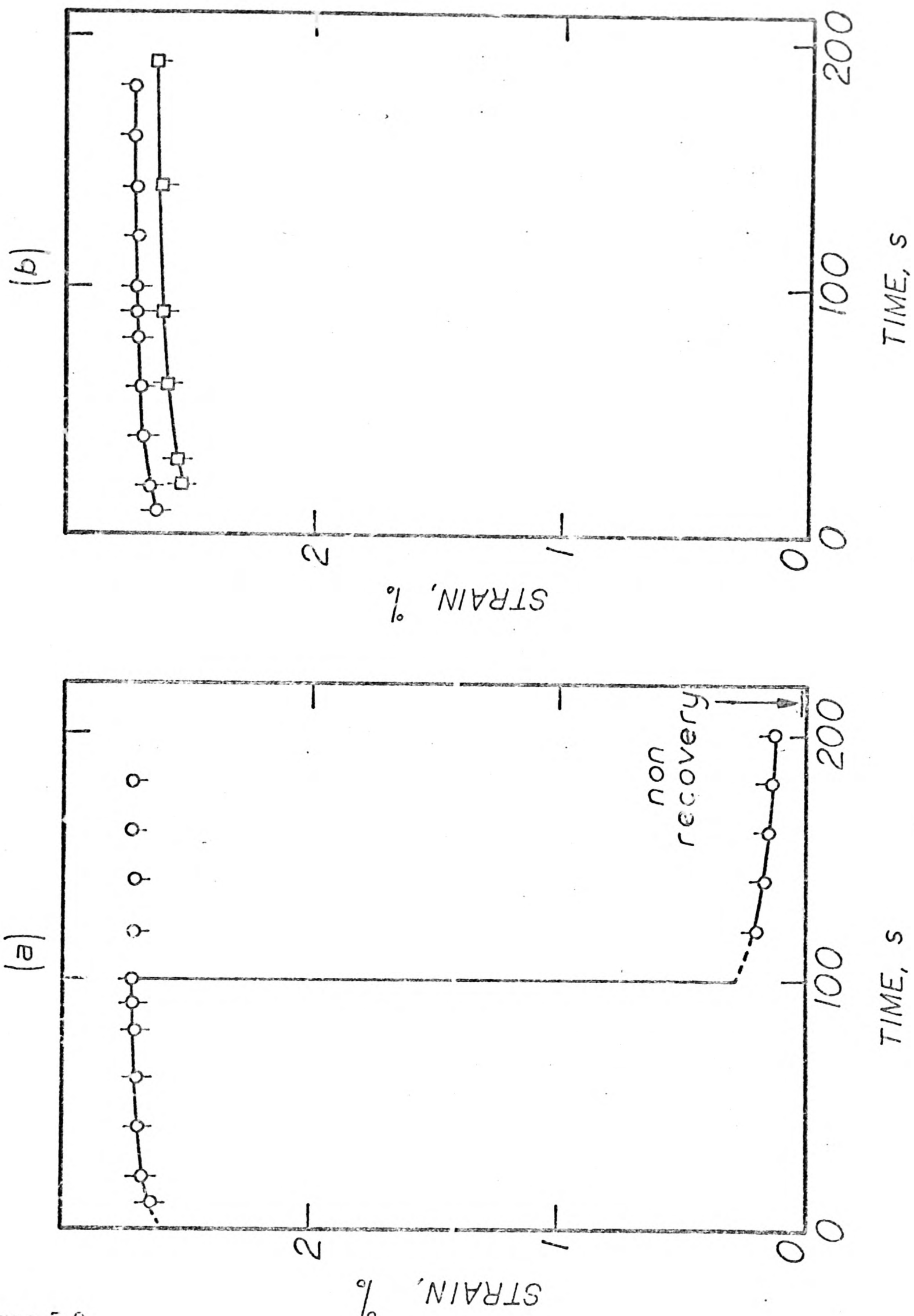


Figure 5-9

Dependence of a) strain on time in creep-recovery experiment and b) creep strain (o) and recovery strain (□) on time.
pip up: load 2 kg, loading time t_o = 100s. pip down: load 2 kg, loading time t_o = 200s. Also shown is the amount of non-recovery after the experiment. specimen CH2-16-1(m71,Hfh).

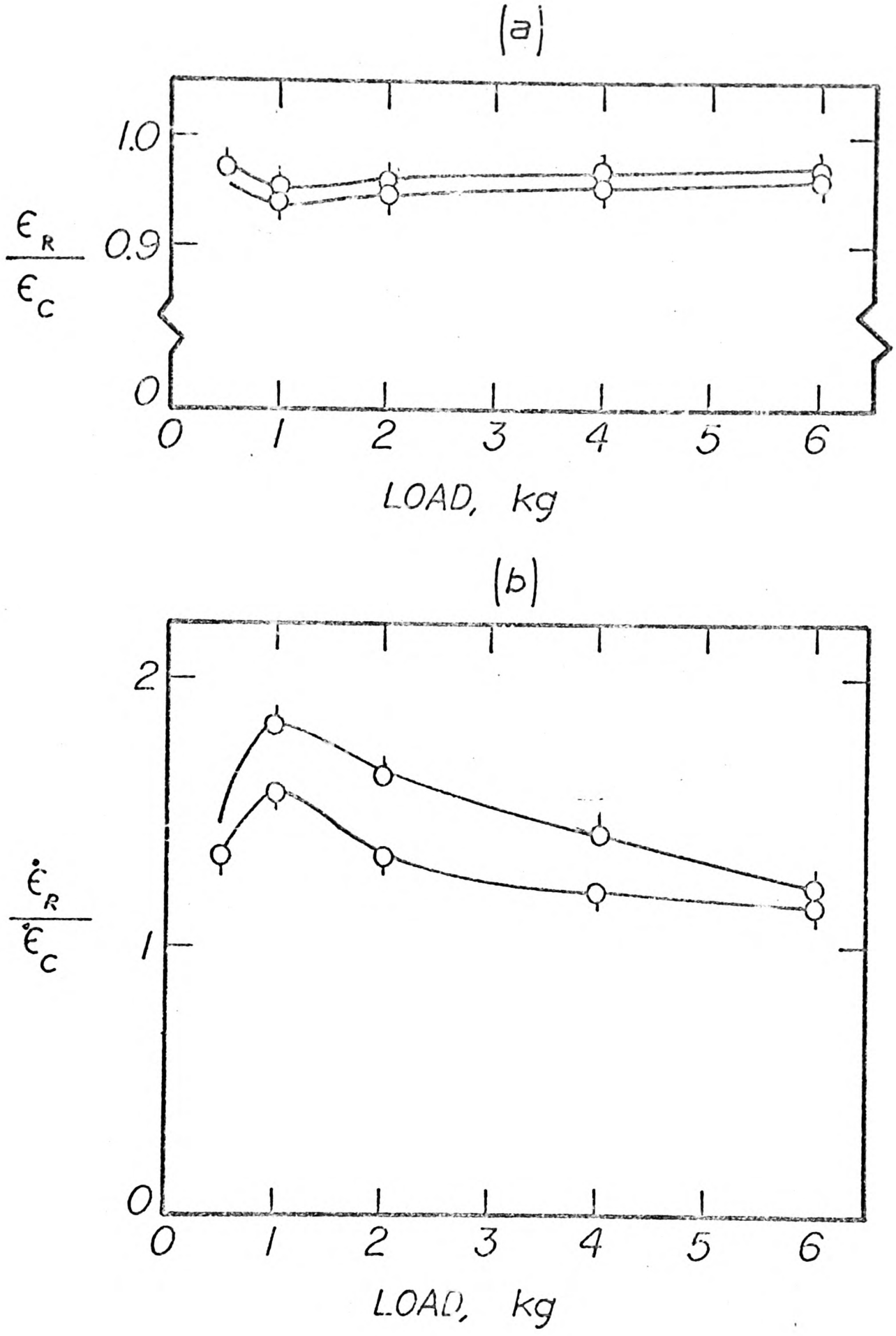


Figure 5-10

Dependence of a) the ratio isochronal ϵ_R/ϵ_C on load
b) the ratio isochronal $\dot{\epsilon}_R/\dot{\epsilon}_C$ on load

♀ t=20s; ♂ t=90s. specimen CH2-16-1(m71,Hfh).

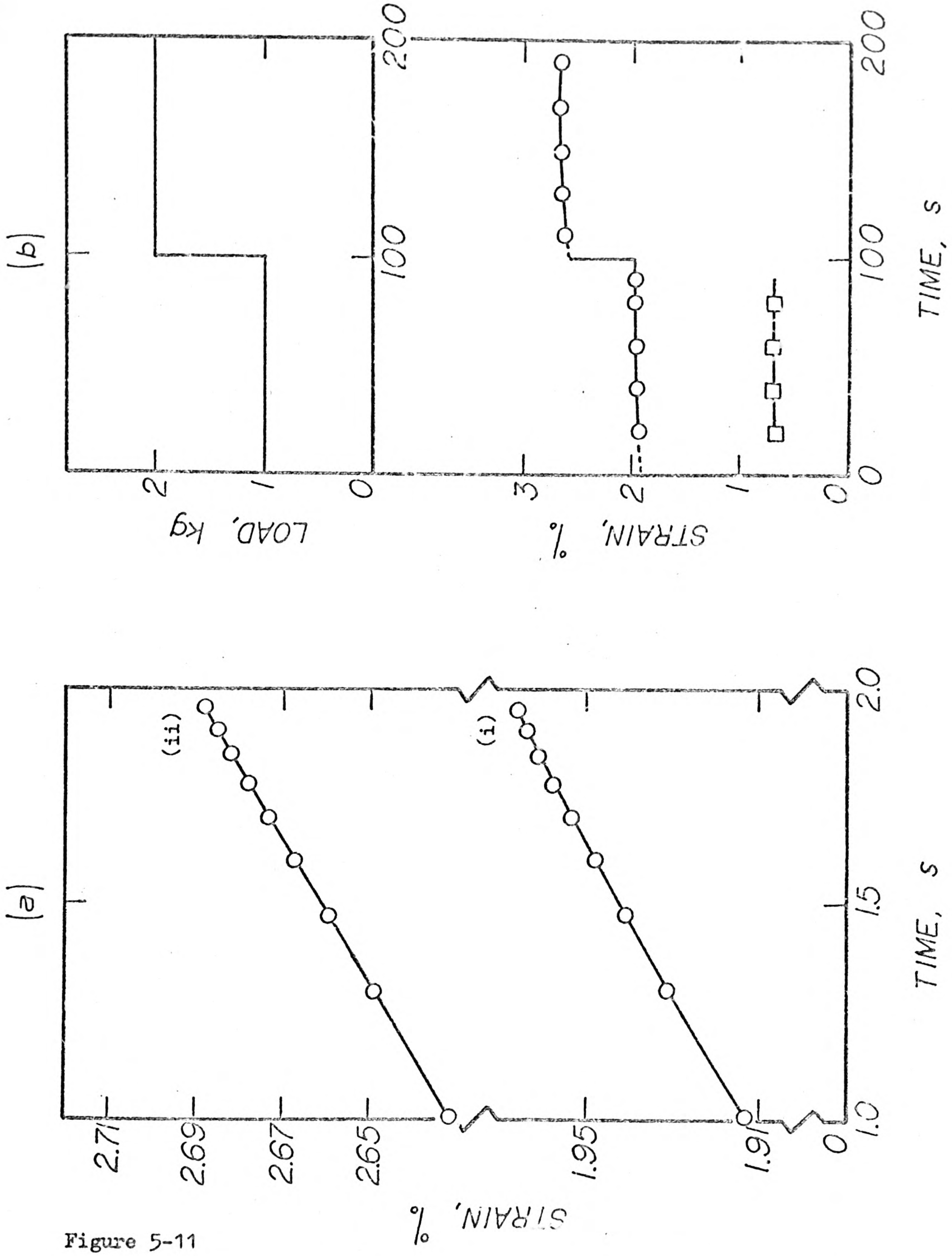


Figure 5-11

a) dependence of creep strain on log time in 2-step loading experiment (i) after first step and (ii) after 2nd step.
b) the loading programme and the creep strain dependence (circled points) on time for the same experiment. Squared points: calculated 'additional' strain.

specimen CH2-16-1(m71,Hfh)

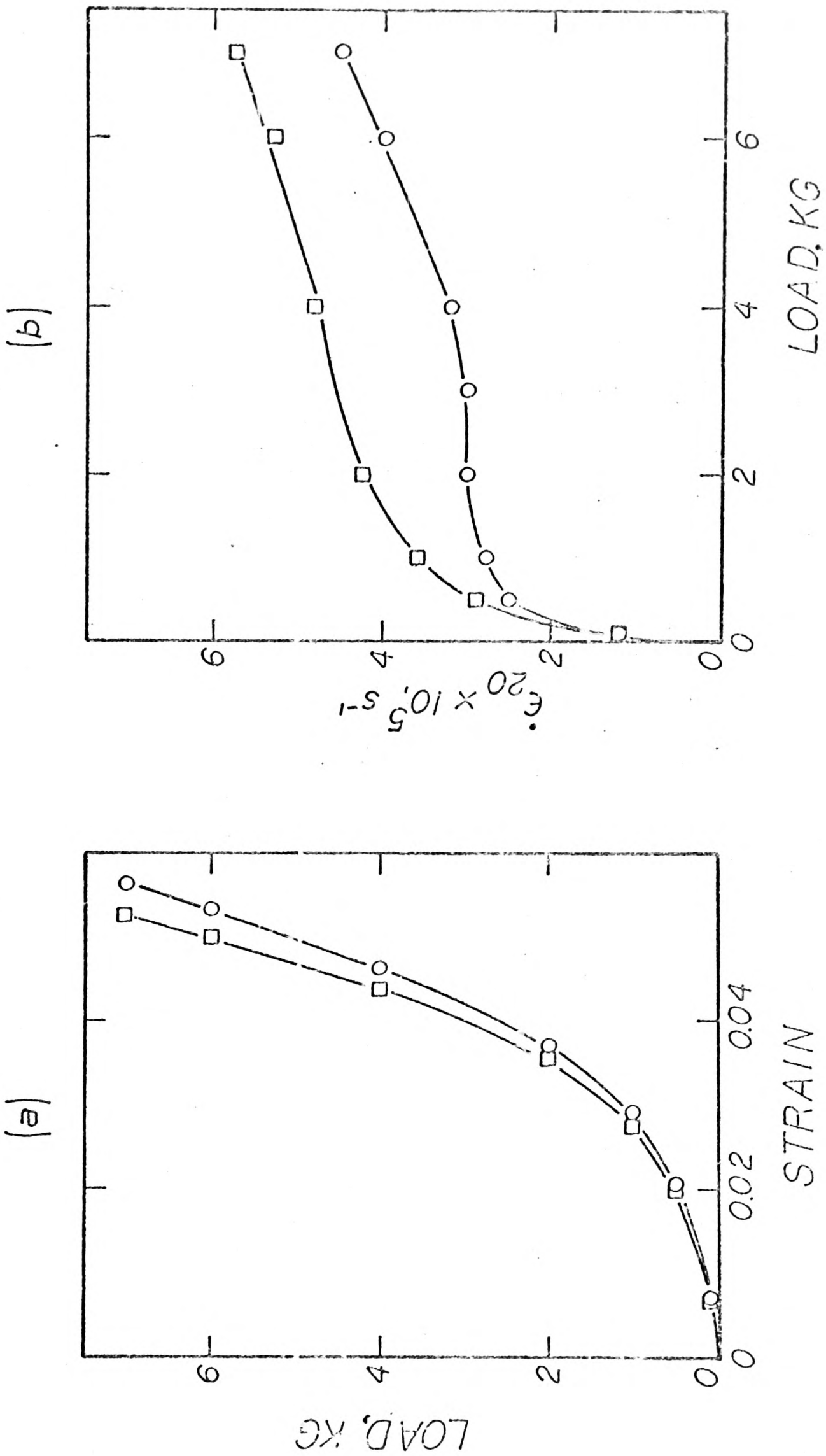


Figure 5-12

a) 20s isochronal load against strain curve
b) 20s isochronal rate against load curve
o creep; □ recovery. Specimen Ch2-16-4(x71,Hfh), t_o= 30s.

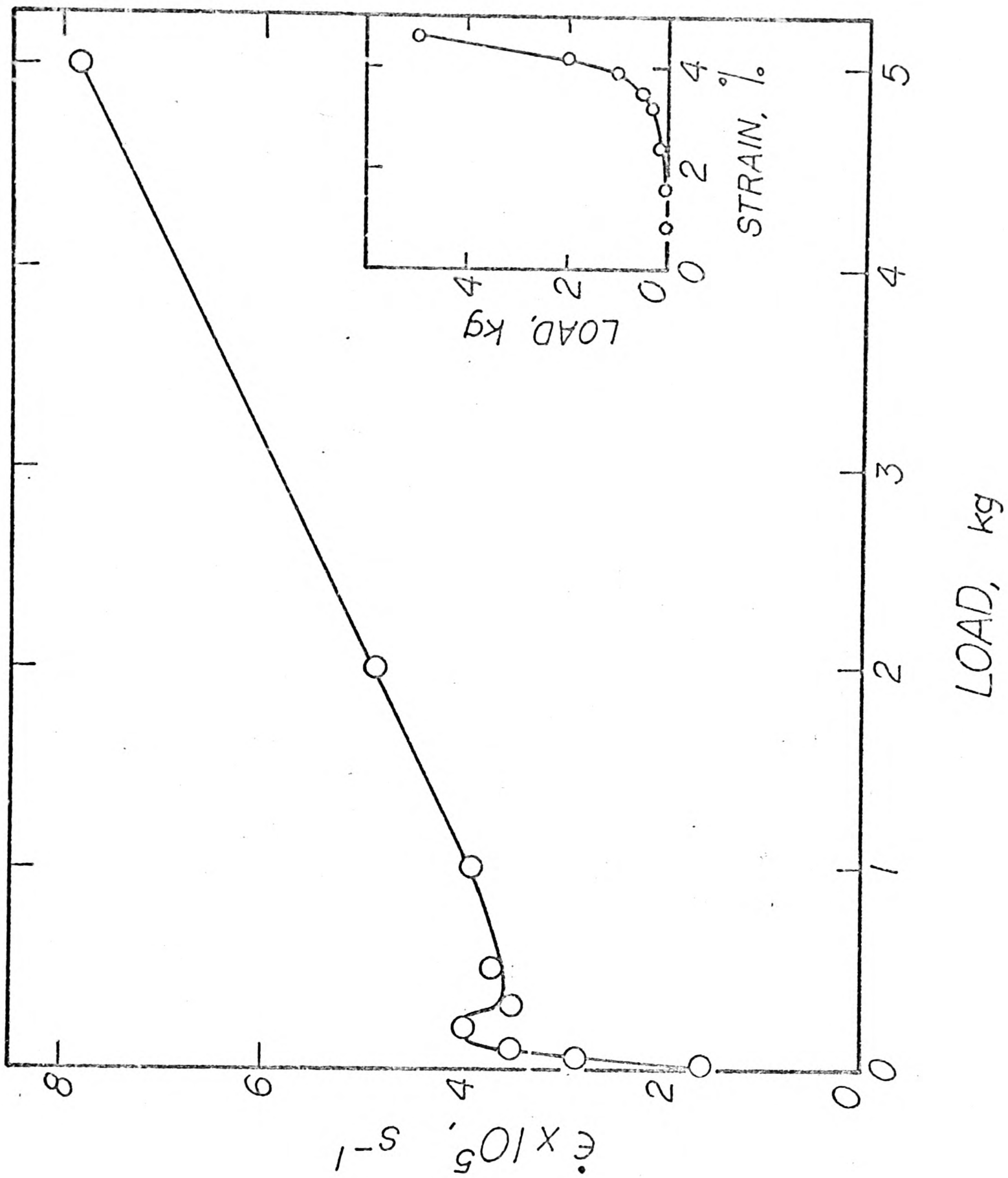


Figure 5-13

Dependence of 20s creep rate on load for specimen CH2-9-1(m77,Hfh), T_o = 28 °C. Inset shows the 20s isochronal load-strain curve.

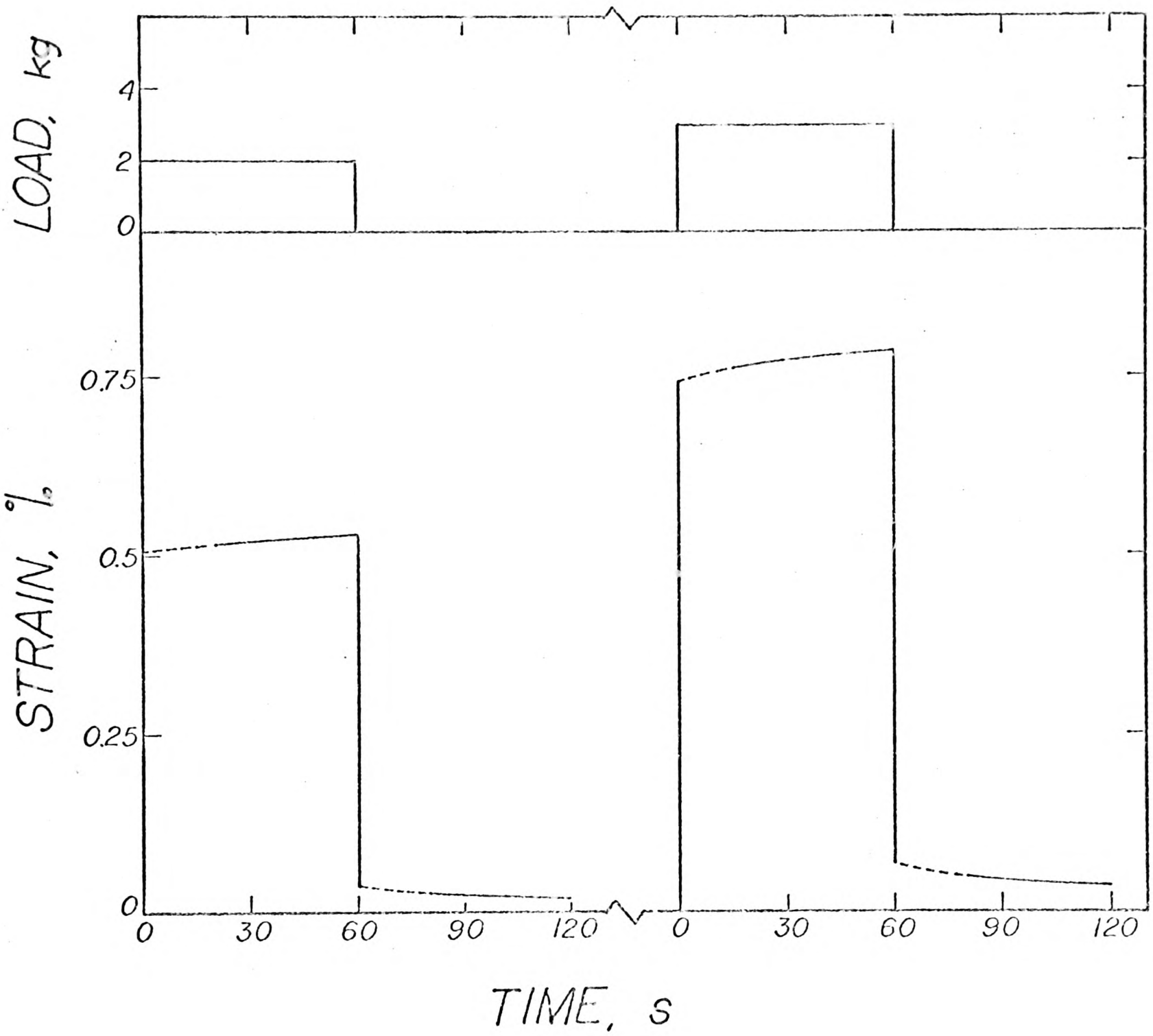


Figure 5-14

Dependence of strain on time for the loading programme shown.
Specimen CH2-16-4(m71,Hfh), preload 3 kg.

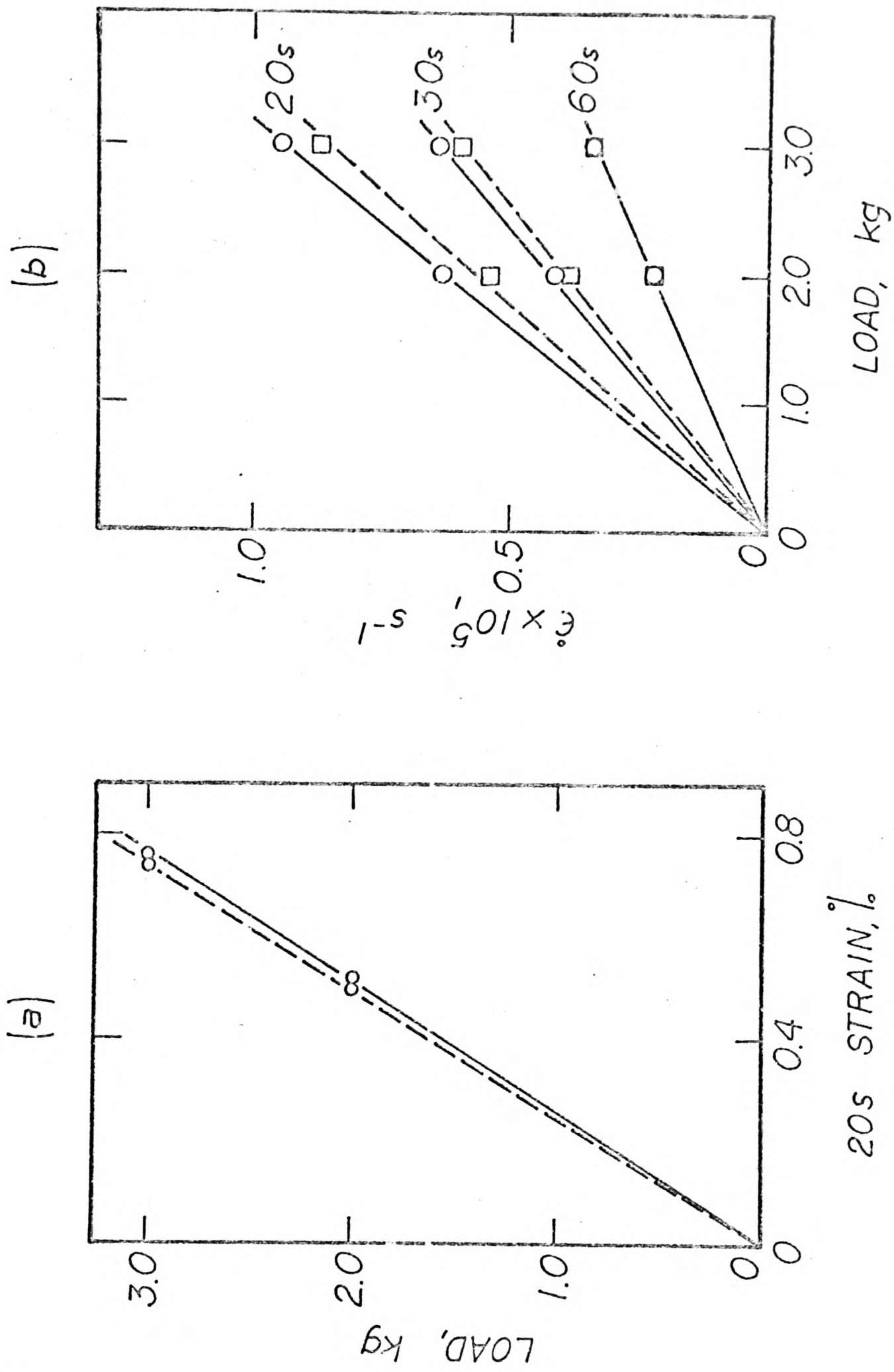


Figure 5-15

a) 20s isochronal load-strain curve
b) 20s isochronal rate against load curve
specimen CH2-16-4(m71,Hfh), preload = 3kg, T_o=28 °C,
——— creep; ---- recovery

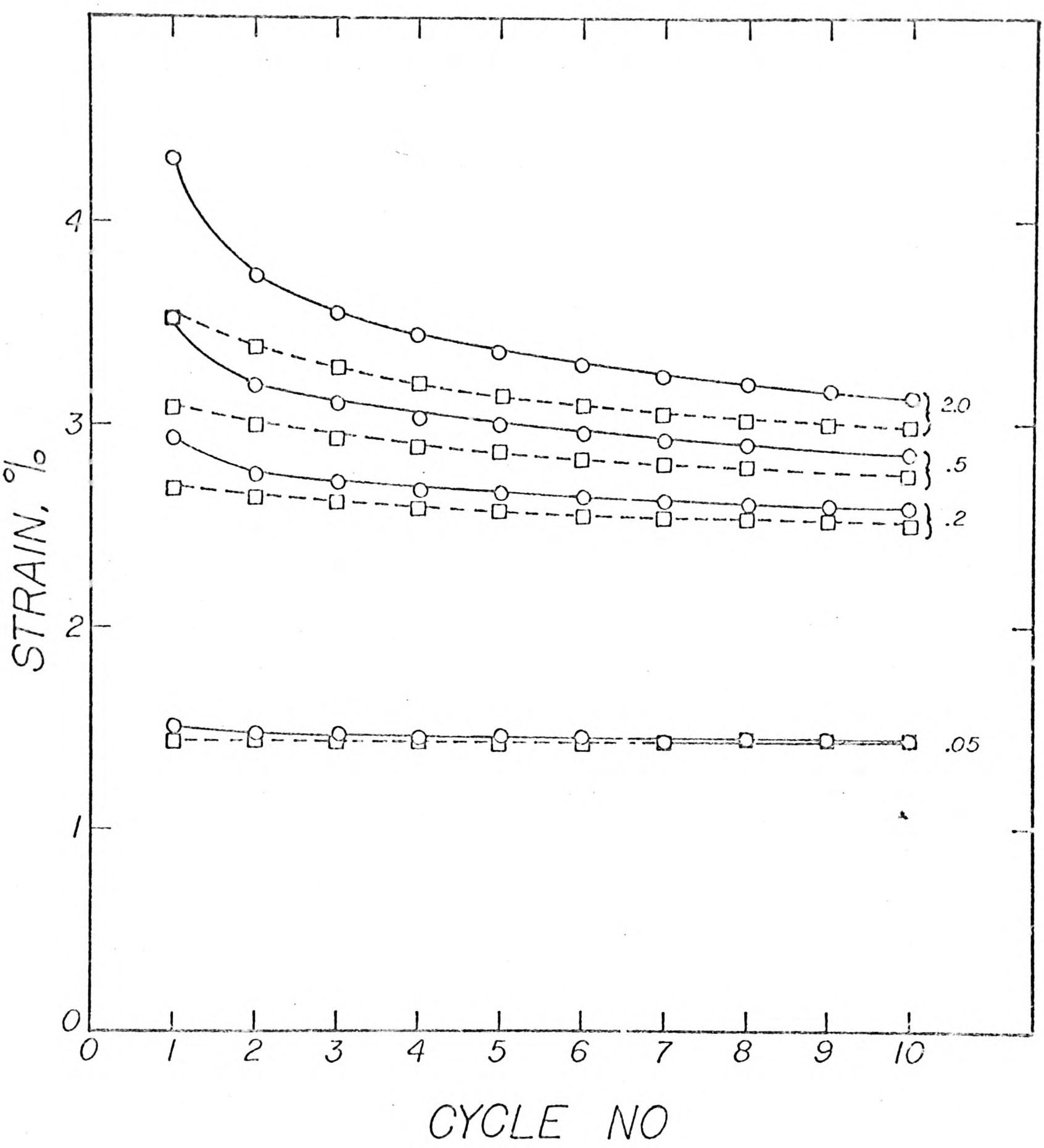


Figure 5-16

Dependence of 20s strain on the number of cycles in creep cycling experiments for various loads as shown, specimen CH2-9-1(m77,Hfh). o creep strain, ϵ_C; □ recovery strain, ϵ_R. loads are in kg.

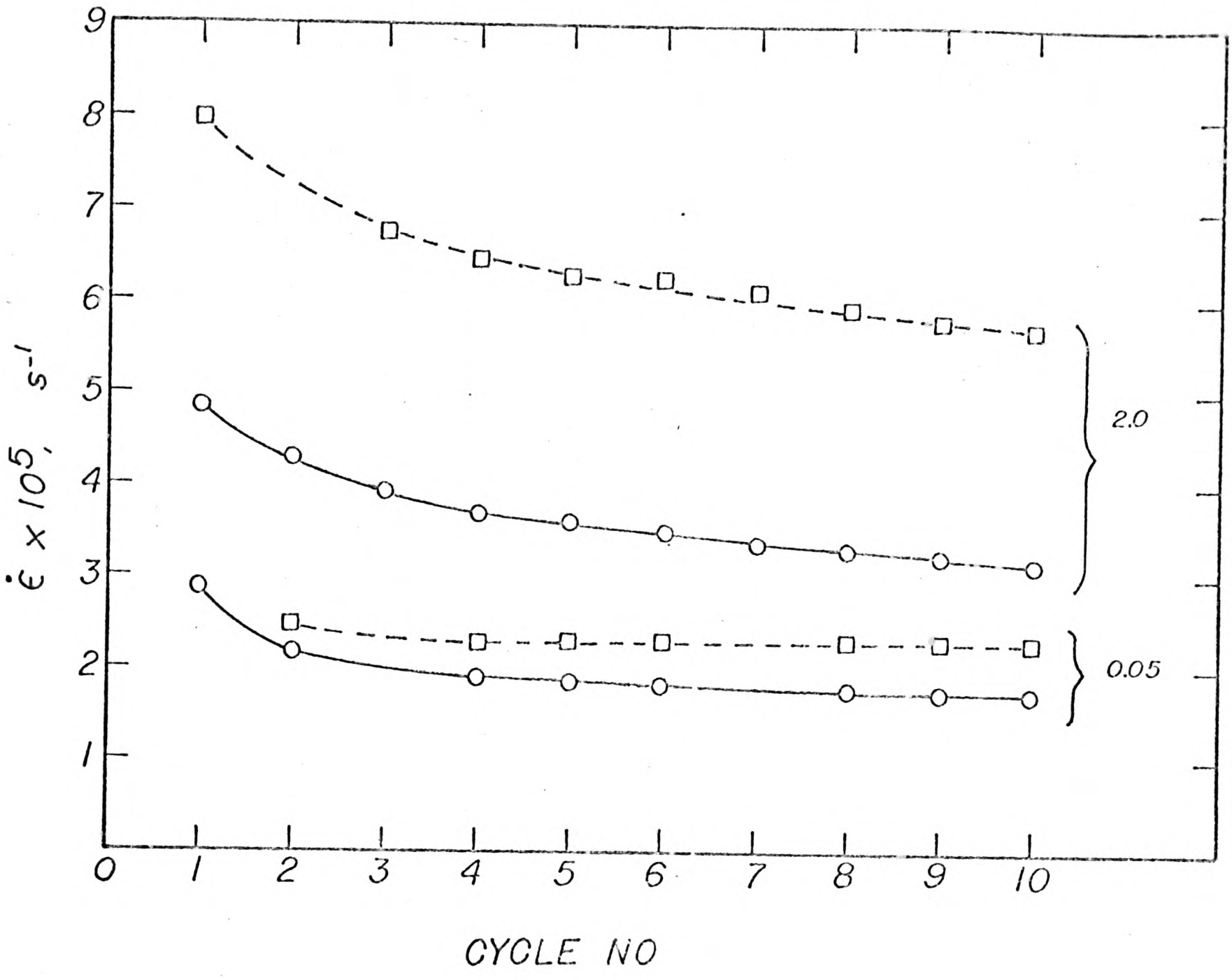


Figure 5-17

Dependence of 20s rate on the number of cycles in creep cycling experiments for various loads as shown, specimen CH2-9-1 (m77, H6b)
o creep rate, $\dot{\epsilon}_C$; □ recovery rate, $\dot{\epsilon}_R$. loads are in kg.

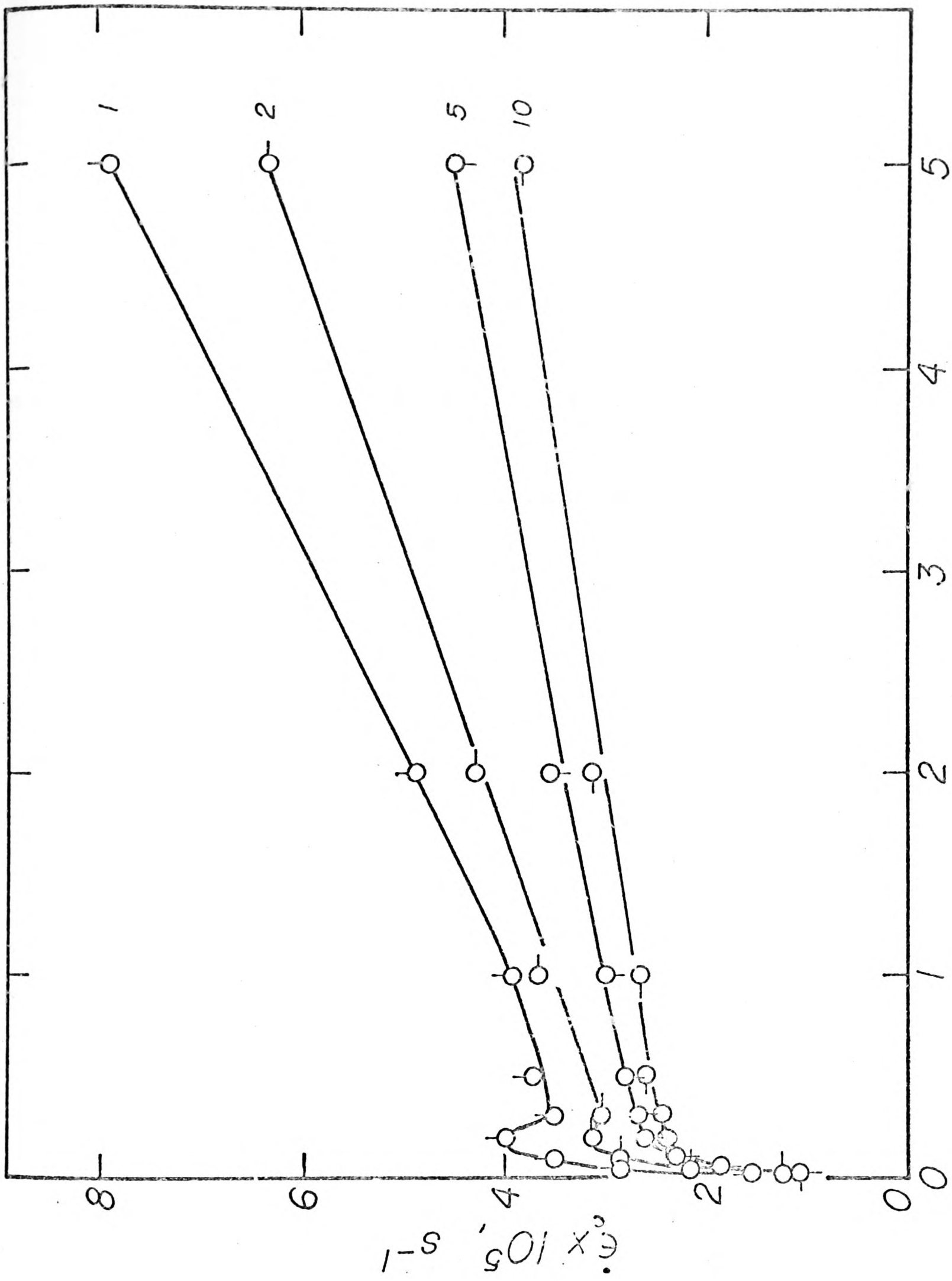


Figure 5-18

Dependence of 20s creep rate, $\dot{\varepsilon}_c$, on load for various cycles, specimen CH2-9-1(m77,Hfh).
♂ 1st; o- 2nd; ♀ 5th; -o 10th cycle.

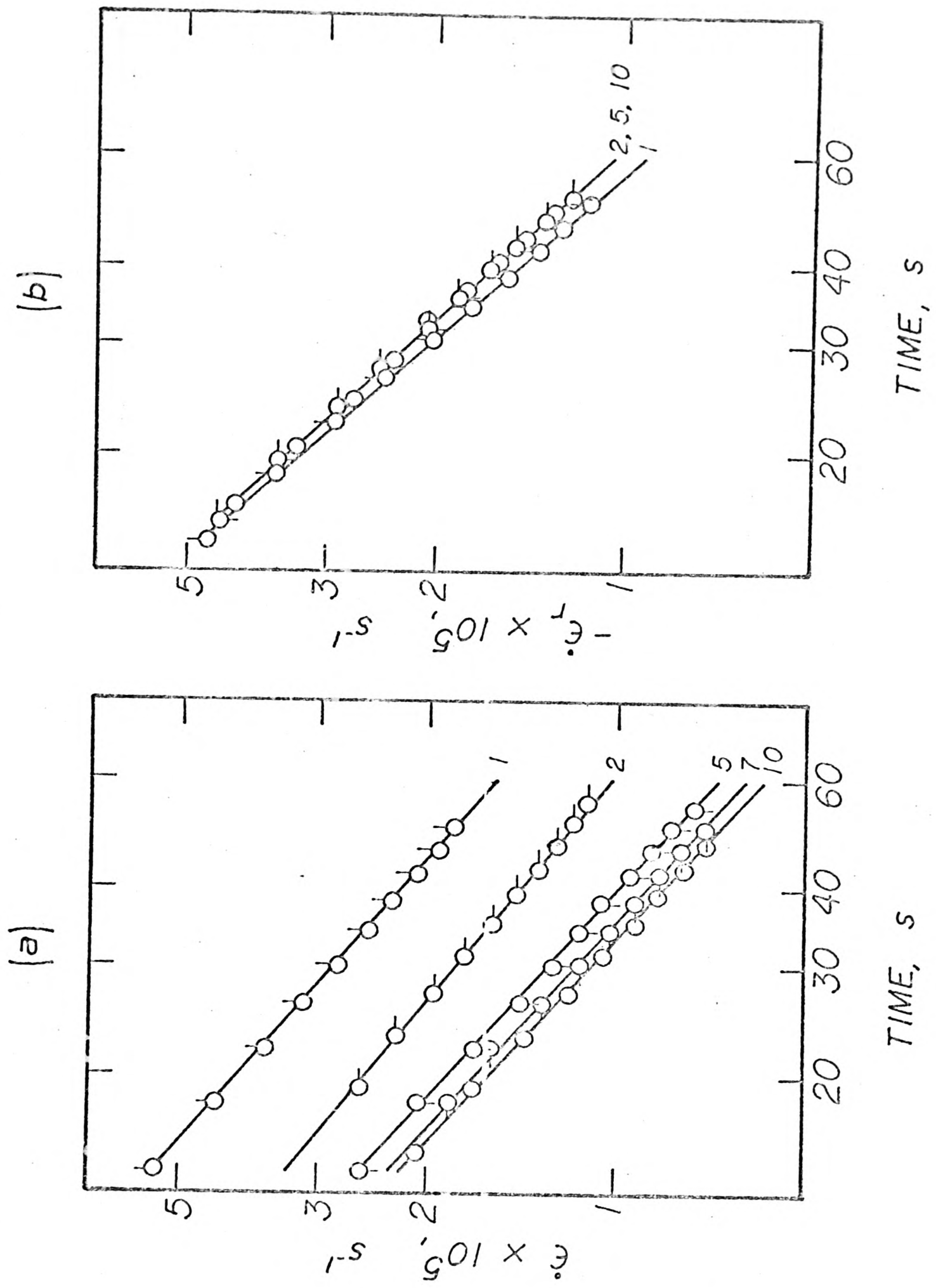


Figure 5-19

Experimental data in creep cycling experiments for the dependence of a) log (creep rate) on log (time after the application of the load) and b) log (residual rate) on log (time after removal of the load) for the number of cycles shown, loading time = 60s, specimen CH2-9-1 (m77,Hfh), load = 200 gm.

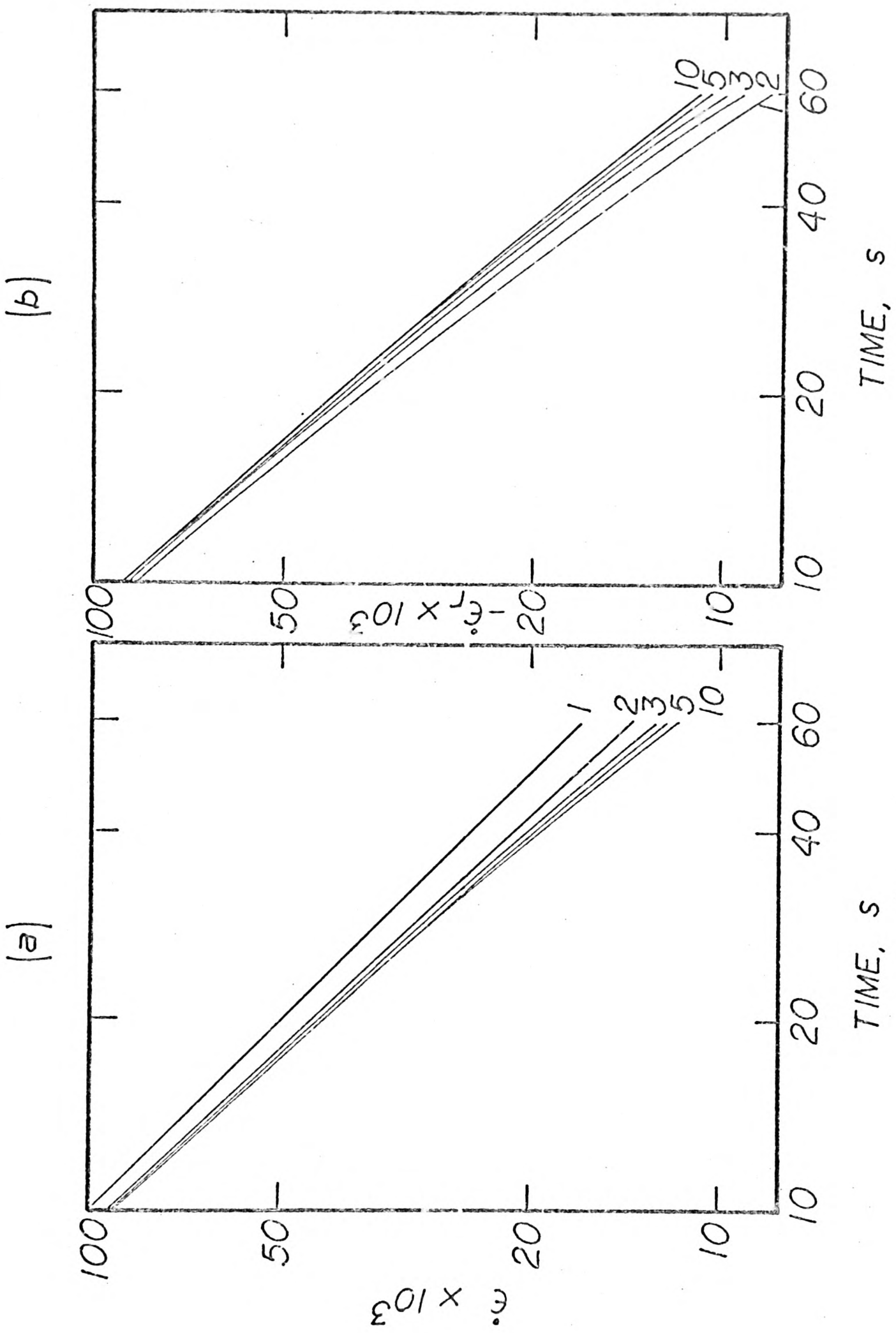


Figure 5-20

Theoretical dependence of
a) log (creep rate) on log (time after the application of the load) and
b) log (residual rate) on log (time after removal of the load)
for creep cycling experiments for the number of cycles shown,
loading time = 60s, n = C = 1.

Chapter 6

The Non-isothermal Viscoelastic Behaviour of Tendon in Creep

6.1 Introduction

We have dealt so far with the isothermal creep behaviour of tendon at 28°C under various loads from the 'toe' region to the 'linear' region of the stress-strain curve. i.e. in the normal operating range of the tendon in vivo. We can now turn our attention to the thermorheological properties of the tendon. Why is there a need for this information?. In the previous chapter, all the data suggests that two types of deformation may be occurring. Further than that it is difficult to know what the mechanism of the deformation might be. This is where the non-isothermal viscoelastic behaviour becomes useful and in particular the T-jump experiment. Each mechanism of deformation will have a temperature dependence, the magnitude of which is given by the a_T time-temperature shift factor, which can be related to the activation energy, ΔH_a, by the Arrhenius equation(3.4). If we find two widely different temperature dependences in the two deformation regions of tendon at the high and low loads, then we can clearly say that there are different deformation processes taking place in these two regions. The form of the temperature dependence,(i.e the values of ΔH_a) for the two mechanisms will give us an indication of the type of mechanism occurring.

In order to determine the apparent activation energy of the deformation process for tendon, we employed both the T-jump technique[1] and the method of time-temperature superposition.[2] It was found that the T-jump method was a far superior technique. A critical examination of the reproducibility required to give good data for time-temperature superposition revealed the worthlessness of this technique for tendon. Creep T-jumps were performed to determine the value of ΔH_a in the 'toe' and 'linear' regions of the stress-strain curve for a variety of specimens. Recovery T-jumps were conducted to find the activation energy for the recovery process and

to ascertain if there was any significant b_T effect in the creep data. Creep T-jumps were also performed on a preloaded tendon and a sample of collagen tape to obtain the value of ΔH_a for the collagen fibres. Finally the T-jump technique was used to obtain the value of ΔH_a for a denatured tendon specimen, i.e. one which was composed mainly of gelatin.

6.2 The Apparent Activation Energy, ΔH_a, for Tendon.

6.2.1 ΔH_a in the 'Toe' Region

a) The T-jump Experiment

We will first consider the temperature dependence of the deformation of tendon in the 'toe' region using the T-jump experiment. The isochronal load-20s strain curve was obtained for specimen CH2-O-1(m21,Hfh) as shown in figure 6-1. From this curve, the load to be used for the T-jumps was determined and was chosen as 0.76 kg, i.e. at a point within the 'toe' region but large enough that the rate would be high enough to obtain accurate extrapolation of the T-jump data. A series of T-jumps were performed on this specimen at the load 0.76 kg for various values of ΔT, with T_o=28 °C and t'=60s. Sufficient time was allowed for recovery and the specimen was annealed at 34 °C between experiments. The natural logarithm of the ratio of the rates at t', (ln r), determined for each T-jump by the method of extrapolation outlined in chapter 2 is shown in figure 6-2. It is seen that the points lie on a straight line, the best fit of which was found by least squares. The value obtained for the slope in this way gave a value of $\Delta H_a = 12 \pm 1.5$ kcal/mol.

A second series of T-jump experiments was performed to determine whether ΔH_a was dependent on certain experimental variables, namely the concentration of NaCl in the thermostating fluid, or the period of immersion of the specimen. The same tendon was immersed in distilled water (pH 6) at 28 °C and on the first day, 8 T-jumps were performed at the same load

0.76 kg and 8 determinations of ln r were obtained. One determination of ln r for a particular value of ΔT was made per day on the next seven days with the specimen continuously immersed in distilled water. Figure 6-3 shows a plot of these values of ln r against ΔT for these eight days. It can be seen that the points again fall approximately on a straight line and yield a value of ΔH_a=12 kcal/mol.

The effect of age of the specimens on the value of ΔH_a was also considered. The results of the T-jumps performed on specimen CH2-2-1 (f89,Heh) and CH2-1-1(m55,Heh) are shown in figure 6-4 along with those found earlier for the specimen CH2-0-1(m21,Hfh). No difference in the value of ΔH_a can be discerned, indicating that the mechanism of deformation does not change with age. Experiments were also performed on these samples to determine whether ΔH_a was a strong function of temperature. Data were obtained for specimens CH2-0-1(m21,Hfh) with T_o=10 °C, for CH2-1-1(m55,Heh) with T_o=1.3 °C and for CH2-2-1(f89,Heh) with T_o=0.8 °C. The resulting ln r- ΔT plots were all straight lines, the values of ΔH_a obtained from the slopes being equal to 13.5, 10.0 and 10.0 kcal/mol respectively. Hence ΔH_a is a weak function of temperature which is to be expected and is useful for biological purposes.

Creep T-jumps were also performed on bovine deep flexor tendon (specimen BT2) to see if the source of the tendon made any difference to the value of ΔH_a. The ln r- ΔT plot is shown in figure 6-5 for a load of 0.8 kg and T_o=28 °C. The value of the best straight line through the points is ΔH_a=14.5 $\pm$ 1.5 kcal/mol.*

---

* It has been reported earlier that ΔH_a for the bovine tendon was equal to 20 kcal/mol.[3] An error had been made in this calculation. The creep rates were not corrected for thermal expansion in the earlier evaluation, and since the creep rates were lower for this tendon than had been previously seen for other tendons, this introduced an error of ~5 kcal/mol.

To ascertain the mechanism of deformation in recovery for these low loads in the 'toe' region and to see if there might be any significant effect due to b_T[4] (see chapter 4), recovery T-jumps[5] were performed on the specimen CH2-2-2(f89,Het) at a load 0.3 kg, well within the extent of the 'toe' region of the load-strain curve. The specimen was allowed to creep for 60s (i.e. t_o=60s) when the load was removed and the temperature changed 60s later (i.e.t'=60s). The ln r- ΔT plot is shown in figure 6-6. It was only possible to obtain the values of ln r for +ve ΔT T-jumps with any degree of accuracy because of the low rates and the increased effect on the output of the fluid flow past the unloaded specimen. The three recovery T-jump points (squared points) agree well with those obtained for the creep T-jumps (circled points) on the same specimen and can be fitted by a straight line. A value of $\Delta H_a = 12 \pm 2$ kcal/mol is again found.

The effect of cycling on the value of ΔH_a in the 'toe' region was obtained on specimen CH2-10-1(m44,Heh) by performing 10 cycles of creep and recovery at a load of 0.2 kg, each cycle 120s long with the load on for 60s in each cycle. On the 11th cycle, a creep T-jump was performed at t'=60s. The ln r- ΔT plot obtained from these creep T-jumps is shown in figure 6-7 (circled points). Recovery T-jump data were obtained in a similar manner. This time the specimen was subjected to 10 cycles of creep and recovery and the temperature change took place 60s after removal of the load on the 11th cycle. These points are also shown in figure 6-7 (squared points). A best fit straight line through both creep and recovery data gives $\Delta H_a = 15 \pm 1.5$ kcal/mol. Although this is slightly higher than that found earlier, it is still not a significant change.

To summarise, we have obtained values of ΔH_a for various experimental conditions in the 'toe' region of the stress-strain curve,

These values are tabulated in Table 6-1. The value of ΔH_a was found to be equal to 12 $\pm$ 3 kcal/mol for the creep T-jumps for all of the following variables: age, NaCl concentration, length of time in the apparatus, the value of T_o, cycling, and type of tendon. Recovery T-jumps also gave the same result. We thus have a considerable amount of evidence that the value of the apparent activation energy for the deformation process in the 'toe' region is 12 kcal/mol.

6.2.1-(b) Time-Temperature Superposition

Isothermal creep experiments were performed on specimen CH2-0-1 (m21,Hfh) in the temperature range 14.5 to 35.1 °C in the 'toe' region at a load of 0.76 kg, the same as that used for the T-jumps on this specimen. The strain obtained at four temperatures in this range are shown in figure 6-8. It will be seen that there is a systematic increase in compliance at a given time as the temperature is increased. The data of figure 6-8 were differentiated and the plots of $\frac{d\epsilon}{d \log t} = t \frac{d\epsilon}{dt}$ against log time are shown in figure 6-9. The data of figures 6-8 and 6-9 were shifted horizontally to the reference temperature 29 °C and satisfactory master curves were obtained for both ϵ and $\frac{d\epsilon}{d \log t}$ shifts yielding a value of $\Delta H_a = 8$ kcal/mol, a value slightly lower than that found by T-jump. This is a result achieved probably more by luck than good management. To qualify this statement, it will be necessary to give some measure of the change in strains with temperature necessary to obtain the value of $\Delta H_a = 12$ kcal/mol.

Let us take the specimen CH2-16-1(m71,Hfh) for example,(figures 5-1 and 5-2). For four creep tests at load 1 kg, the 20s strain was 0.0195 with a standard deviation of 2.3×10^{-4}, i.e.1.2%. For the 2 kg load, four creep tests were performed and the standard deviation was also 1.2%. For the 4kg load, 7 tests were performed giving the strain 0.0368 with a standard deviation of 3.5×10^{-5} i.e. 0.1%, and for the 6 kg load, the standard deviation was

0.6%. In all cases, the specimen recovered to within 1% of the 20s strain achieved in the creep tests at a given load. Taking an activation energy of say 30 kcal/mol, then for a change in temperature of $\Delta T=5\,^{\circ}C$, this will give $a_T \sim 0.4$ and $\log a_T \sim -0.36$. From the data for 4kg load, for specimen CH2-16-1(m71,Hfh), figure 5-2, this shift would require the strain at 30s, say, to be 0.0005 greater at the higher temperature than at the lower temperature. Since the strain at this load is ~ 0.04, this is an increase of $\sim 1.25\%$ of that strain, which is also of the order of the error in the strain measurements from one test to the next for most of the above loads. For the case where the error in strain is as low as 0.1%, errors in ΔH_a will be ~ 5 kcal/mol. Even for the case of an error of only 0.6% in the value of strains from one experiment to the next at the same load, which certainly seems acceptable for this type of material, will mean that a_T could vary between 0.66 and 0.25 instead of 0.4 giving ΔH_a between 15 and 50 kcal/mol when superposition of the strains is attempted. This is an error of 50%. Similarly, for the rates which were found to differ by about 4% for the 7 creep tests for the 4 kg load. This will give errors of $\sim 50\%$ for superposition of $\frac{d\epsilon}{d \log t}$.

If we choose $\Delta H_a = 15$ kcal/mol and $\Delta T=5\,^{\circ}C$, then $a_T=0.66$ and $\log a_T = -0.178$. This means that for the data of figure 6-8, (specimen CH2-1-1(m21,Hfh)) the strain at the higher temperature at a given time will be greater than that at the lower temperature by ~ 0.0002. For a standard deviation of 1% in the strain from one experiment to another at the same load, and for the strain ~ 0.013 as in figure 6-8, this will mean that a variation of strain of 0.00025 from experiment to experiment will occur, which again is of the order of that required for superposition. Hence errors of $\sim 100\%$ will occur and a value of ΔH_a from 0 to 30 kcal/mol could be obtained.

It is clear from the previous discussion that to find a_T by means of time-temperature superposition requires extreme accuracy and reproducibility in the strain and creep rates, and the conditions imposed are far greater than those attainable for tendon specimens. To achieve reproducibility of ~1% for the strain values at a given load for a biological material of this sort is extremely good and to get recovery of the strain to within 1% is quite an achievement. But to obtain an accurate measure of a_T from time-temperature superposition requires reproducibility in the strain values to less than 0.1%, which is not possible. The nature of the structure of the material and the fact that the amount of creep is small means that a small deviation of the starting point and thus the initial crimp angle, θ_o, from one experiment to the next introduces an error in the measured strain and strain rates of the order of that required for superposition. It is the combination of two factors

(1) the slight change in the substructure at time t=0 due to the crimp angle change and

(2) the small amount of creep in the material when stressed,

that contribute to the inaccuracy of the superposition technique. If the amount of creep were higher, then superposition would be possible with the above variation in the strain measure.

From the above analysis, it can be seen how Rigby et al[6], who performed time-temperature superposition on rat-tail tendon in the 'toe' region in stress relaxation, observed no change in the measured strain with temperature below 35 °C, i.e. they found ΔH_a equal to zero for all temperatures. Above 35 °C, they found a non zero value for ΔH_a. With the errors involved in their load readings of the order described above, they could easily have found any other value of ΔH_a up to 30 kcal/mol. We can thus see that time-temperature superposition is not a technique to be attempted on tendons and results obtained should be viewed with caution.

In fact, any experiment on tendon which requires the determination of a quantity from data obtained in two separate experiments should be avoided, or else a careful determination of the errors involved calculated.

This also shows the advantage of the T-jump experiment on a material of this sort. In this experiment, we are comparing quantities (the creep rates immediately before and after the temperature change) obtained from a single experiment. Since the rates are obtained at the same time in the same experiment, then the rates will refer to the same substructure of the specimen,i.e. that which occurs at the time of the temperature change. The substructure at t' may vary slightly from experiment to experiment at a given load, but unless there is a change in the deformation mechanism involved in the deformation process, this will not alter the value obtained for the ratio ln r in the T-jump experiment. That this is so can be seen in the T-jump data presented so far, since all points observed are close to the theoretical straight line. Even if the T-jump is initiated before the specimen has recovered completely from an earlier experiment, as for instance for the T-jumps performed on the 11th cycle in the cycling experiments, we will still obtain the value of a_T and ΔH_a for the deformation process at the substructure at which the T-jump was performed. In this case, in the 'toe' region, it was found equal to that on the first creep cycle. The accuracy of the T-jump at these low values of activation energy has been demonstrated since we have found the same value of ΔH_a for a large number of different samples.

We persevered with time-temperature superposition for a while. Superposition of the strain data of specimen CH2-10-1(m44,Heh) on the first and tenth cycle was tried, giving ΔH_a=10.5 kcal/mol and 16 kcal/mol respectively. The rate data $\frac{d\epsilon}{d \log t}$ was too flat to obtain anything meaningful. Superposition of the rates and strains for specimen BT2 (bovine,

flexor,foot) gave values anywhere between 0 and 20 kcal/mol and for specimen CH2-1-1(m55,Heh) superposition over the temperature range 35°C to 55°C gave ΔH_a=6 kcal/mol. Time-temperature superposition was also tried in stress relaxation on specimen CH2-5-1(m54,Heh) in the 'toe' region, and after a value of 45 kcal/mol was obtained, no further attempts at using time-temperature superposition were made.

6.2.2 ΔH_a at High Loads

We have determined the activation energy for the deformation process in the 'toe' region to be 12 $\pm$ 3 kcal/mol. If there is a change in the deformation mechanism with increasing strain as the specimen is loaded into the 'linear' region, then there should be a change in the value of ΔH_a. We thus used the T-jump technique to study the variation in the apparent activation energy, ΔH_a, with applied load. Figures 6-10 to 6-13 show the ln r- ΔT plots obtained for the sample CH2-16-1(m71,Hfh) at various loads from 1 kg to 6 kg. This range of load takes the specimen from approximately the end of the 'toe' region to the 'linear' region of the load-strain curve. On all the graphs, a best fit straight line can be drawn through the points, the slope of which gives the values for ΔH_a as shown in Table 6-1.

These values of ΔH_a are plotted against load and strain along with the load-strain curve for this material in figure 6-14. As has been mentioned before, the isochronal load-strain curve for each material must be determined in order to compare the various regions of deformation. The format of figure 6-14 will be used again later. On the right of the load-20s strain curve is the plot of ΔH_a against load and above the load-20s strain curve is the ΔH_a against 20s strain plot. All divisions on the axes for ΔH_a, strain and load are kept consistent throughout. Figure 6-14 shows

at a glance that the change of ΔH_a with load coincides with the transition from the 'toe' to the 'linear' region, and once in the 'linear' region, a value of ΔH_a=32 kcal/mol is attained which remains constant as the load is increased.

It was not possible to obtain, for this material, the values of ΔH_a in the 'toe' region since the rates were too low at the low loads to obtain accurate extrapolation of the log rate-log time curves. The dashed circle on figure 6-14 is shown for the value found earlier for ΔH_a in the 'toe' region, and the dashed line is of the form anticipated if we had been able to obtain points in that region. It will be seen in figures 6-10 and 6-11 that no values could be found for the down T-jumps at these loads because the rates were too low. This was also the case for recovery T-jumps on this specimen. Accurate data were obtained for the down T-jumps at the higher loads of 4 and 5.9 kg. Typical log creep rate-log time data for these loads are shown in chapter 8 (figures 8-11 and 8-12) where they are fitted with the linear viscoelastic theory.

An attempt was made to obtain the whole of the ΔH_a dependence on load and strain. It was thought that the time to do this by performing several T-jumps at each load would be too long as the specimen may be degrading by the time the experiments were completed. Instead, it was decided to perform just one T-jump with a ΔT=5 to 6°C at each load. By keeping the load increments small, any errors introduced by taking the value of ΔH_a from the single experiment at a given load instead of from a ln r- ΔT plot as done previously were minimised. Since all ln r- ΔT plots found so far were straight lines, this procedure was considered valid.

The result for specimen CH2-8-2(m23,Heh) is shown in figure 6-15. The 20s isochronal load-strain curve is shown in the centre to compare the change in the value of ΔH_a as the applied load increases with the transition

from the 'toe' to 'linear' region. The plots of ΔH_a against load and 20s strain are shown on the right and top respectively as in figure 6-14. Also included in this figure are the 20s creep rates against load and 20s strain curves on the left and bottom respectively. All plots in the vertical plane have 20s strain as the abscissa and all plots in the horizontal plane have the load on the same axis. In this way, the dependence of the experimental parameters ΔH_a, 20s strain and creep rate on load can be seen clearly from right to left, and likewise for the dependence of ΔH_a, load and 20s creep rate on 20s strain from top to bottom. The divisions on the axes remain constant throughout.

On each graph, the transition from one type of curve to another can be seen to occur as the applied load (or the 20s strain) increases; in the load-strain curve, it is the transition from the 'toe' to the 'linear'; with the creep rate curve it is from the 'hump' shape to an almost linear region; and for the ΔH_a curves, it is a transition from one constant value of ΔH_a=15 kcal/mol to a higher constant value of 33 kcal/mol. This graph shows in a nutshell the essence of the viscoelastic mechanical deformation of tendon, namely its isothermal load-strain characteristics, its creep rate-load dependence and its non-isothermal viscoelastic behaviour, all of which indicate that there are two mechanisms occurring in the deformation process and there is a gradual transition from one to the other as the applied load increases.

Data was also obtained during the course of cycling experiments on another specimen CH2-8-3(m23,Heh) which was subjected to the loading pattern as shown in figure 6-16. For each load a recovery T-jump was performed on the second cycle followed 30 minutes later by a creep T-jump. The results are shown in figures 6-17 and 6-18 and are presented in the same form as for figure 6-15. The creep T-jumps of figure 6-17 show the same behaviour

as for specimen CH2-8-2(m23,HeL) with ΔH_a changing from 15 to 29 kcal/mol as the load increases, and with the 'hump' followed by the linear portion on the 20s creep rate-load curve. For the recovery T-jumps of figure 6-18, the change in ΔH_a is from 14 to 34 kcal/mol. The 1st cycle recovery strains and rates are shown and the recovery rates are again seen to be greater than the creep rates of figure 6-17. Plots such as figures 6-15, 6-17 and 6-18 can be considered as the fingerprint for the viscoelastic properties of tendon in creep.

6.2.3 ΔH_a of a Preloaded Tendon By T-jump

In order to look more closely at the deformation in the 'linear' region or, as thought, the region due to the fibre extension, and to minimise the effect of the 'toe' deformation mechanism on the determination of ΔH_a in the 'linear' region, we performed T-jumps on the specimen CH2-16-4 (m71,Hfh) to which a preload had been applied as described in chapter 5. This 3 kg preload took the specimen to the start of the 'linear' region. Once the specimen had reached mechanical equilibrium at this preload, we performed the various isothermal tests as described earlier and also creep T-jumps for the various values of ΔT and for loads 2 kg and 3 kg applied on top of the preload. The values of ln r found for the various values of ΔT are shown in figures 6-19 and 6-20. A straight line through the points gives $\Delta H_a = 34 \pm 2$ kcal/mol for the 2 kg load and 32 ± 2 kcal/mol for the 3 kg load. Both values are in excellent agreement with those found before for the normal unpreloaded sample in the high load region. Hence it appears that we are now looking at the mechanism dominated by the collagen fibre stretching.

6.3 ΔH_a of Collagen Tape.

Further evidence to support the above hypothesis was found by performing experiments on a 3500 denier (ca 0.09 mm thick, 4.8 mm wide) strip of collagen tape which was manufactured by Ethicon Corporation, N.J. by extrusion of a steer tendon homogenate. This material, which is devoid of all mucopolysaccharides was immersed in 0.9 wt % NaCl at pH 7 as for the tendons. The 60s isochronal load-strain and strain rate-load curves are shown in figure 6-21. The 'toe' region up to the 0.2 kg load is here due to the geometry of the woven fabric and similar to that observed for other two dimensional meshes[7]. The 60s creep rate-load curve is linear after 0.2 kg. T-jump experiments were performed at a load of 0.8 kg, i.e. in a region where the geometry effects of the weave are negligible. The ln r- ΔT plot obtained is shown in figure 6-22 and the points lie close to a straight line, the best fit giving $\Delta H_a = 33 \pm 3$ kcal/mol, agreeing well with the data obtained in all previous high load experiments on tendon.

6.4 ΔH_a of Gelatin

As a final application of the T-jump in creep on tendon, we performed experiments to find the value of ΔH_a for denatured collagen, or gelatin[8]. The bovine tendon, BT2, was heated to 65 °C for 48 hours and a contraction of the specimen was observed. This occurs as a result of the melting of the collagen crystals and the triple helix of the tropocollagen molecule being unwound to give a random coil structure. The tendon contracted to over $\frac{1}{3}$ of its original length and when no further contraction could be observed, the specimen was cooled to 28 °C. The T-jump experiments were performed on this specimen at one value of load and various values of ΔT. The small load of 0.2 kg gave rise to a strain of ~30%, (compare this with the ~2% strain found before the contraction for this same load before

heating, in figure 6-5). The specimen is thus highly extensible. Its rubberlike behaviour can be seen from the thermal expansion when undergoing a T-jump. Typical creep strain against time curves are shown in figure 6-23 for this specimen and a T-jump occurs at 60s after the load is applied. As can be seen for the +ve temperature change, the specimen contracts, and for the -ve temperature change it expands. This is typical for rubberlike behaviour above the thermo-elastic inversion point[2,9]. The values of ln r found for the T-jumps are shown in figure 6-24 and a straight line through the points gives a value of $\Delta H_a = 9 \pm 4$ kcal/mol. This value coincides with that obtained for lightly crosslinked cis 1-4 polybutadeine[10]. The mechanism attributed to the latter material was one of the slippage of the entanglements within the lightly crosslinked network. It is likely that the same mechanism is applicable here.

6.5 Discussion

The T-jump experiment has been used to determine the apparent activation energy of tendon in the 'toe' and 'linear' regions of the stress-strain curve for a variety of specimens and experimental conditions. The time-temperature superposition technique used to obtain ΔH_a has been shown to be grossly inaccurate in its use on tendon, producing errors up to 100% for a value of $\Delta H_a = 15$ kcal/mol. Consequently, the results of Rigby et al[6] (who found ΔH_a to be zero in the 'toe' region by time-temperature superposition), should be viewed with caution.

A summary of all the T-jumps performed on tendon is shown in Table 6-1. Since the values of ΔH_a for creep and recovery are the same, and there is no curvature on the ln r- ΔT plots, it is clear that the effect of b_T[4,5] is negligible in both the 'toe' and 'linear' regions. The apparent activation energy of tendon was found to be 12 ± 3 kcal/mol in the 'toe' region and 33 ± 3 kcal/mol in the 'linear' region in both creep and recovery

T-jumps for a variety of specimens. A transition was observed from the low activation energy mechanism (~12 kcal/mol) to the high activation energy mechanism (~32 kcal/mol) which coincided with the changes observed in two other sets of data, as shown in figures 6-15, 6-17 and 6-18, reinforcing the idea that we are in fact seeing two viscoelastic processes. These figures are the fingerprint for each specimen and show

(i) a change from the 'toe' to the 'linear' region on the isochronal load-strain curve.

(ii) a change from the 'hump' to a 'linear' region on the isochronal rate-load curve.

(iii) a change from a value of $\Delta H_a = 12 \pm 3$ kcal/mol to $\Delta H_a = 35 \pm 3$ kcal/mol over the same region of stress and strain as the changes in (i) and (ii).

It has been suggested by Stromberg and Wiederhielm[11] that the creep in tendons resulted from a lag in the fibrillar elements due to the viscous resistance to movement of these elements by the ground substance. Gibbs and Balazs[12] also suggested a possible role of the mucopolysaccharides in the deformation of connective tissue. The value of the activation energy for hyaluronic acid, which is the main component of the mucopolysaccharides of the tendon, was 9 kcal/mol at concentrations, ionic strength and pH close to those found in the body.[13] This value of ΔH_a is very close to that found by our T-jumps for the low strain behaviour of tendon in the 'toe' region. The value of 12 ± 3 kcal/mol was obtained for so many different experiments that this is hard to dispute. The indication is clear: the mucopolysaccharides of the tendon are involved in the viscoelastic process. What is the likely mechanism? It is postulated that viscoelastic deformation, when the fibres are crimped, will be due to a shearing of the viscoelastic gel which is located between the crimped ribbons of the collagen fibres.[14] The ribbons may be considered as a stack of cards which slide and rotate under the action

of a shear stress on the gel when a tensile stress is applied to the tendon along the tendon axis. The recovery process will also be dominated by the same mechanism.

The value of $\Delta H_a = 32 \pm 3$ kcal/mol for the 'linear' region of the load-strain curve indicates that another mechanism is involved in this region. The value was obtained for a variety of specimens, not only for tendon in the 'linear' region and when preloaded, but also for collagen tape(which is devoid of mucopolysaccharides). In all cases, the value of $\Delta H_a = 32 \pm 3$ kcal/mol was found. The mechanism for recovery seems to be the same as for creep since ΔH_a for creep and recovery are the same in all regions of the load-strain curve.

Although the mechanism in the 'linear' region cannot so easily be associated with a given process, indications are possible. It is almost certain that the collagen fibres are themselves taking the load at these high strains, since the value of $\Delta H_a = 32 \pm 3$ kcal/mol which we have found in the'linear' region is of the order of that found for semi-crystalline polymers, e.g. a value of $\Delta H_a = 35$ kcal/mol has been determined for polypropylene[15] and $\Delta H_a = 30$ kcal/mol for linear polyethylene.[16] It is difficult to say which of the viscoelastic deformation processes usually associated with crystalline polymers will occur in collagen. The most likely are[17]

a) an intralamellar shear process where the collagen crystals themselves deform by shearing movements in the direction parallel to the chain axis of the tropocollagen molecule, or

b) an interlamellar shear process where the collagen crystals slip relative to each other.

Further research is necessary to determine which mechanism is occurring in collagen.

In the next chapter, we will develop a viscoelastic model of

the tendon behaviour based on these two mechanisms, i.e. the shear of the gel between the collagen ribbons for low strains and fibrillar extension, (whether interlamellar, intralamellar or otherwise) at the high strains. The gradual transition between the two mechanisms will be seen to result from the difference in the initial crimp angle from one fibrillar element (or ribbon) to another.

References

1 McCrum N.G. and Morris E.L., Phil.Mag.,7,2115,1962.

2 Ferry J.D., Viscoelastic Properties of Polymers, Wiley, New York, 1970.

3 Cohen R.E., Hooley C.J. and McCrum N.G., J. Biomech.,9,175,1976.

4 McCrum N.G. and Pearce D.L., Nature, Physical Sci., 243,52,1973.

5 Hutchinson J.M., McCrum N.G. and Pearce D.L., J.Polymer Sci., Polymer Phys.,12,1255,1974.

6 Rigby B.J., Hirai N., Spikes J.D. and Eyring H., J.Gen.Physiol.,43,265,1959.

7 Bull H., In Tissue Elasticity, (ed. Remington J.W.) Amer.Physiol.Soc. Washington D.C.,1957.

8 Yannas I.V., J.Macromol.Sci.-Revs.Macromol.Chem.,C7(1),49,1972.

9 Caruthers J.M. and Cohen R.E., Polym.Eng.Sci.,16,41,1976.

10 Caruthers J.M. and Cohen R.E., J.Polymer Sci.,14,1891,1976.

11 Stromberg D.D. and Wiederhielm C., J Appl.Physiol.,26,857,1969.

12 Gibbs D.A., and Balazs E.A., In Chemistry and Mol.Biol. of Int.Matrix, vol 2, (ed. Balazs E.A.) Academic Press, New York, 1970.

13 Gibbs D.A., Merrill E.W., Smith K.A. and Balazs E.A., Biopolymers,6,777, 1968.

14 Baer E., Gathercole L.J. and Keller A., In Colston Papers, Structure of Fibrous Biopolymers, (ed Atkins E.D.T. and Keller A.) 26,189,1975. Butterworths, London.

15 Hutchinson J.M., D. Phil. Thesis, Oxford University, 1974.
Morgan C.J. and Ward I.M., J.Mech.Phys.Sol.,19,165,1971.
McCrum N.G. and coworkers, To be published.

16 Pearce D.L., D.Phil. Thesis, Oxford University, 1976.
McCrum N.G. and Morris E.L., Proc.Roy.Soc.,A292,506,1966.
McCrum N.G., Read B.E. and Williams G., 'Anelastic and Dielectric Effects in Polymeric Solids' Wiley, London, 1967.

17 Arridge R.G.C, 'Mechanics of Polymers', Clarendon Press, Oxford. 1975.

Table 6-1 The Apparent Activation Energy of Tendon by T-jump

Specimen	Region	Load (kg)	Pre-load (kg)	20s Strain %	Creep ΔH_a kcal/mol	Recovery ΔH_a kcal/mol	Figure
CH2-0-1	toe	0.76		1.46	12		6-2,3
CH2-1-1	toe	0.72		1.40	12		6-4
CH2-2-1	toe	0.30		1.42	12		6-4
BT2	toe	0.8		3.40	14.5		6-5
CH2-2-2	toe	0.3		1.5	12	12	6-6
CH2-10-1	toe	0.2		1.48	15	15	6-7
CH2-16-1	transition	1.0		1.94	25.5		6-10
"	transition	2.0		2.67	26.5		6-11
"	linear	4.0		3.68	32		6-12
"	linear	5.9		4.515	33		6-13
CH2-8-2	toe	<0.6		<4.5	16		6-15
"	linear	>2.0		>6.5	33		6-15
CH2-8-3	toe	<1.1		<3.8	15		6-17
"	linear	>3.5		>4.8	29		6-17
CH2-8-3	toe	<0.7		<3.2		15.5	6-18
"	linear	>3.0		>4.1		34	6-18
CH2-16-4	linear	2.0	3.0	0.515	34		6-19
"	linear	3.0	3.0	0.76	32		6-20
Collagen Tape	linear	0.8		5.0	33		6-22
Gelatin (BT2)		0.2		28.1	9		6-24

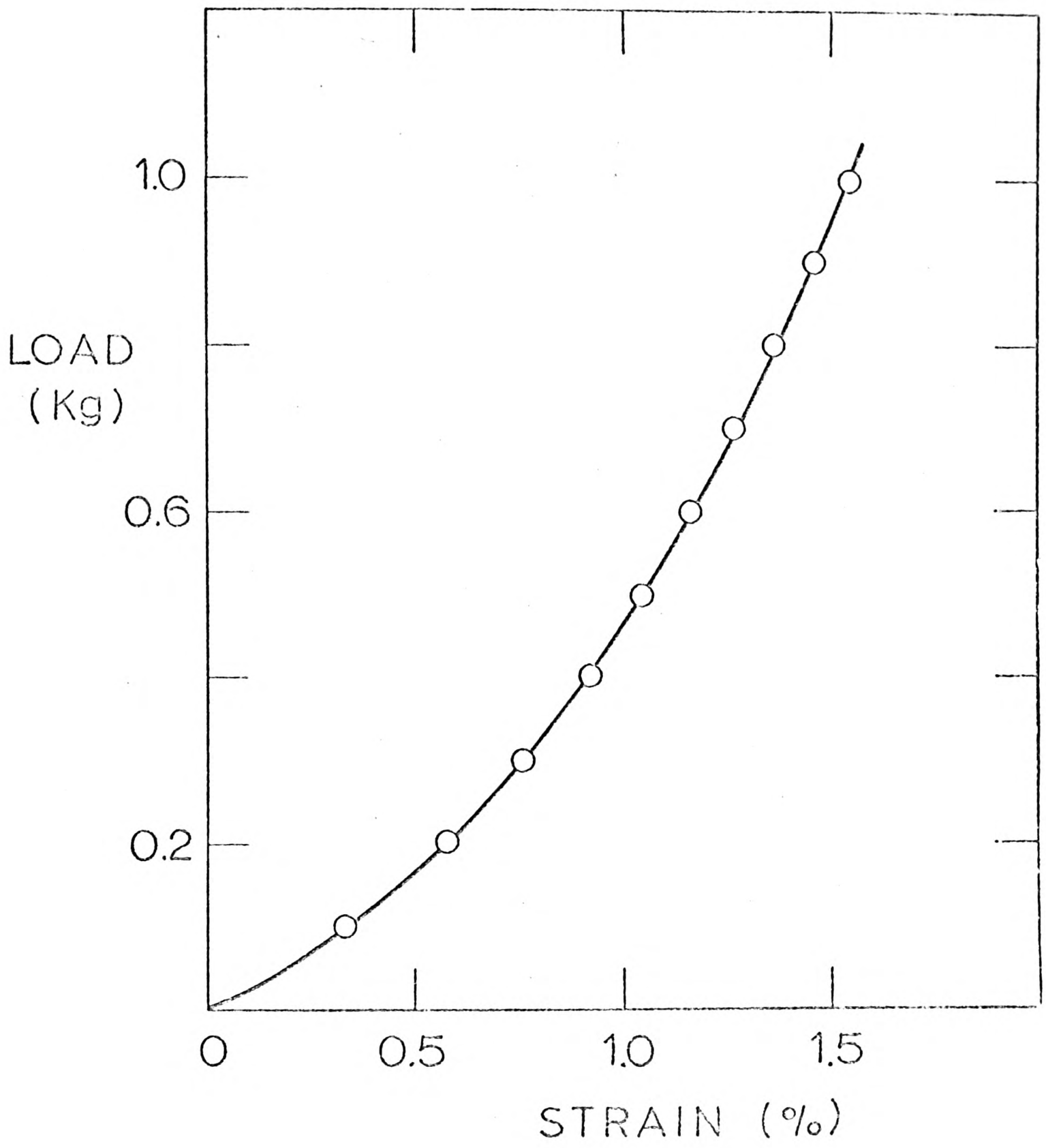


Figure 6-1

20s isochronal load-strain curve, specimen CH2-0-1(m21,Hfh), T_a = 30°C.

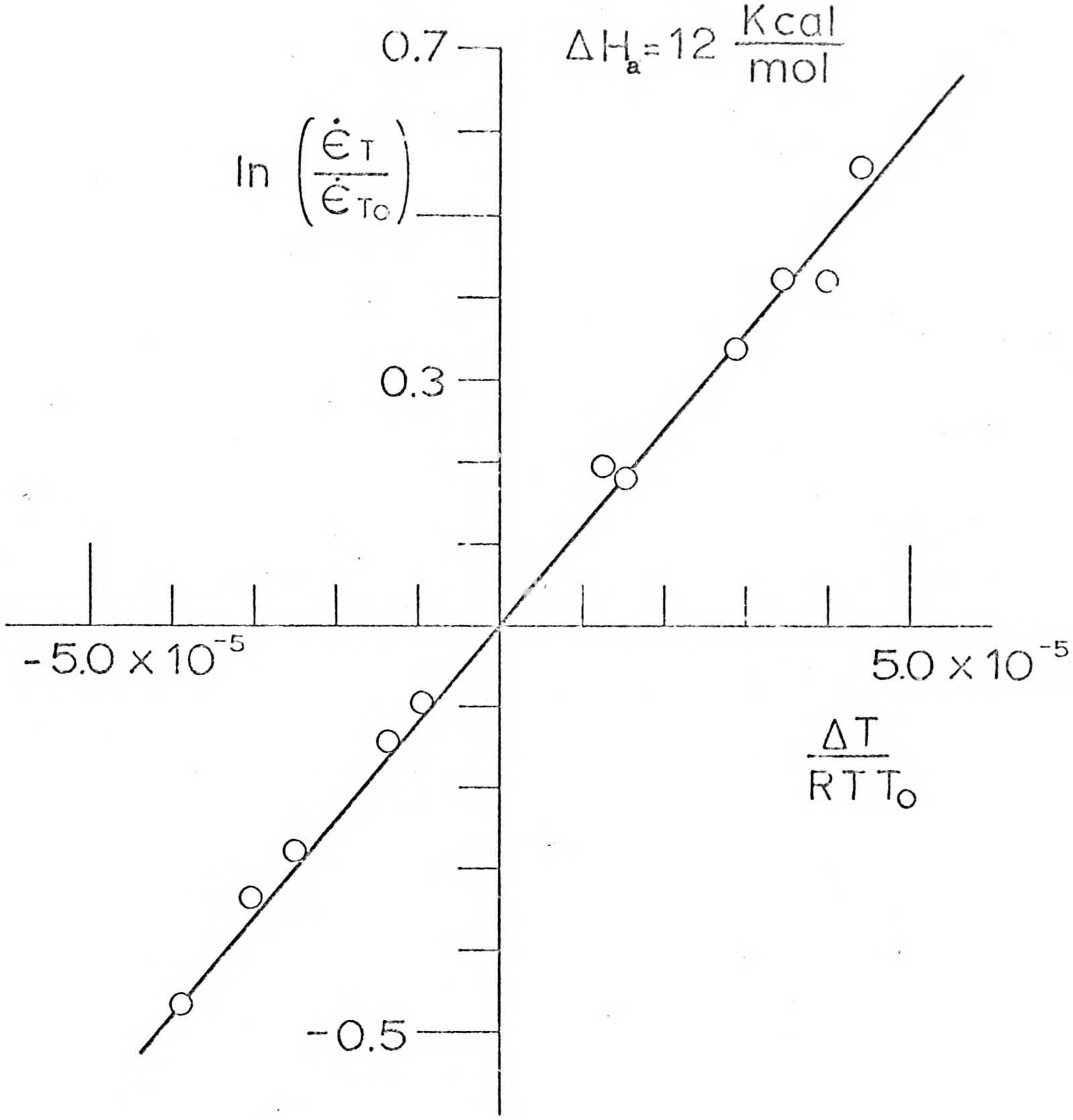


Figure 6-2

Dependence of ln ($\dot{\epsilon}_T(t')/\dot{\epsilon}_{T_o}(t')$) on $\Delta T/RTT_o$, creep T-jump, specimen CH2-O-1(m21,Hfh), T_o= 28 °C, best fit straight line through the points gives ΔH_a = 12 kcal/mol.

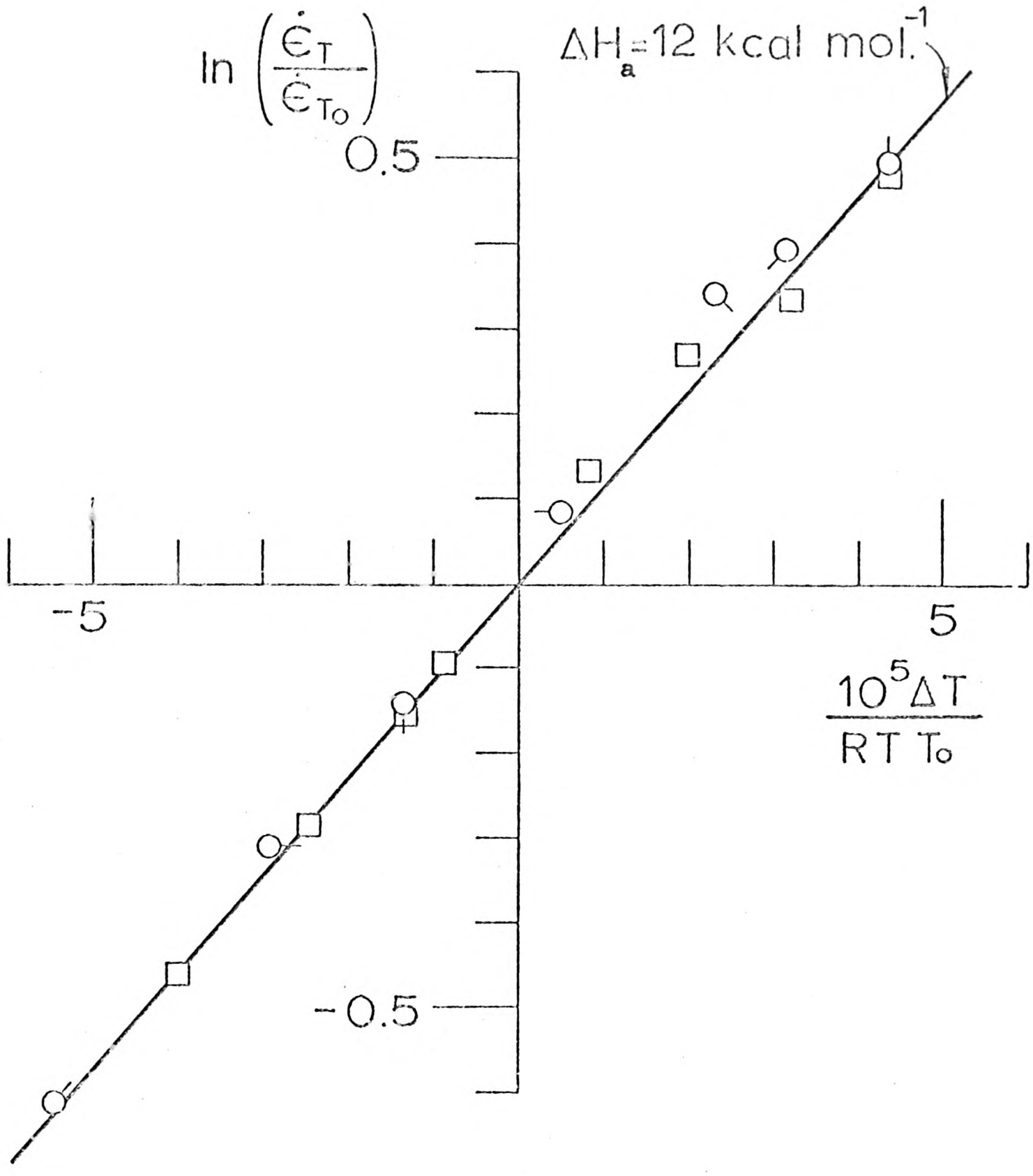


Figure 6-3

Dependence of ln r on $\Delta T/RTT_o$ for creep T-jumps on specimen CH2-0-1(m21,Hfh) in distilled water at pH 6 and T_o = 28 °C.
squared points; all 8 points taken on the day the specimen was immersed in distilled water
circled points: a point taken each day for the next seven days with the specimen continuously immersed in distilled water. Pips on the circled points indicate the day of measurement. ♁ day 2; ♂ day 3; etc..

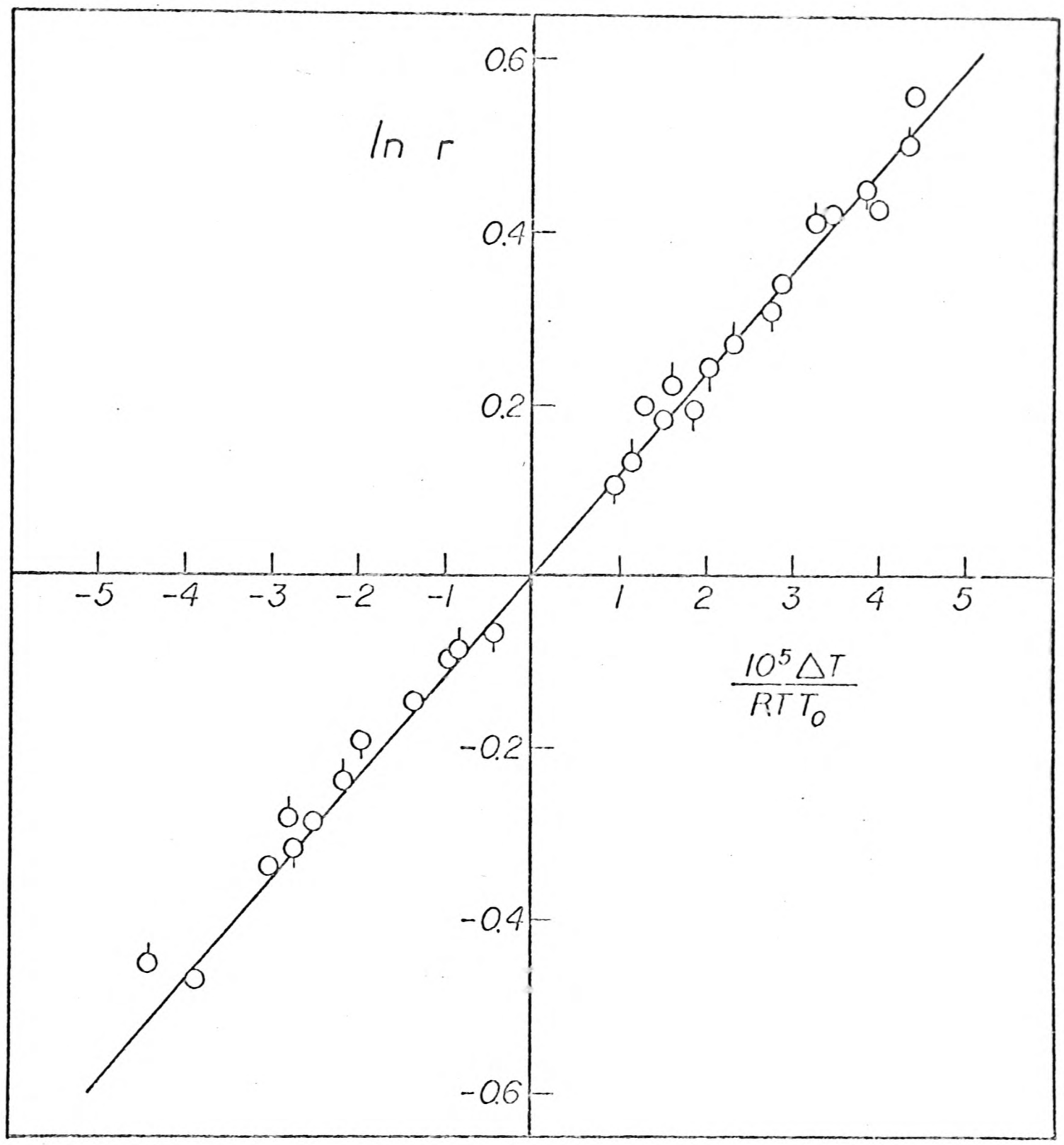


Figure 6-4

Dependence of ln r on $\Delta T/RTT_o$ for creep T-jumps on specimens

o CH2-0-1(m21mHfh), at load 0.76 kg.
ȯ CH2-1-1(m55,Heh), at load 0.72 kg.
♀ CH2-2-1(f89,Heh), at load 0.30 kg.
T_o = 28 °C, straight line drawn through the points for ΔH_a = 12 kcal/mol.

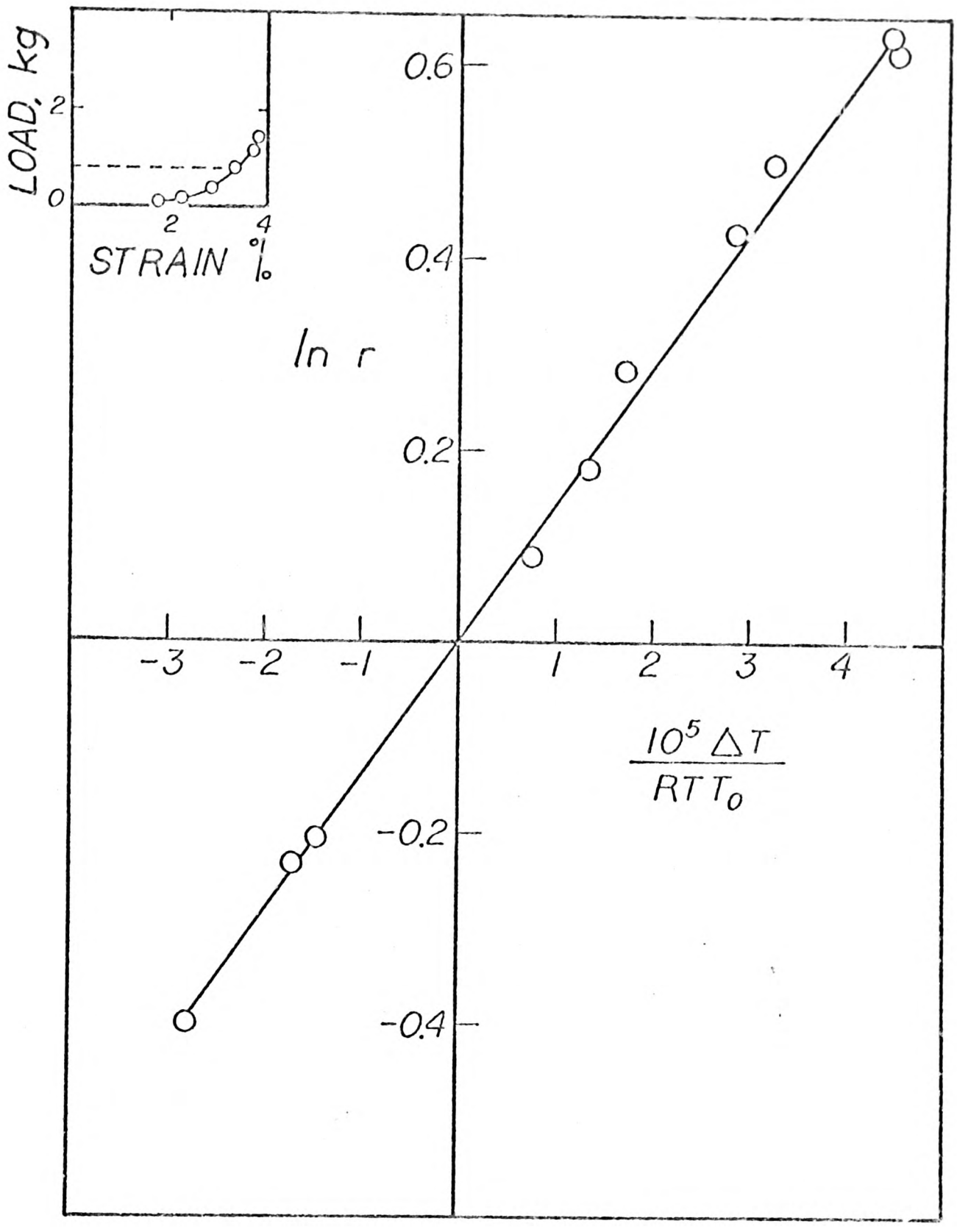


Figure 6-5

ln r- ΔT plot for bovine deep flexor tendon (BT2), creep T-jumps, T_o = 28 °C, inset shows the 20s isochronal load-strain curve. load 0.8 kg, ΔH_a = 14.5 kcal/mol.

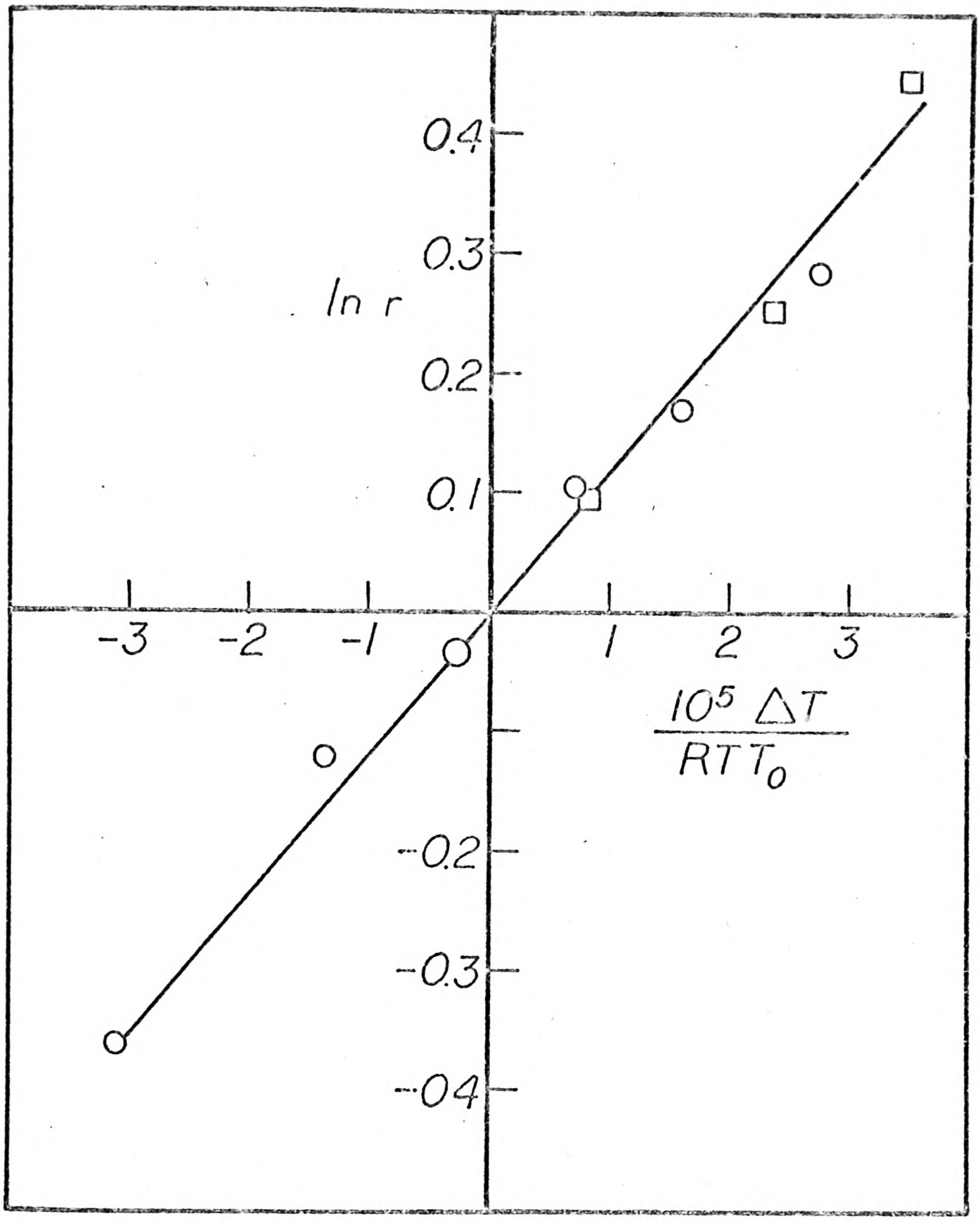


Figure 6-6

ln r- ΔT plot for the toe tendon CH2-2-2(f89,Het), load = 0.3 kg, $\epsilon_{20} \sim 1.5\%$. ΔH_a = 12 kcal/mol.

o creep T-jumps; □ recovery T-jumps.

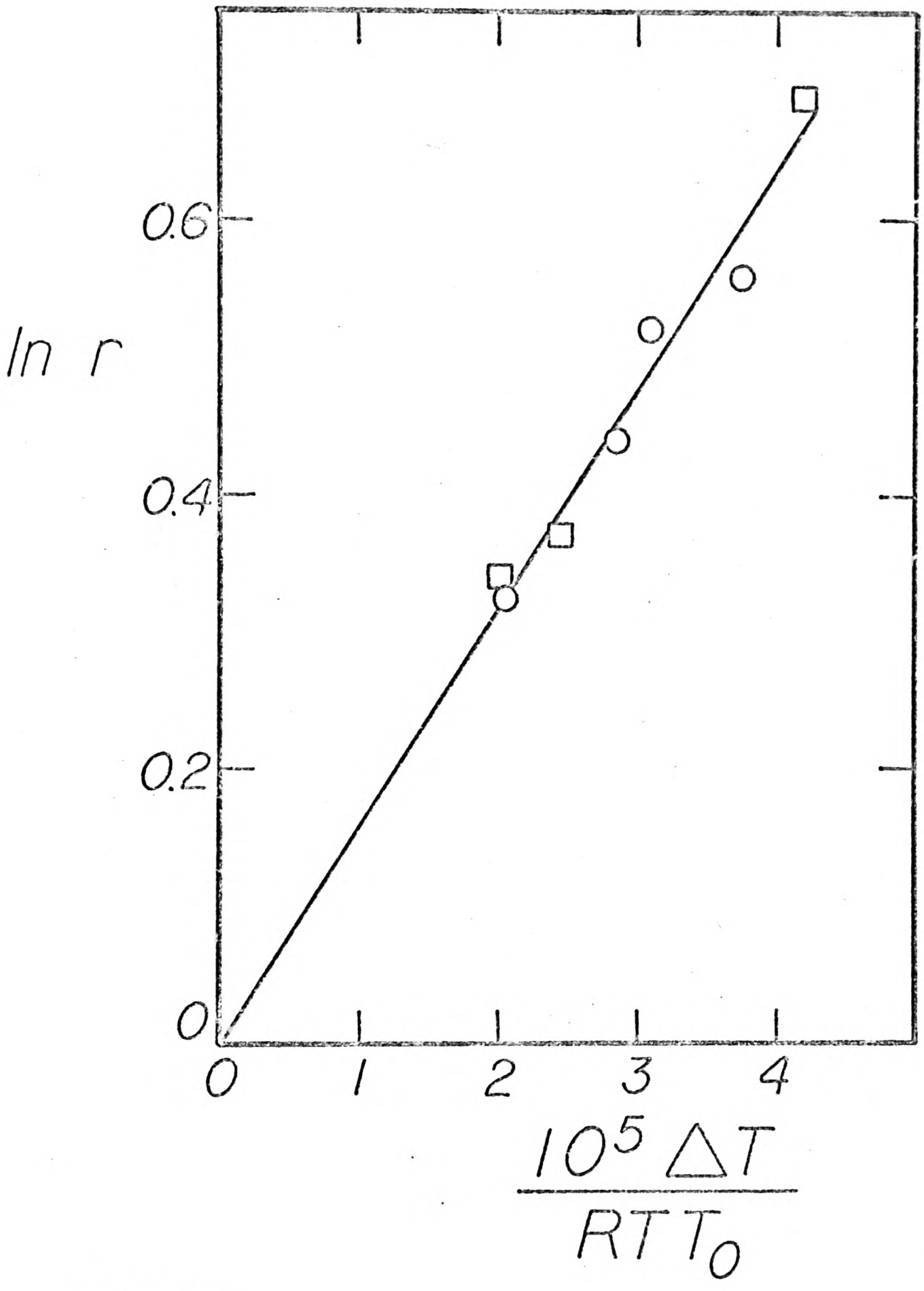


Figure 6-7

ln r- ΔT plot for CH2-10-1(m44,Heb) after 10 cycles of creep-recovery of duration 120s under a load of 200 gm, ΔH_a = 15 kcal/mol.

o creep T-jumps; □ recovery T-jumps.

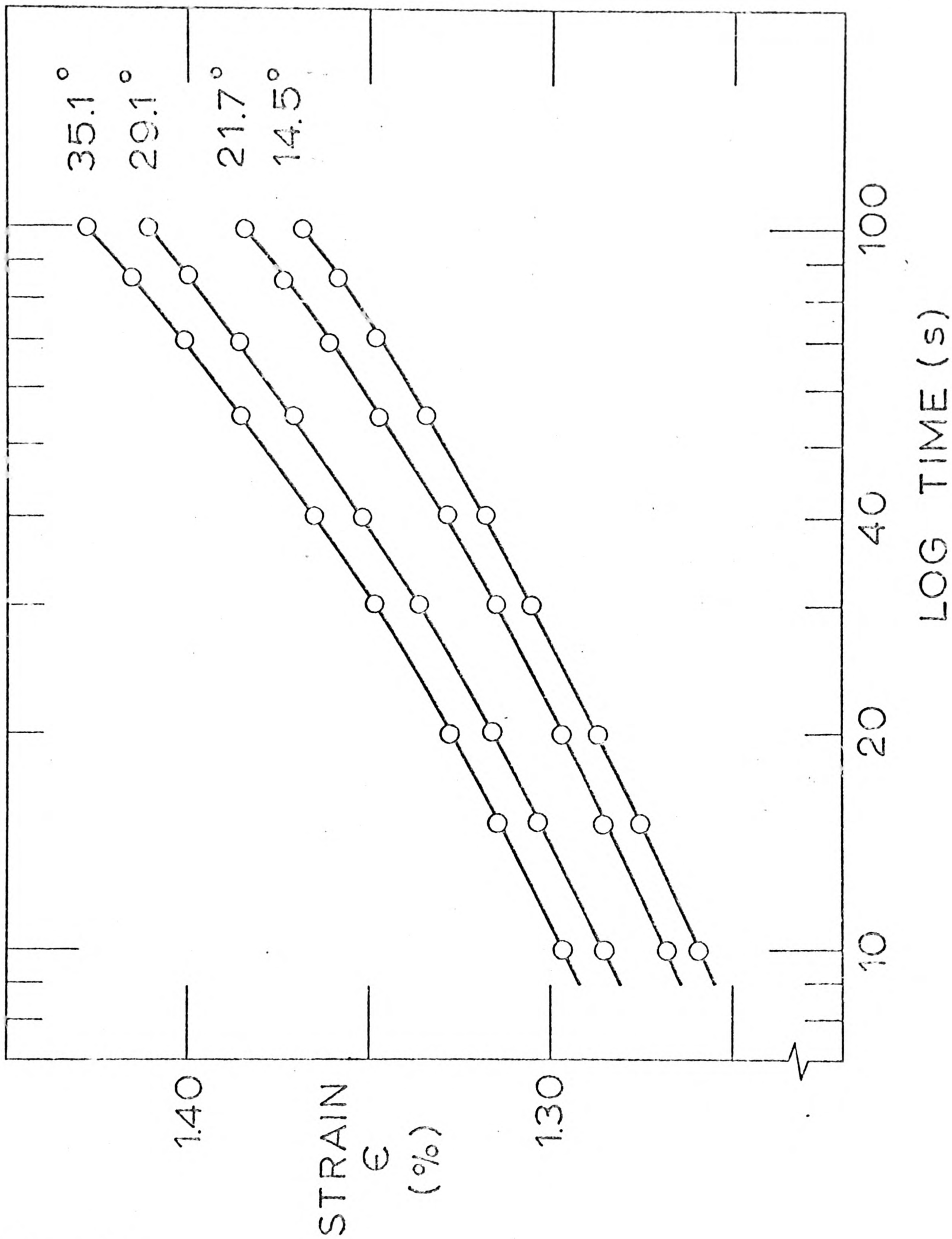


Figure 6-8

Strain dependence on log time at constant load of 0.76 kg at temperatures 35.1, 29.1, 21.7 and 14.5 °C. Specimen CH2-O-1(m21,HFn).

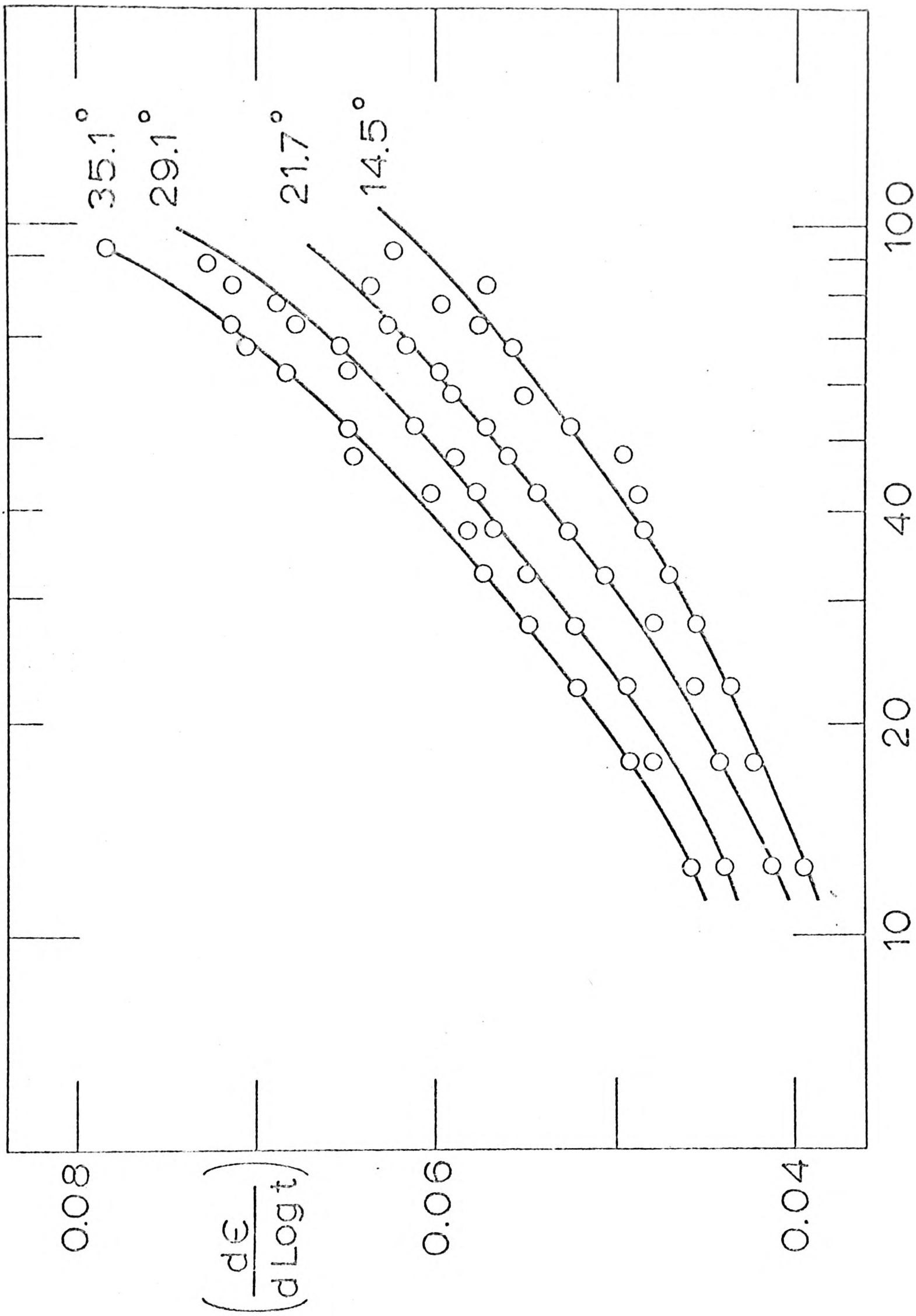


Figure 6-9

Dependence of (dε/d log t) on log time at constant load at the temperatures shown, specimen CH2-0-1(m21,Hfh). load = 0.76 kg.

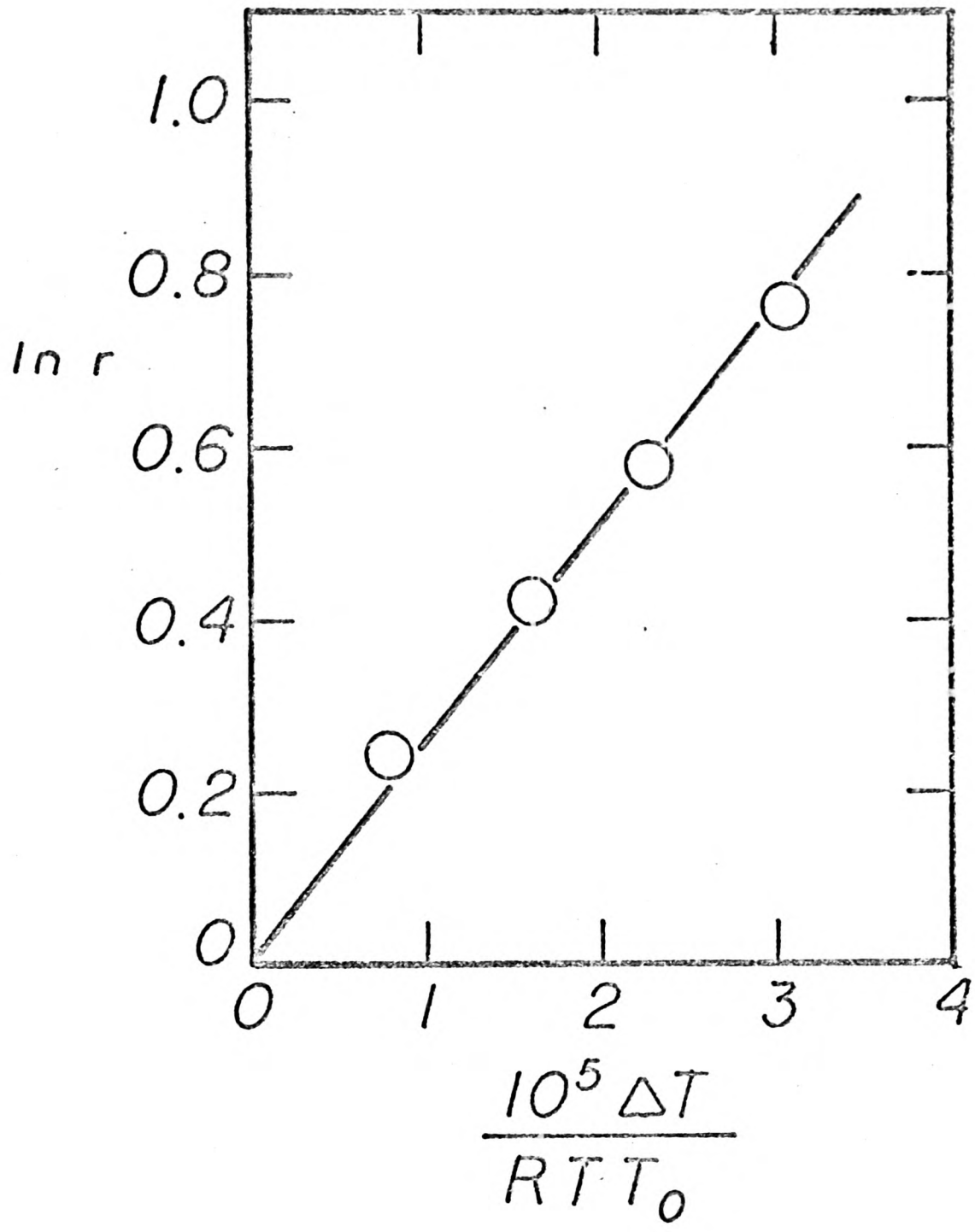


Figure 6-10

ln r- ΔT plot for specimen CH2-16-1(m71,Hfh), creep T-jumps, load = 1 kg, $\Delta H_a = 25.5 \pm 1.0$ kcal/mol.

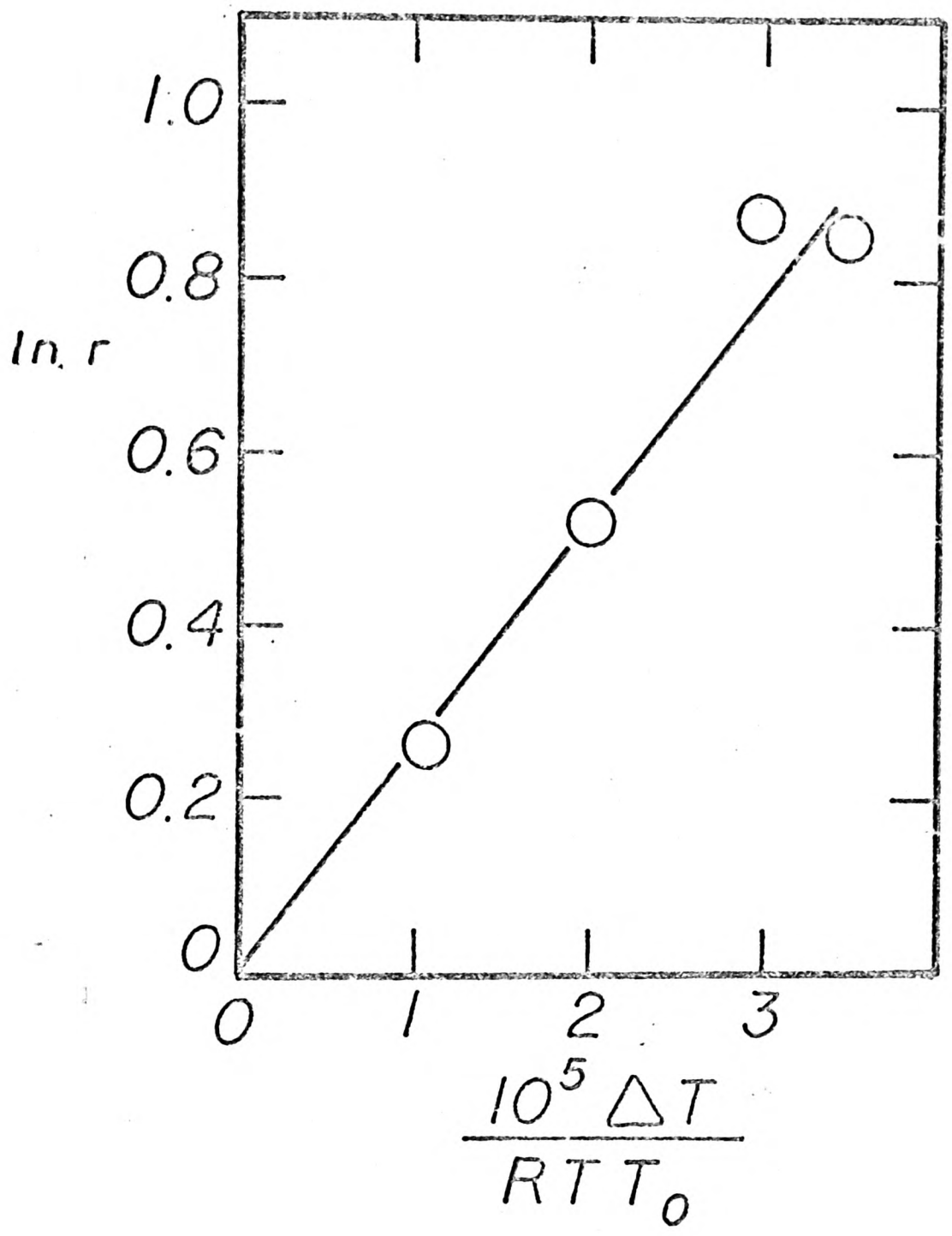


Figure 6-11

ln r- ΔT plot for specimen CH?-16-1(m71,Hfh), creep T-jumps, load = 2 kg, $\Delta H_a = 26.5 \pm 1.5$ kcal/mol.

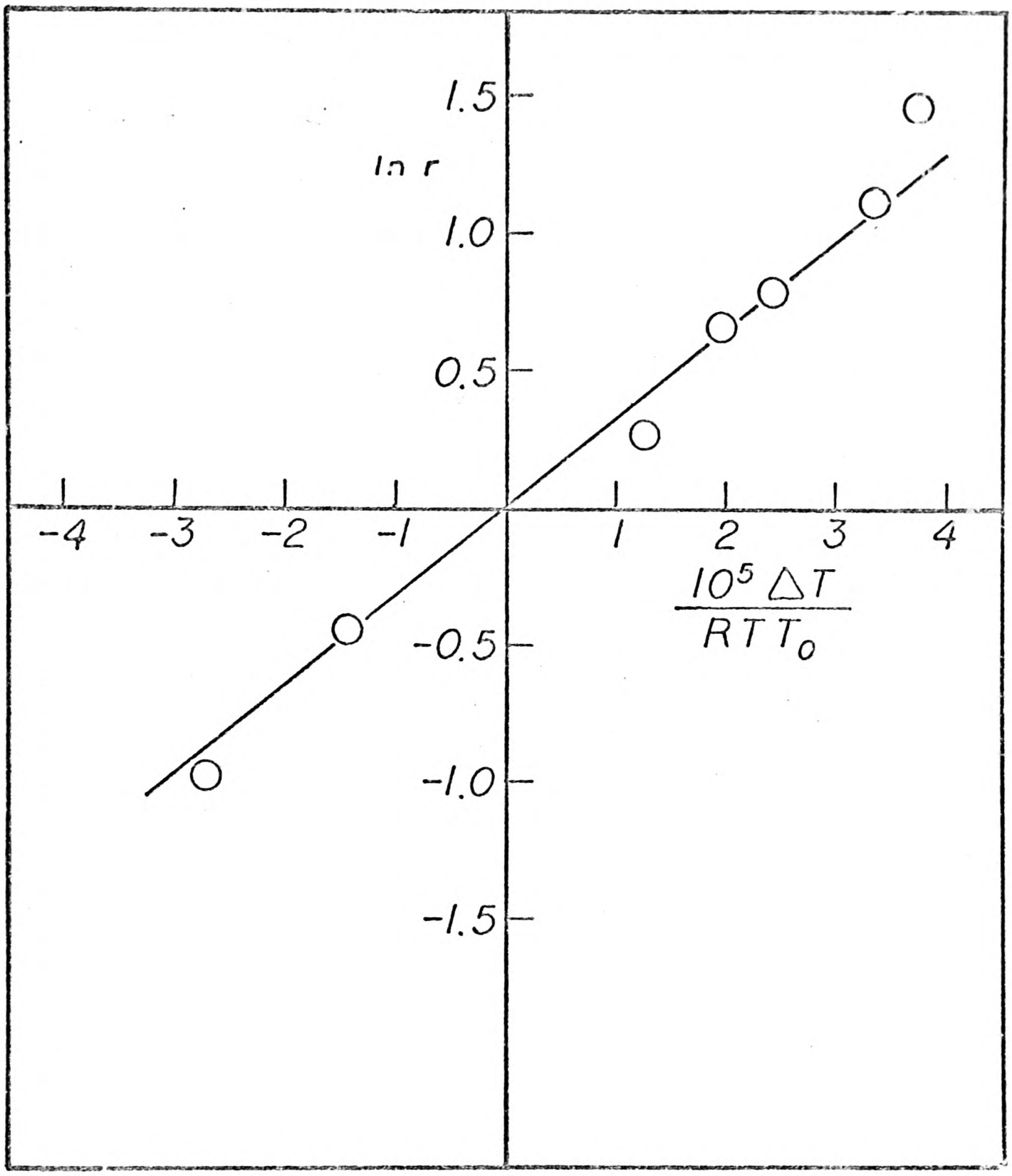


Figure 6-12

ln r- ΔT plot for specimen CH2-16-1(m71,Hfh), creep T-jumps, load = 4 kg, $\Delta H_a = 32 \pm 3$ kcal/mol.

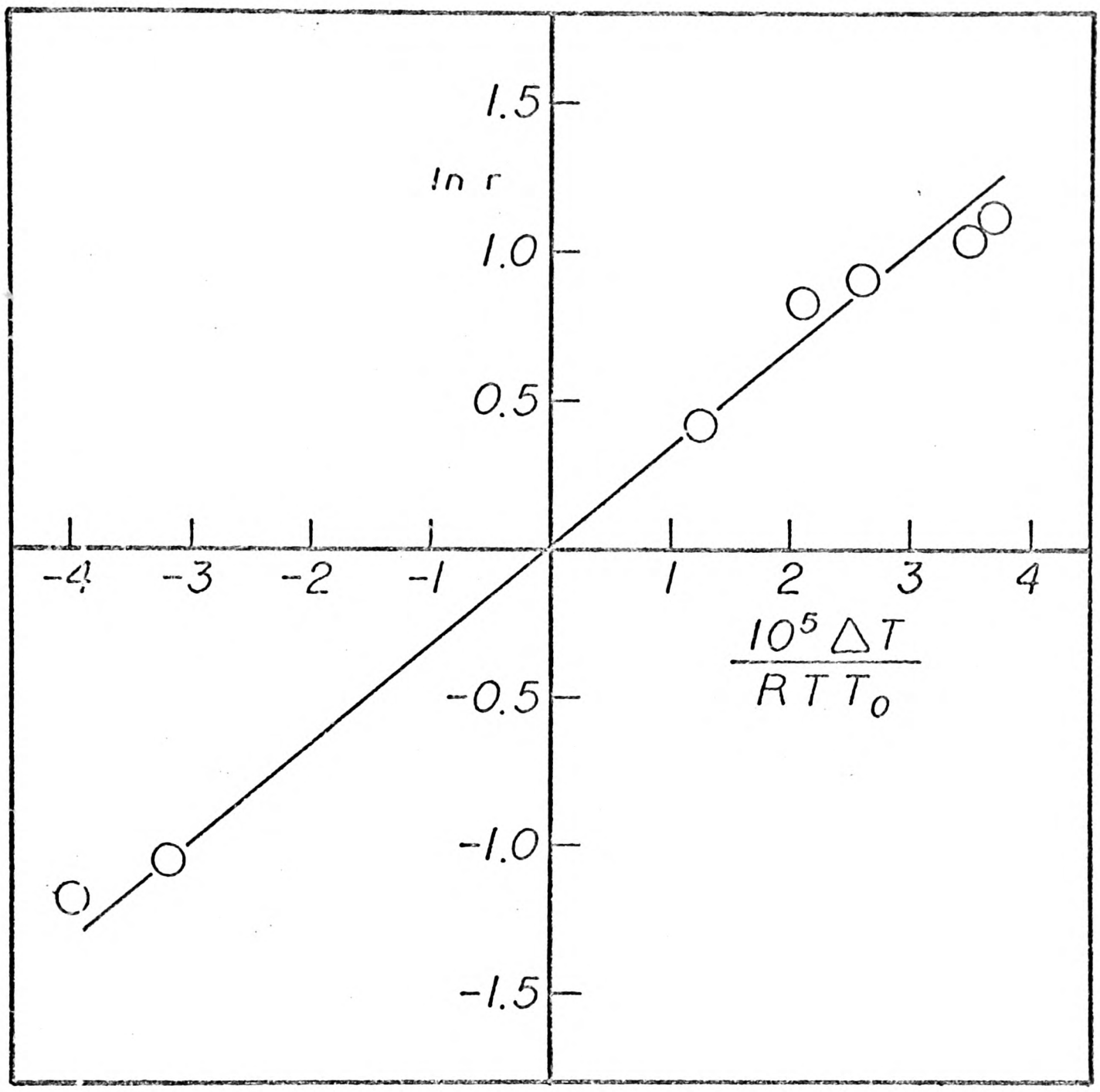


Figure 6-13

ln r- ΔT plot for specimen CH2-16-1(m71,Hfh), creep T-jumps, load = 5.9 kg, $\Delta H_a = 33 \pm 3$ kcal/mol

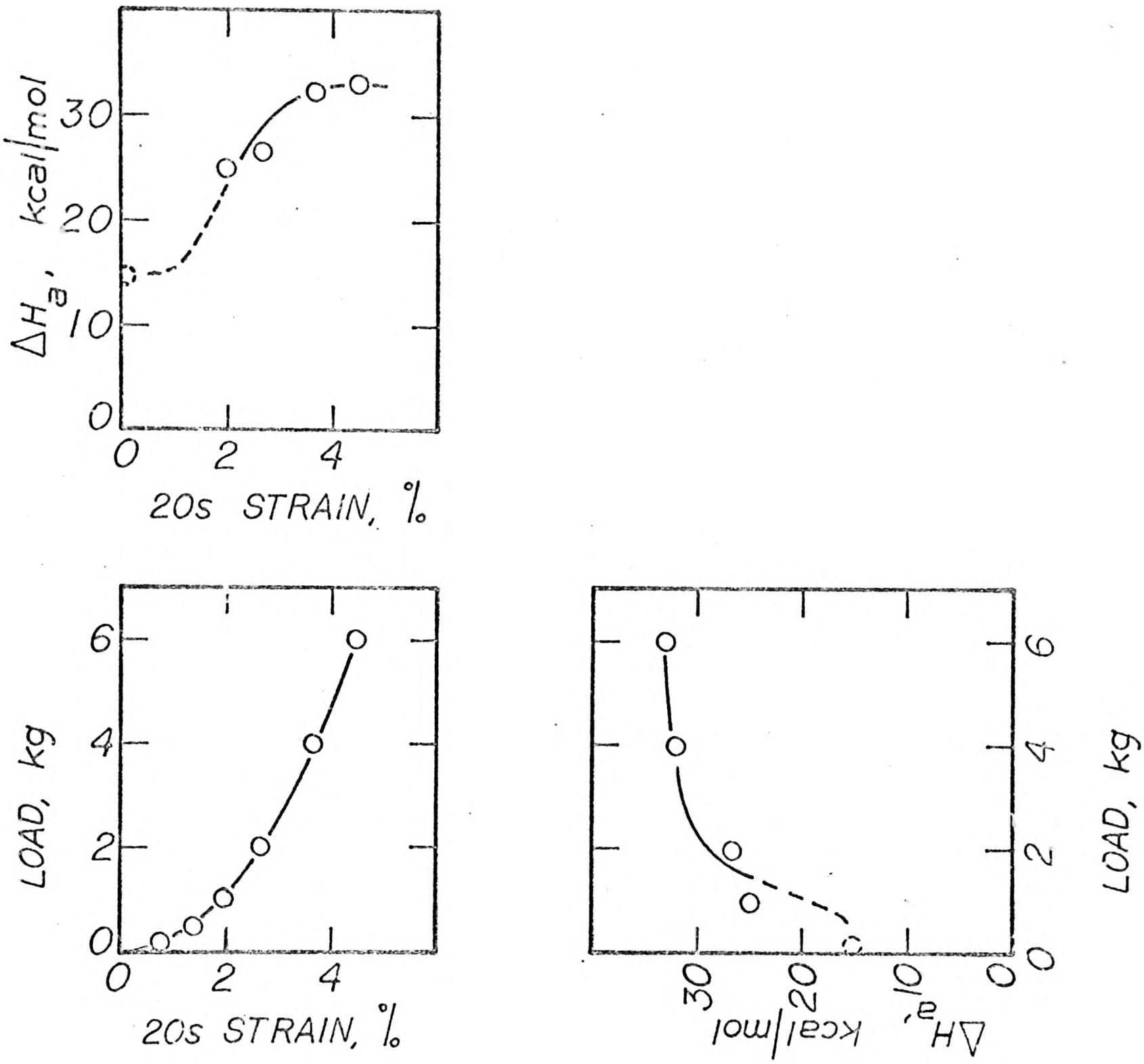


Figure 6-14

Bottom left: 20s isochronal load-strain curve

Right : dependence of ΔH_a on load

Top : dependence of ΔH_a on 20s strain

Specimen CH2-16-1(m71,Hfh), T_o = 28 °C, creep T-jump.

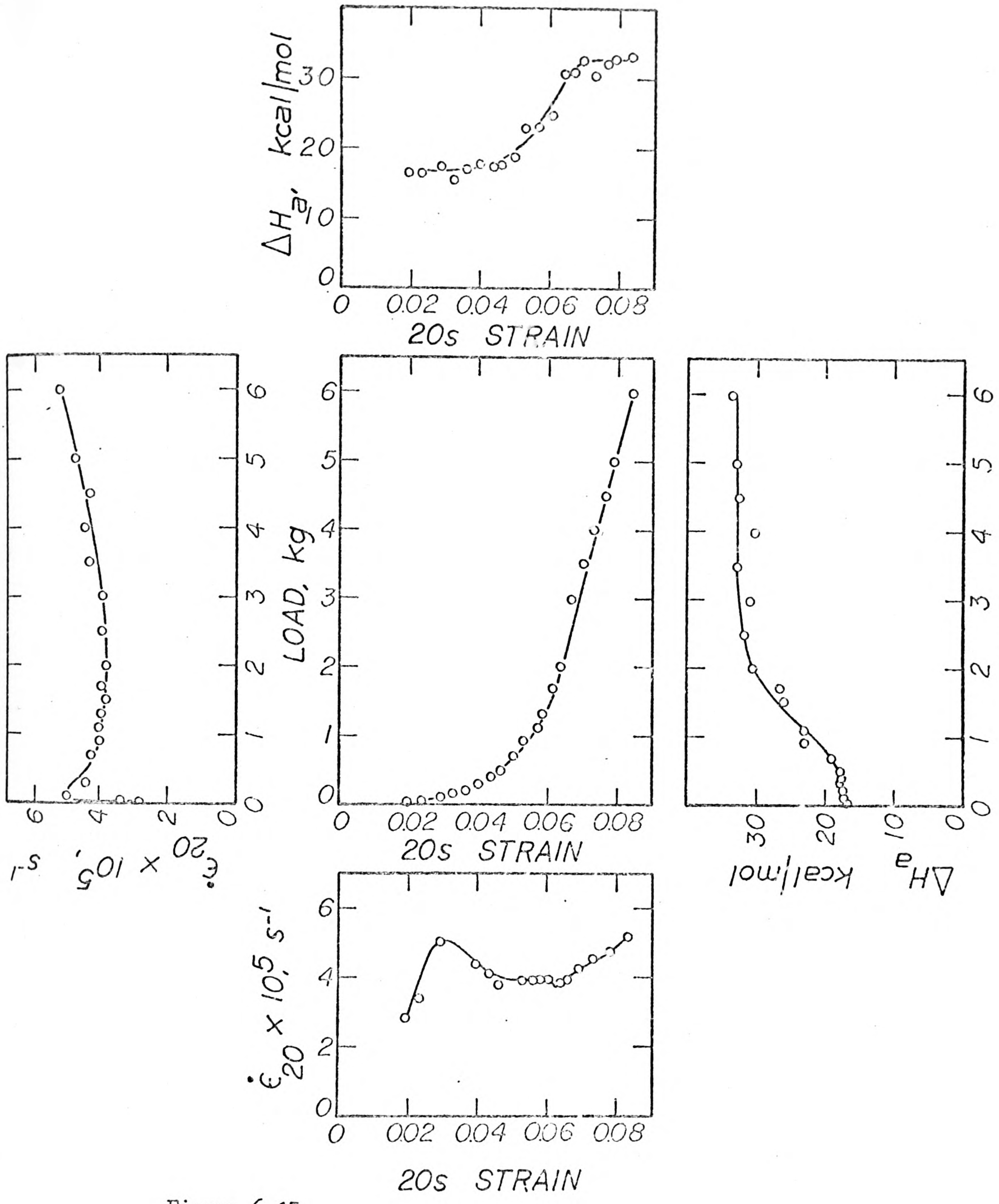


Figure 6-15

Centre: 20s isochronal load-strain curve
Right : dependence of ΔH_a on load
Left : dependence of 20s creep rate on load
Top : dependence of ΔH_a on 20s strain
Bottom: dependence of 20s creep rate on 20s strain.
specimen CH2-8-2(m23,Heh), T_o = 28 °C, creep T-jumps.

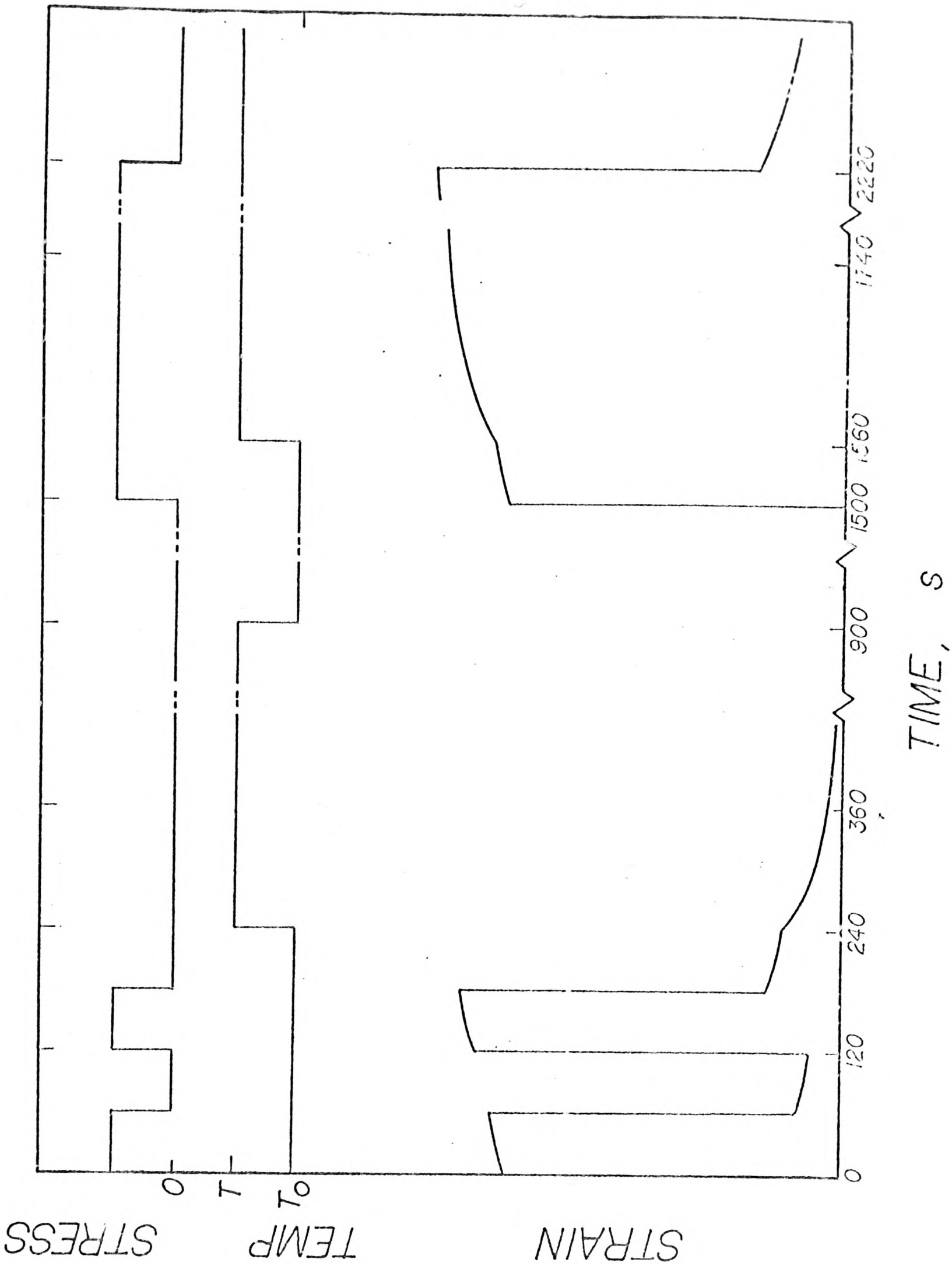


Figure 6-16

Schematic diagram of loading and temperature histories and creep response for specimen CH2-8-3(m23,Heh).

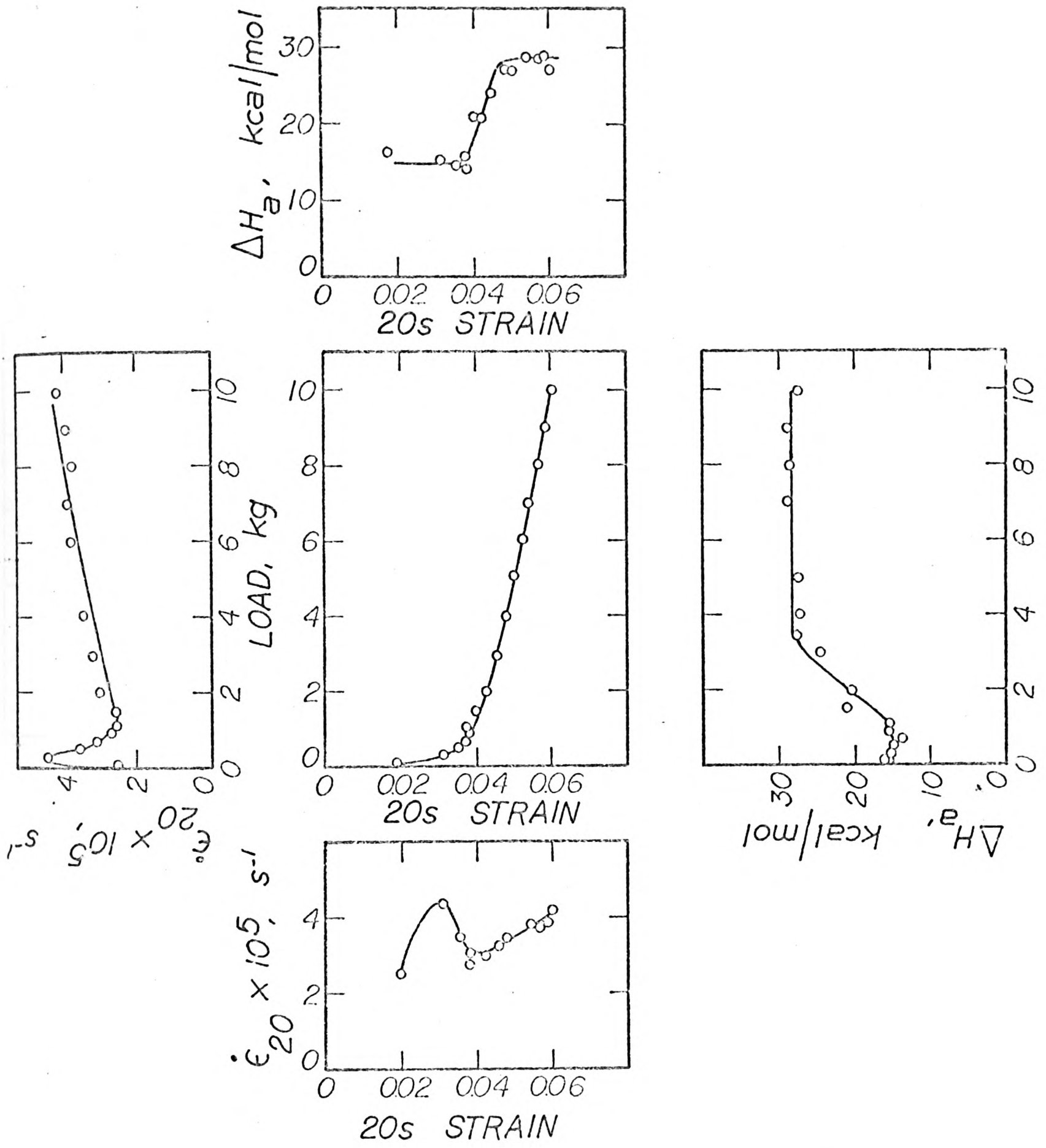


Figure 6-17

Centre: 20s isochronal load-strain curve
Right : dependence of ΔH_a on load
Left : dependence of 20s creep rate on load
Top : dependence of ΔH_a on 20s strain
Bottom: dependence of 20s creep rate on 20s strain.
specimen CH2-8-3(m23,Heh), T_o = 28 °C, creep T-jumps.

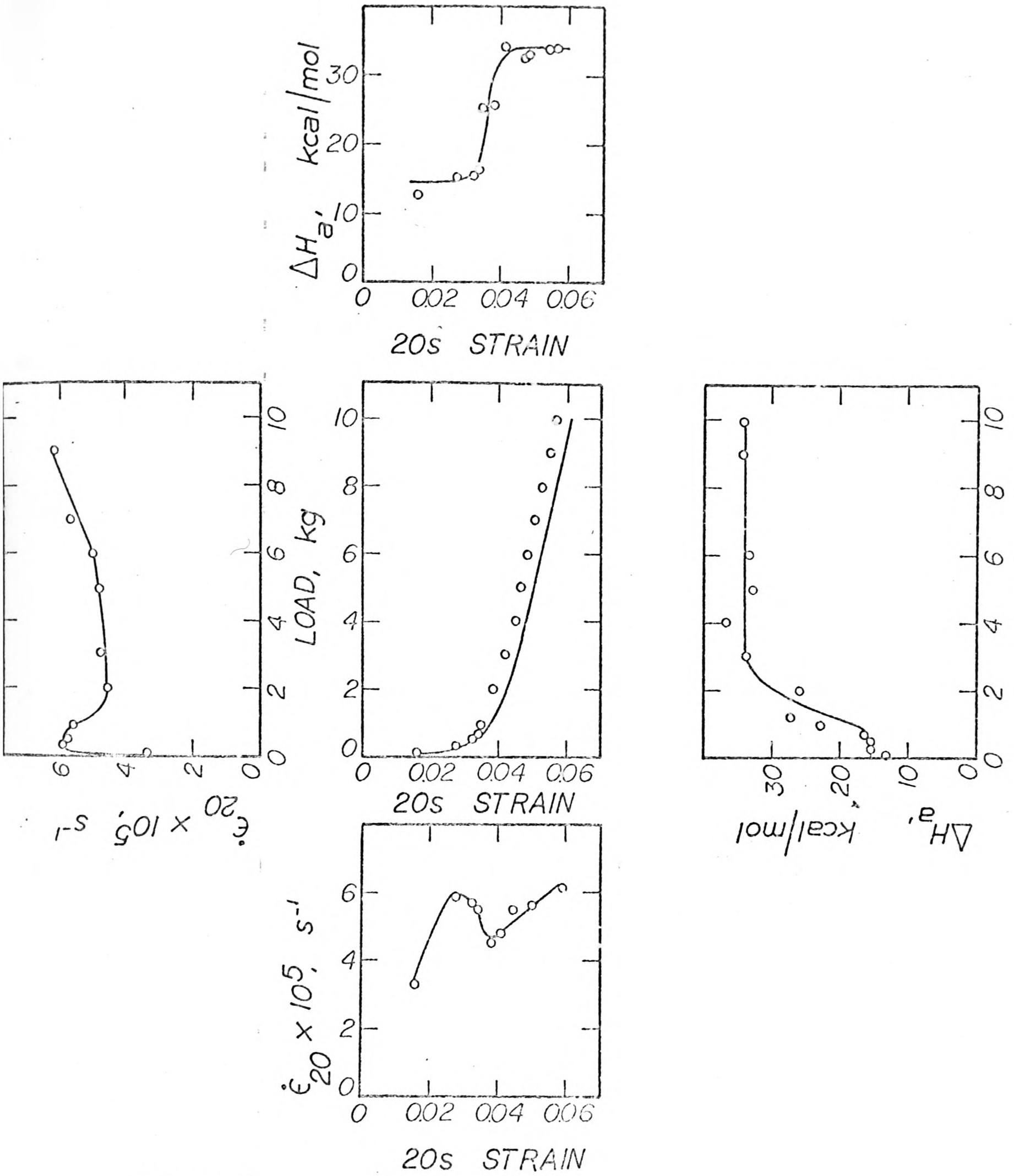


Figure 6-18

Centre: 20s isochronal load-recovery strain curve (circled points). (also shown is the 20s load-creep strain curve of figure 6-17, continuous line).
Right : dependence of ΔH_a on load
Left : dependence of 20s recovery rate on load
Top : dependence of ΔH_a on 20s recovery strain
Bottom: dependence of 20s recovery rate on 20s recovery strain.
specimen CH2-8-3(m23,Heh) T_o = 28 C, recovery T-jumps.

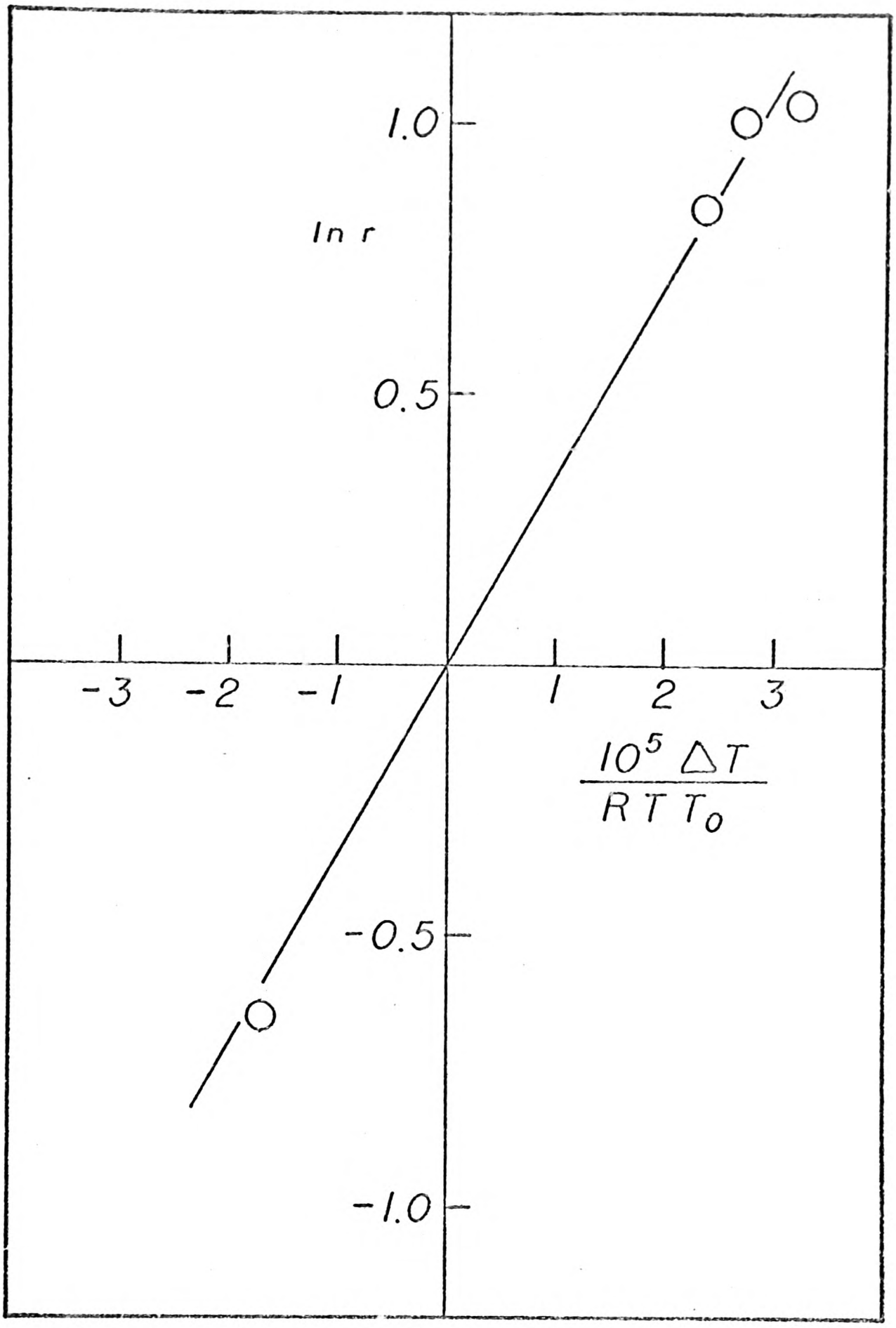


Figure o-19

ln r-- ΔT plot for specimen CH2-16-4(m71,Hfh), creep T-jumps, preload = 3 kg, load = 2 kg, ΔH_a = 34 kcal/mol.

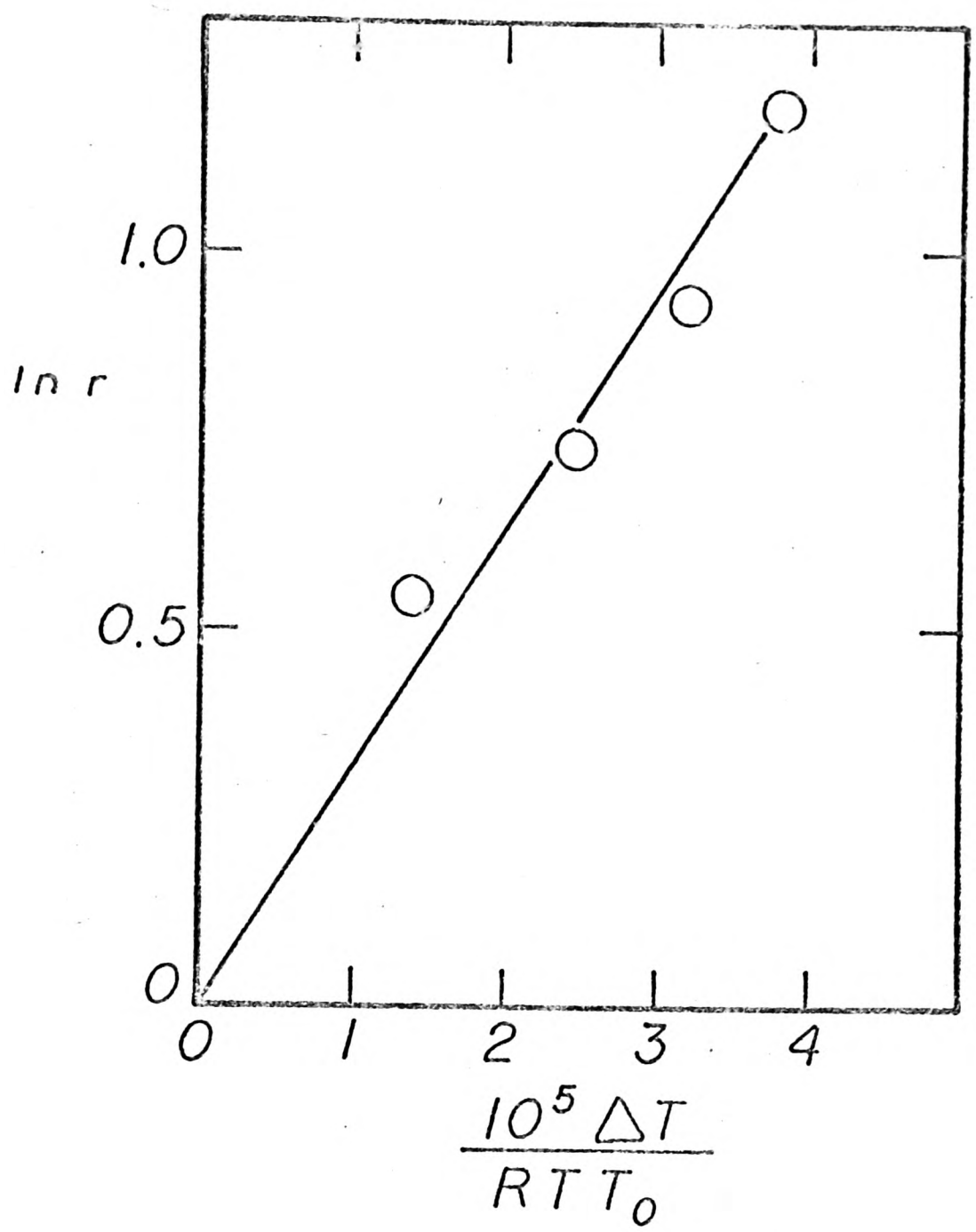


Figure 6-20

ln r- ΔT plot for specimen CH2-16-4(m/1,Hfh), creep T-jumps, preload = 3 kg, load = 3 kg, ΔH_a = 32 kcal/mol.

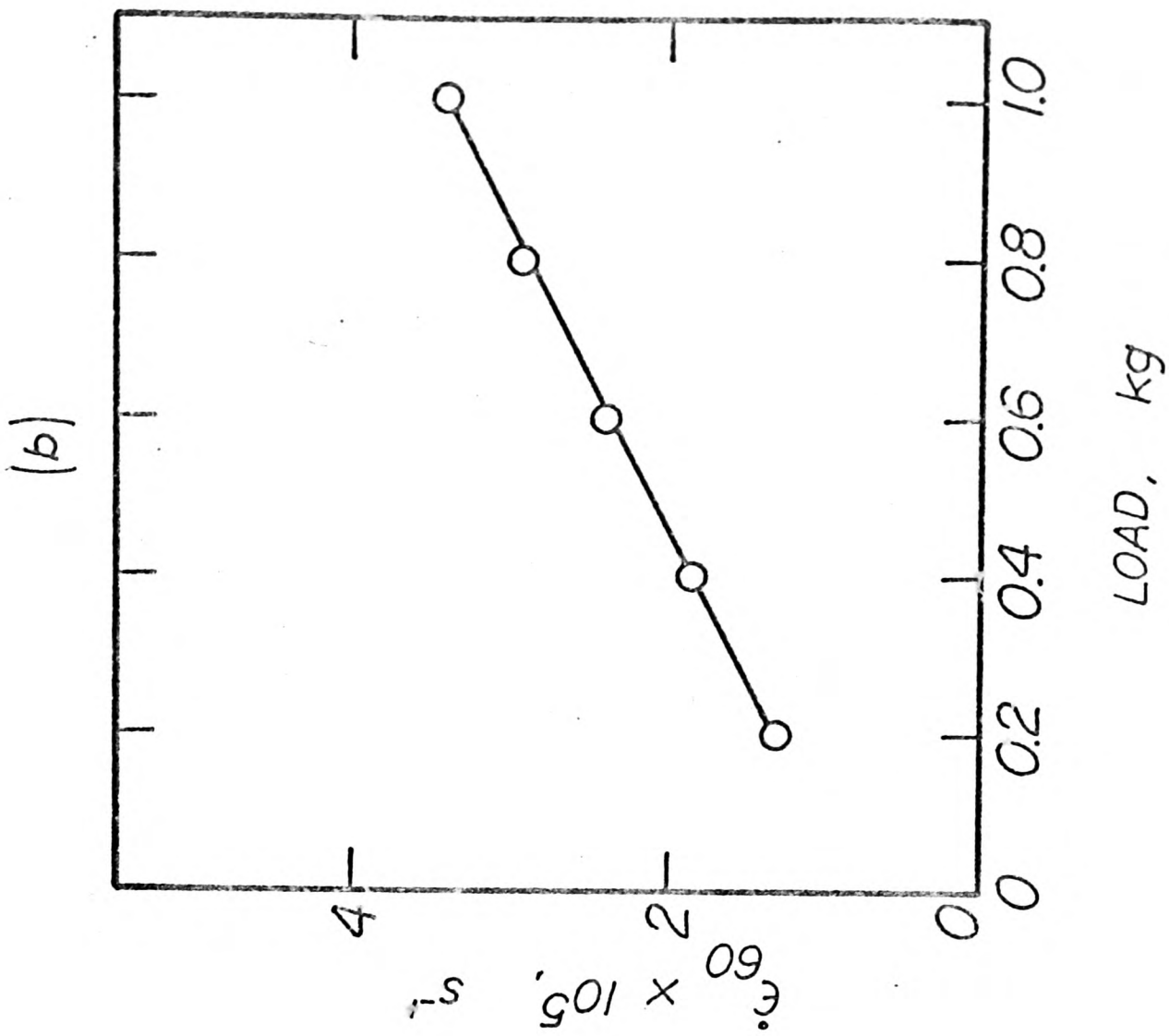


Figure 6-21

a) 60s isochronal load-strain curve
b) 60s isochronal creep rate against load curve
for collagen tape, 3500 denier, T_o = 28°C.

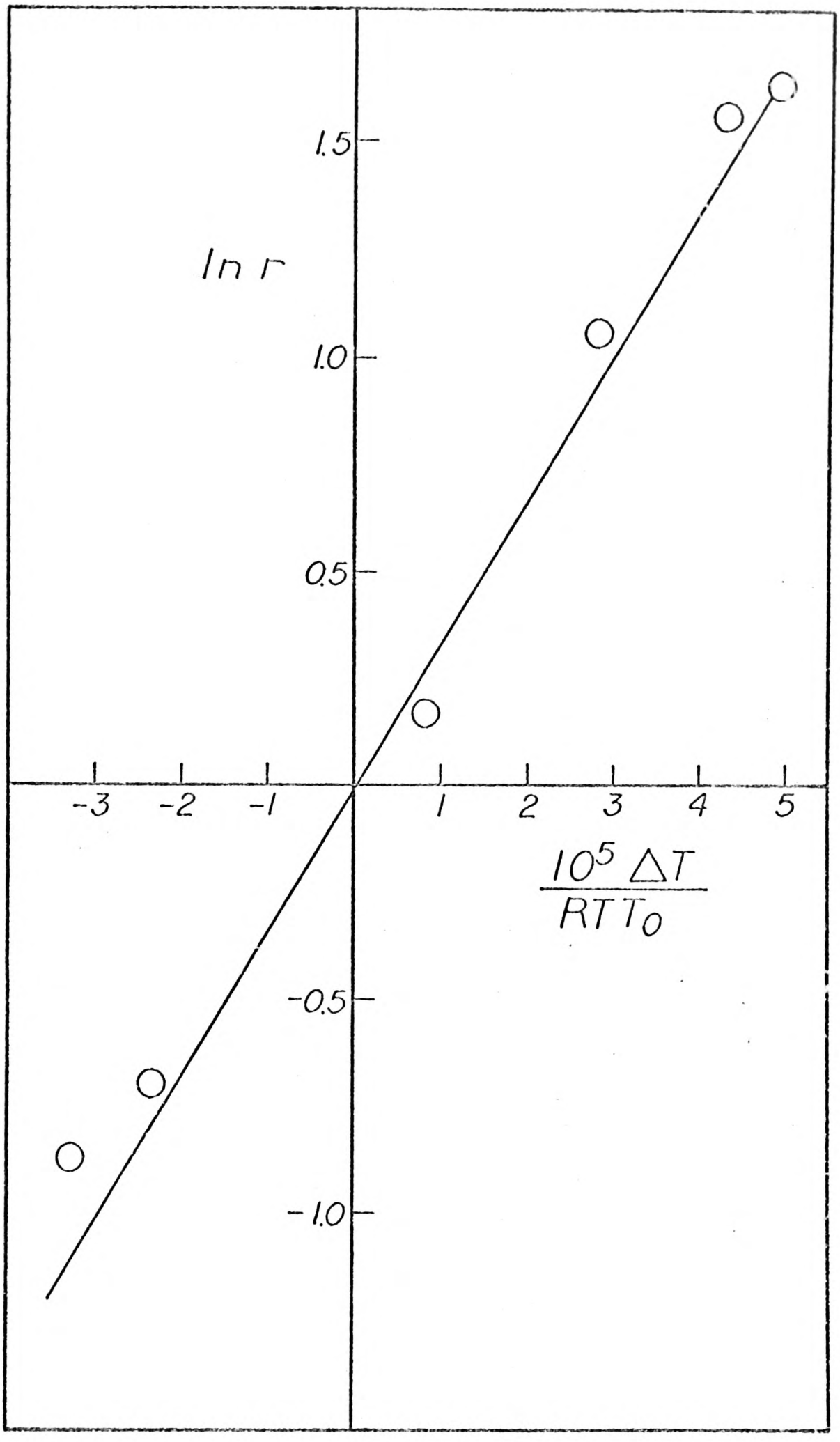


Figure 6-22

ln r- ΔT plot for creep T-jumps on collagen tape, 3500 denier, load = 0.8 kg, T_o = 28 °C, ΔH_a = 33 kcal/mol.

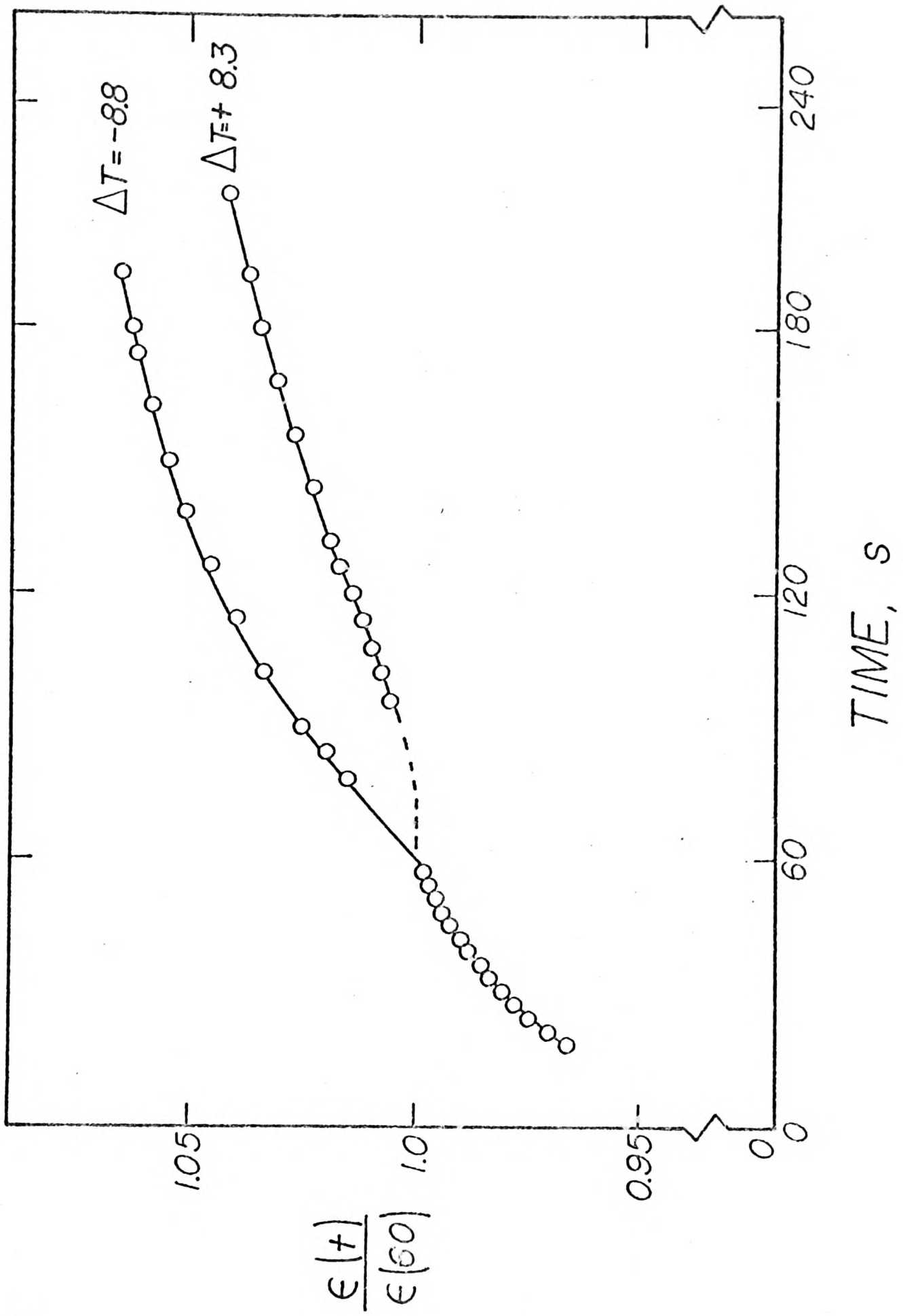


Figure 6-23

Dependence of strain ($\epsilon(t)/\epsilon(t=60s)$) on time during creep T-jumps on contracted bovine deep flexor foot tendon (specimen BF2) after being heated to 65 °C for 48 hours.
ΔT = +8.3 °C ($\epsilon(60s)$ = 29.7%), and ΔT = -8.8 °C ($\epsilon(60s)$ = 28.79%)
load = 0.2kg, T_o = 28 °C.

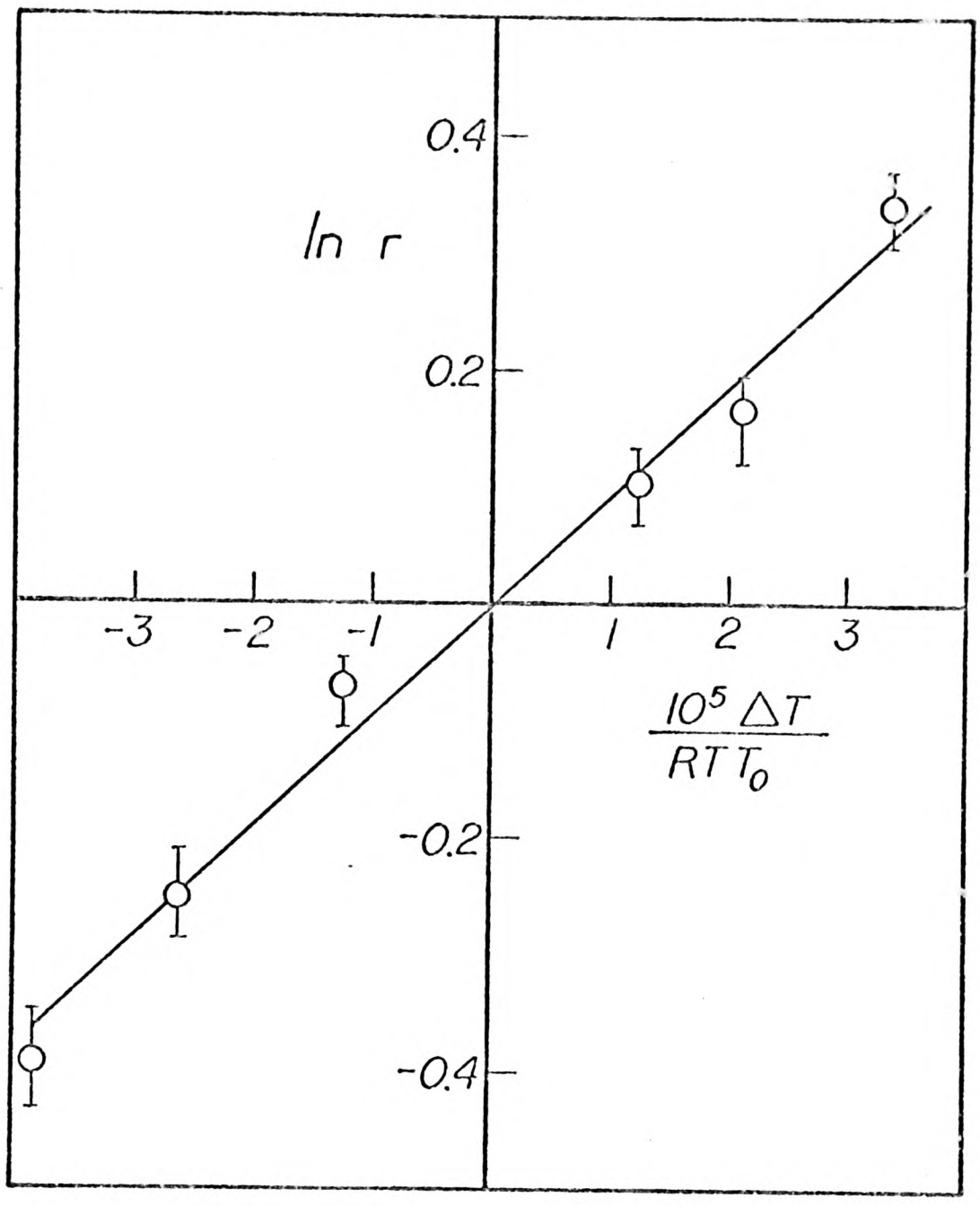


Figure 6-24

ln r- ΔT plot for tendon BT2 after contraction, creep T-jumps, load = 0.2 kg, $\Delta H_a = 9 \pm 4$ kcal/mol.

Chapter 7

Theoretical Model for the Creep Behaviour of Tendon

7.1 Introduction

The results of a variety of experiments conducted on various tendon specimens at low strains suggests that the mechanism involved in the deformation process is related in some way with the mucopolysaccharides of the connective tissue. Gibbs[1] has found a value of ΔH_a=9-10 kcal/mol for the activation energy of hyaluronic acid at pH, concentration, ionic strength and temperature close to those found in the body. The value for ΔH_a in the low strain region is close to this. The high strain value of 32 kcal/mol suggests that the fibres themselves make the major contribution to the deformation in this region. It is reasonable to assume that there is a gradual change from one mechanism to the other.

The most likely way in which the mucopolysaccharides and the fibres combine to elicit the overall observed behaviour can be seen by considering the structure of the tendon. As stated earlier, the tendon consists of collagen fibres which are made up of smaller units of collagen ribbons[2] and fibrils, (figure 1-4) in between which is the mucopolysaccharide gel.[3] When unstressed, the fibres, ribbons and fibrils are crimped,[2] i.e. they are in the form of a planar zig-zag, (figure 7-1). The initial value of the crimp angle, θ_o, between the crimped ribbon (or crimped fibre or fibril) plane, (see figure 7-1(a)) and the tendon axis has been found to lie in the range 13° to 20°[2] for rat-tail tendons, the value depending on the age of the animal. On stretching, the crimp straightens out, and the crimp angle, θ, decreases until a level of strain is reached at which the fibres are straight. For increasing strain, it is likely that the fibres are being stretched. The shape of the stress-strain curve can be correlated to these various features of the geometry of the tendon, namely the 'toe' region which

corresponds to the straightening crimp,[2,4,5] followed by the 'linear' region of the fibre stretching.

Most mechanical models have been concerned with the elastic behaviour of the tendon and collagen.[2,6,7] To explain the viscoelastic properties of tendon, workers have concentrated on phenomenological models with non-linear springs and dashpots.[8-12] The drawback with such models is that they lose their physical significance since the parameters associated with the non-linear springs and dashpots cannot be related to the physical constants or viscoelastic parameters of the actual tendon and its constituents.

In the model to be developed to explain the viscoelastic properties of the tendon, we will begin with the basic 3-parameter standard linear viscoelastic solid approach; each of the springs and dashpots will have parameters related to material constants of either the fibres or the gel. We will then extend the treatment to consider the more realistic case of a distribution of retardation times and use this to predict experimental behaviour.

7.2 Creep Deformation with a Single Retardation Time.

7.2.1 The 'Toe' Region

The low activation energy found for the low strain behaviour suggested that at these low strains the deformation mechanism was one of shearing of the viscoelastic gel between the ribbons* of the collagen fibres. In the following model, we assume that this shearing process is the

---

*It is not clear as yet whether the crimped ribbon structure is present down to the level of the dimensions of the fibril, although it is likely that it does since it has been estimated that the fibril is the load bearing unit.[2] Hence, we will continue to use the term 'ribbon' for any fibrous entity which is crimped.

dominant viscoelastic process until the fibres are straight. During the shearing process, we assume that the ribbons are not being sheared, (i.e. their shear compliance is essentially infinite compared to that of the gel), and that they are not subjected to any tensile stress which would result in them being stretched.

Consider a parallel array of tendon ribbons under zero stress. The initial angle between the crimped ribbons and the fibre (or tensile) axis is θ_o as shown in figure 7-1(a). If a tensile stress, σ , is applied along the fibre axis, then the initial tensile strain which results decreases the crimp angle to θ . The shear stress, Σ , on the plane at angle θ to the fibre axis is [13]

$$\Sigma = \sigma \sin\theta \cos\theta \qquad (7.1)$$

Under this shear stress, the ribbons will slide and rotate and the angle θ will change by a small amount $d\theta$. To a first approximation, the point P (figure 7-1(b))will move a distance $ad\theta$ relative to Q, where a is the sum of the width of the ribbon and the distance between them as shown. Since P' does not move relative to Q (as we assume that there is no shear of the ribbons), then the displacement of P relative to P' is $ad\theta$. The shear strain of the gel is thus $\frac{ad\theta}{b}$ (where b is the distance in between the ribbons) and the shear rate, $\dot{\gamma}$, of the gel is

$$\dot{\gamma} = -\frac{a}{b}\frac{d\theta}{dt} \qquad (7.2)$$

(with a -ve sign as the shear stress is +ve in the direction of increasing θ). In the region where the ribbons are crimped, we can relate the tensile strain to the angle θ by considering the straightening of the ribbons as shown in figure 7-1(c), where it can be seen that the isochronal strain, ϵ , in the direction of the tensile axis is

$$\epsilon = \frac{\cos\theta - \cos\theta_o}{\cos\theta_o} \tag{7.3}$$

and differentiating

$$\frac{d\epsilon}{dt} = -\frac{\sin\theta}{\cos\theta_o}\frac{d\theta}{dt} \tag{7.4}$$

and hence

$$\dot{\gamma} = \frac{a}{b}\frac{\cos\theta_o}{\sin\theta}\dot{\epsilon} \tag{7.5}$$

where $\dot{\epsilon}$ is the strain rate in the tensile direction. Note that, since we have assumed that in this 'toe' region the major deformation mechanism is this shearing mechanism, then $\dot{\epsilon}$ is the strain rate of the gel and of the whole material. Even though the initial ($t=0^+$) elastic deformation may result from a different mechanism, equation (7.5) is still valid if the assumption of the shearing process being the dominant viscoelastic mechanism is true.

We can now determine the viscoelastic response for this mechanism from the 3-parameter model of figure 7-2.[14] The differential equation relating the shear strain rate to the shear stress is

$$\frac{d\gamma_G}{dt} + \frac{\gamma_G}{\eta_G \Delta J_G} = \frac{\Sigma}{\eta_G}\left(\frac{J_{U_G}}{\Delta J_G} + 1 + \dot{J}_{U_G}\eta_G\right) + J_{U_G}\frac{d\Sigma}{dt} \tag{7.6}$$

where the subscript G refers to the gel and J_U, ΔJ and η are the unrelaxed compliance, compliance difference and the shear viscosity respectively. Σ is essentially constant over the time period in which we are interested and equal to Σ_o. (Over a time interval of 60s, say, the change in θ (obtained from experimental data using equation (7.3)), produces a change in Σ (from equation(7.1)) of $< 0.5\%$). With this assumption, we can integrate equation (7.6) to give the shear strain as

$$\frac{\gamma}{\Sigma_o} = J_{U_G} + \Delta J_G \left(1 - \exp\left(- \frac{t}{\tau_G} \right) \right) \qquad (7.7)$$

and differentiating

$$\frac{\dot{\gamma}}{\Sigma_o} = \frac{\Delta J_G}{\tau_G} \exp\left(- \frac{t}{\tau_G} \right) \qquad (7.8)$$

where $\tau_G = \eta_G \Delta J_G$ is the retardation time of this model. Substituting equations (7.5) and (7.1) in equation (7.8) we obtain the relation between the tensile stress and the tensile creep rate as

$$\frac{\dot{\epsilon}_G(t)}{\sigma_o} = \frac{\Delta J_G}{\tau_G} f(\theta) \exp\left(- \frac{t}{\tau_G} \right) \qquad (7.9)$$

where

$$f(\theta) = \frac{b}{a} \frac{\sin^2\theta \cos\theta}{\cos\theta_o} \qquad (7.10)$$

Hence we see that the solution is similar to that for a normal linear viscoelastic material[14] except for the term $f(\theta)$ which decreases to zero as θ decreases to zero. Equation (7.9) becomes more manageable if we use equation (7.3) relating the strain to the angle θ and we obtain

$$\frac{\dot{\epsilon}_G(t)}{\sigma_o} = \frac{\Delta J_G}{\tau_G} f(\epsilon) \exp\left(- \frac{t}{\tau_G} \right) \qquad (7.11)$$

where

$$f(\epsilon) = \frac{b}{a} \left\{ 1 - \cos^2\theta_o (1 + \epsilon)^2 \right\} (1 + \epsilon) \qquad (7.12)$$

This equation is similar in form to that used by various workers on elastomers[15] where the strain and time dependence of the non-linearity are separable.

Certain things are immediately apparent from equations (7.11) and (7.12). If the isochronal values of $\dot{\epsilon}_G / \sigma_o$ of equation (7.11) are plotted against $(1+\epsilon)$ for values of $\epsilon \geq 0$, an approximate straight line will result

as shown in figure 7-3. The importance of this will be seen when considering the experimental data in chapter 8. We chose a value of $\theta_o = 16^\circ$ for figure 7-3 which is a realistic value since it is (i) in the range found by Diamant et al[2] for rat-tail tendon and (ii) is of the order of that found from fitting equation (7.11) to the tendon data as shown in chapter 8, (figure 8-1). The intercept of the best straight line through the experimental data in the toe region on an isochronal(creep rate/ σ_o) against $(1+\epsilon)$ plot yields, from equation (7.11), a value equal to $1/\cos\theta_o$. (It should be remembered that in the 'toe' region, $\dot{\epsilon}_G(t)$ will be equal to the creep rate of the whole specimen).

In order to find the shape of the creep rate against load curve for the gel as described in equation (7.11) we must first assume a functional form for the isochronal stress-strain curve. A convenient one, which also nicely approximates the observed experimental stress-strain curve, is the parabola[16]

$$\sigma_o = c_o \epsilon^2 \qquad (7.13)$$

where c_o is a constant determined from fitting the isochronal stress-strain curve and ϵ, as before is the strain at a particular time, usually 20s in this modelling. This will be found not to detract from the findings of the subsequent modelling. Using this equation(7.13) in equation (7.11) we obtain the equation

$$\dot{\epsilon}_G(t) = \frac{b}{a} c_o \frac{\Delta J_G}{\tau_G} \chi_G \qquad (7.14)$$

where

$$\chi_G = \epsilon^2 (1+\epsilon) \left\{ 1 - \cos^2\theta_o (1+\epsilon)^2 \right\} \exp\left(-\frac{t}{\tau_G}\right) \qquad (7.15)$$

In figure 7-4, the function $\chi_G \left(= \dot{\epsilon}_G / \frac{b}{a} c_o \frac{\Delta J_G}{\tau_G}\right)$ of equation (7.15) is plotted against (σ_o / c_o) for a given value of t. t/τ_G

is assumed small enough that exp $(-\frac{t}{\tau_G})$ is equal to unity. This effectively represents a plot of creep rate against stress with the various parameters $\tau_G/\Delta J_G$, $\frac{a}{b}$, and c_o equal to unity. It can be seen from figure 7-4(a) that the model predicts a peak (or 'hump') in the creep rate against load dependence for tendon. This agrees with the experimental data of figures 5-13, 6-15 and 6-17 where a'hump' was seen on the creep rate-load plot at low strains in the 'toe' region. Hence, here is another qualitative correlation of the simple model with experimental data.

7.2.2 The 'Linear' Region

Once the crimp has straightened out, we assume that the fibres themselves contribute solely to the viscoelastic process. We assume that the fibres exhibit linear viscoelastic behaviour,i.e. the isochronal creep rate is linear with stress. The equation for the creep rate of the fibre for a single retardation time model shown in figure 7-2 is

$$\frac{\dot{\epsilon}_F(t)}{(\sigma_o - \sigma')} = H(\sigma_o - \sigma') \frac{\Delta D_F}{\tau_F} \exp(-\frac{t}{\tau_F}) \qquad (7.16)$$

where σ' is the value of the stress at which the fibres just become straight, subscript F refers to the fibre and ΔD is the tensile compliance difference. H is the Heaviside unit step function. Using equation (7.13) we obtain for the isochronal creep rate

$$\dot{\epsilon}_F(t) = H(\sigma_o - \sigma') c_o \frac{\Delta D_F}{\tau_F} \chi_F \qquad (7.17)$$

where

$$\chi_F = (\epsilon^2 - \epsilon'^2) \exp(-\frac{t}{\tau_F}) \qquad (7.18)$$

and ϵ' is the isochronal strain at which the fibres become straight.

In figure 7-4(b) we have plotted the fibre creep rate of equation (7.17) (i.e. isochronal $\dot{\epsilon}_F(t) / \frac{b}{a} c_o (\frac{\Delta J_G}{\tau_G}) = \chi_F(\frac{\Delta D_F}{\tau_F}) / \frac{b}{a} (\frac{\Delta J_G}{\tau_G}))$ against stress (σ_o / c_o) with an arbitrary value of ($\frac{\Delta D_F}{\tau_F}$)/($\frac{b}{a} \frac{\Delta J_G}{\tau_G}$) to give the approximate order of magnitude of the fibre rate to that of the gel. (We again assume that t/τ_F is small enough that exp ($-\frac{t}{\tau_F}$) is equal to unity). The total creep rate due to both fibres and gel will be assumed to be given by the sum of the two contributions, and is , (using equations (7.11) and (7.16))

$$\dot{\epsilon}(t) = \dot{\epsilon}_G(t) + H(\sigma_o - \sigma') \dot{\epsilon}_F(t)$$

$$= \frac{\Delta J_G}{\tau_G} f(\theta) \exp(-\frac{t}{\tau_G}) \sigma_o + H(\sigma_o - \sigma') \frac{\Delta D_F}{\tau_F} \exp(-\frac{t}{\tau_F}) (\sigma_o - \sigma') \quad (7.19)$$

Using equation (7.13), we obtain the creep rate as

$$\dot{\epsilon}(t) = \frac{b}{a} c_o \frac{\Delta J_G}{\tau_G} \chi_G + H(\sigma_o - \sigma') c_o \frac{\Delta D_F}{\tau_F} \chi_F \quad (7.20)$$

In figure 7-4(c) we have plotted the total isochronal creep rate given by

$$\chi_T = \dot{\epsilon}(t)/(\frac{b}{a} c_o \frac{\Delta J_G}{\tau_G}) = \chi_G + H(\sigma_o - \sigma') \left\{ (\frac{\Delta D_F}{\tau_F}) / (\frac{b}{a} \frac{\Delta J_G}{\tau_G}) \right\} \chi_F \quad (7.21)$$

against stress (σ_o / c_o)*. Note that this plot is beginning to resemble the creep rate against load curves of specimens CH2-8-2 and CH2-9-1 shown in figures 6-15 and 5-13 respectively.

---

*In all plots of rate against load for the single retardation time model, we assume for convenience that t/τ_G and t/τ_F are small so that both exp($-\frac{t}{\tau_G}$) and exp($-\frac{t}{\tau_F}$) are equal to unity.

7.2.3 Distribution of Crimp Angles.

One striking difference between the experimental and theoretical curves of the simple model developed so far is that in the experimental curves, there is a smooth transition between the gel behaviour and the linear fibre behaviour. This difference arises almost certainly from the fact that in the tendon as a whole, not all of the fibres and ribbons will have the same initial crimp angle. This has been observed for the fibres in the polarising light microscope by Viidik.[4] There will obviously be a distribution of initial crimp angles, θ_o. Such a distribution of values of θ_o was introduced into the model in the form of a Gaussian (or normal) distribution[17] in which each rate for a given initial crimp angle, θ_o', is multiplied by the probability of that rate occurring, $p(\theta_o')$, given by

$$p(\theta_o') = \frac{1}{(2\pi\bar{\lambda}^2)^{\frac{1}{2}}} \exp\left\{ - \frac{(\theta_o' - \theta_o)^2}{2\bar{\lambda}^2} \right\} \qquad (7.22)$$

where θ_o is still defined as before but now takes on the added significance of the mean value of the distribution of initial crimp angles. $\bar{\lambda}$ is the standard deviation* and is a constant which takes different values for distributions of various broadness. Values of $p(\theta_o')$ for various values of $\bar{\lambda}$ are shown in figure 7-5. It is difficult to know which might apply to the tendon, so a variety of values of $\bar{\lambda}$ were tried in our model. The procedure was as follows:

for a given value of ϵ, θ_o', $\bar{\lambda}$ and $\left(\frac{b}{a}\frac{\Delta J_G}{\tau_G}\right) / \left(\frac{\Delta D_F}{\tau_F}\right)$

the value of χ_T in equation (7.21) was found and multiplied by $p(\theta_o')$. This

---

* It is unfortunate that in statistics, the usual symbol for the standard deviation is the same as that used for stress. We have thus used $\bar{\lambda}$ for the standard deviation in all the equations.

was repeated at that same value of ϵ for enough values of θ_o' such that integration of the resulting function $p(\theta_o')\,\dot{\epsilon}(t, \theta_o')\,d\theta_o'$ could be performed by an incremental parabolic rule technique using the equation [18]

$$\int_o^N f(x)\,dx = \frac{\Delta x}{3}\left\{f(0)+4f(1)+2f(2)+4f(3)+.....2f(N-2)+4f(N-1)+f(N)\right\} \qquad (7.23)$$

where Δx is the constant difference between the values of x taken. The resulting values of the isochronal creep rate χ_T are shown in figure 7-6 for values of $\bar{\lambda}$ ranging from 1.0 to 4.0 and with $\theta_o = 16^\circ$. Also shown is the dashed curve for a single ribbon with $\theta_o = 16^\circ$. A value of $(\frac{b}{a}\frac{\Delta J_G}{\tau_G})/(\frac{\Delta D_F}{\tau_F})$ =160 was taken to give the right order of magnitude relation between the gel and the fibre rates. It should be noted that by introducing the distribution of initial crimp angles, the creep rate against stress curve now becomes smooth and of the form observed in experimental data. As can be seen from figure 7-6, the 'hump' in the rate against stress curve disappears as the distribution in θ_o gets wider, (i.e. as $\bar{\lambda}$ gets larger). This is an important prediction of the model and is a feature never considered previously. Measurements of the parameter $\bar{\lambda}$, (the standard deviation of the distribution of crimp angles) will provide support for our model. If changes in the value of $\bar{\lambda}$ occur with disease, age, etc., this will produce important changes in the viscoelastic behaviour as seen in figure 7-6.

The value of ths slope of the approximately straight part of the creep rate-stress curve at the higher stresses for the larger values of $\bar{\lambda}$ is not equal to that of the fibres and only approaches that of the fibres as the stress increases. This is another feature seen in experimental data (specimen CH2-8-2(figure 6-15), CH2-9-1 (figure 5-13), CH2-16-4 (figure 5-12), CH2-16-1 (figure 5-5)). The 'hump' will also be more or less prominent for two other reasons;

(i) if the value of $(\frac{b}{a}\frac{\Delta J_G}{\tau_G})/(\frac{\Delta D_F}{\tau_F})$ is lower as can be seen in figure 7-7

where a value of 80 was used, or

(ii) if the value of θ_o is smaller as seen in figure 7-8, where values of $\bar{\lambda}=2.0$ and $\left(\frac{b}{a}\frac{\Delta J_G}{\tau_G}\right)/\left(\frac{\Delta D_F}{\tau_F}\right)=120$ and $\theta_o = 12^\circ, 14^\circ, 16^\circ, 18^\circ$, were used. These theoretical graphs compare favourably with the behaviour observed with figures 5-5, 5-12, 5-13, 6-15 and 6-17 of earlier chapters.

If the value of either ΔD_F of the fibres, or ΔJ_G of the gel is altered as a result of disease, (e.g. Ehlers Danlos, Lathyrism, Arthritis), or if the tendon is treated in various ways (e.g. tanning) or if θ_o is changed with age, it is clear from figures 7-7 and 7-8 that there will be a marked change in the viscoelastic properties of the tendon. It should be possible in the future to measure the values of θ_o, ΔJ_G and ΔD_F and to relate these to changes in the viscoelastic behaviour.

7.3 Creep Behaviour with a Distribution of Retardation Times

7.3.1 Isothermal Behaviour

The next stage in the model is to find the correct form of the time dependence of the creep rates. The single retardation time model gives a straight line on a log creep rate against time plot but a curve on a log creep rate against log time plot. We have observed experimentally a straight line on a log rate-log time plot for all our tests on tendon. This can be predicted if we introduce a distribution of retardation times.

For the fibres, which we have assumed to be linear viscoelastic, this is straightforward and takes the form as shown in chapter 4. When the retardation spectrum $L(\ln \tau)$ is taken to be of the form

$$\ln L_F(\ln \tau_F) = m_F \ln \tau_F + \ln C_F \qquad (7.24)$$

(where m_F is the slope and C_F is the intercept on the $\ln L$-$\ln \tau$ plot), then the rate for the fibres is

$$\frac{\dot{\epsilon}_F(t)}{(\sigma_o - \sigma')} = H(\sigma_o - \sigma')\ \Delta D_F(\tau_F=1)\ \frac{\Gamma(n_F)}{(t)^{n_F}} \qquad (7.25)$$

where $-n_F$ is the slope of the log creep rate-log time curve for the fibres and $1-m_F=n_F$. C_F is the value of $L_F(\ln\ \tau_F)$ when $\tau_F=1$, and since $L_F = \Delta D_F\ \tau_F$ then $C_F = \Delta D_F(\tau_F=1)$. Γ is the Gamma function.

We must perform a similar analysis for the gel. We have to go back to the equation (7.8) to introduce the distribution of retardation times of the gel. This equation becomes

$$\frac{\dot{\gamma}}{\Sigma_o} = \int_{-\infty}^{\infty} \frac{L_G(\ln \tau_G)}{\tau_G} \exp\left(-\frac{t}{\tau_G}\right)\ d \ln \tau_G \qquad (7.26)$$

which for $\ln L_G(\ln \tau_G) = m_G \ln \tau_G + \ln C_G$ becomes

$$\frac{\dot{\gamma}}{\Sigma_o} = \Delta J_G(\tau_G=1)\ \frac{\Gamma(n_G)}{(t)^{n_G}} \qquad (7.27)$$

and on using equation (7.1) and (7.5)

$$\frac{\dot{\epsilon}_G(t)}{\sigma_o} = \Delta J_G(\tau_G=1)\ f(\theta)\ \frac{\Gamma(n_G)}{(t)^{n_G}} \qquad (7.28)$$

where $f(\theta)$ is the same as before (equation (7.10)) and effectively reduces the observed height of the retardation spectrum as the stress increases. The total creep rate will now be

$$\dot{\epsilon}(t) = \Delta J_G(\tau_G=1)\ f(\theta)\ \frac{\Gamma(n_G)}{(t)^{n_G}}\ \sigma_o + H(\sigma_o-\sigma')\ \Delta D_F(\tau_F=1)\ \frac{\Gamma(n_F)}{(t)^{n_F}}\ (\sigma_o-\sigma') \qquad (7.29)$$

and

$$\chi \equiv \dot{\epsilon}(t)/\left(\frac{b}{a}\Delta J_G(\tau_G=1)\right)$$

$$= (1+\epsilon)\left\{1-\cos^2\theta_o(1+\epsilon)^2\right\}\frac{\Gamma(n_G)}{(t)^{n_G}}\ \sigma_o + H(\sigma_o-\sigma')\ \frac{\Delta D_F(\tau_F=1)}{\frac{b}{a}\Delta J_G(\tau_G=1)}\ \frac{\Gamma(n_F)}{(t)^{n_F}}\ (\sigma_o-\sigma') \qquad (7.30)$$

where as before σ' is the stress at which θ becomes zero.

It is obvious that this equation will produce a graph of isochronal creep rate against stress of exactly the same form as that shown in figure 7-4 from equation (7.21) for the single value of θ_o and a single τ and the same as figures 7-6, 7-7 and 7-8 for the distribution of θ_o and a single τ, but we now have a time dependence of the correct form. Equation (7.29) will give a straight line on a log creep rate-log time plot of slope $-n_G$ for the low strains and of slope equal to $-n_F$ at high strains once the fibres have straightened out. For the case of a distribution of θ_o's, there will be a gradual transition from one to the other as shown in figure 7-9. In this graph, the slope of the log creep rate-log time curve is plotted against isochronal strain, for values of $\theta_o=16^\circ$, $n_G=1.0$ and $n_F=1.2$ and values of $\bar{\lambda}$ and $(\frac{b}{a}\Delta J_G)/(\Delta D_F)^*$ as shown. It can be seen that with $(\frac{b}{a}\Delta J_G)/(\Delta D_F)$ =120 then as the width of the θ_o distribution increases, so the change from the one slope to the other becomes more gradual. It can also be seen that for a given $\bar{\lambda}$ an increase in the value of $(\frac{b}{a}\Delta J_G)/\Delta D_F$ shifts the curve along the strain axis. This should be compared to figure 5-4 for specimen CH2-8-2.

The dependence of the creep rate against stress curve on both time and the slopes n_G and n_F is shown in figure 7-10, where χ in equation (7.30) (and using equation(7.13) for the stress, with c_o and ϵ taken at t=20s) is plotted against stress σ_o/c_o for two times 20s and 60s and for values of a) $n_G=n_F=1.0$ and b) $n_G=1.0$ and $n_F=1.2$. It can clearly be seen that the values

---

* In future, $\Delta J_G(\tau_G=1)$ and $\Delta D_F(\tau_F=1)$ of equation (7.28) will be written as ΔJ_G and ΔD_F where it is implicit that they are evaluated at $\tau_G=1$ and $\tau_F=1$ respectively.

of the slopes, n, and thus the slopes m of the retardation spectra, play an important role in determining the shape of the creep rate-stress curve. In this particular case, the shape of the curve at larger strains is changed significantly with the change of n_F from 1.0 to 1.2. The values of n_G=1.0 and n_F=1.2 were chosen to be similar to those found experimentally.

7.3.2 Temperature Dependence in Creep; Distribution of Retardation Times

We can now turn our attention to the temperature dependence of the model. Since there are two distinct types of deformation in this model, then each mechanism will have its own temperature dependence, the form of which will manifest itself in the time-temperature shift factor a_T. We denote the shift factor of the gel and fibres as a_{T_G} and a_{T_F} respectively. If we perform a T-jump experiment on the creeping tendon at time t', then if we assume the wedge distribution for the spectrum of retardation times, as in the previous section, the creep rate before t' will be given from equation (7.29) by

$$\dot{\epsilon}_{T_o}(t) = \Delta J_G\, f(\theta)\, \frac{\Gamma(n_G)}{(t)^{n_G}}\, \sigma_o + H(\sigma_o-\sigma')\, \Delta D_F\, \frac{\Gamma(n_F)}{(t)^{n_F}}\, (\sigma_o-\sigma') \qquad (7.31)$$

and the ratio of the rate at time t before t' to that at t=t' at the initial temperature T_o will be

$$\frac{\dot{\epsilon}_{T_o}(t)}{\dot{\epsilon}_{T_o}(t')} = \frac{\Delta J_G\, f(\theta)\, \frac{\Gamma(n_G)}{(t)^{n_G}}\, \sigma_o + H(\sigma_o-\sigma')\, \Delta D_F\, \frac{\Gamma(n_F)}{(t)^{n_F}}\, (\sigma_o-\sigma')}{\Delta J_G\, f(\theta) \frac{\Gamma(n_G)}{(t')^{n_G}}\, \sigma_o + H(\sigma_o-\sigma')\, \Delta D_F\, \frac{\Gamma(n_F)}{(t')^{n_F}}\, (\sigma_o-\sigma')} \qquad (7.32)$$

After t' the ratio of the creep rate at any time, t, at temperature T to that at time t' at temperature T_o is (from equation (4.31), (assuming $(b_T-1)A$ is negligible) and from equation(7.29))

$$\frac{\dot{\epsilon}_T(t)}{\dot{\epsilon}_{T_o}(t')} = \frac{\frac{\Delta J_G}{a_{T_G}} f(\theta) \frac{\Gamma(n_G)}{(t_G^*)^{n_G}} \sigma_o + H(\sigma_o-\sigma') \frac{\Delta D_F}{a_{T_F}} \frac{\Gamma(n_F)}{(t_F^*)^{n_F}} (\sigma_o-\sigma')}{\Delta J_G f(\theta) \frac{\Gamma(n_G)}{(t')^{n_G}} \sigma_o + H(\sigma_o-\sigma') \Delta D_F \frac{\Gamma(n_F)}{(t')^{n_F}} (\sigma_o-\sigma')} \qquad (7.33)$$

where $t^* = t' + \left(\frac{t-t'}{a_T}\right)$ as defined in equation (4.5) and subscripts F and G refer to the fibre and gel respectively. Equation (7.33) reduces at $t=t'$ to

$$r \equiv \frac{\dot{\epsilon}_T(t')}{\dot{\epsilon}_{T_o}(t')} = \frac{\frac{\Delta J_G}{a_{T_G}} f(\theta) \frac{\Gamma(n_G)}{(t')^{n_G}} \sigma_o + H(\sigma_o-\sigma') \frac{\Delta D_F}{a_{T_F}} \frac{\Gamma(n_F)}{(t')^{n_F}} (\sigma_o-\sigma')}{\Delta J_G f(\theta) \frac{\Gamma(n_G)}{(t')^{n_G}} \sigma_o + H(\sigma_o-\sigma') \Delta D_F \frac{\Gamma(n_F)}{(t')^{n_F}} (\sigma_o-\sigma')} \qquad (7.34)$$

For one value of θ_o this equation(7.34) would give a sudden transition from one value of a_T to the other at the value of strain at which $\theta=0$. However, the distribution of the crimp angle θ_o will give a gradual change from a_{T_G} to a_{T_F}. This is shown in figure 7-11 for various values of $\bar{\lambda}$. We again assume that changes in ΔT are small enough that a_T can be written in the form of the Arrhenius equation (3.4) and that a_T of the gel and fibre can be described by a similar Arrhenius equation, with ΔH_{a_G} and ΔH_{a_F} being the apparent activation energies of the gel and fibres respectively. By choosing appropriate values of ΔH_{a_G} and ΔH_{a_F} and again assuming the parabolic relation between stress and strain (equation (7.13)) we can model the material behaviour and obtain values of ln r for various values of ΔT from equation (7.34). These values of ln r will be related to the a_T and ΔH_a observed for the whole process and the value of ΔH_a found will be equal to ΔH_{a_G}, ΔH_{a_F} or somewhere in between depending on the level of stress, and will be given by

$$r \equiv \frac{\dot{\epsilon}_T(t')}{\dot{\epsilon}_{T_o}(t')} = \frac{1}{a_T} = \exp\left(\frac{\Delta H_a \Delta T}{RTT_o}\right) = \text{Right Hand Side of Equation (7.34)} \qquad (7.35)$$

The values of ΔH_a found in this way are shown in figure 7-11. Here we chose ΔH_{a_G}=9 kcal/mol and ΔH_{a_F}=35 kcal/mol, the former being taken to coincide with that found by Gibbs et al [1] for hyaluronic acid and the latter to be close to that found experimentally (as in fact was ΔH_{a_G}). One value of $\Delta T=T-T_o$ was chosen as 6.0 °C to be of the same order as that used for specimen CH2-8-2. Various values for $\bar{\lambda}$ of the distribution of crimp angles were chosen. ($\frac{b}{a}\Delta J_G/\Delta D_F$) was taken to be 120 and θ_o=16°. It can be seen that for $\bar{\lambda}$=1.0, there is a fairly rapid change from the initial value of ΔH_a= 9 kcal/mol to the higher value of 35 kcal/mol over the region of isochronal strain 0.035 to 0.04. As the width of the θ_o distribution increases,(i.e. $\bar{\lambda}$ increases), this transition occurs over a wider range of strain as seen for $\bar{\lambda}$=2.0 and 3.0. This behaviour is again in agreement with that found experimentally (see figures 6-14, 6-15 and 6-17).

We are also interested in the ln r- ΔT plot for the model. Equation (7.34) can be used to give us figure 7-12 where we have the same parameters as in figure 7-11 except we have taken various values of ΔT and $\bar{\lambda}$=2.0. For isochronal strains less than ~0.035, the value of ΔH_a obtained from the best straight line through the data would be ~10 kcal/mol. As the strain increases, past 0.04, there is a change in the slope of the ln r- ΔT plot until at a strain of about 0.06 the slope shows little further increase with strain and the apparent activation energy becomes constant at 35 kcal/mol. In the 'transition' region between the low and high values of ΔH_a, the ln r- ΔT plot is curved, but an approximate straight line can be drawn through the data for $\Delta T>0$. This was in effect done to obtain figure 7-11. A straight line could also be drawn through the data for $\Delta T<0$, which in the 'transition' region will be slightly different from that obtained for $\Delta T>0$. However, by taking one slope or the other, we will have a measure of the temperature dependence in this region, as long as it is realised that in this region

the value of ΔH_a cannot be associated with a particular mechanism but is an intermediate value between that of the gel and fibres, the magnitude of which depends on the stress and on whether we choose ΔT to be +ve or -ve.

It was found that if the slopes n_F and n_G were altered, there was negligible change in both the ΔH_a against stress curve and the ln r- ΔT plot. What these parameters do is alter the shape of the log creep rate-log time curve. In figure 7-13, the values of log normalised creep rate, $(\dot{\epsilon}(t)/\dot{\epsilon}_{T_o}(t'))$, against log normalised time, (t/t'), are plotted from equations (7.32) and (7.33) for $\theta_o = 16^\circ$, $\Delta H_{a_G} = 9$ kcal/mol, $\Delta H_{a_F} = 35$ kcal/mol, $\frac{b}{a}\Delta J_G/\Delta D_F = 120$, $\bar{\lambda} = 2.0$ as for figure 7-12 and strain < 0.03 with $n_G = 1.0$ and various values of ΔT. In this region, the curves are unaffected by the value of n_F. The curve before t' is a straight line of slope = -1. It can be seen from figure 7-13 that the curves after t' approach the continuation of the line before t' at larger values of t/t'. For values of $n_G < 1.0$, the curves, for equal +ve and -ve ΔT, will move away from the line of slope unity, similar to that shown in figure 4-14, and for $n_G > 1.0$ they will cross over each other. This latter feature is shown in figure 7-14 for the high strain mechanism of the fibres, (using the same parameters as in figures 7-11 to 7-13) with strain > 0.07 and n_F chosen as 1.2 (the same as for figures 7-11 and 7-12), and $\Delta H_{a_F} = 35$ kcal/mol. This cross over feature was also observed experimentally (as will be seen in figures 8-9 to 8-12).

It should be noted from figure 7-13 that there is little curvature to the lines and in an experiment for these low activation energies it would be extremely difficult to distinguish between the curve and the straight line (see figure 2-3). At the higher activation energies of figure 7-14, the curvature is again clear, agreeing with the experimental behaviour, (see figure 2-4, 8-11, and 8-12). As is to be expected, the lines on the log creep rate-log time curve obtained for a single mechanism of

ΔH_a=35 kcal/mol and n=1.2 using equation (4.31) will produce the exact same curves as in figure 7-14. The same holds for figure 7-13. It can also be seen from these two figures that if we plot log($\dot{\epsilon}_T(t)/\dot{\epsilon}_{T_o}(t')$) against log (t/t') for various values of strain and one value of ΔT with n_G=1.0 and n_F=1.2, then as the strain increases there will be a cross over of the curves. This was observed for specimen CH2-8-2 and will be seen in the next chapter (figure 8-7).

7.4 Discussion

We have seen excellent qualitative agreement between the curves obtained from our modelling and those obtained experimentally for a variety of different experimental circumstances, both for isothermal and non-isothermal deformation. The major points of agreement are:

(i) the creep rate dependence on stress (or strain) shows

(a) a 'hump' at low strains associated with the shearing of the gel as the waves straighten out, and

(b) a transition from the gel behaviour to an approximately linear region of creep rate vs. stress, the latter being associated with the creep of the fibres. The gradual nature of this transition is explained by introducing a distribution of initial crimp angles, θ_o.

(ii) the distribution of retardation times gives the correct time dependence in that the log rate against log time curves are straight lines, the slope of which shows a gradual transition from that of the gel mechanism to that of the fibre.

(iii) the model predicts that the apparent activation energy, measured from a T-jump experiment should go through a transition from a low value associated with the gel at low strains to a higher value at larger

strains associated with the fibre, the width of the transition depending on the width of the Gaussian distribution of initial crimp angles.

(iv) the log creep rate-log time curves after the T-jump cross over for the case of

(a) +ve and -ve ΔT T-jumps at one value of strain and

(b) T-jumps at different strains and one value of ΔT,

when values of n_G and n_F are used of the order of those found experimentally.

The parameters which are important in order to determine the experimental behaviour are the following:

(i) θ_o; the mean value of the initial crimp angle. This can be found experimentally from a (creep rate/load) against $(1+\epsilon)$ plot.

(ii) n_G and n_F; the values of the slopes of the log creep rate against log time curves for the gel and fibre respectively. These can be estimated from experimental creep rate-time data at a given stress and are related to the shape of the retardation spectrum.

(iii) ΔH_{a_G} and ΔH_{a_F}; these can be found from the limiting low strain and high strain behaviour respectively.

(v) the ratio $\frac{b}{a}\ \Delta J_G / \Delta D_F$ and the measure of the width, $\bar{\lambda}$, of the Gaussian distribution of crimp angles, θ_o. There is at present no experimental data to provide this directly and these are the parameters which have to be found from a best fit of the experimental data obtained in this work. Clearly such data represents a challenge for future work and once obtained will offer a severe test of the model presented here.

The important thing to see from this model is that all the parameters in the model relate either to structural constants of the material,

like θ_o, $\bar{\lambda}$ and $\frac{b}{a}$ or to the usual (and in principle, measurable) viscoelastic parameters, e.g. the compliance differences ΔJ_G and ΔD_F, and a_T and not to an arbitrary array of springs and dashpots. In the next chapter, we will try to obtain quantitative agreement with the experimental data by finding values for the constants above which give the best fit to the experimental data. The degree of agreement of these values with those expected based on existing knowledge of tendon structure and mechanical behaviour will represent a measure of the predictive capabilities of the mathematical model (equations (7.29), (7.33) and (7.34)) of tendon which was formulated here.

References

1 Gibbs D.A., Merrill E.W., Smith K.A. and Balazs E.A., Biopolymers, 6,777,1968.

2 Diamant J., Keller A., Baer E., Litt M. and Arridge R.G.C., Proc.Roy.Soc., London,B180,293,1972.

3 Torp S., Baer E. and Friedman B., In Colston Papers, Structure of Fibrous Biopolymers, (ed. Atkins E.D.T. and Keller A.) 26,223,1975. Butterworths, London.

4 Viidik A., Z. Anat. Ent., 136.204,1972.

5 Yannas I.V. and Huang C., J.Polymer Sci.,10,577,1972.

6 Comninou M. and Yannas I.V., J.Biomech.,9,427,1976.

7 Viswenadham R.K., Agrawas D.C. and Kramer E.J., J.Polymer Sci., Polym. Phys.,12,2195,1976.

8 Viidik A., J. Biomech.,1,3,1968.

9 Viidik A., Int.Rev.Conn.Tiss.Res.,6,127,1973.

10 Frisen M., Magi M., Sonnerup L. and Viidik A., J.Biomech.,2,13,1969.

11 Frisen M., Magi M., Sonnerup L. and Viidik A., J.Biomech.,2,21,1969

12 Frankel V.H. and Burstein A.H., 'Orthopaedic Biomechanics', Lea and Febiger, Philadelphia, Penns,1970.

13 Case J. and Chilver A.H., 'Strength of Materials', Arnold, London,1959.

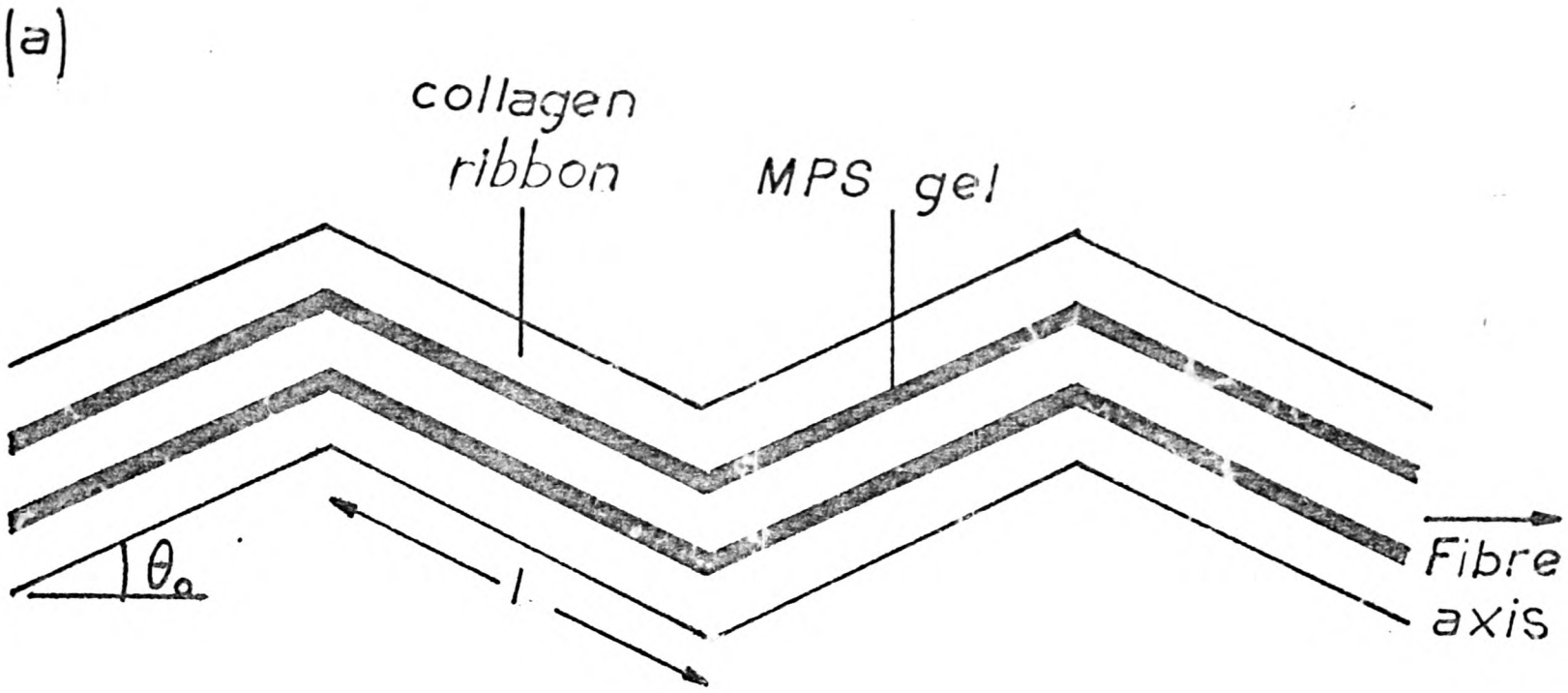
14 Ward I.M.,Mechanical Properties of Solid Polymers, Wiley, London,1971. Arridge R.G.C., Mechanics of Polymers, Clarendon Press,1975.

15 Ferry J.D., Viscoelastic Properties of Polymers, Wiley, New York, 1970. Smith T.L., Trans. Soc.Rheol.,6,61,1962.

16 Haut R.C. and Little R.W., J.Biomech.,5,423,1972.

17 Barford N.C.,'Experimental Measurements: Precision, Error and Truth' Addison Wesley, London,1967.

18 Hildebrand F.B., 'Introduction to Numerical Analysis', 2nd ed., McGraw Hill, New York,1974.



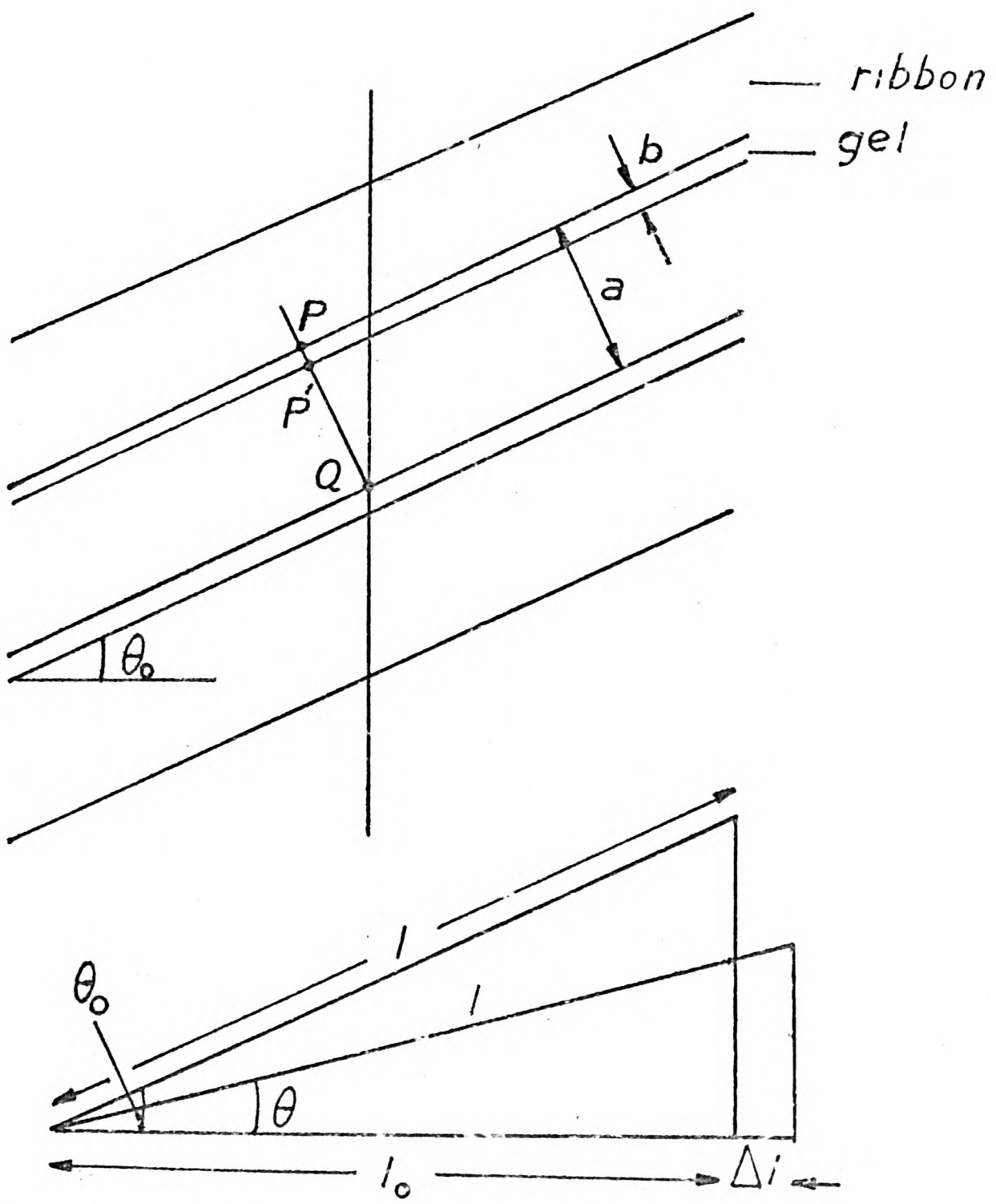


Figure 7-1

a) Schematic diagram of tendon with crimped collagen ribbons at an angle θ_o to the tensile exis and the mucopolysaccharides in between.
b) Closer view of the ribbons to define the various parameters shown
c) Diagram to show the method of calculating the strain in the tensile direction as the crimp angle, θ, reduces.

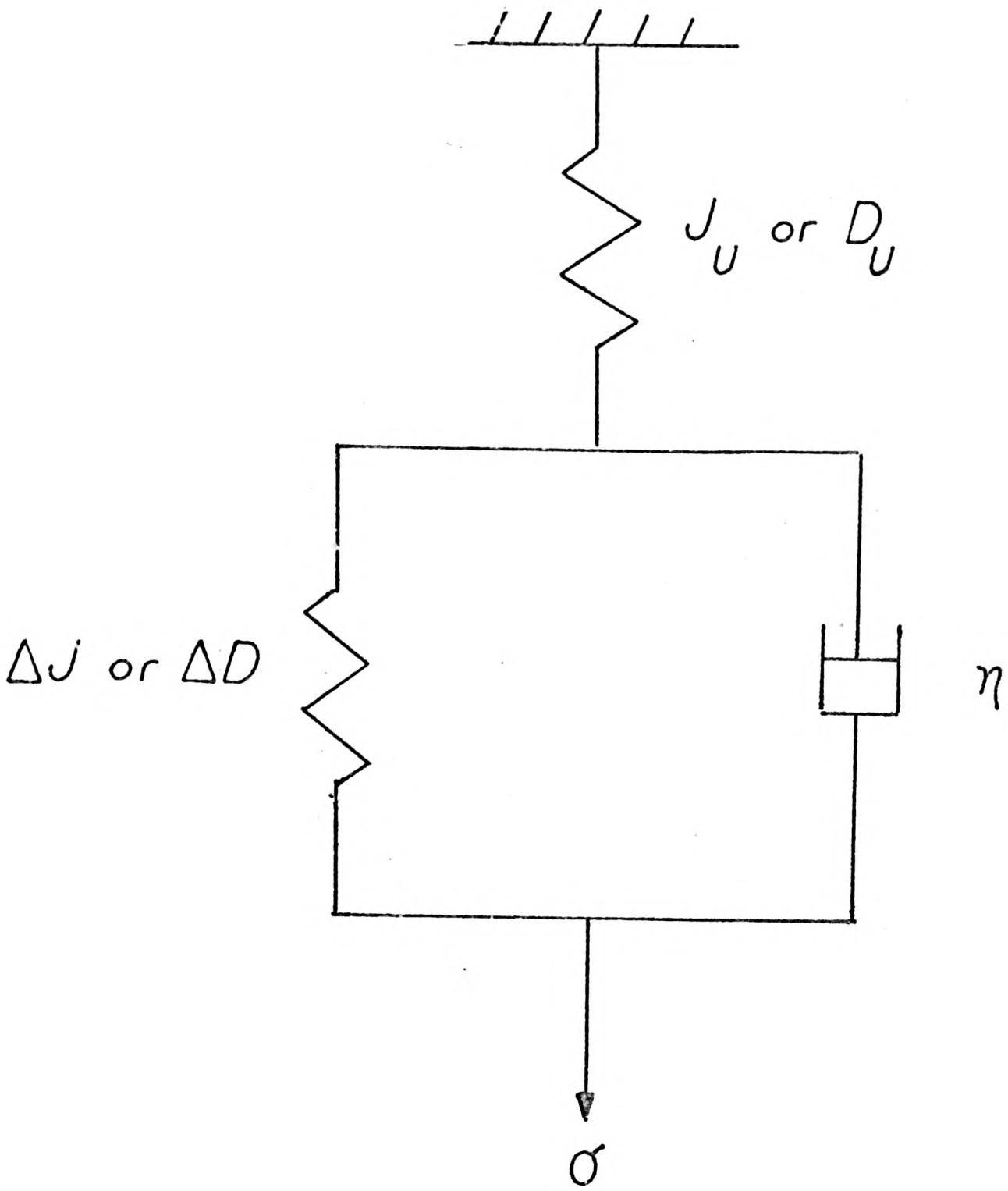


Figure 7-2

3-parameter model with elastic compliance, D_U or J_U, compliance difference, ΔD or ΔJ, and viscosity η .

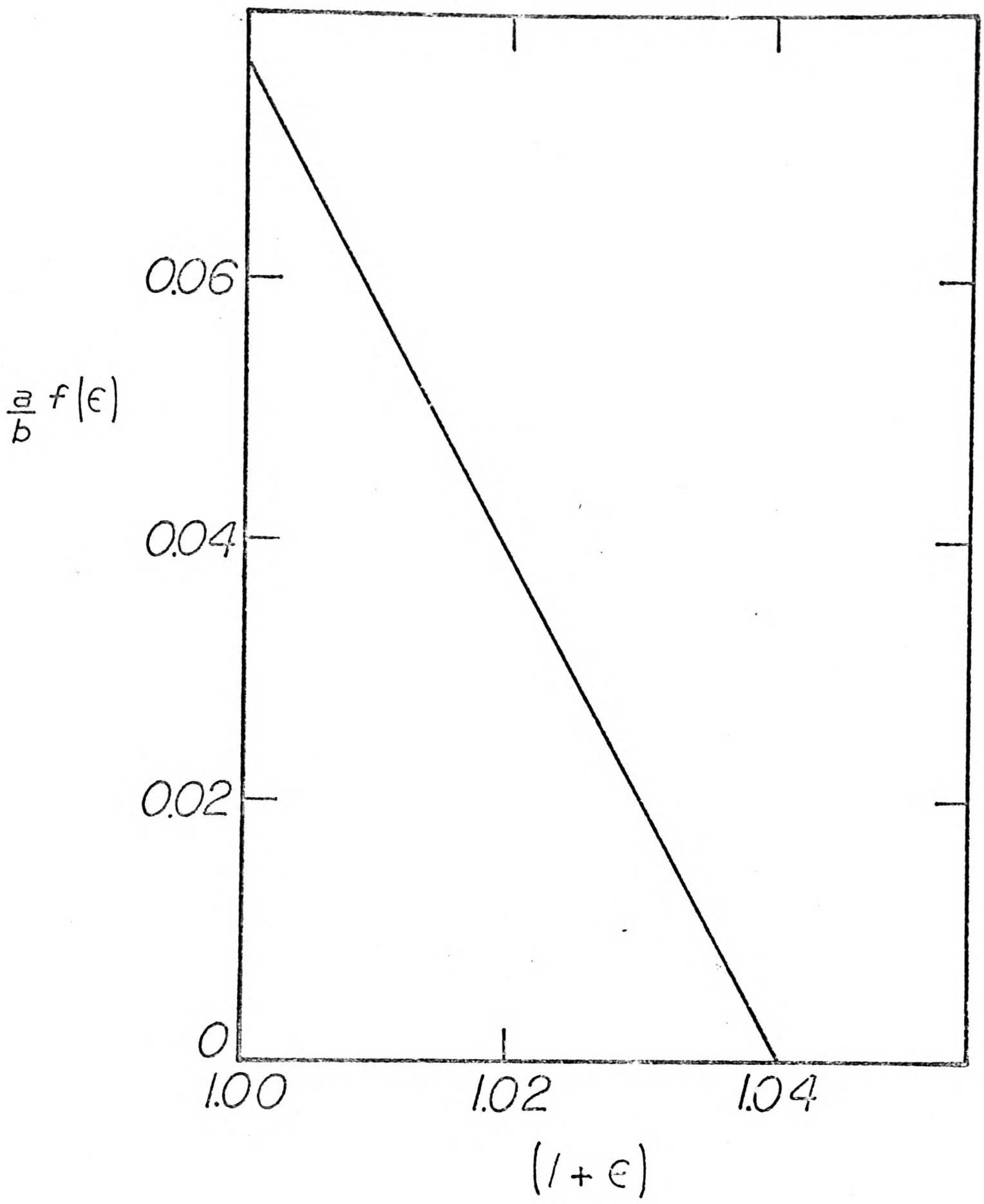


Figure 7-3

Plot of theoretical function $(1+\epsilon)\ (1-\cos^2\theta_o(1+\epsilon)^2)$ of equation (7.12) against $(1+\epsilon)$ with $\theta_o = 16^\circ$.

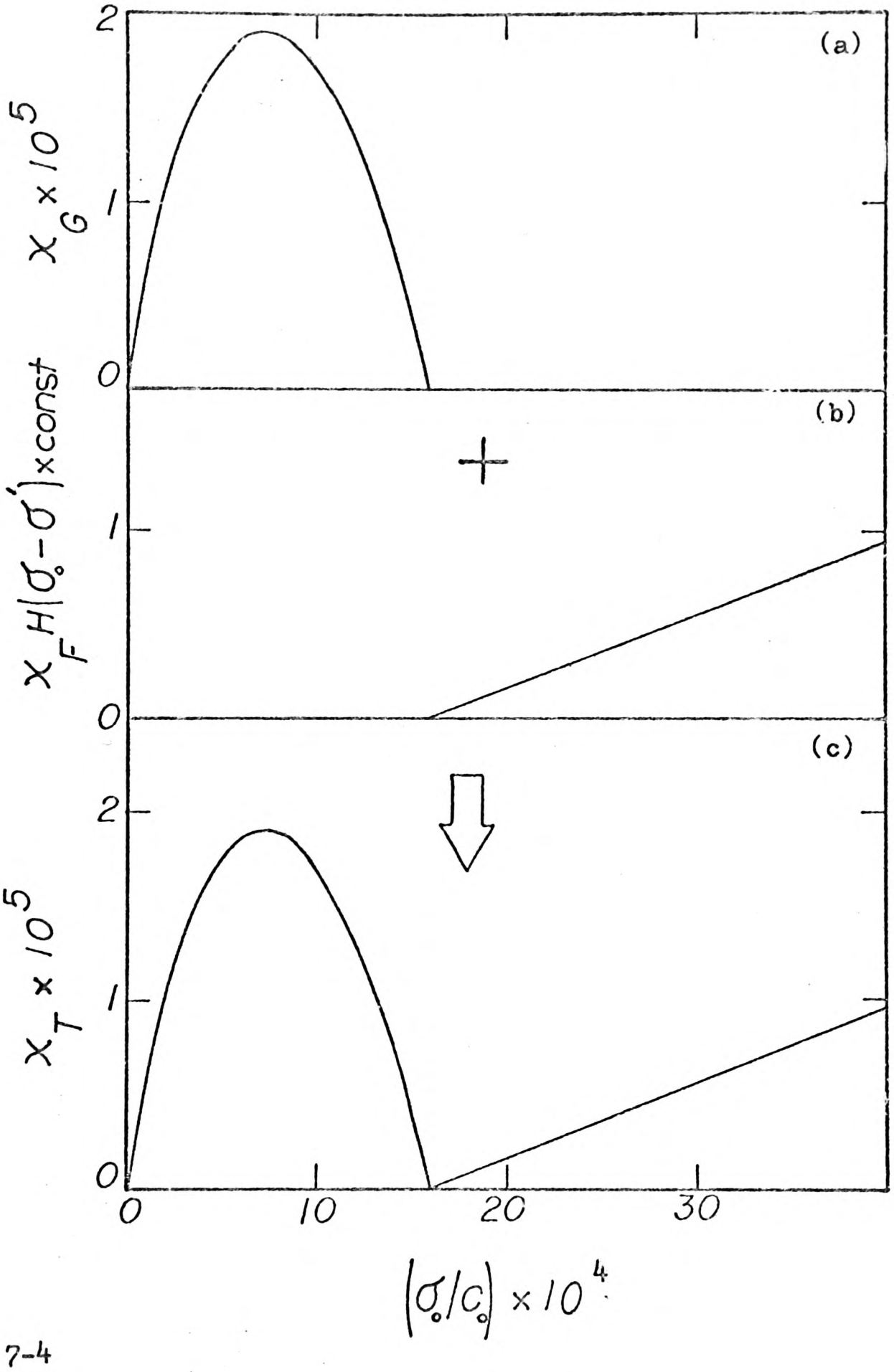


Figure 7-4

Theoretical deperdence on load for
a) the isochronal creep rate for the gel given by equation (7.15)
b) the isochronal creep rate for the ribbon given by equation (7.18)
c) the total isochronal creep rate given by the sum of (a) and (b) and equation (7.21)

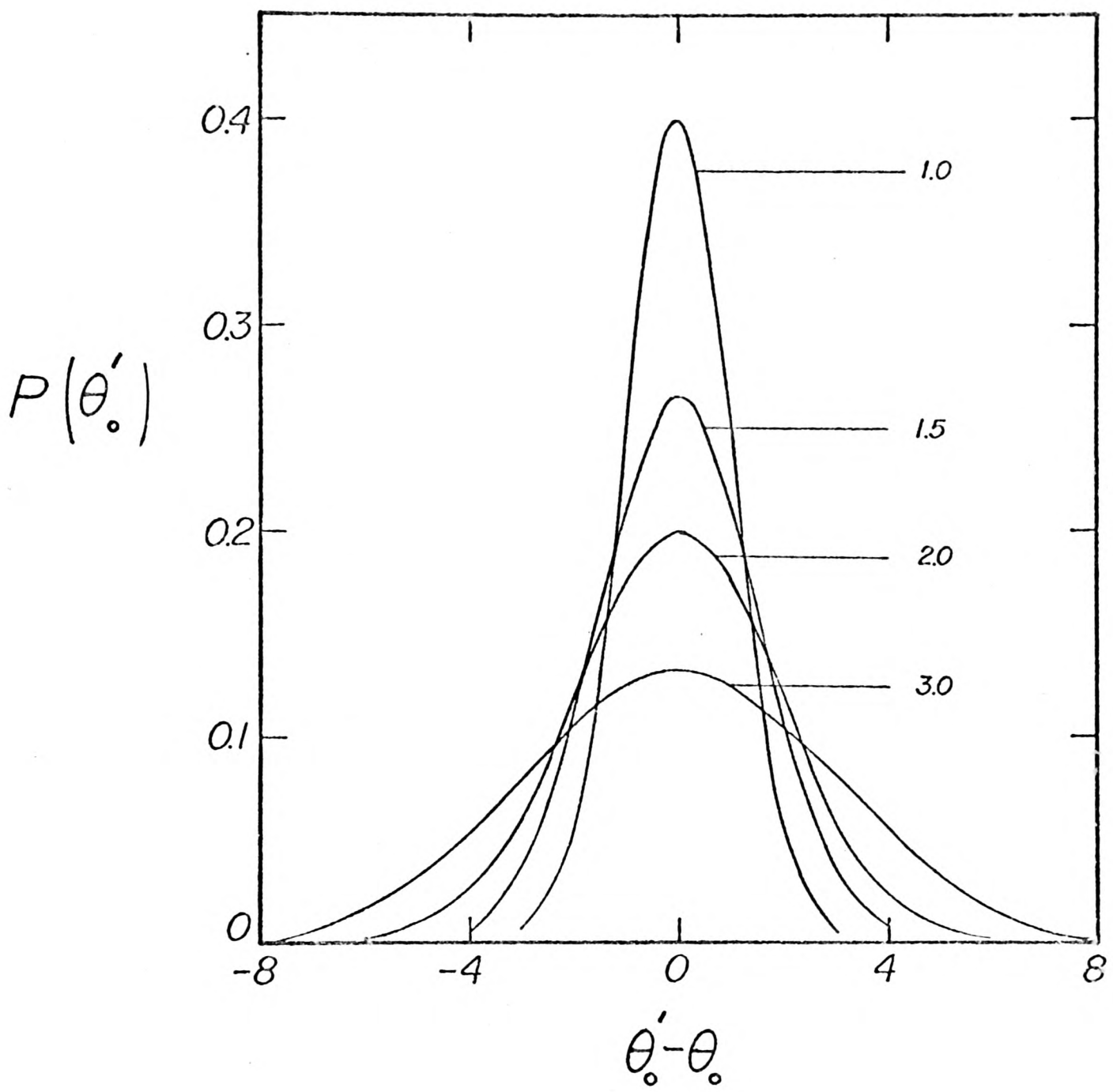


Figure 7-5

The shape of the Gaussian distribution for various values of $\bar{\lambda}$. as shown.

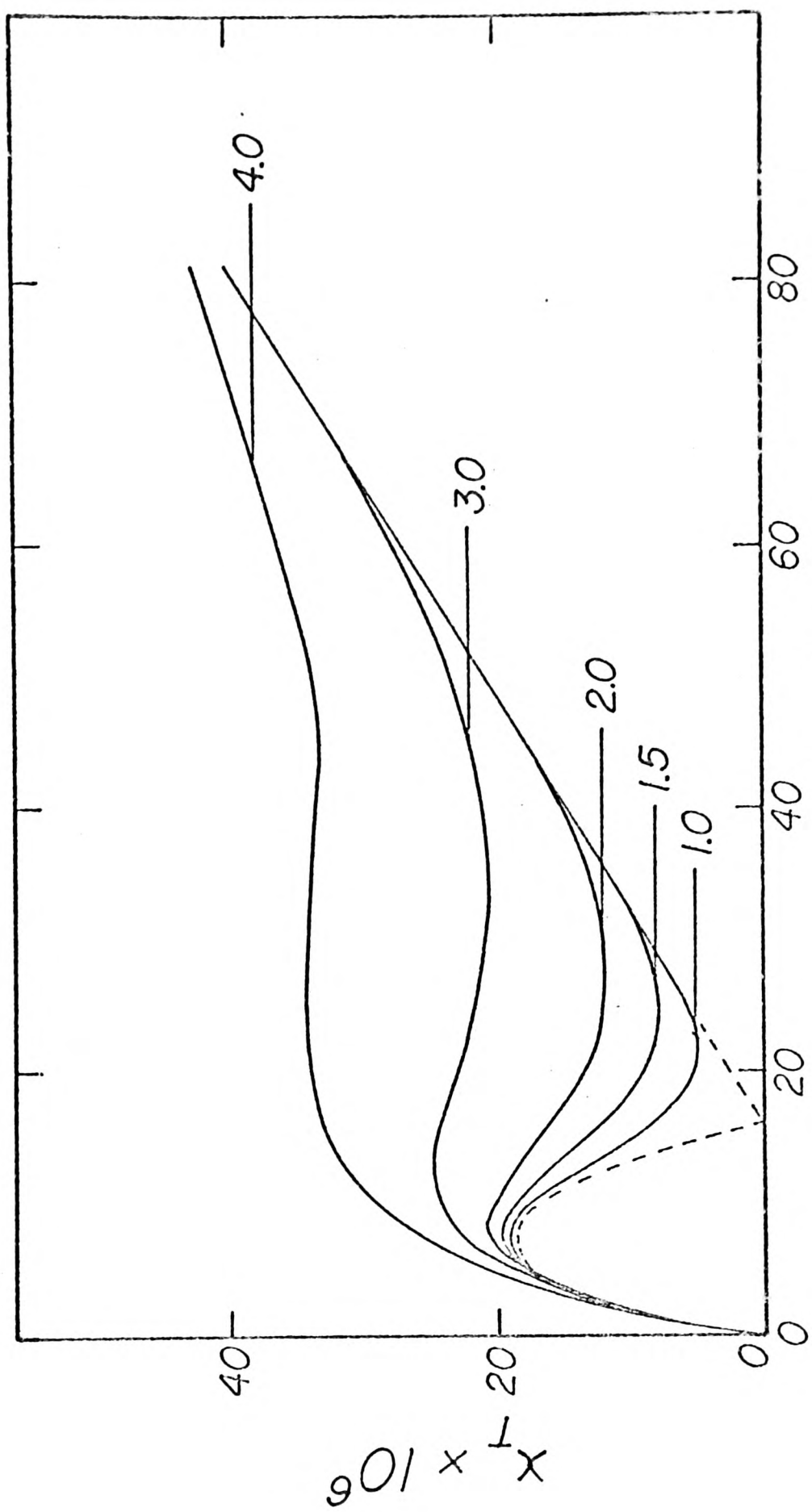


Figure 7-6

Theoretical plot of χ_T (isochronal creep rate) against σ_o/c_o, (stress) from equation (7.21) for the distribution of crimp angles, $\bar{\lambda}$ = 1.0, 1.5, 3.0, 4.0. $\frac{b}{a}(\Delta J_G / \Delta D_F) = 160$, $\theta_o = 16^\circ$.
Dashed line for single crimp angle of 16°.

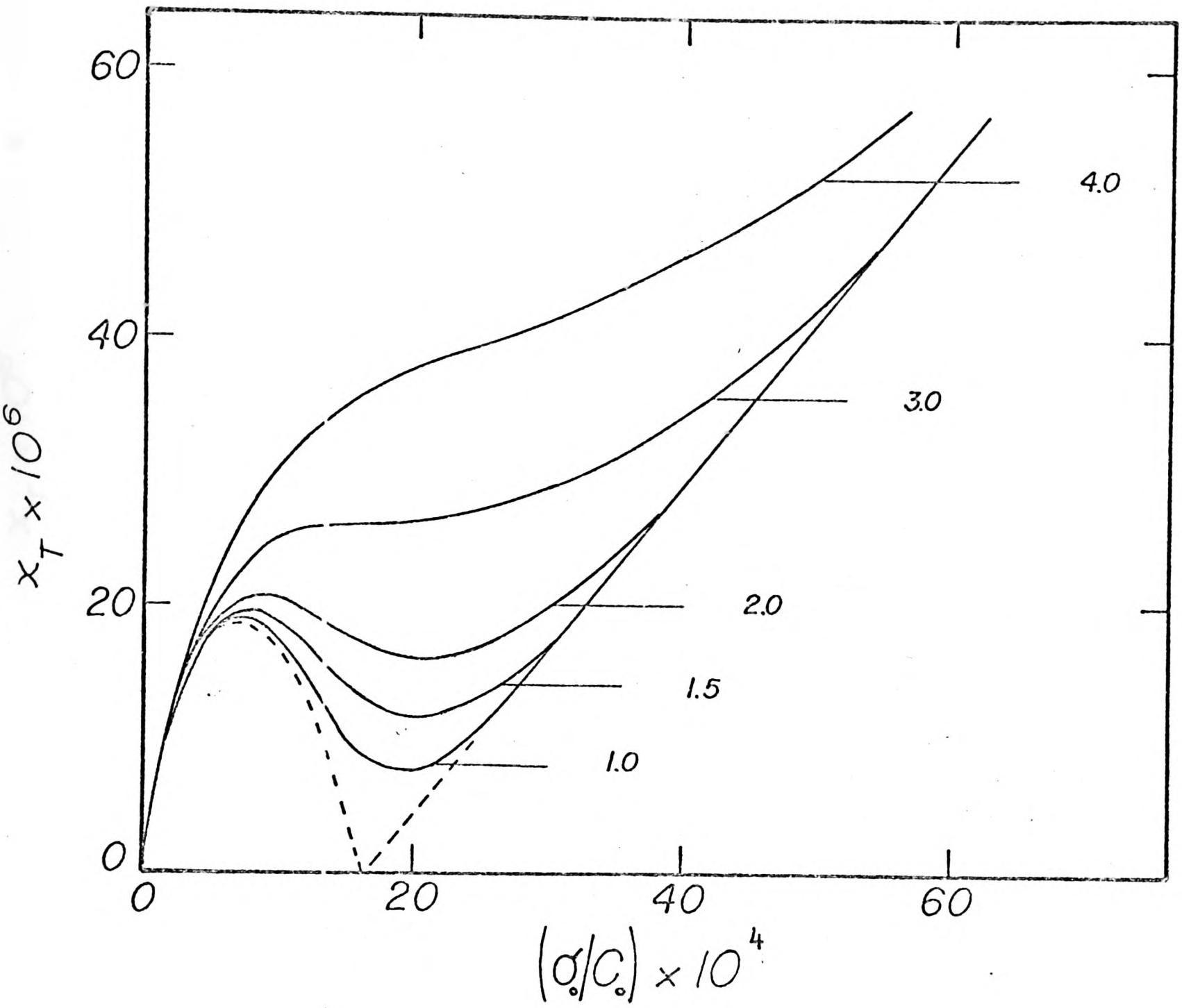


Figure 7-7

Theoretical plot of X_T (isochronal creep rate) against σ_o/c_o (stress) from equation (7.21) for the distribution of crimp angles for values of $\bar{\lambda}$ = 1.0, 1.5, 2.0, 3.0, 4.0. $\frac{b}{a}(\Delta J_G/\Delta L_F) = 80$, $\vartheta_o = 16^\circ$. Dashed line is for a single crimp angle of 16°.

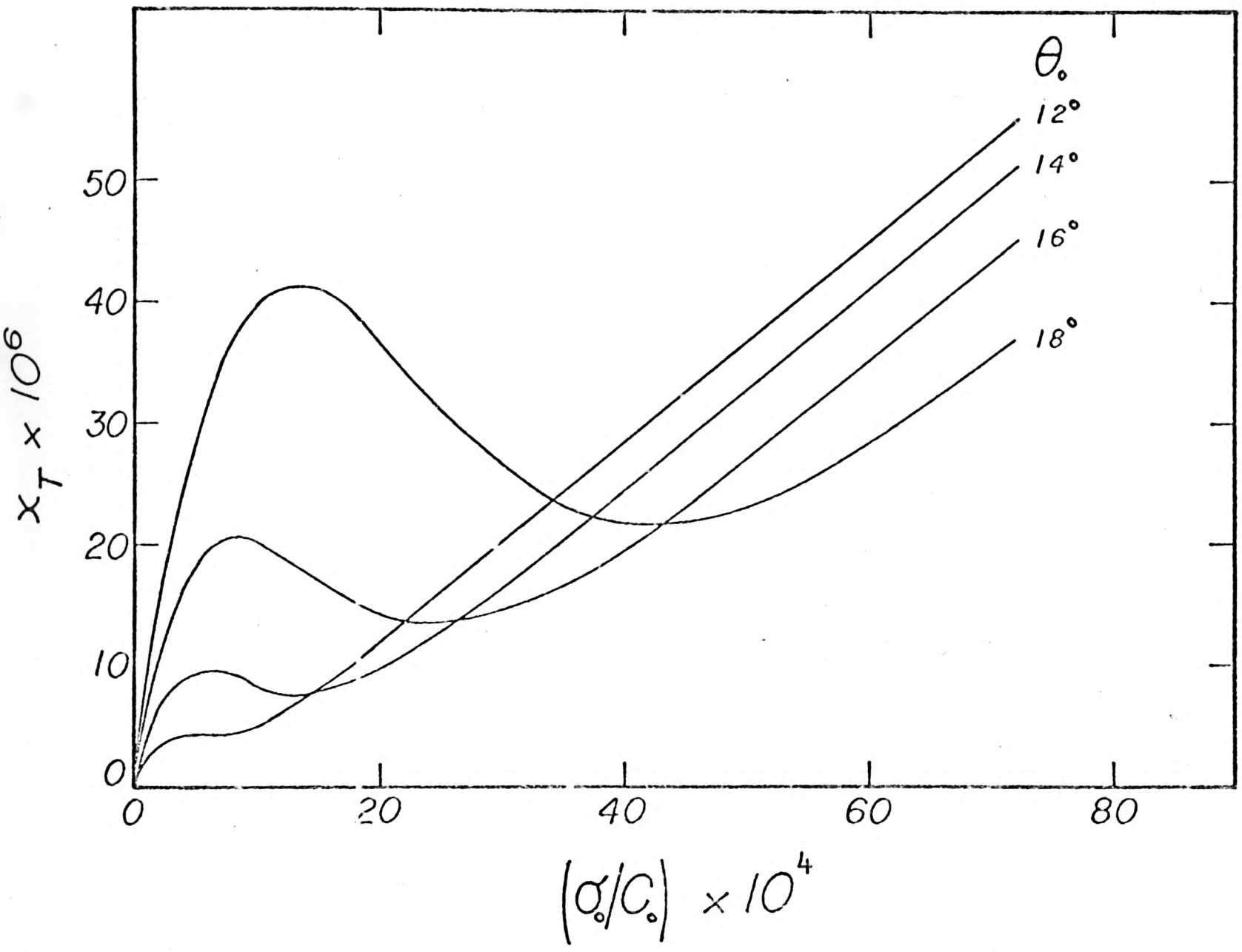


Figure 7-8

Theoretical plot of X_T (isochronal creep rate) against σ_o/c_o (stress) from equation (7.21) with $\frac{b}{a}(\Delta J_G/\Delta D_F) = 120$, $\theta_o = 12^\circ$, 14°, 16°, 18°, and $\bar{\lambda} = 2.0$.

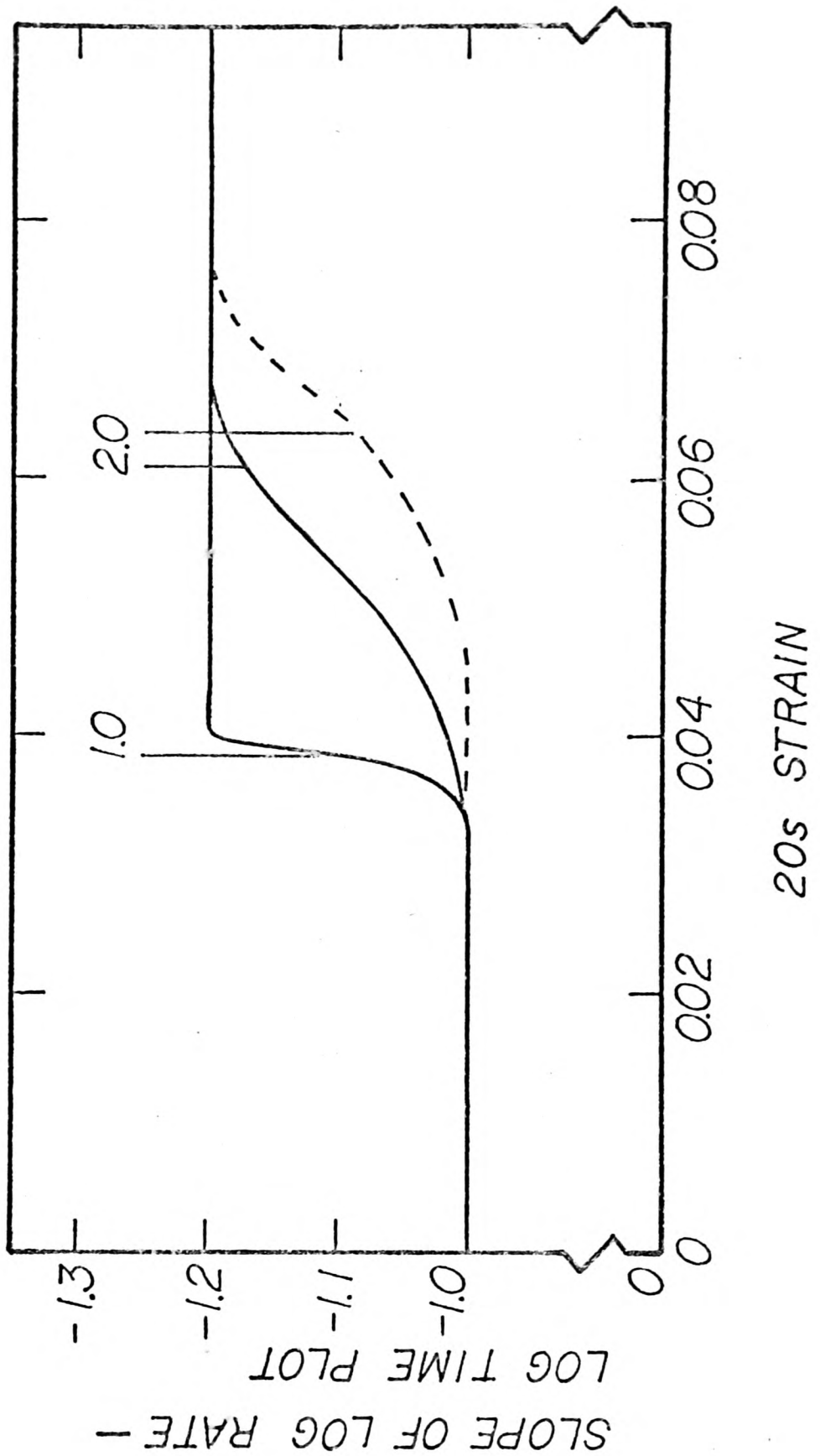


Figure 7-9

Theoretical plot of (slope of the log creep rate- log time curve) against isochronal strain from equation (7.29) for $\bar{\lambda}$ = 1.0, 2.0, $\theta_o = 16^\circ$, $n_G = 1.0$, $n_F = 1.2$, —— $\frac{b}{a}(\Delta J_G/\Delta D_F) = 120$;

---- $\frac{b}{a}(\Delta J_G/\Delta D_F) = 1200$.

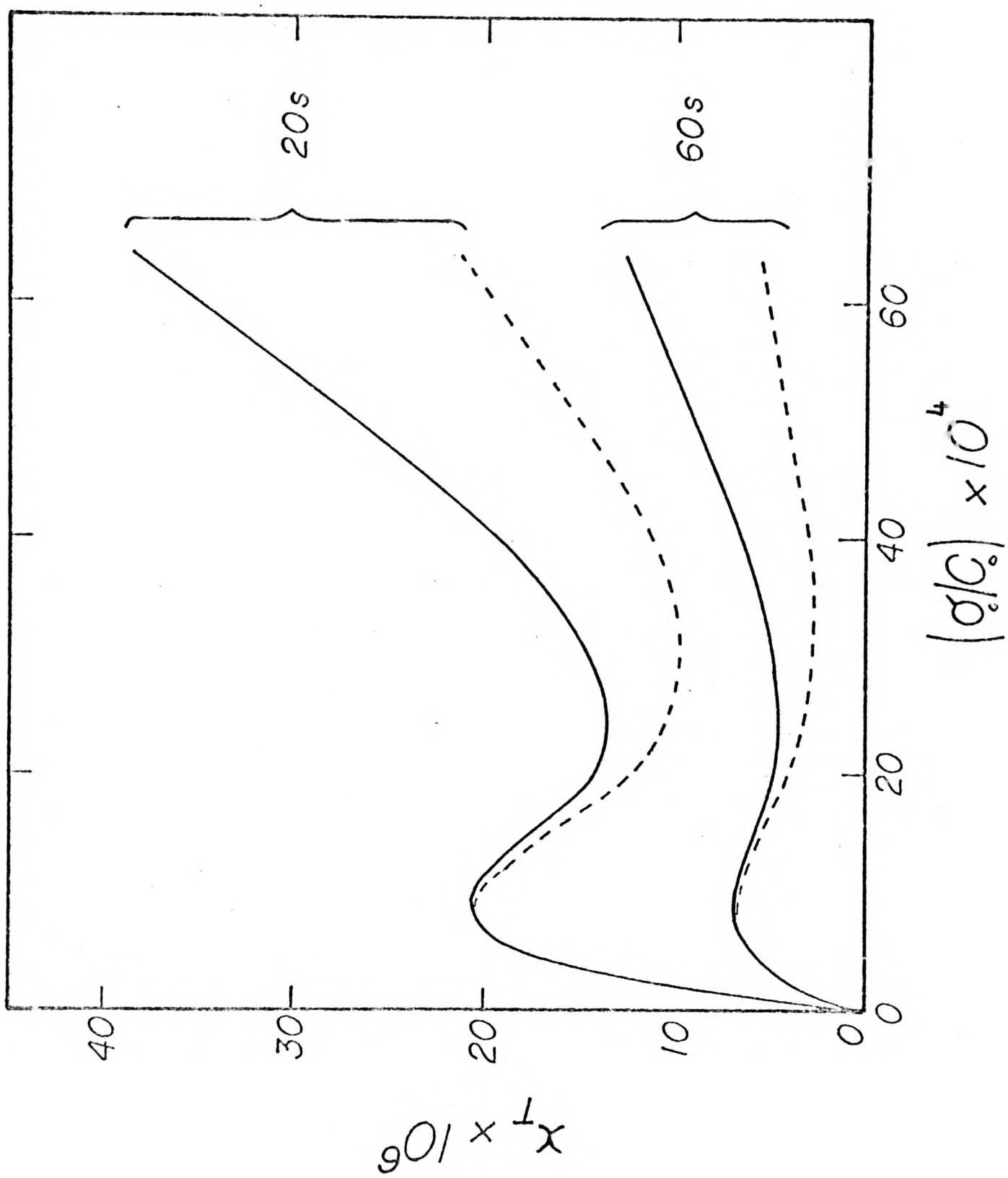


Figure 7-10

Theoretical plot of χ (isochronal creep rate) against σ_o/c_o (stress) from equation (7.30) for a distribution of crimp angles, and τ's, with $\theta_o = 16^\circ$, $\bar{\lambda} = 2.0$, $\frac{b}{a}(\Delta J_G/\Delta D_F) = 120$ and times 20s and 60s.

——— $n_G = n_F = 1.0$.

---- $n_G = 1.0$, $n_F = 1.2$.

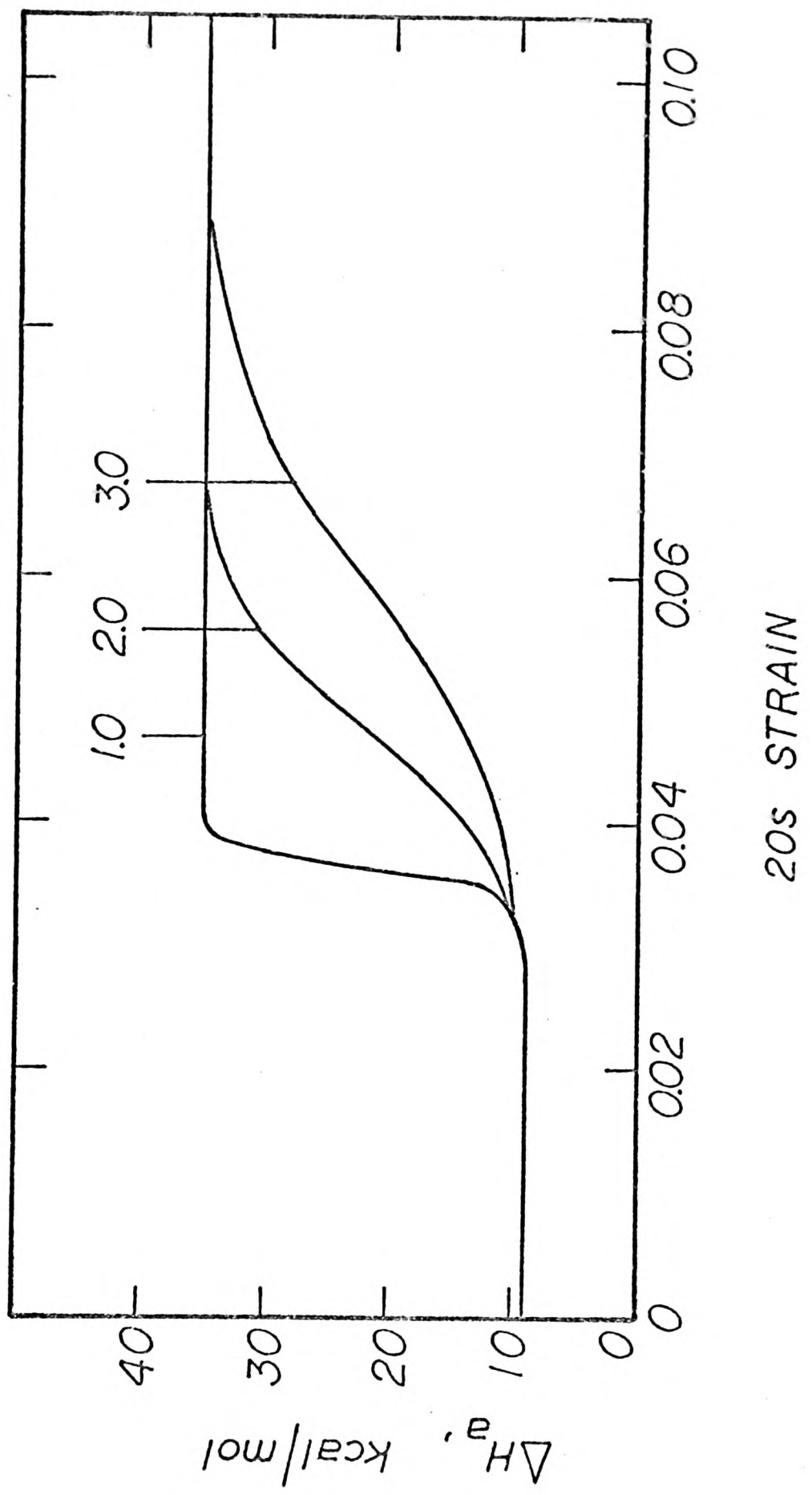


Figure 7-11

Theoretical plot of ΔH_a against isochronal strain from equation (7.34) for $\bar{\lambda}$ = 1.0, 2.0, 3.0. $\frac{b}{a}(\Delta J_G/\Delta D_F) = 120$, $\theta_o = 16^\circ$, ΔH_{a_G} = 9 kcal/mol, and ΔH_{a_F} = 35 kcal/mol.

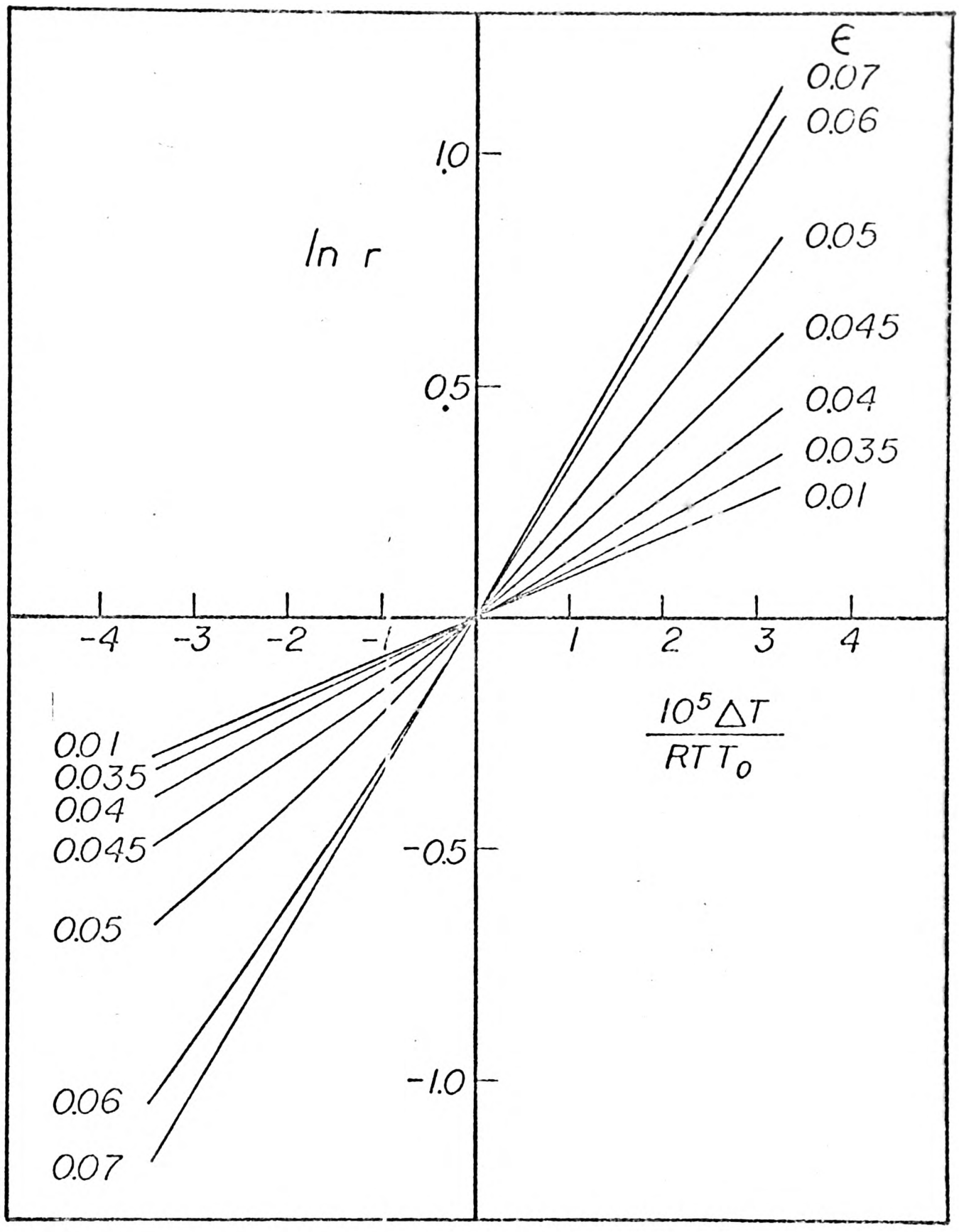


Figure 7-12.

Theoretical ln r- ΔT plot for various values of isochronal strain from equation(7.34). $\theta_o = 16^\circ$, $\bar{\lambda} = 2.0$, $\frac{b}{a}(\Delta J_G/\Delta D_F) = 120$, $\Delta H_{a_G} = 9$ kcal/mol, $\Delta H_{a_F} = 35$ kcal/mol.

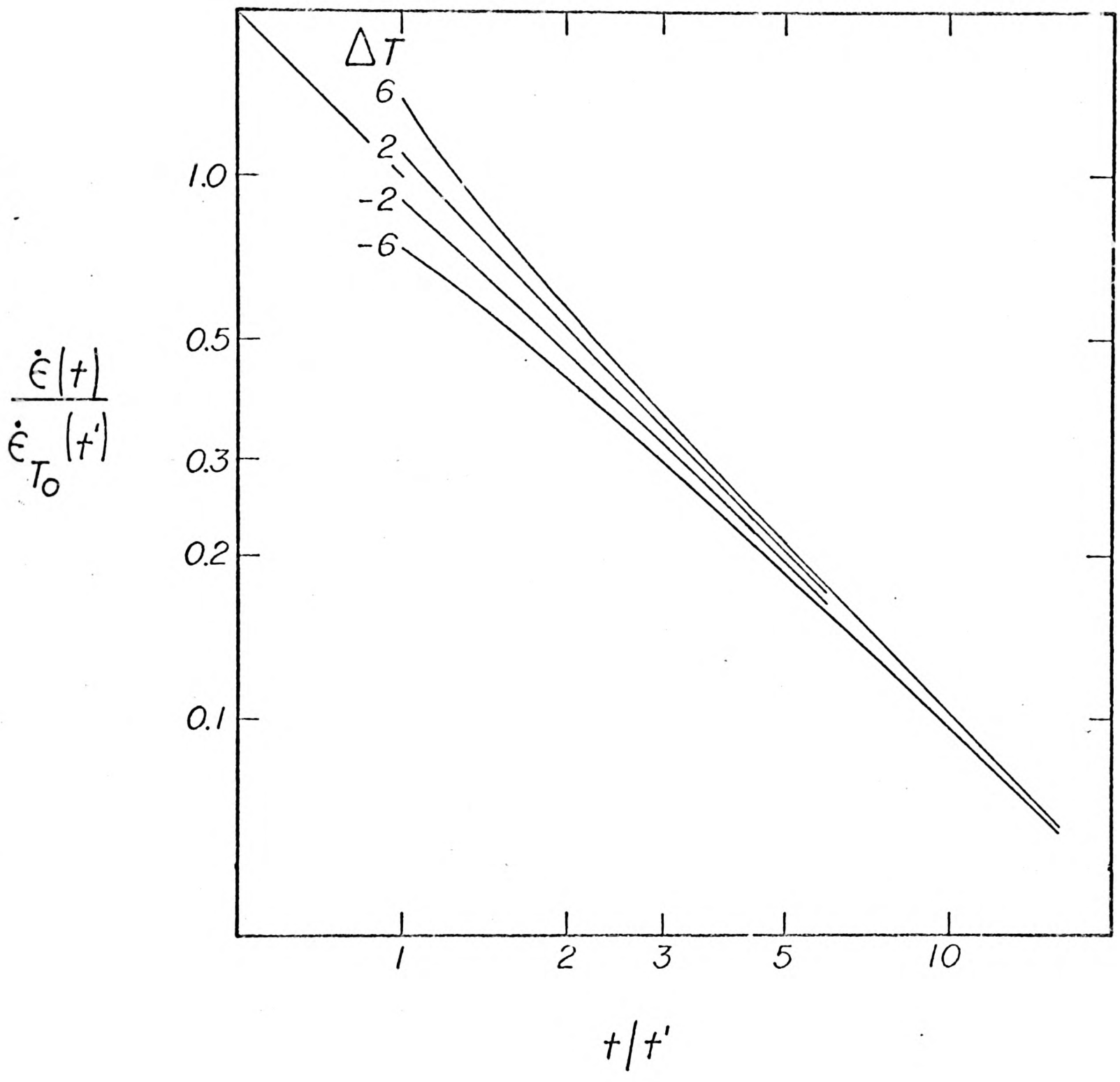


Figure 7-13

Dependence of theoretical log (normalised creep rate, $\dot{\epsilon}(t)/\dot{\epsilon}_{T_o}(t')$) on log (normalised time, t/t') from equations (7.32) and (7.33) for various values of ΔT = 6, 2, -2, -6 °C. θ_o = 16°, $\bar{\lambda}$ = 2.0, $\frac{b}{a}(\Delta J_G/\Delta D_F)$ = 120, n_G = 1.0, n_F = 1.2, ΔH_{a_G} = 9 kcal/mol, ΔH_{a_F} = 35 kcal/mol and $\epsilon < 0.03$.

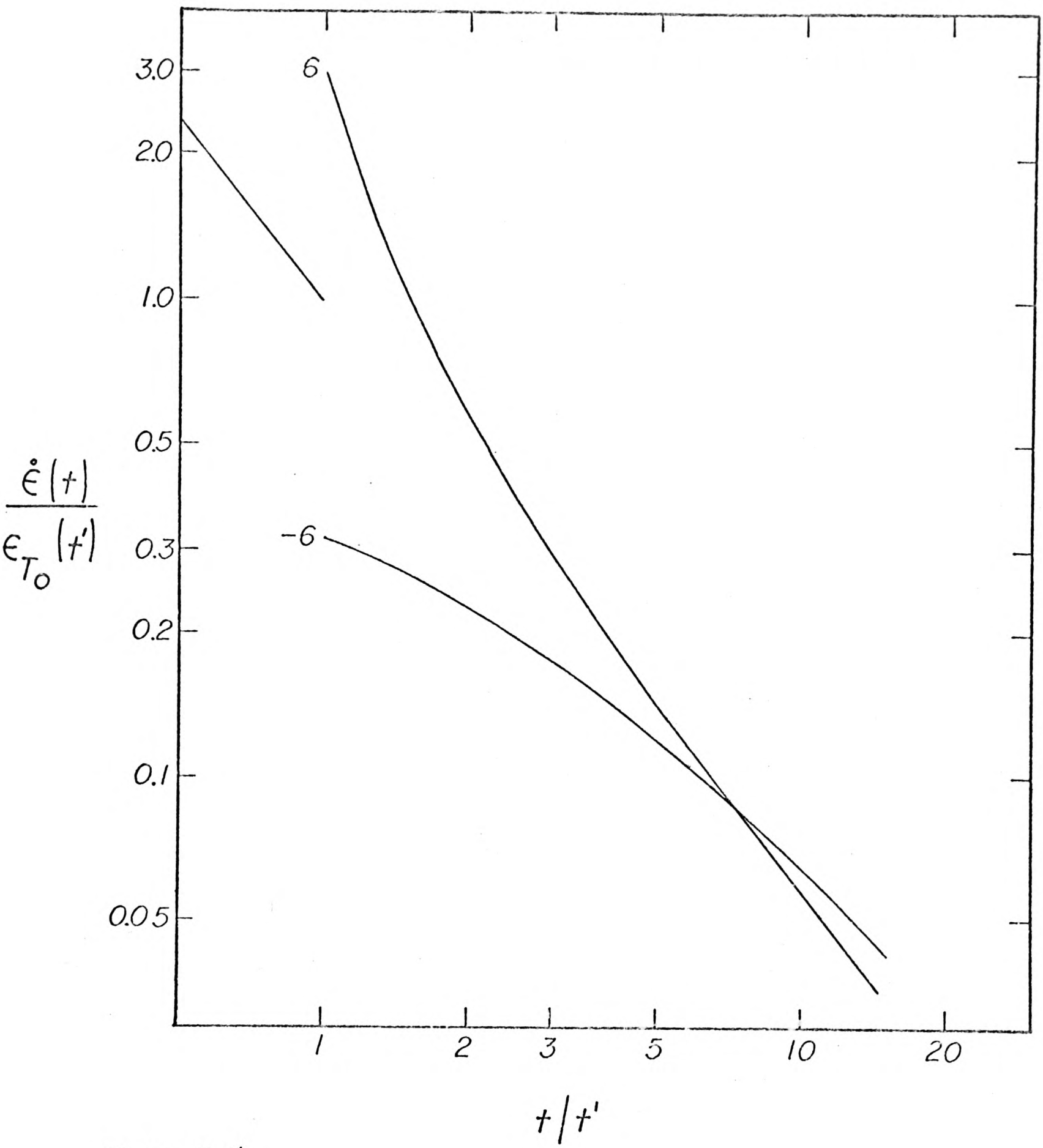


Figure 7-14

Dependence of theoretical log (normalised creep rate, $\dot{\epsilon}(t)/\dot{\epsilon}_{T_o}(t')$) on log (normalised time, t/t') from equations (7.32) and (7.33) for various values of $\Delta T = +6, -6\,^{\circ}C$, $\theta_o = 16^{\circ}$, $\bar{\lambda} = 2.0$, $\frac{b}{a}(\Delta J_G/\Delta D_F) = 120$, $n_G = 1.0$, $n_F = 1.2$, $\Delta H_{a_G} = 9$ kcal/mol, $\Delta H_{a_F} = 35$ kcal/mol, and $\epsilon > 0.07$ is in the high strain region.

Chapter 8

Experimental Verification of the Predictions of the Theoretical Model for the Creep of Tendon

8.1 Introduction

The model described in the previous chapter allows for the prediction of the viscoelastic behaviour of tendon in five separate ways.

(i) the strain dependence of the isochronal creep rate normalised by the stress (i.e. $\dot{\epsilon}/\sigma_o$).

(ii) the dependence of the observed isochronal creep rate on the applied load.

(iii) the dependence on isochronal strain (or load) of the slope of the log creep rate-log time plot.

(iv) the dependence of the activation energy, ΔH_a, on load or isochronal strain.

(v) the shape of the log creep rate against log time curves for various levels of strain for both isothermal and creep T-jump experiments.

In this chapter, we will obtain experimental verification of the predictions of the theoretical equations developed in chapter 7 by applying these equations to the 5 sets of experimental data described above. From the best fit of the theory to the first two sets of data ((i) and (ii)) above, we will be able to determine the following parameters for various tendon specimens, namely the crimp angle, θ_o, the standard deviation of the Gaussian distribution of crimp angles, $\bar{\lambda}$, and the compliances ΔJ_G and ΔD_F of the gel and fibres respectively. Once these parameters have been found for each specimen, we can apply the equations of chapter 7 to a variety of experimental circumstances ((iii) to (v) above) and the extent to which the equations can be used to predict the experimental behaviour can be determined. We will try to extend the use of the model to fit creep-recovery

and creep cycling data; in these latter cases, the limitations of the theory will become apparent.

8.2 Application of the Theoretical Model to Experimental Data

8.2.1 Determination of the Crimp Angle

First we consider the plot of the ratio (creep rate/load) against $(1+\epsilon)$ for various specimens. Figure 8-1 shows this for specimens CH2-8-2 (m23,Heh) and CH2-9-1(m77,Hfh) and the straight lines through the data points, predicted by equation (7.11) give values for θ_o, the initial crimp angle, from the intercept on the $(1+\epsilon)$ axis as shown in Table 8-1. The different values found between specimens ties in with the differences in the creep rate against load characteristics of each specimen as mentioned in chapter 5. These values are also in general agreement with those found by Diamant et al[1] who found values of θ_o, for rat-tail tendon, ranging from 20° to 13° depending on the age of the animal. It is seen from figure 8-1 that as the strains increase, there is a bending away of the curve from the straight line. This is due to the fact that not all the fibres will have the same θ_o and some will straighten before others.

8.2.2 Determination of the Distribution of Crimp Angles and the Compliance Differences for the Fibres and Gel.

We can use the values of θ_o found above to determine the creep rate dependence on load as described by equation (7.29) or (7.30). For this purpose, we used the same three specimens as in Table 8-1. The creep rate against load curves are shown in figures 8-2, 8-3 and 8-4 for these specimens CH2-16-4(m71,Hfh), CH2-8-2(m23,Heh) and CH2-9-1(m77,Hfh) and the best fit lines from the theory are drawn through the experimental (circled) points. The fit was obtained with the use of an IBM 1130 computer. The initial

value of θ_o used was as in Table 8-1. The procedure was briefly as follows: we started with a value of θ_o, the mean initial crimp angle as found above. Taking a value of θ_o', (any other initial crimp angle), the 20s isochronal load-strain behaviour of the specimen was used in equation (7.3) to calculate the value of θ (the crimp angle during creep) corresponding to each level of isochronal strain for this particular θ_o'. If θ was equal to or less than zero, then the rate contribution from the gel was zero and only the second term in equation (7.30) contributed to the rate. To compute the contribution from the fibre, a value of $\frac{b}{a}\frac{\Delta J_G}{\Delta D_F}$ was chosen. The value of σ' (i.e. the value of the load at which θ is zero) for each value of θ_o' was also obtained from the experimental load-strain data and used to compute the contribution from the fibre term. It was necessary to work in loads rather than stresses. The 20s isochronal rate (or in fact the value of χ) given by equation (7.30) was then multiplied by the probability $p(\theta_o')$ of the crimp angle θ_o' occurring, where $p(\theta_o')$ is again given by equation (7.22) as a Gaussian distribution.This procedure was repeated for enough values of θ_o' so that the value of $\int p(\theta_o')\,\dot{\epsilon}(t,\theta_o')\,d\theta_o'$ could be obtained using the parabolic rule as in the previous section. This was done for all the values of 20s strain from the load-strain curve. The values obtained for the 20s rate (χ) in this way at the various levels of strain were compared to the experimental values of 20s creep rate by multiplying χ by a number which in fact is equal to $\frac{b}{a}\Delta J_G$ (although it will be an inverse load term rather than an inverse stress in the ΔJ term) to give $\dot{\epsilon}(t)$ as in equation (7.29) and the sum of the squares of the differences between the theoretical and experimental values of the creep rates calculated. This procedure was repeated using different values of $\frac{b}{a}\Delta J_G/\Delta D_F$ (the ratio of the compliance difference of the gel and fibre multiplied by the shape factor b/a), $\bar{\lambda}$,(the standard deviation of the Gaussian distribution)

and of θ_o, (the initial mean crimp angle).

The values of these parameters, $\frac{b}{a}\Delta J_G / \Delta D_F$, $\bar{\lambda}$, and θ_o which gave the least value for the sum of the squares was found for each specimen. These values were used to determine the creep rate at each level of isochronal strain and load on the load-strain curve of each specimen. The best fit values for the specimens CH2-16-4, CH2-8-2 and CH2-9-1 are shown in Table 8-2 and the lines corresponding to these values drawn on figures 8-2, 8-3 and 8-4.* Even though all the specimens are from different donors, the values lie within the same order of magnitude as each other; $\frac{b}{a}\ \Delta J_G/\ \Delta D_F$ ~300 to 1200, $\bar{\lambda}$ ~1.6 to 2.6 and θ_o ~ 14° to 16°. Hence from our data and the model described above, we have obtained important and physically meaningful parameters relevant to the viscoelastic behaviour of tendon, namely

(i) the value of θ_o

(ii) the width of the distribution of crimp angles, i.e. $\bar{\lambda}$

(iii) the value of the ratio $\frac{b}{a}\ \frac{\Delta J_G}{\Delta D_F}$ from which ΔJ_G and ΔD_F can be estimated.

Note also how a change in θ_o of one degree and the change in $\bar{\lambda}$ can change the shape of the creep rate-load curve.

The best fit of all is the data of CH2-16-4(m71,Hfh), figure 8-2, which gives excellent agreement for all points on the curve. The parameters found for this specimen can give us further information on the material parameters. For instance, from the multiplying constant to convert χ from the theory to obtain $\dot{\epsilon}$ and from the ratio $\frac{b}{a}\ \frac{\Delta J_G}{\Delta D_F}$ we can obtain the rate which would result from the fibres if they were all straight at the start of the experiment. This is shown as the dotted line on figure 8-2 and can be seen to compare favourably with the rates determined experimentally on this specimen after a preload had been applied to straighten the fibres. The creep tests performed on the sample after mechanical equilibrium had

---

* The values of n_G and n_F used in these figures were found from a least squares fit of the log creep rate-log time curves before t' at the low and high loads respectively.

been reached are shown as the straight line through the solid points in figure 8-2 and lie close to the theoretical dotted line.

Hence we have extremely good correlation with theory and experiment not only in the fitting of the creep rate-load curve, but also using the same parameters to give the fibre behaviour determined in an independent experiment. From the fit of the data of specimen CH2-16-4(m71,Hfh) we can obtain an estimate of ΔJ_G and ΔD_F and the shear rate $\dot{\gamma}$. The values from the programme gave

$$\frac{b}{a} \quad \Delta J_G(\tau_G=1) \left(\frac{g}{A_o} \right) = 4.14 \times 10^{-2} \quad kg^{-1}$$

where ΔJ_G is in Pa^{-1}, and A_o is the cross-sectional area of the specimen. For $A_o \sim 10^{-5}$ m^2 then

$$\frac{b}{a} \quad \Delta J_G(\tau_G=1) \sim 10^{-7} \quad Pa^{-1}$$

and for $b/a \sim 10^{-2}$, then

$$\Delta J_G(\tau_G=1) \sim 10^{-5} \quad Pa^{-1}$$

which is of the right order of magnitude for polymeric fluids of high molecular weight[2] and compares favourably with that found by Parsons and Black[3] for the shear modulus of the polysaccharides of articular cartilage of $\Delta G_G = 10^5$ Pa.

We can also calculate ΔD_F, since for this specimen, we found

$$\frac{b}{a} \quad \frac{\Delta J_G(\tau_G=1)}{\Delta D_F(\tau_F=1)} = 300$$

and hence

$$\Delta D_F(\tau_F=1) = 10^{-9} - 10^{-10} \quad Pa^{-1}$$

which is again of the right order of magnitude for a retardation process for a crystalline polymer.[4,5,6]

The value for the shear rate of the gel may be obtained from the relation

$$\dot{\gamma} = \frac{a}{b} \frac{\cos \theta_o}{\sin \theta} \dot{\epsilon} \qquad (7.5)$$

For the first point of CH2-16-4, this gives a value for $\dot{\gamma}_1 = 5.5\text{x}10^{-3}$ s^{-1}, and for the second point $\dot{\gamma}_2 = 1.7\text{x}10^{-2}$ s^{-1} and this will decrease to zero. Comparing this with the data of Gibbs[7] for the dependence of viscosity on the shear rate for hyaluronic acid at pH 7, T_o=25 °C and concentration 3.99 gm/ml, it is found that the viscosity remains constant at a level of 10^2 Pa s for $\dot{\gamma} < 10^{-3}$ s^{-1} and decreases from then on with a relaxation time of ~1s. So, the viscosity of the gel changes to some extent with shear rate, a feature we have not considered in the present model.

8.2.3 The Dependence on Strain of the Slope of the Log Creep Rate-Log Time Curve.

We next consider specimen CH2-8-2 (m23,Heh) on which we performed T-jumps at various levels of strain from which we obtained the creep rate against load curve. The fit of this curve is shown in figure 8-4 and is not as good as for CH2-16-4(m71,Hfh) but the parameters obtained from these data will be useful in determining the ΔH_a against isochronal strain and load behaviour and the variation of the slope of the (log rate-log time) curve with isochronal strain. These results are shown in figures 8-5 and 8-6 where in both figures we used the same parameters as those found to fit the creep rate against load curve for specimen CH2-8-2(m23,Heh). The line of figure 8-5 was obtained from equation (7.29) using the 20s isochronal load-strain data of this material in a similar manner to that described earlier to determine $f(0)$ and σ' and hence the creep rate at a given value of time, t. This was done for a series of values of t and the slope of the line through

these points was determined from a least squares fit. In fact no discernable deviation from a straight line was observed. The resulting values of the (slope of the (log creep rate-log time) curve)and their variation with strain are shown by the line in figure 8-5 and seen to be in excellent agreement with the circled experimental data of specimen CH2-8-2(m23,Heh). Also shown is the dotted line for $\bar{\lambda}=2.8$ which shows how important the width of the distribution of crimp angles is in determining the experimental behaviour. It should be remembered that the slope of the log rate-log time curve for the fibre and the gel is related to the form of the distribution of retardation times spectrum of these components.

8.2.4 The Dependence of ΔH_a on Strain

The dependence of the apparent activation energy, ΔH_a, on isochronal strain for specimen CH2-8-2(m23,Heh) is shown in figure 8-6 and the line through it determined from equations(7.34) and (7.35), using the same parameters as before(as in Table 8-2) for this specimen. Again, excellent agreement is observed between theory and experiments. We have thus fitted 3 different sets of data with the same constants and found good to excellent agreement in all three cases.

8.2.5 The Dependence of the Log Creep Rate on Log Time

We can now turn our attention in more detail to the log creep rate against log time data for the various specimens. The form of these data has been neglected in previous work on T-jumps[8] which was only concerned with the value of the rates at t=t' found by extrapolating the log creep rate-log time curve to t'. From chapters 4 and 7 we now know what shape of curve will be expected on the log creep rate-log time plot both before and after t', the exact form depending on the value of ΔH_a and on the slope

of the retardation spectrum. With this information, it will be possible to make better and less arbitrary extrapolations. The following features are to be expected;

(i) Before t', we expect a straight line

(ii) After t',(see figures 4-5 and 4-6)

a) for low values of ΔH_a (<15 kcal/mol) we expect an approximate straight line.

b) as the value of ΔH_a increases, the curvature of the line increases and is quite marked at times close to t' ($t/t' < 5$) for $\Delta H_a > 25$ kcal/mol.

(iii) the value of n,(- the slope of the log rate-log time curve),before t' will determine whether the log creep rate-log time curves at a given load and various ΔT will cross ($n > 1$) or not ($n < 1$) as seen in figure 4-14.

We will see that our data exhibits all of these features and that we can use the equations developed in chapter 4 and 7 to fit the data extremely well, thus giving further support to our theory of the T-jump and to our values of ΔH_a presented.

First let us consider specimen CH2-8-2(m23,Heh), on which we performed a number of T-jumps at different levels of strain and one value of ΔT. Using the same parameters found earlier (Table 8-2) for this specimen in equation (7.33) we obtain the theoretical curves of figure 8-7 where the normalised creep rate is plotted against normalised time for t'=60s. It will be seen that the curves cross over as the transition from one mechanism to another takes place as a result of the value of n changing from the 'toe' region value ($n_G < 1$) to that in the 'linear' region ($n_F > 1$). This is to be compared with the experimental data for specimen CH2-8-2 shown in figure 8-8 for loads 0.05, 0.5, 1.1, and 1.7 kg where as expected the curves cross over as the applied load increases and as the value of ΔH_a

increases.

Even if the parameters θ_o, $\bar{\lambda}$, $\frac{b}{a}$ and $\frac{\Delta J_G}{\Delta D_F}$ are unknown, we can still fit the experimental log creep rate-log time curve by using equation (4.31) (with $(b_T-1)A$ negligible) instead of equation (7.33). Equation (4.31) is for a single activation energy mechanism and was found to be identical to equation (7.33) when used in the 'toe' region and the 'linear' region using the relevant values of ΔH_a and n in those regions. In the region in between (e.g. for values of strain from 0.04 to 0.07 of figure 8-7) a slight difference between equation (4.31) and equation (7.33) was found. For example, for specimen CH2-8-2, taking the values of ΔH_a and n in figures 8-5 and 8-6 appropriate to a level of strain 0.06, say, and using them in equation (4.31), the dashed line of figure 8-7 results which differs from the line from equation (7.33) only at times $t/t' > 4$. If a lower value of n had been used, this would have fitted the data exactly.

With this in mind, we fitted the log creep rate-log time data after t' for a number of specimens, using equation (4.31)i.e. the equation for the single activation energy mechanism given by

$$\frac{\dot{\epsilon}_T(t)}{\dot{\epsilon}_{T_o}(t')} = \frac{1}{a_T}\,\frac{1}{(t^*/t')^n} = \exp\left(\frac{\Delta H_a \Delta T}{RTT_o}\right)\,\frac{1}{(t^*/t')^n} \qquad (4.31)$$

where $t^* = t' + \left(\frac{t-t'}{a_T}\right)$

The experimental log creep rate against log time data (circled points) for specimen CH2-16-1(m71,Hfh) and the best fit theoretical lines through the experimental points found from equation (4.31) are shown in figures 8-9 to 8-12 for various values of load and ΔT. It can be seen from these figures that the lines predicted by equation (4.31) are in close agreement with the experimental points for a variety of loads. The values of ΔH_a and n used in equation (4.31) to produce these lines are given in Table 8-3. These

values of ΔH_a are compared in Table 8-3 with those found earlier from values of $\ln r$ obtained by the normal extrapolation of the experimental creep rate curves, and close agreement is found between the theoretically predicted and experimental values. The values of n found from a least squares fit of the experimental data before t' is also shown in Table 8-3.

Further support for the use of equation (4.31) was found by fitting the creep rate data of specimen CH2-16-4(m71,Hfh) to which a preload of 3kg was applied to the specimen to straighten out most of the crimped fibres. After mechanical equilibrium had been achieved under this preload, creep T-jumps were performed and the results indicated that we were looking at the fibre mechanism, as the apparent activation energy obtained was ~33 kcal/mol, the same as that for the high stress values without the preload. The log(normalised creep rate ($\dot{\epsilon}(t)/\dot{\epsilon}_{T_o}(t')$)) against log (t/t') curves for these experiments are shown in figures 8-13 to 8-15 (circled points) and the best fit lines through them from equation (4.31) are drawn for the values of ΔH_a and n shown in Table 8-3. Excellent agreement is again found between these values of ΔH_a found from the fitting of equation (4.31) to the data and those obtained previously in chapter 6 from extrapolation of the experimental creep rate data.

The degree of agreement in all cases above is remarkable considering the nature of the material as a biological polymer, where obtaining reproducible results is an achievement in itself, and considering the complexity of the structure and the difficulty in measuring such small creep rates. This lends considerable support to the method of the T-jump experiment for determining the apparent activation energy of both synthetic and biological materials.

The data of specimen CH2-16-1 for the down T-jumps (ΔT -ve) was not good enough to determine whether the $\ln r$- ΔT plot showed the

curvature to be expected in the 'transition' region from the gel to fibre behaviour. What we do know is that for the low strains of the gel behaviour and for the higher strains at which the fibre behaviour predominates, the ln r- ΔT plots were straight lines.

8.2.6 Cycling and Recovery Behaviour

All the previous cases give excellent agreement with the theory. When applying the theory to recovery and creep cycling experiments, we cannot fit the data accurately, but certain important trends will be seen which again agree with experimental data.

We have already fitted the creep rate against load data of specimen CH2-9-1(m77,Hfh) with equation (7.29) as shown in figure 8-3 and the agreement is extremely good. The fitting parameters are shown in Table 8-2. For the cycling experiments on this specimen, we saw in chapter 5 that the isochronal creep rate reduced with cycling. For a linear viscoelastic material, the isochronal rate should be the same for each cycle. Since we have assumed linear viscoelastic behaviour in our model, then it may be possible to explain the behaviour in cycling using the fact that the crimp angle at the start of each cycle is smaller than at the start of the previous one.

We thus obtained the creep rate on the second cycle from equation (7.29) by finding the value of θ at the end of the recovery part of the first cycle and using this as the θ_o for the 2nd cycle. The isochronal creep rates on the 2nd and subsequent cycles, found by this method, are shown for specimen CH2-9-1(m77,Hfh) in figure 8-16 for cycles 1,2 and 10. Although the theoretical lines do not exactly fit the experimental data, the theory does predict that the creep rate will decrease on cycling as a result of the uncrimping of the fibres.

In order to predict the recovery rate behaviour of tendon, we assumed that

(i) creep recovery results from the application of a negative load equal to the original load so as to make the net load equal to zero.

(ii) since the fibres are linear viscoelastic, the contribution to the rate from the fibres in recovery is the same as in creep.

(iii) the contribution from the gel results from the negative load acting on the crimp planes at angles θ determined from the actual strain of the material during recovery. The initial crimp angle, θ_{c_R}, to be used in the equations during recovery will be determined from the value of strain at the time of removal of the load. Hence the gel contribution will be different in recovery from that in creep since the crimp angle of the fibres will be less in recovery than it was in creep and hence the shear stress on the gel between the ribbons will be different from creep. In some cases, the crimps will be totally straightened out in creep, but during recovery, the crimps will have returned.

For example, for specimen CH2-9-1, taking t=20s at a load of 50gm, $\theta_o = 14.5^\circ$, $\theta_{o_R} = 11.1^\circ$, and the value of θ after removal of the load is 14.17° since the 20s strain is 0.147%. Using this and the load-strain data at other strains we obtained the recovery rate as shown in figure 8-17 (solid line). This compares with the experimental creep rate on the same plot, (dashed line) and can be seen to be two orders of magnitude larger than the creep rate at the larger strains. Even though the values for the recovery rate are much larger than those found experimentally, the theory nevertheless predicts that the recovery rate will be greater than the creep rate.

8.3 Summary

We have obtained excellent agreement between the theory and various types of experimental data for a number of specimens. We have found

(i) the value of θ_o from the best fit straight line through the $\dot{\epsilon}/\sigma_o$ against $(1+\epsilon)$ data for the specimens CH2-16-4(m71,Hfh), CH2-9-1(m77,Hfh), and CH2-8-2(m23,Heh).

(ii) the values of $\bar{\lambda}$ and $\frac{b}{a}\frac{\Delta J_G}{\Delta D_F}$ from the best fit of the theoretical equations to the creep rate against load data for the same specimens CH2-16-4, CH2-9-1 and CH2-8-2. Values for ΔJ_G and ΔD_F were also found for specimen CH2-16-4.

Using the values of these parameters found above, we have obtained good fit of the theory to

(iii) the fibre creep rate against load data of the preloaded specimen CH2-16-4.

(iv) the ΔH_a-isochronal strain data and the slope,n, of the(log rate-log time curve)against isochronal strain data for the specimen CH2-8-2

(v) the log (normalised creep rate, $(\dot{\epsilon}_T(t)/\dot{\epsilon}_{T_o}(t'))$ against log (normalised time,(t/t')) data for

a) specimen CH2-8-2 at various stresses and one ΔT.

b) specimen CH2-16-1 at stresses (and strains) in the'transition' region and in the fibre dominant region.

c) specimen CH2-16-4 for stresses producing small strains on a preloaded sample.

The parameters of the model are to be emphasised as they reflect the true nature of the tendon material and thus are structural constants which do not alter from one type of mechanical test to another. They are

(i) the ratio $\frac{b}{a}\frac{\Delta J_G}{\Delta D_F}$

(ii) the initial crimp angle, θ_o.

(iii) the measure of the width of the Gaussian distribution, $\bar{\lambda}$.

(iv) the slopes of the (log rate-log time) curves for the gel and fibre, i.e. n_G and n_F, which are related to the slope m of the retardation spectrum on a ln L- ln τ plot by n=1-m.

Even though the cycling and recovery predictions do not fit the experimental data precisely, we have been able to model some important qualitative trends which agree with experiment, namely

(i) the creep rate reduces with cycling

(ii) the recovery rate is greater than the creep rate.

References

1 Diamant J., Keller A., Baer E., Litt M. and Arridge R.G.C., Proc.Roy.Soc., London, B180,293,1972.

2 Bird B.R., Armstrong R.C. and Hassager O., 'Dynamics of Polymeric Liquids', vol 1, Wiley, New York, 1977.

3 Parsons J.R. and Black J., J.Biomech.,10,21,1977.

4 Ferry J.D., 'Viscoelastic Properties of Polymers', Wiley, New York, 1970.

5 McCrum N.G., Read B.E. and Williams G.,'Anelastic and Dielectric Effects in Polymeric Solids', Wiley, London, 1967.

6 Arridge R.G.C., 'Mechanics of Polymers', Clarendon Press, Oxford,1975.

7 Gibbs D.A., Sc.D. Thesis, M.I.T., 1966.

8 Hutchinson J.M. and McCrum N.G., Nature, Physical Sci.,236,115,1972.
Hutchinson J.M., D.Phil. Thesis, Oxford University, 1974.
Pearce D.L., D.Phil. Thesis, Oxford University, 1976.
McCrum N.G. and Pearce D.L., Nature, Physical Sci.,243,52,1973.
Caruthers J.M. and Cohen R.E., J.Polymer Sci.,14,1891,1976.

Table 8-1 Values of Crimp Angles Determined from Fitting Equation (7.11) to Experimental Data.

Specimen	θ_o
CH2-9-1(m77,Hfh)	15°
CH2-8-2(m12,Heh)	16°
CH2-16-4(m71,Hfh)	14°

Table 8-2 Values of Crimp Angle, (θ_o), Standard Deviation of the Gaussian Distribution of Crimp Angles, ($\bar{\lambda}$), Compliance Differences of the Gel, (ΔJ_G) and Fibres (ΔD_F) found from fitting equation (7.29) to the Experimental Data.

Specimen	θ_o	$\bar{\lambda}$	$\frac{b}{a}\frac{\Delta J_G}{\Delta D_F}$
CH2-16-4	14°	2.6	300
CH2-8-2	15°	2.2	1200
CH2-9-1	14.5°	1.6	800

Table 8-3 Comparison Between Values of ΔH_a and n Found From (i) Experimental Creep Rates, and Extrapolation to time t', and (ii) Fitting of Equation (4.31) to the Experimental Creep Rate Data.

Specimen	Figure	$\dot{\epsilon}_{T_o}(t')$ $\times 10^5 s^{-1}$	Load (kg)	ϵ_{20} (%)	Pre-Load (kg)	ΔT °C	(i)Experimental -slope before t',(n)	(i)Experimental ΔH_a kcal/mol	(ii)Theoretical n	(ii)Theoretical ΔH_a kcal/mol
CH2-16-1	8-9	0.40	1.0	1.990		1.4	1.13	27	1.25	27
	8-9	0.38	"	1.965		2.9	1.15	27	1.25	27
	8-10	0.545	2.0	2.679		5.45	1.15	28	1.20	28
	8-10	0.555	"	2.636		1.9	1.15	25	1.20	25
	8-11	0.71	4.0	3.686		4.45	1.19	32	1.25	38
	8-11	0.76	"	3.683		-4.9	1.18	31	1.30	32
	8-11	0.72	"	3.679		-2.6	1.20	31	1.30	35
	8-12	0.83	5.9	4.415		2.3	1.25	33	1.225	38
	8-12	0.81	"	4.423		6.45	1.25	30	1.225	38
	8-12	0.75	"	4.489		-7.1	1.25	30	1.225	30
CH2-16-4	8-13	0.23	2.0	0.516	3.0	5.9	0.98	31	0.975	32
	8-13	0.24	"	0.513	"	-3.1	0.98	37	0.95	35
	8-14	0.35	3.0	0.749	"	2.5	0.95	38	0.93	36
	8-15	0.315	"	0.759	"	4.5	1.00	30	0.95	32

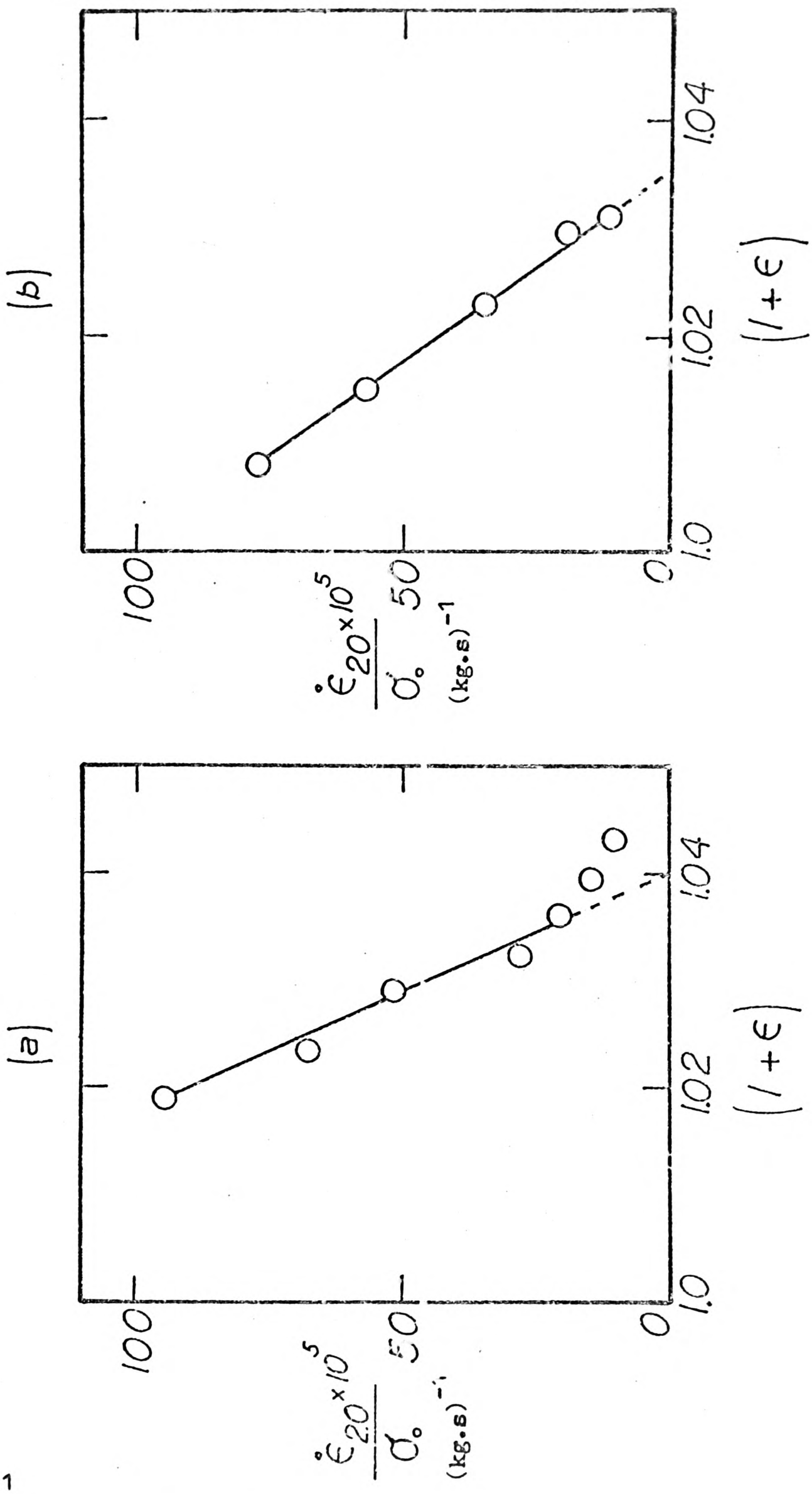


Figure 8-1

Plot of $\dot{\epsilon}_{20}$/load against $(1+\epsilon_{20})$ for specimens a) CH2-8-2(m23,Heh) and b) CH2-9-1(m77,Hfh) giving the intercept on the $(1+\epsilon_{20})$ axis as $1/\cos\theta_0$ = 1.04 and 1.035 respectively.

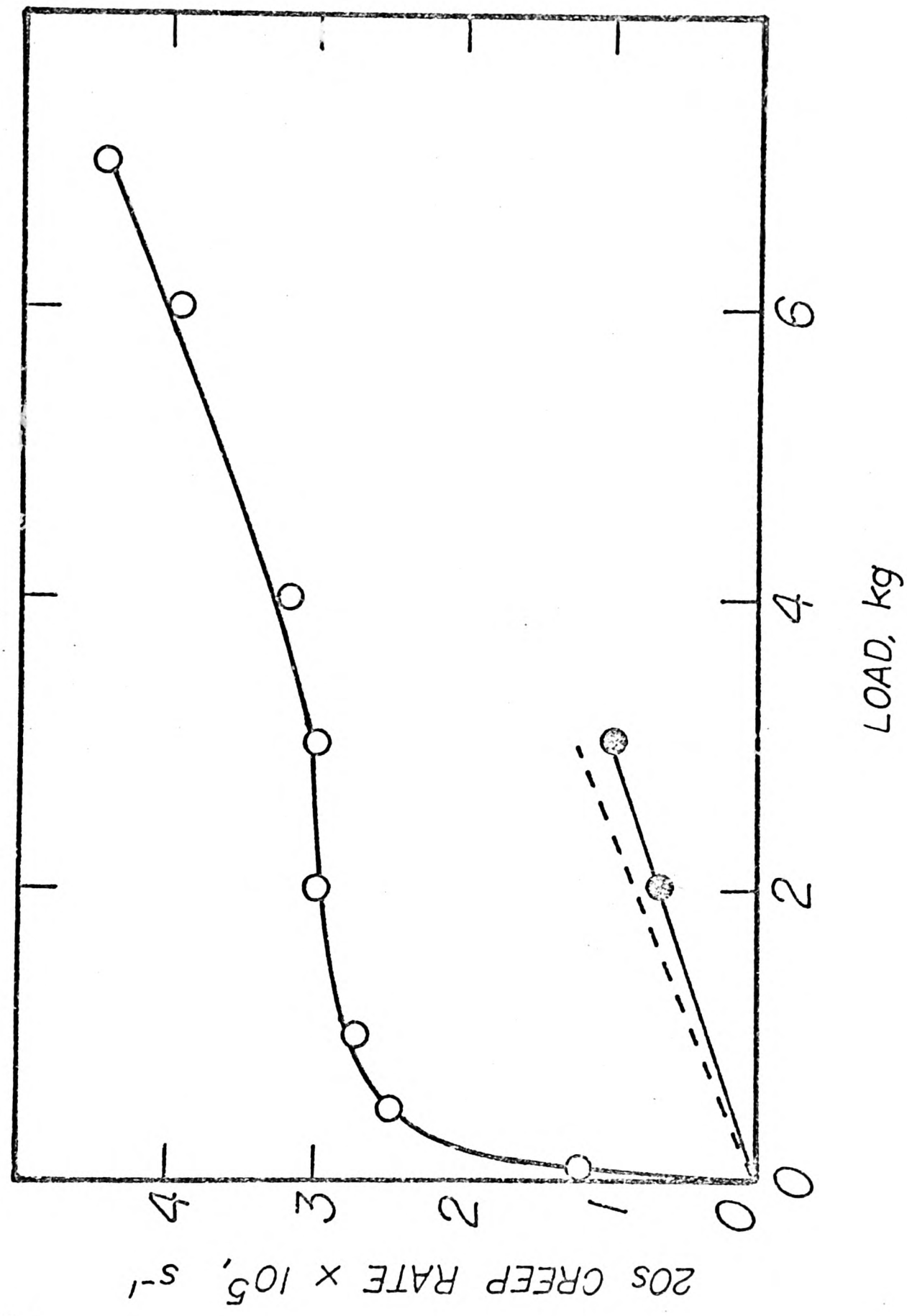


Figure 8-2

Open circles: plot of the 20s creep rate against load for CH2-16-4(m71,Hfh). Theoretical line drawn through the experimental points for $\theta_o = 14^\circ$, $\bar{\lambda} = 2.6$, $\frac{h}{a}(\Delta J_G/\Delta D_F) = 300$. Values of $n_G = 1.0$ and $n_F = 1.05$ were used as found from the log rate-log time curves at low and high loads respectively.

Solid circles: experimental 20s creep rate against load curve under 3 kg preload; theoretical line for the fibres with constants as above.

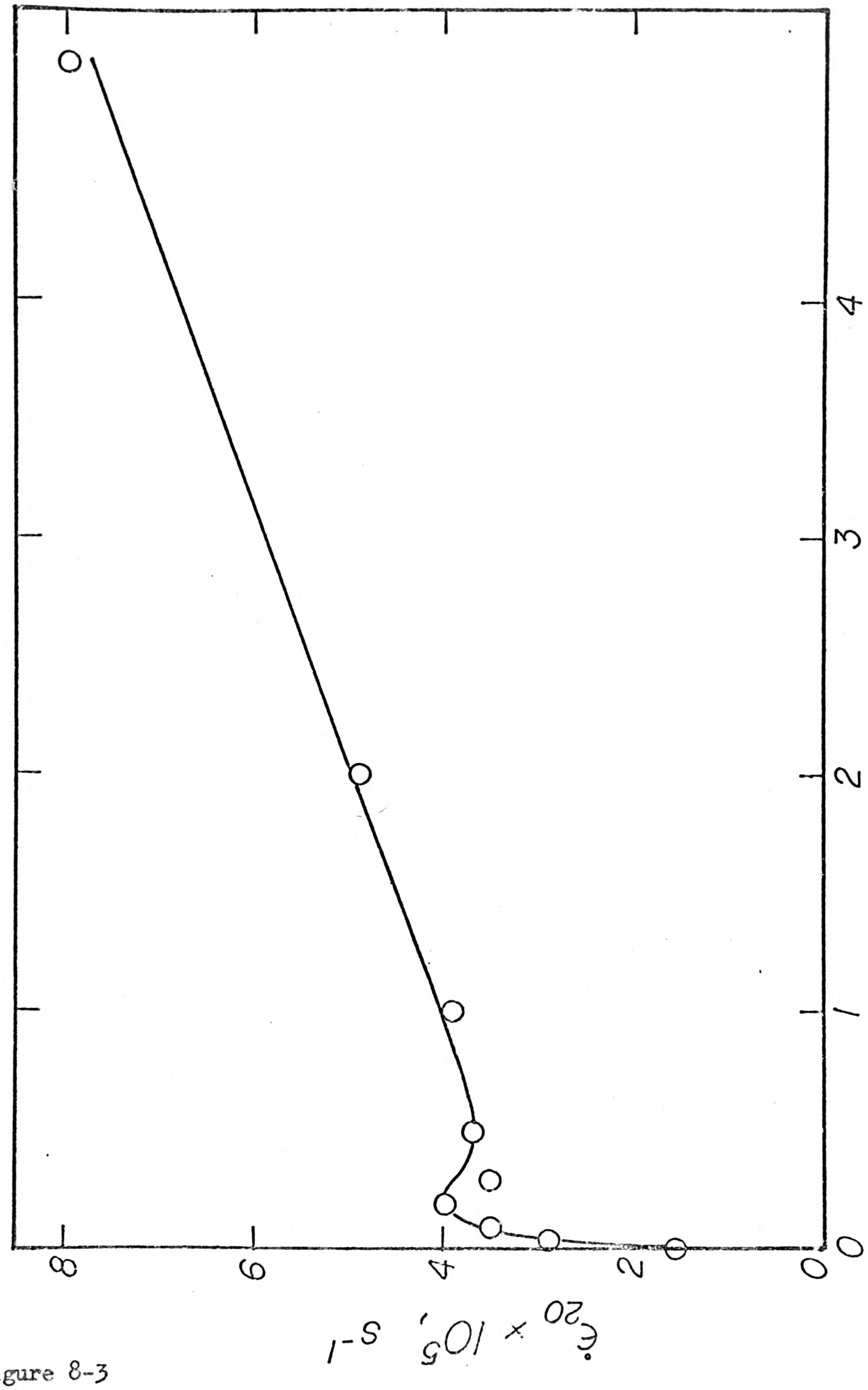


Figure 8-3

Dependence of 20s creep rate on load (open circles) for specimen CH2-9-1 (m77,Hfh) with the theoretical line drawn through the experimental points for $\theta_o = 14.5°$, $\bar{\lambda} = 1.6$ and $\frac{b}{a}(\Delta J_G/\Delta D_F) = 800$, and with values of $n_G = 0.87$ and $n_F = 0.93$.

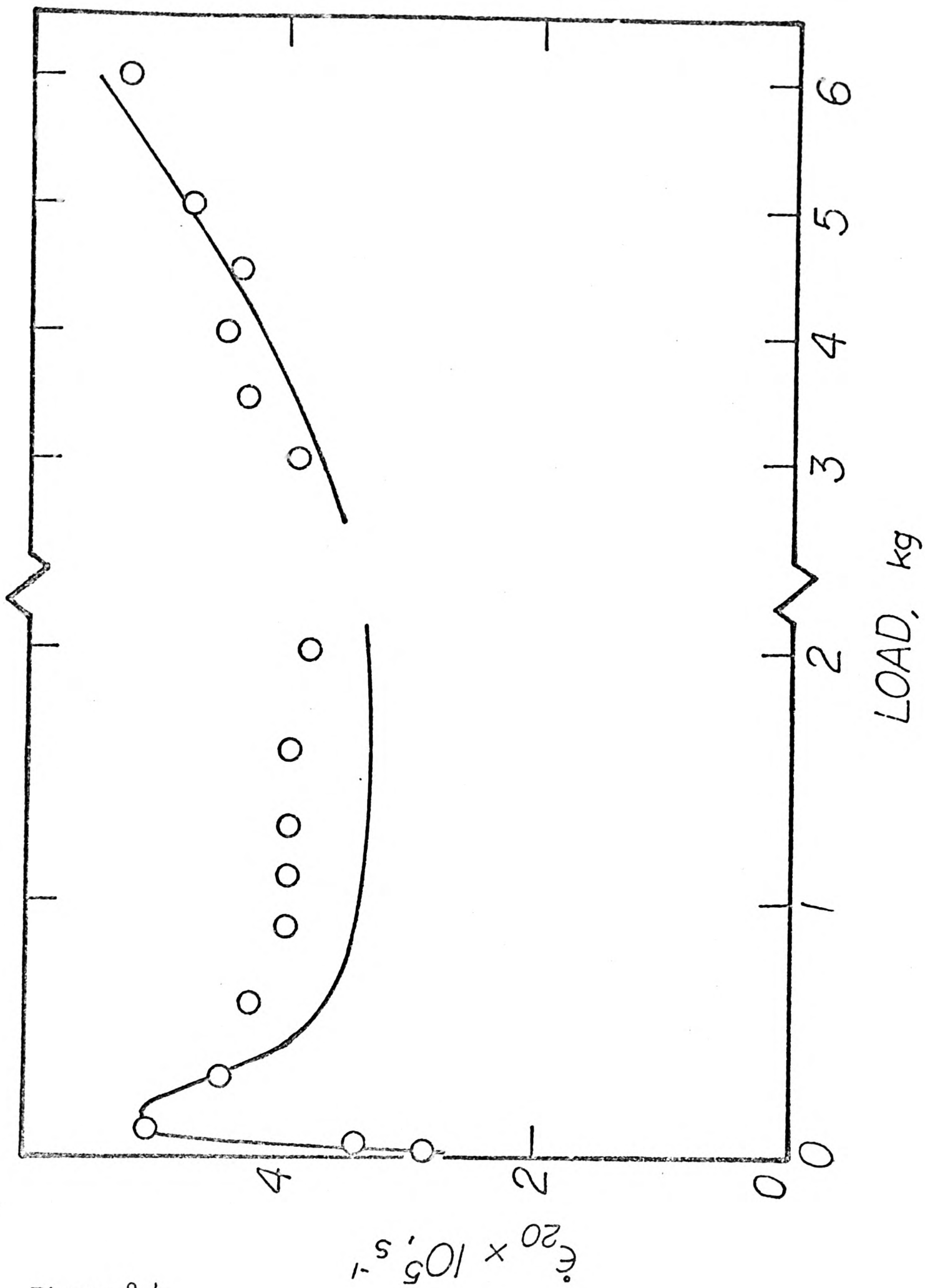


Figure 8-4

Dependence of 20s creep rate on load (open circles) for the specimen CH2-8-2 (m23,Heh) with the theoretical line drawn through the experimental points for $\theta_o = 15°$, $\bar{\lambda} = 2.2$, and $\frac{b}{a}(\Delta J_G/\Delta D_F) = 1200$. Values of n_G=0.95 and n_F = 1.17 were used.

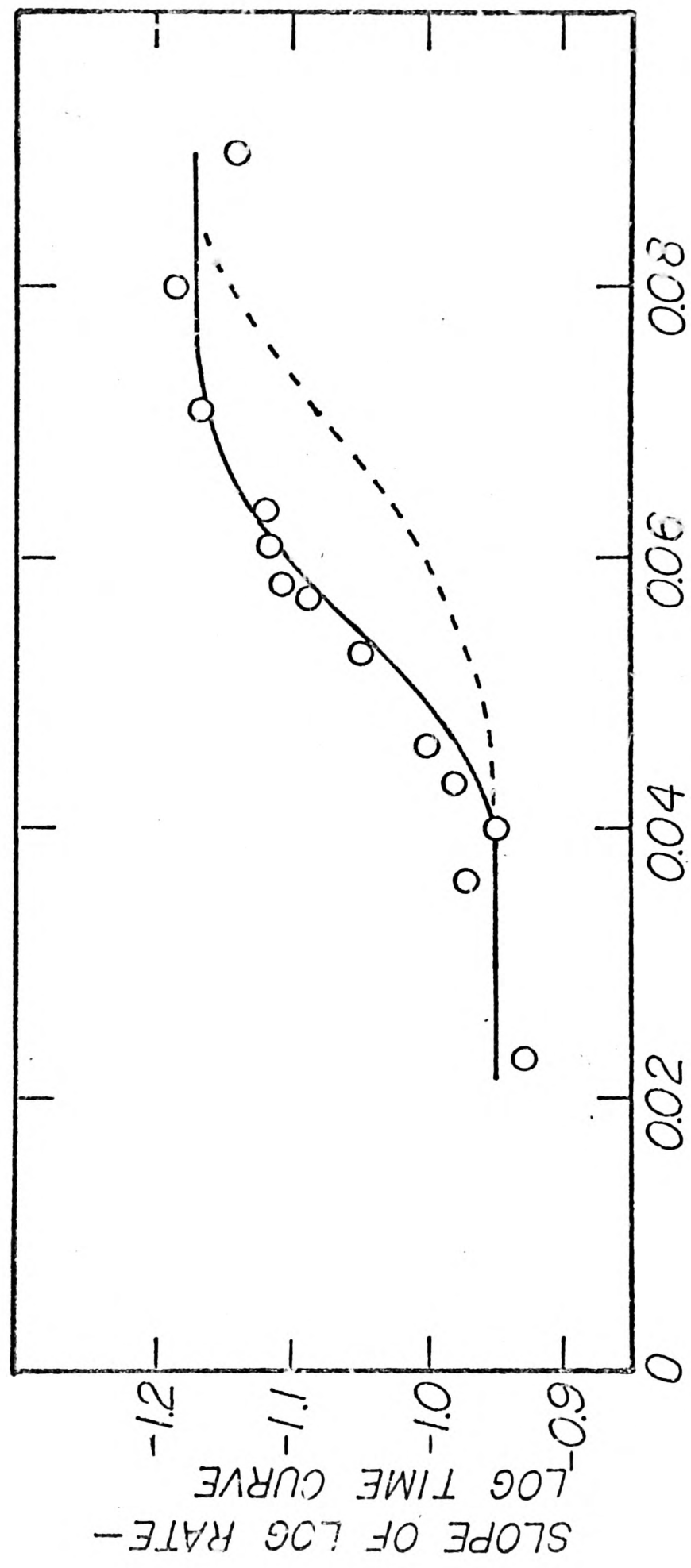


Figure 8-5

Dependence of n, the slope of the log rate-log time curve, on the 20s isochronal strain (circled points) for specimen CH2-8-2(m23,Heh).
——— theoretical line for $\theta_o = 15^\circ$, $\bar{\lambda} = 2.2$ and $\frac{b}{a}(\Delta J_G/\Delta D_F) = 1200$
----- theoretical line for $\theta_o = 15^\circ$, $\bar{\lambda} = 2.8$ and $\frac{b}{a}(\Delta J_G/\Delta D_F) = 1200$

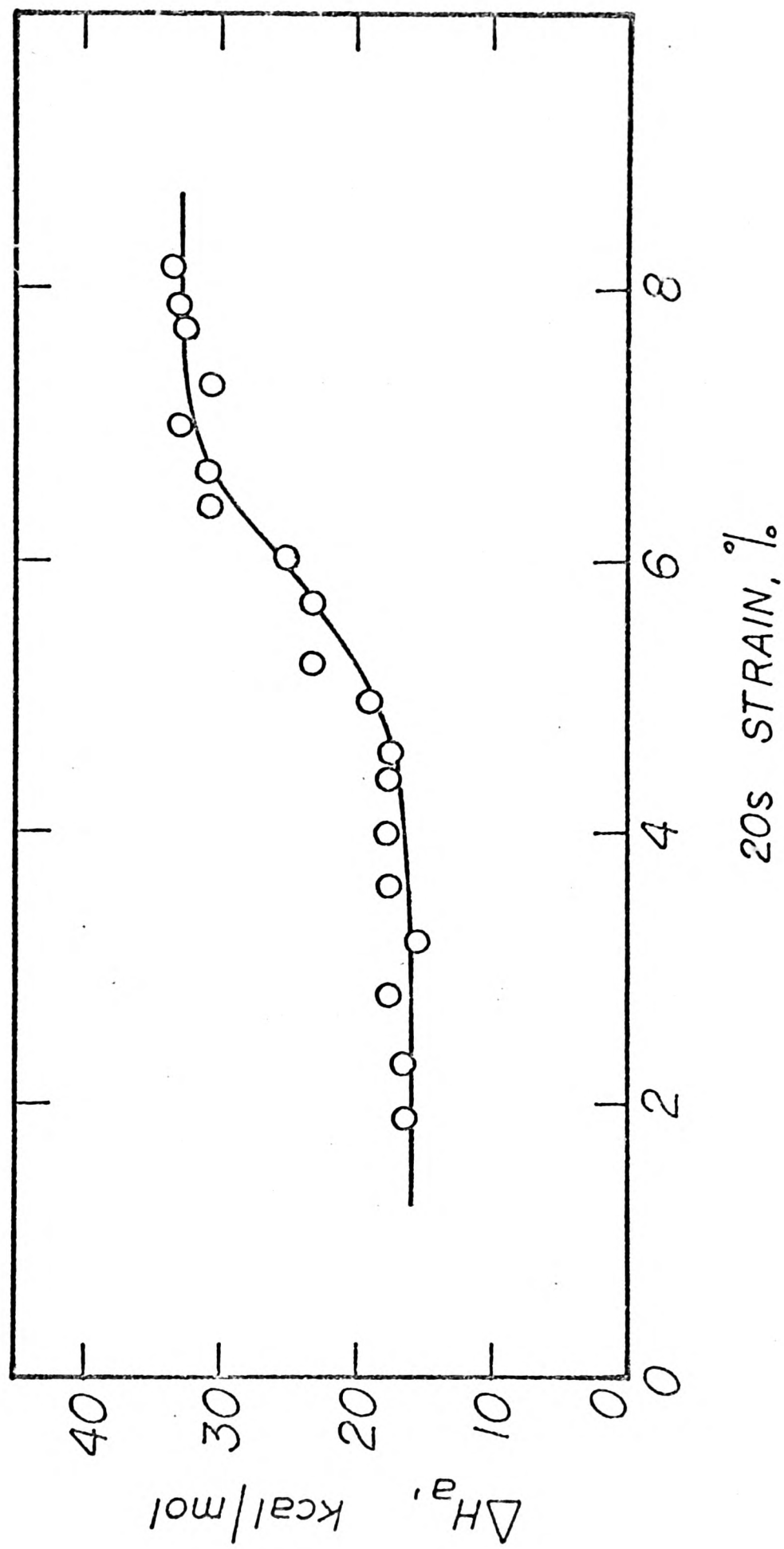


Figure 8-6

Dependence of ΔH_a on the 20s isochronal strain (open circles) for specimen CH2-8-2(m23,Heh). —— theoretical line through the experimental points for $\theta_o = 15^\circ$, $\bar{\lambda} = 2.2$, $\frac{b}{a}(\Delta J_G/\Delta D_F) = 1200$. Values of $n_G = 0.95$ and $n_F = 1.17$ were used.

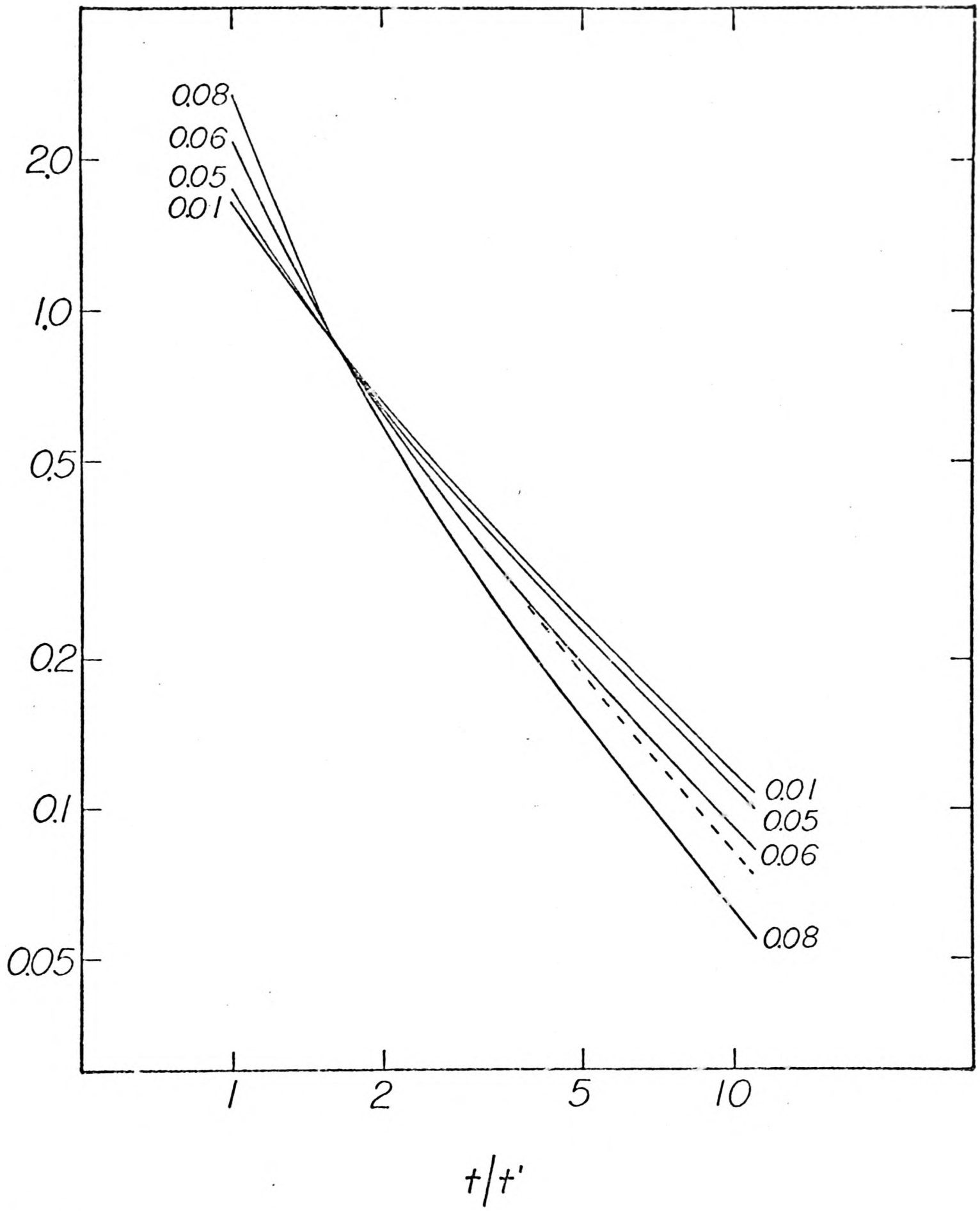


Figure 8-7

Theoretical dependence of log (normalised creep rate) on log (normalised time), after a creep T-jump using the parameters found before for specimen CH2-8-2(m23,Heh), namely θ_o = 15°, $\bar{\lambda}$= 2.2, $\underline{b}(\Delta J_G/\Delta D_F)$ = 1200, n_G=0.95, n_F = 1.17 for various levels of strain, and using equation(7.33).

----- is for a single activation energy mechanism, using equation (4.31) with ΔH_a = 25.5 kcal/mol and n = 1.10.

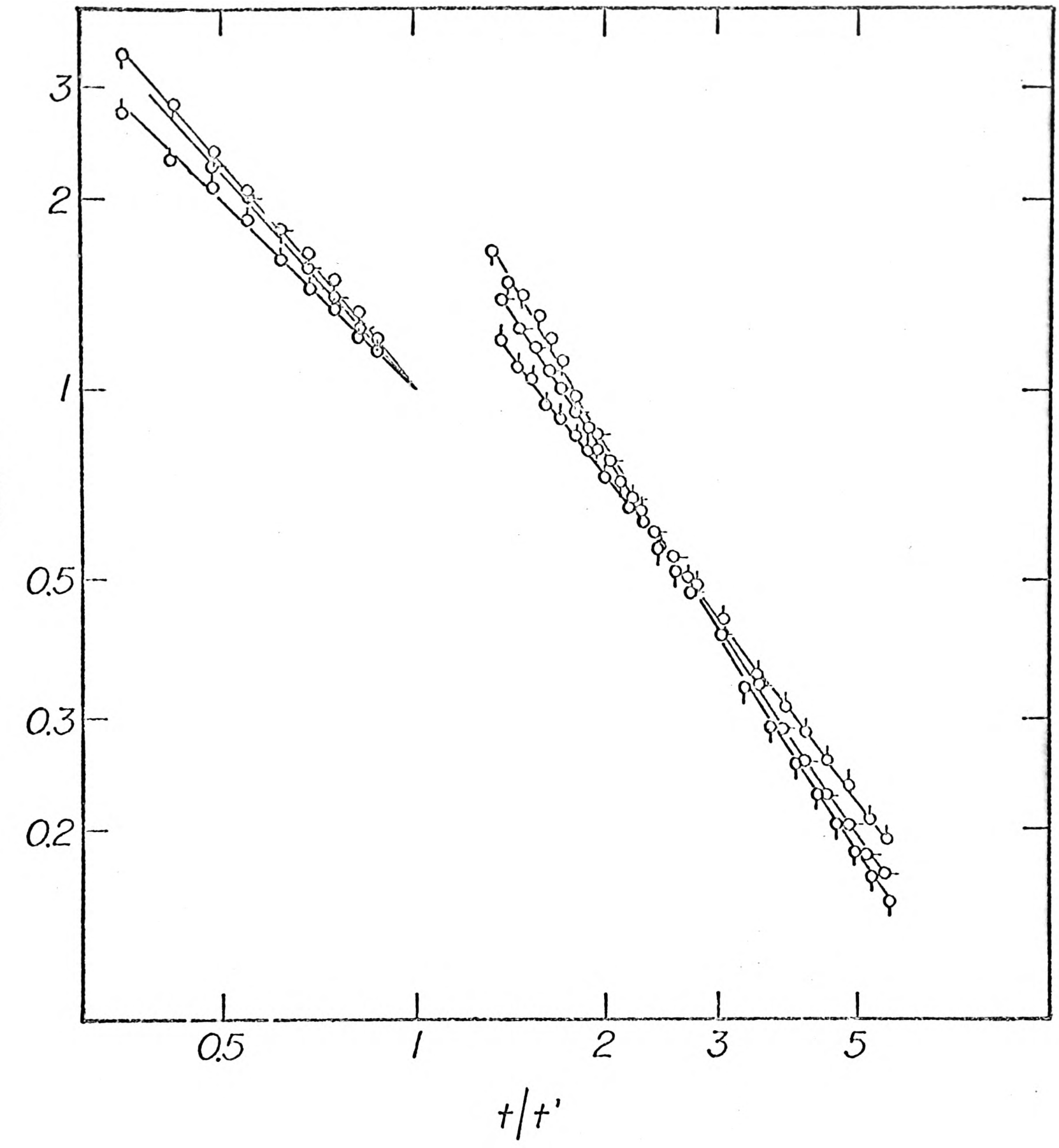


Figure 8-8

Dependence of experimental log (normalised creep rate, $\dot{\epsilon}(t)/\dot{\epsilon}_{T_0}(t')$) on log normalised time(t/t') before and after a T-jump for specimen CH2-8-2 (m23,Heh) at various loads as shown.

ò 0.05 kg and 0.5 kg; o- 1.1 kg; ọ 1.7 kg.

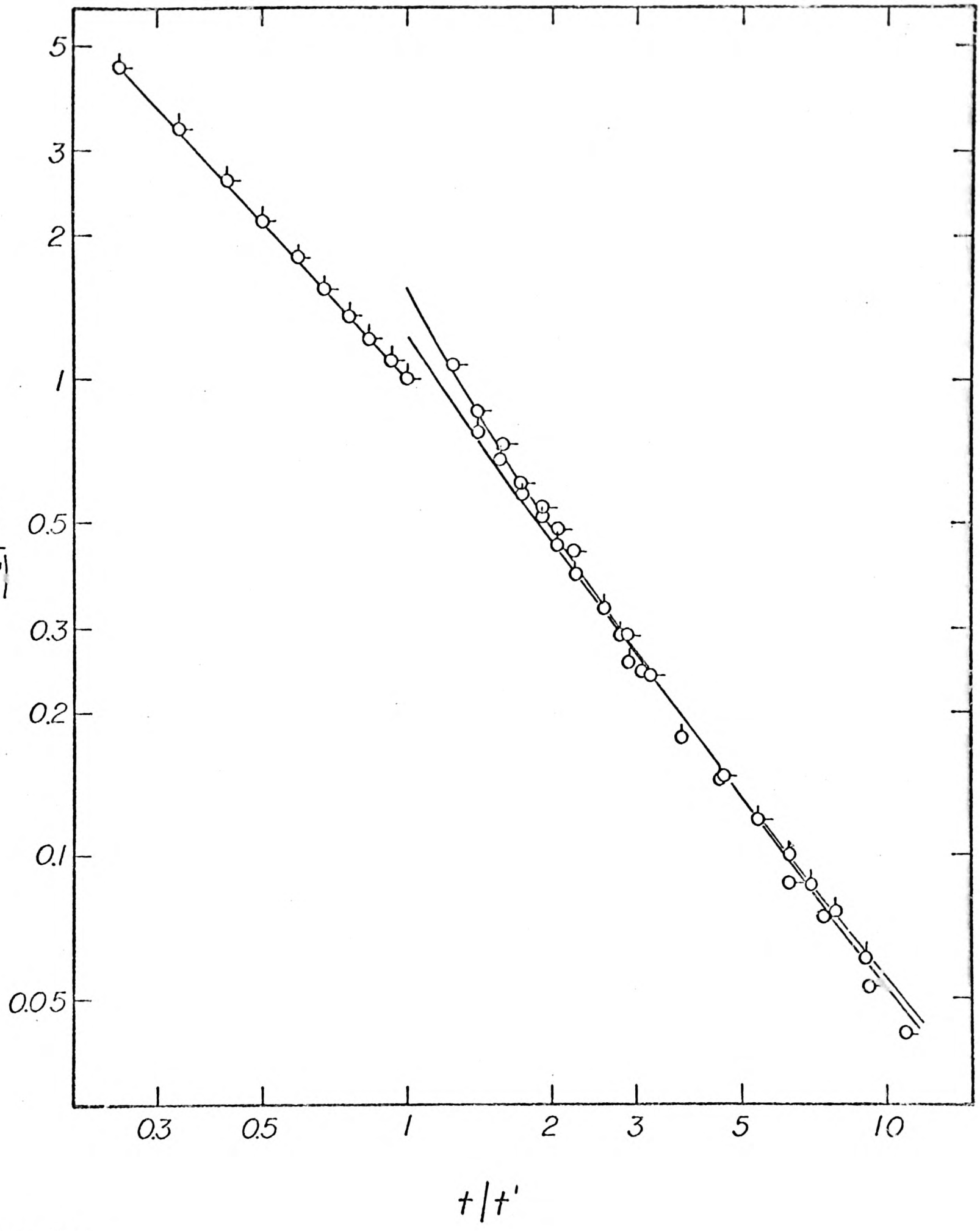


Figure 8-9

Dependence of log (normalised creep rate, $\dot{\epsilon}(t)/\dot{\epsilon}_{T_o}(t')$) on log (normalised time, t/t') in creep T-jumps for specimen CH2-16-1(m71,Hfh), load = 1 kg, ♁ $\Delta T = 1.4\,^{\circ}C$; o- $\Delta T = 2.9\,^{\circ}C$.

Theoretical lines drawn through the experimental points after t' calculated from equation (4.31) with $\Delta H_a = 27$ kcal/mol and n = 1.25

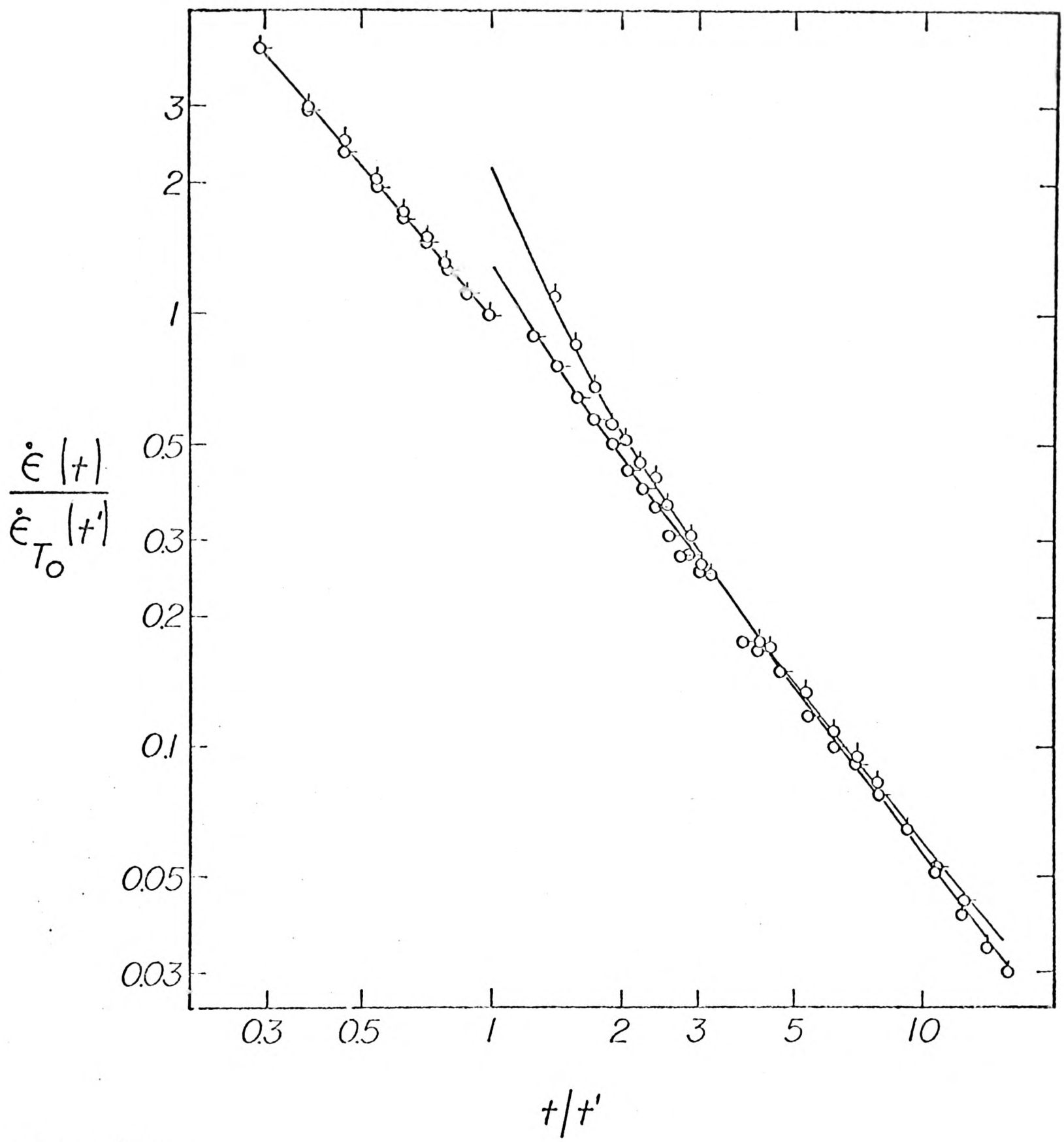


Figure 8-10

Dependence of experimental log (normalised creep rate, $\dot{\epsilon}(t)/\dot{\epsilon}_{T_0}(t')$) on log(normalised time, t/t'), (open circles), in creep T-jumps for specimen CH2-16-1(m71,Hfh), load = 2 kg, for various values of ΔT; o- ΔT = 1.9 °C; ó ΔT = 5.45 °C.
Theoretical lines through the data after t' calculated from equation (4.31) with the parameters ΔH_a and n given below.

Experimental points o- ; theoretical line with ΔH_a = 25 kcal/mol, n = 1.20

Experimental points ó ; theoretical line with ΔH_a = 28 kcal/mol, n = 1.20

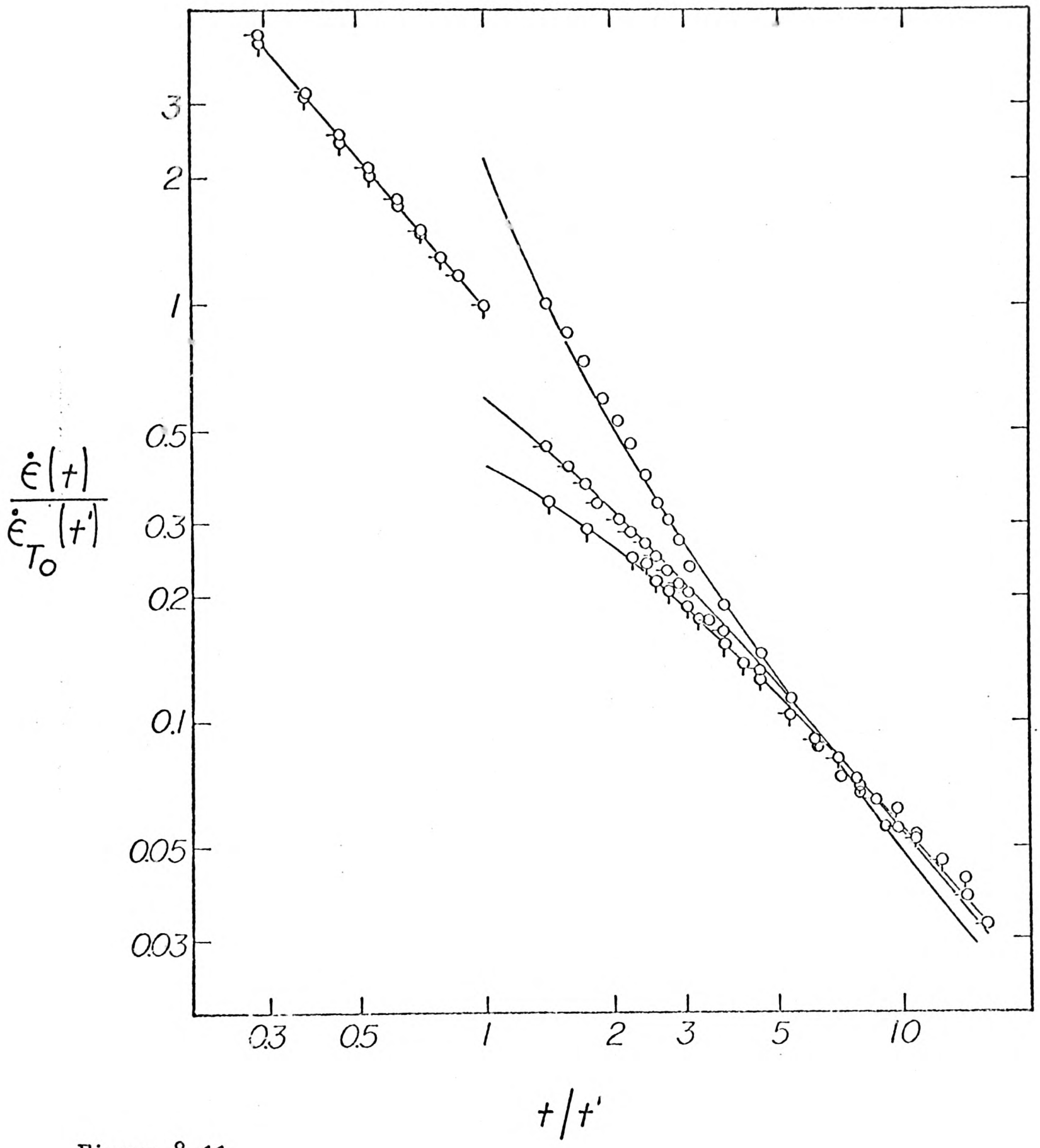


Figure 8-11

Dependence of experimental log (normalised creep rate, $\dot{\epsilon}(t)/\dot{\epsilon}_{T_0}(t')$) on log (normalised time, t/t'), (open circles), in creep T-jumps for specimen CH2-16-1(m71,Hrh), load = 4 kg, for various values of ΔT; o $\Delta T = 4.45\,^{\circ}C$; -o $\Delta T = -2.6\,^{\circ}C$; ϙ $\Delta T = -4.9\,^{\circ}C$.
Theoretical lines through the data after t' calculated from equation (4.31) with the values of ΔH_a and n given below:

Experimental points o ; theoretical line with $\Delta H_a = 38$ kcal/mol, n = 1.25

Experimental points -o ; theoretical line with $\Delta H_a = 35$ kcal/mol, n = 1.30

Experimental points ϙ ; theoretical line with $\Delta H_a = 32$ kcal/mol, n = 1.30

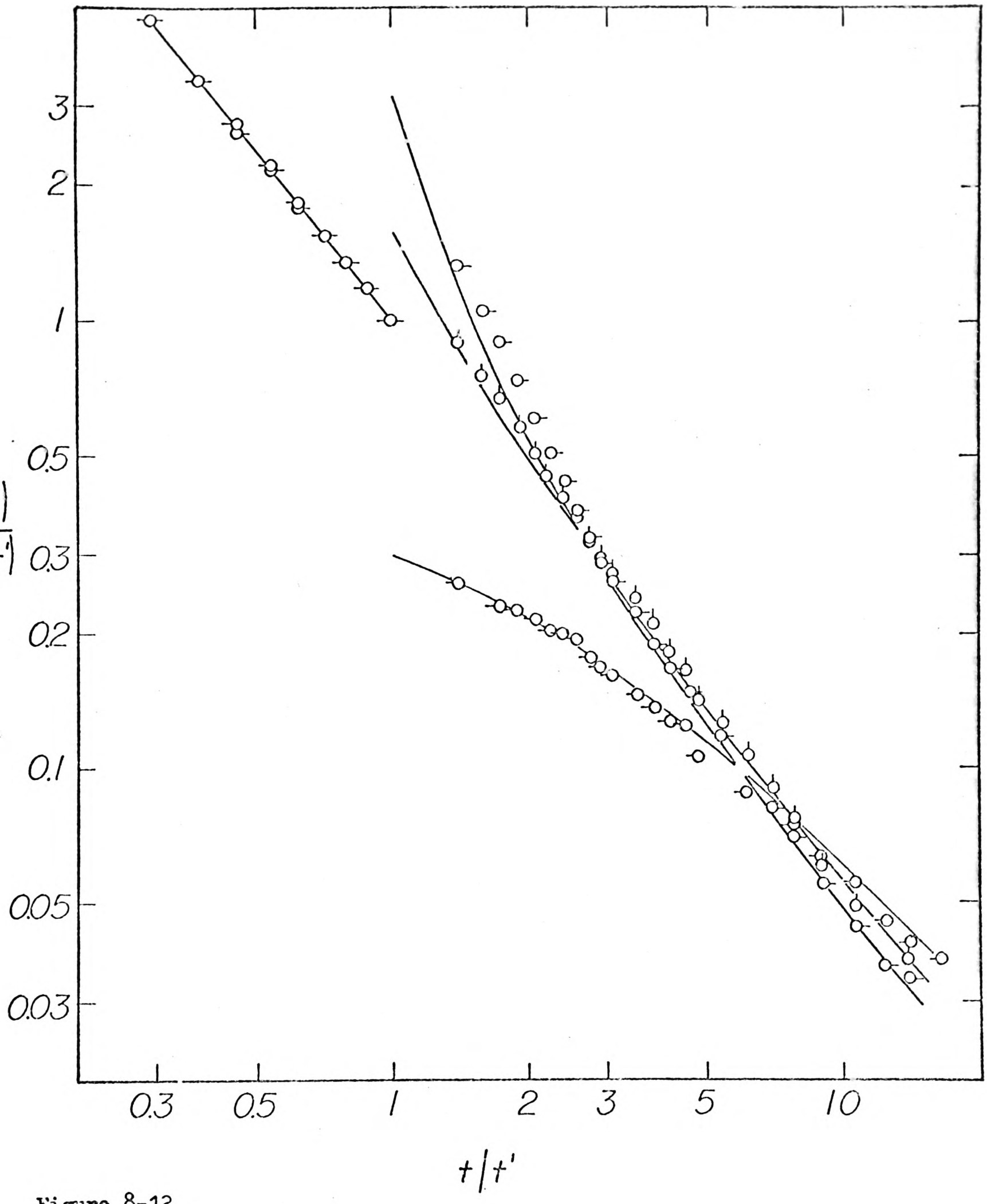


Figure 8-12

Dependence of experimental log (normalised creep rate, $\dot{\epsilon}(t)/\dot{\epsilon}_{T_0}(t')$) on log (normalised time, t/t'), (open circles), in creep T-jumps for specimen CH2-16-1(m71,Hfh), load = 6 kg, for various values of ΔT; ó $\Delta T = 2.3^{\circ}C$; o- $\Delta T = 6.45^{\circ}C$; -o $\Delta T = -7.1^{\circ}C$. Theoretical lines through the data after t' calculated from equation (4.31) with the values of ΔH_a and n given below:

Experimental points ó ; theoretical line with $\Delta H_a = 38$ kcal/mol, n = 1.225

Experimental points o- ; theoretical line with $\Delta H_a = 38$ kcal/mol, n = 1.225

Experimental points -o ; theoretical line with $\Delta H_a = 30$ kcal/mol, n = 1.225

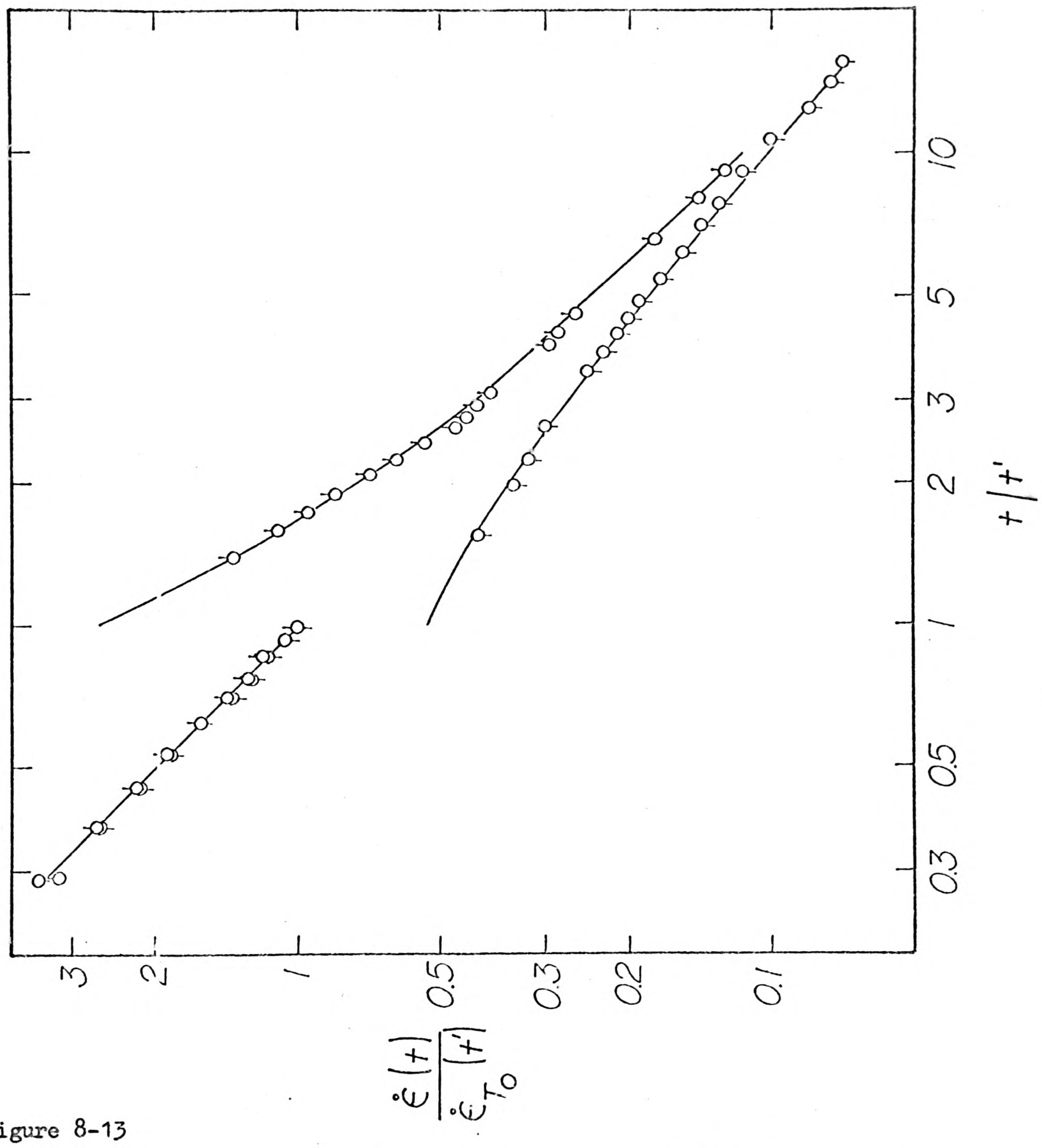


Figure 8-13

Dependence of experimental log (normalised creep rate, $\dot{\epsilon}(t)/\dot{\epsilon}_{T_o}(t')$) on log (normalised time, t/t') in creep T-jumps for specimen CH2-16-4($^{\circ}$m71,Hfh), load = 2 kg, preload = 3 kg, for various values of ΔT: ♁ ΔT= 5.9 °C; ♀ ΔT= -3.1 °C. Theoretical lines through the data after t' calculated from equation (4.31) with the values of ΔH_a and n given below:

Experimental points ♁ ; theoretical line with ΔH_a = 32 kcal/mol, n = 0.975.

Experimental points ♀ ; theoretical line with ΔH_a = 35 kcal/mol, n = 0.95

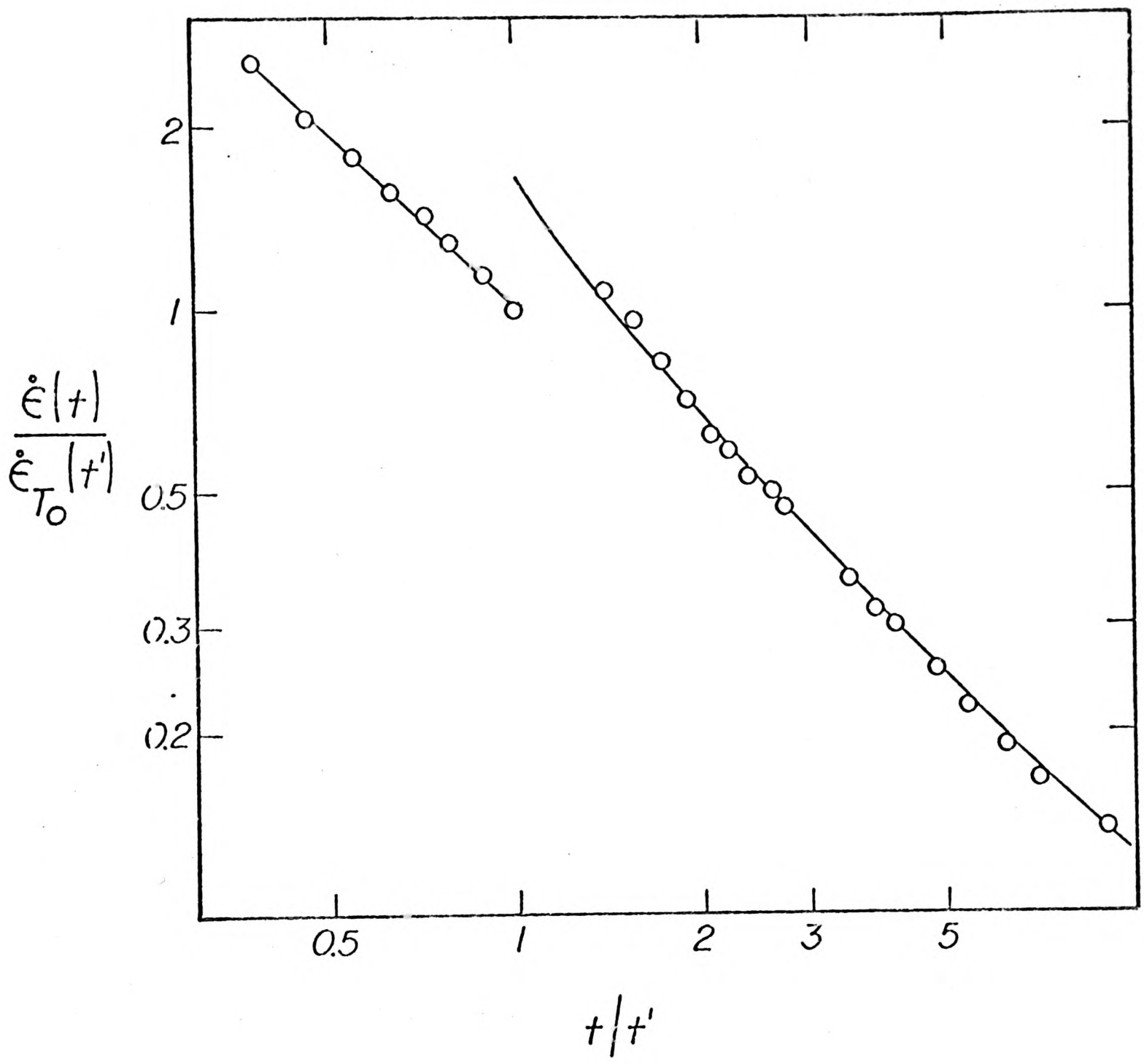


Figure 8-14

Dependence of experimental log (normalised creep rate, $\dot{\epsilon}(t)/\dot{\epsilon}_{T_o}(t')$) on log (normalised time, t/t') , (open circles), in creep T-jumps, for specimen CH2-16-4(m?:,Hfh), load = 3 kg, preload = 3 kg, with $\Delta T = 2.5\,^{\circ}C$.

Theoretical line through the data after t' calculated from equation (4.31) with ΔH_a = 36 kcal/mol and n = 0.93.

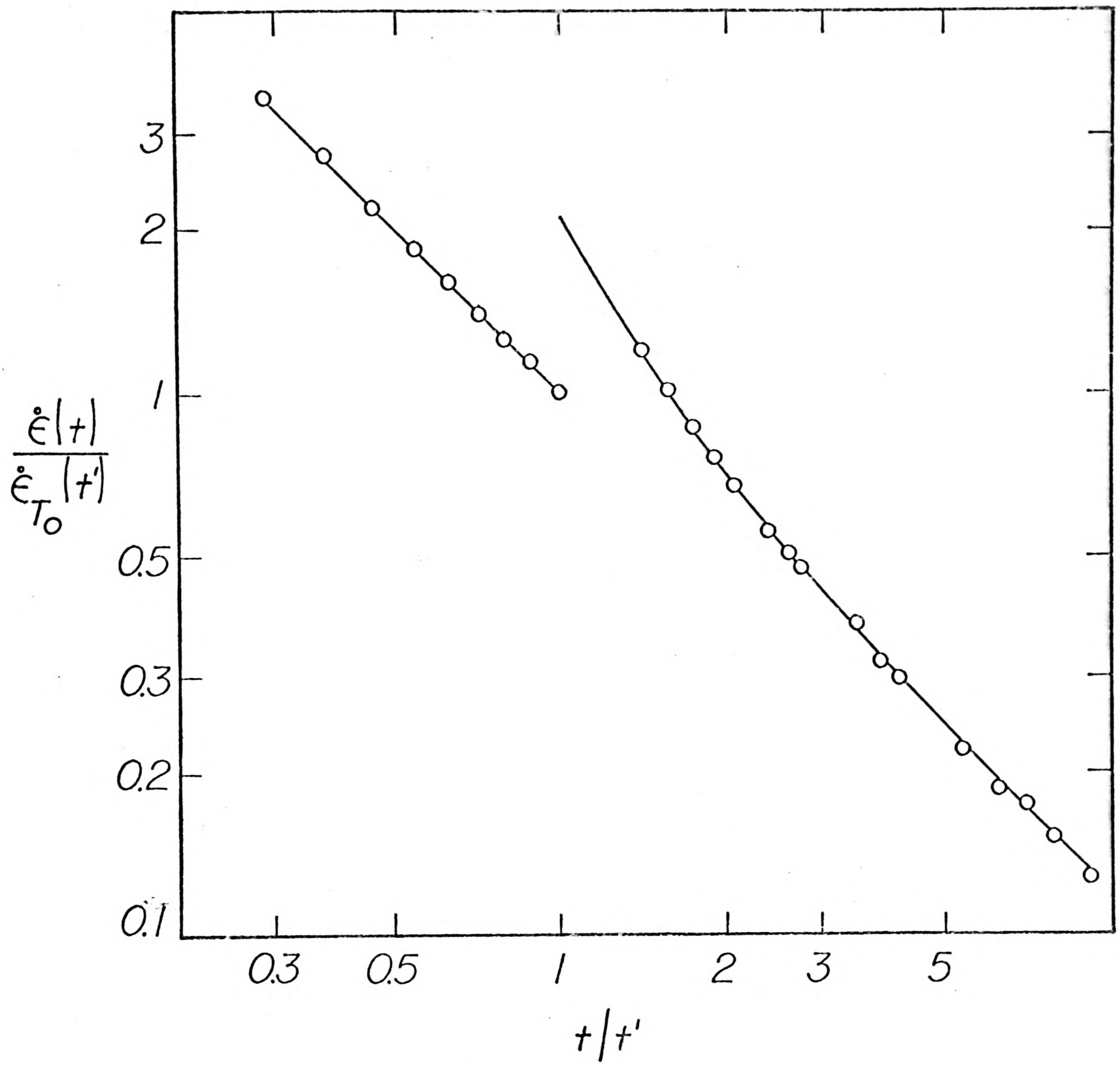


Figure 8-15

Dependence of experimental log (normalised creep rate, $\dot{\epsilon}(t)/\dot{\epsilon}_{T_o}(t')$) on log (normalised time, t/t'), (open circles), in creep T-jump for specimen CH2-16-4(m71,Hfh), load = 3 kg, preload = 3 kg, with $\Delta T = 4.5\,^{\circ}C$.

Theoretical line through the data after t' calculated from equation (4.31) with ΔH_a = 32 kcal/mol and n = 0.95.

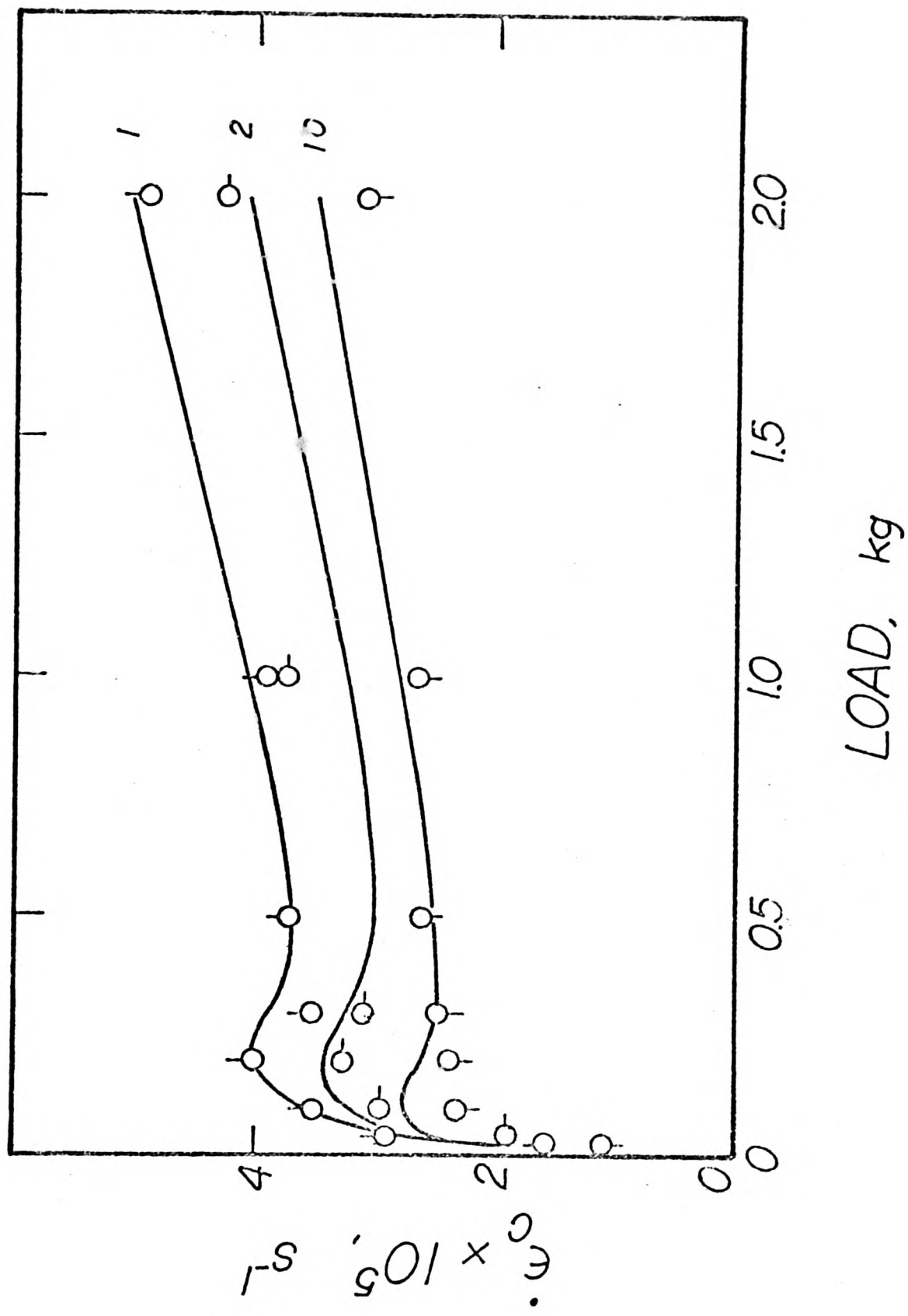


Figure 8-16

Plot of experimental 20s creep rate against load for specimen CH2-9-1 (m77,Hfh) for creep cycling experiments.
ȸ 1st cycle; o- 2nd cycle; ϙ 10th cycle.

Theoretical lines through the points with $\theta_o = 14.5^\circ$, $\bar{\lambda} = 1.6$, $\frac{b}{a}(\Delta J_G/\Delta D_F) = 800$, $n_G = 0.87$ and $n_F = 0.93$.

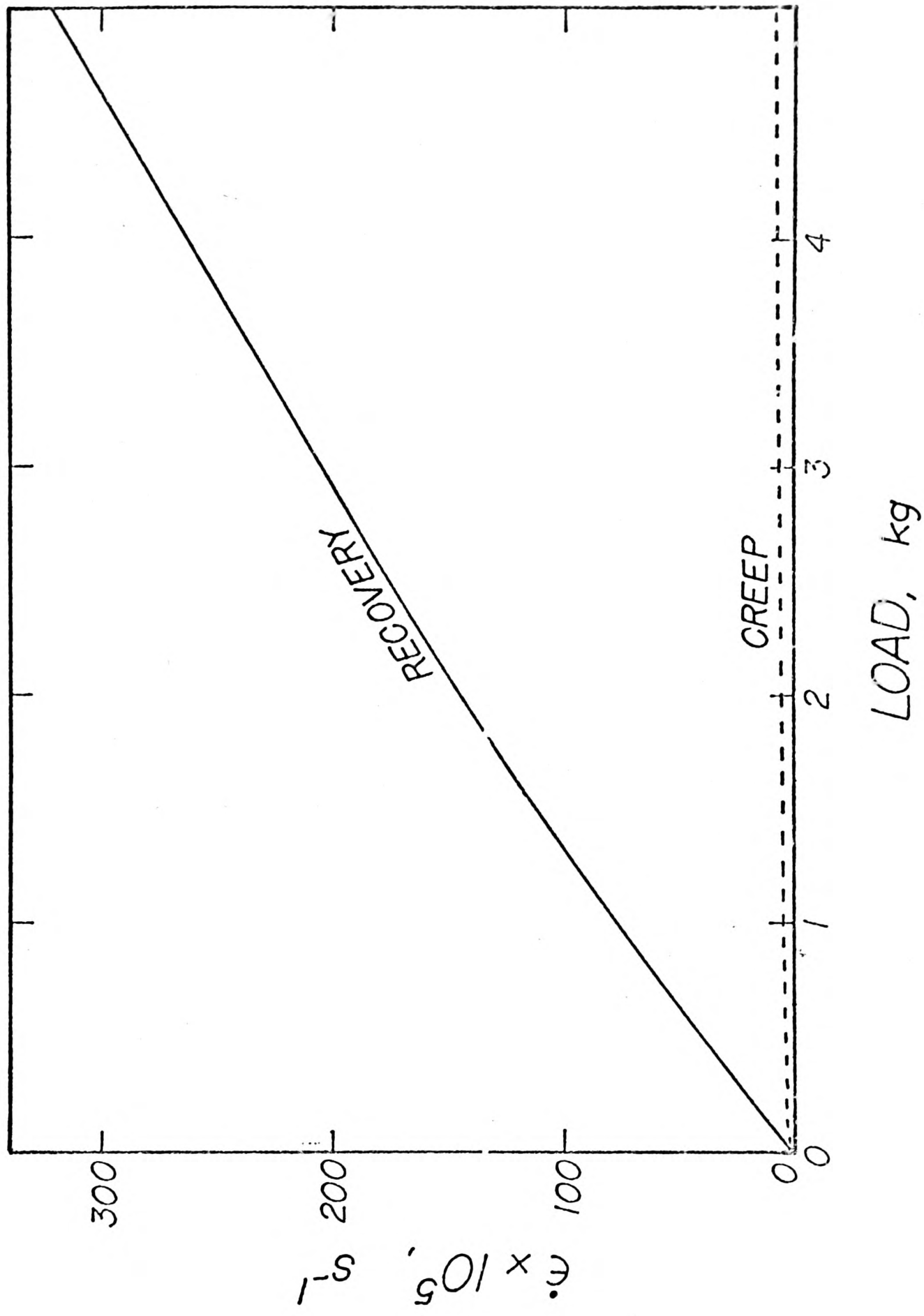


Figure 8-17

Dependence of theoretical recovery rate on load for data from specimen CH2-9-1(m77,Hfh), continuous line.

$\frac{b}{a}(\Delta J_G/\Delta D_F) = 800$, $\bar{\lambda} = 1.6$, $\theta_o = 14.5°$.

Also shown is the dashed line for the experimental creep rate.

Chapter 9

The Stress Relaxation Behaviour of Tendon

9.1 Introduction

Most of the experiments on tendon by various workers have been performed in stress relaxation[1-6]. Our purpose in carrying out stress relaxation experiments was to test the validity of the T-jump theory in this mode of deformation. The linear viscoelastic theory as outlined in chapter 4 predicts exactly similar behaviour in creep and stress relaxation for the case where the b_T terms of equations (4.38) and (4.42) are negligible. But if we cannot neglect those terms, the stress relaxation curves on a log rate-log time plot will be similar to those of figure 4-16 and the value of ΔH_a will be less than that in creep as shown in figure 4-17 for $\lambda = 0.005$.

9.2 Isothermal Behaviour

Typical stress relaxation curves with time for various strains are shown for specimen CH2-16-3(m71,Hfh) in figure 9-1 where the strain was applied for 60s and removed. The conditioning procedure as described for creep had already been carried out. Figure 9-1 shows clearly that for equal increments in strain, the load increments become larger. The values of load are plotted against log time in figure 9-2 and are seen to be approximately straight lines,as found for creep. The relaxation rate for these loads is calculated and plotted on a log (-load rate)-log time curve in figure 9-3. As was seen for creep, straight lines are found of slopes close to -1. The 20s isochronal load-strain curve for specimen CH2-5-1(m54,Heh), in the low strain region is shown in figure 9-4. The load-strain curve as expected shows a 'toe' region. The 20s load rate against strain curve is of a similar shape with a concave upwards region where the relaxation rate increases faster than that expected from the tangent to the curve to the

origin. For higher strains (figure 9-5, specimen CH2-16-3) the 'toe' for the 20s relaxation rate against strain curve changes into a 'linear' region as does the isochronal load-strain curve. Hence the two regions of behaviour are again displayed.

For specimen CH2-16-3(m71,Hfh), we applied a prestrain of 0.0496 which,as can be seen from figure 9-5, took it into the 'linear' region. Once mechanical equilibrium was achieved by observing no further decrease in load with time, we performed stress relaxation tests on this prestrained sample, the results of which are shown in figure 9-6. Both the 20s relaxation load and load rate against strain curves are straight lines(for the imposed strains of 0.295 and 0.58%) as found for creep. In this respect, the behaviour might be thought to be linear viscoelastic. However, non-linear viscoelastic behaviour of a similar nature to that observed in creep was seen when 2-step strain experiments were performed.

9.3 T-jumps in Stress Relaxation

We performed a series of T-jumps on a number of specimens at strains ranging from the 'toe' region through to the 'linear' region, as before for creep. For specimen CH2-5-1(m54,Heh) we used a strain of 3.44% which we have just seen to lie in the 'toe' region, (figure 9-4). The resulting log (-load relaxation rate) against log time curve gave values of the ratio of the load rates immediately before and after the time of the T-jump. The ln r- ΔT plot (where r is now the ratio of the load rates) is shown in figure 9-7. A straight line can be drawn through the points as predicted by equation (4.35) (without the b_T terms) and a value of $\Delta H_a = 12 \pm 1.0$ kcal/mol results, identical with that found for creep.

The dependence of ΔH_a with strain was also attempted as before for creep. For reasons of experimental expedience, it was not possible to

obtain the complete range of the ΔH_a dependence on strain on a single specimen. Thus we used two specimens; CH2-5-1(m54,Heh) in the low load region as above and CH2-16-3(m71,Hfh) at high loads. A sample of the relaxation load rate against time curve has already been shown for the specimen CH2-16-3 in figure 2-8. The values of ln r found from such curves are plotted against ΔT as shown in figures 9-8, 9-9 and 9-10 for various values of strains from the 'toe region upwards to the 'linear' region. All points were found to lie on straight lines and a least squares fit of each line gave the values of ΔH_a for each level of strain. Even though we could not obtain data in the lower end of the 'toe' region we still managed to obtain two values in the upper end of this region as shown in figure 9-8. The apparent activation energies were 13 ± 2 and 14 ± 2 kcal/mol respectively. Figure 9-9 shows a point in the transition region with $\Delta H_a = 26.5 \pm 1.0$ kcal/mol and figure 9-10 shows the results of T-jumps for two values of strain in the 'linear' region with $\Delta H_a = 30 \pm 3$ and 32 ± 3 kcal/mol respectively. Few values could be obtained for down temperature jumps due to low relaxation rates.

These results for ΔH_a are shown in figure 9-11 in the same format as used for creep, with the 20s load-strain curve on the left and the variation of ΔH_a with strain above and ΔH_a with 20s load on the right. The correlation of the change in ΔH_a with the transition from the 'toe' to the'linear' region is clear. The values obtained for ΔH_a in the 'toe' region and in the 'linear' region are identical with those found for creep.

One further series of T-jumps were performed on specimen CH2-5-2(m54,Heh) to gain confirmation of the previous results. This time only one T-jump was performed at each level of strain, from which ΔH_a at that load was obtained. The ΔH_a dependence on strain and load is shown for this material in figure 9-12. Exactly the same behaviour is observed as before.

Since the values found for ΔH_a in stress relaxation are exactly the same as for creep, this indicates that the process of deformation for stress relaxation is the same as that for creep in both the regions of deformation studied, i.e. the 'toe' and 'linear'. It also gives one more piece of evidence to support the assumption that the effect of b_T in equation (4.42) is negligible.

We also tried to fit the theory of the T-jump equations as described in chapter 4 (equations (4.41) and (4.42)) to the log rate-log time data as was done for creep. We chose data for the 'linear' region where one mechanism was predominant. Figures 9-13 and 9-14 show the log normalised load rate against log normalised time curves for the two values of ΔT = 2.05 and -2.1 °C respectively with the applied strain equal to 0.0496. The curves after t' were fitted with equation (4.42) (assuming the b_T terms could be neglected) and the values of ΔH_a and n which gave the best least squares fit of the data are shown in Table 9-2. For figure 9-13, the best fit line shown through the points is from equation (4.42) with ΔH_a=36 kcal/mol and slope n=1.17, and for figure 9-14, the best fit values are ΔH_a= 31 kcal/mol and n=1.23. These values agree well with those found experimentally as shown in Table 9-2. Hence once again the data can be fitted reasonably closely by the linear viscoelastic theory. This is again remarkable considering the nature of the material and once more gives us confidence in the use of T-jumps for this material.

9.4 Theoretical Model for Stress Relaxation.

It would be useful if we could apply the creep theory of the deformation process to describe the stress relaxation behaviour. For stress relaxation, and again taking the standard 3-parameter, single relaxation time model,[7] we obtain for the shear stress, Σ, on the gel

$$\dot{\Sigma}_G + \frac{\Delta G_G}{\eta_G} \Sigma_G = \gamma_o \frac{\Delta G_G}{\eta_G} G_{R_G} \qquad (9.1)$$

where γ_o is the shear strain of the gel, ΔG is the shear modulus difference $G_U - G_R$, where G_R and G_U are the relaxed and unrelaxed shear moduli, η_G is the shear viscosity and subscript G refers to the gel. This equation integrates to

$$\frac{\Sigma_G}{\gamma_o} = G_{R_G} + \Delta G_G \exp(-\frac{t}{\tau_G}) \qquad (9.2)$$

where $\tau_G = \eta_G / \Delta G_G$ and differentiating

$$\frac{\dot{\Sigma}_G}{\gamma_o} = -\frac{\Delta G_G}{\tau_G} \exp(-\frac{t}{\tau_G}) \qquad (9.3)$$

which for a distribution of relaxation times is

$$\frac{\dot{\Sigma}_G}{\gamma_o} = -\Delta G_G(\tau_G=1) \frac{\Gamma(n_G)}{(t)^{n_G}} \qquad (9.4)$$

where $-n_G$ is the slope of the log relaxation rate-log time curve of the gel (and $1-n_G=m_G$ where m_G is given by the equation $\ln H_G(\ln \tau_G) = m_G \ln \tau_G +$ ln constant, and $H(\ln \tau)$ is the relaxation spectrum). Now, γ_o, the shear strain is given by [8]

$$\gamma_o = \epsilon_o \sin\theta \cos\theta \qquad (9.5)$$

which can be substituted in equation (9.4), but it is not clear how Σ_G is related to the relaxation stress, σ, in the tensile direction. If this were known, then we could model as before.

The contribution from the fibres will be of a similar form to equation (9.3) and is

$$\left(\frac{\dot{\sigma}_F}{\epsilon_o - \epsilon'}\right) = H(\epsilon_o - \epsilon')\left(-\frac{\Delta E_F}{\tau_F}\right) \exp\left(-\frac{t}{\tau_F}\right) \qquad (9.6)$$

where ϵ_o is the applied strain, ϵ' is the strain when the fibres are straight, $-n_F$ is the slope of the log rate-log time curve of the fibre, H is the Heaviside unit step function. For a distribution of relaxation times, this equation becomes

$$\frac{\dot{\sigma}_F}{(\epsilon_o - \epsilon')} = -H(\epsilon_o - \epsilon')\ \Delta E_F(\tau_F=1)\ \frac{\Gamma(n_F)}{(t)^{n_F}} \qquad (9.7)$$

Until the fibres straighten, the gel mechanism will be the major viscoelastic mechanism as before for creep, after which the relaxation of the fibres will be the dominant mechanism.

Since we do not know the exact form of the equation for the relaxation rate of the gel, we have come across a stumbling block. It may be possible to proceed as follows. In the 'toe' region for creep, the relation for the gel was given by equation (7.28)

$$\dot{\epsilon}_G = \sigma_o\ f(\theta)\ \Delta J_G(\tau_G=1)\ \frac{\Gamma(n_G)}{(t)^{n_G}} \qquad (7.28)$$

By assuming that the $f(\theta)$ term stays with the stress term, we obtain for the case of the stress relaxation of the gel

$$f(\theta)\,\dot{\sigma}_G = -\epsilon_o\ \Delta G_G(\tau_G=1)\ \frac{\Gamma(n_G)}{(t)^{n_G}} \qquad (9.8)$$

Plotting $\frac{\epsilon_o}{\dot{\sigma}_G}$ against $(1+\epsilon_o)$ for the various values of ϵ_o will give the value of θ_o from the intercept on the $(1+\epsilon_o)$ axis for $\epsilon_o/\dot{\sigma}_G = 0$. This was done for specimen CH2-5-1 for data in the 'toe' region as shown in figure 9-15 and a value of $\theta_o = 14.5^\circ$ was found. This is the same order of magnitude as found before for creep.

The shape of equation (9.8) for the isochronal load rate against strain curve is shown in figure 9-16 for two values of $\theta_o = 14.5^\circ$ and 16° and

with $\frac{a}{b}\ \frac{\Delta G_G\ \Gamma(n_G)}{(t)^{n_G}} = 1$. It can be seen that the shape of the stress rate against strain curve is similar to that found experimentally as seen in figures 9-4 and 9-5 in the 'toe' region and fits exactly the first part of the curve of figure 9-4 up to a strain of 2.5%. The problem here is that the theoretical relaxation rate of equation (9.8) increases asymptotically to infinity as θ approaches zero. The shear strain on the gel will, however, be approaching zero and from equation (9.4) the rate will go to zero as $\theta \to 0$. The equation (9.8) above is not valid for values of θ close to zero and it has dubious validity for the rest of the curve, but it will serve to illustrate how a concave upward curve combined with a linear curve will produce the sort of curve observed experimentally if we again introduce a distribution of crimp angles. The combination of the two curves of figure 9-17, i.e. the curve concave upwards given by equation (9.8) for $\theta > 5$ and the straight line of equation (9.7) gives

$$\dot{\sigma} = -\frac{\Delta G_G}{f(\theta)}\frac{\Gamma(n_G)}{(t)^{n_G}}\epsilon_o - H(\epsilon_o - \epsilon')\,\Delta E_F\frac{\Gamma(n_F)}{(t)^{n_F}}(\epsilon_o - \epsilon') \qquad (9.9)$$

Using a Gaussian distribution of the initial crimp angle, θ_o, as before for creep, we can obtain the shape of the curve as shown in figure 9-18 which is similar to that observed for specimen CH2-16-3 (see figure 9-5). If the exact equation for the rate as a function of strain in the 'toe' region was known, then we could fit the experimental curves in a similar manner as for creep and also predict the transition from one mechanism to another in the T-jump equations.

9.5 The Stress-Strain Curve of Tendon

As a final note on this modelling we can obtain the form of the observed stress-strain curve of tendon by using an equation which gives a concave upward curve with increasing strain as the crimp straightens out,

(curve (i) of figure 9-19) along with a straight line for the fibre deformation (curve (ii) of figure 9-19) which adds in once the crimps are straight, and again using the distribution of crimp angles. For want of an exact form for the concave upward curve that is easy to handle, we used a function similar to that used before in figure 9-17, for the curved part of the stress-strain curve, namely

$$\frac{\sigma}{\epsilon} = C_1 \left(\frac{\cos\theta_o}{\sin^2\theta \cos\theta} \right) = \frac{C_1}{(1+\epsilon)\left\{1-\cos^2\theta_o(1+\epsilon)^2\right\}} \qquad (9.10)$$

In this equation, only values of $\theta > 5^\circ$ were used. For $\theta < 5^\circ$, the value remained constant at the final value for $\theta = 5^\circ$ (figure 9-19(i)). At $\theta = 5^\circ$, the straight line of figure 9-19(ii) begins. The equation used was thus

$$\sigma = C_1 \frac{\epsilon}{(1+\epsilon)\left\{1-\cos^2\theta_o(1+\epsilon)^2\right\}} + H(\epsilon-\epsilon')\, C_2\, (\epsilon-\epsilon') \qquad (9.11)$$

A Gaussian distribution of initial crimp angles was again used, with $\theta_o = 16^\circ$ and various values were chosen for C_1/C_2. The result is as shown in figure 9-20, where σ/C_1 is plotted against strain. The curved section at the low strains merges smoothly into the linear section which was also seen in the experimental curves. Although the equation used for the curved portion is not the one which will be found experimentally, it serves to illustrate three points:

(i) in order to have a smooth transition from the 'toe' region to the 'linear' region, a distribution of initial crimp angles is necessary. This means that at all points along the curve, there will be a combination of the two types of behaviour, crimp straightening and fibre extension.

(ii) the fibres do not take the stress until a certain strain is reached, otherwise the straight line portion of figure 9-20 would pass through

the origin of the load-strain curve.

(iii) the value of the modulus of the fibre is important in determining the stress-strain curve. If it is too low, the deformation of the type shown in figure 9-20 for $C_1/C_2 = 0.05$ will occur, which indicates an unacceptable tendon.

9.6 Discussion

A summary of the T-jump data is found in Table 9-1 and a transition from a value of ΔH_a=12 kcal/mol to 33 kcal/mol can be seen as the strain increases from the 'toe' region to the 'linear' region. From these results, it has been seen that the values for ΔH_a found from stress relaxation are identical with those in creep. This gives support for our main purpose in performing the experiment, namely that the linear viscoelastic T-jump equations apply equally well for both creep and stress relaxation and that for tendon the b_T terms in these equations are negligible. The stress relaxation experiment is,however, less satisfactory even though the use of the Instron tensile tester is widespread, because of the difficulty in obtaining thermal expansion measurements. The method by which this is done was described in chapter 2, but it is a more difficult procedure than in creep since, for tendon, the thermal expansion will cause a different decrease in the observed load level for each level of strain for a given ΔT.

We have also obtained the values for the stress relaxation rate as a function of strain showing a curved region followed by a linear region similar to the load-strain curve. Once the theoretical relationship for the curved portion can be obtained, the data can be fitted for the various parameters as was done for the case of creep in chapter 8.

The modelling of the stress-strain curve also indicates the importance of both the distribution of crimp angles and the modulus of the

collagen fibres in determining the mechanical behaviour of the tendon. It is clear that if the modulus of the collagen fibres is lowered as a result of disease, for instance, then this can drastically alter the shape of the stress-strain curve and will show itself in the manner seen in figure 9-20.

References

1 Rigby B.J., Hirai N., Spikes J.D. and Eyring H., J. Gen.Physiol., 43,265,1959.

2 Rigby B.J., Nature, 202,1072,1964.

3 Abrahams M., Med.Biol.Eng.,5,443,1967.

4 Van Brocklin J.D. and Ellis D.G., Arch.Phys.Med.,46,369,1965.

5 Baer E. and Coworkers, Proc.Roy.Soc., London,B180,293,1972.
" Colston Papers, Structure of Fibrous Biopolymers, (ed. Atkins E.D.T. and Keller A.) vol 26, 1975. Butterworths, London.

6 Viidik A., Int.Rev. Conn.Tiss.Res.,6,127,1973.

7 Ward I.M., 'Mechanical Properties of Solid Polymers', Wiley, London, 1971.

8 Case J. and Chilver A.H., 'Strength of Materials', Arnold, London, 1959.

Table 9-1 Summary of the Instron T-jump Data

Specimen	Region	Strain (%)	20s Load (kg)	ΔH_a kcal/mol	Figure
CH2-5-1	toe	3.44	0.433	12	9-7
CH2-16-3	toe	3.72	0.37	13	9-8(a)
	toe	4.03	0.80	14	9-8(b)
	transition	4.34	1.59	26.5	9-9
	linear	4.96	3.27	30	9-10(a)
	linear	5.58	5.88	32	9-10(b)
CH2-5-2	toe	<2.6	<0.6	16	9-12
	linear	>3.5	>2.0	33	9-12

Table 9-2 Comparison of Values of ΔH_a and n found from (i) Experimental Rate Data and (ii) from Fitting of the Log Rate-Log Time Curve by Equation (4.42).

Specimen	Region	Strain (%)	20s Load (kg)	$-\dot{\sigma}_{T_o}(t')$ (gm/s)	ΔT °C	(i) Experimental ΔH_a kcal/mol	(i) Experimental n	(ii) Theoretical ΔH_a kcal/mol	(ii) Theoretical n
CH2-16-3	linear	4.96	3.27	1.85	2.05	36	1.10	36	1.17
"	linear	4.96	3.30	2.05	-2.25	32	1.10	31	1.23

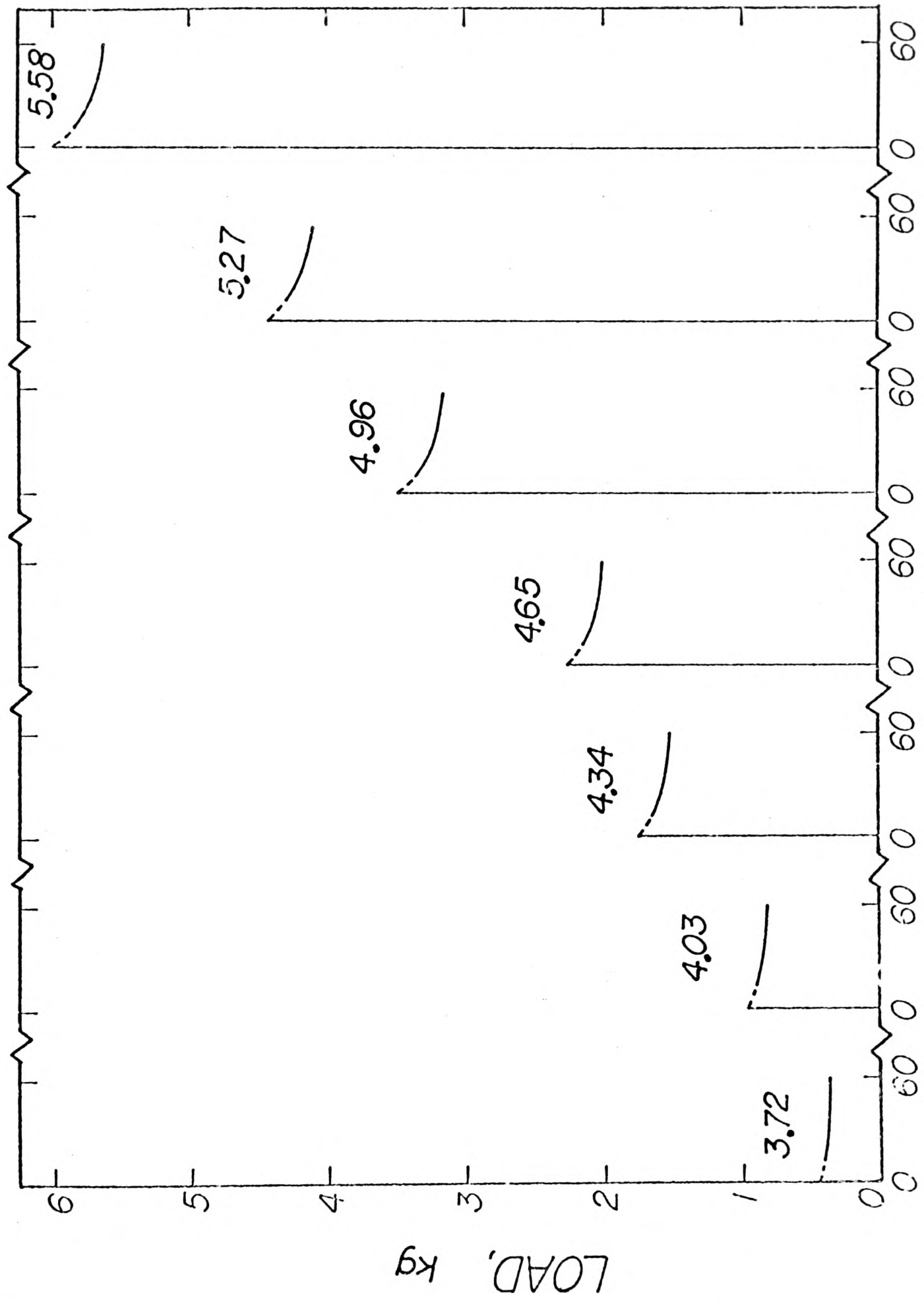


Figure 9-1

Dependence of load on time for various values of strain, ϵ_o = 0.0372, 0.0403, 0.0434, 0.0465, 0.0496, 0.0527, 0.0558. Specimen CH2-16-3 (m71,Hfh), T_o = 28 °C.

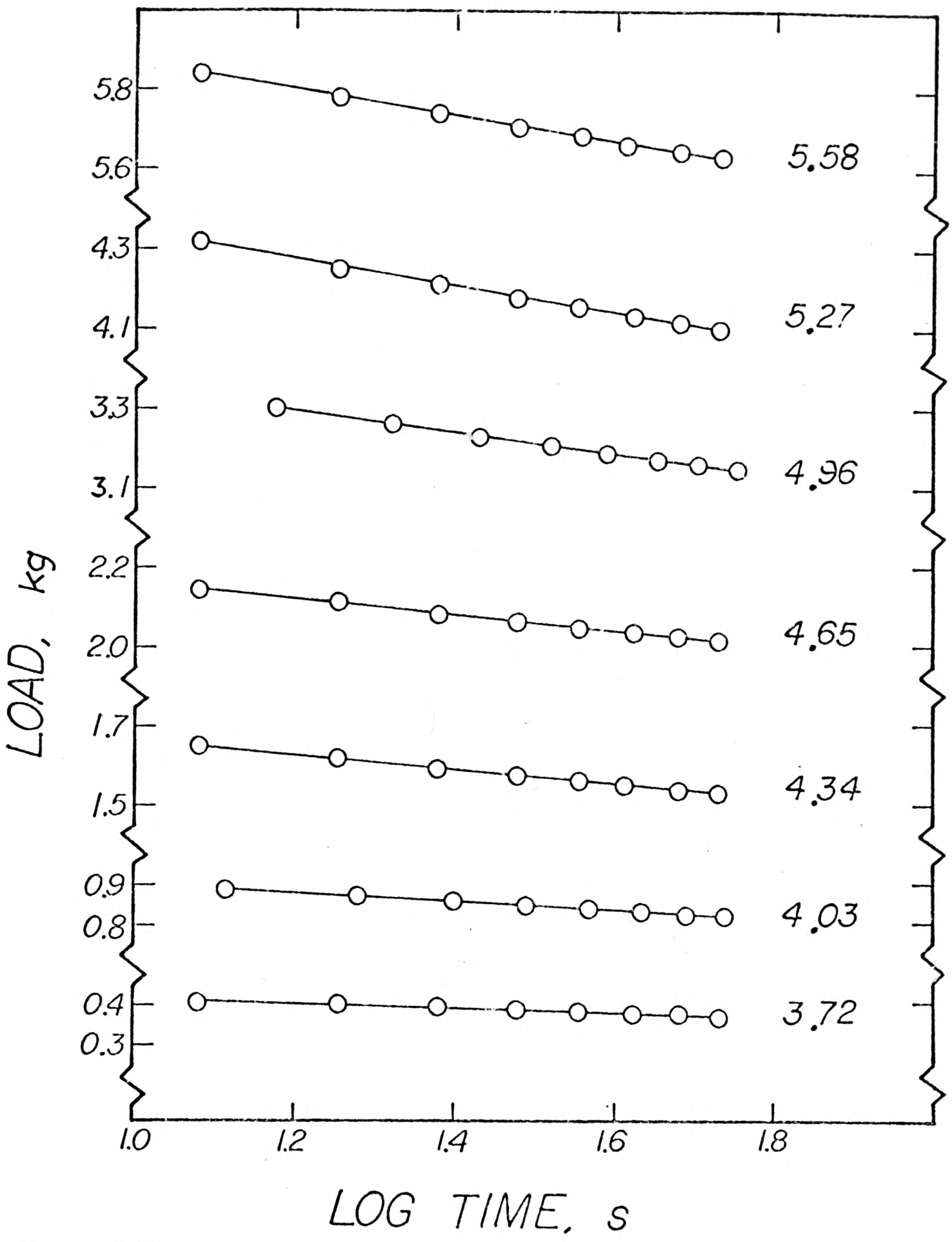


Figure 9-2

Dependence of load on log time for various values of strain for the same experiments as in figure 9-1, Specimen CH2-16-3(m71,Hfh), T_o = 28 °C. Strains are in %.

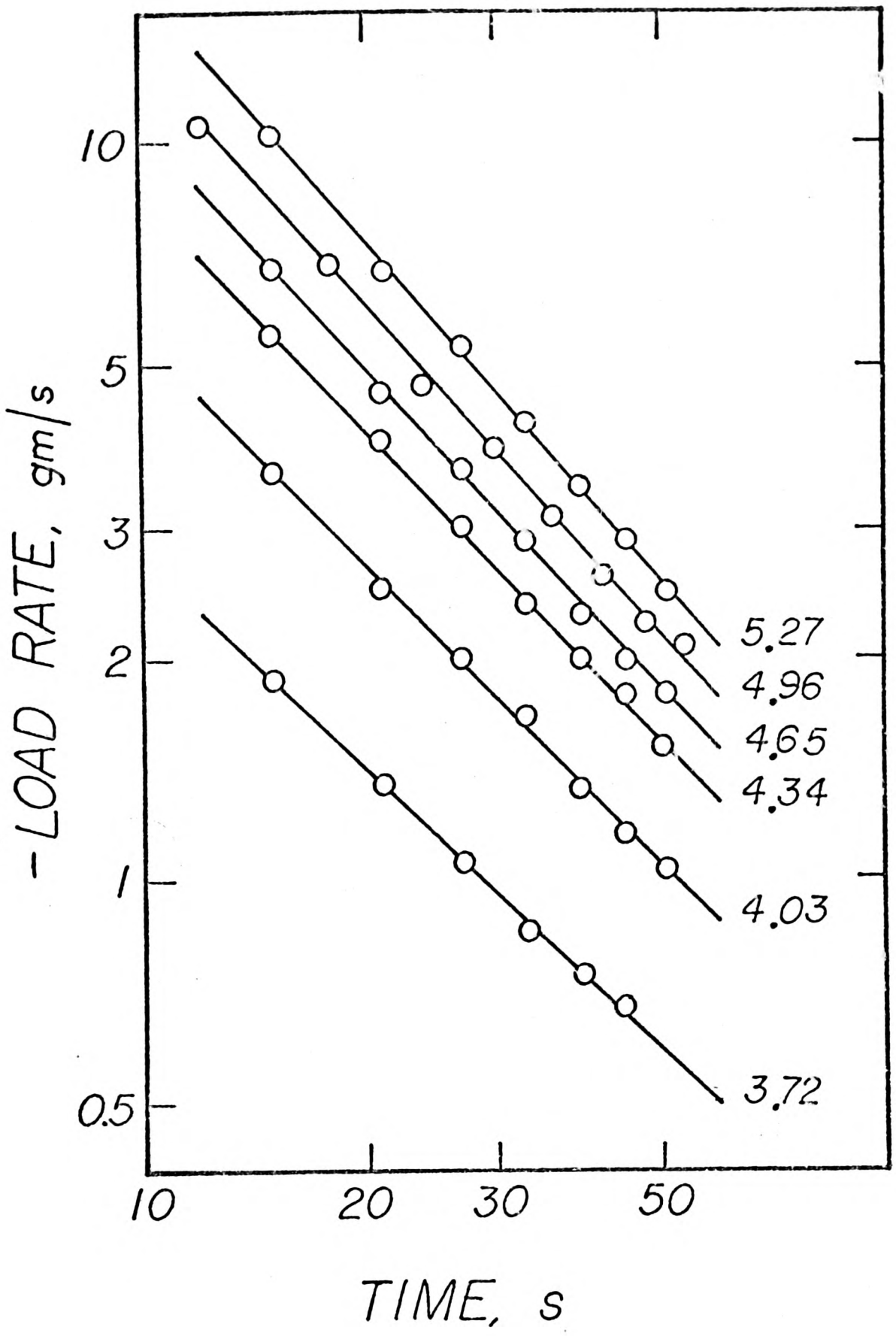


Figure 9-3

Dependence of log (-load relaxation rate) on log time for specimen CH2-16-3(m71,Hfh) for the same values of strain as in figure 9-1. T_o = 28 °C. Strains are in %.

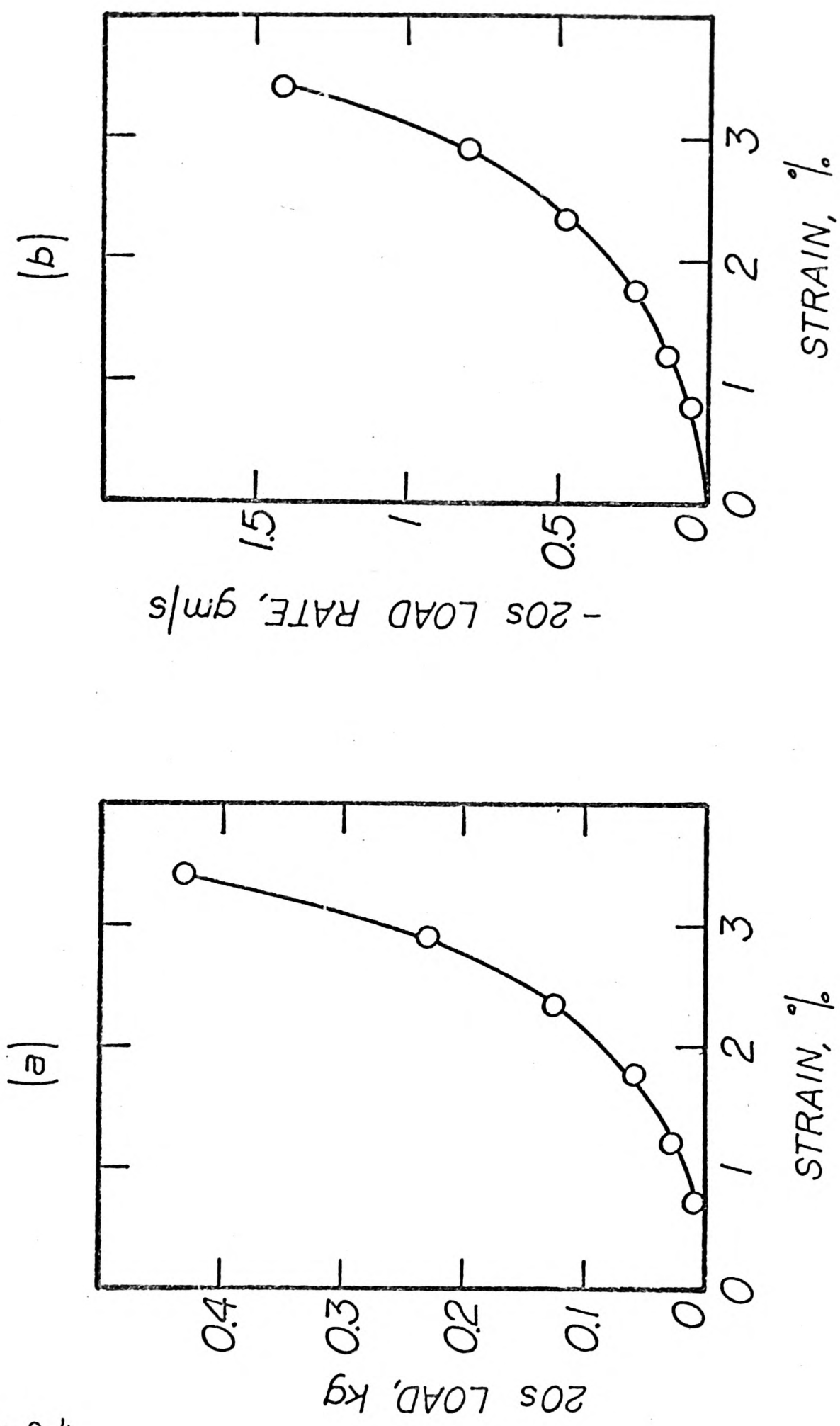


Figure 9-4

Dependence of a) 20s load on strain and
b) 20s load rate on strain
for specimen CH2-5-1(m54,Heh), T_o = 28°C.

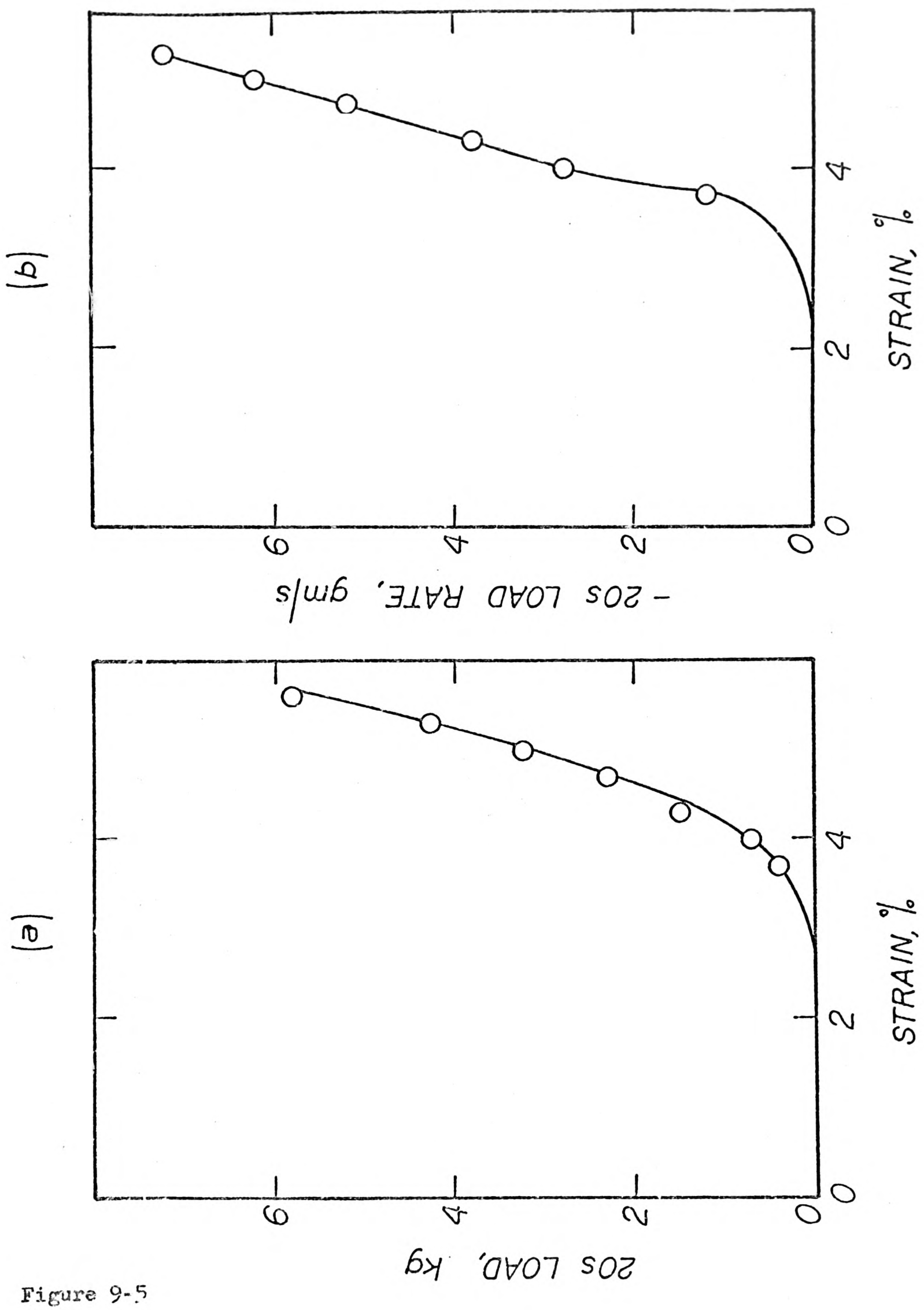


Figure 9-5

Dependence of a) 20s load on strain and
b) 20s load rate on strain
for specimen CH2-16-3(m71,hfh), T_o = 28 °C.

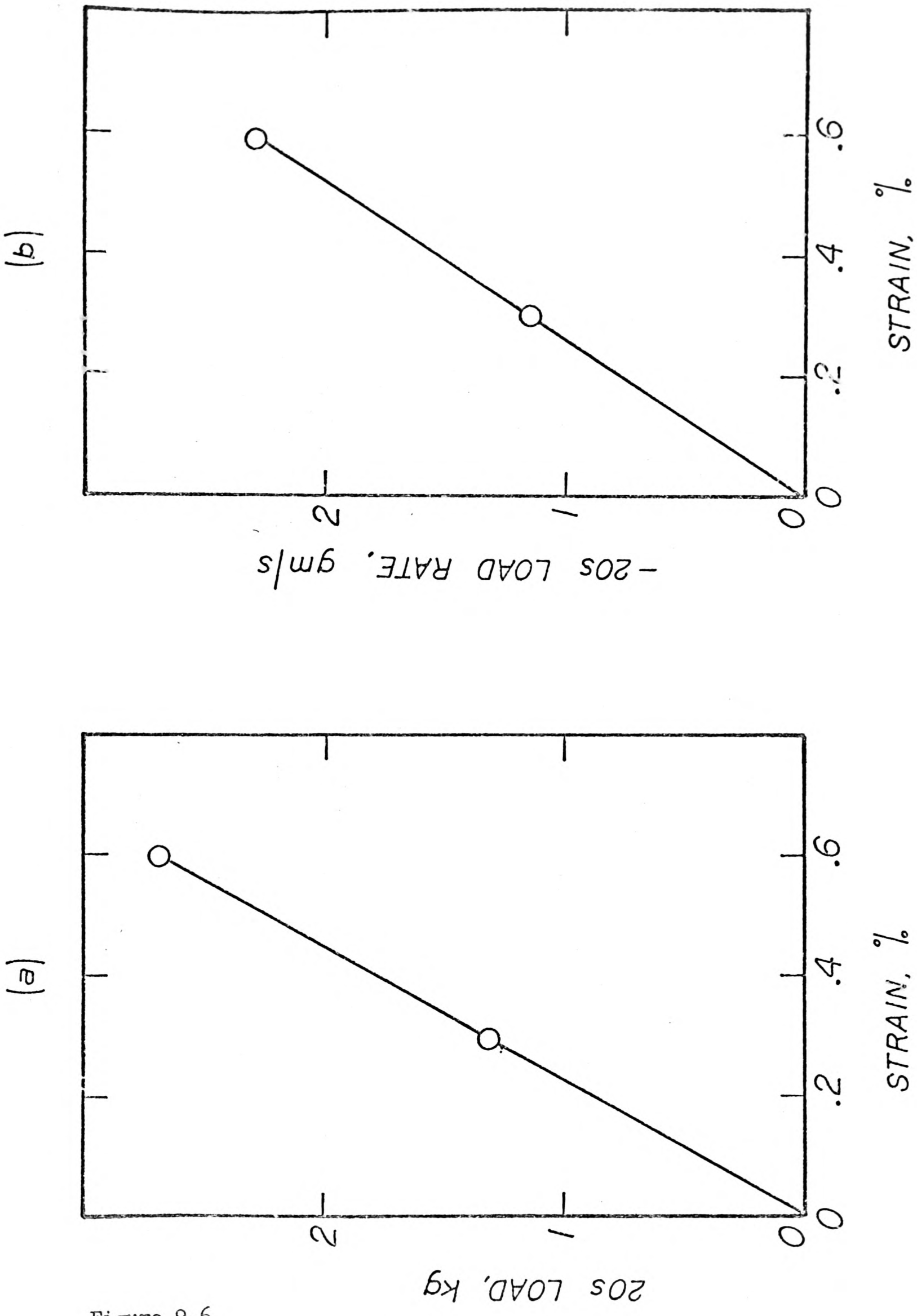


Figure 9-6

Dependence of a) 20s load on strain
b) 20s load rate on strain
for specimen CH2-16-3(m71,Hfh) prestrained to 0.0496, T_o = 28 °C.

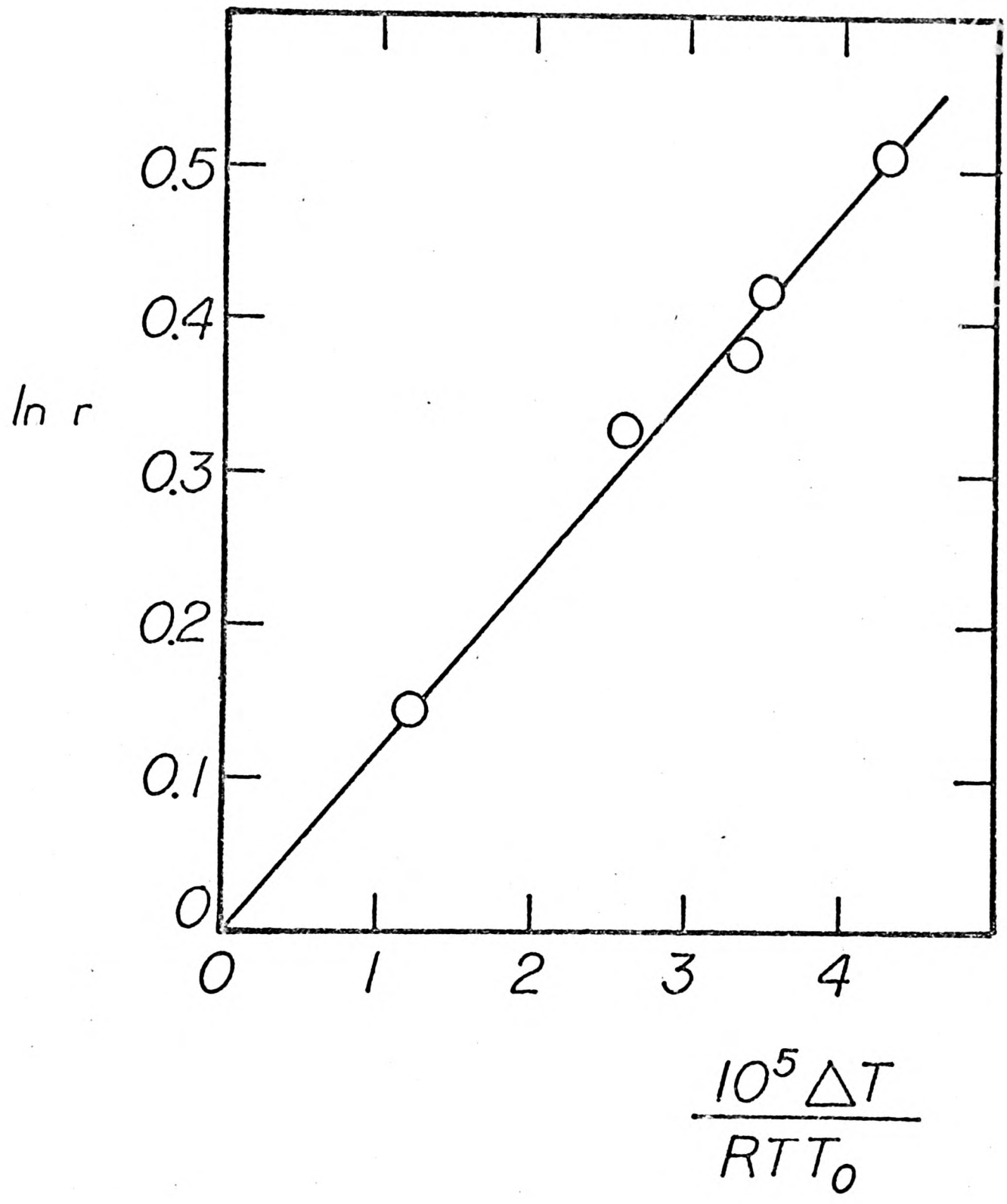
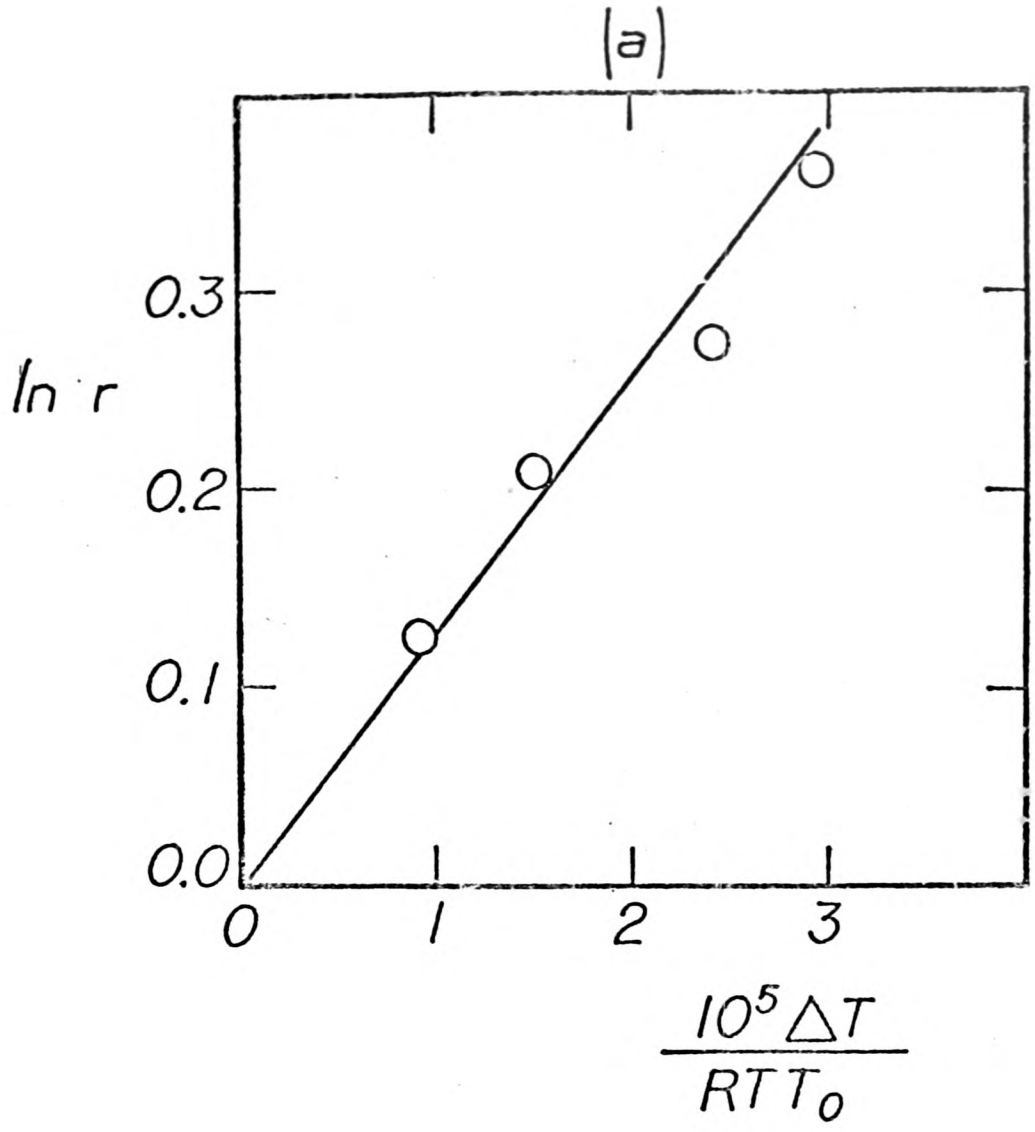


Figure 9-7

Plot of ln r against $\Delta T/RTT_o$ for specimen CH2-5-1(m54,Heh), ϵ_o = 3.44%, σ_{20} = 0.433 kg. The best fit straight line through the points gives ΔH_a = 12 kcal/mol.



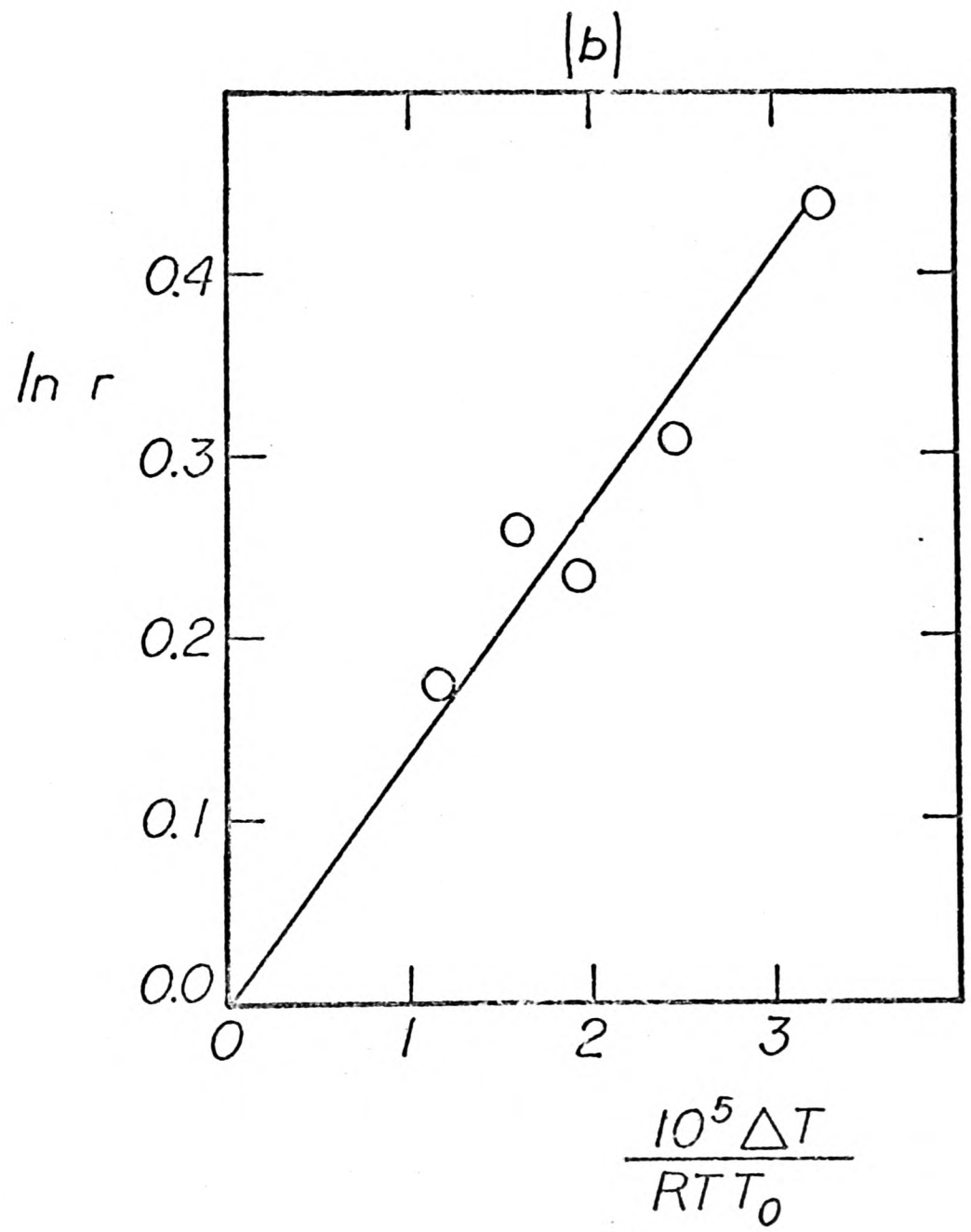


Figure 9-8

ln r- ΔT plot for specimen CH2-16-3(m71,Rfh)
a) σ_{20} = 0.37 kg; ϵ_o = 0.0372; ΔH_a = 13 kcal/mol.
b) σ_{20} = 0.80 kg; ϵ_o = 0.0403; ΔH_a = 14 kcal/mol.

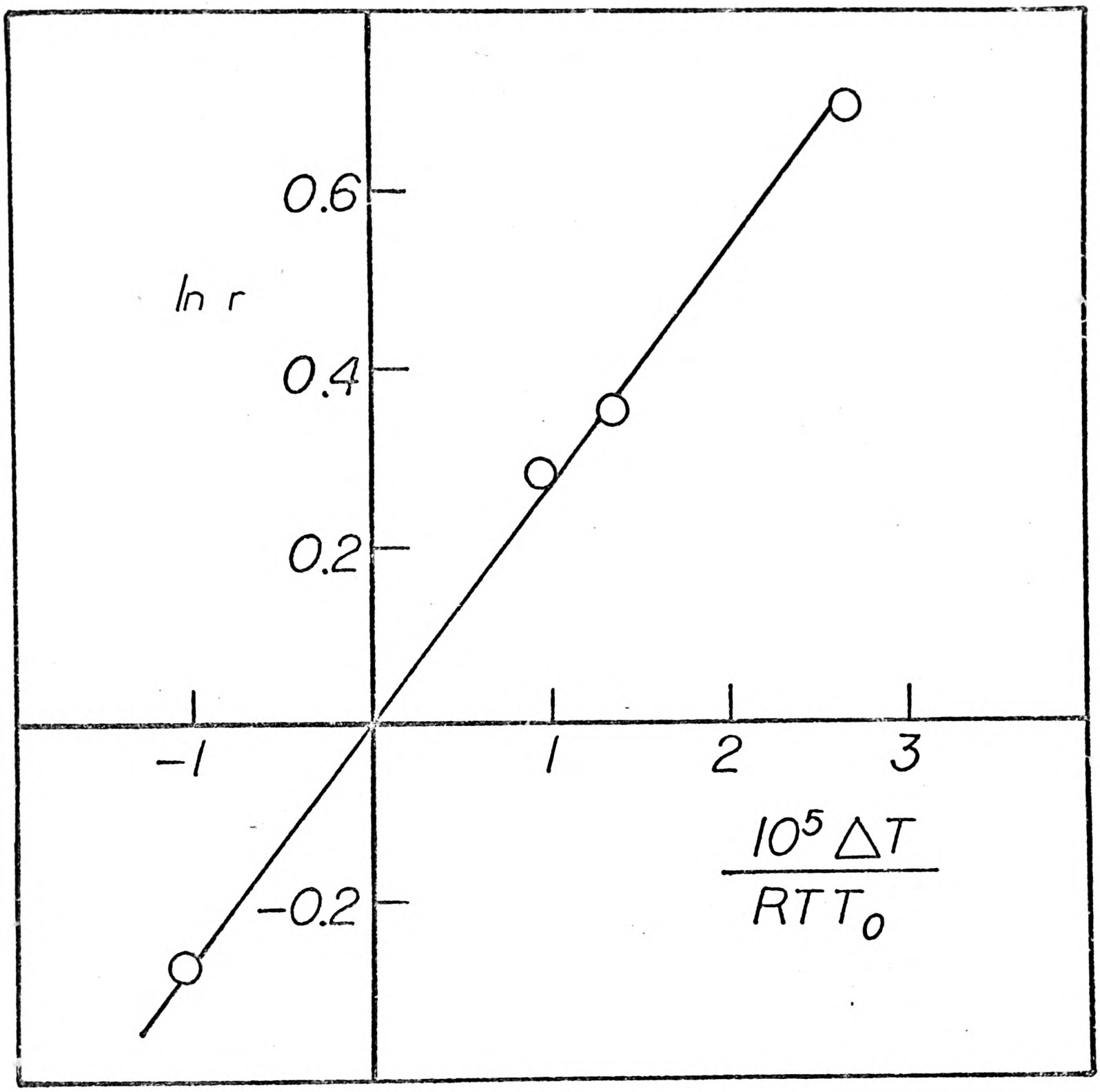
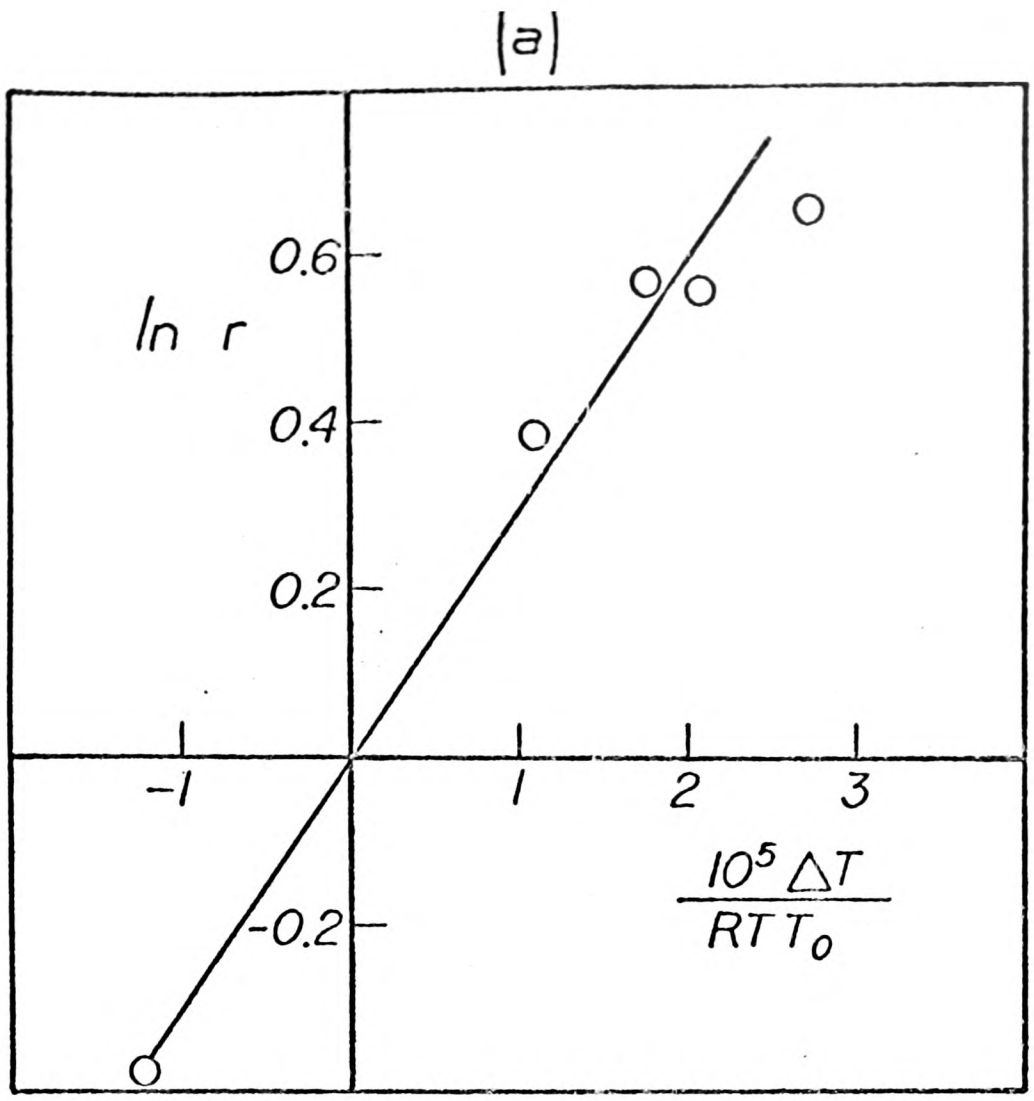


Figure 9-9

ln r- ΔT plot for specimen CH2-16-3(m71,Hfh)

σ_{20} = 1.59 kg; ϵ_o = 0.0434; ΔH_a = 26.5 kcal/mol.



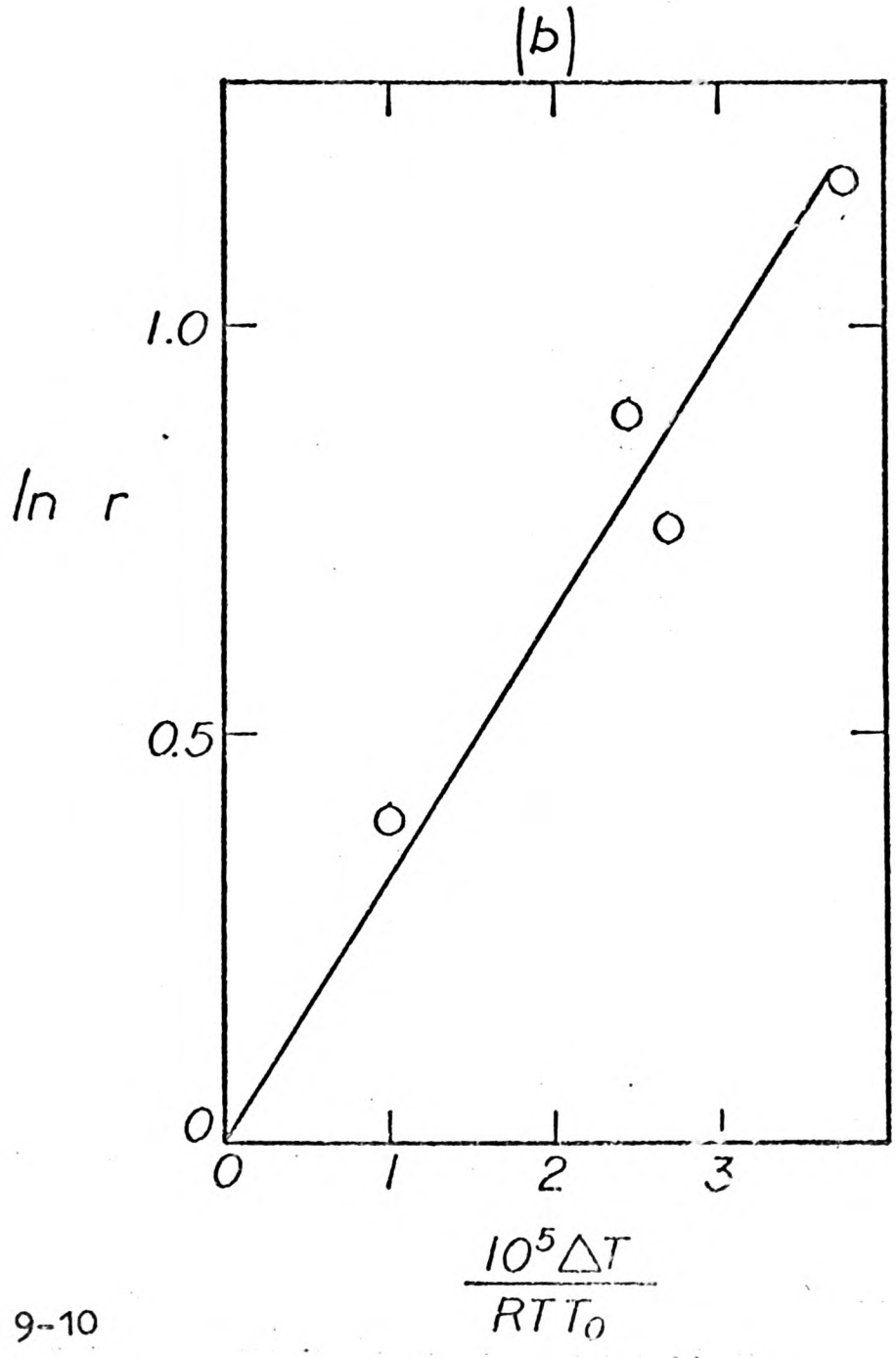
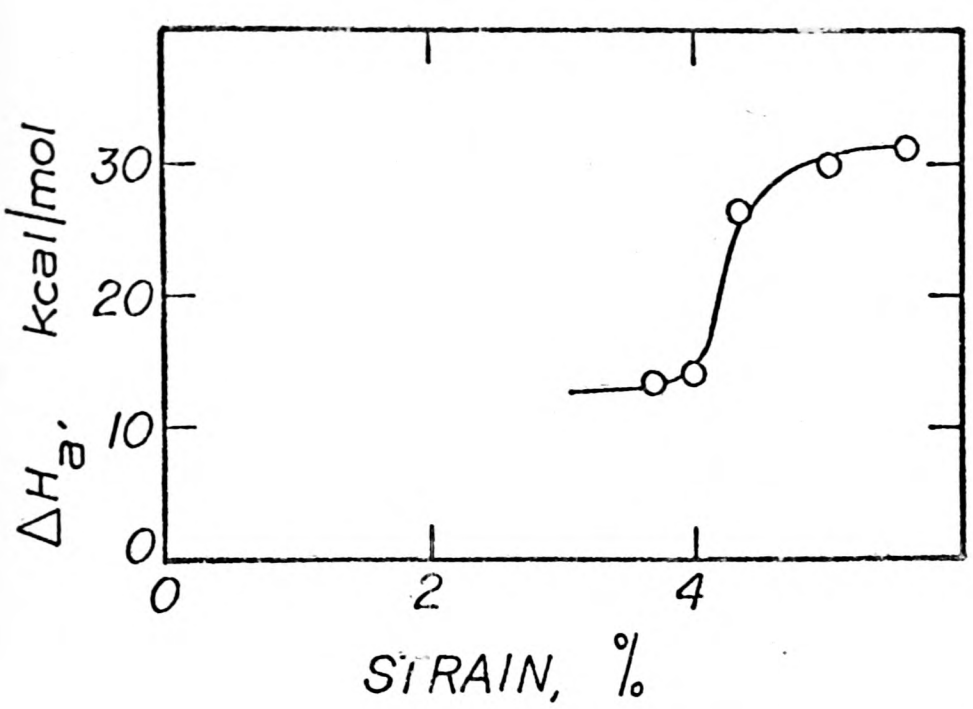
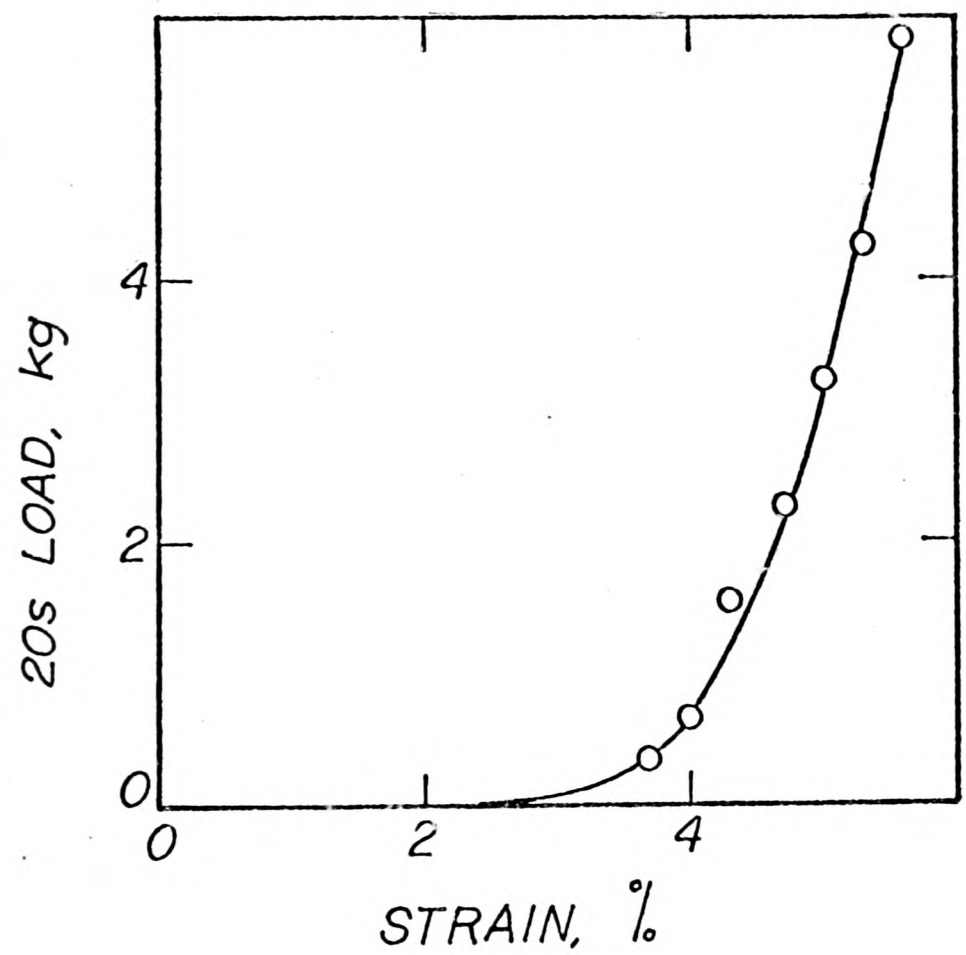


Figure 9-10

ln r- ΔT plot for specimen CH2-16-3(m71,Hfh)
a) σ_{20} = 3.26 kg; ϵ_o = 0.0496; ΔH_a = 30 kcal/mol.
b) σ_{20} = 5.88 kg; ϵ_o = 0.0558; ΔH_a = 32 kcal/mol.





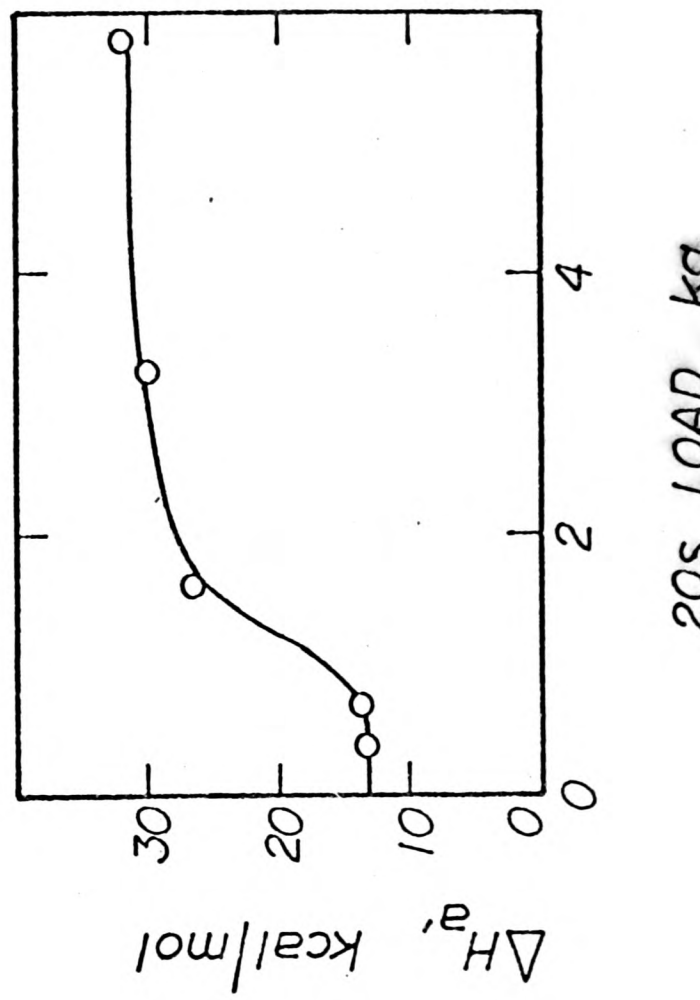


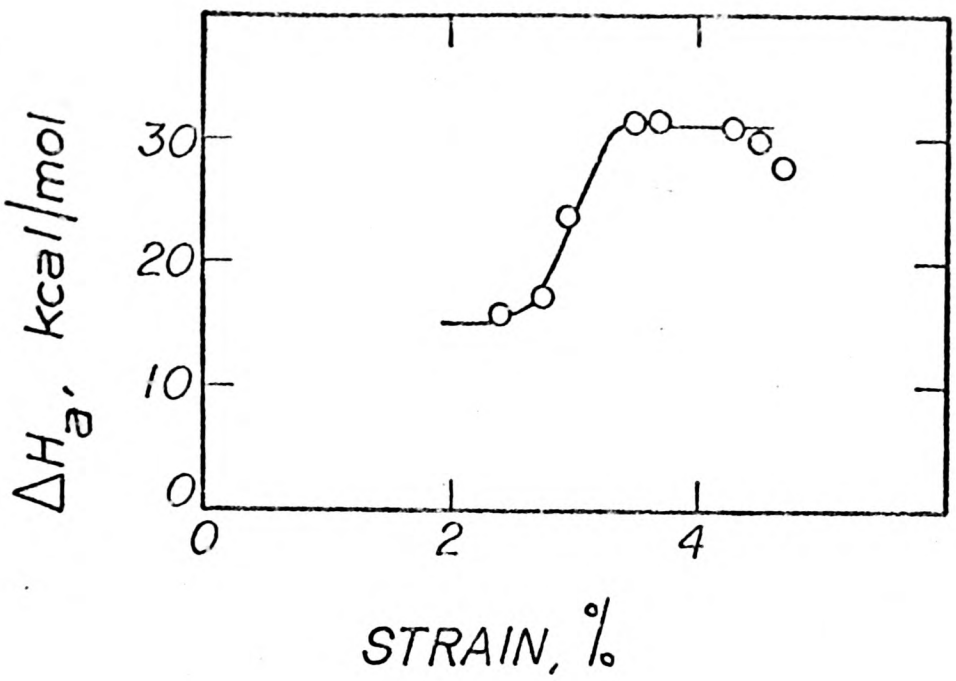
Figure 9-11

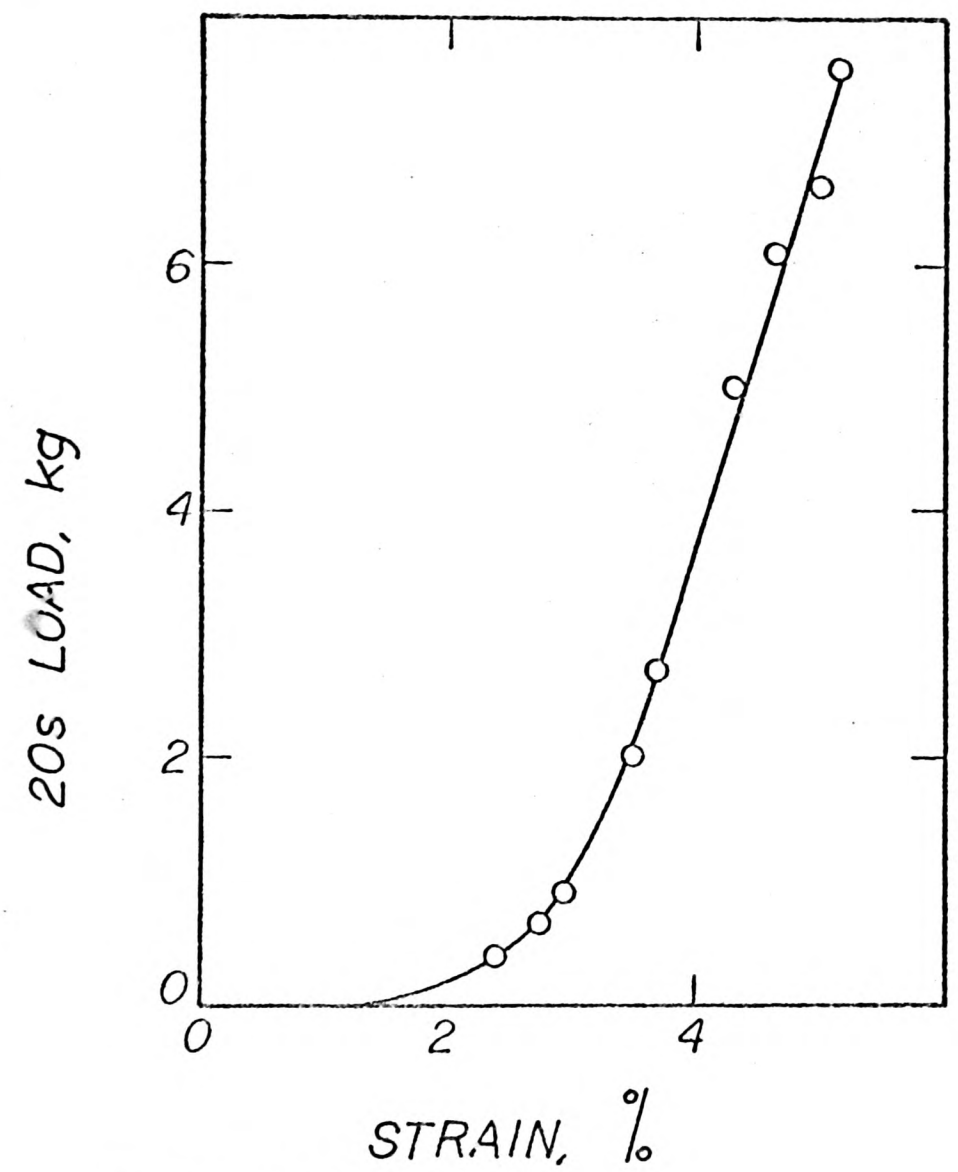
Bottom left: 20s isochronal load-strain curve.

Right : dependence of ΔH_a on 20s load.

Top : dependence of ΔH_a on strain.

Specimen CH2-16-3(m71,Nfh)





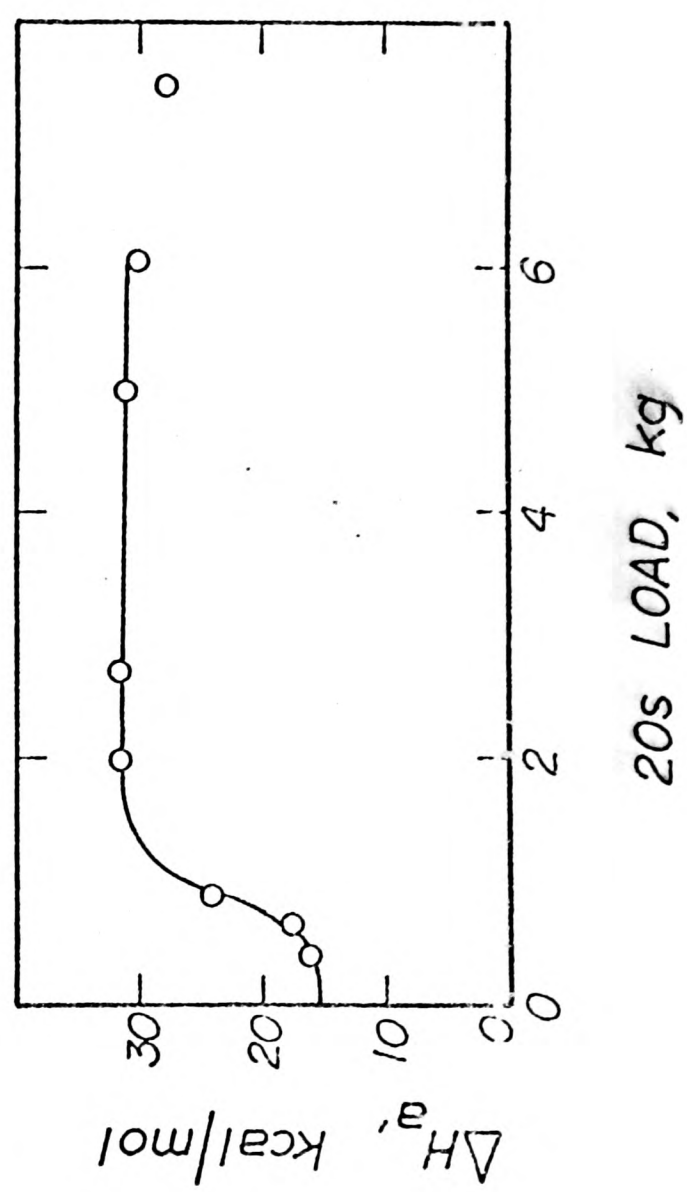


Figure 9-12

Bottom left: 20s isochronal load-strain curve.

Right : dependence of ΔH_a on 20s load

Top : dependence of ΔH_a on strain

Specimen CH2-5-2(m54,Heh)

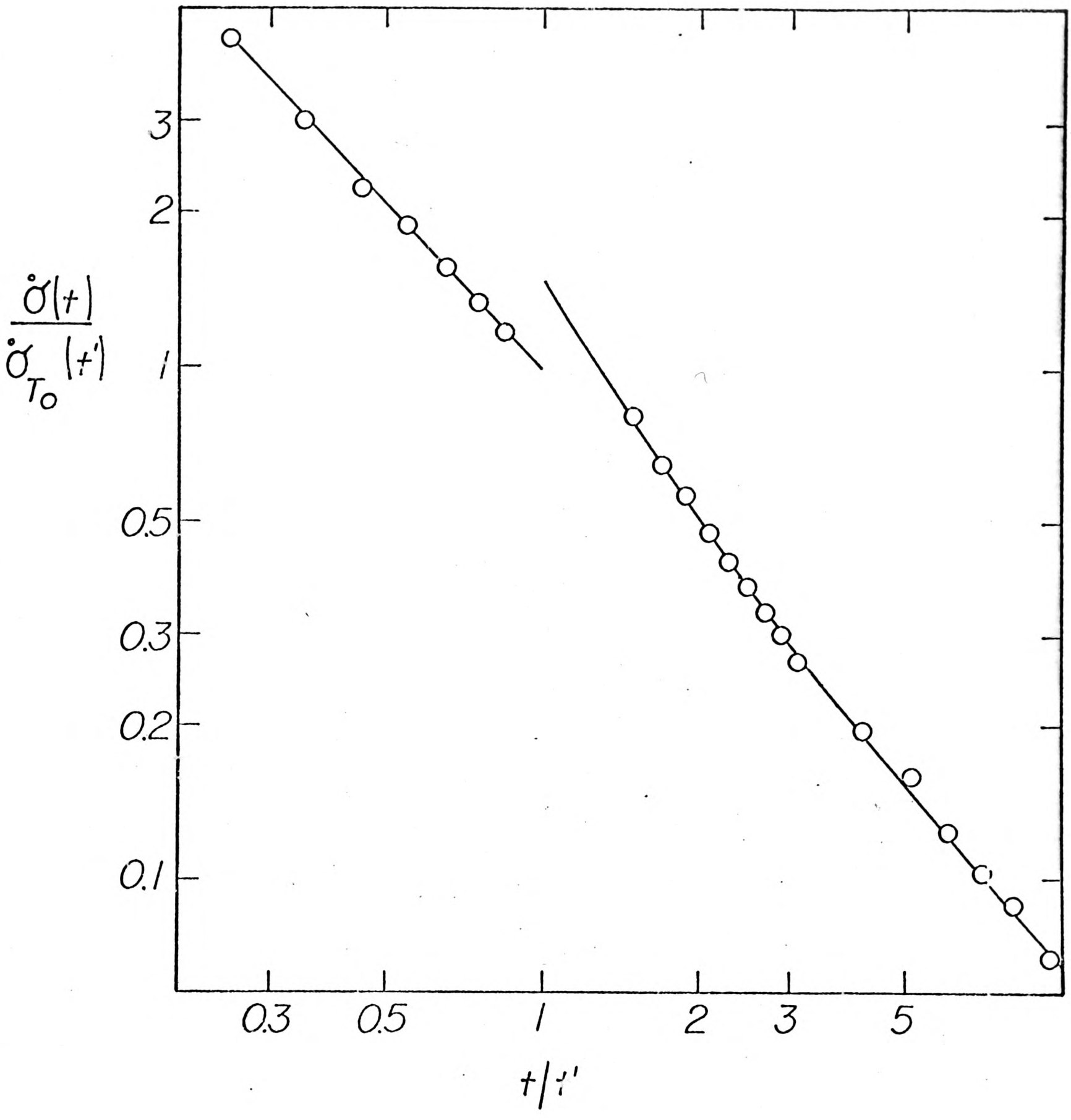


Figure 9-13

Dependence of log (normalised load relaxation rate, $\dot{\sigma}(t)/\dot{\sigma}_{T_o}(t')$) on log (normalised time, t/t') for specimen CH2-16-3(m71,Hfh).
strain = 0.0496, ΔT = 2.05 °C
Theoretical line through the experimental points calculated from equation (4.42) with ΔH_a = 36 kcal/mol and n = 1.17.

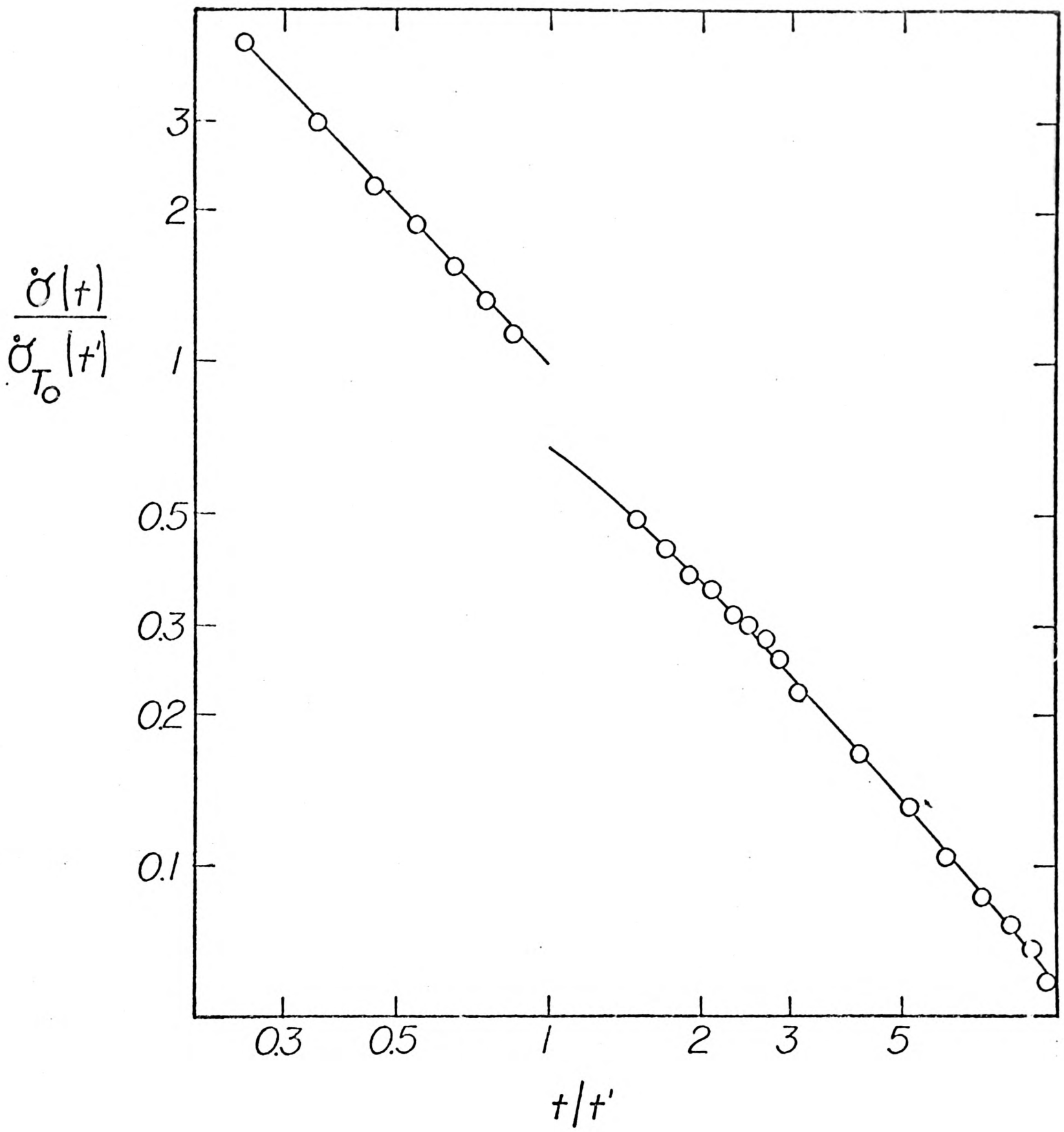


Figure 9-14

Dependence of log (normalised load relaxation rate, $\dot{\sigma}(t)/\dot{\sigma}_{T_o}(t')$) on log (normalised time, t/t')
for specimen CH2-16-3(m71,Hfh).
strain = 0.0496, ΔT = -2.25°C.
Theoretical line through the experimental points calculated from equation (4.42) with ΔH_a = 31 kcal/mol and n = 1.23.

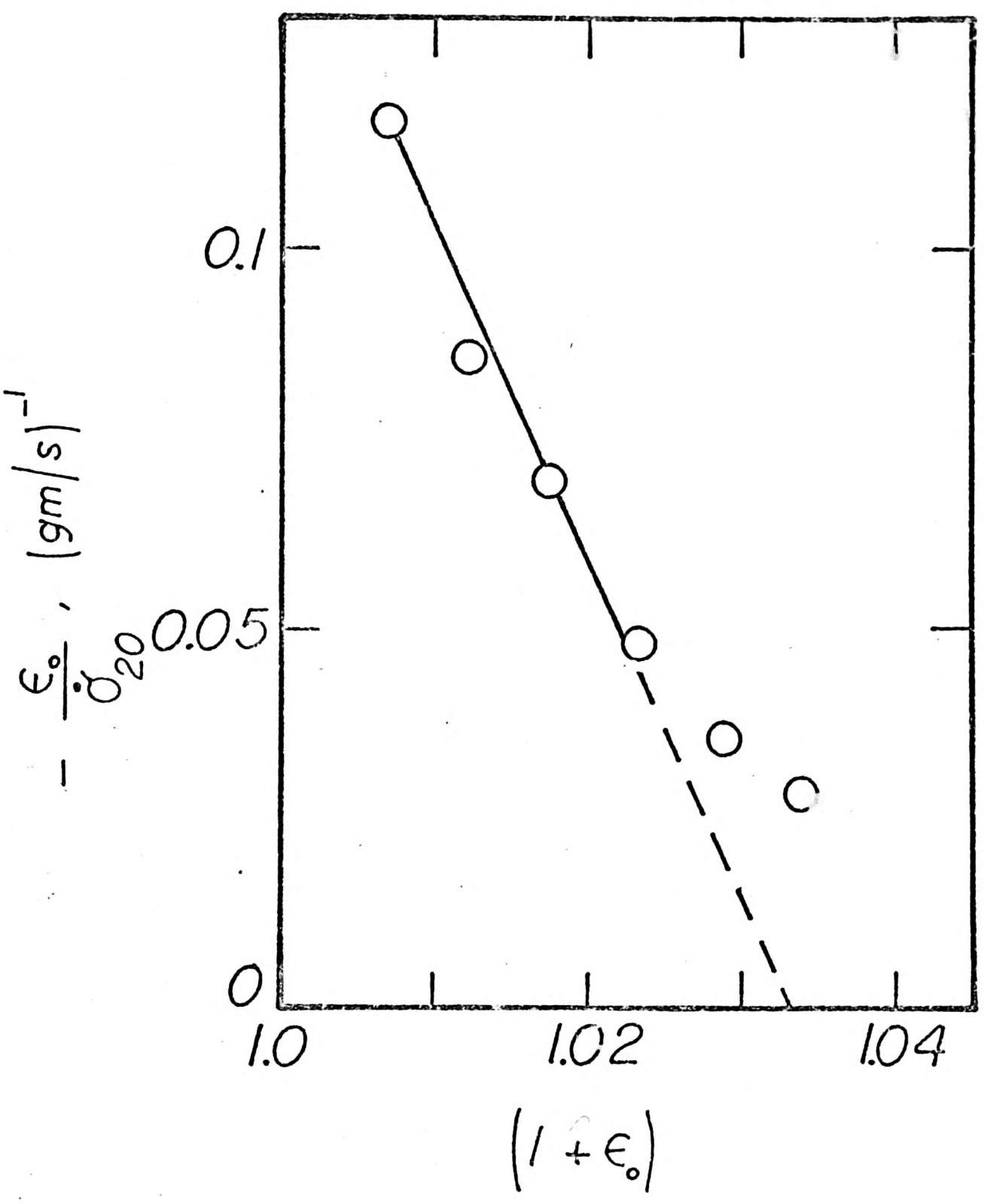


Figure 9-15

Plot of (strain/20s load rate) against $(1+\epsilon_o)$ for specimen CH2-5-1(m54,Heh), Intercept on abscissa gives $\theta_o = 14.5^\circ$ from equation (9.8)

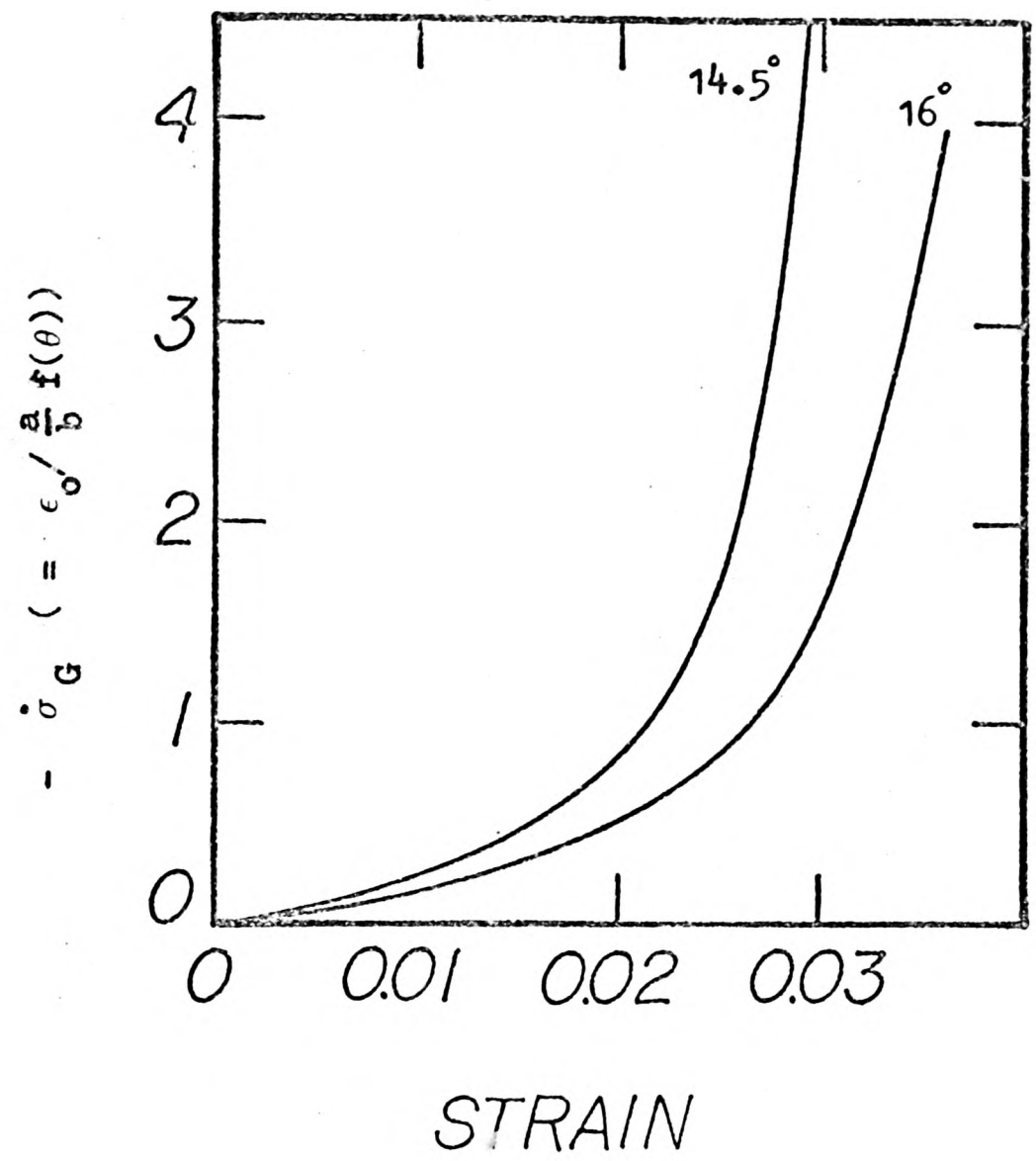


Figure 9-16

Theoretical plot of isochronal load rate against strain given by equation (9.8) with $\frac{a}{b}\Delta G_G \, \Gamma(n_G)/(t)^{n_G} = 1$ for two values of $\theta_o = 14.5^\circ$ and 16°.

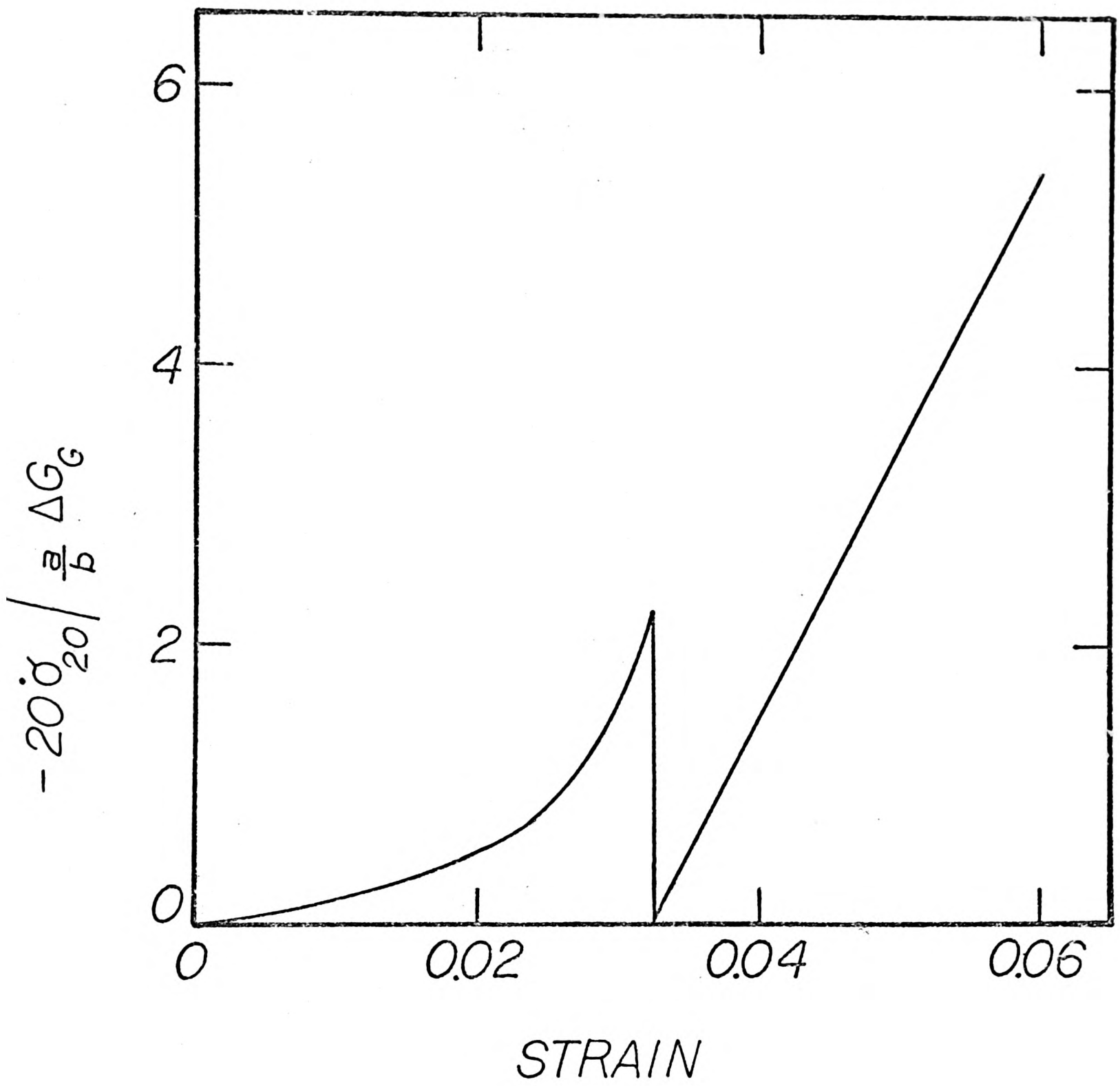


Figure 9-17

Theoretical plot of 20s load rate ($\dot{\sigma} / \frac{a}{b} \Delta G_G$) against strain given by equation (9.9) for one $\theta_o = 16^{\cdot}$, $\frac{a}{b}(\Delta G_G / \Delta E_F) = 0.005$, $n_F = n_G = 1.0$.

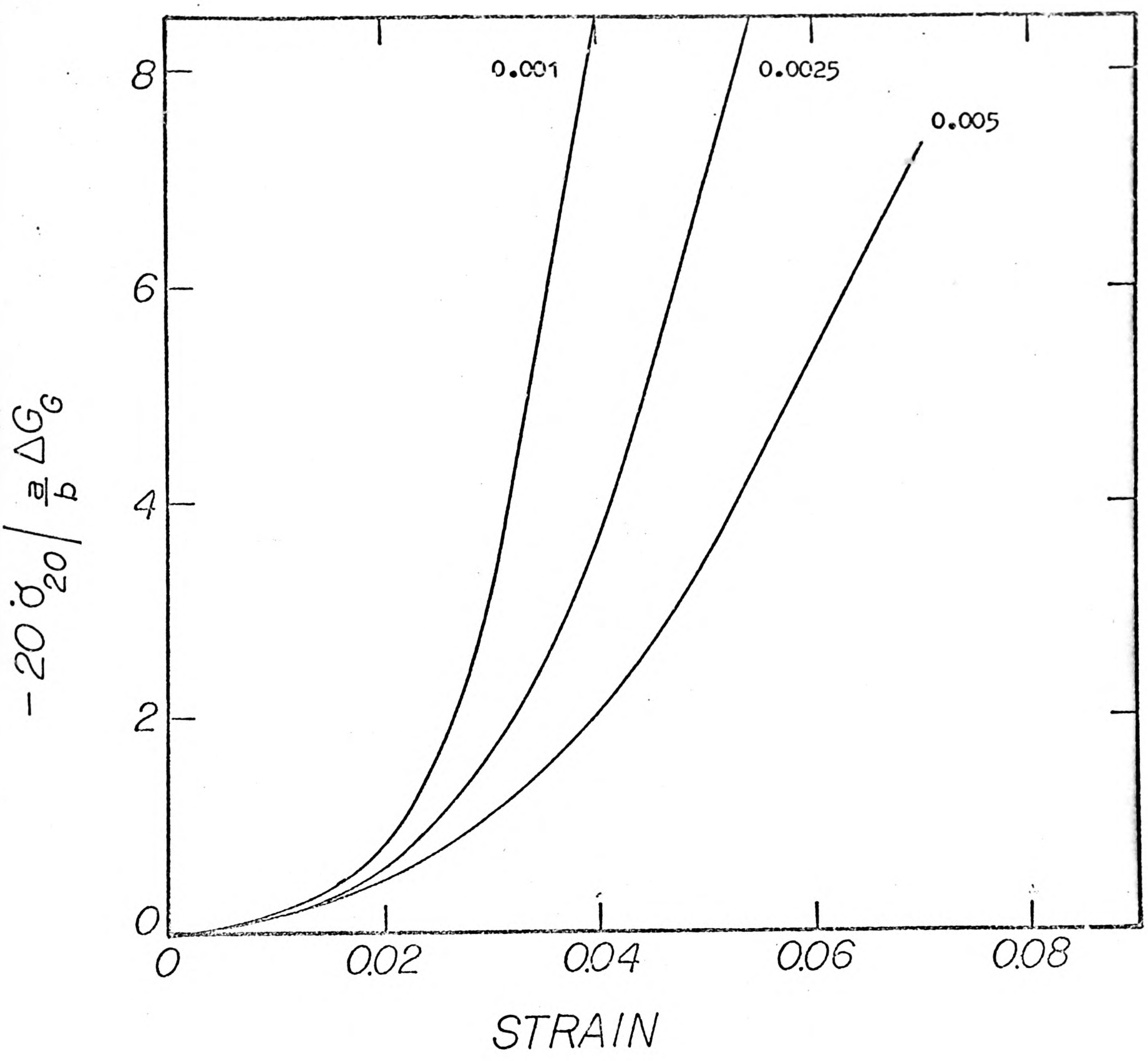


Figure 9-18

Theoretical plot of 20s load rate ($\dot{\sigma}/\frac{a}{b}\Delta G_G$) against strain given by equation (9.9) for a Gaussian distribution of crimp angles. $\bar{\lambda} = 2.0$, and values of $\frac{a}{b}(\Delta G_G/\Delta E_F) = 0.001, 0.0025, 0.005$, $n_F = n_G = 1.0$

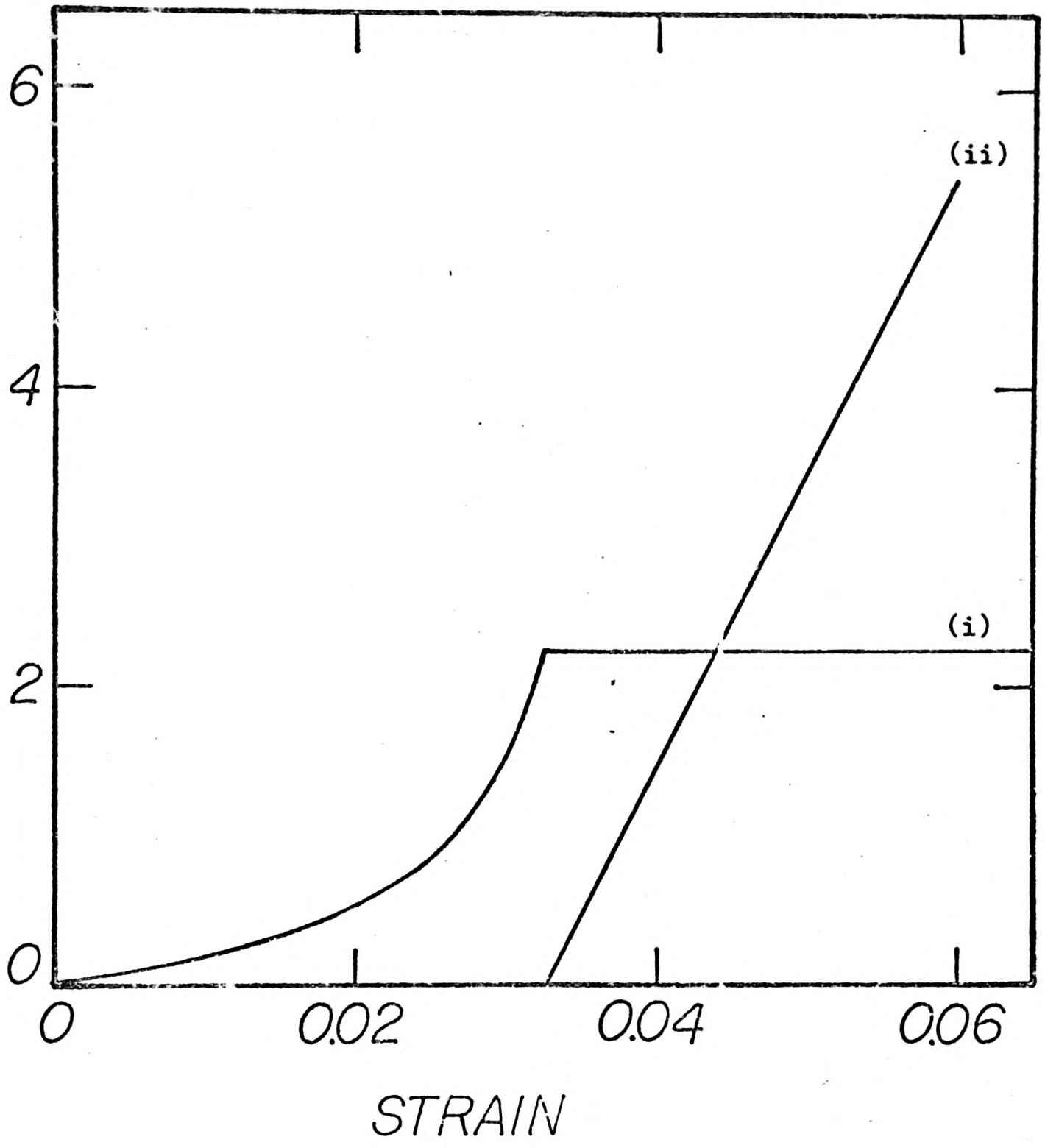


Figure 9-19

Theoretical plot of load against strain curve from equation (9.11) with a single value of $\theta_o = 16^\circ$, $C_1/C_2 = 0.005$
(i) curve due to crimp straightening
(ii) curve due to fibre stretching.

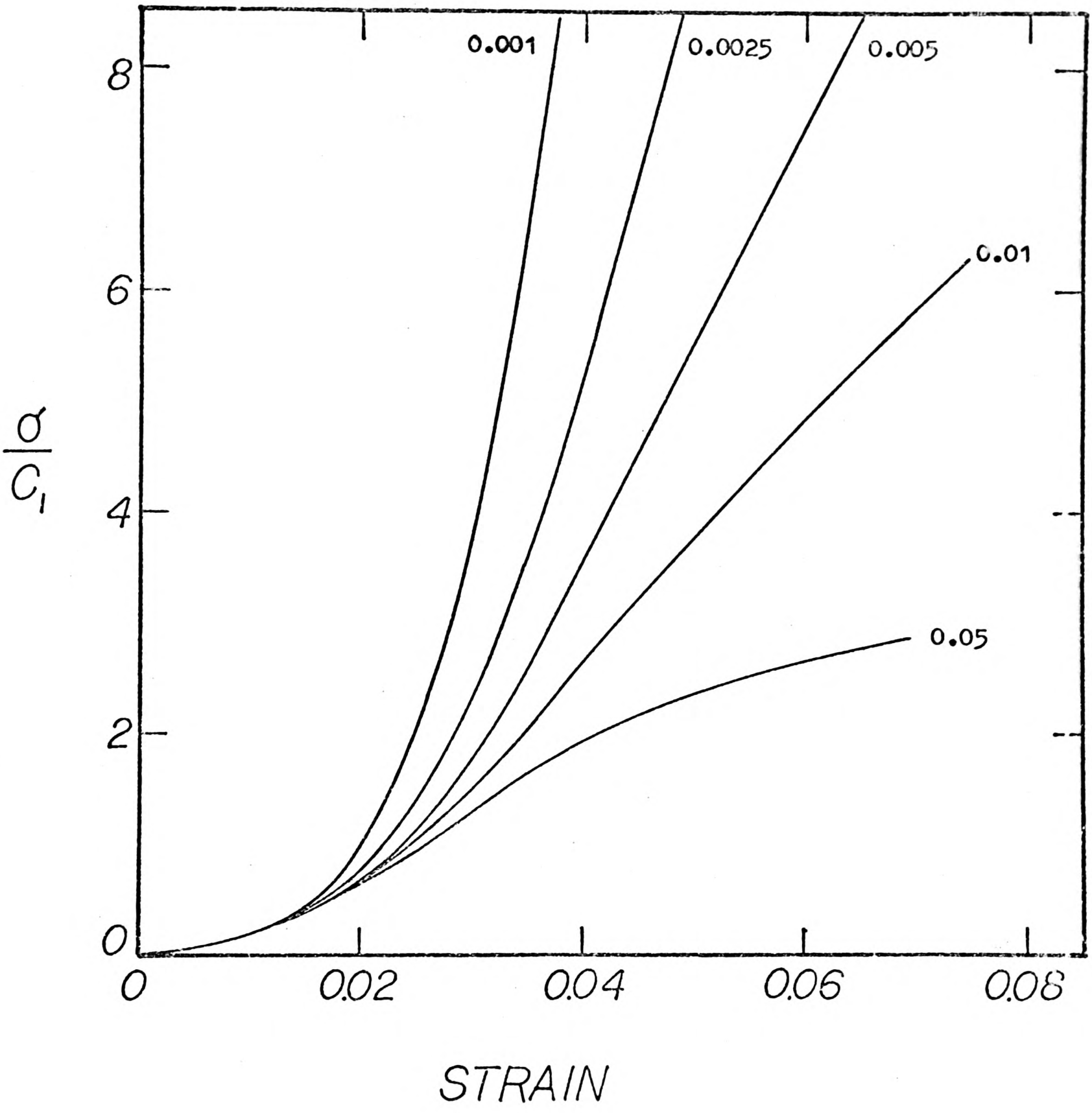


Figure 9-20

Theoretical plot of load against strain from equation (9.11) with a Gaussian distribution of θ_o's, $\bar{\lambda} = 2.0$, $\theta_o = 16^\circ$, and various values of $C_1/C_2 = 0.001, 0.0025, 0.005, 0.01, 0.05$.

Suggestions for Further Work

On the Viscoelastic Behaviour of Tendon

The modelling in chapters 7 and 8 provides a challenge for the future to find the standard deviation of the distribution of initial crimp angles of the collagen ribbons and fibres throughout the tendon in order to test the validity of the theoretical model. It would be interesting to see whether the predictions of the model correlate with changes in the crimp angle distribution. It would also be helpful to find the other unknown parameters of the model, namely ΔJ_G, ΔD_F, $\frac{b}{a}$, and the shape of the retardation spectrum, and to compare these with the values found from our model. Future work on tendon could also be concerned with the region beyond the 'linear' portion of the stress-strain curve where the fibres are thought to break down into smaller units.[1] It would be expected that the value for ΔE_u would change if the mechanism is changed in this region.

The ultimate aim is an artificial tendon. Some thought and time was spent on this and the following prototype developed. Crimplene fibres (2.8 denier) were wrapped around a metal former (~1000 strands/cm^2). The former was suspended in a solution of water, HEMA (2-hydroxy-ethyl methacrylate) and a crosslinking agent (ethylene glycol dimethacrylate) for sufficient time to allow the solution to permeate in between the fibres. (The contents of the solution were 70% H_2O, 0.5% crosslinking agent, 29.5% HEMA, based on original composition). It was subsequently crosslinked with a dose of 0.25 Mrad/hr for 4 hours at room temperature in air. This prototype was used for two reasons:

(i) it has crimped fibres as does tendon and

(ii) the hydrogel, PHEMA, which is considered to be highly blood compatible, contains ~75% water, (similar to that of body tissues), and as a gel may perform a similar function to that of the mucopolysaccharide gel.

Preliminary tests on this prototype, which was approximately the same size as the tendons employed in our earlier investigations were performed in an Instron tensile tester in constant strain rate experiments (strain rate ~1.7%/min). The stress-strain curve showed a 'toe' region of extent ~1% strain and a linear region, reproducible up to ~3 kg. It would be interesting to compare the viscoelastic properties of a synthetic composite of this type with those of the natural tendon, since the prototype contains the essential features of the natural tendon, i.e. a crimped fibre and a gel.

From the modelling of the previous chapters, certain other conditions for the artificial tendon must be met.

(i) the fibres must have a certain modulus as shown in figure 9-20.

(ii) the various combinations of the model parameters, e.g. ΔJ_G, and ΔD_F must be satisfied.

(iii) there must be a distribution of initial crimp angles, θ_o, the broadness of which could be varied and the resulting changes in the viscoelastic properties measured.

(iv) there should be a smooth transition from the low value of ΔH_{a_G} to that of the fibres, ΔH_{a_F}.

Even though PHEMA is particularly suitable for body implantation and the above type of artificial tendon might be useful for replacing damaged tendons, the problems involved in this, in particular, the need for a sheath in which the tendon can move and also the fact that fibrous tissue forms at the suture points which prevents easy sliding of the tendon within the sheath, may be difficult to overcome.

From the discussion of the T-jump equation in chapter 4, it is evident that a more rigorous analysis of the effect of b_T in creep of linear polyethylene[2] in the linear viscoelastic region would be useful. In particular,

it would now be possible to take the log creep rate-log time curves and fit them for the parameters a_T (or ΔH_a) and b_T from equations (4.29) and (4.31). Hence the parameter A in the McCrum and Morris[3] equation (4.6) which is a large problem in determining ΔH_a from the ln r- ΔT plot will not enter into the calculations. A check on the values of a_T and b_T can be obtained from the ln r- ΔT plot when it is fitted for these parameters and A'.

Confirmation of a b_T effect will be obtained in stress relaxation experiments. For the magnitude of this effect found by McCrum and Pearce[2], there should be a significant change in the shape of the curves on a log relaxation rate-log time plot from the case where b_T can be neglected. This will tell us for certain whether the b_T terms of equation (4.6) are significant for this material, since the curves bend in opposite directions in creep and stress relaxation. The values of a_T and b_T should again be obtained from fitting the log relaxation rate-log time curve and compared with those found from fitting the ln r- ΔT plot.

References

1 Torp S., Baer E. and Friedman B., Colston Papers (ed. Atkins E.D.T. and Keller A.) 26,223,1975. Butterworths, London.

2 McCrum N.G. and Pearce D.L., Nature, Physical Sci.,243,52,1973.

3 McCrum N.G. and Morris E.L., Phil.Mag.,7,2115,1962.

Appendix

Non-isothermal Viscoelastic Constitutive Equations

Case 1

To formulate the general non-isothermal constitutive equations, we considered a linear viscoelastic solid with a single retardation time, τ and relaxed and unrelaxed tensile compliances D_R and D_U respectively, and compliance difference $\Delta D = D_R - D_U$. All four of τ, ΔD, D_R and D_U are temperature dependent, but it is only necessary to consider τ and two of the compliance functions, which we choose to be ΔD and D_U. The temperature dependence of τ and ΔD are given in equations (3.2) and (3.3) and c_T is defined as

$$c_T = \frac{D_{U_T}}{D_U} \qquad (A.1)$$

where as in chapter 3, D_{U_T} and D_U are the unrelaxed compliances at temperatures T and T_o respectively. The material is subjected to an arbitrary temperature profile as shown in figure A-1, and, at time $u=t_o$ when the temperature is T_o, a constant stress, σ_o, is imposed. In this case, a_T, b_T and c_T are functions of time as shown schematically in figure A-1. After a small interval of time, $\Delta t = t_1 - t_o$ has elapsed, the strain $\epsilon(t_1)$ is given by

$$\frac{\epsilon(t_1)}{\sigma_o} = c_{T_1} D_U + \int_{t_o}^{t_1} \frac{b_{T_1}}{a_{T_1}} \frac{\Delta D}{\tau} \exp\left[-\left(\frac{t_1 - u}{a_{T_1}\tau}\right)\right] du \qquad (A.2)$$

where a_{T_1} and b_{T_1} are the values of a_T and b_T at time $t_o + \Delta t = t_1$ respectively, i.e. at temperature T_1.

In general, at time $t_n > t_{n-1} > t_{n-2}$ etc.,

$$\frac{\epsilon(t_n)}{\sigma_o} = c_{T_n} D_U + \int_{t_o}^{t_1} \frac{b_{T_1}}{a_{T_1}} \frac{\Delta D}{\tau} \exp\left[-\left(\frac{t_n - t_{n-1}}{a_{T_n}\tau}\right) - \left(\frac{t_{n-1} - t_{n-2}}{a_{T_{n-1}}\tau}\right) \cdots \left(\frac{t_2 - t_1}{a_{T_2}\tau}\right)\right]$$

$$\exp\left[-\left(\frac{t_1 - u}{a_{T_1}\tau}\right)\right] du + \int_{t_1}^{t_2} \frac{b_{T_2}}{a_{T_2}} \frac{\Delta D}{\tau} \exp\left[-\left(\frac{t_n - t_{n-1}}{a_{T_n}\tau}\right) - \left(\frac{t_{n-1} - t_{n-2}}{a_{T_{n-1}}\tau}\right) \cdots\right.$$

$$\ldots\ -\left(\frac{t_3-t_2}{a_{T_3}\tau}\right)\Bigg]\exp\left[-\left(\frac{t_2-u}{a_{T_2}\tau}\right)\right]du \;+\; \ldots\ldots + \int_{t_{n-1}}^{t_n} \frac{b_{T_n}}{a_{T_n}}\,\frac{\Delta D}{\tau}\,\exp\left[-\left(\frac{t_n-u}{a_{T_n}\tau}\right)\right]du$$

(A.3)

This can be integrated, and in the limit of the summation over n becoming the integral, this expression gives

$$\frac{\epsilon_1(t)}{\sigma_o} = c_T D_U + \Delta D \int_0^t \frac{b_T(\xi)}{a_T(\xi)\tau}\left[\exp - \int_\xi^t \frac{d\zeta}{a_T(\zeta)\tau}\right] d\xi \qquad \text{(A.4)}$$

where the subscript on ϵ refers to case 1. Hence, if the variation of a_T and b_T with time is known, then the strain $\epsilon(t)$ can be determined. Differentiation of equation (A.4) with respect to t and neglecting $\frac{d}{dt}(c_T D_U)$ which will in general be small,

$$\frac{\dot{\epsilon}_1(t)}{\sigma_o} = \frac{\Delta D}{a_T(t)\tau}\left\{ b_T(t) - \int_0^t \frac{b_T(\xi)}{a_T(\xi)\tau}\left[\exp - \int_\xi^t \frac{d\zeta}{a_T(\zeta)\tau}\right] d\xi \right\} \qquad \text{(A.5)}$$

Defining a normalised creep rate as

$$\Upsilon_1(t) = \frac{\left[\frac{d}{dt}\epsilon_1(t)\right]_{t=t}}{\left[\frac{d}{dt}\epsilon_1(t)\right]_{t=0}}$$

$$= \frac{a_T(t=0)}{b_T(t=0)}\,\frac{1}{a_T(t)}\left[b_T(t) - \int_0^t \frac{b_T(\xi)}{a_T(\xi)\tau}\,\exp\left\{ - \int_\xi^t \frac{d\zeta}{a_T(\zeta)\tau} \right\} d\xi \right]$$

(A.6)

Both a_T and b_T are unity at t=0, if T at t=0 is the reference temperature.

Case 2

A generalised retardation spectrum model with a temperature dependent limiting compliance difference.

For a single element of the generalised model, we have from equation (A.4) that

$$\frac{\epsilon_2(t)}{\sigma_o} = c_T D_U + \Delta D_i \int_0^t \frac{b_T(\xi)}{a_T(\xi)\tau_i} \exp\left\{ - \int_\xi^t \frac{d\zeta}{a_T(\zeta)\tau_i} \right\} d\xi \qquad (A.7)$$

where the subscript on ϵ refers to case 2. In the limit of a continuous distribution of retardation elements,

$$\frac{\epsilon_2(t)}{\sigma_o} = c_T D_U + \int_o^\infty \Delta D(\tau) \left[\int_o^t \frac{b_T(\xi)}{a_T(\xi)\tau} \exp\left\{ - \int_\xi^t \frac{d\zeta}{a_T(\zeta)\tau} \right\} d\xi \right] d\tau \qquad (A.8)$$

It should be noted that a_T and b_T weight equally all the retardation times and compliance differences respectively, i.e. $a_T \neq a_T(\tau)$. This is an assumption of thermorheological simplicity.

For a retardation spectrum $L(\tau) = \Delta D(\tau)\,\tau$ and remembering that both τ and $\Delta D(\tau)$ are taken at the reference temperature,

$$\frac{\epsilon_2(t)}{\sigma_o} = c_T D_U + \int_{-\infty}^\infty L(\ln \tau) \left[\int_o^t \frac{b_T(\xi)}{a_T(\xi)\tau} \exp\left\{ - \int_\xi^t \frac{d\zeta}{a_T(\zeta)\tau} \right\} d\xi \right] d \ln \tau \qquad (A.9)$$

and the creep rate is

$$\frac{\dot{\epsilon}_2(t)}{\sigma_o} = \int_{-\infty}^\infty \frac{1}{a_T(t)\tau} \frac{L(\ln \tau)}{\tau} \left[b_T(t) - \int_0^t \frac{b_T(\xi)}{a_T(\xi)\tau} \exp\left\{ - \int_\xi^t \frac{d\zeta}{a_T(\zeta)\tau} \right\} d\xi \right] d \ln \tau \qquad (A.10)$$

and the normalised creep rate is

$$T_2(t) = \frac{\left[\frac{d}{dt}\,\epsilon_2(t)\right]_{t=t}}{\left[\frac{d}{dt}\,\epsilon_2(t)\right]_{t=0}}$$

$$= \frac{a_T(t=0)}{b_T(t=0)}\;\frac{1}{a_T(t)}\;\frac{\int_{-\infty}^{\infty}\frac{L(\ln\tau)}{\tau}\left[b_T(t) - \int_0^t \frac{b_T(\xi)}{a_T(\xi)\tau}\,\exp\left\{-\int_\xi^t \frac{d\zeta}{a_T(\zeta)\tau}\right\}d\xi\right]d\ln\tau}{\int_{-\infty}^{\infty}\frac{L(\ln\tau)}{\tau}\,d\ln\tau} \qquad (A.11)$$

Case 1 with a Ramp Temperature Profile

For the ramp in temperature used in equation (3.8) and with a_T and b_T given by equations (3.9) and (3.10), then the expressions obtained for the creep rate are as follows:

$t < t'$

$$\frac{\dot\epsilon(t)}{\sigma_o} = \frac{\Delta D}{\tau}\,\exp\left(-\frac{t}{\tau}\right) \qquad (A.12)$$

$t' < t < t''$

$$\frac{\dot\epsilon(t)}{\Delta D\,\sigma_o} = \frac{1}{a_{T_2}\tau}\left[(b_{T_2}-1) + \exp-\left\{\frac{t'}{\tau} + \frac{C_1}{\tau}\left(\frac{1}{a_{T_2}}-1\right)\right\}\right.$$

$$\left.-\frac{\lambda\,\Delta T}{(t''-t')}\left[(t-t')\left(1-\exp\left(\frac{-C_1}{a_{T_2}\tau}\right)\right) - C_1\exp\left(\frac{-C_1}{a_{T_2}\tau}\right)\right.\right.$$

$$\left.\left.\left\{\frac{C_1}{\tau}\left(\left(\frac{1}{a_{T_2}}\right)-1\right) + \frac{1}{2.2!}\left(\frac{C_1}{\tau}\right)^2\left(\left(\frac{1}{a_{T_2}}\right)^2 - 1\right) + \ldots\ldots\right\}\right]\right] \qquad (A.13)$$

$t > t''$

$$\frac{\dot{\epsilon}(t)}{\Delta D\,\sigma_o} = \frac{1}{a_{T_3}\tau}\exp-\left(\frac{t-t''}{a_{T_3}\tau}\right)\left[(b_{T_3}-1) + \exp-\left\{\frac{t'}{\tau}+\frac{C_1}{\tau}\left(\frac{1}{a_{T_3}}-1\right)\right\}\right.$$

$$-\frac{\lambda\Delta T}{(t''-t')}\left[(t''-t')\left(1-\exp\left(\frac{-C_1}{a_{T_3}\tau}\right)\right) - C_1\exp\left(\frac{-C_1}{a_{T_3}\tau}\right)\right.$$

$$\left.\left.\left\{\frac{C_1}{\tau}\left(\left(\frac{1}{a_{T_3}}\right)-1\right)+\frac{1}{2.2!}\left(\frac{C_1}{\tau}\right)^2\left(\left(\frac{1}{a_{T_3}}\right)^2-1\right)+\ldots\ldots\right\}\right]\right] \qquad (A.14)$$

where $C_1 = \dfrac{RT_o^{\,2}(t''-t')}{\Delta H_a\,\Delta T}$

and a_{T_2}, b_{T_2} are the values of a_T and b_T in the region $t' < t < t''$

and a_{T_3}, b_{T_3} are the values of a_T and b_T in the region $t > t''$.

Equation (A.14) can be written as

$$t > t'' \qquad \ln\frac{\epsilon(t)}{\Delta D\,\sigma_o} = K_1 + K_2 t \qquad (A.15)$$

where K_1 and K_2 are independent of time and

$$K_1 = -\ln a_{T_3}\tau + \frac{t''}{a_{T_3}\tau} + \ln\left[\exp-\left\{\frac{t'}{\tau}+\frac{C_1}{\tau}\left(\frac{1}{a_{T_3}}-1\right)\right\} + (b_{T_3}-1)\right.$$

$$-\frac{\lambda\Delta T}{(t''-t')}\left[(t''-t')\left(1-\exp\left(-\frac{C_1}{a_{T_3}\tau}\right)\right) - C_1\exp\left(\frac{-C_1}{a_{T_3}\tau}\right)\left\{\frac{C_1}{\tau}\left(\frac{1}{a_{T_3}}-1\right)+\ldots.\right.\right.$$

$$\left.\left.\left.+\ldots.\right\}\right]\right] \qquad (A.16)$$

and

$$K_2 = -\frac{1}{a_{T_3}\tau} \qquad (A.17)$$

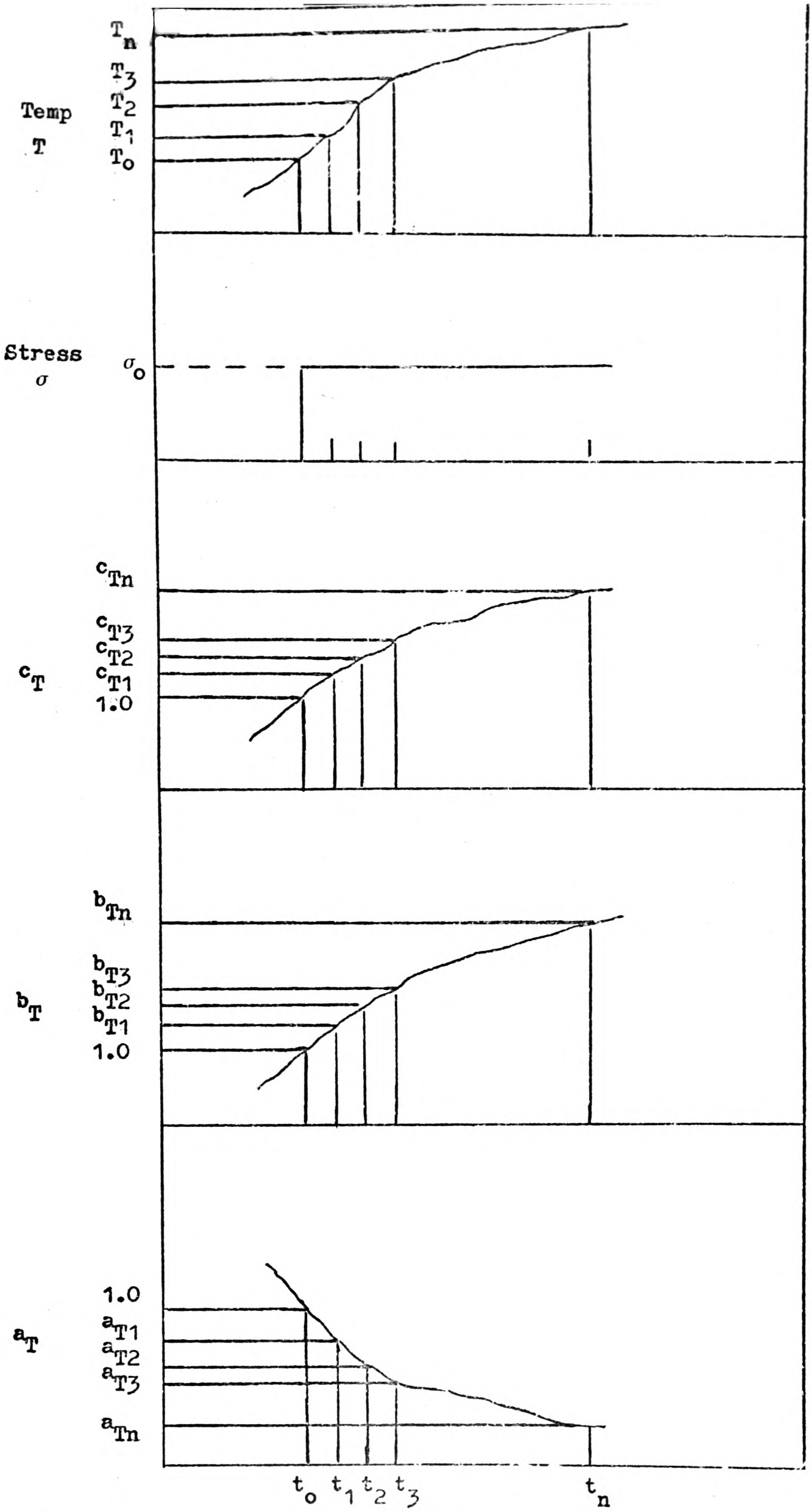


Figure A-1

Schematic diagram showing the temperature profile, (T against u) and the variation with time, u, of the parameters a_T, b_T, c_T and stress, σ. The stress is applied at time t_o when the temperature is the reference temperature T_o. The values of a_T, b_T, c_T at the various temperatures T_1 T_2, T_3, T_4, etc. are also shown.